PHYS

VOLUME 61

THE PHYSICAL REVIEW

A journal of experimental and theoretical physics established by E. L. Nichols in 1893

Published by the American Physical Society
at the
AMERICAN PHYSICAL SOCIETY
Editorial
President
I. I. RABI
Columbia University
New York, New York
Vice-President
C. C. LAURITSEN
California Institute of Technology
Pasadena, California
Secretary
E. E. DARROW
Bell Telephone Laboratories
Office:
Columbia University
New York 27, New York
Treasurer
C. S. PEGRAM
Columbia University
New York 27, New York
Local Secretary
for the Pacific
J. KAPLAN
University of California at Los Angeles
Los Angeles, California
Managing Editor
E. L. HILL
University of Minnesota
Minneapolis, Minnesota

BOARD OF EDITORS

Editor
E. L. HILL

Assistant Editor
J. W. BUCHTA

Associate Editors

S. A. GOUDSMIT — W. E. LAMB, JR. — HARVEY BROWN
E. M. PURCELL — R. G. HERB — R. F. CHRISTY
V. F. WEISSKOPF — J. BARDEEN — RAOUL K. KIRKWOOD

Manuscripts for publication should be submitted to E. L. Hill, University of Minnesota, Minneapolis, Minnesota. The authors' institutions are requested to pay a publication charge of $5 per page which, if honored, entitles them to 100 free reprints. Instructions will be sent with galley proof.

Proof and all correspondence concerning papers in the process of publication should be addressed to the Publication Manager, American Institute of Physics, 57 East 55 Street, New York 22, New York.

Subscription Price

United States and Canada $15.00
Elsewhere $17.00

Back Numbers[1]

Yearly back number rate when complete year is available:
Prior to 1940: $26.00
Thereafter: $27.00
Single copies: $2.00 each, prior to July, 1929;
$1.00 each, July, 1929–December, 1941;
$2.00 each, January, 1942–December, 1945;
$1.00 each, January, 1946–December, 1948;
$1.25 each, thereafter.
General index, 1893–1970: $4.00.

Subscriptions, renewals, and orders for back numbers should be addressed to the American Institute of Physics, 57 East 55 Street, New York 22, New York.

Changes of address in the case of members of the American Physical Society should be addressed to the Treasurer; in the case of other subscribers to the American Institute of Physics.

[1]For Series I (replies of Physics Department, Cornell University, Ithaca, New York)

The Physical Review is published semi-monthly at Prince and Lemon Streets, Lancaster, Pennsylvania.

Entered as second class matter March 6, 1941, at the Post Office at Lancaster, Pennsylvania, under the Act of March 3, 1879.

Acceptance for mailing at special rate of postage provided for in paragraph (d-2), section 34.40, P. L. & R. of 1948, authorized January 26, 1949.

THE
PHYSICAL REVIEW

A journal of experimental and theoretical physics established by E. L. Nichols in 1893

SECOND SERIES, VOL. 81, NO. 2 JANUARY 15, 1951

On the Nucleon-Nucleon Interaction*

ROBERT JASTROW**
Institute for Advanced Study, Princeton, New Jersey
(Received August 18, 1950)

A charge-independent interaction between nucleons is assumed, which is characterized by a short range repulsion interior to an attractive well. It is shown that it is then possible to account for the qualitative features of currently known n-p and p-p scattering data. Some of the implications for saturation are discussed.

I. INTRODUCTION

RECENT experiments[1] on p-p scattering at 340 Mev indicate a cross section roughly isotropic between 20° and 90° with a mean magnitude of approximately 4 mb/sterad. This result is in strong contrast to that obtained in n-p experiments at comparable energies where a marked anisotropy is observed, the cross section at 260 Mev rising from approximately[2] 1.2 mb at 90° to 10 mb at 180°. At low energies, however, a complete charge independence is observed in the singlet state, within the limits of error in the determination of the singlet scattering parameters.[3,4]

A striking feature of the p-p observations lies in their qualitative disagreement with the results expected from a central attractive potential consistent with the low energy scattering, as shown in Fig. 3, curve I. This potential predicts strong forward scattering at 340 Mev, with a cross section of 0.2 mb at 90° which rises steeply[5] to 11 mb at 0°. The appearance of strong forward scattering at high energies is indeed a characteristic of the scattering from any central potential which does not change sign, as can be seen from the expressions for the differential cross sections,

$$\sigma_{np}(\theta)=\tfrac{1}{4}|f_s(\theta)|^2+\tfrac{3}{4}|f_t(\theta)|^2$$
$$=\tfrac{1}{4}\lambda^2\sum_l\sum_{l'}(2l+1)(2l'+1)\sin\delta_l^s\sin\delta_{l'}^s\cos\delta_{ll'}^s P_lP_{l'}$$
$$+\tfrac{3}{4}\lambda^2\sum_l\sum_{l'}(2l+1)(2l'+1)$$
$$\times\sin\delta_l^t\sin\delta_{l'}^t\cos\delta_{ll'}^t P_lP_{l'}; \quad (1a)$$

$$\sigma_{pp}(\theta)=\tfrac{1}{4}|f_s(\theta)+f_s(\pi-\theta)|^2+\tfrac{3}{4}|f_t(\theta)-f_t(\pi-\theta)|^2$$
$$=\lambda^2\sum_{\substack{l,l'\\ \text{even}}}\sum(2l+1)(2l'+1)\sin\delta_l^s\sin\delta_{l'}^s\cos\delta_{ll'}^s P_lP_{l'}$$
$$+3\lambda^2\sum_{\substack{l,l'\\ \text{odd}}}\sum(2l+1)(2l'+1)$$
$$\times\sin\delta_l^t\sin\delta_{l'}^t\cos\delta_{ll'}^t P_lP_{l'}. \quad (1b)$$

Here the superscripts s and t refer to singlet and triplet states, respectively. Successive even Legendre polynomials alternate in sign at 90°, hence the interference terms between states of successive even angular momenta in the p-p cross section, such as the $S-D$ term, for example, are negative at 90° and positive at 0°, provided the potential is everywhere of the same sign and the phases are therefore all of the same sign. The scattering is, consequently, predominantly forward at energies sufficiently high to excite a number of angular momenta. The contribution from states of odd angular momentum is zero at 90° and rises to a maximum at 0°, increasing the forward effect.

We wish to show that it is possible, nonetheless, by means of a charge-independent static potential,[6] to

* Supported by the AEC by a grant to the Institute for Advanced Study.
** Now at the Radiation Laboratory, University of California, Berkeley, California.
[1] O. Chamberlain and C. Wiegand, Phys. Rev. 79, 81 (1950), and private communication with E. Segrè, through whose kindness I am able to quote unpublished values on the mean magnitude of the 340 Mev p-p cross section.
[2] Kelly, Leith, Segrè, and Wiegand, Phys. Rev. 79, 96 (1950).
[3] H. A. Bethe, Phys. Rev. 76, 38 (1949).
[4] H. A. Bethe and C. Longmire, Phys. Rev. 77, 647 (1950).
[5] R. S. Christian and H. P. Noyes, Phys. Rev. 79, 85 (1950).
[6] The velocity-dependent spin-orbit interaction has been investigated by K. M. Case and A. Pais [Phys. Rev. 80, 203 (1950)],

account for the isotropic distribution observed in p-p scattering at high energies while maintaining the anisotropy in n-p scattering at comparable energies.

II. THE INTERACTION

A charge-independent interaction is assumed, the differences in n-p and p-p scattering then being only those determined by the exclusion principle in (1a) and (1b), namely, the domination of σ_{pp} over σ_{np} by a factor of four and the elimination in the former of the odd singlet and even triplet states.

We adopt an interaction characterized in the singlet states by a short-range repulsion and a surrounding attractive well, the parameters in the combination being chosen for agreement with low energy scattering constants.[7] The attractive part of the field is perhaps to be associated with the π-meson and the short-range repulsion with a heavier particle.

The small magnitude of the triplet effective range (1.7×10^{-13} cm) precludes the possibility of a triplet repulsion larger than 0.2×10^{-13} cm. Since the effects of a core of this size are unimportant at the energies considered, we may simplify the interaction by taking the triplet radius of repulsion to be zero.

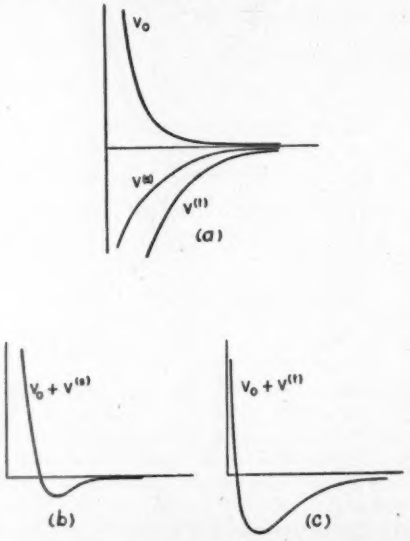

FIG. 1. Composition of the potential from a repulsion constant in all states and a spin-dependent attractive well. V_0=repulsion potential, V_t=triplet attraction, V^s=singlet attraction.

who conclude that it is possible by means of a singular interaction of this type to represent qualitatively the n-p and p-p cross sections on a charge-independent basis. Some consequences of spin-orbit coupling have also been considered by Blanchard, Avery, and Sachs [Phys. Rev. 78, 292 (1950)].

[7] A similar type of interaction has been considered by N. M. Kroll in connection with p-p scattering. P. O. Olsson has examined the possibility of introducing a repulsion into the n-p interaction, as have also G. Parzen and L. Schiff [Phys. Rev. 74, 1564 (1948)].

The assumption of a spin-dependent core radius is somewhat artificial. However, the absence of the core in the triplet states may also be considered as arising from the superposition of an attractive well of spin-dependent depth on a repulsive interaction constant in all states (Fig. 1).

The triplet interaction is assumed to be the same as that fitted by Christian and Hart[8] to the deuteron constants and low energy n-p scattering parameters, except for the addition of a weak tensor force in the odd states.

The repulsive field is represented by a hard sphere for convenience in calculation. An exponential radial dependence is chosen for the attractive well since the S phase may then be expressed analytically.[9] The interaction then takes the form:

$$\text{Singlet: } V=\infty, \quad r<r_0;$$

$$V=V_{0s}\exp\left(-\frac{r-r_0}{r_s}\right)\left(\frac{1+P_x}{2}\right), \quad r>r_0. \tag{2}$$

$$\text{Triplet: } V=\{a+(1-a)P_x + [b+(1-b)P_x]\gamma S_{12}\}V_{0t}\exp(-r/r_t).$$

If one chooses $r_0=0.60\times10^{-13}$ cm, the remaining parameters are then fixed at the following values by the deuteron constants and by n-p and p-p scattering at various energies:

$r_0=0.60\times10^{-13}$ cm	$V_{0s}=375$ Mev[10]
$r_s=0.40\times10^{-13}$ cm	$V_{0t}=69$ Mev
$r_t=0.75\times10^{-13}$ cm	$\gamma=1.84$
$a=0.50$	$b=0.30$

III. P-P SCATTERING

A. Qualitative Effect of the Core

The introduction of a short-range singlet repulsion has the following effect on p-p scattering. When energies are reached comparable with or greater than the depth of the surrounding attractive well, the S wave will be affected less by the well than by the inner core, and the sign of the S phase shift will change from positive to negative in this energy region. States of higher angular momentum are, however, affected more by the outer or attractive region of the potential, and the corresponding phase shifts will remain positive until energies are reached which are greater than that at which the S phase changes sign. Thus, there will

[8] R. S. Christian and E. W. Hart, Phys. Rev. 77, 441 (1950).

[9] The exponential well possesses this advantage over the Yukawa well. With regard to the possibility of other radial forms, the only important requirement is that the tail of the well be approximately as long as that of the exponential or Yukawa wells.

[10] The magnitude of the singlet well depth arises from the narrow range employed. Although large in comparison with the customarily quoted well depths for square wells without repulsion, the figure of 375 Mev appears to be more reasonable when compared with the singlet and triplet depths of 100 and 160 Mev, respectively, which occur when the exponential well without core is used.

always exist an energy region in which the sign of the S phase is opposite to that of states of higher angular momentum. In this region the $S-D$ interference term in (1b) will be positive at 90° and negative at 0°, tending to destroy the forward scattering and build up the scattering[11] at 90°.

These effects are illustrated in Fig. 2, where the singlet p-p cross sections are plotted for three sets of parameters in the neighborhood of those given in (2).

The dip in the singlet cross section at intermediate angles is a consequence of the vanishing of the Legendre polynomial, P_2, at 55°. Tensor scattering fills in this gap, resulting in the 340-Mev p-p cross section shown in Fig. 3, curve II, for $r_0=0.60\times10^{-13}$ cm. Between 90° and 30° curve II agrees with the experimental values of 4.0 ± 0.6 mb.[1] At 20°, however, it has risen to 6.2 mb in disagreement with observation. An increase of this order of magnitude at small angles is characteristic of the interaction. It is possible that the rise may be diminished by the assumption of a more complicated potential of the same general type. However, in view of the neglect of nonstatic forces and relativistic effects an emphasis on precision of fit is probably unjustified in comparison with the importance of simplicity in the potential.

The central phases entering into the p-p cross sections were computed by numerical integration with the exception of $L=2$ at 30 Mev and $L=4$ at higher energies, where the Born approximation was permissible. Tensor scattering was computed in the Born approximation with the exception of 30 Mev where tensor-Coulomb interference was included.[12]

B. The Scattering at 30 Mev

The comparison of the scattering experiments at 30 Mev with the scattering expected from an attractive well consistent with the low energy data has been made by Christian and Noyes,[8] and we mention here only the most important points. The experiments indicate a cross section with a mean magnitude of approximately 14 mb on which is superposed a drop of 2 mb between 90° and 25°. On the other hand, the scattering from a Yukawa well consistent with the low energy data consists of S scattering of mean magnitude 15 mb on which is superposed a *rise* of approximately 2 mb having its origin in a large D phase shift. The magnitude of the D phase results from the long-tailed character of the Yukawa well.[13]

An important effect of the hard core at 32 Mev lies in the diminution of the D phase shift. The origin of this decrease can be seen as follows. In general, the

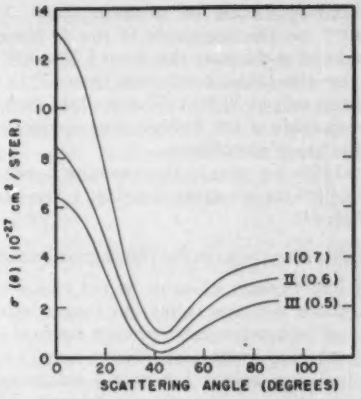

FIG. 2. Singlet p-p cross section at 340 Mev, calculated from potential (2) for several core radii: I. $r_0=0.70$. II. $r_0=0.60$. III. $r_0=0.50$ (units of 10^{-13} cm).

introduction of the hard sphere interaction increases the effective range of the potential,[14] and one has, in fact, the approximate relation valid for large scattering length,

$$r_{eff}\sim2(r_0+2r_1) \tag{3}$$

where r_{eff} is the effective range, r_0 the core radius and, r_1 the range of the surrounding well. In order to keep

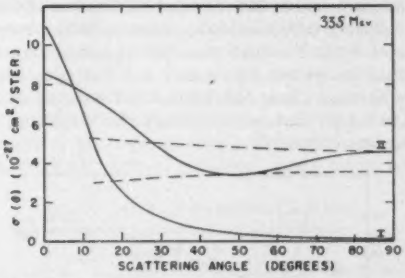

FIG. 3. Differential p-p cross section at 340 Mev calculated from potential (2) assuming I. $r_0=0.60\times10^{-13}$. II. $r_0=0$.

the effective range at the value determined by low energy scattering it is necessary to decrease the range of the surrounding attractive well below its value without the core. The consequent contraction of the tail of the well reduces the phase shifts of all states with $L>0$. With $r_0=0.60\times10^{-13}$ cm the range of the

[11] Only the $S-D$ interference term is mentioned because singlet states with L greater than 2 do not make important contributions at the energies with which we are concerned.

[12] I am indebted to R. S. Christian and H. P. Noyes for communication of their results on the calculation of this term.

[13] The long-tailed exponential and Yukawa wells lead to D phase shifts of 1.2° and 1.4°, respectively, at 32 Mev. The square well is superior in this respect, predicting a D phase shift of only 0.6°.

[14] This can be seen from the useful formula of H. A. Bethe for the effective range (reference 3),

$$\tfrac{1}{2}r_0=\int_0^\infty(v_0^2-u_0^2)r^2dr$$

where u_0 and v_0 are the zero-energy wave functions in the presence and absence, respectively, of the nuclear potential. It is clear that the introduction of a short-range repulsion, keeping the volume of the surrounding well constant, will decrease u_0 in the region occupied by the repulsion, thereby increasing r_0.

exponential well must be decreased from 0.72 to 0.40×10^{-13} cm the magnitude of the D phase shift being reduced at the same time from 1.2° to 0.6°.

The core also causes a reduction from 47° to 42° in the S phase shift at 30 Mev. The resultant drop in the mean magnitude of the 30-Mev cross section is made up by the tensor contribution.

The 30-Mev p-p cross section assuming a core radius of 0.60×10^{-13} cm is compared in Fig. 4 with the data at 29.4 Mev.[15]

C. Possible Variations in the Interaction Parameters

An initial freedom exists as to the choice of core radius. When the core radius has been selected the singlet well parameters in even states are fixed by the singlet scattering length and effective range, as determined from low energy n-p or p-p scattering. The triplet interaction in even states is determined by the deuteron constants and by the n-p triplet scattering parameters and must be identical with the Christian-Hart interaction in these states, once the possibility of a triplet repulsion of appreciable radius has been excluded. N-p scattering at high energies indicates that there is no appreciable central force in odd states, thus determining the amount of space exchange in the singlet and triplet wells.[8] The core is considered as a phenomenological manifestation of nucleonic structure and probably not subject to ordinary exchange effects. The strength of the tensor force in odd states is fixed by the requirement that at 340 Mev and 90° the sum of tensor and singlet contributions to σ_{pp} must equal the observed value of 4 mb. The form of radial dependence is somewhat arbitrary, but high energy n-p scattering apparently requires a long-tailed well,[8] and it seems reasonable to require that this be the same for the central and tensor interactions.

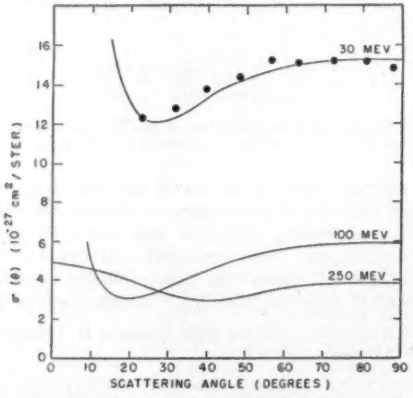

FIG. 4. Differential p-p cross sections at intermediate energies calculated from (2) with $r_0=0.60\times10^{-13}$ cm.

[15] W. K. H. Panofsky and F. Filmore, UCRL Report 481, unpublished.

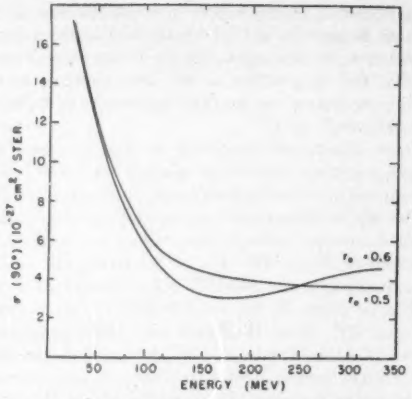

FIG. 5. p-p cross section at 90° vs. energy, calculated from (2) for core radii of 0.50 and 0.60×10^{-13} cm.

Thus, on the assumption of a given radial dependence, the only important free parameter is the core radius. The effect of variations in the core radius on the singlet cross section at 340 Mev is shown in Fig. 2. The choice of $r_0=0.60$ (curve II) represents the best compromise between the demand for a flat cross section at 340 Mev and for the correct mean magnitude at 30 Mev.

An increased core radius (curve I) results in an increase in the singlet cross section at 90° and below 40°. In order that the 90° cross section at 340 Mev shall remain 4 mb, it is necessary to decrease the tensor strength. Consequently, the singlet dip in the neighborhood of 55° is less completely filled, while at the same time the singlet scattering below 40° has been increased, the net effect being the destruction of the desired isotropy.

For the same reason, a decrease in the core radius (curve III), and consequently in the 90° singlet cross section at 340 Mev, requires an increase in tensor strength. The effect of the singlet dip at intermediate angles is thereby removed while at the same time the singlet forward scattering is reduced, resulting in a materially greater degree of isotropy. However, the necessary increase in tensor strength is accompanied by an excessive tensor contribution at lower energies, destroying the agreement with observation at 30 Mev. With $r_0=0.50\times10^{-13}$ cm the 30-Mev cross section is 17 mb at 90°, decreasing to 11.5 mb at 25°. (Compare with Fig. 4.)

D. Energy Dependence of the 90° Cross Section

In the neighborhood of 150 Mev the S phase shift changes sign in consequence of the interference between positive and negative regions of the potential. The small magnitude of $\delta_0{}^s$ in this region results in the appearance of a minimum in the singlet cross section between 100 and 200 Mev, which is partially compen-

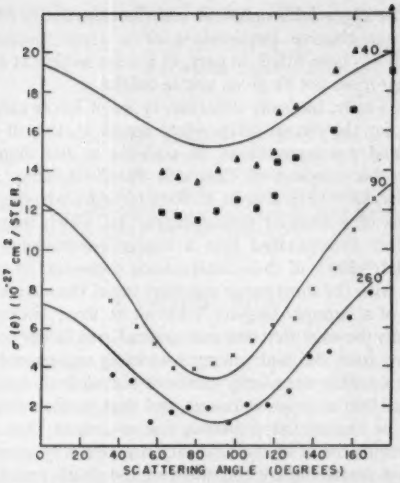

FIG. 6. Differential n-p cross sections calculated from (2) for a core radius of 0.60×10^{-13} cm. The experimental distributions are taken from reference 2. ■ 40-Mev distribution normalized to the total cross section measurement of Segrè, *et al.* (reference *a* of Table I). ▲ 40-Mev distribution normalized to the total cross section measurement of Hildebrand and Leith (reference *b* of Table I) × 90 Mev (reference *a* of Table I). ● 260 Mev (see reference 2).

sated by a rise in the tensor cross section. The variation of the resultant 90° cross section with energy is shown in Fig. 5 for core radii of 0.50 and 0.60×10^{-13} cm. It is seen that the effect of the dip in the singlet cross section becomes more pronounced with increasing core radius.

The angular distributions at 100 Mev and 250 Mev are shown in Fig. 4, with the effect of the Coulomb field included at the lower energy. One sees that the variation of the cross section with energy and with angle is surprisingly small between 100 Mev and 350 Mev.

IV. *N-P* SCATTERING

The principal contribution to the n-p cross section comes from the triplet states because of their statistical weight,[16] hence the n-p cross section predicted by (2) may be expected to have the same general characteristics as the Christian-Hart cross section. Figure 6 compares the n-p cross sections calculated from (2) with the observed distributions.[2]

The major effect on the n-p cross section of the changes introduced into the Christian-Hart interaction appears in the total cross sections, which are seen to be relatively larger at high energies (Table I). The experimental value at 40 Mev is rather uncertain. The angular distribution at 40 Mev in Fig. 6 has been normalized both to the value of 170 mb determined by Segrè, *et al.*,[2] as well as to the value of 203 mb obtained by Leith, *et al.*[17]

The effect of odd tensor forces has not been included in Fig. 6. Calculations by Christian[18] indicate that the major effect of these forces on the angular distribution is a decrease of the order of 10° in the position of the minimum in the cross section. Their contribution to the total cross section varies from 10 percent at 40 Mev to 25 percent at 260 Mev and has been included in the figures of Table I.

Figure 6 indicates that at 40 Mev the theoretical value of $\sigma(\pi)/\sigma(\pi/2)$ is 1.3 as compared to the experimental value of 1.55. The discrepancy can be removed by assuming a triplet well with a longer tail, [$\sigma(\pi)/\sigma(\pi/2)=1.4$ for the Yukawa well], but only at the expense of a further increase in the already excessive figure for the predicted total cross section, as can be seen from a comparison of columns B_1 and B_2 in Table I. It appears to be difficult to introduce a reasonable modification of the Christian-Hart triplet interaction which will at the same time lower the total cross section and increase the $\sigma(\pi)/\sigma(\pi/2)$ ratio. The disagreement is the more serious in that it is most pronounced at 40 Mev where little help can be expected from non-static forces.

V. IMPLICATIONS FOR SATURATION

On the assumption of a short-range repulsion it is clear that saturation will result, of the type existing in classical liquids. However, since the radius of repulsion assumed is smaller by a factor of four than the observed nucleonic spacing in the heavy nuclei, it appears to be questionable whether reasonable values of nuclear density and binding energy will result from (2). In this connection it is important, however, to note that the effect of the impenetrability interaction contained in (2) is greater than the classical liquid model leads

TABLE I. Total n-p cross sections (10^{-27} cm²).

Energy	Theoretical A	B_1	B_2	Experimental
40	222	217	231	170±15[a] 203± 7[b]
90	95	87	102	76±10[c] 83± 4[d] 73± 2[d] (95 Mev)
260	41	31	37	35± 9[e]

A. Hard core potential (2)
B. Christian-Hart potential:
1. Exponential
2. Yukawa

[a] Hadley, Kelly, Leith, Segrè, Wiegand, and York, Phys. Rev. **75**, 351 (1949).
[b] See reference 17.
[c] Cook, McMillan, Peterson, and Sewell, Phys. Rev. **75**, 7 (1949).
[d] J. Dejuren and N. Knable, Phys. Rev. **77**, 606 (1950).
[e] See reference 2.

[16] This is not true for σ_{pp} because of the exclusion of triplet even states by the Pauli principle.

[17] R. H. Hildebrand and C. E. Leith, Phys. Rev. **80**, 842 (1950).
[18] Private communication.

one to expect, because of the quantum-mechanical zero-point energy resulting from the exclusion by the hard sphere interactions of the part of the volume available in the nucleus for each nucleon.[19] An analogy can be drawn with liquid helium, where the particles are coupled by an interaction similar to (2) except for scale. The radius of repulsion in liquid helium is approximately 2A and the mean spacing 4A, the difference in these figures having its origin in the zero point energy associated with the repulsion. Moreover, the radius of repulsion may be expected to be greater for the thermal collisions occurring in nuclei than for collisions at energies of several hundred Mev which were made the basis for setting the repulsive range at 0.60. In a potential of more realistic form than that used in these calculations the hard sphere may be replaced by a potential which crosses the axis with finite slope, as in Fig. 1, and at a distance greater than the range of repulsion effective at higher energies.

VI. CONCLUSIONS

It is seen thus that the introduction of a short-range repulsive force permits one to reconcile the preservation of charge independence with the qualitative features of n-p and p-p scattering over the energy range thus far explored. This type of interaction may have, furthermore, desirable characteristics with respect to the saturation properties of the heavy nuclei. Several points must, however, be emphasized in considering the significance of these results:

(1) The omission of non-static forces is not to be taken as implying that such forces are negligible, but only, as the results of this calculation indicate, that a rough description of the scattering in terms of static forces cannot be excluded by present data. Since there may be appreciable nonstatic contributions at 350 Mev, the quantitative implications of a static potential which has been fitted, in part, to a cross section at that energy must not be given undue weight.

(2) Other, basically different, types of forces can be used for the charge-independent representation of the n-p and p-p interactions. In addition to the singular spin-orbit coupling of Case and Pais,[6] Christian and Noyes[5] have been able to account for p-p scattering by means of a singular tensor interaction which may be possibly incorporated into a charge-independent potential.[20] Each of these interactions possesses, in common with the short-range repulsive force, the characteristic of a strongly singular behavior at short distances. It may be said that the one general conclusion to be drawn from the high energy scattering experiments is that a strong singularity exists in the nucleon-nucleon interaction at small distances, and that on the assumption of charge independence one can show that the consequences of this singularity are partially masked in n-p scattering by the effect of the Pauli principle. It does not seem to be possible to obtain more definite information on the nature of this short-range force until nonstatic and relativistic effects are understood well enough to permit a quantitative comparison of the calculations with experiment.

I should like to express my thanks to Drs. K. M. Case, J. R. Oppenheimer, and A. Pais for stimulating discussions throughout the course of this work. The criticism of Mr. R. S. Christian and of Professors N. M. Kroll and R. Serber concerning the analysis of the calculations was extremely valuable. I am in addition grateful to Drs. E. M. Hart and P. Noyes and, in particular, to Mr. Christian, for their cooperation in supplying information and results relating to tensor scattering which made possible a considerable abbreviation of the computations.

[19] The magnitude of the zero-point energy is reduced by the fact that the wave function of a system of nucleons is symmetric with respect to the interchange of only $\frac{1}{4}$ of the relative coordinates.

[20] N. M. Kroll (private communication).

Upper Limit for the Time between Fission and the Emission of Neutrons*

THOMA M. SNYDER† AND ROBERT W. WILLIAMS‡
Los Alamos Scientific Laboratory, University of California, Los Alamos, New Mexico
(Received October 17, 1949)

The Baker experiment to detect times of delay greater than $\sim 5\times10^{-9}$ sec for the emission of fission neutrons has been performed by observing the change in fission neutron counting rate when fission fragments are allowed to fly away from a neutron counter as compared to the counting rate when the fragments are kept in the vicinity of the counter. The fission neutrons were detected by observing proton recoils in a thick-paraffin-lined proportional counter. The percent of neutrons delayed by a time of at least 8×10^{-9} sec was found to be (3.6 ± 2.8) percent.

I. INTRODUCTION

A VERY small number (about 0.8 percent) of the neutrons which accompany nuclear fission are delayed by times of the order of seconds.[1] These neutrons are associated with beta-processes in the fission products. It has been assumed that the rest of the neutrons (the "prompt" neutrons) are emitted within the short times characteristic of ordinary nuclear reactions ($<10^{-15}$ sec). Wilson[2] has shown that there is a strong correlation between the direction of a fission fragment and the direction of a fission neutron, indicating that a considerable number of the neutrons are emitted before the fragments are brought to rest. The purpose of the present experiment was to ascertain whether all of the "prompt" neutrons (the ones which are not delayed by at least many milliseconds) are emitted in less than 10^{-8} sec.

The method, originally proposed by C. P. Baker, uses the high speed of the fission fragments to measure the neutron emission time. A foil of U^{235} is wrapped around a counter sensitive only to fast neutrons and the whole immersed in a flux of thermal neutrons. The counter and foil are placed within a chamber that can either be evacuated or filled with a gas of high stopping power. The chamber wall is 3.46 cm away from the foil. Thus when the chamber is evacuated, most of the fission fragments (which have a velocity of $\sim10^9$ cm/sec) can travel from the foil to the chamber wall in $\sim5\times10^{-9}$ sec. On the other hand, when the chamber is filled with the gas, the fragments are brought to rest very close to the counter. If there is a delay in neutron emission, as long as or longer than 5×10^{-9} sec, the neutrons emitted by those fragments which escape from the U^{235} will come from the outer wall of the chamber, far from the counter, when the chamber is evacuated, but from just outside the counter when the chamber is filled with gas. Because the solid angle subtended by the counter is much less at a point on the chamber wall than on the surface of the counter itself, one expects a difference in the neutron counting rates in the two cases if an appreciable number of neutrons are emitted 5×10^{-9} sec or more after fission occurs.

II. APPARATUS

The fast-neutron detector actually used in these experiments was a thick-paraffin-lined proportional counter, illustrated in Fig. 1. The counter cylinder was 17 in. long and 2 in. o.d. with a $\frac{1}{16}$-in. duralumin wall. This large counter was considered desirable because of its high counting rate, since good statistics are imperative in an experiment whose "background" is inevitably greater than 50 percent (because at least half of the fission fragments must remain in the foil). The axial collecting electrode was a Kovar wire 0.005 in. in diameter. The entire counter cylinder was lined with a cerecin-impregnated nickel gauze. The wires of the gauze were scraped free of paraffin on both sides after coating to insure good electrical contact with the counter wall on the one side and to insure an electrical field undistorted by charge accumulation on the other. Cleanliness was important in minimizing the boron contamination since boron gives alpha-particles in a slow-neutron flux which are difficult to distinguish from recoil protons. In addition to boron, any nitrogen present gives an undesirable background owing to protons from the slow-neutron (n,p) reaction. For this reason the counter was filled with spectroscopic argon. With a pressure of 15 cm, the counter was found to operate well at about 820 v.

The counter was placed on the axis of a steel cylinder $4\frac{7}{8}$ in. i.d., $\frac{1}{32}$-in. wall, which could be evacuated or filled

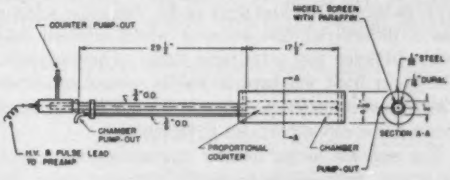

FIG. 1. The recoil counter and gas chamber.

* This document is based on work performed in 1943 at Los Alamos. A more complete account can be found in the declassified document LADC-252.

† Present address: Knolls Atomic Power Laboratory, General Electric Company, Schenectady, New York.

‡ Present address: Massachusetts Institute of Technology, Cambridge, Massachusetts.

[1] See, for example, de Hoffmann, Feld, and Stein, Phys. Rev. 74, 1330 (1948); Hughes, Dabbs, Cahn, and Hall, Phys. Rev. 73, 111 (1948).

[2] R. R. Wilson, Phys. Rev. 72, 189 (1947).

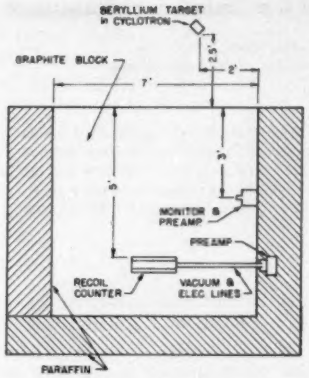

FIG. 2. Plan view of the graphite block, showing location of the counter and monitor.

with commercial propane to a pressure of one atmosphere (see Fig. 1).

To minimize slow-neutron absorbing materials in and near the counter its wire was used both as the collecting and high voltage electrode, and electrical connections were made by a long coaxial lead through the counter filling tube. By using a glass-insulated central wire of sufficient size, spurious electrical effects were avoided. This lead was made long enough so that the pulse preamplifier was far away and had negligible effect on the slow-neutron flux near the counter.

In operation, the counter was placed across the axis of a graphite block 7×5.7 ft on the front face and 7 ft long (see Fig. 2). Fast neutrons from a cyclotron with internal beryllium target were incident on the front face. At a depth of 5 ft, where the counter was located, these neutrons had been slowed down to give a thermal flux $(nv)_{th}=10^5$ per cm² per sec. The ratio of this flux to the flux of neutrons above 100 kev was 25,000. It is important in this experiment to have the number of fast neutrons already present in the block as small as possible compared to the number of fast neutrons produced by fission, which one is attempting to measure. Under the conditions described, background (from all sources) was less than half the total counting rate.

The circuits used in counting consisted of a regulated high voltage supply for the counter, a one-stage preamplifier and cathode follower mounted just outside the graphite block, a stabilized amplifier of the Waddell type, pulse selector, and scale of 32. The pulse selector was a differential discriminator which selected only pulses between two adjustable limits of pulse height. The upper limit was kept as low as seemed consistent with a good counting rate in order to eliminate as many of the boron alpha-particles as possible.

The response of the counter was calibrated by bombardment with monochromatic neutrons from the Li(p,n) source of the Los Alamos electrostatic generator. The purpose of the calibration was to determine whether or not the counter responded selectively to neutrons of certain energies and thus gave preference to some of the fission neutrons while ignoring others. The response was found to be satisfactory for our purposes. The sensitivity had a threshold at about 300 kev, and remained approximately constant on going to higher energies. One Mev was the maximum neutron energy obtained during this calibration. The presence of a plateau beginning at 700 kev means that the counter responds impartially to nearly all the fission neutrons since few have lower energies than 700 kev. The sensitivity of the counter in counts per incident neutron was found from this same calibration to be 9×10^{-5}.

The U^{235} being investigated was a sample of enriched material containing 15.7 percent U^{235} and 84.3 percent U^{238}. It was electroplated onto the outside of a platinum foil 16×6 in. which fitted around the outside of the counter. The average weight of metal deposited (in the form of the fluoride) was about 1 mg of UF_4 per cm². Although this deposit was not thin to fission fragments, but rather about one-fourth of their range, it nevertheless permitted most of the fragments to escape with a large part of their initial velocity retained. The disadvantage caused by the inability of all fragments to escape with full velocity was offset by the large number of neutrons produced which gave an improved ratio of fission neutrons counted to background.

For quantitative interpretation of the experiment, it was necessary to know the fraction, E, of fission fragments which escape from the foil. (E would be one-half if the foil were perfectly thin.) The method of determining E and of measuring the uniformity of the foil is described in the Appendix. The value found for the escape fraction was $E=0.435$.

III. PROCEDURE

To compensate for variations in cyclotron output, it was necessary to monitor the thermal-neutron flux incident on the counter. For this purpose a fission ionization chamber employing a semithick foil of unseparated U was placed in the graphite block at a distance of 3 ft from the front face, 3 ft from the bottom, and 1 ft from one side. Any change in intensity and distribution of neutrons incident on the face of the block would therefore be expected to have the same effect on the monitor and on the number of fissions in our apparatus.

The significant quantity for the experiment is therefore the number of recoil counts per unit monitor count. This will be referred to as the counting rate.

In order to learn how sensitive the counting rate is to the point of origin of fission neutrons we observed the counting rate with the U^{235} foil in its normal position, surrounding the counter, then moved the U^{235} foil to the inner surface of the outer cylinder and observed the decrease in counting rate which this caused. These measurements were made with the stopping gas in the

chamber. To eliminate any error which might arise from the change in slow-neutron flux with distance from the front face of the graphite block, the foil was placed symmetrically with respect to a plane perpendicular to the axis of the block. It is evident that this measurement, which we have called the "in-out measurement" would correspond approximately to the change in counting rate which would be expected if somehow *all* the fission fragments could escape from the foil, and all the fission neutrons were delayed by at least the time required for the fragments to reach the wall. Of course not more than half the fragments can escape at best, and their arrangement upon striking the wall will be more spread out than it is possible to make the foil, but the result of the experiment expressed in terms of this measurement is, to a first approximation, independent of the *calculation* of the change in counting efficiency as the source of neutrons moves from the surface of the counter to the outer wall of the chamber. This is important because it seems likely that considerations other than the change in solid angle subtended by the counter enter into this efficiency change, making an exact calculation difficult.

Knowing the fraction of fragments that escaped to the walls, we have now a measure of the change in counting rate to be expected from the delayed neutrons when the foil was on the outside of the counter and the stopping gas was removed from the surrounding chamber. The experiment then consisted of repeatedly comparing the counting rate with gas in the chamber (and fragments therefore all confined to the neighborhood of the foil) to the counting rate with the chamber evacuated (and some fraction, less than one-half, of the fragments therefore going to the walls).

If the stopping gas has appreciable absorption for slow neutrons a correction must be made, since the slow-neutron flux on the U^{235} and hence the number of fissions per unit monitor count would then be greater when the gas was removed, and the decrease in counting rate resulting from delayed neutrons might be masked. Propane, having eight hydrogen atoms per molecule, has a small but appreciable probability for slow-neutron capture, and the "gas effect" correction was therefore measured quite carefully and accurately, by covering the U^{235} foil with a foil of Al thick enough to stop the fission fragments, and then comparing the counting rate with and without the gas. A reduction of (0.7 ± 0.2) percent of the total counting rate was observed. About half of this can be attributed to absorption of slow neutrons, according to a simple diffusion calculation, and the rest may reasonably be attributed to slowing of residual fast neutrons.

IV. RESULTS

Table I summarizes the results of this experiment. The first column gives the average for each run of the "in-out" ratio, $I=100\ (\text{C.R.}_{\text{in}}-\text{C.R.}_{\text{out}})/\text{C.R.}_{\text{in}}$. C.R._{in} is the counting rate with the U^{235} foil in its normal position, C.R._{out} the rate with the foil against the outer wall of the chamber. This quantity was measured three times during Run I, twice during Runs II and III, and once during Run IV. It is a criterion of the sensitivity of the experiment and depends, in part, on the background counting rate. Its fluctuations arise from changes in the background, and the improvement between Runs II and III was made by reducing the fast-neutron background. The graphite block was lengthened by adding 12 in. of graphite to its front face; and the hole which contained the recoil counter was changed from a $5\frac{1}{4}$-in. cylinder to an 8×8-in. square channel, in the center of which the counter was supported. The latter change was made to reduce back-scattering into the counter of fast neutrons originating in the U^{235} since such scattering would have a tendency to decrease the change in counting efficiency for delayed neutrons.

The quantity of interest for our experiment is the difference between the counting rate with propane in the outer chamber and the counting rate with outer chamber evacuated. This quantity was converted to percent by multiplication by 100/(C.R. with propane) and designated by P. Each run consisted of about 10 pairs of measurements, a value of P being found for each pair. The average of these values of P for each run is tabulated in the second colum of Table I. The standard deviation of P_{av}, calculated in the usual way from the counting statistics, is given as σ_{calc}. The many values of P for each run permit a determination of the observed value of the standard deviation of P_{av},

$$\sigma_{\text{obs}}=\{\sum_{i=1}^{n}\Delta_i^2/n(n-1)\}^{\frac{1}{2}}.$$

This quantity is given, for each run, in the fourth column of Table I. It will be seen that the internal consistency is satisfactory.

TABLE I. Summary of the measurements on delayed neutrons.

Run no.	I_{av}	P_{av}	σ_{calc}	σ_{obs}
I	28.2%	0.45%	0.46%	0.85%
II	24.8%	−0.16%	0.39%	0.44%
III	35.3%	−0.58%	0.58%	0.62%
IV	35.9%	−0.54%	0.51%	0.38%

Table II gives the results of two runs on the gas absorption effect. The results and errors were obtained in the same way as were those of the delayed neutron

TABLE II. Gas absorption. Foil on counter, covered with 0.001-in. aluminum.

Run no.	Percent difference	σ_{obs}	σ_{calc}
I	0.79%	0.30%	0.28%
II	0.62%	0.32%	0.25%
Average	0.71%	0.22%	

TABLE III. Percentage of delayed neutrons.

Run no.	P, corrected for gas abs.	σ	100f = percent delayed >8×10^{-9} sec	σ
I	1.15%	0.88%	12.2%	9.3%
II	0.55%	0.49%	6.6%	5.8%
III	0.13%	0.66%	1.1%	5.5%
IV	0.17%	0.55%	1.4%	4.5%

Average percent delayed 3.6 ± 2.8 percent.

experiments. The values of P after adding the gas absorption correction and combining errors are given in Table III.

V. DISCUSSION

To a first approximation there is a very simple relation between the in-out measurement, I (defined as the percentage decrease in counting rate when the U^{235} foil is moved from the surface of the counter out to the wall of the chamber, the latter being filled with propane); the fraction E of fission fragments which escape from the foil; the observed counting rate reduction P; and the fraction f of neutrons delayed by at least the time necessary for all the fragments to reach the wall of the chamber. EI is just the counting rate reduction expected if *all* the neutrons were delayed, and f is therefore given by $f=P/EI$. Actually, since the effective length of the counter is about 40 cm, and the average velocity of the fragments about 0.9×10^9 cm/sec, the time for the fragments which take the longest path to reach the wall is 5×10^{-8} sec, which is unnecessarily long. Also, a correction must be made for the finite range of the fragments in the stopping gas. Some knowledge of the efficiency of the counter as a function of the distance of the neutron source from its axis is therefore necessary.

The details of these rather tedious calculations are given in the original paper[3] and will not be repeated here. The results can be expressed to a good approximation by writing the fraction delayed longer than a time Δt after fission as $f=(P/EI)K(\Delta t)$. For times Δt long enough so that all the fission fragments have come to rest, $K(\Delta t)$ is of course constant, and is equal to 1.3 (it differs from unity mainly because of the finite range of fission fragments in propane, about 1.3 cm). For shorter times, $K(\Delta t)$ involves the spacial distribution of the flying fission fragments.[4]

Figure 3 is a graph of $K(\Delta t)$ against $\log(\Delta t)$. From this graph it is seen that the experiment has very nearly reached its maximum sensitivity, $K=1.3$, at $\Delta t=8\times10^{-9}$ sec. Thus, one can say that $f=1.3\times P/EI$ is the fraction of fission neutrons delayed by at least 8×10^{-9} sec. Table III gives the corrected values of P and corresponding values of f for the four runs. The weighted mean is (3.6 ± 2.8) percent delayed.

This result would include most of the 0.8 percent of fission neutrons which are delayed by long times, although their energies are somewhat lower than those of the normal fission neutrons. There remains (2.8 ± 2.8) percent delayed. The most reasonable interpretation is that this corresponds to zero: within an accuracy of three percent, and excluding the well-known delayed neutrons, none of the neutrons from fission are emitted at times greater than 8×10^{-9} sec after the fission process.

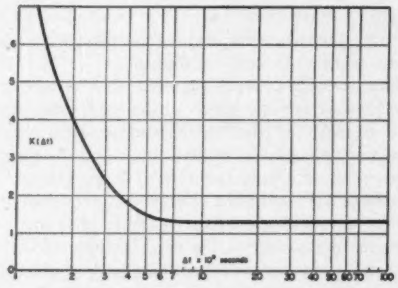

FIG. 3. The function $K(\Delta t)$. $1/K$ is a measure of the sensitivity of the experiment to neutrons emitted at a time Δt after fission.

ACKNOWLEDGMENTS

The authors are indebted to Miss E. E. Anderson for performing the difficult electrodeposition of the UF_4. Mr. E. D. Klema was associated with the work in its early stages.

This paper is based on work performed at the Los Alamos Scientific Laboratory of the University of California under U. S. Government Contract W-7405-Eng-36.

APPENDIX

At the conclusion of the experiment, the fraction of fission fragments which escape from the foil was measured by cutting two 2×2-in. samples from representative parts of the foil and comparing the number of fission fragments of energy >6 Mev from them with the number from a thin foil of known weight and the same isotopic constitution. The average E obtained in this way was 0.41. We correct for the fragments of <6 Mev as follows: Let the thickness of the UF_4 deposit be $\beta\leqslant\rho$, where ρ is the range of fragments in the UF_4. Then the fraction of fragments which escape after traversing a thickness less than l is given by the

[3] Declassified document LADC 252. It is shown there that the probability for a neutron to make a count is approximately proportional to $1/r$, where r is the distance from the neutron source to the counter axis. This law was checked by calculating the value of the in-out ratio, I. The value expected from geometrical considerations was 53 percent. A background measurement (made with the foil removed) showed that 54 percent of the counting ratio with foil in "in" position was due to fission neutrons. One would therefore expect the in-out ratio to be $0.54\times53=28.6$ percent. The measured value at this time was 28 percent.

[4] This calculation included the distribution in velocity of the fission fragments as they emerge from the foil, and therefore involved the range-velocity relation given in the Appendix. It was simplified by assuming that all delayed neutrons were emitted after the same time Δt. An estimate shows that the corresponding mean life for an exponential decay law would be larger than Δt, but by less than a factor of two.

expression

$$1-\beta/2l \text{ when } l \geqslant \beta; \quad l/2\beta \text{ when } l \leqslant \beta. \tag{1}$$

In particular, the total fraction that escape; i.e., the fraction that have traversed any thickness of material up to ρ is

$$1-(\beta/2\rho). \tag{2}$$

We may use the above formulas together with a range-velocity relationship to find both the total fraction of fragments that escape and the thickness of the foil relative to the range; i.e., β/ρ.

A range-velocity relation which agrees with experiment well enough for these purposes is $(v/v_0)=(1-l/\rho)$. From this equation we calculate the value of l/ρ corresponding to 6 Mev, taking an average initial energy of the fragments to be 81 Mev. From Eq. (1) and the measured escape fraction we find $\beta/\rho=0.26$. Inserting this value of β/ρ in Eq. (2) we find that the total fraction of fragments which escape from the foil is $E=0.435$.

The uniformity of the UF_4 deposit was measured by cutting 24 one-inch squares from the foil and alpha-counting them. The standard deviation in thickness of the foil was 18 percent. We have assigned an uncertainty of this magnitude to E in computing the error of our final result.

PHYSICAL REVIEW VOLUME 81, NUMBER 2 JANUARY 15, 1951

Distribution of Slow Neutrons in Free Atmosphere up to 100,000 Feet*†

LUKE C. L. YUAN‡
Palmer Physical Laboratory, Princeton University, Princeton, New Jersey

(Received July 27, 1950)

Two identical proportional counters filled with boron trifluoride of 96 percent B^{10} have been sent aloft up to an altitude of 102,000 ft at a geomagnetic latitude of 51° 46′ N by means of free balloons. One counter was shielded with 0.030 in. of cadmium, and the other enclosed in tin of the same thickness for the compensation of possible effects caused by "stars" produced in the cadmium shield. The difference in the counts of the two counters is due only to slow neutrons ($E \leqslant 0.4$ ev). The counts and the pressure and temperature were radioed down by an FM telemetering system. Up to about 20 cm of Hg the counts increase exponentially with altitude according to an absorption depth $\lambda=156$ g/cm², in agreement with previous measurements, and roughly with the increase of "stars" in the atmosphere. The counts of both counters as well as their difference show a maximum at high altitude, as expected theoretically. The maximum for the cadmium difference counts appears at about 8.5-cm Hg pressure and drops down sharply to about one-fourth of its maximum value at 1 cm Hg. The counter sensitivity was calibrated against a standard neutron source and the absolute number of slow neutrons absorbed per gram and second in the atmosphere is computed and compared with the number of protons produced at the same altitudes.

I. INTRODUCTION

A CONSIDERABLE number of measurements have been made on the neutron intensity in cosmic radiation by various investigators in this field.[1–9] The essential results thus far show an exponential increase of the neutron intensity as a function of altitude. Since neutrons in the cosmic radiation cannot be considered as primary particles because of their short lifetime, they must be produced in the atmosphere. Thus one can expect that there exists a maximum in neutron intensity distribution as a function of altitude. The position of the maximum has been calculated by Fluegge[10] and recently by Bagge and Fincke[11] on a theoretical basis by considering the absorption, scattering, and diffusion of neutrons in the atmosphere. This maximum is expected to exist at about 10 cm Hg, assuming that the atmospheric neutrons are originally produced in the processes of nuclear disruptions or "stars." However, measurements in the past[7] show a continuous increase in the neutron intensity up to 2 cm Hg. This discrepancy between theory and experiment[7] can probably be attributed to spurious counts obtained at high altitudes because of corona discharge at the high voltage terminals of the proportional counter. As will be described later, a completely pressurized system for the high voltage supply and the counters was employed[12] in the present experiment to eliminate such possible corona effects.

The object of the present experiment is not only to obtain the intensity distribution of the slow neutrons ($E \leqslant 0.4$ ev) in the atmosphere, but also to attempt to measure their absolute intensities at various altitudes.

* Assisted by the joint program of the AEC and ONR.

† A preliminary report of the present work appeared in Phys. Rev. 77, 728 (1950); Phys. Rev. 74, 504 (1948).

‡ Now at Brookhaven National Laboratory, Upton, New York.

[1] For references up to 1939, see Bethe, Korff, and Placzek, Phys. Rev. 57, 575 (1940).

[2] S. D. Chatterzee, Indian J. Phys. 14, 435 (1940).

[3] S. A. Korff and E. T. Clarke, Phys. Rev. 61, 422 (1942).

[4] S. A. Korff and B. Hamermesh, Phys. Rev. 69, 155 (1946).

[5] S. A. Korff and B. Hamermesh, Phys. Rev. 71, 842 (1947).

[6] Agnew, Bright, and Froman, Phys. Rev. 72, 203 (1947).

[7] S. A. Korff and A. Cobas, Phys. Rev. 73, 1010 (1948).

[8] C. L. Yuan and R. Ladenburg, Bull. Am. Phys. Soc. 23, No. 2, 21 (1948).

[9] J. A. Simpson, Jr., Phys. Rev. 73, 1389 (1948).

[10] S. Fluegge, Sec. 14 of *Lectures on Cosmic Radiation*, edited by W. Heisenberg, translated by T. H. Johnson (Dover Publications, New York, 1946).

[11] Von Erich Bagge and Karl Fincke, Ann. Physik 6, Folge, Bd. 6, 21 (1949).

[12] Luke C. L. Yuan, Phys. Rev. 74, 504 (1948).

A complete description of the measurements made at high altitudes will be given here. Experimentation at lower altitudes is still in progress.[12]

II. APPARATUS

A. Gondola Equipment

The present measurements were carried out at Princeton, New Jersey (geomagnetic latitude 51° 46′ N), by sending aloft two identical proportional counters 5 cm in diameter and 20 cm in length up to an altitude of 102,000 ft (corresponding to a pressure of 0.75 cm Hg) by means of free balloons. The counters were made of glass of low boron content (less than 0.02 percent boron) and they were filled with purified boron trifluoride gas containing 96 percent B^{10} at a pressure of 20 cm Hg in the first flight (April, 1948) and at a pressure of 50 cm Hg in the second (July, 1948) and third (January 8, 1949) flights. They were operated at

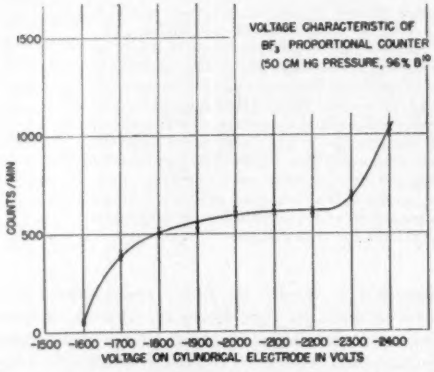

FIG. 1. Voltage plateau characteristic of proportional counter.

a voltage plateau centered at 800 v and 1850 v, respectively. A preliminary report on the results of the first flight has appeared.[13]

A typical voltage plateau characteristic of the proportional counter is shown in Fig. 1, where the counting rate is plotted against the negative high voltage on the outer electrode (cathode) of the counter. The width of the plateau is about 200 volts with a slope of about 3 percent per 100 v. A counter operated at such a plateau region has a very high alpha-to-gamma-ray discrimination, and so pulses due to single gamma-rays are easily biased off.

Of the two counters used in the flight, one counter was shielded with 0.030 in. of cadmium. Owing to the possibility of stars being produced in the cadmium shield at high altitudes, a tin shield of the same mass as the cadmium shield was put around the second counter to compensate for any such effect. Tin was

[13] For preliminary results, see reference 8, also Luke C. L. Yuan, Phys. Rev. 76, 1267 (1949) and Phys. Rev. 76, 1268 (1949).

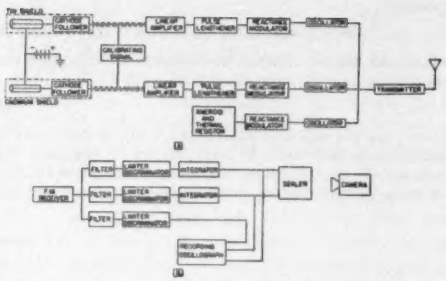

FIG. 2. Block diagram of telemetering and receiver system.

chosen as the material for the compensating shield simply because its atomic number ($Z=50$) is close to that of cadmium ($Z=48$) and because its absorption cross section for neutrons is exceedingly small. The calculated absorption of the tin shield for thermal neutrons amounts to about two percent.

The output pulse amplitude of these counters due to disintegration of B^{10} by neutrons at 1850 volts is of the order of a few millivolts, which is a thousand times smaller than that of a Geiger-Mueller counter. In view of this fact, a series of tests were made to determine the possible effect of corona on the counter at high altitudes and the means of eliminating such effect. This was done by putting the counter and its high voltage battery supply in a large vacuum chamber. Various methods of insulation were applied to the high voltage leads and terminals and to the battery itself, and corona effects were determined as the chamber was pumped down. With the best insulation method tried, corona still began to show up at about 4- or 5-cm Hg pressure, and its effect increased as the pressure decreased. This would give rise to a false increase in the neutron counts as the altitude increased if the corona effect were not completely eliminated.

In order to eliminate any possible corona discharge under high altitude conditions, a pressurization system was adopted such that both counter shields as well as the high voltage battery container were sealed airtight and were maintained at atmospheric pressure throughout the flight. The high voltage leads were fed through long pressurized copper tubings which connected the high voltage battery container with the two counter shields.

A cathode follower stage using a 2E41 subminiature tube was placed at one end of each counter shield. The output from the counter tube was fed directly from the anode (the axial wire) of the counter, which was at approximately ground potential, to the grid of the 2E41. The output of the cathode follower was then fed through Kovar seals and long shielded leads to the input of a three-stage inverse-feedback linear amplifier, which was placed about 2½ ft away from the counter. Each counter was followed by a separate cathode

follower and linear amplifier channel as shown in the block diagram in Fig. 2(A).

The output of each amplifier was fed into a pulse lengthening circuit which converted a pulse of a certain amplitude into a corresponding square pulse such that the width of the latter was made to vary as the logarithm of the amplitude of the original pulse. These square pulses were employed to drive a reactance tube which frequency modulated a subcarrier oscillator. The frequency of the subcarrier oscillator was thus changed by a small, fixed amount for a time proportional to the logarithm of the original counter pulse amplitude.

The gain of the amplifiers was so adjusted that the amplitudes of gamma-ray pulses from a 15-mc Ra-Be source at one foot away from the counter were just below the threshold voltage required to operate the pulse lengthener. Thus, the gamma-ray pulses, as well as the noise background of the amplifier circuits, were not transmitted through the telemetering system.

A calibrated fixed signal of constant amplitude was switched into the input circuit of the linear amplifiers every 15 min for a period of 8 sec. This served as a check on the constancy of the amplifier gain and the performance of the whole system during the course of the flight. The calibrated fixed signal was produced by a relaxation oscillator employing a small neon bulb painted black which gave a constant signal output over a long period of time and a wide temperature range.

The above described frequency-modulated telemetering system has a very good noise discrimination characteristic which is independent of signal fading and frequency drift within wide limits. A circuit diagram of the complete system[14] employed in the balloon flight is shown in Fig. 3.

Before each flight the whole gondola containing the entire system was put into a vacuum tank which was pumped down gradually to $\frac{1}{2}$-cm Hg pressure to detect the presence of any possible corona discharge. When the background counts of the two counters remained unchanged during a period of one hour at $\frac{1}{2}$-cm Hg as well as during the pumping down period, the gondola was then ready for flight.

The gondola frame was made of magnesium angle strips. The total weight of the gondola, including all of its equipment, was about 43 lb. The gondola was wrapped in a thin sheet of cellophane paper painted partially black, and the temperature inside remained fairly constant throughout the flight.

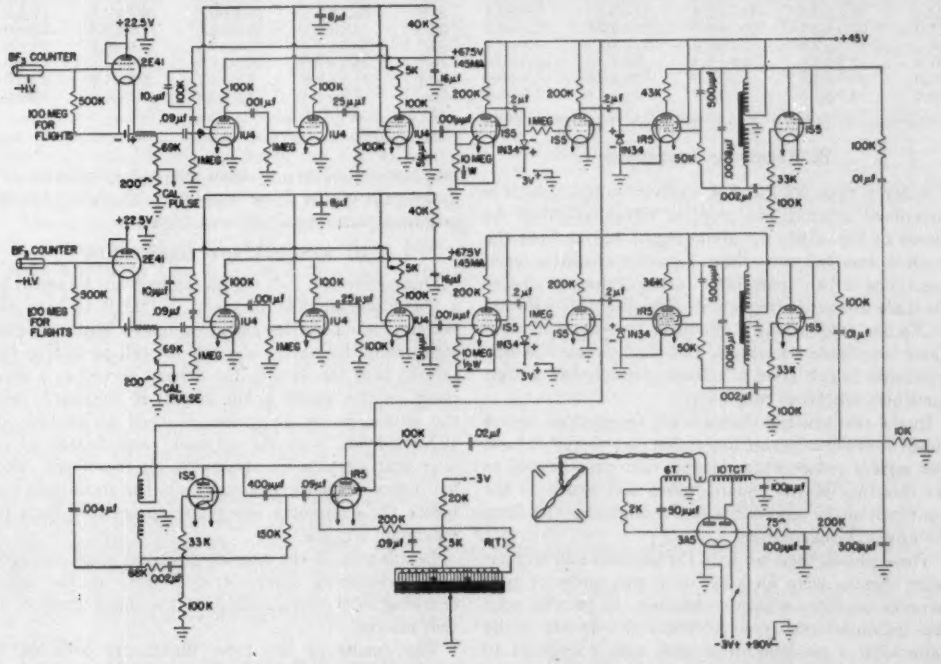

FIG. 3. Schematic circuit diagram of counters and associated telemetering system.

[14] A detailed description of the telemetering system is given in a paper by T. Coor which has been submitted for publication in Rev. Sci. Instr.

TABLE I. June 9, 1948, balloon flight. Counting rates in counts per minute (counter background subtracted).

(1) Pressure in cm Hg	(2) Tin-shielded counter	(3) Cd-shielded counter	Cd difference (2)−(3)	Cd ratio (2)/(3)
69.0	1.5±0.8			
57.4	0.9±0.8	0.4±0.6	0.5±1.0	2.3±3.9
47.5	3.3±1.0	0.5±0.6	2.8±1.2	6.6±6.9
38.3	7.5±1.5	3.3±1.1	4.2±1.9	2.3±0.9
30.8	13.5±1.7	6.3±1.3	7.2±2.1	2.1±0.5
24.7	24.1±2.2	11.5±1.6	12.6±2.7	2.1±0.4
19.7	35.9±2.7	14.7±1.8	21.2±3.2	2.4±0.4
15.8	50.5±3.2	18.3±2.0	32.2±3.8	2.8±0.4
12.7	54.5±3.3	20.7±2.1	33.8±3.9	2.6±0.3
10.2	61.7±3.6	26.1±2.4	35.6±4.4	2.4±0.3
8.27	65.5±3.6	32.7±2.6	37.8±4.4	2.0±0.2
6.75	68.1±3.7	29.3±2.5	38.8±4.5	2.3±0.2
5.45	62.9±3.6	33.9±2.6	29.0±4.4	1.8±0.2
4.5	62.2±3.2	32.3±2.3	29.9±3.9	1.9±0.2
4.17	63.5±3.6	31.5±2.6	32.0±4.4	2.0±0.2
4.17	60.9±3.5	28.9±2.5	32.0±4.3	2.1±0.2
4.36	65.9±3.7	32.5±2.6	33.4±4.5	2.0±0.2
4.8	68.5±3.7	28.1±2.4	40.4±4.4	2.4±0.2
5.38	60.1±3.5	31.5±2.6	28.6±4.4	1.9±0.2
6.05	70.9±3.8	28.5±2.4	42.3±4.5	2.5±0.3
6.83	60.2±3.1	35.6±2.4	24.6±3.9	1.7±0.1
7.75	58.9±3.4	34.1±2.7	24.8±4.4	1.7±0.1
9.92	59.7±3.5	30.7±2.5	29.0±4.3	1.9±0.2
10.7	63.9±3.6	25.9±2.4	28.0±4.4	2.5±0.3
12.5	58.5±3.4	25.3±2.3	33.2±4.1	2.3±0.3
14.5	50.5±3.2	24.1±2.3	26.4±3.9	2.1±0.2
16.8	43.7±3.0	18.3±2.0	25.4±3.6	2.4±0.3
19.3	39.1±2.8	17.1±1.9	22.0±3.4	2.3±0.3
22.1	29.5±2.5	14.7±1.8	14.8±3.1	2.0±0.3
25.0	22.7±2.2	10.1±1.5	12.6±2.6	2.2±0.4
28.2	19.5±2.0	8.5±1.4	11.0±2.4	2.3±0.4
31.8	10.9±1.6	6.9±1.3	4.0±2.1	1.6±0.4
36.0	12.7±1.7	4.3±1.1	8.4±2.0	2.9±0.9
40.6	4.9±1.3	2.3±0.9	2.6±1.6	2.1±1.0

TABLE II. July 25, 1948, balloon flight. Counting rates in counts per minute (counter background subtracted).

(1) Pressure in cm Hg	(2) Tin-shielded counter	(3) Cd-shielded counter	Cd difference (2)−(3)	Cd ratio (2)/(3)
60	2.2±0.8	1.6±0.7		
51	3.8±1.0	4.4±1.0		
42.5	10.6±1.5	7.0±1.3	3.6±2.0	1.5±0.4
35.5	18.2±2.0	10.8±1.5	7.4±2.5	1.7±0.3
29	31.2±2.5	20.0±2.0	11.2±3.2	1.6±0.2
23	63.8±2.9	31.0±2.5	32.8±4.6	2.1±0.2
18.2	82.8±4.1	52.0±3.2	30.8±5.2	1.6±0.1
14	118.3±5.4	64.8±4.0	53.5±6.7	1.8±0.1
11	130.4±5.1	73.6±3.8	56.8±6.3	1.8±0.1
8.5	128.2±5.1	79.4±4.0	48.8±6.5	1.6±0.1
7	149.0±5.5	80.0±4.0	69.0±6.8	1.9±0.1
5.9	145.2±5.4	82.6±4.1	62.6±6.8	1.8±0.1
5.5	135.4±5.2	81.4±4.0	54.0±6.5	1.7±0.1
4.9	138.6±5.3	79.4±4.0	59.2±6.6	1.8±0.1
4.7	122.0±2.3	77.2±1.8	44.8±2.9	1.6±0.1
5	131.0±5.7	82.0±5.2	49.0±7.7	1.6±0.1
5.3	134.2±5.2	87.2±4.2	47.0±6.7	1.5±0.1
6.1	141.2±5.3	86.6±4.2	54.6±6.8	1.6±0.1
6.8	136.0±3.9	82.0±3.0	54.0±4.9	1.7±0.1
7.5	139.0±3.9	88.2±3.2	50.8±5.0	1.6±0.1
8.4	130.2±3.6	80.0±2.8	50.2±4.6	1.6±0.1
9.6	131.2±5.8			
11.7	126.0±4.6			
13.2	123.4±5.0			
14.8	105.6±4.6			
16.6	87.0±4.7			
19	84.2±4.1			
21.5	66.8±3.7	40.2±2.9	26.6±4.7	1.7±0.2
24.3	46.2±3.1	25.4±2.3	20.8±3.9	1.8±0.2
27.5	38.0±2.8	19.0±2.0	19.0±3.4	2.0±0.3
32	26.0±2.3	12.4±1.6	13.6±2.8	2.1±0.3
36.3	18.6±2.0	10.0±1.5	8.6±2.5	1.9±0.3
41.4	11.6±1.6	4.8±1.1	6.8±1.9	2.4±0.6
46	7.8±1.3	2.6±0.8	5.2±1.5	3.0±0.1
51	5.0±1.1			

B. Receiving Equipment

A Navy type RBF-3 FM receiver with a rotatable directional antenna was used for signal reception. As shown in Fig. 2(B), the audio signal output from the receiver was fed into three separate channels, each containing a band-pass filter corresponding to one of the three subcarrier frequencies. The filters are followed by limiter stages, which minimize the effect of radio signal amplitude variations, and then by an FM discriminator which gives a voltage proportional to that particular subcarrier frequency.

In the two neutron channels the transmitted square pulses after detection are integrated and converted back into regular pulses whose heights were proportional to the duration of the square pulses and hence to the logarithm of the amplitudes of the original pulses from the proportional counter.

These pulses, together with the pressure and temperature signals, were recorded on a galvanometer type recorder on three separate channels. In parallel with this galvanometer type recorder, two-decade scaler units with a predetermined bias were connected to register the neutron counts from the two counters. The readings of these two scaler units were photographed at one-minute intervals in synchronization with the timing signals of the galvanometer recorder. Thus, the counting rate can be read directly from the photographic records if the gain of the linear amplifiers, as shown by the calibrated fixed signal, remains constant.

III. RESULTS AND DISCUSSION

During the first two flights the balloons ascended to a maximum altitude of about 67,000 ft (4.2-cm Hg pressure) and then descended gradually. Measurements were made during the descent as well as during the ascent; thus the data in the descent served as a good check on the results in the ascent. In the third flight the balloon-borne equipment reached an altitude of 102,000 ft (0.75-cm Hg pressure) and floated at or near that altitude for approximately two hours. After five hours of continuous reception, the signal was lost before the equipment descended appreciably from its maximum altitude.

In analysis of the results, counting rates averaged over five-minute intervals were used as the mean counting rate corresponding to the mean pressure in that interval.

The results of the three flights are collected in Tables I, II, and III, where the background counts of each counter were subtracted from the actual counting rate. These background counts were measured at ground level by shielding the counters with a cadmium shield;

TABLE III. January 8, 1949, balloon flight. Counting rates in counts per minute (counter background subtracted).

(1) Pressure in cm Hg	(2) Tin-shielded counter	(3) Cd-shielded counter	(4) Cd difference (2)-(3)	(5) Cd ratio (2)/(3)
60.3	1.6±0.7	0.4±0.6	1.2±0.9	4.0±6.3
54.3	4.6±1.1	1.0±0.7	3.6±1.3	4.6±3.4
48.3	8.4±1.4	4.2±1.0	4.2±1.7	2.0±0.6
43.3	13.0±1.7	6.0±1.2	7.0±2.0	2.2±0.5
38.7	18.8±2.0	7.2±1.3	11.6±2.4	2.6±0.5
34.3	29.2±2.5	12.0±1.6	17.2±3.0	2.4±0.4
30.3	35.6±2.7	19.0±2.0	16.6±3.4	1.9±0.2
26.7	51.6±3.2	17.8±1.9	33.8±3.7	2.9±0.4
23.5	64.2±3.6	28.0±2.4	36.2±4.3	2.3±0.2
20.3	84.1±4.1	40.4±2.9	44.4±5.0	2.1±0.2
17.5	95.6±4.4	45.6±3.1	50.0±5.4	2.1±0.2
15.2	126.3±5.2	52.6±3.3	74.2±6.2	2.4±0.2
12.7	144.4±5.4	65.0±3.6	79.4±6.5	2.2±0.1
11.1	148.6±5.5	75.2±3.9	73.4±6.7	2.0±0.1
9.5	165.8±5.7	79.4±4.0	86.4±7.0	2.1±0.1
8.1	173.6±5.9	82.4±4.1	91.2±7.2	2.1±0.1
7.0	172.2±5.9	91.0±4.3	81.2±7.3	1.9±0.1
5.8	168.6±5.7	87.1±4.1	81.5±7.0	1.9±0.1
5.0	153.4±5.5	82.4±4.1	71.0±6.9	1.9±0.1
4.3	161.8±5.7	85.8±4.2	76.0±7.1	1.9±0.1
3.5	136.6±5.2	84.0±4.1	52.6±6.6	1.6±0.1
3.0	130.8±5.1	81.2±4.0	49.6±6.5	1.6±0.1
2.5	125.4±5.0	67.4±3.7	58.0±6.2	1.9±0.1
2.2	108.8±4.7	56.6±3.4	52.2±5.8	1.9±0.1
1.8	103.4±4.6	56.8±3.4	46.8±5.7	1.8±0.1
1.6	98.0±4.4	56.8±3.4	41.2±5.6	1.7±0.1
1.4	98.6±4.5	63.0±3.6	35.6±5.8	1.6±0.1
1.3	86.0±4.2	55.8±3.4	30.2±5.4	1.5±0.1
1.2	81.4±4.1	53.8±3.3	27.6±5.2	1.5±0.1
1.1	77.4±4.0	55.2±3.4	22.2±5.3	1.4±0.1
1.0	101.3±3.2	65.2±2.6	36.1±4.1	1.6±0.1
0.9	82.6±2.9	61.1±2.5	21.5±3.8	1.4±0.1
0.8	83.0±4.1	53.0±3.3	30.0±5.3	1.6±0.1
0.9	93.1±0.6	67.2±0.5	25.9±0.8	1.4±0.01

they amount to about one count per minute for the counters employed. They were due mainly to the alpha-contamination of the surface of the counter electrode.

The altitude dependence of the neutron intensity in the atmosphere obtained during the three balloon flights is shown in Figs. 4, 5, and 6, where the counting rate is plotted against the pressure in centimeters of Hg. Figure 4 represents the data obtained by means of two identical 20-cm-Hg-pressure BF_3 counters with a calibrated effective cross section of 6.3 ± 0.6 cm^2 for thermal neutrons (see Appendix A). The upper curve *A* gives the counting rates obtained from the tin-shielded counter, curve *B* that from the cadmium-shielded counter, and curve *C* that from the difference of the two. Figures 5 and 6 show the results obtained with similar BF_3 counters but with 50-cm Hg pressure, i.e., counters with about twice as great efficiency. The results obtained from the three flights agree well among themselves in the positions of the maxima as well as in the rate of increase, which is also in good agreement with that obtained previously at lower altitudes.[8,9]

The tin-shielded counter (curve *A*) shows a maximum counting rate at 7.5 cm Hg; the cadmium-shielded counter (curve *B*) shows a maximum at 6.5 cm Hg; and the cadmium difference (curve *C*) has a flat maximum around 8.5 cm Hg. The slow neutron ($E\leqslant0.4$ ev) intensity, N, increases exponentially with decreasing atmospheric depth to a pressure of about 20 cm Hg. The absorption depth, i.e., the quantity λ in the expression $N=N_0e^{-x/\lambda}$, is $\lambda=156$ g cm^{-2}. The corresponding absorption coefficient is $\mu=1/\lambda=6.4\times10^{-3}$ cm^2/g. Both the tin counter (which measures fast as well as slow neutrons plus the effect due to recoils and stars produced in the shield, etc.) and the cadmium counter (which measures only the fast neutrons plus the effect due to recoils, stars, etc.), show the same slope of increase in counting rate[14a] up to about 20 cm Hg. Above the maximum, the counting rate of the tin counter decreases much more rapidly with increasing altitude than that of the cadmium counter, with the result that the slow neutron intensity (curve *C*, Fig. 6) drops sharply to about one-fourth of its maximum value at 0.75 cm Hg. If one extrapolates this curve up to the very top of the atmosphere, approaching zero pressure, one finds that the slow neutron intensity drops almost to zero.

For comparison, the values of absorption depth λ, obtained in other processes involving the production of neutrons, are as follows. (1) For ionization bursts by Rossi, Williams, Bridge, and Hulsizer[15] below 20-cm Hg pressure, $\lambda=138$ g/cm^2; by Coor,[14] $\lambda=160$ g/cm^2. (2) For nuclear disruptions or stars in photographic plates by Perkins[16] between sea level and 44 cm Hg, $\lambda=140$ g/cm^2, and by George,[17] $\lambda=150$ g/cm^2.

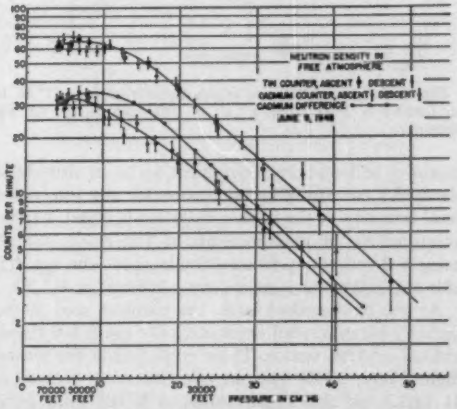

FIG. 4. Balloon flight made at geomagnetic latitude 51° 46′ N on June 9, 1948, using a pair BF_3 counters (20 cm Hg pressure).

[14a] The balloon floated at an altitude corresponding to about 0.9-cm Hg pressure for nearly two hours and the average value for the cadmium difference obtained for this altitude was 25.9 ± 0.8 counts per minute.

[15] B. Rossi and R. W. Williams, Phys. Rev. **72**, 172 (1947); H. Bridge and B. Rossi, Phys. Rev. **71**, 379 (1947); R. I. Hulsizer, Phys. Rev. **73**, 1252 (1948).

[16] D. H. Perkins, Nature **160**, 707 (1947); Nature **163**, 319 (1949).

[17] E. P. George, private communication.

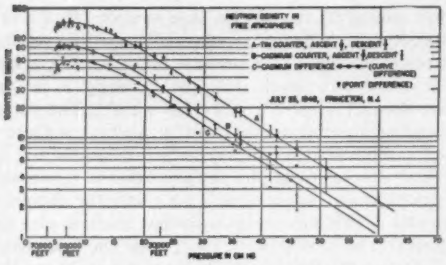

FIG. 5. Balloon flight made at geomagnetic latitude 51° 46′ N on July 25, 1948, using a pair of BF_3 counters (50 cm Hg pressure).

For further comparison, the position of the maximum in the vertical intensity distribution for the soft component of the cosmic radiation at geomagnetic latitudes greater than 45° N is at about[18] 11.5 cm Hg and that for the total radiation[18] is at about 10 cm Hg, according to measurements made by Millikan, Pfotzer, *et al.*,[19] by

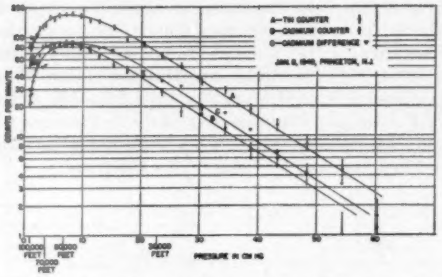

FIG. 6. Balloon flight made at geomagnetic latitude 51° 46′ N on January 8, 1949, using a pair of BF_3 counters (50 cm Hg pressure).

means of balloon-borne equipment up to an altitude of about 2.5 cm Hg. The maximum for the integrated total intensity of the cosmic radiation is about 4.1 cm, according to the measurements of Van Allen, *et al.*,[20] using V-2 rockets up to an altitude above the appreciable atmosphere at a geomagnetic latitude of 41° N.

As will be described later, the counters used in the flights were calibrated experimentally against a standardized neutron source. Those employed in the second flight (July, 1948) had an effective cross section of 11.3 ± 1.1 cm² and those employed in the third flight (January, 1949) had an effective cross section of 12.6 ± 1.2 cm², all for neutrons of thermal energy. Division of the observed counting rates by these effective cross sections would give the neutron flux in particles per cm² and per unit time, if the neutrons had thermal energy. Actually they do not. The $1/v$ absorption of nitrogen cuts out the lowest energies, and the most probable energies will be of the order of 0.1 ev, instead of 0.02 ev. This circumstance greatly complicates the determination of the absolute neutron flux. Fortunately, a quantity of greater physical interest than the flux, *the number of neutrons, s, absorbed per gram of air and per second*, is much less affected by uncertainties in the form of the spectrum of slow neutrons. More specifically, one may note that 193 grams of air have the same absorption cross section for thermal neutrons as does a counter with an effective response cross section of 10.6 cm² for thermal neutrons. For slow neutrons of other energies the boron trifluoride counter will of course have a *different* cross section, but will still be equivalent in neutron absorbing power to the *same* mass of air. This result is an obvious consequence of the fact that both nitrogen and boron follow the $(1/v)$ law at the low energies which are of interest here. We conclude that the number of counts in the boron counter gives directly the number of neutrons absorbed per second in a certain mass of air which is fixed once and for all and which may be considered for our purposes to be independent of the shape of the neutron spectrum.

However, when the cadmium-difference counts are used instead of the counting rate obtained from a single unshielded counter, the air mass equivalent of the counter as described above must be corrected in order that it may be applied to the cadmium-difference counts. A brief description of the correction procedure is given below.

Let $A(E)=(1/v_{\text{thermal}})\Sigma_a v\sigma_a$ for all atoms in one gram of air, where v is the velocity of neutrons and σ_a is the absorption cross section of air atoms. For low energy neutrons $A(E)$ is constant and is found to be 0.055 cm²/gm, since σ_a follows $(1/v)$ law in this energy region.

Let $B(E)=(v/v_{\text{thermal}})\times$effective cadmium-difference response cross section of boron counter to an isotropic flux. Then the air mass equivalent of the cadmium-difference counter is given by

$$\int B(E)(df_a/dE)dE \Big/ \int A(E)(df_a/dE)dE = \int B(E)(df_a/dE)dE/0.055, \quad (1)$$

where (df_a/dE) represents the fraction of the neutrons in 1 cc of air which lie in a unit energy range at E. [The same result can be expressed alternatively by introducing the conception of "sweepage," that is, the product of cross section by neutron velocity. This quantity is the most convenient measure of absorbing power of an atom or material which follows the $1/v$ law. It has the physical dimensions of cm/sec. In the present considerations what matters is, of course, the ratio of

[18] B. Rossi, Rev. Mod. Phys. **20**, 537 (1948).
[19] Millikan, Neher, and Pickering, Phys. Rev. **63**, 234 (1943); G. Pfotzer, Z. Physik **102**, 23 (1936); H. Carmichael and E. G. Dymond, Proc. Roy. Soc. (London) **A171**, 321 (1939).
[20] J. A. Van Allen and H. E. Tatel, Phys. Rev. **73**, 245 (1948); Gangnes, Jenkins, Jr., and Van Allen, Phys. Rev. **75**, 57 (1949).

the sweepage by the counter and the sweepage by one gram of air. The ratio will obviously be unaltered by dividing the two sweepages by the same constant. The quotient of the sweepage of a gram of air divided by thermoneutron velocity, which received above the name $A(E)$, this quantity having the dimension of square centimeters, is a little easier to visualize than the sweepage itself. Similarly, B represents the counter-sweepage divided by the same constant.]

For convenience, we compute the effective cadmium-difference response cross section $(v_{\text{thermal}}/v)B(E)$, for two limiting idealized cases: *viz*, (a) for a boron counter of spherical geometry and (b) for the opposite limiting case of a layer of BF_3 gas confined between two infinite parallel sheets.

(*a*) *Spherical counter.* Consider a spherical boron trifluoride counter of radius R. The response cross section of the whole counter with no cadmium present is equal to $(v_{\text{thermal}}/v)\times 10.6$ cm². Therefore, the response cross section of one cm³ of counter $=(v_{\text{thermal}}/v)\times(3\times 10.6/4\pi R^3)$cm², which holds either for isotropic flux or for flux in the x-direction because of the spherical symmetry.

Now consider the case of unit flux in the x-direction with cadmium present. Then the effective response cross section owing to neutrons striking surface between angular limits θ to $\theta+d\theta(0<\theta<\pi/2)$ is

$$4\pi R^3\cos^2\theta\sin\theta d\theta\frac{v_{\text{thermal}}}{v}\frac{3\times 10.6}{4\pi R^3}\times\exp\frac{-\text{Cd}(E)}{t}\{[R^2\cos^2\theta+t(2R+t)]^{\frac{1}{2}}-R\cos\theta\}$$

where $\exp[-\text{Cd}(E)]$ is the fraction of a normally incident neutron beam of velocity v which penetrates a sheet of cadmium of thickness t. Hence, the response cross section of the cadmium covered counter is, after substituting $u=\cos\theta$,

$$\frac{v_{\text{thermal}}}{v}10.6\int_0^1 3u^2\exp\frac{-\text{Cd}(E)}{t}\times\{[R^2u^2+t(2R+t)]^{\frac{1}{2}}-Ru\}du. \quad (2)$$

Consequently, we conclude that in the idealized case of spherical geometry the cadmium-difference response cross section of the boron counter is

$$\frac{v_{\text{thermal}}}{v}B(E)=\frac{v_{\text{thermal}}}{v}10.6\left(1-3\int_0^1 u^2\exp\frac{-\text{Cd}(E)}{t}\times\{[R^2u^2+t(2R+t)]^{\frac{1}{2}}-Ru\}du\right). \quad (3)$$

The quantity $B(E)$ is plotted as a function of energy in Fig. 7 (curve A) by taking $R=5$ cm, which was obtained from the effective volume of the cylindrical counter used in the measurements. The values of the exponential integral were obtained by numerical integration. The quantity $\text{Cd}(E)$ represents the decrement in napiers of a normally incident neutron beam and was calculated from the thickness, 0.305 g/cm², of the cadmium foil, and from the curve of cadmium cross section as a function of energy given by Rainwater, Havens, and Wu.[21]

From the values of $B(E)$ given in Eq. (3) and using the values for the neutron distribution in the atmosphere calculated by Kouts,[22] we get,

$$\int_0^\infty B(E)(df_a/dE)dE=2.78\text{ cm}^2. \quad (4)$$

(*b*) *Parallel plane counter.* Now consider the limiting idealized case of a layer of boron trifluoride gas confined between two infinite parallel sheets of cadmium, the analogous calculation gives, for case of isotropic incidence the cadmium-difference response cross section

$$(v_{\text{thermal}})(B(E)=(v_{\text{thermal}}/v)10.6\times\left\{1-\int_0^{\pi/2}\sin\theta\exp[-\text{Cd}(E)/\cos\theta]d\theta\right\} \quad (5)$$

or by substituting $u=\cos\theta$, we have

$$B(E)=10.6\left[1-\text{Cd}(E)\int_{\text{Cd}(E)}^\infty u^{-2}\exp(-u)du\right]. \quad (6)$$

The values of $B(E)$ given by Eq. (6) are also plotted in Fig. 7 (curve B). Hence

$$\int_0^\infty B(E)(df/dE)dE=2.93\text{ cm}^2. \quad (7)$$

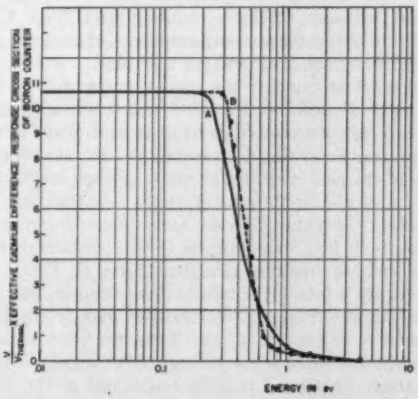

FIG. 7. Calculated effective *cadmium-difference* response cross section of a spherical and a parallel plate counter. Curve A is for the spherical counter, and curve B is for the parallel plate counter.

[21] Rainwater, Havens, and Wu, Phys. Rev. 71, 65 (1947).
[22] Kouts, Wheeler, and Whyte, to be published.

TABLE IV. Air mass equivalents of counters used, calculated on basis of thermal neutron cross section of 5.30×10^{-3} cm² per gram of air.*

Counter name	Observed effective response cross section for thermal neutrons from pile (cm²)	Calculated air mass equivalent (grams)
Standard	10.6	52.0
June, 1948, flight	6.3	30.8
July, 1948, flight	11.3	55.5
January, 1949, flight	12.6	62.0

* This value was given as the most probable absorption cross section of nitrogen for thermal neutrons by H. H. Goldsmith, Committee on Nuclear Science, National Research Council.

It is seen from Fig. 7 that the difference between the curves for the idealized spherical and plane counters is small. Moreover, in the energy range where the difference is greatest, the equilibrium neutron density in air has fallen to a very low value. From Eqs. (4) and (7) the integral $\int B(E)(df_a/dE)dE$ has in the two idealized limiting cases, respectively, the values 2.78 cm² and 2.93 cm², a difference of only 5 percent. We adopt the average value

$$\int_0^\infty B(E)(df_a/dE)dE=2.86 \qquad (8)$$

for the actual intermediate case of cylindrical geometry. Thus, we get the air mass equivalent of the particular cadmium difference counter:

$$2.86/0.055=52.0 \text{ g}. \qquad (9)$$

Similar calculations for the air mass equivalent of other counters used in these experiments give the results listed in Table IV.

Thus it is only necessary to divide the tabulated air mass equivalent of the appropriate counter into the observed cadmium difference counting rates (Figs. 4, 5, and 6) to obtain the absolute number, s, of neutrons absorbed per gram of air and per unit time.

In order to compare the results represented by the curves A, B, and C in Figs. 4, 5, and 6, one must take into account the respective air mass equivalents in the two cases. From Fig. 6, curve C, the actual counting rate of the slow neutrons at the maximum (at 8.5 cm Hg) is 86±4 counts/min (January counter), and its counting rate reduced to the same July counter sensitivity as in Fig. 5 amounts to 78±7 counts/min. The slow neutron counting rate from curve C, Fig. 7, at 8.5 cm Hg is 60±6 counts/min (June counter) and the counting rate from Fig. 6(c) reduced over to the July counter is 63±5 counts/min. Thus, the slow neutron intensity measured in the January, 1949, flight is higher by about 20 percent than that obtained in the June and July, 1948, flights; but the difference between these results is so close to the statistical error of the experiment that one cannot draw a definite conclusion, even though the June and July results are in very good agreement. On the other hand, if this difference is real, it might conceivably be attributed to the time variation of the neutron component of the cosmic radiation. In regard to the time variation of cosmic radiation, Jesse[33] found an approximate 14 percent increase in the total cosmic radiation intensity at high altitude in early spring over early summer at Chicago between October, 1938 and November, 1939. Millikan and Neher[34] observed a similar increase in the total intensity of about 9 percent in December, 1938, over September, 1937, at Omaha, Nebraska.

The cadmium ratio, obtained by taking the ratio between the counts from the tin-shielded counter to those from the cadmium-shielded counter is of the order of 2 over the depth of 50 cm Hg to 4 cm Hg. Figure 8 (A, B, and C) shows the values of the cadmium ratio obtained at various altitudes for the three flights, respectively. It seems to show that the cadmium ratio is approximately constant above 4 cm Hg, having a

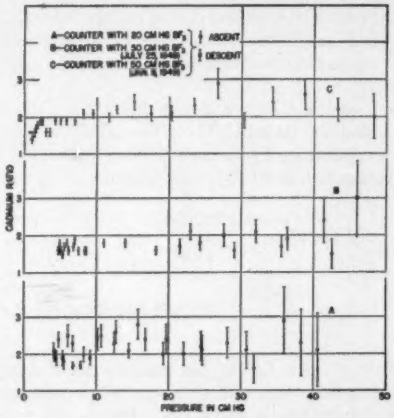

FIG. 8. Cadmium ratio as a function of altitude.

value of about 2, but then decreases gradually as the pressure decreases and reaches a ratio of 1.4 at 0.9 cm Hg. This is probably due to the increasing contribution of the non-neutron counts and to the decrease in the slow neutron counts when approaching the top of the atmosphere. On the other hand, the cadmium ratio calculated from Eq. (8) is $10.6/(10.6-2.86)=1.4$, which is lower in value than the experimental ratio of 2. This difference is probably due to the neglect of the molecular scattering of slow neutrons in the moderation process in calculating the energy distribution of the air neutrons.[32] The molecular scattering effect is difficult to estimate but Bagge and Fincke[11] have shown that such effects can improve the agreement between the theoretical and experimental cadmium ratios.

In the present experiments two identical counters were used simultaneously, one enclosed in tin, the other

[33] W. P. Jesse, Phys. Rev. **58**, 281 (1940).
[34] R. A. Millikan and H. V. Neher, Phys. Rev. **56**, 491 (1939).

in cadmium. The non-neutron counts are of the same magnitude in both counters, and they cancel out. Consequently, the difference of the counts should give the true counting rate due to slow neutrons.

From the above results and from the air mass equivalents of the counters one can calculate the absolute number of slow neutrons absorbed in one gram of air per second. For example, at a pressure of 20 cm Hg there were observed 0.83 counts per second, in the January counter, for which the equivalent air mass is calculated to be 62.0 cm²; thus, *we find for s, the slow neutron absorption rate in air amounts to* 1.3×10^{-2} *per gram per second.* This would be, in equilibrium, the neutron production rate in the atmosphere if (1) no fast neutrons were captured by nitrogen and oxygen and (2) no fast neutrons were lost (or gained) by diffusion to (or from) other levels in the atmosphere. At the 20-cm level the curve of neutron intensity (not the logarithm of neutron intensity) as a function of altitude is neither strongly convex upward, as at the maximum, nor strongly concave upward as lower in the atmosphere. Consequently, it is reasonable to conclude that neutron diffusion has relatively little effect at this altitude in redistributing the neutrons. In view of the losses during moderation it is therefore to be expected that the slow neutron absorption rate at 20 cm is a lower limit on the neutron production rate at this elevation.

It is of some interest to compare this value with the proton production rate in the atmosphere. At 8.9-cm Hg pressure the value for the proton production rate obtained by Coor[14] is 0.015/g-sec and the lower limit of the neutron production rate extrapolated to this altitude is 0.034/g-sec. The ratio of the proton to neutron production rate thus calculated is 0.015/0.034 = 0.44. Actually, the ratio must be smaller still because the figure 0.034 employed here is the lower limit of the neutron production rate.

By integration of the slow neutron counts from the ground up to the top of the atmosphere, one finds the number of *slow* neutrons absorbed per cm² of the earth's surface per second at the latitude of Princeton is 7.1.

The author wishes to express his sincere gratitude to Professor R. Ladenburg, with whom this series of neutron experiments was initially started, for his generous advice and helpful suggestions; to Professor John A. Wheeler for his constant encouragement and many valuable discussions; to Messrs. T. Coor and F. J. Darago for their technical assistance in the construction and adaptation of the telemetering system to the present experiment; to Mr. David Hill for his kind assistance in carrying out the measurements and calculations of the counter calibration at the pile of the Argonne National Laboratory and for the contribution of Appendix B; to Mr. Herbert Kouts, who kindly let the author use his theoretical results on the energy distribution of air neutrons; to Dr. N. Hilberry, Associate Director of the Argonne Laboratory, for the opportunity to secure a calibration of our counters; to Dr. D. J. Hughes and Mr. C. Eggler for their help in fitting this measurement into the Argonne program.

APPENDIX A. STANDARDIZATION

Although the cross section of boron for neutrons of various energies is well known and one can calculate the efficiency of a BF_3 counter theoretically, it is necessary in practice, owing to factors such as the geometry and the effective volume of the counter, absorption due to counter walls, etc., to calibrate the counter sensitivity experimentally. In this way were obtained the values of counter cross section which are referred to in the preceding section.

Through the courtesy of the Argonne National Laboratory, the sensitivity of the BF_3 counters used here was calibrated against its standardized neutron source. A brief description of the calibration procedure is given below. The detailed computation for the calibration was carried out by D. Hill, and is described in Appendix B.

The counter to be calibrated was placed in a beam of thermal neutrons of known intensity distribution emitted from the pile at the Argonne Laboratory. It was a 50-cm-Hg-pressure BF_3 counter (96 percent B^{10}) and was operated at its voltage plateau region under the same conditions under which it was being used in the experiment.

The counter was checked with a Ra-Be source (15 mc) surrounded by a paraffin cylinder at a fixed geometry both before and after the standardization to make certain that the performance of the counter remained unchanged throughout the calibration.

A similar counter used by Agnew, Bright, and Froman[6] was lent to the author and was put beside our counter separated by a distance of one foot.

A comparison of the sensitivities of the two counters was made by using the same electronic circuits and by operating in the respective plateau regions. An average of six measurements at six different angular positions of the counters was taken in order to eliminate the effect due to anisotropy of the neutron beam. For the same neutron flux, the counter used by the author was found to give 2.32 times the counting rate of that used by Agnew, Bright, and Froman, whereas the ratio of the sensitivities calculated from gross volume and pressure is 2.48.

The above measurement with the 15-mc Ra-Be source also gave a secondary standardized neutron source for subsequent calibrations.

APPENDIX B. CALIBRATION OF BF_3 COUNTER

The BF_3 counter was calibrated by observation of its counting rate in a spray of thermal neutrons scattered by a graphite wall 10 cm thick placed in a beam emerging from the Argonne heavy water pile, and by comparison of this counting rate with the saturated beta-activity acquired by indium foils placed about the boron counter in such a manner that their average activation should correspond to the average neutron flux impinging upon the counter. It was found that the bare counter presented an effective cross section of 9.6 cm² to thermal neutrons; but this result is subject to two small corrections deriving from the fact that the response of the indium foils (1) involves the influence of the moderator present upon the self-absorption in the foils, and (2) depends upon the isotropy of the neutron atmosphere.

The calibration of the indium foils themselves is made by irradiating them in a solid graphite pile at a position in which the thermal neutron flux is known and isotropic. On the other hand, in our counter calibration the foils under irradiation are supported upon a light sheet metal structure suspended in mid-air. The difference in scattering materials about the foils in the two cases must be expected to change the perturbation in the neutron density caused by the absorption of neutrons in indium. To

establish the amount of this effect, Mr. C. Eggler kindly performed a subsidiary measurement in which he compared the specific saturated activity for irradiations in air and in graphite of a standard indium foil (92.3 mg/cm²) with that of a very thin indium deposit (0.423 mg/cm²; negligible self absorption) on an iron foil finding

$$\frac{(A \text{ thin})}{(A \text{ stan})}\Big/\frac{(A \text{ thin})}{(A \text{ stan})}=0.95.$$
$$\text{(air)} \qquad \text{(graphite)}$$

If all of the neutrons striking the boron counter-indium foil assembly were monodirectional, proceeding from the primary scatterer only, the activity induced in the indium foils would be, as is easily computed, 1.29 times greater for the arrangement chosen, in which the normal to the indium foils made an angle of 55° with the line from the foils to the primary scatterer, than the activity if the neutrons were isotropic. The degree of isotropy was easily checked by observation of the counting rate in a boron counter which was sheathed in cadmium over all of its surface except one end; it was found that the counting rate changed in a gradual manner from a maximum when the counter window pointed directly toward the primary scatterer to a minimum, equal to one-fourth the maximum, when the window pointed away from the primary scatterer. We thus conclude that most of the neutrons striking the indium foil assembly have been scattered in by objects other than the primary graphite scatterer. We also note that the unshielded boron counter responds in approximately the same manner as do the indium foils to deviations from isotropy, since the arrangement kept the axis of the counter parallel to the planes in which the foils were mounted; but the effect in the counter is smaller from the circumstance that neutrons passing perpendicularly through the counter along a diameter experience a fractional reduction in intensity of 0.05, whereas for neutrons passing perpendicularly through a standard indium foil the reduction is 0.092. This study leads us to estimate the effect of nonisotropy in the neutron atmosphere as producing a correction of about 5 percent.

These two corrections then lead us to write for the detection cross section of the counter: 10.6 ± 1 cm².

Adopting for the mean cross section of a nitrogen molecule for absorption of thermal neutrons the figure $2\times1.7\times10^{-24}$ cm², we may say that the number of counts is the same as the number of neutrons absorbed in a mass of air of 10.6 cm²/(0.055 cm²/gm air) = 193 gm air (for single unshielded counter).

This air mass equivalent of the counter is derived from calibration for thermal neutrons. As the cross sections of both boron and nitrogen follow the $1/v$ law, the same air mass equivalent will apply for unshielded counters to slow neutrons of all energies.

PHYSICAL REVIEW VOLUME 81, NUMBER 2 JANUARY 15, 1951

$(n,2n)$ and (n,p) Cross Sections*

BERNARD L. COHEN†‡
Carnegie Institute of Technology, Pittsburgh, Pennsylvania
(Received July 26, 1950)

Cross sections of several $(n,2n)$ and (n,p) reactions were measured by bombarding samples with a known flux of neutrons and measuring the induced beta-activity, making elaborate corrections for self-absorption of the beta-rays. Using the known energy spectrum of the incident neutrons, calculations were made of the cross sections to be expected from Weisskopf's statistical theory, and the agreement was satisfactory. The results indicate that level densities in odd-odd nuclei are greater than those in even-even nuclei by a factor of 3 ± 1. Applications of the method to shielding and the use of threshold detectors are discussed.

I. INTRODUCTION

An interesting result of nuclear statistical theories is the prediction of cross sections of nuclear reactions which predominantly proceed through energy states of excitation sufficiently high that resonances are very closely spaced and can thus be meaningfully averaged over. $(n,2n)$ and (n,p) reactions are particularly simple examples of these, since the incident particle faces no Coulomb barrier, whence the cross section for the formation of the compound nucleus is πr^2 (r is the nuclear radius). The cross section for an $(n,2n)$ reaction is then πr^2 times the probability that the compound nucleus will decay by emission of two neutrons which, considering neutron emission as much more probable than any other mode of decay, is just the probability that the first neutron is emitted with low enough energy to leave emission of a second neutron energetically possible. Considering the first neutron to be emitted with an energy spectrum approximating a Maxwell distribution with temperature, T, gives[1]

$$\sigma(n,2n)=\pi r^2[1-(1+\Delta E/T)\exp(-\Delta E/T)], \quad (1)$$

where $\Delta E=E-B$, E=energy of incident neutron, and B=threshold of the reaction.

In the case of (n,p) reactions, emission of a proton is impeded by the coulomb barrier, causing it to be much less probable than emission of a neutron (inelastic scattering) with which it competes, whence

$$\sigma(n,p)=\pi r^2 f_p/(f_n+f_p)\simeq\pi r^2 f_p/f_n, \quad (2)$$

where f_p and f_n are the relative probabilities of the compound nucleus decaying by emission of a proton and neutron. Methods of calculating these quantities are given by Weisskopf.[1]

* Assisted by the ONR.
† A section of doctoral dissertation submitted in partial fulfillment of the requirements for the degree of Doctor of Science.
‡ Present address: Oak Ridge National Laboratory, Oak Ridge, Tennessee.

[1a] V. Weisskopf, *Lecture Series in Nuclear Physics* (U. S. Govt. Printing Office, Washington, D. C., 1947). [b] V. Weisskopf and Ewing, Phys. Rev. 57, 472 (1940). [c] V. Weisskopf and J. M. Blatt, M.I.T. Technical Report No. 42 (May 1, 1950), unpublished.

TABLE Ia. $(n,2n)$ reactions studied.

Original nucleus	Material used	Half-life	Method	Other activities observed
N^{14}	NH_4NO_3 Urea	10.1 min	1	None
F^{19}	LiF	112 min	1	None
P^{31}	Ca_3P_2 Red phos.	2.55 min	1–2	2.5-hr $Ca(n,\gamma)$; 170-min $P(n,p)$
K^{39}	K_2CO_3 KCOOH	7.5 min	3	12.4 hr (n,γ); 38.5-min (n,α)
Ti^{46}	Ti metal powder	3.08 hr	1–2	57-hr (n,p); 44-min (n,p)
Cr^{50}	Cr_2O_3	42 min	2	3.9 min (n,p)
Fe^{54}	Fe metal	8.9 min	2	2.59-hr (n,p); (8.9-min not observed)
Ni^{58}	Ni metal	36 hr	(1)–3	2.6-hr (n,γ); 72-day (n,p)
Cu^{63}	$Cu^{63}O$[a]	10.1 min	2	5-min (n,γ); 12.8-hr (n,γ)
Zn^{64}	Zn metal	38.3 min	3	13.8-hr (n,γ); $5M(n,p)$; 57-min (n,γ)
Ga^{69}	Ga_2O_3	68 min	2	20-min (n,γ); 14.1-hr (n,γ)
As^{75}	As_2O_3	16 days	(1)–2	26.8-hr (n,γ)
Rb^{85}	Rb_2CO_3	6.5 hr	2	17.8-hr (n,γ); 19.5-day (n,γ) (6.5 hr not observed)
Zr^{90}	ZrO_2	78 hr	3	62-hr (n,p); 17-hr (n,γ)
Ru^{94}	Ru metal powder	20 min	3	Long; (20 min not observed)
Ag^{107}	Ag metal	24.5 min	1–2	2.3-min (n,γ); 13-hr (n,p); ~40 day ???
Sb^{121}	Sb_2O_3	16 min	1	2.8-day (n,γ)
I^{127}	NH_4I	13 days	(1)–2	25-min (n,γ)
Pr^{141}	Pr_6O_{11}	3.5 min	2	Long

[a] Obtained from Isotope Division, AEC, Oak Ridge, Tennessee.
Methods designated as 1, 2, and 3 described in Sec. II. Parenthesis indicates method was not carried out thoroughly.

TABLE Ib. (n,p) reactions studied.

Original nucleus	Material used	Half-life	Method	Other activities observed
O^{18}	Sugar	8 sec	3	2.1-min $(n,2n)$; long
Mg^{24}	Mg metal	14.8 hr	1	10.2-min (n,γ)
Al^{27}	Al metal	10.2 min	1	2.4-min (n,γ)
Si^{28}	H_2SiO_3	2.4 min	1	170-min (n,γ); 6.7-min (n,p)
Si^{29}	H_2SiO_3	6.7 min	1	170-min (n,γ); 2.4-min (n,p)
P^{31}	NH_4PO_4 Red phos.	170 min	1–2	2.5-min $(n,2n)$
S^{32}	Flower of sulfur	14.3 day	1–2	None
Ca^{42}	CaOH	12.4 hr	(1)–2	2.5-hr (n,γ)
Ti^{48}	Ti metal powder	44 hr	1	3.08-hr $(n,2n)$; 57-min (n,p)
Ti^{49}	Ti metal powder	57 min	1–2	3.08-hr $(n,2n)$; 44-hr (n,p)
Cr^{52}	Cr_2O_3	3.9 min	(1)–2	42-min $(n,2n)$; long
Fe^{56}	Fe metal	2.59 hr	(1)–2	None
Ni^{58}	Ni metal	72 day	(1)–3	2.6 hr (n,γ); 36-hr $(n,2n)$
Cu^{65}	Cu metal	2.6 hr	(2)–3	10.1-min $(n,2n)$; 5-min (n,γ); 12.8 hr (n,γ)
Zn^{66}	Zn metal	5 min	1	57 min (n,γ); 13.8 hr (n,γ); 38 min $(n,2n)$
Ge^{70}	GeO_2	20 min	2	89 min (n,γ)
Se^{76}	Se metal powder	26.8 hr	2	None
Se^{77}	Se metal powder	40 hr	3	26.8-hr (n,p); (40 hr not observed)
Rb^{87}	Rb_2CO_3	74 min	3	17.8-min (n,γ); long (74-min not observed)
Sr^{88}	SrC_2O_4	17.8 min	1	2.7-hr (n,γ)
Zr^{90}	ZrO_2	62 hr	3	78-hr $(n,2n)$
Mo^{97}	Mo metal	75 min	3	14.6-min (n,γ); long (75-min not observed)
Ru^{101}	Ru metal powder	14 min	2	Long; (14-min not observed)
Ag^{109}	Ag metal	13 hr	2	2.3-min (n,γ); 24.5-min $(n,2n)$; 40 day ???
Ba^{138}	BaOH	33 min	3	85-min (n,γ); long (33 min. not observed)
La^{139}	La_2O_3	85 min	3	40-hr (n,γ); (85-min doubtfully observed)

II. EXPERIMENTAL PROCEDURE

Incident Neutrons

The cross sections of several $(n,2n)$ and (n,p) reactions, as given in Table I, were obtained by irradiating samples with neutrons and measuring the induced beta-activity. The neutrons were obtained by bombarding an internal thick beryllium target with 15-Mev deuterons in the University of Pittsburgh cyclotron. Their energy distribution was determined by observing recoil protons in photographic emulsions[2] and in a triple coincidence anticoincidence counter telescope,[3] and is shown in Fig. 1. The beam intensity was monitored by the 24.5-min activity due to $Ag^{107}(n,2n)Ag^{106}$, except for a few long-lived activities which were monitored by the 14.8-hour activity from $Mg^{24}(n,p)Na^{24}$.

The absolute intensity was determined from the known cross section[4] of $S^{32}(n,p)P^{32}$, which gives results shown[5] to be in agreement with determinations based on the cross sections of uranium and thorium fission, and the reaction $P^{31}(n,p)Si^{31}$. A confirmation in the high energy region is discussed in Sec. IV.

[2] B. Cohen, Carnegie Inst. Tech. Report No. 4 (May 20, 1950), unpublished.
[3] Falk, Carnegie Inst. Tech. Report No. 5 (June 1, 1950), unpublished.
[4] E. D. Klema and A. O. Hanson, Phys. Rev. 73, 106 (1948).
[5] Allen, Nechaj, Sun, and Jennings, Phys. Rev. 76, 188 (1949).

Correction for Self-Absorption of Beta-Rays

The samples, which were in the form of $1\frac{1}{4}$ in. diameter pills, were counted with a thin windowed end counter. By insertion of various thicknesses of aluminum between the pills and the counter, it was found that beta-rays were absorbed according to

$$N \sim \varepsilon^{-y}, \tag{3}$$

where N is the counting rate with a thickness of aluminum, t (in mg/cm^2), interposed, and $y=t/\alpha$. Here, α is a constant which was found to be independent of absorber material. For calculation of self-absorption, Eq. (3) must be integrated through the thickness of the pill, giving the percentage transmission, T, as

$$T=(1-\varepsilon^{-y})/y. \tag{4}$$

Equations (3) and (4) form the basis of two methods of determining α: (1) by measuring relative activities with various thickness of aluminum between the pill

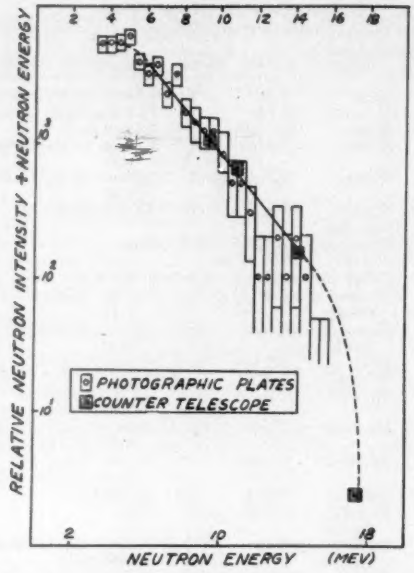

FIG. 1. Energy distribution of incident neutrons (from references 2 and 3).

and window (aluminum absorption), and (2) by measuring the relative activities from pills of various thickness (thin pill). Determinations of α by the two methods are shown plotted against the maximum beta-energies of the activities in Fig. 2.

The following methods were then used for determining cross sections:

Method 1. The best value of α was obtained by averaging the values from thin pill and aluminum absorption determinations, giving some weight to line A of Fig. 2. The corrected activity was then found by an extrapolation of the thin pill activities to zero thickness by use of Eq. (4).

Method 2. As can be shown from Eq. (4) (see reference 2), the ratio of the observed to the corrected activity of a thick pill ($I \gg \alpha$) is dependent only on α, which was determined by aluminum absorption. Corrections were applied for the change in pill to counter distance, and for deviations from Eq. (3). This method was used where sufficiently thin pills ($I \ll \alpha$) were difficult to prepare or could not be given sufficient activity for good counting statistics.

Method 3. In cases where determinations of activities were not sufficiently accurate (due to large corrections for background activities) for a determination of α, it was obtained from line A of Fig. 2, and used to correct thin pill or thick pill activities.

Other Corrections

Studies were made of the effect of backscattering from the pans on which the samples were supported, and of beta-absorption in air and in the counter window, and corrections for these (seldom more than 10 percent) were applied.

III. (n, p) CROSS SECTIONS

The experimentally observed (n,p) cross sections in the cyclotron beam are listed in Table II and plotted[6] *vs* atomic number in Fig. 3. The first conclusion obtainable from Table II is that even-even elements have larger (n,p) cross sections than even-odd and odd-even ones. This can be understood in view of the fact that the density of levels in odd-odd nuclei (the result of an (n,p) reaction in an even-even element) is larger than in even-even nuclei (the result of an $(n$-$n)$ reaction) owing to the Pauli exclusion principle. Analysis of the data gives the difference as a factor of 3 ± 1, which is in agreement with the factor of 4 predicted by Weisskopf in an earlier paper.[1b] For this reason, the observed (n, p) cross sections of even-even nuclei were divided by 4 in Fig. 3.

The lines in Fig. 3 represent theoretical calculations based on various values of the parameter r_0 (used in calculating nuclear radii by $r = r_0 A^{\frac{1}{3}} \times 10^{-13}$ cm) and of nuclear temperatures. Proton capture cross sections [used in calculating f_p in Eq. (2)] are taken from reference 1c.

Curve A represents $r_0 = 1.3$ and nuclear temperatures from reference 1a; Curve B uses the same temperatures and $r_0 = 1.5$; and curves C and D were calculated with $r_0 = 1.3$ and temperatures 25 percent lower and higher, respectively. From these curves, the predictions of any other assumptions can be estimated. For example, curve E represents $r_0 = 1.3$ and Weisskopf's most recent estimation of nuclear temperatures.[1c] (Curve F was obtained from an old calculation of penetration factors[1b]

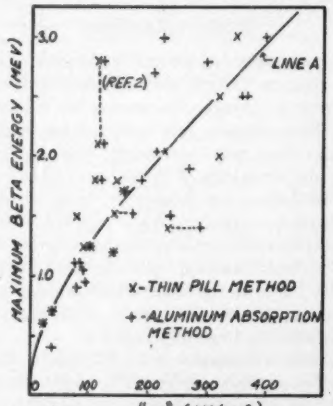

FIG. 2. Determinations of α by thin pill and aluminum absorption methods.

[6] The nucleus O^{16} is omitted from Fig. 3 because it has a very low atomic number and the (n,p) reaction has a high threshold; P^{31} and S^{32} are also omitted because excitation functions for (n,p) reactions in these nuclei have been measured and found to exhibit resonances which explain the large value of the total cross section. Clark Goodman, Editor, *The Science and Engineering of Nuclear Power* (Addison-Wesley Press, Cambridge, 1948–49).

TABLE II. Observed (n,p) cross sections.[a]

(1) Element	(2) Atomic number	(3) Threshold (Mev)	(4) Observed cross section (mb)	(5) Max. error (%)
O^{16}	8	9.3	8	200
Mg^{24}	12	2.1	39	10
Al^{27}	13	2.1	25	10
Si^{28}	14	3.9	45	12
Si^{29}	14	1.8	36	15
P^{31}	15	1.1	120	10
S^{32}	16	1.0	285	5
Ca^{42}	20	2.9	120	10
Ti^{48}	22	1.3	23	15
Ti^{49}	22	1.1	6.5	10
Cr^{52}	24	2.8	15	10
Fe^{54}	26	2.9	18.5	8
Cu^{65}	29	2.3	3.2	40
Zn^{64}	30	3.5	11.0	10
Ge^{70}	32	1.8	14.5	15
Se^{76}	34	2.3	16.5	10
Se^{77}	34	0.0	<8[b]	...
Rb^{87}	37	3.3	<2[b]	...
Sr^{88}	38	4.3	0.93	8
Zr^{90}	40	1.8	3.1	30
Mo^{97}	42	1.5	<1[b]	...
Ru^{101}	44	0.9	<0.8[b]	...
Ag^{109}	47	0.4	2.0	30
Ba^{138}	56	3.1	<0.2[b]	...
La^{139}	57	2.1	<0.2[b]	...

[a] From neutron energy spectrum shown in Fig. 1.
[b] Activity not observed.

and is included because Wäffler's data[7] are compared with it. His values of $\sigma(\text{obs})/\sigma(\text{cal})$ are in substantial agreement with the data of Table II if $\sigma(\text{cal})$ is taken from curve F.)

All curves in Fig. 3 are calculated for zero threshold. The effect of thresholds can be taken into account in one of two ways:

(1) Assuming that level densities depend on the excitation energy above the average of ground states of nuclei of similar mass,[8] the correction is very small and the circles can be compared directly with the curves in Fig. 3.

(2) Assuming that level densities depend on the excitation energy above the ground state of the particular nucleus involved introduces a large correction factor which depends sensitively on the threshold. This calculation is shown by correcting the observed values by the inverse of these correction factors, giving the crosses in Fig. 3, which can then be compared with the curves.

One might expect the first assumption to be valid for highly excited levels—these are important in (n,p) reactions in light elements—and the second to be valid for levels near the ground state which are the major contributors in heavy elements. From Fig. 3, however, it appears that the first assumption can have only limited validity for energies as high as 5 Mev (these are important contributors) for elements of atomic number $\sim$30. It might also be noted that curve E agrees exceptionally well with the calculation from assumption (2).

From Fig. 3 it can be concluded that even the best statistical theory can predict only trends in (n,p) cross sections, with considerable variations to be expected; but the general basis for calculating (n,p) cross sections, and their dependence on atomic number can probably be considered to be satisfactorily verified.

IV. $(n,2n)$ CROSS SECTIONS

The observed and calculated $(n,2n)$ cross sections are listed in Table III. The errors correspond to about two standard deviations and were estimated from a detailed study of the factors involved. The calculated values for columns (5) and (6) were obtained using temperatures from reference 1a (T_1) and reference 1c (T_2) and were corrected for K-capture from curves given by Trigg.[9]

The Cu^{63} cross section is in substantial agreement with the result obtained by integration of the experimental excitation function of Fowler and Slye[10] over the incident neutron spectrum; this serves as a check on the absolute calibration. (Wäffler's[7] calibration is in bad disagreement with these, probably owing to an error in the measurement of the neutron flux.) The calculations using T_2 seem to give better agreement with the experimental data than those using T_1, but the excitation function for $(n,2n)$ in Cu^{63} is in better agreement with

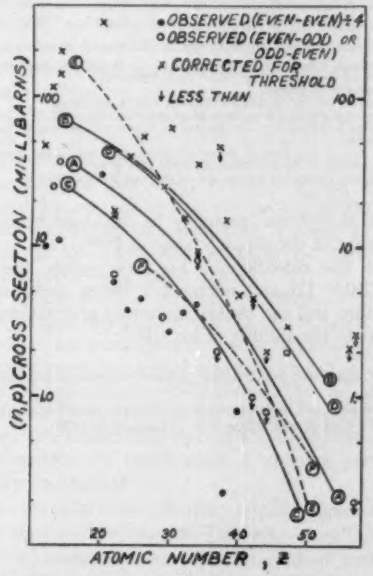

FIG. 3. (n,p) cross sections in cyclotron beam. Lines show calculated values according to various assumptions described in text.

[7] H. Wäffler, Helv. Phys. Acta 23, 239 (1950).
[8] H. Bethe, Revs. Modern Phys. 9, 90 (1937).
[9] G. L. Trigg, private communication.
[10] J. L. Fowler and J. M. Slye, Phys. 77, 787 (1950).

the latter. When the latter are used, there is a tendency for calculated cross sections to be too large. This has also been reported by Taschek[11] and possible explanations have been advanced.[2,12] With the exception of the four lightest elements, for which the theory fails completely, only Zn^{64} and Pr^{141}, show disagreement beyond the expected error. (The excessive activity in Zr was probably due to impurities, as that element is very difficult to purify.) A possible explanation for Zn^{64} was given in reference 2, and the small observed cross section of Pr^{141} can probably be explained by lack of knowledge of the decay scheme of Pr^{140}.

With due consideration for these points, the data from Table III and reference 7 (when corrected for K-capture and the calibration error) give satisfactory support to the validity of Eq. (1).

TABLE III. $(n,2n)$ cross sections.

(1) Element	(2) Threshold (Mev)	(3) σ(obs) (mb)	(4) Error in (3)(±)	(5) σ(obs)/σ(cal) (T_1)	(6) σ(obs)/σ(cal) (T_2)	(7) Percent error in (5) and (6)
N^{14}	10.6	0.255	0.02	0.04	0.2	50
F^{19}	10.4	2.27	0.23	0.24	0.8	50
P^{31}	12.3	14.4	1.5	3.3	10	50
K^{39}	13.2	0.113	0.02	0.045	0.10	60
Ti^{46}	12.3[a]	≥7.7	0.8	≥1.07	≥2.0	50
Cr^{50}	13.4	1.07	0.15	0.31	0.9	70
Fe^{54}	13.9	<2.0	...	<1.0	<3	80
Ni^{58}	11.7	2.9	0.7	0.57	0.9	55
Cu^{63}	10.9	19.6	2.0	0.67	1.2	45
Zn^{64}	11.8	1.6	0.4	0.14	0.25	55
Ga^{69}	10.5[b]	25.8	4.0	0.69	1.2	50
As^{75}	10.3	50	10	1.3[d]	2[e]	60
Rb^{85}	11.5[b]	<4.0[e]	...	...[e]	...[e]	...
Zr^{90}	12.0	14.0	2.0	2.1	3.0	50
Ru^{96}	13.0[b]	<3.1[e]	...	<1.0	<1.0	90
Ag^{107}	9.6	42	3	0.97[f]	1.0[f]	40
Sb^{121}	9.25	40	4	0.99	1.0	40
I^{127}	9.45	31	3	1.9[g]	1.9[g]	60
Pr^{141}	9.4	39	4	0.49	0.5	40

[a] Threshold calculated from masses in L. Rosenfeld, *Nuclear Forces* (Interscience Publishers, Inc., New York, 1948–49).
[b] Thresholds estimated.
[c] Decay scheme of product nucleus not well investigated.
[d] Decays by $\beta+$ and $\beta-$. Branching ratio estimated.
[e] Maximum beta-energy not known, so that K-capture correction could not be made.
[f] Only one of two isomers observed. Branching ratio taken from D. J. Tendam and H. L. Bradt, Phys. Rev. 72, 1118 (1947).
[g] K-capture correction inaccurate, as β-decay is forbidden.

[11] Gittings, Ogle, and Phillips, privately communicated by R. F. Taschek.
[12] V. Weisskopf, in Symposium on Nuclear Shell Structure, New York Meeting of Am. Phys. Soc. (February 4, 1950).

TABLE IV. Favorable threshold detectors.

Approximate threshold (Mev)	Approximate half-lives (minutes) 3	30	300	3000
9.5	Pr	Ag		I
10.5	N	N	F	AS
11.5			Ni	
12.5	P			
13.5		Cr		
16	O			
21		C		

V. APPLICATIONS

Shielding

Since $(n,2n)$ cross sections are an indirect measure of the energy distribution of inelastically scattered neutrons, columns (5) and (6) of Table III, can be taken as a rough index of inelastic scattering efficiency (aside from the factor πr^2). Phosphorous seems to be especially efficient, while nitrogen and potassium are hopelessly inefficient. A useful method of shielding neutrons of energies above 3 Mev might be based on the large (n,p) cross section in sulfur.

Selection of Threshold Detectors

Since almost all high energy neutron threshold detectors employ $(n,2n)$ reactions, Tables Ia and III can be considered as a detailed study of threshold detectors giving suitable chemical compounds to use (often not a simple matter), the half-life of the activity, the other activities that must be corrected for, the threshold, and the cross section. An approximate absolute calibration can be arrived at by correcting for self-absorption by Eq. (4) with an approximate value for "α" obtainable from Fig. 2.

Table IV lists some favorable threshold detectors (i.e., those which have no seriously interfering activities) by threshold and activity half-life. It may be noted from Table IV that, for most purposes, several other detectors are more favorable than is copper, which has been used quite commonly.

The author would like to acknowledge the extensive help of Professor E. Creutz and L. Wolfenstein in carrying out these experiments and calculations, and the cooperation of Professor A. J. Allen and the operating personnel of the University of Pittsburgh cyclotron in the use of that instrument.

Production of Mesons by Photons on Nuclei*

MELVIN LAX
Department of Physics, Syracuse University, Syracuse, New York

AND

HERMAN FESHBACH
Department of Physics

AND

Laboratory for Nuclear Science and Engineering, Massachusetts Institute of Technology, Cambridge, Massachusetts

(Received July 19, 1950)

The total cross section, energy spectrum, and angular distribution of mesons produced by photons incident on a target nucleus have been expressed in terms of the nucleon momentum distribution within the nucleus. The theory used here is valid for photon energies greater than approximately 1.2 times threshold, and for all but the lightest nuclei. These results have been applied to carbon employing Goldberger and Chew's momentum distribution for the protons in carbon. Excellent agreement is obtained for the meson energy spectrum at 90° and the decrease in efficiency of meson production compared to free protons as targets. The change in efficiency with photon energy, and the meson spectrum at various angles can be used to determine the internal nucleon momentum distribution. Positive mesons yield the proton distribution, negative mesons the neutron distribution.

I. INTRODUCTION

WE shall estimate here the total cross section, angular distribution, and energy spectrum of π-mesons produced in a photo-nuclear collision. We assume that the matrix elements for the basic process in which the target nucleus is a free proton or neutron are known. Actually this is not quite so; the nature of the π-meson is not yet definitely settled, and matrix elements in the available theories are known only in the Born approximation.[1] We shall therefore make use of these matrix elements in a schematic way, without committing ourselves to any particular form of meson theory. We shall, for example, express the cross section for positive meson production with a nuclear target in terms of the cross section with a free proton as target. In fact we shall show that the ratio of these cross sections is *essentially independent of the matrix elements* and depends primarily on the proton momentum distribution within the struck nucleus (providing only that the matrix elements have a smooth energy and angle dependence). Thus the measurement of the meson production cross section in hydrogen and other nuclei can be used as a tool for investigating the momentum distribution within these nuclei.

The angular dependence of the nuclear cross section for photo-meson production also yields fairly direct information concerning the momentum distribution with the nucleus. If the target nucleus is hydrogen, there is no appreciable internal momentum; the energy of the meson and its angle of production are precisely related by a "Compton law." For other target nuclei, the internal momenta of the nucleons leads to a broadening of the Compton line. The shape of the Compton line, half-width, etc., are measures of the momentum distribution with the nucleus. These results, of course, are also influenced by the meson matrix elements.

Experimental results for the total cross section and the meson spectrum at 90° are available for carbon and hydrogen.[2] Instead of using these experiments to calculate the internal momentum distribution, we prefer to check our theory by making use of an approximate distribution available from deuteron pick-up reactions.[3] Both the 90° spectrum and the total cross-section ratio are found to be in excellent agreement with experiment.

The experimental result that seems most startling at first sight is "that the cross section of six bound protons in a carbon atom is only about twice as large as that of a single free proton." In other words, the efficiency $\epsilon=\sigma/(Z\sigma_p)$ ratio of the positive meson cross section to that for Z free protons is only $\frac{1}{3}$ in carbon. This result is explained by our theory. It will be shown that the efficiency is zero at threshold, rises to unity at high energies, and has intermediate values in good agreement with the experimental result quoted.

The reason for the decrease in efficiency at low energies is that only a portion of the proton momentum distribution can participate in the reaction. The region in momentum space energetically possible will generally intersect the momentum region occupied by the protons in the nucleus. As the photon energy increases, the common volume increases so that eventually the entire proton momentum distribution is covered and the efficiency becomes unity.

The evaluation of the efficiency requires some knowledge of the nuclear states. We shall see that sufficiently far above threshold the momentum transfer goes primarily to the struck proton so that only one particle in

* Assisted in part by the Joint Program of the ONR and AEC.

[1] H. Feshbach and M. Lax, Phys. Rev. 76, 134 (1949).

[2] J. Steinberger and A. S. Bishop, Phys. Rev. 78, 494 (1950); McMillan, Peterson, and White, Science 110, 579 (1949).

[3] G. F. Chew and M. L. Goldberger, Phys. Rev. 77, 470 (1950).

the nucleus changes its state. This "single-particle" cross section is then computed using the Hartree approximation to describe the nucleus. This procedure yields results which essentially could be surmised on the basis of the physical ideas given in the preceding paragraph.

It is not actually necessary to assume that the other particles do not change state, but merely that the most important residual states have a small energy spread. The summation over all possible residual states is then equivalent to closure over (A-1) variables. The result is then identical to that obtained by the Hartree approximation except for a binding energy correction.

II. MATRIX ELEMENTS. FREE PROTON CROSS SECTION

The matrix element for positive meson production can always be written in the form

$$\langle n|T(\mathbf{x},\mathbf{p},\boldsymbol{\sigma},\boldsymbol{\tau})|p\rangle, \tag{1}$$

where $|n\rangle$ represents the final neutron state, $|p\rangle$ the initial proton state and T is an operator which is a function of the common space coordinate $\mathbf{x}$, the momentum operator $\mathbf{p}=-i\hbar\nabla$ and the spin and isotopic spin operators $\boldsymbol{\sigma}$ and $\boldsymbol{\tau}$. This matrix element can be assumed to be exact; i.e., the result of an infinite order relativistic perturbation calculation from which divergences have been removed. It will in general depend on the photon, meson, proton, and neutron energies as well as on the spins and polarizations of the various particles. The corresponding matrix element for a nuclear target can be written:

$$(\Psi_f,\textstyle\sum_r T_r\Psi_i), \tag{2}$$

where Ψ_i and Ψ_f are the initial and final nuclear states and T_r acts on the coordinates of particle r:

$$T_r=T(\mathbf{x}_r,\mathbf{p}_r,\boldsymbol{\sigma}_r,\boldsymbol{\tau}_r). \tag{3}$$

The operator T in a relativistic calculation will in general depend on all 16 Dirac operators; and this could be included in our notation, and subsequent procedure. Since both final and initial energy states involve positive energies only, only the terms in 1, $\boldsymbol{\sigma}$, β, and $\beta\boldsymbol{\sigma}$ will survive our evaluation of the matrix element. The matrix elements of the operators β and $\beta\boldsymbol{\sigma}$ may be expanded in a power series in $(1/M)$ with terms involving $\mathbf{p}$ and $\boldsymbol{\sigma}$. Equivalently, a contact transformation to nucleon states involving only the two spinors (1 0 0 0) and (0 1 0 0) may be applied to obtain a new operator T which may then be expressed in terms of 1, $\boldsymbol{\sigma}$ and $\mathbf{p}$ only.

The dependence of T on space must be of the plane wave form $\exp[i(\boldsymbol{\nu}-\boldsymbol{\mu})\cdot\mathbf{x}]$ so that insertion of the neutron and proton wave functions in (1) leads to the usual conservation of momentum factor $\delta(\boldsymbol{\mu}+\mathbf{n}-\mathbf{p}-\boldsymbol{\nu})$. Here $\boldsymbol{\mu}$, $\mathbf{n}$, $\mathbf{p}$, $\boldsymbol{\nu}$ are the momenta of the meson, neutron, proton, and photon respectively. The dependence on $\boldsymbol{\sigma}$ and $\boldsymbol{\tau}$ can at most be linear. The isotopic spin dependence must be given by $\tau^+=(\tau_x+i\tau_y)/2$ since it converts a proton into a neutron. Thus we can write

$$T=\exp[i(\boldsymbol{\nu}-\boldsymbol{\mu})\cdot\mathbf{x}]\tau^+(\mathbf{K}\cdot\boldsymbol{\sigma}+L), \tag{4}$$

where $\mathbf{K}$ and L are abbreviations for matrices $\langle n|\mathbf{K}|p\rangle$ and $\langle n|L|p\rangle$ that depend on the photon and meson momenta and polarizations in addition to the nucleon momenta. The matrix element in the negative meson case is similar: τ^+ is replaced by τ^-, and $\mathbf{K}$ and L are replaced by other functions approximately but not exactly equal to the positive meson matrix elements.[4] This difference is important in calculating the ratio of negative to positive meson production. If scalar, pseudoscalar or vector mesons are treated in the first Born approximation, and the nucleons are treated nonrelativistically, $\mathbf{K}$ and L will be independent of the nucleon momenta. This assumption is unnecessary for the subsequent theory but is utilized in the numerical comparison with experiment. We also mention that to terms of order meson mass/nucleon mass $\mathbf{K}=0$ in the scalar case, and $L=0$ in the pseudoscalar case, but neither $\mathbf{K}$ nor L vanishes in the vector meson case.

The matrix elements (4) are similar to those in beta-decay problems with a combination of Fermi and Gamow-Teller selection rules. However, the phase $(\boldsymbol{\nu}-\boldsymbol{\mu})\cdot\mathbf{x}$ is much larger than in the beta-decay case, and the exponential cannot be approximated by a power series.

The matrix element in the free proton case (1) can be integrated to give momentum conservation. Take the absolute square of (1) and perform the spin sums. The free proton cross section is then:

$$\sigma_p=(2\pi)^{-2}\int(K^2+L^2)d\boldsymbol{\mu}I_p, \tag{5}$$

$$I_p=\int d\mathbf{n}\,\delta(\mathbf{n}+\boldsymbol{\nu}-\boldsymbol{\mu}-\mathbf{p})\delta(n_0+\mu_0-\nu_0-p_0) \tag{6}$$

in units $\hbar=c=$ meson mass $=$ unity. Here $\mu_0=(1+\mu^2)^{\frac{1}{2}}$ is the meson energy, $n_0=(M^2+n^2)^{\frac{1}{2}}$ is the neutron energy, $p_0=(M^2+p^2)^{\frac{1}{2}}$ is the proton energy and $\nu_0=\nu$ is the photon energy. In what follows we shall take the struck proton to be at rest: $p=0$, $p_0=M$.

The momentum-energy conditions expressed by (6) reduce after integrating over $\mathbf{n}$ to a single condition

$$I_p=\delta[(M^2+(\boldsymbol{\nu}-\boldsymbol{\mu})^2)^{\frac{1}{2}}+\mu_0-\nu_0-M] \tag{7}$$

equivalent to the "Compton" relation between the meson momentum and its angle θ relative to $\boldsymbol{\nu}$:

$$2\nu(\mu_0-\mu\cos\theta)=1+2M(\nu_0-\mu_0). \tag{8}$$

This relation reduces to the usual one for photons if we set $\mu\simeq\mu_0=$ degraded photon energy and omit the 1 (the meson rest mass).

The integrations over $d\boldsymbol{\mu}=2\pi d(\cos\theta)\mu\mu_0 d\mu_0$ can be performed in either order according to whether the final

[4] K. A. Brueckner and M. L. Goldberger, Phys. Rev. **76**, 1725 (1949).

result is to be expressed as a meson spectrum or as an angular distribution. For the meson spectrum we need

$$\int I_\nu d(\cos\theta) = (M+\nu_0-\mu_0)/\mu\nu. \tag{9}$$

For the angular distribution we need

$$\int I_\nu d\mu_0 = (\partial\mu_0/\partial E_f)_\theta = \mu n_0/[\mu n_0+\mu_0(\mu-\nu\cos\theta)]. \tag{10}$$

It is understood that μ is to be eliminated from (5) and (10) with the help of the Compton Law. For future reference, we note that if I_ν is replaced by (6) and the integrations in (10) over $d\mathbf{n}$ and $d\mu_0$ are performed in reverse order:

$$\int I_\nu d\mu_0 = |\partial\mathbf{n}/\partial\mathbf{k}|_{E_f=E_i}, \tag{11}$$

where $\mathbf{k}=\mathbf{n}+\boldsymbol{\nu}-\mathbf{v}$ and the Jacobian does not take on the value unity because μ_0 depends on n_0 through energy conservation.

III. CLOSURE APPROXIMATION TO THE CROSS SECTION

Using matrix (2) the cross section for a nuclear target can be written as

$$\sigma = (2\pi)^{-2}\int d\boldsymbol{\nu}\sum_f |(\Psi_f, \sum_\tau T_\tau\Psi_i)|^2\delta(E_f-E_i). \tag{12}$$

E_f and E_i are the final and initial energies of the entire system. In comparison with the free particle case (5) $\mathbf{p}+\mathbf{v}\neq\mathbf{n}+\boldsymbol{\nu}$ and the integration over $\mathbf{n}$ is now replaced by a summation over the final states of the residual nucleus. These final states are limited by energetic considerations as indicated by the δ-function in (12). To obtain a closure approximation to the cross section we relax the energy conservation sufficiently to permit the summation to be made over all final states of the nucleus. This is performed by dropping the energy of the initial and final nucleus from the argument of the δ-function in (12) and replacing the final meson energy μ_0 by some average value over the emergent meson energy distribution. Sufficiently far above threshold this average is approximately given by the "Compton" relation (8); i.e., the replacement given below is approximately valid:

$$\delta(E_f-E_i)\rightarrow\delta\{[M^2+(\mathbf{v}-\boldsymbol{\nu})^2]^{\frac{1}{2}}+\mu_0-\nu_0-M\}. \tag{13}$$

The closure approximation should be accurate when the photon energy exceeds the threshold energy by a sufficiently large amount. (At lower energies, particularly near threshold, the closure approximation should give an upper bound to the cross section, inasmuch as it includes many final states which are not energetically possible.) We can then employ closure to obtain

$$M = \sum_f |(\Psi_f, \sum T_\tau\Psi_i)|^2 = (\Psi_i, \sum_{\tau,s} T_\tau^\dagger T_s\Psi_i). \tag{14}$$

We now consider the diagonal terms and the non-diagonal terms in this sum separately. The diagonal terms involve just one nuclear particle at a time so that we shall call their contribution to the cross section the single particle cross section and the corresponding matrix element M_1. The non-diagonal terms involve two nucleons at a time, and are therefore called the two particle contribution; the corresponding matrix element is M_2. It is clear that the two-particle matrix element can have a contribution only inasmuch as there is some correlation in the location of nucleons in the nucleus. Correlation is of course a necessary but not a sufficient condition for $M_2\neq 0$.

Consider now the single-particle terms. These are given by

$$\langle i|\sum_\tau T_\tau^\dagger T_\tau|i\rangle = \langle i|\sum_\tau (\mathbf{K}\cdot\boldsymbol{\sigma}_\tau+L)^2\tau_\tau^-\tau_\tau^+|i\rangle. \tag{15}$$

This result may be averaged over all orientations of the nucleus:

$$\langle(\mathbf{K}\cdot\boldsymbol{\sigma}_\tau+L)^2\rangle_{Av} = K^2+L^2. \tag{16}$$

The equivalence between an orientation average and a spin sum can also be regarded as a consequence of the principle of spectroscopic stability. Furthermore $\langle i|\sum_\tau \tau_\tau^-\tau_\tau^+|i\rangle = Z$, the number of protons in the nucleus. Combining Eqs. (12) to (16) we find that in the region where (13) is valid, the one-particle contribution is simply

$$\sigma_1 = Z\sigma_p, \tag{17}$$

the result to be expected from Z free protons. The off-diagonal or two-particle contributions are given by:

$$M_2 = \sum_{\tau\neq s}\langle i|\tau_\tau^-\tau_s^+(\mathbf{K}\cdot\boldsymbol{\sigma}_\tau+L)(\mathbf{K}\cdot\boldsymbol{\sigma}_s+L) \times\exp[i(\mathbf{v}-\boldsymbol{\nu})\cdot(\mathbf{x}_\tau-\mathbf{x}_s)]|i\rangle. \tag{18}$$

M_2 can be evaluated exactly if the pair correlation function $\rho(\mathbf{x}_\tau, \mathbf{x}_s)$ is known for all spin, isotopic spin states. In general, however, we do not have such detailed information concerning the nuclear state. We shall therefore make the following assumptions.

(1) There are only two independent correlation functions, one for space symmetric, and one for space antisymmetric states. In other words, the spin, isotopic spin state of a pair of particles influences their space correlation only through the Pauli principle.

(2) These correlation functions depend only on the separation $|\mathbf{x}_\tau-\mathbf{x}_s|$ between particles. Thus, any odd dependence on $\mathbf{x}_\tau-\mathbf{x}_s$ which is present in (18) will disappear on averaging.

Making use of the second assumption we can replace the exponential by an orientation average:

$$V_{\tau s} = \langle\exp[i(\mathbf{v}-\boldsymbol{\nu})\cdot(\mathbf{x}_\tau-\mathbf{x}_s)]\rangle_{Av} = \sin(|\mathbf{v}-\boldsymbol{\nu}||\mathbf{x}_\tau-\mathbf{x}_s|)/(|\mathbf{v}-\boldsymbol{\nu}||\mathbf{x}_\tau-\mathbf{x}_s|).$$

It is now permissible to average over the spin orientation of the nucleus

$$\langle(\mathbf{K}\cdot\boldsymbol{\sigma}_\tau+L)(\mathbf{K}\cdot\boldsymbol{\sigma}_s+L)\rangle_{Av} = \tfrac{1}{3}K^2(\boldsymbol{\sigma}_\tau\cdot\boldsymbol{\sigma}_s)+L^2$$

and to symmetrize on indices r and s:

$$M_2=\sum_{r\neq s}\langle i|O_{rs}V_{rs}|i\rangle,$$

$$O_{rs}=\tfrac{1}{2}(\tau_r^-\tau_s^++\tau_s^-\tau_r^+)[\tfrac{1}{3}K^2(\sigma_r\cdot\sigma_s)+L^2].$$

Employing methods similar to those of Wigner and Feenberg[5] we split the state $|i\rangle$ into its space symmetric and antisymmetric parts:

$$|i\rangle=|s\rangle+|a\rangle,$$
$$|s\rangle=\tfrac{1}{2}(1+P_{12})|i\rangle;\quad |a\rangle=\tfrac{1}{2}(1-P_{12})|i\rangle, \tag{19}$$

where P_{12} is the space exchange operator

$$-P_{12}=\tfrac{1}{4}(1+\sigma_1\cdot\sigma_2)(1+\tau_1\cdot\tau_2).$$

Thus a typical term in the sum (18) is:

$$\langle i|O_{12}V_{12}|i\rangle=\langle s|O_{12}V_{12}|s\rangle+\langle a|O_{12}V_{12}|a\rangle$$

and cross terms vanish because O_{12} commutes with P_{12}. Making use of assumption (1) and (19) we can simplify this matrix element:

$$\langle i|O_{12}V_{12}|i\rangle=V_s\langle s|O_{12}|s\rangle+V_a\langle a|O_{12}|a\rangle$$
$$=\tfrac{1}{2}(V_s+V_a)\langle i|O_{12}|i\rangle+\tfrac{1}{2}(V_s-V_a)\langle i|O_{12}P_{12}|i\rangle.$$

The spin matrix elements are evaluated by methods similar to those of Wigner:[6]

$$\langle i|\sum_{r\neq s}O_{rs}|i\rangle=-Z(K^2+L^2)+L^2[T(T+1)-T_s(T_s+1)]$$
$$+\tfrac{1}{3}K^2[P^2+(P')^2+(P'')^2+4P+2P'-S(S+1)$$
$$-T(T+1)-3T_s-S-\langle Y_s^2\rangle]\simeq-Z(K^2+L^2),$$

$$\langle i|\sum_{r\neq s}O_{rs}P_{rs}|i\rangle=-\tfrac{1}{6}(K^2+L^2)(A^2-4T_s^2)$$
$$-\tfrac{1}{6}(3L^2-2K^2)(S^2-\langle Y_s^2\rangle)\simeq-\tfrac{1}{6}(K^2+L^2)A^2$$

where $\langle Y_s^2\rangle$ is the mean value of the operator $(\frac{1}{2}\sum_r\sigma_{rs}\tau_{rs})^2$ in the state with quantum numbers, P, P', P'', T, T_z, S, $S_z=S$ (compare reference 5 for notation). The approximate values contain all terms of order A^2 and A. Thus the complete matrix element is given approximately by:

$$M_1+M_2\simeq(K^2+L^2)\{Z[1-\tfrac{1}{2}(V_s+V_a)]$$
$$-\tfrac{1}{16}A^2(V_s-V_a)\}$$

and the ratio of the two particle to the one-particle contribution is approximately

$$M_2/M_1\simeq-\tfrac{1}{2}(V_s+V_a)-\tfrac{1}{2}(A^2/8Z)(V_s-V_a). \tag{20}$$

The order of magnitude of V_s and V_a can be obtained from a simple model in which the two particle densities ρ_a^s are proportional to $\exp[-(x_{12}/R)]\pm\exp[-(x_{12}/r_0)]$ respectively, where R is the nuclear radius and r_0 the range of nuclear forces. The results neglecting the fixed position of the center of mass of the nucleus are given below. The more precise calculations in which this approximation has not been made have been performed and give very similar numerical results.

$$V_a^s=\left\{\frac{R^3}{[1+(|\nu-\mu|R)^2]^2}\pm\frac{r_0^3}{[1+(|\nu-\mu|r_0)^2]^2}\right\}(R^3\pm r_0^3)^{-1},$$

$$\tfrac{1}{2}(V_s+V_a)\simeq[1+(|\nu-\mu|R)^2]^{-2},$$

$$\tfrac{1}{2}(V_s-V_a)\simeq(r_0/R)^3[1+(|\nu-\mu|r_0)^2]^{-2}. \tag{21}$$

In our units $r_0\simeq1$ and $R^3\simeq Ar_0^3$. Except in the forward direction $|\nu-\mu|R\gg1$ and the two-particle contributions are small. An estimate of their effect on the integrated cross section can be obtained by averaging the V's over the angular distribution associated with free proton targets. The result is

$$\langle(V_s+V_a)/2\rangle=[(R^2-1)^2+(2\nu R)^2]^{-1}\sim[A^{4/3}+4\nu^2A^{2/3}]^{-1}$$
$$\langle(V_s-V_a)/2\rangle=(r_0/R)^3[(r_0^2-1)^2+(2\nu r_0)^2]^{-1}\sim(4\nu^2A)^{-1},$$
$$|M_2/M_1|\sim(A^{4/3}+4\nu^2A^{2/3})^{-1}+(16\nu^2)^{-1}.$$

Thus the one-particle contribution is an adequate description away from the threshold, in all but the lightest nuclei. How closely may threshold be approached before M_2 starts to make significant contributions? In the next section we shall make a closer estimate of M_1. Combining this with the estimate of M_2 contained herein, it is estimated that M_2 may be neglected for $\nu>1.2$ or $\nu>170$ Mev. This estimate, which is rigorous only at a considerable energy above threshold, has been checked by the calculation of the two-particle contribution for the deuteron as target nucleus.[7]

IV. THE SINGLE-PARTICLE CONTRIBUTIONS IN THE HARTREE APPROXIMATION

The closure procedure used in the preceding section is not based on any model of the nucleus, or on any assumptions concerning nuclear forces. However, it overestimates the cross section by extending the sum over final states to include some which are not energetically possible. In order to estimate the energies at which the closure approximation is valid as well as the decrease in cross section below these energies we shall introduce the Hartree approximation. We shall consider in detail the one-particle contributions, the main term in the cross section.

We shall show that the relation between the bound and the free-particle cross sections depends primarily on the momentum distribution in the nucleus, and not on a more detailed knowledge of the nuclear wave functions. This result undoubtedly has a validity greater than that of the Hartree model with which it will be obtained.

[5] E. P. Wigner and E. Feenberg, "Reports on progress in physics," Phys. Soc., London **8**, 308 (1941).
[6] E. P. Wigner, Phys. Rev. **56**, 519 (1939).
[7] M. Lax and H. Feshbach, unpublished.

The initial nuclear state can be represented by the anti-symmetrized product:

$$\Psi_i=(A!)^{-\frac{1}{2}}\sum \epsilon_\alpha\varphi_{\alpha_1}(x_1)\varphi_{\alpha_2}(x_2)\cdots\varphi_{\alpha_n}(x_n), \quad (22)$$

and the final nuclear state is represented by a similar product. The one-particle contributions are obtained by using a final wave function in which only one state, say $\varphi_j(x)$ has been changed. The ejected particle may be represented approximately by a plane wave $(2\pi)^{-\frac{1}{2}}\exp(i\mathbf{n}\cdot\mathbf{x})$. In doing so we have of course neglected the interaction of the emergent neutrons and the residual nucleus. We have also assumed that the final neutron has sufficient energy to leave the nucleus. Terms involving the nucleons remaining in the nucleus are, except for small energy transfers, included in the two particle terms; an estimate for these was obtained in Sec. III.

The spin sum yields the same result as in the free case if we neglect the variation of the space dependence of φ_j with spin direction. It is easy to include this dependence, but in view of the large uncertainties in the nuclear wave function, the choice of an average seems to be more appropriate. In terms of the normalized momentum wave function

$$c_j(\mathbf{k})=(2\pi)^{-\frac{1}{2}}\int \exp(-i\mathbf{k}\cdot\mathbf{x})\varphi_j(\mathbf{x})d\mathbf{x},$$

the matrix element takes the form $c_j(\mathbf{n}+\boldsymbol{\mu}-\boldsymbol{\nu})$. Squaring and summing over the contributions of the various one-particle transitions we find that

$$M_1=\sum_j \int |c_j(\mathbf{n}+\boldsymbol{\mu}-\boldsymbol{\nu})|^2 d\mathbf{n} \quad (23)$$

takes the place of the closure expression (14). Because of the isotopic spin operator τ^+ the sum over j includes only the proton states. In effect, M_1 replaces the conservation of momentum factor $\delta(\mathbf{n}+\boldsymbol{\mu}-\boldsymbol{\nu})$ in the free particle case (6). Introducing the normalized momentum density:

$$\rho(\mathbf{k})=Z^{-1}\sum_j |c_j(\mathbf{k})|^2,$$

$$M_1=Z\int d\mathbf{n}\int d\mathbf{k}\rho(\mathbf{k})\delta(\mathbf{n}+\boldsymbol{\mu}-\boldsymbol{\nu}-\mathbf{k}),$$

the one-particle contributions to the nuclear cross section can now be written in a form directly comparable with the free particle result (5):

$$\sigma_1=Z(2\pi)^{-2}\int (K^2+L^2)d\boldsymbol{\mu}I, \quad (24)$$

$$I=\int \rho(\mathbf{k})d\mathbf{k}\int d\mathbf{n}\delta(\mathbf{n}+\boldsymbol{\mu}-\boldsymbol{\nu}-\mathbf{k}) \times\delta(n_0+\mu_0-\nu_0-M+\epsilon)$$
$$=\int \rho(\mathbf{k})d\mathbf{k}\delta\{[(\boldsymbol{\nu}+\mathbf{k}-\boldsymbol{\mu})^2+M^2]^{\frac{1}{2}} -M+\mu_0-\nu_0+\epsilon]\}. \quad (25)$$

By inserting the correct (rather than Hartree) energy conservation condition in (25) we obtain the same cross section as that yielded by the partial closure method discussed in the introduction. The correct condition is $\delta(n+\mu_0+$*mass of residual nucleus*$-\nu_0-$*mass of struck nucleus*$)$. We may therefore interpret $\epsilon=$(*mass of residual nucleus*$+M-$*mass of struck nucleus*) as approximately (*binding energy of the proton*$+$*average excitation energy of the residual nucleus*). Since the struck proton energy does not appear in the energy conservation we cannot interpret the cross section as simply that due to a distribution of free protons.

The choice $\rho(\mathbf{k})=\delta(\mathbf{k})$ corresponding to a proton at rest reduces I to its free proton value I_p in (6) if we neglect binding energy corrections (set $\epsilon=0$). In the free case, I_p vanishes unless the Compton law relating μ and θ is obeyed—i.e. at each angle θ the meson energy takes a definite value. If a distribution of momenta $\rho(\mathbf{k})$ is available, the Compton line will be broadened. The extent to which this occurs can be investigated by integration, over the directions of $\mathbf{k}$ using $\boldsymbol{\nu}-\boldsymbol{\mu}$ as a polar axis and $d\mathbf{k}=k^2dk2\pi d(\cos\chi)$. The integration over $\cos\chi$ can then be evaluated as:

$$I=2\pi\frac{M+\nu_0-\mu_0}{a}\int_{(b-a)\text{ or }(a^2-\delta\nu)^{\frac{1}{2}}}^{a+b}\rho(k)kdk, \quad (26)$$

$$a=|\boldsymbol{\nu}-\boldsymbol{\mu}|, \quad b=[(\nu_0'-\mu_0)(2M+\nu_0'-\mu_0)]^{\frac{1}{2}},$$

where $\nu_0'=\nu_0-\epsilon$. Limits on k are set by the conservation condition given by (25) subject to $|\cos\chi|=1$. Equation (26) exhibits the direct relationship between the shape of the Compton line and the momentum distribution in the nucleus.

We have assumed that $\rho(\mathbf{k})$ is spherically symmetric. It will, in general, be large out to some momentum α and decrease rapidly thereafter. The closure approximation will therefore be valid only if both conditions

$$|\boldsymbol{\nu}-\boldsymbol{\mu}|-[2M(\nu_0'-\mu_0)]^{\frac{1}{2}}<\alpha,$$
$$|\boldsymbol{\nu}-\boldsymbol{\mu}|+[2M(\nu_0'-\mu_0)]^{\frac{1}{2}}>\alpha,$$

can be met. The first condition with α and ϵ equal to zero is the Compton condition. This condition can be met if one particle can absorb all the available momentum $|\boldsymbol{\nu}-\boldsymbol{\mu}|$. This is always possible above the free particle threshold. Above the free particle threshold this condition simply describes the width of the Compton line. The second condition $(a+b)>\alpha$ is sufficient to make the integral independent of its upper limit, since it then covers the significant region of integration. In this case, the integrated intensity of the broadened Compton line will be the same as the corresponding unbroadened line.

A quantitative investigation of the decrease in total cross section when these conditions are not fulfilled requires an integration over $d\boldsymbol{\mu}$. This integration cannot be performed unless the dependence of K and L is specified, and some form is given to $\rho(k)$. An alternative

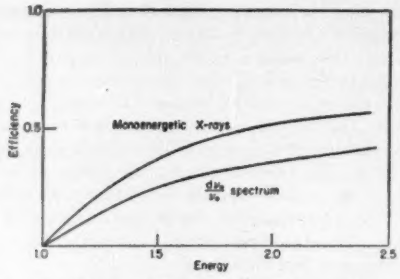

FIG. 1. Efficiency of meson production. The abscissa gives (1) photon energy for the upper curve (2) maximum photon energy for $d\nu_0/\nu_0$ bremsstrahlung spectrum.

procedure is to perform the integration over $d\boldsymbol{\mu}$ *before* that over $d\mathbf{k}$. We shall therefore introduce the following definition:

$$\sigma(\boldsymbol{\nu}+\mathbf{k},\ \nu_0')=(2\pi)^{-2}Z\int(K^2+L^2)d\boldsymbol{\mu}$$
$$\times\delta\{[(\boldsymbol{\nu}+\mathbf{k}-\boldsymbol{\mu})^2+M^2]^{\frac{1}{2}}-M+\mu_0-\nu_0'\},\quad(27)$$

so that the total cross section can be rewritten as:

$$\sigma=\int\sigma(\boldsymbol{\nu}+\mathbf{k},\ \nu_0')\rho(\mathbf{k})d\mathbf{k}.\quad(28)$$

Roughly speaking, the situation is equivalent to having a distribution of photons with momenta $\boldsymbol{\nu}+\mathbf{k}$ and a fixed energy ν_0'. Only a certain portion of these "photons," however, can contribute to the cross section, since the momentum the neutron can absorb is limited by energy considerations. Since $\boldsymbol{\mu}$ has already been integrated over, the limit on $|\boldsymbol{\nu}+\mathbf{k}|$ is to be set using the most favorable value of $\boldsymbol{\mu}$. The most favorable direction for $\boldsymbol{\mu}$ is parallel to $\boldsymbol{\nu}+\mathbf{k}$ since the meson then helps to absorb the "excess" momentum. With this direction $|\boldsymbol{\nu}+\mathbf{k}|\leq\mu+b$. The most favorable value of μ_0 is then $\mu_0=1+(\nu_0-1)/M$ and we obtain the condition

$$|\boldsymbol{\nu}+\mathbf{k}|\lesssim[2M(\nu_0'-1)]^{\frac{1}{2}}=d.$$

The quantity d is just the nucleon momentum available if all of the incident photon energy is absorbed by the nucleon. When $\sigma(\boldsymbol{\nu}+\mathbf{k},\ \nu_0')$ varies slowly with $\mathbf{k}$, the decrease in cross section due to lack of closure is then simply:

$$\sigma_1/(Z\sigma_p)=\int_{|\boldsymbol{\nu}+\mathbf{k}|\leq d}\rho(\mathbf{k})d\mathbf{k}.\quad(29)$$

In short, the cross section is reduced because only a portion of the momentum distribution is energetically capable of contributing to the cross section. The region of integration is a sphere of radius $[2M(\nu_0-1)]^{\frac{1}{2}}$ centered at $-\boldsymbol{\nu}$. However, $\rho(\mathbf{k})$ is appreciable over the sphere $|\mathbf{k}|<p_F$ and small outside, where $p_F=(2M\epsilon_F)^{\frac{1}{2}}$ is the Fermi momentum. These two spheres will overlap fairly completely if

$$[2M(\nu_0-1)]^{\frac{1}{2}}>\nu_0+p_F.\quad(30)$$

Thus the cross section may be expected to approach the closure cross section at an energy of about 320 Mev, $\nu_0\simeq 2.3$.

Near threshold the sphere of integration shrinks to a point at $\mathbf{k}=-\boldsymbol{\nu}=-1$. $\sigma(\boldsymbol{\nu}+\mathbf{k},\ \nu_0)$ becomes $\sigma(0,\ 1)$ and the closure correction is simply

$$\sigma_1/(Z\sigma_p)\simeq\frac{4\pi}{3}[(2M)^{\frac{1}{2}}(1+(1/2M))]^3\rho(-1)$$
$$\times\frac{\sigma(0,\ 1)}{\sigma(1,\ 1)}(\nu_0-1)^{\frac{1}{2}}.\quad(31)$$

Since the free proton cross section behaves like $(\nu_0-1)^{\frac{1}{2}}$ the nuclear cross section varies as $(\nu_0-1)^2$. We note that the threshold is actually 1 (aside from a small binding energy correction). The reason for this is that protons of momentum $\mathbf{k}=-1$ are available to absorb the photon impact so that no recoil energy need be absorbed.

A previous analysis of the nuclear cross section near threshold[6] led to a behavior of $(\nu_0-1)^{5/2}$; i.e., an additional factor of $(\nu_0-1)^{\frac{1}{2}}$. This calculation was based, however, on the Fermi statistical model of the nucleus. On this model $\rho(\mathbf{k})$ vanishes abruptly for $k>p_F$. Thus $\int\rho(\mathbf{k})d\mathbf{k}$ is the intersection volume of two spheres. And the latter will vary as $(\nu_0-\nu_t)^2$ in the neighborhood of the threshold energy ν_t at which the spheres begin to overlap.

It should be emphasized that energy dependence given by (31) may be modified if $\sigma(0,\ 1)$ should vanish. For the deuteron as target nucleus,[7] if $\mathbf{K}=0$, the Pauli exclusion principle yields $\sigma(0,\ 1)=0$, so that the energy dependence of the cross section becomes $(\nu_0-1)^3$.

V. COMPARISON WITH EXPERIMENT

At present the only available data[2] involve carbon as the target nucleus. The incident beam is the bremsstrahlung spectrum from the Berkeley synchrotron. The measurements include the meson energy distribution at 90° with respect to the incident photon beam, and the efficiency of production. This latter is (1/3); the energy distribution at 90° is given in Fig. 3.

Comparison with the theory of Sec. IV involves a knowledge of the normalized momentum density, which fortunately has been evaluated for similar momentum transfers by Goldberger and Chew.[8] These authors give

$$\rho(\mathbf{k})=\alpha_p/\pi^3(\alpha_p^2+k^2)^2.\quad(32)$$

This expression is not expected to be valid for the large values of k for one would expect that $\rho(\mathbf{k})$ decreases more rapidly than indicated by (32).

We now introduce (32) into (29) to obtain the efficiency of positive meson production, and into (24) and

[8] D. ter Haar, Science **108**, 57 (1948).

(26) for the energy distribution at 90°. We neglect binding energy effects. These results must then be integrated over the brehmsstrahlung spectrum to obtain values comparable with experiment. Strictly speaking, such a calculation gives only the one-particle contribution to the cross section. The two-particle terms, which give the coherence effects, are small except for ν_0 near threshold. However, the cross section will generally increase with energy more rapidly than the photon-spectrum decreases, so that the integration over the photon-spectrum will emphasize the larger values of ν_0. Hence the error involved in including only the single-particle contribution should be small.

Let us consider the efficiency of positive meson production. From (29) and (32)

$$\varepsilon=\frac{\sigma_1}{Z\sigma_p}=\frac{1}{\pi}\left[\tan^{-1}\frac{d-\nu_0}{\alpha_p}+\tan^{-1}\frac{d+\nu_0}{\alpha_p}\right]+\frac{\alpha_p}{2\pi\nu_0}\ln\frac{\alpha_p^2+(d-\nu_0)^2}{\alpha_p^2+(d+\nu_0)^2}. \quad (33)$$

A plot of ε as a function of ν_0 is given in Fig. 1. The relatively slow rate of increase for large ν_0 is directly attributable to the long tail of distribution (32) and is suspect.

If the incident photon spectrum is $f(\nu_0)d\nu_0$ the average efficiency is

$$\bar{\varepsilon}=\left(\int\sigma_1 f(\nu_0)d\nu_0\right)\Big/\left(Z\int\sigma_p f(\nu_0)d\nu_0\right). \quad (34)$$

In this paper, we have approximated the spectrum by $f(\nu_0)=1/\nu_0$ and have employed the σ_p calculated in an earlier publication.[1] The consequent $\bar{\varepsilon}$ is also plotted in Fig. 1. The value at $\nu_0=2.4$ is 0.4, which is 20 percent higher than the estimated experimental value, but well within the experimental error. It is quite clear that an accurate determination of the excitation curve for either monochromatic x-rays or for a spectrum will yield information about the nucleon momentum distribution.

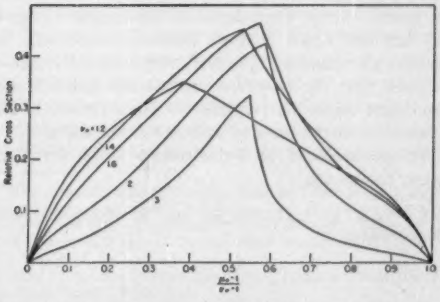

FIG. 2. Meson energy spectra at 90° with respect to photon beam for monoenergetic x-rays incident on carbon. The abscissa is the ratio of the meson kinetic energy to the excess of photon energy over threshold.

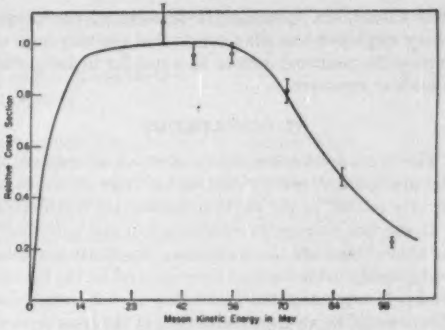

FIG. 3. Meson energy spectrum at 90° with respect to photon beam for a $d\nu_0/\nu_0$ bremsstrahlung spectrum incident on carbon. The experimental points are taken from Steinberger and Bishop.

The energy distribution at 90° is obtained by inserting momentum distribution (32) into (24) and (26). The integral I is given by

$$I=\frac{\alpha_p}{\pi}\frac{M+\nu_0-\mu_0}{a}\left[\frac{1}{\alpha_p^2+k_i^2}-\frac{1}{\alpha_p^2+(a+b)^2}\right], \quad (35)$$

where

$$k_i^2=\begin{cases}a^2-b^2 & a\geqslant b\\ (b-a)^2 & a\leqslant b\end{cases}.$$

I must then be multiplied by the statistical factors $\mu\mu_0$ and by the energy dependence of K^2+L^2. This must at least be $1/(\mu_0\nu_0)$ from the normalization of the meson and photon wave functions and indeed is closely that for pseudoscalar mesons though not precisely so. Hence the spectrum is given by

$$g(\mu_0)d\mu_0\sim[(\mu_0^2-1)^{\frac{1}{2}}I(\mu_0)/\nu_0]d\mu_0. \quad (36)$$

The function $g(\mu_0)$ is plotted in Fig. 2 for some values of ν_0 ranging from $\nu_0=1.2$ to $\nu_0=3$. The salient features are (1) the discontinuity in slope at $a=b$, i.e., at the meson energy obtained from Compton law (8); (2) the relatively rapid decrease of g with μ_0 for μ_0 greater than the value at the discontinuity. For these meson energies only those protons whose momenta are in a direction opposite to the direction of the incident photon can contribute.

In Fig. 3 the energy distribution average over a $d\nu_0/\nu_0$ spectrum is given, together with experimental values. The scale for the ordinate for the theoretical curve has been chosen as unity at a meson kinetic energy of 0.3. Comparison of the predicted absolute magnitude with experiment has already been made above. The agreement of the predicted and experimental energy distributions is remarkably close. Because of the many approximations and the experimental errors such agreement must be regarded as fortuitous. However, the agreement of prediction both with efficiency and the energy distribution indicates that the qualitative, and to

some extent, the quantitative features of the simple theory employed here are correct; that one may hope to employ the produced mesons as a tool for investigation of nuclear structure.

VI. CONCLUSIONS

The cross section for the production of mesons by photons incident upon a nucleus has been shown to be directly related to the nucleon momentum distribution ρ. It was first necessary to demonstrate that sufficiently far above threshold the correlation effects are small except possibly in the forward direction and for the lightest nuclei. It was estimated that below $\nu \sim 1.2$, correlation effects would be an appreciable part of the cross section. These estimates were based on the closure approximation (Sec. II). Once this result was established, the efficiency of meson production was calculated, as well as the meson energy distribution at a given angle. In both of these, the assumption is made that the recoil nucleon can be described by a plane wave. From the efficiency it is possible to estimate the energy at which the closure approximation is valid and the efficiency is essentially one. In the absence of a tail to the momentum energy distribution, this photon energy is 320 Mev. Since the tail may still make an appreciable contribution, the efficiency will actually be one at some energy well above 320 Mev depending upon the shape of the tail. In calculating the efficiency it was assumed that the matrix elements varied smoothly with photon momentum; i.e., with the space phase of the photon wave. The dependence of the meson energy distribution on the momentum distribution ρ is given in (24, 26). This meson energy distribution has its maximum for each angle at the meson energy given by the Compton law for a free nucleon. The distribution is asymmetric, falling off more rapidly at higher energies. The width of the energy distribution is roughly determined by the nucleon momentum at which ρ starts to decrease rapidly. Finally the cross section at threshold was estimated. It was assumed that the photon energy dependence of the correlation contributions will be more rapid than the single particle term. The single particle contribution behaves as $(\nu-\nu_t)^2$ at threshold ν_t.

These calculations have been applied to carbon employing Goldberger and Chew's momentum distribution. Astonishingly good agreement with experiment is obtained for both the efficiency of meson production and the energy distribution of mesons produced at 90° with respect to the incident beam. This agreement, while partly accidental does indicate that at least a semi-quantitative understanding of the production is possible. More important, it strongly suggests that meson production may be employed as a tool for the investigation of nuclear structure, particularly of the momentum distribution inside the nucleus. *Indeed by observing the energy distribution at various angles, and by observing the efficiency as a function of photon energy, it should be possible to describe this momentum distribution very closely even without reference to any other experimental information.*

The interpretation at higher photon energies than are presently available would be somewhat simpler for here many of our assumptions become strictly valid. However, it would be necessary to have more complete information on the fundamental matrix element. This may be obtained empirically by employing hydrogen as a target nucleus. In the present paper the dependence of the matrix elements on the nucleon momenta have not been used in the calculations. Equation (24), however, is correct if K and L are replaced by matrices $\langle n|K|k\rangle$ and $\langle n|L|k\rangle$. If these matrices have a smooth energy dependence, for both negative and positive mesons, the negative positive cross-section ratio will be practically the same as for free nucleon targets. Some difference may be expected, however, in heavier nuclei where the neutron and proton momentum distributions are not equal.

We have also neglected the meson-nucleon interaction on the meson as it passes through the nucleus after its production. This should be unimportant for the lighter nuclei but may be significant for nuclei of large radius. Indeed if a nucleon momentum distribution should be known from other considerations, experiments with heavy nuclei might yield information on the meson-nucleon interaction.

Calculations[7] have been made for H^2 as a target nucleus where the correlation effects are important. These will be reported shortly. Calculations[8] are in progress in which the momenta dependent terms are included for both H^2 and heavier nuclei permitting then a calculation of the ratio of positive to negative meson production.

One point may be emphasized in closing. The energy distribution of mesons at 90° as calculated is sensitive to the meson energy dependence of the matrix elements and this nice check that we obtain is valid only for pseudoscalar mesons. However, this is not conclusive evidence that the observed mesons are pseudoscalar. Agreement might be possible for other mesons if the momentum distribution in carbon were modified.

We are indebted to Dr. Geoffrey Chew for some cogent comments.

[8] F. Villars, M. L. Goldberger, and H. Feshbach, private communication.

Rotational Magnetic Moments in Polyatomic Molecules*

C. K. JEN†
Cruft Laboratory, Harvard University, Cambridge, Massachusetts
(Received August 21, 1950)

There is generally present in a molecule a small magnetic moment associated with its rotational degree of freedom. The rotational g-factor can be measured by an experimental method based upon the Zeeman effect. Previously, the most successful measurements have been made with the molecular beam resonance technique. More recently, the microwave Zeeman splitting of molecular rotation lines has offered another method for the determination of rotational g-factors. With this method, the g-factors of several molecules such as NH_3, H_2O, OCS, etc. have been measured. The quantum mechanical theory of the rotational magnetic moment of the symmetric top molecule has been developed, and the experimental results are discussed qualitatively in the light of this theory.

I. INTRODUCTION

SINCE a molecule is composed of charged particles, a molecular rotation can result in the existence of a magnetic moment. However, the magnetic effects of the positively charged nuclei and the negatively charged electrons would tend to cancel each other, thus leaving a residual moment due to the difference in the distribution and motion of the two kinds of charge. Because of this cancellation effect and the influence of large nuclear masses, the resulting rotational moment in a molecule is generally a very small quantity (of the order of one nuclear magneton or less).

One of the earliest theoretical investigations of the magnetic effect of charged particles in a rotating molecule was made by Condon.[1] He assumed a charged particle rigidly attached to a symmetric rotor and gave a wave-mechanical expression for the perturbed energy in a magnetic field. Several years later, Estermann and Stern[2] measured the rotational moment of the hydrogen molecule by the molecular beam deflection method and obtained a g-factor between 0.8 and 0.9 in the units of nuclear magnetons per rotational quantum number. They found the rigid rotor theory could not account for this result since it would give a g-factor of about 3. This difficulty was resolved by Wick,[3] who showed that the wave-mechanical perturbation theory did account for the experimental value if an appropriate wave function was employed. This explanation was made even more convincing when Ramsey[4] repeated the measurement of the H_2 rotational moment by the more powerful method of molecular beam resonance. Ramsey not only supplied a more accurate measurement for the H_2 rotational moment, the g-factor of which was given as 0.8787, but definitely established the sign of the moment as positive. This result gave, at least for the special case of H_2 molecule, a strong support for Wick's theory and a direct contradiction to the rigid rotor theory for the effect of the electrons. The rigid rotor theory predicted a net rotational moment which was incorrect in magnitude and also incorrect in sign.

The development of microwave spectroscopy in recent years has led to another method of measuring rotational magnetic moments.[5] This method depends on the existence of rotational quantum transitions in the microwave frequency range. The energy level of each rotational state is in general perturbed by a magnetic field and is split into a number of sublevels. From the Zeeman spectrum for a rotational line, information can be obtained on the over-all magnetic moment of the molecule. This over-all magnetic moment is the rotational moment if the molecular rotation has no coupling with any electron or nucleus in the molecule. This requirement is satisfied if the spin of each nucleus is zero and if the molecule is in the $^1\Sigma$-state, as most molecules are in their ground states. Under these conditions, the rotational moment is the only unknown quantity and can be directly determined. If, however, the molecular rotation has a coupling with either an electron or a nucleus, or both, then the determination of the rotational moment must depend either upon the detailed knowledge of the coupled systems or some means of removing the coupling as in the Paschen-Back effect.[6]

II. EXPERIMENTAL METHOD AND APPARATUS

The measuring apparatus and experimental techniques have been described in previous papers.[5,6] The difference between the present method and other current spectroscopic arrangements lies in the use of a resonant cavity as the absorption cell. The microwave generator is simultaneously frequency modulated at two different frequencies in order for the microwave spectral lines to be observed. The higher frequency modulation is used to obtain a high signal-to-noise ratio. The lower fre-

* The research reported in this document was made possible through support extended Cruft Laboratory, Harvard University, jointly by the Navy Department, ONR, the Signal Corps of the U. S. Army, and the U. S. Air Force, under ONR Contract N5ori-76, T. O. 1.

† Now at Applied Physics Laboratory, Johns Hopkins University, Silver Spring, Maryland.

[1] E. U. Condon, Phys. Rev. **30**, 781 (1927).
[2] I. Estermann and O. Stern, Z. Physik **85**, 17 (1933).
[3] G. C. Wick, Z. Physik **85**, 25 (1933).
[4] N. F. Ramsey, Phys. Rev. **58**, 226 (1940).
[5] C. K. Jen, Phys. Rev. **74**, 1396 (1948).
[6] C. K. Jen, Phys. Rev. **76**. 1494 (1949).

quency modulation (actually a saw-tooth wave) is used for the spectral presentation.

A magnetic field continuously variable up to about 10,000 oersteds is used. The field strength is obtained by measurement of the flux change in a stationary coil as the direction of the magnetic field is reversed. The accuracy of the magnetic field measurement is about two percent. The measurement of small frequency differences is accurate to about 50 kc/sec. The average accuracy of a g-factor determination, with the exception of very small g-values, is thus estimated to be about ± 5 percent.

This equipment does not, in its present form, provide means for determining the sign of the magnetic moment.

III. DESCRIPTION OF THE ZEEMAN SPECTRA

It will prove useful for the following sections to describe qualitatively the characteristics of the Zeeman spectra caused by the rotational moment only. The rotational energy, W, in a magnetic sublevel, is, to the first-order approximation,

$$W = W_R - Mg\mu_0 H, \tag{1}$$

where W_R = the energy of a rotational state at $H=0$, designated by the rotational quantum numbers (J, K, etc.), M = magnetic quantum number for J along the field direction, g = g-factor for the rotational state, μ_0 = nuclear magneton, and H = magnetic field. The transition frequency for any Zeeman component is

$$\begin{aligned} \nu &= [(W_R' - W_R)/h] - (M'g' - Mg)\mu_0 H/h \\ &= \nu_R - [\Delta M g' + M(g'-g)]\mu_0 H/h, \end{aligned} \tag{2}$$

where the primed quantities refer to the upper state and the unprimed to the lower state, $\nu_R = (W_R' - W_R)/h$ is the rotational transition frequency (h = Planck's constant), and $\Delta M = M' - M$ is the change in M during transition.

For a given rotational transition, the selection rules for its Zeeman components are:

$$\Delta M = 0, \quad \text{for } \pi\text{-transitions, and}$$
$$\Delta M = \pm 1, \quad \text{for } \sigma\text{-transitions.}$$

Even without a detailed knowledge of the intensity distribution, explicit expressions for which are readily available in standard references,[7] some qualitative description of the nature of the Zeeman spectrum can be made in relation to the rotational g-factors. It can be seen from Eq. (2) that, if $g' = g$, the π-transition has no splitting and the σ-transition results in a doublet, symmetrically displaced relative to the origin (zero-field position). In case g' is not equal to g but $|(g'-g)/g'| \ll 1$, the π-transition results in a group of evenly spaced lines centered at the origin. The σ-transition results in two similar groups (each consisting of lines equally spaced as in the π-group but in general having a different intensity distribution), again symmetrically displaced relative to the origin. Each one of these groups would appear as a single broad "line" for an observation in which the spectral resolution is not sufficiently high. If, however, g' is sensibly different from g, then the lines in each group would be so far separated from one another that they should be treated as individual components.

It should be specifically noted that the Zeeman pattern based on the first-order theory as in Eq. (2) would be invariant to the reversal of the signs of the two g-factors. Hence, the sign of the moment will remain indeterminate. This indeterminacy of sign can be resolved in either one of the following ways. (1) The sign can be determined experimentally with respect to the polarization of the radiation. For an absorption experiment, circularly polarized radiation can cause one branch of the Zeeman pattern or the other to disappear according to the sense of rotation. (2) In the case of a coupling with a nucleus, the sign as well as the magnitude of the rotational moment can be determined, provided the sign and the magnitude of the nuclear moment are known.[5]

IV. RESULTS OF MEASUREMENT

The Zeeman effect in the microwave rotational spectra of some polyatomic molecules has been investigated. The choice of molecules has been dictated primarily by the known presence of rotational lines in the working frequency range of the equipment. To date, measurements have been made on a few representatives of linear, symmetric, and asymmetric types of molecules. The following results refer to the σ-transitions. The g-factors are calculated by Eq. (2). The g-factor in each case is computed from the observed doublet separation and is, therefore, necessarily the average value (denoted by $\bar{g}$) between the true g-factors of two rotational states involved in the transition. The sign of any g-factor is understood to be either plus or minus, unless a definite sign is given.

OCS

Zeeman splitting in the spectra of this linear molecule was measured for OCS^{32} ($J=1\rightarrow 2$, $v=0$) line at 24,325.9 Mc/sec and for the OCS^{34} ($J=1\rightarrow 2$, $v=0$) line at 23,731.3 Mc/sec. Zeeman components were not resolvable for fields below 7000 oersteds. A completely resolved weak doublet has a separation of about 0.36 Mc/sec at $H=8000$ oersteds. Assuming the g-factors for $J=1$ and $J=2$ states are not drastically different, the calculated g-factor for these states is 0.029 ± 0.006. The difference between g-factors of OCS^{32} and OCS^{34} is not detectable in the present experiment.

N_2O

This linear molecule was previously studied with respect to the Paschen-Back effect.[6] Because of the smallness of the electric quadrupole coupling due to the

[7] E. U. Condon and G. H. Shortley, *The Theory of Atomic Spectra* (Cambridge University Press, 1935), p. 387.

N nuclei, decoupling was almost complete at $H=10{,}000$ oersteds. The Paschen-Back components for the σ-transition of the $J=0\rightarrow1$ rotation line were two very strong doublets. The rotational g-factor is calculated to be 0.086 ± 0.004.

NH_3

The Zeeman effect in the inversion spectra of NH_3 (symmetric top) has been studied previously perhaps more thoroughly than for any other molecule.[5,6] Since $N^{15}H_3$ does not have a nuclear quadrupole coupling, its Zeeman spectrum supplies direct information on the rotational magnetic moment. In the case of $N^{14}H_3$, the molecular rotational moment acts in conjunction with the N^{14} nuclear magnetic moment because of the electric quadrupole coupling. The rotational moment of $N^{14}H_3$ can be deduced from its Zeeman spectra with the aid of the known N^{14} nuclear moment or more directly through the Paschen-Back effect. The results for both $N^{15}H_3$ and $N^{14}H_3$ Zeeman data were found to be mutually consistent within the limits of experimental error.

Since the selection rules for the inversion spectra are $\Delta J=0$ and $\Delta K=0$, there is every reason to believe that $g'=g$. Therefore, the σ-transition for an $N^{15}H_3$ line is expected to be a strong and sharp doublet even at a very strong field strength. This expectation proved to be true. Furthermore, the Zeeman splitting at a constant field for lines bearing different J and K values did not seem to change appreciably. This fact leads to the conclusion that the dependence of the g-factor on the rotational quantum numbers is at most rather slight, and the rotational moment of NH_3 is almost exactly proportional to the total rotational angular momentum.

Although the sign of the rotational moment cannot be established through the first-order Zeeman effect in the $N^{15}H_3$ spectra, the relative sign between the nuclear and rotational moments in the $N^{14}H_3$ spectra can be determined. It turned out that the rotational moment of $N^{14}H_3$ must have the same sign as the N^{14} nuclear moment, which is known to be positive. The g-factor for $N^{15}H_3$, calculated directly from the Zeeman data, is $+0.477\pm0.03$. The present experimental accuracy is not sufficient to differentiate between the g-factors for $N^{14}H_3$ and $N^{15}H_3$.

H_2O and HDO

These asymmetric top molecules have only three known rotational lines in the convenient range of the present apparatus, one for H_2O and two for HDO. Using the conventional designation (J_τ stands for a rotational state), the rotational frequencies are $\nu(H_2O\colon 5_{-1}-6_{-5})=22{,}235.2$ Mc/sec; $\nu(HDO\colon 5_0-5_1)=22{,}307.7$ Mc/sec; and $\nu(HDO\colon 4_{-3}-3_1)=20{,}460.4$ Mc/sec. The Zeeman splitting showed in each case a clear-cut doublet pattern at low field strengths. Figure 1 is a plot of the doublet frequency separation as a function of the magnetic field. It is seen that each of the three curves shows a linear

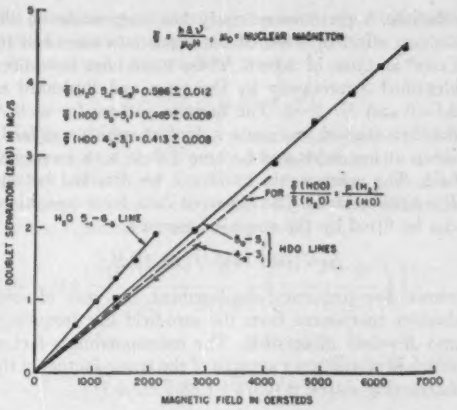

FIG. 1. Zeeman splitting of H_2O and HDO rotational lines.

relation between the doublet separation and the field, thus indicating a first-order perturbation effect. However, there is a large difference between one curve and the other two for the range of indicated field strengths. For the two curves ($H_2O\colon 5_{-1}-6_{-5}$ and $HDO\colon 4_{-3}-3_1$), the doublet components became rapidly weaker and broader with increasing field and could not be detected beyond the range indicated on the graph. For the curve with longer range ($HDO\colon 5_0-5_1$), the doublet components preserved their intensity and sharpness up to a much higher field. It should be noted that the "short-range" curves are associated with $\Delta J=\pm1$ and large change in τ, while the "long-range" curve is associated with $\Delta J=0$ and a small change in τ. This evidence points to the fact that there is a definite, though probably slight, dependence on J and τ for the g-factors.

It is also worth noting that the two curves for HDO give an average g-factor, which is smaller than that for H_2O by a factor approximately equal to the inverse ratio of the reduced masses (μ) of H_2 and HD. This indicates that the rotation of the hydrogen or deuterium atoms contributes significantly to the rotational moment.

The measured g-factor for each transition, as determined by the slope of each curve in Fig. 1, represents a value between g' and g of the interacting states. The average value (denoted by $\bar{g}$) for each transition is given in the same figure.

CH_3OH

This molecule is a slightly asymmetric top. The spectral lines observed in the microwave range are attributed by Dennison and Burkhard[8] to a hindered internal

[8] D. M. Dennison and D. G. Burkhard, Symposium on Molecular Structure and Spectroscopy, Ohio State University (June, 1948). A private communication from Professor D. M. Dennison, concerning a preliminary theory on the Zeeman effect in the CH_3OH microwave spectra, is gratefully acknowledged by the author.

rotation. A preliminary study has been made on the Zeeman effect of a few of the transitions identified by Coles[9] as those of $\Delta J=0$. These same lines have been identified theoretically by Dennison and Burkhard as $\Delta J=0$ and $K=2\rightarrow1$. The Zeeman pattern for each of the lines studied was again a doublet, which was fairly sharp at low fields and became diffuse with increasing field. The components could not be detected beyond $H=3000$ oersteds. The observed data for σ-transitions can be fitted by the empirical formula

$$\Delta\nu=\{60+1440/J(J+1)\}H,$$

where $\Delta\nu$=frequency displacement (in cps) of each doublet component from the zero-field line frequency, and H=field in oersteds. The corresponding g-factor, which is probably an average of the true g-factors of the interacting states, is $0.078+1.88/[J(J+1)]$.

SO_2

The microwave rotational spectra of this asymmetric top have been observed by other investigators.[10] Only a few out of many observed lines could be identified tentatively with quantum number specifications. The Zeeman spectra of these tentatively assigned lines were very complex. In general, each line began to show appreciable weakening at a low field (about 2000 oersteds) and split into weak components, starting from an intermediate field (about 4500 oersteds). The Zeeman components are usually too many and too weak to be measured. In one instance, however, a spectral line at about 25,392 Mc/sec (assigned as $7_{2,6}-8_{1,7}$) showed a measurable doublet-like splitting in the range from 5000 to 9000 oersteds. The doublet separation was found to be proportional to the field strength. At $H=6000$ oersteds, for example, the frequency separation between the apparent doublet components was about 0.76 Mc/sec. The approximate g-factor is 0.084 ± 0.010.

The data for $\bar{g}$ (average value of the g-factors of two rotational states described above) are summarized in Table I.

TABLE I. Summary of data.

Molecule	$\bar{g}$
H_2O	0.586 ± 0.012
NH_3	$+0.477\pm0.030$
HDO[a]	0.439 ± 0.009
N_2O	0.086 ± 0.004
SO_2	0.084 ± 0.010
OCS	0.029 ± 0.006

[a] Average of two transitions.

V. THEORY OF THE ROTATIONAL MAGNETIC MOMENT OF SYMMETRIC TOP MOLECULES

The quantum mechanical theory of the magnetic effect of a charged particle rigidly attached to a symmetric rotor was first derived by Condon.[1] The rigid rotor theory is certainly applicable to the effect of the nuclear charges and should be reasonably accurate for the electrons in the inner shells of atoms. Its validity, however, cannot be extended to those electrons which are loosely attached to the atoms. This fact has been clearly demonstrated by Wick's theory of the rotational moment of diatomic molecules.[3,11] For loosely attached electrons, a nonrigid rotor theory must be used to obtain agreement with experimental data. Since a polyatomic molecule has, in effect, both rigid and nonrigid constituents, a general theory will be worked out in this paper.

The molecule under consideration is assumed to be a symmetric top, having two equal moments of inertia, A, about axes perpendicular to the figure axis and a third moment of inertia, C, about the figure axis. This consideration will automatically include the whole class of linear polyatomic molecules as a special case. The molecule is assumed to rotate about its center of mass as a rigid body.

Let a charge, ϵ, be rigidly attached to the molecule and thus be representative of a nuclear charge (intrinsically positive) or the charge of a firmly bound electron (intrinsically negative). Its position is described by the distance, a, measured from the figure axis and another distance, b, from the center of mass along the figure axis. In the case of a firmly bound electron, these coordinates are considered as being averaged over a static distribution function. Let there be also an electron, having charge, $-e$, and mass, m. This electron is taken to be representative of those loosely attached to the molecule. The effects of nuclear and electron spins are neglected.

Let the Cartesian coordinate system x, y, z be fixed in space and another system x', y', z' be fixed in the molecule, where z' is chosen to be coincident with the figure axis. Both systems have a common origin at the center of mass and their relative orientation is specified by the Eulerian angles (θ, ϕ, ψ) in the usual manner. The constant magnetic field H is assumed to be along the z-axis of the space-fixed system.

The Lagrangian function for the rigid body with a bound charge and a "free" electron in a magnetic field is

$$L=T_1+T_2-V+(\epsilon/c)\mathbf{v}_\epsilon\cdot\mathbf{A}_\epsilon-(e/c)\mathbf{v}_e\cdot\mathbf{A}_e, \qquad (3)$$

where T_1 and T_2 are, respectively, the kinetic energies of the rigid rotor and the electron, V the total potential energy, $\mathbf{v}$ the velocity of a charged particle, and $\mathbf{A}$ the vector potential. The vector potential $\mathbf{A}$ has the components $A_x=-yH/2$, $A_y=xH/2$, and $A_z=0$ in the space-fixed system.

The Lagrangian function in Eq. (3) can be expressed in the coordinates of (θ, ϕ, ψ) and (x', y', z') and their time derivatives $(\dot{\theta}, \dot{\phi}, \dot{\psi})$ and $(\dot{x}', \dot{y}', \dot{z}')$ by an orthogonal transformation. Here, the primed quantities are

[9] D. K. Coles, Phys. Rev. **74**, 1194 (1948).
[10] B. P. Dailey, S. Golden, and E. B. Wilson, Jr., Phys. Rev. **74**, 1537 (1948).
[11] G. C. Wick, Phys. Rev. **73**, 51 (1948).

the coordinates of the electron alone. The nonrigid nature of the electronic motion is provided by the presence of x', y', and z'. Let q_k stand for one of the coordinates θ, ϕ, ψ, x', y', z', and p_k for the generalized momentum conjugate to that coordinate. Thus, there are six such generalized momenta determined by the relation $p_k=\partial L/\partial\dot{q}_k$. The Hamiltonian of the whole system is then $\mathcal{H}=\sum_k p_k\dot{q}_k-L$. The complete result of these transformations is

$$\mathcal{H}=\frac{\mathcal{P}_\theta(\sin\theta\mathcal{P}_\theta)}{2A\sin\theta}+\frac{\mathcal{P}_\phi^2}{2C}+\frac{(\mathcal{P}_\phi\cos\theta-\mathcal{P}_\psi)^2}{2A\sin^2\theta}+\frac{1}{2m}\{p_{x'}^2+p_{y'}^2+p_{z'}^2\}+\frac{eH}{2mc}p_\psi+\frac{1}{2m}\left(\frac{eH}{2c}\right)^2\rho^2+V, \quad (4)$$

where

$\mathcal{P}_\theta=P_\theta-p_\theta-(eH/2c)[-a\cos\phi(b\cos\theta+a\sin\theta\sin\phi)]$,
$\mathcal{P}_\phi=P_\phi-p_\phi-(eH/2c)[a(a\cos\theta-b\sin\phi\sin\theta)]$,
$\mathcal{P}_\psi=P_\psi-p_\psi-(eH/2c)[a^2\cos^2\phi+(b\sin\theta-a\cos\theta\sin\phi)^2]$,
P_θ, P_ϕ, P_ψ and $p_{x'}$, $p_{y'}$, $p_{z'}$ are the generalized momenta,
$p_\theta=\cos\phi(y'p_{z'}-z'p_{y'})-\sin\phi(z'p_{x'}-x'p_{z'})$,
$p_\phi=x'p_{y'}-y'p_{x'}$,
$p_\psi=\cos\theta(x'p_{y'}-y'p_{x'})+\sin\theta\sin\phi(y'p_{x'}-z'p_{y'})+\sin\theta\cos\phi(z'p_{x'}-x'p_{z'})$,
$\rho^2=(x')^2+(y')^2+(z')^2-(x'\sin\theta\sin\phi+y'\sin\theta\cos\phi+z'\cos\theta)^2$.

Equation (4) can be expanded, noting the noncommutability of each pair of canonically conjugate variables. For simplicity, only the unperturbed Hamiltonian and those terms which will eventually contribute to the first- and second-order perturbation energies, both linear in H, will be retained. The result can be written as

$$\mathcal{H}=\mathcal{H}_0+\mathcal{H}'+\mathcal{H}''+\cdots, \quad (5)$$

where

$$\mathcal{H}_0=\frac{P_\theta(\sin\theta P_\theta)}{2A\sin\theta}+\frac{P_\phi^2}{2C}+\frac{(P_\phi\cos\theta-P_\psi)^2}{2A\sin^2\theta}+\frac{1}{2m}(p_{x'}^2+p_{y'}^2+p_{z'}^2)+V,$$

$$\mathcal{H}'=-\frac{1}{C}P_\phi p_\phi-\frac{(P_\phi\cos\theta-P_\psi)(p_\phi\cos\theta-p_\psi)}{A\sin^2\theta},$$

$$\mathcal{H}''=-\frac{eH}{2c}\left[\frac{b^2+\frac{1}{2}a^2}{A}P_\psi+\cos\theta\left(\frac{a^2}{C}-\frac{b^2+\frac{1}{2}a^2}{A}\right)P_\phi\right]+\frac{eH}{2mc}p_\psi.$$

The transcription of Eq. (5) into the quantum-mechanical expression is conveniently done by noting $P_{Q_k}=-ih\partial/\partial Q_k$, where $Q_k=\theta$, ϕ, or ψ, and $h=h/2\pi$, and $p_{q_k}=-ih\partial/\partial q_k$, where $q_k=x'$, y', or z'. (6)

The quantities p_θ, p_ϕ, and p_ψ, known as the "internal" angular momenta, will remain unchanged.

The solution of $\mathcal{H}\Psi=W\Psi$, where

$$\Psi=\Psi(\theta,\phi,\psi,x',y',z'),$$

is readily obtained by the perturbation method. The solution for $\mathcal{H}_0\Psi_0=W_0\Psi_0$ may be assumed to be $\Psi_0=\Theta(\theta)e^{iK\phi}e^{iM\psi}f(x',y',z')$. The first-order perturbation energy W_1 in $W=W_0+W_1+W_2+\cdots$ is (retaining only the significant terms linear in H)

$$W_1=-Mh\frac{eH}{2c}\left[\frac{b^2+\frac{1}{2}a^2}{A}+\frac{K^2}{J(J+1)}\left(\frac{a^2}{C}-\frac{b^2+\frac{1}{2}a^2}{A}\right)\right]+\frac{MK}{J(J+1)}\frac{eH}{2mc}(0|p_\phi|0), \quad (7)$$

where

J = total angular momentum quantum number of the molecule,
K = rotational quantum number along figure axis,
M = magnetic quantum number.

The bracketed quantity on the right-hand side of Eq. (7) represents the contribution of the bound charge e to the magnetic perturbation energy. This is the result obtained by Condon for a charge rigidly attached to a symmetric rotor.[1] The second term would be the contribution due to the orbital motion of the electron, if the matrix element $(0|p_\phi|0)$ were not zero. However, for a molecule containing many electrons, it is this quantity summed over all the electrons that is of importance. This sum total is known to be zero[12] if the polyatomic molecule is in the $^1\Sigma$-state, which is the case most frequently encountered. Consequently, the second term in Eq. (7) will be dropped for the present discussion of molecules in the $^1\Sigma$-state.

The second-order perturbation gives an energy change which is, on neglecting terms in H^2,

$$W_2=Mh\frac{eH}{mc}\sum_{n\neq0}\frac{1}{(E_n-E_0)}\left[\frac{\alpha_{n0}^2}{A}+\frac{K^2}{J(J+1)}\left\{\frac{\gamma_{n0}^2}{C}-\frac{\alpha_{n0}^2}{A}\right\}\right], \quad (8)$$

where

$\alpha_{n0}^2=\frac{1}{2}\{|(n|L_{x'}|0)|^2+|(n|L_{y'}|0)|^2\}$,
$\gamma_{n0}^2=|(n|L_{z'}|0)|^2$,
$L_{x'}=y'p_{z'}-z'p_{y'}$,
$L_{y'}=z'p_{x'}-x'p_{z'}$,
$L_{z'}=x'p_{y'}-y'p_{x'}=p_\phi$,
E_0 = energy of the electronic ground state, and
E_n = energy of the nth excited state.

[12] J. H. Van Vleck, *The Theory of Electric and Magnetic Susceptibilities* (Oxford University Press, 1932), p. 274.

Equation (8) represents the contribution from a nonrigid electron in a symmetric top molecule to the magnetic perturbation energy. When applied to the special case of a linear or diatomic molecule, Eq. (8) is reduced to a form in exact agreement with that derived by Wick.[3,11]

For a molecule, it is necessary to sum W_1 in Eq. (7) over all bound charges (nuclear charges and bound electrons) and W_2 in Eq. (8) for all "free" electrons. Let

$$W_H=\sum_i^N (W_1)_i+\sum_j^n (W_2)_j.$$

W_H represents the total contribution of all charged particles in the molecule to the part of the magnetic perturbation energy that is proportional to the magnetic field. Such a procedure is valid only under the assumption that each particle behaves as if it is in a field specified by its space coordinates alone. Then it is possible to express the result in terms of the magnetic moment of the molecule through the equation $W_H=-\mu_H H$, where μ_H is the component of the magnetic moment μ along the magnetic field. Or the result can be even more conveniently expressed in terms of the g-factor in the equation $W_H=-Mg\mu_0 H$, where M is, again, the magnetic quantum number, μ_0 is equal to $eh/2M_pc$ (the nuclear magneton in terms of the proton mass M_p). The final expression for the g-factor is

$$g=\sum_i \frac{\epsilon_i}{e}\left[\frac{b_i^2+\frac{1}{2}a_i^2}{\mathfrak{a}}+\frac{K^2}{J(J+1)}\left(\frac{a_i^2}{\mathfrak{C}}-\frac{b_i^2+\frac{1}{2}a_i^2}{\mathfrak{a}}\right)\right]$$
$$-\frac{2}{m}\sum_i\sum_{n\neq 0}\frac{1}{(E_n-E_0)_j}\left[\frac{\alpha_{n0}^2}{\mathfrak{a}}+\frac{K^2}{J(J+1)}\left(\frac{\gamma_{n0}^2}{\mathfrak{C}}-\frac{\alpha_{n0}^2}{\mathfrak{a}}\right)\right]_j, \quad (9)$$

where $\mathfrak{a}=A/M_p$ and $\mathfrak{C}=C/M_p$.

VI. DISCUSSION OF RESULTS

Although it is seen from the preceding section that it is theoretically possible to calculate the rotational magnetic moment of any linear or symmetric molecule, yet, in practice, only the contribution from the nuclear charges can be handled without difficulty. It is true that a reasonably good approximation should be possible for the effect of inner shell electrons which are tightly bound to an atom in the molecule; but the problem concerning the loosely bound electrons cannot be solved quantitatively unless one has extensive knowledge concerning the electronic wave functions. As such knowledge is still lacking for the molecules under consideration, only a qualitative discussion of the experimental results will be made.

There is, in general, no apparent contradiction between the theory and experiment as regards the order of magnitude of the molecular rotational magnetic moment and its dependence upon the parameters such as the moments of inertia, charge distribution, internal angular velocity, and rotational quantum numbers. According to the theory, the nuclear charges always contribute to a positive g-factor, whose value ranges from about unity for molecules made up of light atoms to approximately one-half for molecules made up of medium heavy atoms. This is primarily due to the smaller charge-to-mass ratio of the heavier nuclei for comparable internuclear distances. This trend of generally descending g-factor for heavier molecules is quite apparent from the experimental data. The theory further asserts that the electronic contribution to the g-factor is a variable quantity depending principally upon the interaction between the electron and the electric field due to the rest of the molecule. If the electron is very tightly bound to the molecule, then its effect could amost completely compensate that of an equal and opposite charge in the neighboring nucleus. If the charge distribution is farther away from the center of mass than the corresponding nuclear charge, the net g-factor could be negative. Experimentally, the linear molecules N_2O and OCS have g-factors which are respectively about seven and seventeen times smaller than the nuclear contributions. The effect of bound charges is evidently very large in both cases. In fact, there is some grounds for believing that the g-factor of OCS may be negative from some recent data on the OCS[33] Zeeman spectra.

If, however, an electron is loosely bound in the molecule, the theory predicts, as first pointed out by Wick, a considerably smaller effect for its magnetic contribution relative to the effect of the nuclear charges. The electron is, to use a physical picture, "slipping" behind the rigid rotation of the nuclei. The slip could be one hundred percent if the nondiagonal matrix elements of $L_{x'}$, $L_{y'}$, and $L_{z'}$ were all zero for a symmetric top molecule. Under this condition, the nuclear charges would produce their full effects in the rotational moment. While in practice such complete slip has never been known to exist in a molecule, the case of the H_2 molecule comes remarkably close to the condition. In the present experiment, the g-factors of H_2O, HDO, and NH_3 have been found to be large. To interpret this result as due to a rigid rotation of electrons would necessitate some distribution of electronic charges abnormally close to the center of mass. It seems much more plausible to picture the electrons associated with the hydrogen atoms in these molecules as being similar to those in the hydrogen molecule. Wick's interpretation of nonrigid rotation of electrons is thus supported by the present evidence.

The theory is also explicit concerning the dependence of the rotational g-factor on the rotational quantum numbers for a symmetric top molecule. The available experimental evidence cannot be said to have established this dependence unambiguously. The only symmetric top molecule dealt with here is the NH_3 molecule. It has

just been shown that the nuclear charge rotation is the principal contributor to the magnetic moment because of the electronic slippage. Calculation shows that the coefficient of the $K^2/J(J+1)$ term in the first summation in Eq. (9) is indeed very small, thus making the g-factor essentially independent of the quantum numbers. However, this situation should be regarded as somewhat accidental. In a more general case, a dependence of the g-factor on rotational quantum numbers is to be expected. The case of the water molecule, discussed in Sec. IV, indirectly supports this viewpoint.

The author is greatly indebted to Professor J. H. Van Vleck for advice concerning the theoretical aspects of this paper.

PHYSICAL REVIEW VOLUME 81, NUMBER 2 JANUARY 15, 1951

Radioactivities of Ru^{105}, Rh^{105}, Br^{84}, and Br^{83}

R. B. Duffield* and L. M. Langer†
University of California,‡ Los Alamos Scientific Laboratory, Los Alamos, New Mexico
(Received September 18, 1950)

A lens spectrometer was used to study the disintegrations of Ru^{105} (4.5 hr), Rh^{105} (36.2 hr), Br^{84} (32 min), and Br^{83} (2.4 hr). Ru^{105} emits a simple beta-spectrum with an end-point energy of 1.150±0.006 Mev. This is followed by a 0.726-Mev gamma-ray to a metastable level in Rh^{105}. The decay to the ground state of Rh^{105} proceeds with a gamma-ray of about 0.1 Mev, with a half-life of 45 seconds. The ground state of Rh^{105} emits a simple beta-spectrum of 0.570±0.005 Mev. No gamma-ray appears to be associated with this decay. Br^{84} emits a complex beta-spectrum which can be resolved into at least four groups with end points and relative intensities of 4.679 Mev (40 percent), 3.56 Mev (9 percent), 2.53 Mev (16 percent), and 1.72 Mev (35 percent). The 4.679-Mev group, which goes directly to the ground state of Kr^{84}, does not have a forbidden spectrum shape. It is suggested that the 32-minute half-life may be associated with an isomeric level above the ground state of Br^{84}. The decay of Br^{83} consists of a single beta-ray group with a maximum energy of 0.940±0.010 Mev.

I. INTRODUCTION

THE availability of a large magnetic lens spectrometer, located close to a nuclear reactor, suggested the possibility of a more detailed investigation of the disintegration of Ru^{105} (4.5 hr), Rh^{105} (36.2 hr), Br^{84} (32 min), and Br^{83} (2.4 hr). The spectrometer measurements have been supplemented by coincidence and absorption studies.

Ru^{105} decays by negatron emission to Rh^{105}, which in turn goes to Pd^{105}. Earlier investigations,[1–3] using absorption techniques, report values for the beta-ray end point of 1.3, 1.4, and 1.5 Mev, and values for the energy of a gamma-ray of 0.7 and 0.76 Mev. The Rh^{105} activity was reported[1,2,4,5] again by absorption methods, to have a beta-ray of end-point energy between 0.5 and 0.78 Mev. A weak gamma-ray of 0.3 Mev has also been reported.[1,5]

In addition to yielding more precise values of the beta- and gamma-ray energies, the present investigation has revealed the existence of a 45-second metastable level located about 0.1 Mev above the ground state of Rh^{105}. The 0.3-Mev gamma-ray previously associated with the Rh^{105} activity was not observed. An energy level scheme for the Ru^{105}—Rh^{105}—Pd^{105} transitions is suggested, which is not inconsistent with the predictions of the nuclear shell model.[6,7]

The investigation of the Br^{84} activity was instituted mainly because earlier considerations, based on the available data and on the predictions of the nuclear shell model,[6,8] suggested that the high energy beta-transition should, if it were between the ground states of Br^{84} and Kr^{84}, exhibit a spectrum shape characteristic of a forbidden transition. Earlier absorption work[9,10] reports values of 5.3 and 4.5 Mev for the maximum energy of the beta-rays. The results of the present investigation show that the Br^{84} beta-decay is complex, consisting of at least four groups. Moreover, the highest energy group, with end-point energy of 4.679±0.010 Mev is found to have an allowed shape. Since coincidence experiments indicate that this transition is directly to the ground state of Kr^{84}, the absence of a forbidden shape is inconsistent with what appear to be very reasonable predictions of the nuclear shell model.

* University of Illinois, Urbana, Illinois.
† Indiana University, Bloomington, Indiana.
‡ This work was performed under the auspices of the AEC.
[1] Sullivan, Sleight, and Gladrow, Plutonium Project Report CC-1493 (1944), unpublished.
[2] H. J. Born and W. Seelmann-Eggebert, Naturwiss. 31, 420 (1943).
[3] E. Bohr and N. Hole, Arkiv Mat. Astron. Fysik 32A, No. 15 (1948).
[4] Nishina, Yasaki, Kimura, and Ikawa, Phys. Rev. 59, 323 (1941).
[5] C. E. Mandeville and E. Shapiro, Phys. Rev. 80, 125 (1950).
[6] M. G. Mayer, Phys. Rev. 78, 16 (1950).
[7] L. W. Nordheim, Phys. Rev. 78, 294 (1950).
[8] E. Feenberg and K. C. Hammock, Phys. Rev. 75, 1877 (1949).
[9] S. Katcoff, Plutonium Project Report CC-2310, 52 (1945), unpublished.
[10] H. J. Born and W. Seelmann-Eggebert, Naturwiss. 31, 201 (1943).

It is suggested that the 32-min half-life may be characteristic of a metastable level feeding the ground state of Br^{84}. Under such conditions, the beta-transition to the ground state of Kr^{84} would be allowed and the half-life would be expected to be less than 5 sec. Such an allowed transition is provided by one interpretation of the shell model.[6,7] An attempt to isolate the lower isomeric state by means of a Szilard-Chalmers separation was unsuccessful.

The measurement of the Br^{83} spectrum was obtained as a by-product of the Br^{84} investigation. End-point values of 1.05 and 0.9 Mev had been obtained earlier by absorption.[11,12] No gamma-radiation was found.[13,14] From the present study, it appears that the beta-spectrum is simple, with an end point of 0.940 ± 0.010 Mev.

II. EXPERIMENTAL PROCEDURE

The energy measurements were made in the large magnetic lens spectrometer described in another paper.[15] A G-M tube with a 3.6-mg/cm² mica end window and a 0.5-inch diameter aperture was employed as a detector. With sources of 0.5-inch diameter, the instrument was operated at resolutions of both 3 and 6 percent. The decay periods of all spectra and lines were checked in the spectrometer.

The beta-gamma- and gamma-gamma-coincidence measurements were made with an arrangement employing two anthracene scintillation counters and an amplifier with a resolving time of 0.2μsec.

The Ru^{105} was made by a (n,γ) reaction on Ru^{104}. Normal ruthenium, previously purified by distillation from perchloric acid was activated by neutron irradiation in the thermal column of a nuclear reactor. Short irradiation times produced a negligible intensity of the 41-day Ru^{103}. The source used for the measurement of the beta-spectrum consisted of powdered ruthenium metal, uniformly deposited on a thin aluminum backing. The thickness of the ruthenium was 12 mg/cm² and of the backing, 1.4 mg/cm². The half-life of 4.5 hours was checked at various points of the spectrum, and also in the coincidence experiments.

The Rh^{105} was prepared by beta-decay of Ru^{105} Purified ruthenium trichloride was irradiated with slow neutrons. The 4.5-hr Ru^{105} was allowed to decay and the ruthenium then was distilled away from the Rh^{105} out of perchloric acid solution. The source used for the measurement of the beta-spectrum consisted of rhodium sulfide with a thickness of 0.7 mg/cm² mounted on aluminum foil of thickness 1.4 mg/cm². The thickness of the deposit was quite uniform. The source decayed with a half-life of 36.2 hours measured over six half-lives.

A 45-second isomeric state of Rh^{105}, found by the decay of the 4.5-hr Ru^{105}, was found by performing a rapid chemical separation of rhodium from ruthenium. Ruthenium trichloride, previously neutron-irradiated to produce Ru^{105}, was oxidized by perchloric acid to volatile RuO_4. The latter was then distilled from the solution and collected on a platinum plate cooled with dry ice. This was allowed to stand for a few minutes; and then the RuO_4 was vaporized by rapid heating, leaving the rhodium decay product on the platinum plate, on which it was counted directly.

Br^{83} and Br^{84} were separated from other uranium fission products. Uranyl nitrate, enriched in U^{235}, was irradiated in the thermal column of a nuclear reactor, then dissolved in nitric acid with the addition of bromine and iodine carriers. The bromine and iodine fission products were then distilled into 0.1*N* nitric acid containing sodium nitrite to reduce the bromine to bromide. The iodine was extracted into carbon tetrachloride and discarded. The bromide was then precipitated as silver bromide. Two sources were prepared for the determination of the Br^{84} beta-spectrum; the first had a thickness of 4 mg/cm² and the second a thickness of 2.5 mg/cm². Each was deposited on 7 mg/cm² of filter paper and mounted on 1 mg/cm² of aluminum. Only the second source was used in determining the Br^{83} spectrum after all Br^{84} had disappeared. The Br^{84} spectrum was found to decay with a half-life of 32 minutes over seven half-lives. The Br^{83} spectrum decayed with a half-life of 2.4 hours.

III. RESULTS

Ru^{105}

Figure 1 is a Fermi plot of the data obtained on the beta-spectrum of Ru^{105}. The resolution of the spectrometer was 6 percent. There is evidently only one group of electrons, and the spectrum is of the allowed form. The end point is 1.150 ± 0.006 Mev. There was no

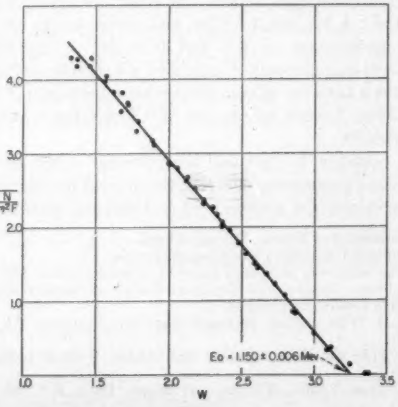

FIG. 1. Fermi plot of the Ru^{105} beta-spectrum.

[11] A. Langsdorf, Jr., and E. Segrè, Phys. Rev. **57**, 105 (1940).
[12] L. E. Glendenin, NNES-PPR, Vol. 9B, No. 7.3.1 (1940), unpublished.
[13] A. H. Snell, Phys. Rev. **52**, 1007 (1937).
[14] L. E. Glendenin, Plutonium Project Report CC-920, 35 (1943), unpublished.
[15] L. M. Langer, Phys. Rev. **77**, 50 (1950).

evidence of any conversion electron lines at energies above 0.250 Mev.

A search was made for gamma-radiation, using both a 0.0006-in. uranium radiator and a 0.002-in. silver radiator and a strong source of Ru^{105} in the spectrometer. Compton and photo-electrons were found corresponding to a gamma-ray of 0.726±0.007 Mev. No other gamma-rays of energy greater than 0.125 Mev could be found.

Beta-gamma-, but no gamma-gamma-coincidences were found. Figure 2 shows an absorption curve on these coincidences. The beta-gamma coincidence rate per beta-particle is independent of absorber thickness, indicating that the 0.726-Mev gamma-ray is in cascade with the beta-ray.

From the absence of any measurable internal conversion, it is inferred that the 0.726-Mev gamma-radiation is of low polarity.

Rh^{105}

Figure 3 is a Fermi plot of the beta-spectrum of the 36.2-hr Rh^{105} taken with a resolution of 6 percent. The spectrum has an allowed shape and the decay evidently consists of only one group. The end point is 0.570±0.005 Mev. A careful search was made for internal conversion electrons in the neighborhood of 0.3 Mev. None were found.

A search was also made for gamma-radiation using a strong source and an anthracene scintillation counter detector. No measurable effect above background could be found.

45-Sec Rh^{105} Isomer

Considerations of the nuclear shell model for the Rh^{105} nucleus suggested the possibility that a short-lived isomer might exist but might have previously escaped detection. Rh^{103}, a similar nucleus, is known to have a 57-min metastable state. A rapid chemical separation of rhodium from Ru^{105} was made by the procedure described above. Figure 4 shows that the rhodium, so isolated, decays with a 45-sec half-life. A crude absorption curve on this activity yielded a range of 15 mg/cm² of Al, corresponding to an energy of approximately 0.1 Mev for the internal conversion electrons from the isomeric transition.§

Br^{84}

Figure 5 shows the momentum distribution of the beta-particles emitted by Br^{84}. The spectrum, taken with a resolution of 3 percent, is obviously complex. The broken curves show the results of an analysis into four groups on the basis of the Fermi plot illustrated in Fig. 6. The end points and relative contributions are: 4.679±0.010 Mev, 40 percent; 3.56 Mev, 9 percent; 2.53 Mev, 16 percent; 1.72 Mev, 35 percent. Because of the errors involved in performing the multiple subtractions in this analysis, it is difficult to estimate the accuracy of the end points and of the percentages to be attributed to the inner groups. On the assumption that the 32-min half-life is that of the ground state of Br^{84}, the log(ft) values to be associated with each group are respectively: 7.75, 7.9, 6.95, 5.9.

It is significant that the highest energy group (4.679 Mev) yields a straight-line Fermi plot corresponding to an allowed spectrum shape. Under essentially identical conditions, the spectrum of Rb^{83}, which has an atomic number and maximum energy not very different from those of Br^{84}, was found to have a shape characteristic of a once-forbidden transition involving a change of two units of angular momentum and a parity change.[16]

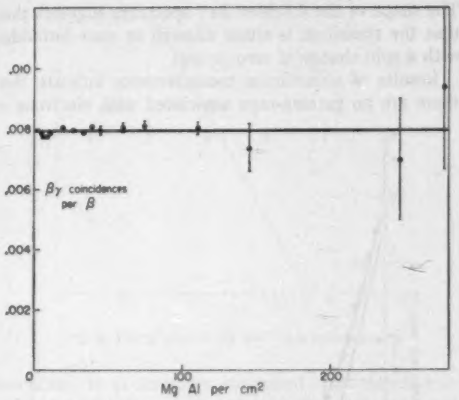

FIG. 2. Beta-gamma coincidence absorption of the Ru^{105} activity.

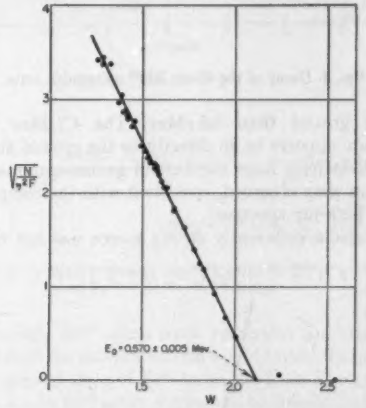

FIG. 3. Fermi plot of the Rh^{105} beta-spectrum.

§ *Note added in proof:* Recently, P. Axel and R. B. Duffield have observed the K and L internal conversion lines in a magnetic spectrometer. From these measurements, the energy of the gamma-transition is 0.130±0.002 Mev. The ratio of K to L conversion is 1.4.

[16] Bunker, Langer and Moffat, Phys. Rev. **81**, 30 (1951).

The shape of the 4.7-Mev Br^{84} spectrum suggests then that the transition is either allowed or once-forbidden with a spin change of zero or one.

Results of coincidence measurements indicate that there are no gamma-rays associated with electrons of energy greater than 3.5 Mev. The 4.7-Mev group therefore appears to go directly to the ground state of Kr^{84}. Relatively large numbers of gamma-gamma-coincidences were observed, consistent with the complexity of the beta-ray spectrum.

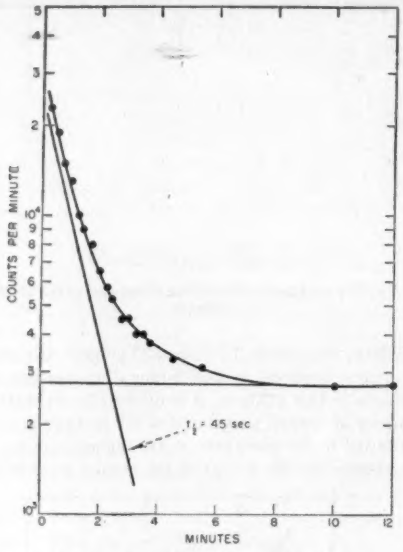

FIG. 4. Decay of the 45-sec Rh^{105} metastable state.

Because a sufficiently strong source was not readily available, no attempt was made to determine the energy of the gamma-rays in the spectrometer.

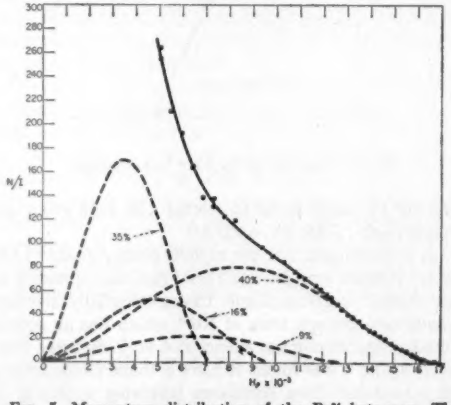

FIG. 5. Momentum distribution of the Br^{84} beta-rays. The broken line curves show the resolution into groups according to the Fermi plot analysis.

An unsuccessful attempt was made to separate the possible isomeric states of Br^{84} by chemical means. The Br^{84}, in the form of BrO_3^- in aqueous solution, was allowed to stand for a few minutes in contact with inactive Br_2. The Br_2 was then extracted into carbon tetrachloride, transferred to a counting cell placed around a Geiger tube, and the activity determined by automatic recording of the output of a scale of 256 unit. Any decay with a half-life between 30 sec and 10 min would have been observed. None was seen. It is concluded that the isomer, if it exists, has a half-life of less than 30 sec, or that the gamma-ray associated with the isomeric transition is not sufficiently converted to give a measurable chemical separation of the isomers.

Br^{83}

Figure 7 shows the momentum distribution of the electrons from Br^{83} taken with a resolution of 3 percent. These data were obtained with the same source as was used for the Br^{84} spectrum determination but after all the Br^{84} had decayed to a completely negligible intensity. Figure 8 is a Fermi plot of the beta-spectrum of Br^{83}. There appears to be only one group with an end point at 0.905 ± 0.010 Mev.

IV. DISCUSSION AND CONCLUSIONS

Figure 9 shows a decay scheme for the $Ru^{105}-Rh^{105}-Pd^{105}$ transitions which accounts for the observed data and which is essentially consistent with present ideas on nuclear shell structure.[6–8] The isomerism of Rh^{105} is understandable, since the $p_{1/2}$ and $g_{9/2}$ states appear to have closely the same energy.[6] The assignment of $g_{7/2}$ or $d_{5/2}$ to the high excited state in Rh^{105} is a guess based upon the assumption that all other states are already filled in the lower shell.

With the assignment of states as indicated in Fig. 9, the observed beta- and gamma-transitions would outcompete all other possibilities, as is required. The only weak point in the scheme appears to be the apparently

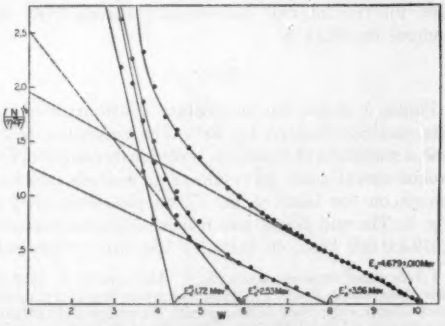

FIG. 6. Fermi plot of the Br^{84} beta-spectrum.

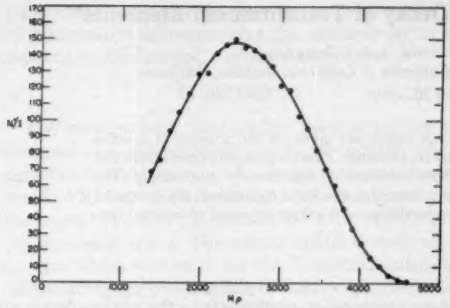

FIG. 7. Momentum distribution of the Br^{83} beta-rays.

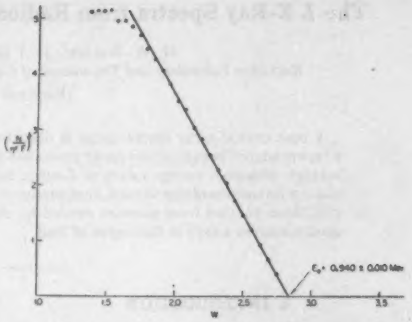

FIG. 8. Fermi plot of the Br^{83} beta-spectrum.

low comparative half-life ($\log ft = 5.5$) to be associated with the once-forbidden $p_{1/2}-s_{1/2}$ transition from Rh^{105} to Pd^{105}. An alternative assignment, which would obviate this difficulty, would be to invert the $g_{9/2}$ and $p_{1/2}$ levels in Rh^{105} and assign $g_{7/2}$ to the ground state of Pd^{105}. This, however, would require a $d_{3/2}$ level for the high excited state of Rh^{105}. Although the $d_{3/2}$ level is rather high up in the next shell, such an assignment for a high excited state is perhaps not unreasonable, so that this scheme may be preferable to that shown in Fig. 9. A measurement of the spin of Pd^{105} would be very informative.

The Br^{84} nucleus contains both an odd proton and an odd neutron. According to the concepts of the nuclear shell model, one might expect the thirty-fifth proton to be $p_{3/2}$ or possibly $f_{5/2}$. The forty-ninth neutron occurs in a region where $p_{1/2}$ and $g_{9/2}$ have about the same energy. If one attempts to form the resultant state for Br^{84} according to the empirical rules of Nordheim,[7] one gets the following possible combinations for the spin and parity:

$f_{5/2}+g_{9/2}$	2, odd
$f_{5/2}+p_{1/2}$	2, even
$p_{3/2}+g_{9/2}$	high, odd
$p_{3/2}+p_{1/2}$	1, even.

The ground state of Kr^{84}, which is an even-even nucleus, is presumably zero, even. One might expect, then, that for any of the first three combinations, the beta-transition from the ground state of Br^{84} to that of Kr^{84} should result in a spectrum with a shape measurably different from that found for allowed transitions.[17] Only the $p_{3/2}-p_{1/2}$ combination would provide for the observed allowed spectrum shape of the 4.679-Mev transition which, according to the coincidence measurements, does go to the ground state of Kr^{84}. However, the high comparative half-life (based upon a 32-min decay) would be inconsistent with the allowed character of such a transition. It is therefore suggested that the 32-min half-life might be associated with an isomeric level somewhat above the $p_{3/2}-p_{1/2}$ ground state of Br^{84}. Excitation of the odd proton to form the $p_{3/2}-g_{9/2}$ combination would provide the conditions necessary for isomerism. The known isomerism in the neighbor odd-

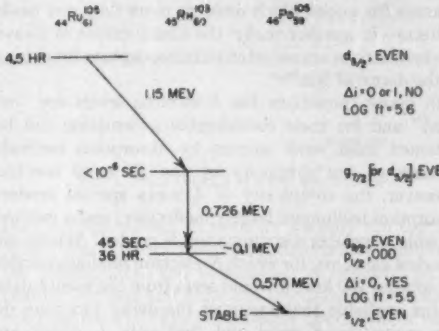

FIG. 9. Energy level diagram for the $Ru^{105}-Rh^{105}-Pd^{105}$ decay.

odd nucleus Br^{80} offers some precedent for this idea. Under such circumstances, one would expect the half-life of the ground state of Br^{84} to be less than 5 seconds.

The 2.4-hr Br^{83} decay appears to be simply that of an allowed transition from the $p_{3/2}$ ground state of Br^{83} to the $p_{1/2}$ ground state of Kr^{83}. On the basis of the 0.94-Mev end point and the 2.4-hr half-life, the $\log(ft)$ for this transition is 5.0.

The authors would like to acknowledge the cooperation of many members of the Los Alamos Scientific Laboratory. In particular, they want to thank Mr. A. Freedman and Mr. R. D. Moffat for help in making some of the measurements.

[17] L. M. Langer and H. C. Price, Jr., Phys. Rev. 76, 644 (1949).

The *L* X-Ray Spectra from Radioactive Decay of Transuranium Elements*

G. W. Barton, Jr.,† H. P. Robinson, and I. Perlman
Radiation Laboratory and Department of Chemistry, University of California, Berkeley, California
(Received September 20, 1950)

A bent crystal x-ray spectrometer is described, and some results are given on the analysis of *L*-series x-rays produced in radioactive decay processes of transuranium elements. There is generally good agreement between measured energy values of *L*-series lines and those predicted by the Moseley relationship. The relative intensities of the various lines produced in this case from γ-ray internal conversion, are compared with those emitted from uranium excited by electron bombardment and values reported of internal conversion excited x-rays in the region of lead.

I. INTRODUCTION

THE x-rays accompanying radioactive decay processes are capable of yielding a considerable amount of information on the nature of these processes. For some purposes simple detection may be adequate, but much potential information can come to light only if the x-ray spectra are resolved. As an example, spectrometry of x-rays enables one to distinguish between electron capture and isomeric transition processes and, in particular, to aid in the resolution of decay schemes for nuclei which undergo more than one mode of decay. In another study[1] the identification of x-rays has revealed an unsuspected electron-capture branching in the decay of Am^{242m}.

In many transitions the *K*-electron levels are "excited" and for these considerable information can be obtained from weak sources by absorption methods because of the simplicity of the *K* x-ray spectra. However, the complexity of *L* x-ray spectra renders absorption techniques largely ineffective; and a method capable of greater discrimination is needed. Among the heaviest elements, for which *K*-electron binding energies are around 100 kev, it would seem from the scanty data so far available that many of the decay processes do not excite the *K* level and that only *L* x-rays are observable.

It is with the measurement of the *L* x-ray spectra from the decay of heavy nuclei that the present communication is concerned. The method used is capable of a moderately high degree of precision and consists of diffraction separation using an oriented thin bent crystal. Since the x-rays examined were those of transuranium elements, the x-ray energies obtained are of interest in themselves, since it may be seen whether or not they agree with extrapolations from lower elements.

The x-rays with which the present report is concerned have their origin in the internal conversion of gamma-rays. In addition to the goals of x-ray spectrometry already mentioned, the measurement of relative intensities of various transitions as they are related to the relative conversion coefficients in the various levels are of obvious importance in understanding the process of γ-ray internal conversion. Kinsey[2] has reviewed the problem in the heavy element region, and in a second paper[3] gives data on ThC and RaD taken by absorption and coincidence counting methods. The data to be reported here are in some details at variance with the generalizations made from the observations on ThC and RaD.

The possibility of making a focusing x-ray spectrometer was examined originally by de Broglie[4] and by Darbord.[5] Later a more complete study of the practical aspects of the problem was made by DuMond and Kirkpatrick.[6] Shortly after this the first generally satisfactory instrument was devised by Cauchois,[7] and her approach is that which has been adopted by a number of others. The essential feature of a Cauchois instrument is the use of an elastically bent crystal to permit focusing of radiation with high resolution and without structural complications.

Abelson[8] was the first to use a bent crystal spectrograph to observe x-rays from a radioactive decay process, and among other measurements he identified molybdenum x-rays from the electron-capture decay of element 43 (technetium). Pool and co-workers[9] have made extensive use of this technique in their identification of radioactive species, as has the group at Zurich.[10] A large radius spectrometer has been built and used by DuMond[11] for precision measurement of photon energies from the conventional x-ray region into the range of a Mev.

The present report describes a bent crystal spectrometer and its use in determining the *L* x-ray spectra of two of the transuranium elements, neptunium, and

* This work was performed under the auspices of the AEC.
† Now at the Argonne National Laboratory, Chicago, Illinois.
[1] O'Kelley, Barton, Crane, and Perlman, Phys. Rev. **80**, 293 (1950).
[2] B. B. Kinsey, Can. J. Research **26A**, 404 (1948).
[3] Reference 2, p. 421.
[4] L. de Broglie, Compt. rend. **158**, 944 (1914).
[5] R. Darbord, J. phys. radium **3**, 212 (1922).
[6] J. W. M. DuMond and H. A. Kirkpatrick, Rev. Sci. Instr. **1**, 88 (1930).
[7] Y. Cauchois, J. phys. radium **3**, 320 (1932); **4**, 61 (1933).
[8] P. Abelson, Phys. Rev. **56**, 753 (1939).
[9] Edwards, Pool, and Blake, Phys. Rev. **67**, 151 (1945); J. E. Edwards and M. L. Pool, Phys. Rev. **72**, 384 (1947); K. D. Coleman and M. L. Pool, Phys. Rev. **72**, 1070 (1947).
[10] Marmier, Blaser, Preiswerk, and Scherrer, Helv. Phys. Acta. **22**, 155 (1949); **21**, 198 (1948).
[11] J. W. M. DuMond, Rev. Sci. Instr. **18**, 626 (1947).

plutonium. These x-rays arise from internal conversion of gamma-rays accompanying the alpha-decay of isotopes of americium and curium, respectively.

II. METHODS

The spectrometer used in the present studies was designed as a monochromator using a counter tube as detector. A scale drawing of the essential parts may be seen in Fig. 1 in which the sample (2), its collimator (4), the crystal (1), and the counter (9) with its collimator (8) are shown in line. The sample holder is mounted on an arm which rotates it on the focal circle of 5-inch radius facing the concave side of the crystal. As pointed out by DuMond,[11] if the counter is placed on the convex side and the source on the concave side, there is a considerable increase in efficiency over the opposite arrangement, since all x-rays from the source are incident upon the crystal at the appropriate angle for diffraction. The crystal used for the measurements to be reported was quartz 0.008 inch thick cut perpendicular to the 310 planes. A tool steel holder with an aperture $\frac{3}{4}$ in. long$\times\frac{1}{4}$ in. high and surfaces machined to a radius of 10 inches clamps the crystal so that its center is tangent to the focal circle and all crystal planes are directed at a point on the opposite side of the focal circle.

In operation on continuous sweep the motor (5) rotates the sample holder arm and at the same time rotates the detector arm so that the angles between crystal planes and sample and between crystal planes and detector are equal. An arrangement of metal bands turns the sample holder so that the sample and its defining slit always face the crystal aperture. The gear changing box (6), operating through the worm gear (7), permits selection of angular speeds of the sample arm of 1, 1/5, 1/20, and 1/100 degree per minute. The position of the sample arm is read on the scale by means of a vernier.

The counter is protected from stray radiation in several ways. The fine lead collimator (8) protects the counter tube from undiffracted x-rays passing through the crystal; in addition, the tube is placed in a lead cylinder and the fixed shield (10) gives still more protection against direct radiation from the sample. The counter used in the measurements to be reported was an end window proportional counter filled with xenon at a pressure of 55 cm Hg and methane at 15 cm. With no sample in place, the background counting rate was in the range 3 to 10 per minute, depending on the amount of activity in the adjacent laboratory. Incoherent scattering contributed an additional background of about $\frac{1}{2}$ percent of the total x-radiation observed. This low background counting rate was made possible by operating the tube in a pulse height selection circuit to discriminate against radiation not in the energy range of the x-rays under measurement.

Figure 2 shows a block diagram of the counting circuits. The tube is operated with the copper cathode

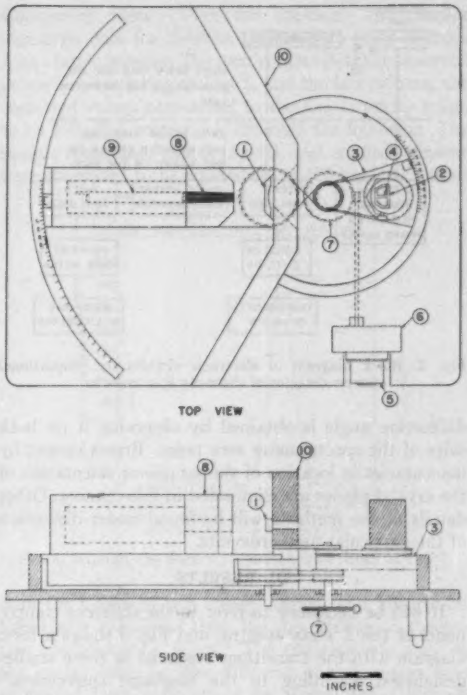

FIG. 1. Scale drawing of x-ray spectrometer.

shell at high voltage in order to simplify the coupling of the small pulses from the proportional counter to the preamplifier. The preamplifier is mounted on the counter housing and amplifies the counter pulse about one hundred fold. The pulse height discriminator which follows the second amplifier can be adjusted both in band width and pass band; and, as mentioned, it is used to eliminate pulses which are not in the range of those produced by the x-rays under measurement. The recording system following the third amplifier includes a scaling circuit, which actuates a recording Streeter-Amet Traficounter, and a counting rate meter connected to an Esterline-Angus graphic milliammeter. The diffraction angle is read and recorded manually on the Traficounter tape at intervals. Points on the milliammeter record chart and on the Traficounter tape are related reliably to the angular position of the sample since all three are driven by synchronous motors.

The method of converting the counting data to x-ray energies is based on the grating spacing of the 310 planes of quartz which was taken to be 1.178A. From the measured diffraction angle and Bragg's law, the wavelength is determined in Angstrom units; and this is converted to energy in kev units by the relation $E=12.395/\lambda$. An internal check on the value of the

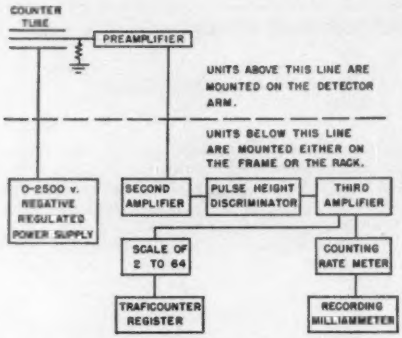
COUNTER TUBE
PREAMPLIFIER
UNITS ABOVE THIS LINE ARE MOUNTED ON THE DETECTOR ARM.
UNITS BELOW THIS LINE ARE MOUNTED EITHER ON THE FRAME OR THE RACK.
0-2500 v. NEGATIVE REGULATED POWER SUPPLY
SECOND AMPLIFIER
PULSE HEIGHT DISCRIMINATOR
THIRD AMPLIFIER
SCALE OF 2 TO 64
COUNTING RATE METER
TRAFICOUNTER REGISTER
RECORDING MILLIAMMETER

FIG. 2. Block diagram of electronic circuits for proportional counter detector of the x-ray spectrometer.

diffraction angle is obtained by observing it on both sides of the spectrometer zero point. Errors caused by inaccuracies in location of the sample or orientation of the crystal planes are eliminated in this manner. Other details of the methods will be found under discussion of the particular measurements.

III. RESULTS

It will be necessary to refer to the different components of the L x-ray spectra, and Fig. 3 shows a term diagram with the transitions observed in these studies designated according to the Siegbahn convention.[12] The particular levels shown are those for plutonium x-rays with energy values obtained by use of the Moseley relation:[13]

$$E^{\frac{1}{2}}=K(Z-\sigma).$$

The values for K and σ were calculated from the level energies of Th and U as given by Siegbahn.[14] The transition energies obtained in this manner have been used to identify the observed x-ray lines. The energies predicted for the major transitions from elements in the atomic number range 90 to 96 are listed in Table I.

A. Plutonium X-Rays from Decay of Cm^{242}

The isotope Cm^{242} is an alpha-particle emitter with 162-day half-life, prepared for the present study by the neutron irradiation of the 475-yr Am^{241} according to the following reactions:

$$Am^{241}(n,\gamma)Am^{242m}, \quad Am^{242m} \xrightarrow[16\text{ hr}]{\beta^-} Cm^{242}.$$

The alpha-decay of Cm^{242} includes fine structure in which roughly 20 percent of the disintegrations go to an excited state of Pu^{238} about 50 kev above the ground state.[15] The accompanying γ-ray transition is largely internally converted in the L-shell and the x-rays measured in this study are those resulting from the refilling of these L-orbit vacancies. The uncertainties in x-ray counting efficiencies allow an estimation of their number only between wide limits, but which for the present we take to be 10 L x-ray quanta per 100 alpha-disintegrations.

A sample[15a] of CmF_3 emitting about 3×10^5 x-rays per second was mounted in a quartz capillary tube making a line source about 1 cm long. This capillary tube was held vertically in a lucite holder in the sample housing. No sample collimator was necessary because of the good definition of the source.

Even so, it is likely that the resolution is limited by the sample width, since with similar samples not so homogeneous in their geometrical distribution, identical "fine structure" appeared in each line, which is interpreted as an image of the sample distribution.

The spectrometer was adjusted to sweep at a rate of 1/20 degree per minute and the counts in each 0.8-min interval were recorded. Figure 4 shows one segment of the spectrum including the $L\alpha_1$ and $L\alpha_2$ lines, in which both the spectrometer scale reading and the energy calibration are indicated. One unit of the spectrometer

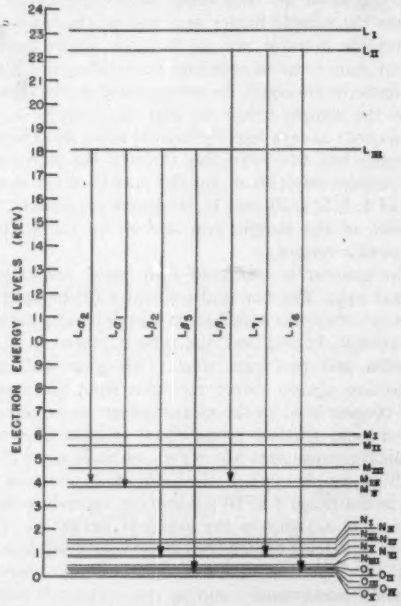

FIG. 3. Term diagram, in which x-ray energy levels in the plutonium transitions observed in this study are indicated.

[12] Compton and Allison, *X-rays in Theory and Experiment* (D. Van Nostrand Company, Inc., New York, 1935), p. 596.
[13] H. G. J. Moseley, Phil. Mag. 27, 703 (1914).
[14] M. Siegbahn, *Spektroskopie der Röntgenstrahlen* (Verlag. Julius Springer, Berlin, 1931).
[15] G. D. O'Kelley and W. W. T. Crane, unpublished work.
[15a] We are grateful to Mr. W. W. T. Crane for placing this sample of curium at our disposal.

TABLE I. Calculated *L*-series x-ray energies.

Line	Transition	Energy (kev) 90Th	91Pa	92U	93Np	94Pu	95Am	96Cm
1	$L_{III}-M_I$	11.14	11.39	11.64	11.90	12.16	12.42	12.69
α_2	$L_{III}-M_{IV}$	12.84	13.15	13.47	13.79	14.11	14.45	14.78
α_1	$L_{III}-M_V$	13.00	13.32	13.65	13.98	14.31	14.66	15.00
η	$L_{II}-M_I$	14.54	14.99	15.43	15.89	16.35	16.81	17.29
β_4	$L_{III}-N_I$	15.00	15.37	15.76	16.14	16.53	16.92	17.32
β_2	$L_{III}-N_{IV}$	15.62	16.01	16.42	16.82	17.29	17.66	18.08
β_4	L_I-M_{II}	15.67	16.14	16.61	17.09	17.58	18.07	18.57
β_3	$L_{III}-O_{II}$	16.24	16.67	17.10	17.54	17.98	18.44	18.89
β_1	$L_{II}-M_{IV}$	16.24	16.75	17.26	17.78	18.30	18.84	19.38
β_3	L_I-M_{III}	16.46	16.97	17.49	18.02	18.56	19.10	19.65
γ_1	$L_{II}-N_{IV}$	19.02	19.61	20.21	20.81	21.43	22.05	22.68
γ_2	L_I-N_{II}	19.34	19.93	20.53	21.13	21.75	22.37	23.00
γ_3	L_I-N_{III}	19.54	20.15	20.76	21.38	22.01	22.65	23.29
γ_4	$L_{II}-O_{IV}$	19.64	20.27	20.89	21.53	22.17	22.83	23.49

scale corresponds to 4 degrees displacement of the sample arm; therefore, the angle traversed between the two peaks shown is only about 0.6 degree.

Figure 5 shows curves obtained for the spectrum in the interval of approximately 14 to 22 kev, in which the two sections represent data taken on the two sides of the zero position. As mentioned, the mean diffraction angle obtained from scale readings on both sides of the zero position is the true value, even though misalignment of the sample or the crystal planes would introduce an error in each of the single position readings. In obtaining these curves a system of curve smoothing was employed which averaged over each five adjacent points and plotted the number so obtained at the center of the smoothing interval. The relative heights of the peaks do not reproduce faithfully the abundances of the emitted x-ray lines, because no corrections have yet been made for the differences in reflection coefficients, counter efficiencies, and several sources of absorption. These will be discussed further below.

Table II lists in the second and third columns the spectrometer scale readings corresponding to the lines of Fig. 5 for some of which there were two measurements. Another series of measurements has been made on a different curium sample and the results agree with those reported here both in energy of the lines and intensities. The last two columns of Table II give the angles of diffraction obtained from these readings and the corresponding energies. The level transition assignments of the lines were made by comparing with the calculated values listed in Table I. Table III compares our measured energy values for the *L*-series x-rays of plutonium (Table II) with those obtained by extrapolation and shown in Table I and with a set calculated by Monk and Allison,[16] who used a formula of Sommerfeld[17] derived by the old quantum theory.

Of interest are the intensity values listed in the last three columns of Table III. The column headed "uranium" gives relative intensities measured by Allison[18] from the electron bombardment of uranium. Comparing these values for uranium with similar measured ones for thorium indicates no gross changes with atomic number. The next column lists the observed intensities according to Fig. 5, and the last column, the corrected values normalized to the $L\alpha_1$ intensity taken to be 100. The corrections involved the following. The sample mounting, quartz crystal, and counter window were estimated to be equivalent to 150 mg/cm² alumi-

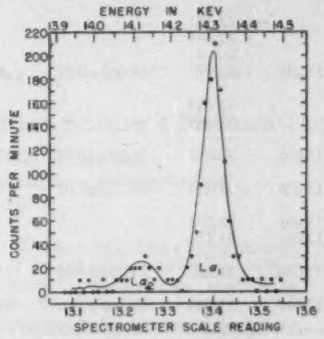

FIG. 4. $L\alpha_1$ and $L\alpha_2$ lines of plutonium from decay of Cm^{242}.

num for x-rays in this energy region, and absorption losses were calculated from the compilation of absorption coefficients by Allen.[19] The counting efficiency of the xenon tube for the different energy x-rays was estimated from calibrations by Crane and Ghiorso[20]

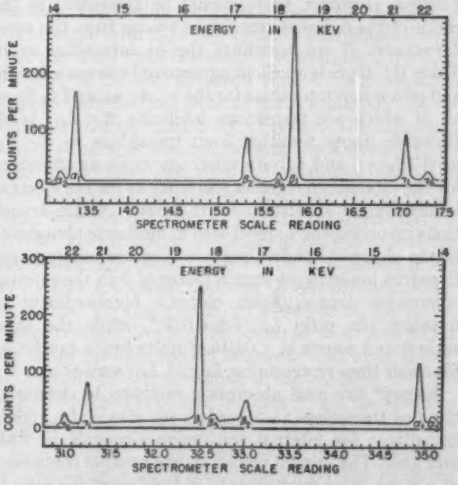

FIG. 5. *L*-series x-ray spectrum of plutonium following decay of Cm^{242}. (Upper and lower plots show identical spectra taken on two sides of spectrometer zero position.)

[16] A. T. Monk and S. K. Allison, Manhattan Project Metallurgical Laboratory Report CP-2120 (September, 1944) (unpublished).
[17] Compton and Allison, reference 12, p. 610.
[18] S. K. Allison, Phys. Rev. 30, 245 (1927); 32, 1 (1928).
[19] S. J. M. Allen, reference 12, p. 800.
[20] W. W. T. Crane and A. Ghiorso, unpublished work.

TABLE II. Plutonium L x-rays from Cm^{242} decay.

X-ray designation	Spectrometer scale reading First position	Second position	Angle of diffraction θ (degrees)	Energy (kev)
$L\alpha_1$		34.932		
		34.947		
	13.404	34.940	21.536±0.02	14.31±0.01
$L\alpha_2$	13.244	35.090	21.846±0.02	14.14±0.01
$L\beta_1$		32.500		
		32.495		
	15.830	32.497	16.667±0.02	18.35±0.02
$L\beta_5$		32.650		
		32.660		
	15.665	32.655	16.990±0.02	17.91±0.02
$L\beta_2$	15.305	33.020	17.725±0.02	17.28±0.02
$L\gamma_1$	17.065	31.262		
	17.067	31.250		
	17.066	31.256	14.190±0.02	21.46±0.04
$L\gamma_5$	17.315	31.025	13.710±0.02	22.20±0.04

and the reflection coefficient of the crystal is assumed to vary[21] as $1/E^2$.

It would not be expected that there should be agreement between all of the relative intensities of x-rays resulting from electron bombardment as compared with those from γ-ray internal conversion because of differences in the relative excitation of different L-levels. However, there should be agreement in the ratios of the different transitions arising from the same L-vacancy. If we normalize the α_1 intensities as in Table III, there is excellent agreement between uranium and plutonium intensities for the α_1, β_2, α_2, and β_5 lines, all of which are transitions involving the L_{III} level. However, those resulting from transitions to the L_{II} level (β_1, γ_1, and γ_5) are relatively twice as abundant for the internal conversion spectrum as for the electron bombardment spectrum. Furthermore, certain transitions involving the L_I level seen in moderate abundance in the electron bombardment source are missing, and therefore lower by at least a factor of 5 in the internal conversion source. From electron bombardment of uranium the ratio $L\beta_3/L\beta_1=0.085$, while the same ratio in our source is <0.016. Similar limits can be set for other lines representing L_I and L_{III} vacancies.

Kinsey[3] has used absorption methods to determine the L_{III} transitions as related to the sum of L_{II} and L_I transitions for internal conversion processes in RaD and ThC. The present results on the internal conversion of a γ-ray of an excited state of Pu^{238} show the ratio of L_{II} to L_{III} x-rays to be in the range reported by Kinsey; but the L_I x-rays were not detected, and a limit of *20 percent* of the number of L_I vacancies formed by electron bombardment could be set. This observation is not consistent with the assumption[2,3] that the L_I level is always most strongly excited in internal conversion. Almost certainly the relative incidence of vacancies is dependent upon both the energy of the γ-emission process and the selection rules, and differences are to be expected for different nuclei.

[21] Lind, West, and DuMond, Phys. Rev. **77**, 475 (1950).

B. Neptunium X-Rays from the Decay of Am^{241}

Through a mechanism similar to that in which plutonium x-rays are present following Cm^{242} alpha-decay, x-rays of neptunium result from the internal conversion of a gamma-ray from an excited state of Np^{237} following the alpha-decay of Am^{241}. The isotope Am^{241} has a half-life of somewhat less than 500 years, emitting alpha-particles measured as 5.45 Mev, a large fraction or all of which go to an excited state[22] of Np^{237}.

TABLE III. Comparison of predicted and observed energies and abundances in L-series x-rays of plutonium from alpha-decay of Cm^{242}.

Line	Transition	Energy (kev) Monk and Allison (ref. 16)	Calc. (this paper)[a]	Measured[b]	Intensity In uranium (ref. 18)	Observed here[c]	Corrected here[d]
α_1	$L_{III}-M_V$	14.30	14.31	14.31	100	160	100
β_1	$L_{II}-M_{IV}$	18.27	18.30	18.35	49.4	276	91
β_3	$L_{III}-N_V$		17.29	17.28	28	78	28
γ_1	$L_{II}-N_{IV}$		21.43	21.46	12	80	23
α_2	$L_{III}-M_{IV}$	14.11	14.11	14.14	11	20	13
β_5	$L_{III}-O_V$		17.98	17.91	6.4	16	6
β_2	L_I-M_{III}	18.55	18.56		4.2		
β_4	L_I-M_{II}	17.60	17.58		4.1		
1	$L_{III}-M_I$	12.12	12.16		3.4		
γ_5	$L_{II}-O_{IV}$		22.17	22.20	2.2	14	4
β_6	$L_{III}-N_I$		16.53		1.6		
γ_2	L_I-N_{II}		21.75		1.5		
γ_3	L_I-N_{III}		22.01		1.4		
η	$L_{II}-M_I$	16.28	16.35		1.0		
β_7	$L_{III}-O_I$		17.73		0.4		

[a] Calculated as explained for Table I and as listed there.
[b] Measured in this work. See Table II.
[c] See Fig. 5.
[d] Corrected as explained in text.

TABLE IV. Neptunium L x-rays from Am^{241} decay.

Line designation	Spectrometer scale reading First setting	Second setting	Angle of diffraction	Energy (kev) (Measured)	(Extrap.)
$L\alpha_1$	35.15	13.05	22.10±0.05	13.98±0.03	13.98
$L\beta_2$	33.12				
	33.15				
	33.14	15.05	18.09±0.06	16.94±0.05	16.82
$L\beta_1$	32.69				
	32.71				
	32.70	15.50	17.20±0.04	17.79±0.03	17.78

[22] Seaborg, James, and Morgan, National Nuclear Energy Series, Plutonium Project Record **14B**, *The Transuranium Elements: Research Papers*, paper No. 22.1 (McGraw-Hill Book Co., Inc., New York, 1949).

The resulting 62-kev transition is highly converted in the L-shell, giving rise to the L x-ray spectrum. The Am^{241} was prepared by neutron capture in plutonium resulting in the β^--emitter Pu^{241}, which decays to the desired product.[22]

[22] Ghiorso, James, Morgan, and Seaborg, Phys. Rev. 78, 472 (1950).

The measurements of the x-rays were made in a manner similar to that already described for the curium sample. However, the americium source was some tenfold weaker, so that not so many lines could be seen, and relative intensities could not be estimated. The data for the three most intense lines ($L\alpha_1$, $L\beta_1$, and $L\beta_2$) are given in Table IV and energies compared with the estimated values as listed in Table I.

PHYSICAL REVIEW VOLUME 81, NUMBER 2 JANUARY 15, 1951

The X-Ray Spectrum Produced by 322-Mev Electrons Striking a Platinum Target*

WILSON M. POWELL, WALTER HARTSOUGH, AND MILTON HILL
Radiation Laboratory, Department of Physics, University of California, Berkeley, California
(Received September 25, 1950)

The differential energy spectrum of the photons produced by 322-Mev electrons striking a 20-mil platinum target was measured by observing the energy of 3467 pairs produced in a one-mil thick lead foil in a Wilson cloud chamber in a magnetic field of 10,000 gauss. The spectrum is found to agree with that predicted by the Bethe-Heitler bremsstrahlung theory using a Thomas-Fermi model with suitable corrections for the thickness of the target. The energy of the 322-Mev electrons was determined by the spectrum of the photons observed in this experiment.

I. INTRODUCTION

THE Berkeley synchrotron produces 322-Mev electrons as estimated from the results of this experiment. These electrons make x-rays by striking a 20-mil thick platinum target inside the quartz vacuum chamber of the machine. The x-rays pass through 1.5 to 2 cm of quartz before reaching the air where practically all experiments are performed. This paper gives the energy distribution of the x-rays as obtained from the measurement of the energy of 3467 pairs produced in a 1-mil thick lead plate placed in the x-ray beam from the synchrotron.

II. APPARATUS

A 16-in. diameter Wilson cloud chamber with a magnetic field of 10,000 gauss was placed in the x-ray beam from the synchrotron, with its center 88.5 ft from the 20-mil thick platinum target of the synchrotron. A six-in. thick lead collimator, 35 ft from the target, collimated the x-rays so that they formed a beam at the chamber approximately 6.5 in. wide and 1 in. high. The beam entered the chamber through a 5-mil aluminum window and passed through a vertical lead plate 1-mil thick across the center of the cloud chamber. Electron-positron pairs were produced in the lead and the gas (a mixture of half argon and half helium with water and ethyl alcohol for the vapor) of the chamber. Only those pairs produced in the lead plate were used in the data given below.

The synchrotron gives a pulse of x-rays six times per sec which can be interrupted at suitable intervals by changing the timing of the high voltage on the synchrotron injector so that it fires too late to produce a beam. The procedure is to monitor the beam by means of a Zeus meter placed just out of the main beam. The beam is run steadily at some low value, interrupted for about a second before and after the pulse used by the cloud chamber. The timing sequence of the cloud chamber is synchronized with the x-ray signal in the following way. First the cloud chamber magnet is energized, reaching full field in 2.3 sec, at which time a ready signal is given so that the next pulse of the synchrotron magnet sends a signal to expand the chamber. The expansion is delayed so that the x-rays from the following pulse reach the chamber just after the expansion. The lights are flashed 0.035 to 0.045 sec after the arrival of the beam. Two General Electric FT-22 flash tubes charged to 1700 v with 250 μf of capacity each are used for illumination and the 127-mm focal length camera lenses were set at f:8 using Eastman Orthochromatic Linagraph film. Because of the early timing of the lights, it was necessary to open the lenses so as to give about four times the light usually required. This early timing and control of the temperature of the chamber to 0.1°C resulted in turbulence free pictures where the spurious radius of curvature was greater than 50 m.

T. C. Merkle, Jr., suggested that a mixture of argon and helium be used in the chamber for the following reasons. Argon gives a larger number of ion pairs per cm length of track than does helium but has the disadvantage of a low heat conductivity and, therefore, takes a long time to reach thermal equilibrium. By mixing in equal amounts of helium, which has a heat

* This work was performed under the auspices of the AEC.

conductivity some nine times greater than that of argon, the heat conductivity of the mixture is increased by a factor of 4 or more and the waiting period necessary to achieve thermal equilibrium in this large chamber is reduced to 45 sec. The tracks are much heavier than they would be with pure helium.

III. EXPERIMENTAL RESULTS

Table I contains the experimental data with column 2 giving the number of pairs observed in the 10-Mev energy intervals indicated in column 1. Column 3 contains numbers proportional to the pair production cross section in lead as calculated from Heitler.[1] Column 4 is obtained by dividing column 2 by column 3 and is a set of numbers proportional to the number of photons in each interval. Column 5 is a set of numbers proportional to the average energy of each interval with unity corresponding to 322 Mev. The numbers in column 6, obtained by multiplying column 4 by column 5, are proportional to the number of photons per Mev multiplied by the average energy of the photons, or they are proportional to the total energy carried by the photons

TABLE I. Experimental differential distribution.

Pair energy interval in Mev	Measured number of pairs N	Calculated relative cross section in lead σ	N/σ	Average pair energy divided by 322 Mev	Experimental differential energy distributoin
0– 10	153	2.0	76.5	0.0155	1.09
10– 20	441	4.9	90.0	0.0466	4.19
20– 30	441	6.4	69.0	0.0777	5.36
30– 40	317	7.2	44.0	0.1088	4.79
40– 50	276	7.7	35.8	0.1399	5.01
50– 60	230	8.0	28.7	0.1710	4.91
60– 70	230	8.4	27.4	0.202	5.54
70– 80	192	8.7	22.1	0.233	5.15
90– 90	136	8.9	15.3	0.264	3.88
90–100	140	9.1	15.4	0.295	4.54
100–110	139	9.2	15.23	0.336	5.11
110–120	124	9.35	13.28	0.357	4.72
120–130	115	9.45	12.18	0.388	4.72
130–140	94	9.55	9.74	0.420	4.07
140–150	90	9.65	9.34	0.451	4.21
150–160	76	9.70	7.85	0.482	3.79
160–170	78	9.80	7.96	0.513	4.08
170–180	89	9.85	9.04	0.544	4.92
180–190	81	9.90	8.19	0.575	4.71
190–200	52	9.95	5.32	0.606	3.23
200–210	51	10.0	5.10	0.627	3.20
210–220	63	10.05	6.26	0.668	4.18
220–230	59	10.10	5.9	0.700	4.13
230–240	51	10.15	5.0	0.732	3.66
240–250	52	10.15	5.1	0.761	3.88
250–260	51	10.20	5.0	0.793	3.96
260–270	38	10.25	3.7	0.824	3.05
270–280	43	10.30	4.2	0.855	3.59
280–290	43	10.35	4.2	0.886	3.72
290–300	34	10.35	3.3	0.917	3.02
300–335	57	10.40	5.5	0.987	5.37

[1] W. Heitler, *Quantum Theory of Radiation* (Oxford University Press, London, 1936), p. 201.

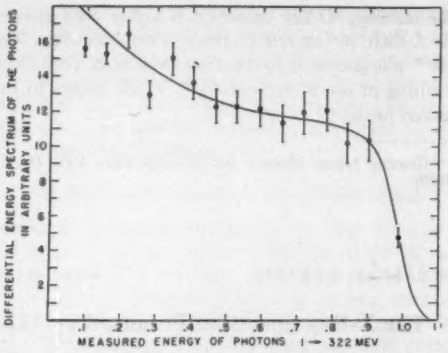

FIG. 1. The differential energy spectrum of the photons from a 40-mil platinum target bombarded by 322-Mev electrons. The solid curve is the energy spectrum predicted by theory.

in each energy interval. This will be called the differential energy spectrum of the photons. The numbers in column 6 were added in pairs so as to give a single number for each 20-Mev interval, and these are shown by the points in Fig. 1. The last energy interval goes from 300 to 335 Mev and was weighted properly by multiplying by 20 and dividing by 35. The errors shown are statistical errors obtained by dividing the values given by the square root of the number of pairs shown in column 2 of Table I but taken in 20-Mev intervals. No estimate of possible systematic errors is included with these errors.

IV. THEORY

The 20-mil platinum target is bombarded by electrons, and the energy distribution of the x-rays produced is a function of this thickness. The spectrum for an infinitely thin target was calculated by R. Christian following the Bethe-Heitler[2,3] bremsstrahlung theory using a Thomas-Fermi model for the atom. The theoretical differential energy spectrum for an infinitely thin target produced by electrons of 322-Mev energy is given in column 2 of Table II. This spectrum is modified by the thickness of the target as the result of the following process. First the original electrons lose energy by radiation so that their original energy is lowered and the x-rays produced by them farther along in the target will show a lower average energy. This lowering in energy would be more marked were it not for another effect which reduces this considerably. The electrons which have been multiply scattered are no longer pointing in their original direction. Using the multiple scattering formulas of E. J. Williams it can be shown that after traversing about the first 4 mils of the target the electrons are sufficiently out of line so as to make most of the photons produced by them miss the cloud chamber altogether. This effect was first pointed out by

[2] H. A. Bethe and W. Heitler, Proc. Roy. Soc. 159, 432 (1937).
[3] B. Rossi and K. Greisen, Rev. Mod. Phys. 13, 253 (1941).

McMillan[4] and its result is to give a spectrum more like that for an infinitely thin target. The spectrum comes almost entirely from the first fifth or quarter of the target and, therefore, these quanta will be absorbed in passing through the remaining three quarters of the target. Only about 10 percent of the quanta are absorbed in the target, and the absorption coefficient changes by only 12 percent from 40 Mev on up. The correction is practically a constant one and reduces the intensity almost uniformly by 10 percent. The spectrum resulting after all these corrections is given in column 3 of Table II.

In order to compare this with the experimental results, it is necessary to assume a pair production cross section for the x-rays in the lead plate and to make any necessary corrections for the passage of the x-rays through the quartz wall of the vacuum chamber and the 88.5 ft of air between it and the cloud chamber. The pair production cross section for x-rays in lead was taken from the curve for lead given by Heitler[1] and is given relative to the cross section at 190 Mev in column 3 of Table I. The pair production cross section for lead was measured by Lawson[5] for 88-Mev x-rays and was found to be 31.3 barns instead of the theoretical value of 34.9 barns, or lower by eleven percent than the simple theory at 88 Mev. Adams[6] measured an absorption coefficient for lead at 19.1 Mev which was 9.6 percent lower than experiment and Walker[7] finds it 9.8 percent lower at 17.6 Mev. Both of these experiments indicate that the cross section for pair production is lower for lead but lower by nearly the same amount from 17 up to 88 Mev. This difference can become appreciable here only if the ratio of the cross sections changes with energy, and since there is no evidence that this occurs no correction has been made.

The one-mil thick lead plate is sufficiently thin so that the probability that a particle produced in the lead will radiate before leaving the lead is very small. Only 0.2 percent of the particles will radiate more than 40 percent of their energy. The absorption of the x-rays by the quartz and the air amounts to 13 percent of the incoming x-rays and is practically uniform over the entire spectrum. The total cross section for 88-Mev x-rays for aluminum as measured by Lawson[5] is 1.128 barns and the theoretical cross section is 1.103 barns. This is a good indication that the theory gives the correct result for light elements and that no large error would result from calculating the absorption of the quartz and the air between the target and the chamber from theory, especially since the maximum percent absorption in the neighborhood of 300 Mev amounts to only 15 percent. In the quartz and the air between the target and the lead plate in the cloud chamber there are 2.7 g/cm^2 of oxygen, 1.7 g/cm^2 of silicon, and 2.5 g/cm^2 of nitrogen. The effect of the argon in the air and the chamber plus the 5-mil-aluminum window on the chamber is neglected. Using the cross sections given by Heitler[1] for the nuclear pair production plus the cross section for the pair production due to the electrons, plus the Compton scattering cross section, the percentage of the x-rays transmitted is found to be 87 percent from 30 to 204 Mev, 88 percent at 15 Mev, and 86 percent at 300 Mev. This has no observable effect on the energy distribution of the x-rays.

In order to be sure that higher energy x-rays absorbed in the quartz and air were not producing secondary quanta which would distort the spectrum at lower energies, the electrons entering the chamber with the x-ray beam were counted for a few pictures taken without magnetic field. The secondary quanta in the beam should be comparable in number with the secondary electrons accompanying the beam. There were 16 electrons accompanying the beam for every pair produced in the lead plates. Since about 4000 photons are necessary to produce one pair, the secondary quanta form a negligible fraction of the x-ray beam.

The theoretical differential energy spectrum given in column 3 of Table II for a 20-mil thick platinum target drops to zero at energies above that of the electrons in the synchrotron. If there is an error in measurement of the energy of the pairs, this will change the shape of the theoretical curve making it less steep and extending it above this energy. The random experimental errors were estimated to give a probable error of 2.5 percent. Actually the errors arise from the fact that the templates used to match curvatures[8] are about four percent apart in radius, and the error due to multiple scattering

TABLE II. Calculated differential energy spectrum.

Average pair energy divided by 322 Mev	Differential energy distribution for an infinitely thin Pt target	Differential energy distribution for a 20-mil thick Pt target	Differential energy distribution for a 20-mil target with 2.5 percent probable error
0.1	18.6	17.5	17.5
0.2	17.0	15.7	15.7
0.3	15.6	14.3	14.3
0.4	14.5	13.1	13.1
0.5	13.8	12.4	12.4
0.6	13.4	11.9	11.9
0.7	13.2	11.6	11.6
0.8	13.1	11.2	11.2
0.9	12.8	10.5	10.5
0.92	12.6	10.3	9.8
0.94	12.3	9.8	9.0
0.95	12.0	9.4	8.3
0.96	11.8	8.9	7.5
0.98	10.0	7.05	5.7
0.99	7.75	5.2	4.7
1.00	0	0	3.7
1.02	0	0	2.0
1.04	0	0	0.87
1.06	0	0	0.30

[4] E. M. McMillan, private communication.
[5] J. L. Lawson, Phys. Rev. 75, 440 (1949).
[6] G. D. Adams, Phys. Rev. 74, 1707 (1948).
[7] R. L. Walker, Phys. Rev. 76, 527 (1949).
[8] Brueckner, Hartsough, Hayward, and Powell, Phys. Rev. 75, 555 (1949).

of the particles in the gas amounts to about one percent. Although the errors arising from the templates are not Gaussian but cut off more rapidly, they were assumed to be Gaussian. The theoretical differential energy spectrum, modified to correspond to one observed with a probable error of 2.5 percent, is given in column 5 of Table II.

The average angle between the direction of the incoming photon and the pair fragments is of the order of the energy of the photon divided by the energy of the electron; since this is very small above energies of 20 Mev, the pair fragments lie very nearly in the same plane which is very nearly perpendicular to the direction of the magnetic field. As a consequence, no correction for large angles is necessary above 20 Mev such as was necessary in the energy spectrum obtained by Koch

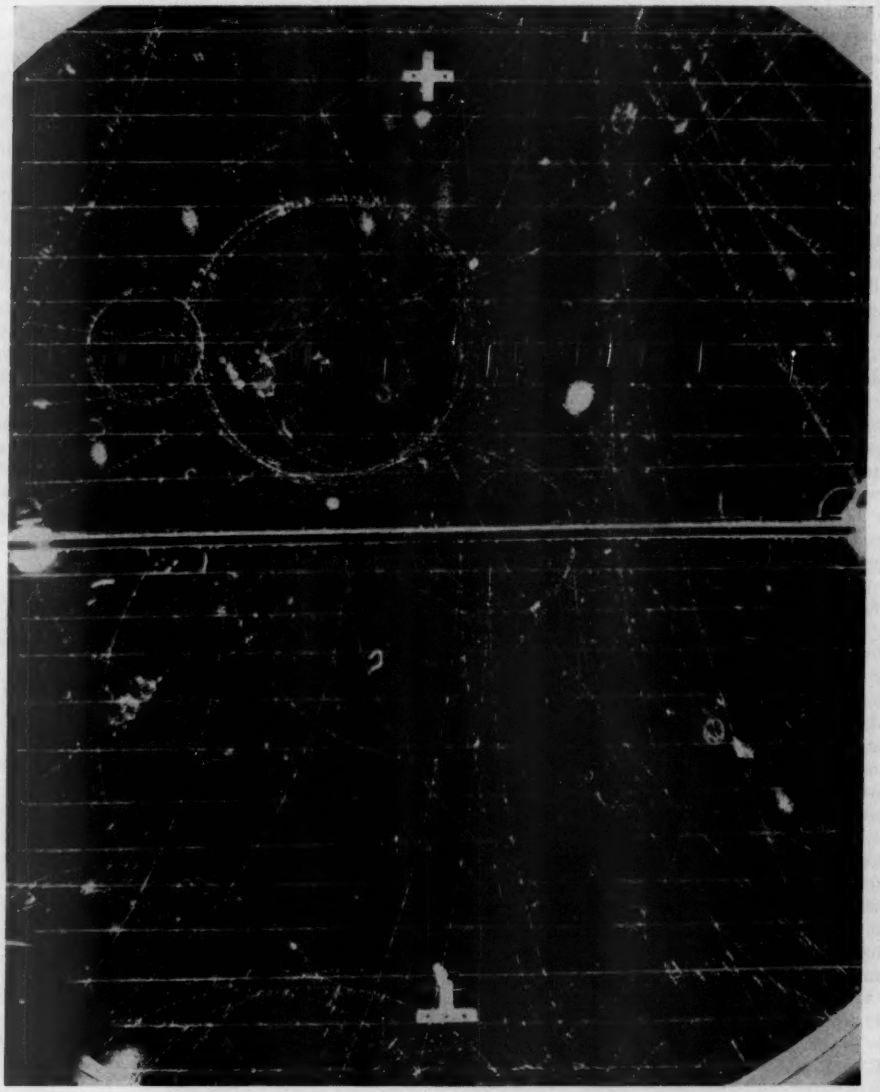

FIG. 2. Pairs produced by the synchrotron x-rays in a 1-mil thick lead target in a Wilson cloud chamber.

and Carter[9] from 19.5-Mev electrons. The first point on the energy spectrum curve disagrees markedly with theory both because no correction was made for these angles and because electrons with energies less than 1 Mev were easily missed because of their very great curvature. Figure 2 shows a typical cloud chamber photograph with seven pairs coming out of the lead and one pair produced in the gas just above the lead. The low energy pair to the left above the plate illustrates how the electrons and positrons stay in nearly the same plane for many revolutions. The illuminated region is only 1.5 in. high.

The normalization of the experimental data involves fitting the data by means of two points and a slope. This is necessary first because absolute intensities are not known, and second because the exact energy of the accelerated electrons is unknown. This experiment can be used to determine the energy of the original electrons if the theory of pair production and x-ray production is assumed to be correct. The first estimate of 335 Mev for the energy of the synchrotron electrons was made from measurements of the magnetic induction around the orbit of the electrons in the synchrotron. Actually the field at a radius of one meter was found to vary by 2.6 percent. The absolute measurement of the field was made with a search coil having an error in effective area of one percent and a voltmeter having an error of 1.5 percent. The voltage on the condensers which discharge into the synchrotron magnet is measured on another voltmeter which was not recalibrated at the time of this experiment and might be in error by two percent. The position of the target is accurately known, but the position of the center of curvature of the beam of electrons has never been determined and might be one or two cm away from the center of the machine. This would make a one or two percent error in the energy. Also the synchrotron magnet has been disassembled twice since the measurement of the magnetic field. The total air gap in the magnet is 2.5 in. and on replacing the top of the magnet this may be changed by as much as 20 mils, 10 mils in the large air gap and 10 mils in changes in the thickness of the Bakelite sheets which insulate the 70-ton top of the magnet from the rest of the magnet. This change might be irregular in azimuth and cause shifting in the center of curvature as well as changes in the average value of the field. Errors of as much as four percent can easily be accounted for by a combination of all of these factors.

The cloud-chamber magnetic field was measured by means of a search coil with effective area accurate to one percent and fluxmeter consisting of an integrator operating into a cathode-ray oscilloscope. Most of the signal from the search coil was bucked out by a secondary flux standard accurate to one percent, and the fluxmeter could be read to a tenth of a percent. Each time a picture was taken, the current going to the cloud-chamber magnet was read from the ammeter used in making the field calibration. The error in magnification of the pictures on reprojection is less than half a percent. The conclusion is that a systematic error in the measurement of the energy of the particles in the chamber could not exceed two percent unless a systematic error were made in comparing the curves on the templates with the tracks. Since the tracks, with a few exceptions, were measured twice by independent observers, a systematic error of a size sufficient to raise this error seems unlikely.

[9] H. W. Koch and R. E. Carter, Phys. Rev. 77, 165 (1950).

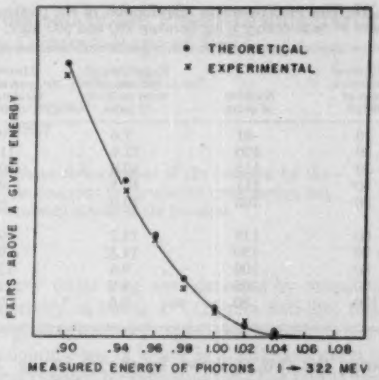

FIG. 3. The integral curve of the photon energy spectrum showing how the normalization was made which determined the energy of the electrons in the synchrotron.

The conclusion is that the electron energy of 322 Mev as determined by the measurements made in the cloud chamber is probably accurate to two percent and is a better value than the 335 Mev estimated from magnetic measurements on the synchrotron.

V. THE ENERGY OF THE ELECTRONS IN THE SYNCHROTRON

In order to be able to compare theory with experiment it is necessary first to determine the energy of the electrons in the synchrotron. As was shown above, the cloud-chamber measurement of the pair spectrum gives a better estimate of this than does the magnetic field measurements made on the synchrotron, if a satisfactory way can be devised for treating the pair spectrum to obtain the energy of the electrons. This comparison was made in the following way. First the theoretical differential energy spectrum adjusted to account for a 2.5 percent random probable error in the measurement of the energy given in column 4 of Table II was divided by the average energy of each set of pairs to give a set of numbers proportional to the actual number of photons. These values were integrated with respect to energy from infinity down and a plot of these values down as far as 0.9 of the full energy of the electrons is shown as the circles in Fig. 3. A similar integral curve was made from the pair data, and on

TABLE III. The relative energy distribution of the positron for pairs of total energy lying between 100 and 300 Mev.

Energy interval of the positrons in percent of pair energy	Number of pairs	Experimental percent of total number of pairs	Theoretical percent of total number of pairs
0– 10	81	7.6	9.0
10– 20	126	11.9	11.0
20– 30	112	10.6	10.4
30– 40	111	10.5	9.9
40– 50	106	10.0	9.7
50– 60	119	11.2	9.7
60– 70	120	11.3	9.9
70– 80	100	9.4	10.4
80– 90	105	9.9	11.0
90–100	80	7.6	9.0

comparing the two as shown by the x's in Fig. 3 the agreement was excellent if the energy of the electrons was assumed to be 322 Mev. Both the experimental and theoretical numbers were integrated down to 60 Mev and normalized as to magnitude at this point. The agreement achieved by these two adjustments is that shown in Fig. 3, and the shape of the foot of the integral curve indicates that the estimate of random errors agrees with the facts.

E. M. McMillan estimated the energy of the electrons by using the ratio of the number of pairs above 290 Mev to the number between 200 and 290 Mev and comparing this ratio to that obtained for the theoretical curve for various assumptions about the energy of the electrons. This comparison should be independent of the errors in measurement if they are random. The result of this calculation gave an energy of 320 Mev with a statistical error of ± 2 Mev. The two methods of determining the energy of the electrons from the data agree well within the experimental errors.

The differential energy distribution of the photons is plotted in 20-Mev groups in Fig. 1. The solid curve is the theoretical curve (column 4 in Table II) modified by the 2.5 percent probable error in the experimental determination of the energies of the pairs. The departure of experiment from theory at the lowest point representing photons with energies up to 20 Mev arises from the fact that the curvature of the tracks was too great to be measurable in many instances for this group. Pairs with energies less than 5 Mev were not measured and were not included in this data. The experimental errors shown in Fig. 2 are statistical errors and it is evident that the experiment shows no appreciable deviation from the theory.

VI. THE FRACTION OF THE PHOTON ENERGY POSSESSED BY THE POSITRON

If we let W be the energy of the photon and U that of the positron belonging to a pair then $F=U/W$ is the fraction of the energy of the photon possessed by the positron. A group of 1060 pairs between 100 and 300 Mev was divided into ten groups according to the value of F and the results are shown in Table III and compared with the theoretical values given by Rossi and Greisen,[3] page 261. The theory and experiment agree well within the limits of error. In the zero to 10 percent group and the 90 to 100 percent group the number of pairs is low, and if no allowance is made for statistical errors, it would appear that 1.6 percent of the pairs were missing in both groups. It has not been possible for us to give any explanation for this low value other than the fact that the number of observations is insufficient to exclude the statistical error.

The number of Compton electrons is negligible in this range of energies. This was borne out by the experimental fact that there were 12 positrons and 10 electrons appearing singly. There should have been about 4 additional electrons over and above positrons from the Compton effect. The numbers observed are not inconsistent with this.

VII. CONCLUSIONS

The differential energy distribution of the photons produced by 322-Mev electrons is that which is predicted by the Bethe-Heitler bremsstrahlung theory using the Thomas-Fermi model for the atom. The fraction of the energy carried by the positron in a group of 1060 pairs agrees with the theoretical predictions.

The energy of the electrons produced by the Berkeley synchrotron for this experiment was 322 ± 6 Mev.

Many of the energy measurements were made by M. Lemmon and Dr. E. Hayward who also helped in the reduction of the results. The cooperation of Mr. Walter Gibbins and numerous others in the operation of the synchrotron and in making the careful adjustments necessary for good cloud-chamber pictures was indispensable in the success of the experiment.

The Angular Distribution of the Neutrons Produced in the Photo-Disintegration of the Deuteron by the 2.51-Mev Gamma-Rays of Ga^{72}

G. R. Bishop, H. Halban, P. F. D. Shaw, and Richard Wilson*
Clarendon Laboratory, Oxford, England
(Received August 23, 1950)†

The angular distribution of the neutrons resulting from the photo-disintegration of the deuteron by the 2.51-Mev gamma-rays of Ga^{72} has been studied. The ratio of the magnetic to the electric cross section has been determined to be 0.61 ± 0.04. A discussion is given of the present status of the problem.

I. PROCEDURE

We have determined the angular distribution of the neutrons produced in the photo-disintegration of deuterons by the 2.51-Mev γ-rays of Ga^{72}. Figure 1 shows the experimental arrangement. A thin-walled (0.2 mm) copper ring R of square cross section (6 mm×6 mm) contained heavy water. It was fixed perpendicular to the plane of an aluminum ring, Al by Nylon threads. Spheres of metallic gallium alloyed with 10 percent Ni (diameter 16 mm) could be placed in positions A, A', and B. The photo-neutrons liberated in the heavy water ring were detected by measuring the radioactivity of iodine I^{128} (25-min half-life) produced in two glass cylinders J_1 and J_2, each of which contained a solution of 5 mg of iodine in 2.5 liters of ethyl iodide, and was covered by cadmium foil. The free radioactive iodine and carrier in J_1 and J_2 were extracted with sodium sulphite solution by a method described elsewhere.[1] Owing to the bulk of the ethyl iodide, it was found necessary to shake the contents of each container consecutively with the same extracting agent, in order to eliminate errors arising from incomplete mixing of

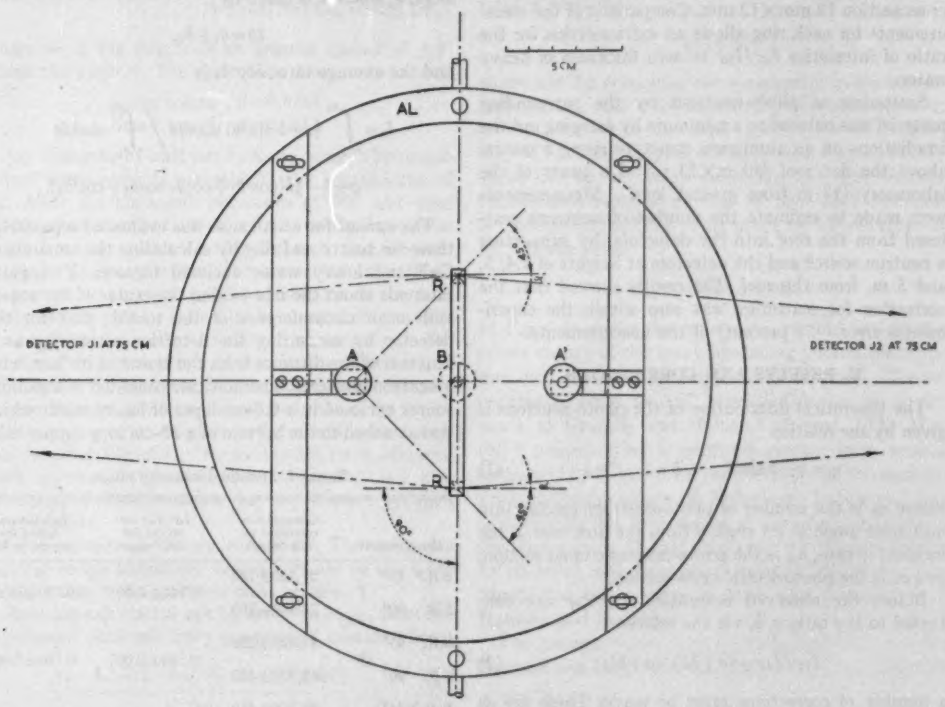

Fig. 1. Experimental arrangement.

* Now at the University of Rochester, Rochester, New York.
† Revised version received September 29, 1950.
[1] P. F. D. Shaw and C. H. Collie, J. Chem. Soc. 264, 1217 (1949).

the two liquids. The radio-iodine and carrier were precipitated as silver iodide; and this was placed, in a brass slide, between two "end-on" Geiger-Müller counters (G.E.C. Type G.M. 4) which were 6 mm apart in a lead castle. The activity was counted for 30 to 45 min.

An average angle of 45° was obtained between the primary rays and the photo-neutrons detected in J_1 and J_2, by placing the two gallium spheres in positions A and A'. For an average angle of 90°, only one source was placed in the position B (consecutive measurements were made on each of the sources used in the 45° position).

The gallium spheres were irradiated in the pile at A.E.R.E. Harwell to a total activity of about three Curies in a neutron flux of 10^{12} neutrons/cm²/sec. Two separate runs were carried out. Each consisted of six measurements in the 45° position, and three for each of the two sources in the 90° position. Each irradiation was made for one hour. In order to evaluate a correction for the scattering of photo-neutrons inside the heavy water ring, a similar series of measurements was made with a ring of the same mean diameter (9 cm) but with cross section 12 mm×12 mm. Comparison of the measurements for each ring allows an extrapolation for the ratio of intensities $I_{45°}/I_{90°}$ to zero thickness of heavy water.

Scattering of photo-neutrons by the surrounding material was reduced to a minimum by carrying out the irradiations on an aluminum structure rising 5 meters above the flat roof (10 m×23 m) of a tower of the laboratory (17 m from ground level). Measurements were made to estimate the number of neutrons scattered from the roof into the detectors, by supporting a neutron source and the detectors at heights of 1.4, 3, and 5 m, from the roof. The results showed that the correction for scattering was zero within the experimental error (<1 percent) of the measurements.

II. RESULTS AND CORRECTIONS

The theoretical distribution of the photo-neutrons is given by the relation

$$\eta_\theta = a + b\sin^2\theta, \quad a/b = 2\sigma_m/3\sigma_e, \tag{1}$$

where η_θ is the number of photo-neutrons ejected into unit solid angle at an angle θ from the direction of the incident γ-rays, σ_m is the photo-magnetic cross section, and σ_e is the photoelectric cross section.

Before the observed intensities, $I_{45°}/I_{90°}$ are converted to the ratio a/b, via the relation

$$I_{45°}/I_{90°} = (a+\tfrac{1}{2}b)/(a+b), \tag{2}$$

a number of corrections must be made. These are as follows.

(1) *The change of solid angle presented by the heavy water ring to the sources in the 45° and 90° positions.* A correction to the inverse square law is made for the finite sizes of ring and sources using a formula derived by integration over the volumes.

$$\text{Mean } (1/r^2) = (1/r^2)[1+(a^2/5r^2)-(x^2/3r^2)],$$

where a is the radius of the source and $2x$ is the thickness of the ring,

(2) *The spread in angle θ about the mean angles defined by the relative positions of ring, sources, and detectors, owing to their finite sizes.* This correction differs for the 45° and 90° positions.

45° position: For the symmetrical arrangement of sources and detector, the mean angles for each source are $45°+\alpha$ and $135°-\alpha$, (Fig. 1) and the sines become $\sin(45°\pm\alpha)$. Since the distribution of Eq. (1) is symmetrical about 45°, the average intensity $\bar{I}_{45°}$ is independent of the angle α, and of the angular spread, because the corrections are equal and of opposite sign and cancel out. Then

$$\bar{I}_{45°} = (a+\tfrac{1}{2}b).$$

90° position: The finite sizes of sources, rings, and detectors introduce a spread in angle about the mean angle θ, where θ is given by

$$2\theta = \theta_1 + \theta_2,$$

and the average intensity I_θ is

$$I_\theta = \int_{\theta_1}^{\theta_2} (a+b\sin^2\theta)\sin\theta d\theta \Big/ \int_{\theta_1}^{\theta_2} \sin\theta d\theta$$

$$= a+b-\tfrac{1}{2}b(\cos^2\theta_1+\cos\theta_1\cos\theta_2+\cos^2\theta_2).$$

The spread for each cause was evaluated separately, those for source and ring by calculating the amounts of Ga^{72} and heavy water enclosed between $\frac{1}{2}°$ angular intervals about the line joining the center of the source and mean circumference of the toroid; that for the detector by measuring the detection sensitivity as a function of the distance from the center of its face, with a neutron howitzer. The howitzer consisted of a gallium source enclosed in a 0.5-cm layer of heavy water which was attached to the bottom of a 35-cm long copper tube

TABLE I. Measured intensity ratios.

Measurement		Counts/min. corrected for all decays	$I_{45°}/I_{90°}$ corrected for solid angle	$I_{45°}/I_{90°}$ corrected for spread at 90°
S.R.[a] 45°	I	27,360±180	0.746±0.005	0.739±0.006
S.R. 90°	I	73,480±350		
S.R. 45°	II	23,620±260	0.748±0.007	0.740±0.007
S.R. 90°	II	63,320±400		
B.R.[b] 45°	I	85,200±450	0.817±0.004	0.809±0.005
B.R. 90°	I	104,630±550		

[a] S.R. = small ring.
[b] B.R. = big ring.

of 2-cm diameter. The tube dipped into a large tank of water, so that in all directions but the axis of the tube the neutrons were slowed down and absorbed. The ethyl iodide containers, covered in cadmium, were placed over this 2-cm opening and irradiated for an hour in each position. The three distributions were then combined, giving a curve of angular spread against the relative weight of over-all neutron efficiency. The curve derived in this manner corresponds to a single source in the $90°+\alpha$ position and *one* detector only; for both detectors two such distributions are added with their peaks symmetrically placed at angle α on either side of the average of 90°. The final distribution is used to supply the correction factor β in the expression

$$I_{90°}=(a+\beta b)$$

by evaluation of the formula,

$$I_{90°}=a+b-\tfrac{1}{2}b\{\Sigma w_\gamma[\cos^2(\gamma-\tfrac{1}{2})+\cos(\gamma-\tfrac{1}{2})\cos(\gamma+\tfrac{1}{2})+\cos^2(\gamma+\tfrac{1}{2})]/\Sigma w_\gamma\}$$
$$=a+b-\tfrac{1}{2}b[1+\cos1°(\Sigma w_\gamma\cos2\gamma/\Sigma\omega_\gamma)+\tfrac{1}{2}\cos1°+\tfrac{1}{2}\Sigma\omega_\gamma\cos2\gamma/\Sigma\omega_\gamma],$$

where w_γ is the weight of an angular spread of $\pm\frac{1}{2}°$ about the angle γ. The corrections are:

Large toroid $\beta=0.9744$;
Small toroid $\beta=0.9813$.

(3) *Scattering of neutrons by heavy water.* The uncorrected measurements overstimate the contribution of σ_m. After the measured intensities at 90° had been corrected as described above, a linear extrapolation was made from the ratios $I_{45°}/I_{90°}$ for each ring, to zero thickness of heavy water. The correction amounts to 10 percent, in agreement with calculations on the scattering of neutrons by D_2O. This is in contradiction with the results of Genevese,[2] who found no variation in $I_{90°}$ for ring thicknesses below 10 mm. It is possible that, at 90°, scattering of neutrons into his detector exactly counterbalances scattering of neutrons out of the beam. If this is so, a large variation in $I_{45°}$ would be expected. Our extrapolation of $I_{45°}/I_{90°}$ avoids this error. Meiners[3] used spheres of 15- and 10-mm diameter and also extrapolated linearly which may be in error for such large spheres.

(4) *Correction for γ-ray momentum.* The value for $I_{45°}/I_{90°}$ in the laboratory system will not be the same as the value in the center-of-mass system.

An exact calculation can be made for σ_m/σ_e from the expression[4] obtained from geometrical considerations.

$$\frac{\sigma_m}{\sigma_e}=\frac{1.5R(1-7\alpha^2/4)-0.75(1+2\alpha^2)}{1-R(1-\frac{3}{4}\alpha^2)}\cdots, \quad (3)$$

[2] F. Genevese, Phys. Rev. **76**, 1288 (1949).
[3] E. P. Meiners, Phys. Rev. **76**, 259 (1949).
[4] I. F. E. Hansson and L. Hulthén, Phys. Rev. **76**, 1163 (1949), and private communication.

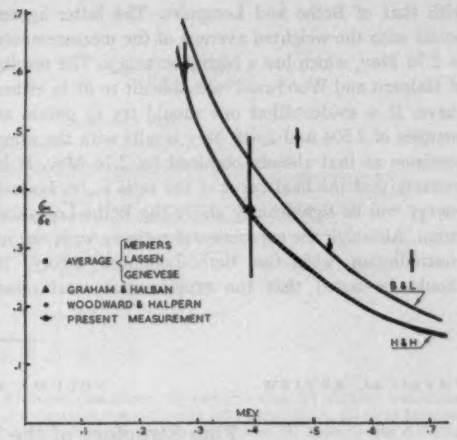

FIG. 2. The dependence of σ_m/σ_e on gamma-ray energy.

where $R=(I_{45°}+I_{135°})/2I_{90°}$, which is the measured ratio of intensities.

$$\alpha=\bar{v}/v,$$

where $\bar{v}$ is the velocity of the mass center in the laboratory system, and v is the velocity of the neutron or proton relative to the mass center. For 2.51 Mev, $\alpha=0.0774$. Table I gives the measured values. Finally σ_m/σ_e can be calculated from Eq. (3). The linearly extrapolated value of $I_{45°}/I_{90°}$ to zero D_2O thickness is $0.654\pm0.015\pm0.011$. This gives by substitution in Eq. (3) the value

$$\sigma_m/\sigma_e=0.61\pm0.04.$$

In Fig. 2 is shown the ratio σ_m/σ_e plotted against the excess energy of the γ-ray producing photo-disintegration over the binding energy of the deuteron. The experimental point at 2.62 Mev (RdTh γ-rays) is the result of Graham and Halban,[5] that at 2.758 Mev (Na^{24} γ-rays) being a weighted average from several authors.[2,3,6–8] The top curve in Fig. 2 was obtained by using the calculations of Bethe and Longmire,[9] but adjusting for the new values of the effective range in the triplet state, $(1.71\times10^{-13}$ cm), the binding energy (2.231 Mev), and the γ-ray energies (2.758, 2.618, 2.504 Mev). The other curve is from the calculations of Hansson and Hulthén.[4]

The present value of σ_m/σ_e falls very close to the Hansson and Hulthén curve, but is not in contradiction

[5] G. A. R. Graham and H. Halban, Revs. Modern Phys. **17**, 297 (1945).
[6] N. O. Lassen, Phys. Rev. **74**, 1533 (1948); **75**, 1099 (1949).
[7] W. M. Woodward and I. Halpern, Phys. Rev. **76**, 107 (1949).
[8] B. Hamermesh and A. Wattenberg, Phys. Rev. **76**, 1408 (1949).
[9] H. A. Bethe and C. Longmire, Phys. Rev. **77**, 647 (1950).

with that of Bethe and Longmire. The latter agrees better with the weighted average of the measurements at 2.76 Mev, which has a higher accuracy. The results of Halpern and Woodward[7] are difficult to fit to either curve. It is evident that one should try to obtain at energies of 2.504 and 2.618 Mev results with the same precision as that already obtained for 2.76 Mev. It is unlikely that the final curve of the ratio σ_m/σ_e against energy will lie significantly above the Bethe-Longmire curve. Although the experimental ratio σ_m/σ_e is not in contradiction with the Bethe-Longmire theory, it should be noted that the experimental total cross section[10] $\sigma_T=\sigma_m+\sigma_e$ lies well above the theoretical values.

The authors would like to express their gratitude to Mr. R. West, Isotope Division, A.E.R.E. Harwell, for arranging the special irradiations; to Mr. V. Round for his ideas and for construction of the source and toroid assembly; to the Iodine Educational Bureau for the gift of some ethyl iodide; and to Lord Cherwell for extending to us the facilities of his laboratory. We are very grateful to Professor L. Hulthén for his guidance on several occasions.

[10] G. R. Bishop, C. H. Collie, H. Halban, A. Hedgsarv, K. Siegbahn, S. DuToit, and R. Wilson, Phys. Rev. **80**, 211 (1950).

PHYSICAL REVIEW VOLUME 81, NUMBER 2 JANUARY 15, 1951

Fine Structure of the Hydrogen Atom.* Part II

WILLIS E. LAMB, JR., AND ROBERT C. RETHERFORD†
Columbia Radiation Laboratory, Columbia University, New York, New York

(Received September 29, 1950)

In the first paper of this series, the shift of the $2^2S_{\frac{1}{2}}$ level of hydrogen was determined to be 1000 Mc/sec. A new apparatus differing from the original one in details, but not in principle, has been built in order to improve the accuracy of the above result. This provides a greater yield of metastable hydrogen atoms, a more homogeneous magnetic field, and more accurate means of measurement of magnetic field and frequency. With these improvements, preliminary measurements of considerably increased accuracy have been made on both hydrogen and deuterium. The transitions observed were $2^2S_{\frac{1}{2}}$, $m=\frac{1}{2}$, to $2^2S_{\frac{1}{2}}$, $m=-\frac{1}{2}$, as well as to $2^2P_{\frac{1}{2}}$, $m=\frac{1}{2}$ and $m=-\frac{1}{2}$. The first transition permits observation of the hyperfine structure of $2^2S_{\frac{1}{2}}$, as well as an accurate calibration of magnetic field. Hyperfine structure was also resolved for the last transition in hydrogen. There was no observable difference between the level shifts for hydrogen and deuterium which may be taken as 1062±5 Mc/sec. Later papers of this series will deal with the numerous experimental and theoretical corrections necessary to obtain a level shift accurate to 1 Mc/sec.

F. NEW APPARATUS

32. Introduction

THE apparatus described[50] in Part I was improvised during the exploratory work necessary to establish the formation and detection of metastable hydrogen atoms. It was geometrically inconvenient and not well suited for precise measurements. In addition, the magnetic field was found to be excessively inhomogeneous, the magnet too small, and the pumping speed inadequate, and no cold traps were provided.

A second apparatus has been built with extensive improvements in the above respects, and in the auxiliary equipment relating to magnetic field, radio-frequency, and power, etc. With this, it has been possible to obtain results having an internal consistency close to 1 Mc/sec. In order to determine the relative positions of the $2^2S_{\frac{1}{2}}$, $2^2P_{\frac{1}{2}}$, and $2^2P_{\frac{3}{2}}$ levels, however, it is necessary to apply many experimental and theoretical corrections to the raw data. Fortunately, it is possible to establish empirically that these corrections can lead to a change of only a few megacycles per second in the results. In this paper, accordingly, we will give an account of the work up to about a year ago, when it was possible to quote a result[60] with a limit of error of ±5 Mc/sec. It is planned to devote Part III of this series to a discussion of the corrections and Part IV to a determination of the precise level shifts from the data.

33. General Features

A cross section of the apparatus in a horizontal plane is shown in Fig. 27 and has the same general features as those shown in Fig. 19 of Part I. Source of atomic hydrogen *a*, electron bombarder *c*, *d*, *e* and detector *j*, *k* are now in separately pumped chambers. The source chamber is pumped by the main pump (DPI-MC 275) and the other chambers by differential pumps (DPI-GF 20W) emptying into the source chamber. There is a

* Work supported jointly by the Signal Corps and ONR.

† Present address: Department of Electrical Engineering, University of Wisconsin, Madison, Wisconsin.

[50] Part I of this series appeared in Phys. Rev. **79**, 549 (1950). Frequent references to this paper are made. Sections, figures, equations, and footnotes of Part II are numbered consecutively after those of Part I. The designation of states by letters α, β, *a*, *b*, *c*, *d*, *e*, *f* is explained in Fig. 14.

[60] R. C. Retherford and W. E. Lamb, Jr., Phys. Rev. **75**, 1325 (1949).

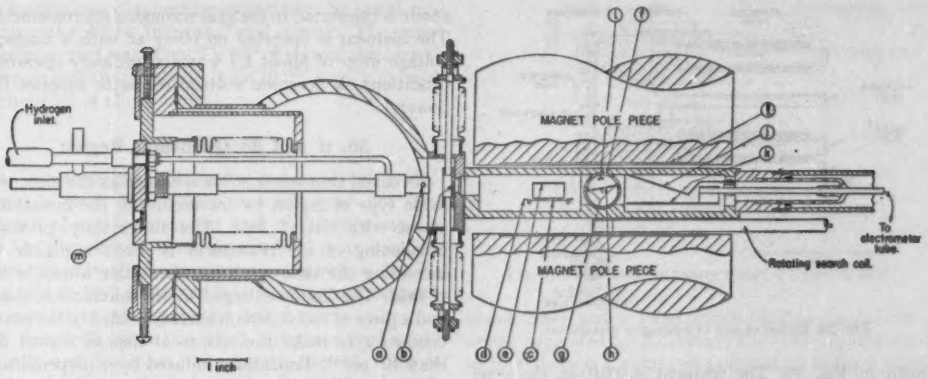

FIG. 27. Cross section of second apparatus: (*a*) tungsten oven of hydrogen dissociator, (*b*) movable slits, (*c*) electron bombarder cathode, (*d*) grid, (*e*) anode, (*f*) transmission line, (*g*) slots for passage of metastable atoms through interaction space, (*h*) plate attached to center conductor of r-f transmission line, (*i*) dc quenching electrode, (*j*) target for metastable atoms, (*k*) collector for electrons ejected from target, (*l*) pole face of magnet, (*m*) window for observation of tungsten oven temperature.

liquid nitrogen trap and baffle between each pump and chamber. The source and electron bombarder chambers are separated by slits *b*, and the electron bombarder and detector chambers by slots *g* in the rf line. The pumps are backed by a booster pump (DPI-MB 100) and by a Kinney (CVD 556) mechanical pump. Ionization gauges are mounted on the source and detector chambers; and, in addition, a Knudsen gauge (DPI-BL 1) is mounted on the source chamber. During operation the detector chamber pressure is monitored by the ionization gauge and the source chamber pressure by the Knudsen gauge. The latter pressure gives an indication of the hydrogen flow.

The electron bombarder and detector chamber and rf line are situated in a rectangular parallelopiped which fits into the magnet gap. The GF-20W pump leads come in at the bottom of this body.

Gas is admitted to the system directly from a hydrogen or deuterium tank through a reducing valve, a hot palladium tube, and a variable leak of the type described by Nier, Ney, and Inghram.[61]

The bellows allow the position of the source *a* to be adjusted for optimum signal strength and the separating slit *b* is adjustable in width and position. The rf line can be rotated to select the best angle of the slits.

34. Hydrogen Dissociator

Hydrogen atoms are produced by thermal dissociation as in Part I, and the dissociator (Fig. 28) is very similar to that shown in Fig. 20. Certain modifications have been made to obtain greater life. A separate lead for hydrogen reduces the chance of leaks at brazed joints in contact with cooling water. A heavy piece of copper was interposed between the molybdenum end and the stainless steel tube, and the size of the molybdenum was increased to $\frac{3}{4}$-in diameter stock to improve cooling.

The tungsten tube is now made from a solid rod by grinding off half of an 0.063-in. diameter rod, grinding a 1/64×1/64-in. groove down its length, and then putting two of these pieces together. A small slit is ground on one side of each piece in the cleavage plane to serve as an exit for the atoms as illustrated in the detail of Fig. 28. This tungsten tube is very much more rugged than the previous type, and usually lasts for several months of laboratory usage at a temperature of 2500°–2600°K. When properly constructed, the two halves of the tungsten tube weld together after a short time and form a true tube. Typical operating conditions are 2.31 v, 188 am, 2520°K. The power is supplied from a large transformer and a Sorensen voltage regulator.

35. Electron Bombarder

At the time this apparatus was designed, it was hoped that most of the electron bombarder troubles previously encountered, especially with the oxide-coated cathode, would be cured by the greatly increased pumping speed. Although there was some improvement, the difficulty with emission poisoning persisted, and the life of a cathode was only a few days with uninterrupted operation of all pumps. This situation was vastly improved by redesigning the electron bombarder with a tungsten wire cathode. No more trouble was encountered with emission poisoning. Despite the great reduction in emitting area, the observed signal was much more stable and ample for our purposes, except under conditions to be described in Sec. 43.

A cross section of the present electron bombarder in a horizontal plane through the filament is shown in Fig. 27 (*d*, *e*, and *c*) and an enlarged cross section in a vertical plane parallel to the magnetic field lines is

[61] Nier, Ney, and Inghram, Rev. Sci. Instr. 18, 191 (1947).

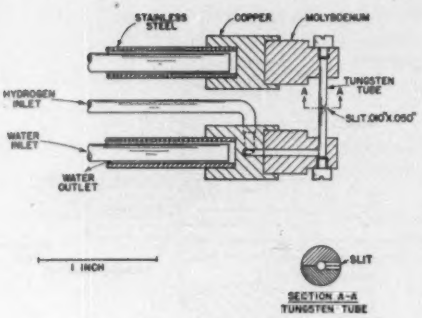

FIG. 28. Detail of end of hydrogen dissociator.

shown in Fig. 29. The filament is 0.010-in. diameter tungsten wire mounted in such a way that it is under tension at all operating temperatures. The grid wires are 0.004-in. diameter tungsten, 67 per inch, and are held at one end only to prevent buckling. The taut filament and nonbuckling grid wires permit very stable operation of the electron bombarder although the grid-filament spacing is 0.010-in. or less. This small spacing permits the control of the anode current by varying the filament temperature without encountering space charge limitation. The anode has the shape of a U and is designed to reduce depression of the potential in the region occupied by electrons. It is made of molybdenum sheet and has a width of about $\frac{5}{8}$ in., a depth of $\frac{5}{16}$ in. and a height of 0.050 in i.d.

On account of the magnetic field, the thickness of the electron beam is effectively the filament diameter, or only slightly larger. The width of the electron beam is equal to the emitting length of the filament or about a centimeter. A very adequate and helpful theory for the behavior of a thin electron beam in a metallic enclosure of this sort has been given by Haeff.[42] Heaters (not shown in the figures) are installed on the top and bottom of the anode for cleaning it while in the apparatus.

The grid is operated at ground potential, the filament at -10.8 v (7 dry cells) to center tap, while the anode is connected to the grid through a microammeter. The filament is operated on 60-cy ac with a filament voltage drop of about 1.7 v rms at ordinary operating conditions. A Sorensen voltage regulator supplies the power.

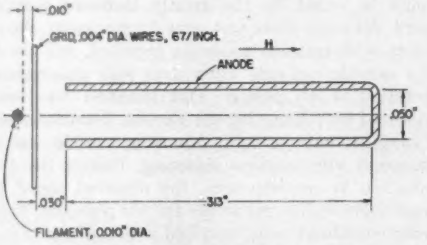

FIG. 29. Cross section of electron bombarder in plane at right angles to beam of hydrogen atoms. The U-shaped anode greatly reduces space charge in the electron beam.

[42] A. V. Haeff, Proc. Inst. Elec. Engrs. 27, 586 (1939).

36. rf and dc Quenching Region

A coaxial transmission line is chosen as the most versatile type of region for interaction of the metastable atoms with the rf field. The uncertainty principle broadening of the resonances is made negligible by increasing the time spent by metastable atoms in the rf field. The line is enlarged in the interaction space, and a piece of molybdenum sheet is welded to the center conductor to make the reciprocal time of transit less than 10^8 sec^{-1}. Transitions induced by a perpendicular component of rf electric field are thereby reduced in intensity, but can still be studied, although less favorably, as there are appreciable fringing field components in the required direction. The stream of atoms passes through slits, g, between inner and outer conductors. The transmission line enters at the top of the apparatus

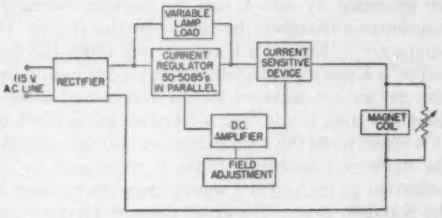

FIG. 30. Block diagram for magnet current stabilizing circuit.

and terminates at the bottom in an unmatched crystal load whose current is used to monitor the rf power. Although this arrangement has great versatility, it has the disadvantage of making it difficult to estimate the rf fields and requiring excessive rf power because of mismatch at the interaction space and at the crystal.

An auxiliary electrode, i, is placed in the interaction region to permit quenching of the metastable atoms by electrostatic fields without breaking the rf circuit. A dc voltage is applied between this electrode and the outer conductor. A potential difference of 125 v suffices to quench essentially all of the metastable atoms at the magnetic fields used here. The corresponding change in electrometer current can be used to monitor the total signal due to metastable atoms.

37. Detector

The detector consisting of tungsten target j and collector k of Fig. 27 differs from that used in the previous apparatus only in nonessential details of construction. The electrometer circuit was changed from balanced to unbalanced type without increased drift or instability. A considerable reduction in galvanometer

fluctuation was obtained by evacuating the vessel containing the FP54 tube and grid circuit. The input resistance used was about 7×10^{10} ohms and the over-all current sensitivity about 1.9×10^{-16} amp/mm with fluctuations of about 1 mm.

38. Magnet

An electromagnet with pole pieces $5\frac{1}{2}$ in. in diameter is used. The pole pieces and yoke are constructed of an electromagnet iron of the type used in the Nevis cyclotron. To make the field more homogeneous, the pole pieces are cut away as shown in Fig. 27. At a field of 1000 gauss, the field is uniform throughout the interaction space to better than $\frac{1}{2}$ gauss.

A circuit illustrated in block diagrams in Fig. 30 controls and stabilizes the magnet current. This is patterned after a similar system devised by Lentz[63] and Katz. The current sensitive device which furnishes the error signal to the dc amplifier is a G.E. 2B23 magnetically controlled diode placed in a solenoid which is energized by the magnet current. A ten-turn helically wound L & N potentiometer is used to adjust the magnetic field. Aside from quite manageable thermal drifts, this circuit holds the magnetic field current steady to one part in fifty thousand.

39. Magnetic Field Measurement

Determination of the level shifts requires knowledge of the magnetic fields used in taking resonance curves. The slopes of the frequency *versus* field curves αe and αf of Fig. 15 are about one and two megacycles per gauss respectively. Consequently, a determination of the level shift to an accuracy of 1 Mc/sec requires an absolute measurement of the magnetic field to an accuracy of 1 or $\frac{1}{2}$ gauss, respectively.

It would have been possible to make such measurements by observing nuclear induction effects in the interaction space; but this would not have been convenient because of the range of magnetic fields, from nearly zero to 4000 gauss, to be covered. Instead, a rotating search coil method was devised which serves this purpose adequately. An hysteresis-type synchronous motor drives two search coils at 30 cps, one in the field of a permanent magnet for a comparison signal and the other in the magnetic field to be measured (Fig. 31). The permanent magnet is mounted inside an iron shield on the motor supporting structure. Search coil No. 2 is shown in position in Fig. 27. The coils have an NA of about 150 cm^2, and fit in a cylinder with an over-all diameter of $\frac{1}{4}$ in. Signals from the search coils are picked up with graphalloy brushes from coil silver slip rings. Three brushes 120° apart are used on each slip ring to minimize brush noise with the brush bearing area adjusted to give low noise. Figure 31 shows the measuring circuit. The 30-cps amplifier has a gain of

[63] J. Lentz and S. Katz, Columbia Radiation Laboratory, Quarterly Report, September, 1947, p. 12.

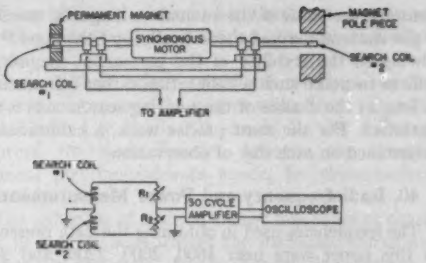

FIG. 31. Apparatus for measurement of magnetic field.

about 5000 and a band width of 5 cy, and is of a design suggested by J. Lentz.[64] The coils are connected so that there is a circulating current at balance which is obtained by observing a Lissajous figure on an oscilloscope. The connection from R_1 to the oscilloscope supplies the horizontal signal required for producing the Lissajous figure. At balance

$$R_2/R_1=\omega(NA)_2H_2/[\omega(NA)_1H_1], \tag{96}$$

or

$$H_2=\text{const}\times R_2. \tag{96a}$$

R_1 and R_2 are G.R. 5-decade resistance boxes and in Eqs. (96) include the lead and search coil resistances. For best results, the relative phase of the signals must be carefully adjusted. This is done by rotation of one of the shafts relative to the other, and requires an adjustment to about 10^{-4} radian.

This method has the advantage of independence of line frequency and stability of relative phase, and it is easily possible to make relative field measurements at a field of 1000 gauss to an accuracy of 1/50 gauss. If two separate motors are used, small erratic relative changes in phase give a great deal of trouble.

In order to make absolute field measurements, it is necessary to have a determination of the constant in Eq. (96a). This can conveniently be obtained from an observation of the sharp transitions $\alpha\beta$ discussed in Sec. 44. Except for small corrections, such as that due to motional Stark effect and incomplete Back-Goudsmit effect of hyperfine structure, the frequency required for this transition is given by the equation

$$h\nu=2(1+\alpha/2\pi)\mu_0H, \tag{97}$$

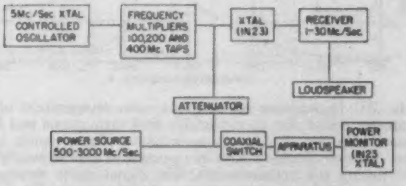

FIG. 32. Circuit for measurement of frequency.

[64] J. Lentz, private communication.

assuming the value of the anomalous magnetic moment of the electron derived theoretically by Schwinger.[65]

Owing to the stability of the permanent magnet, it suffices to make such a calibration rather infrequently as long as the chassis of the rotating search coils is not disturbed. For the most precise work, a calibration is determined on each day of observation.

40. Radiofrequency and Power Measurements

The frequencies used in obtaining the data presented in this paper were near 1600, 2000, 2200, and 2400 Mc/sec, respectively. A 2C39 signal generator was used to produce 1600 and 2000 Mc/sec, and a 2C40 the 2200 and 2400 Mc/sec, although the tube had to be pushed hard to give the required power at the latter frequency. Conventional regulated power supplies are sufficient to give adequate frequency and amplitude stability when the tubes are operated well below their ratings.

The frequency is measured by a beat frequency method as illustrated in Fig. 32, where a signal from the 5-Mc/sec crystal controlled oscillator is multiplied by electronic circuits to 100, 200, or 400 Mc/sec. One of these frequencies is multiplied again by a 1N23 crystal. If the frequency of the signal to be measured is near one of the harmonics, a communications receiver can be used to measure the difference frequency. Care must be taken to avoid one of the false beats due to images, harmonics, and extraneous signals. Nevertheless, this method is quite satisfactory and allows frequency measurements to about 0.01 Mc/sec in the range mentioned. The 5-Mc/sec crystal is standardized against Station WWV.

Rf power supplied to the apparatus is monitored by means of a 1N23 crystal at the end of the transmission line. Although the readings have only a relative significance at any one frequency, they are adequate for the purpose of correcting the data to constant rf power (Sec. 45).

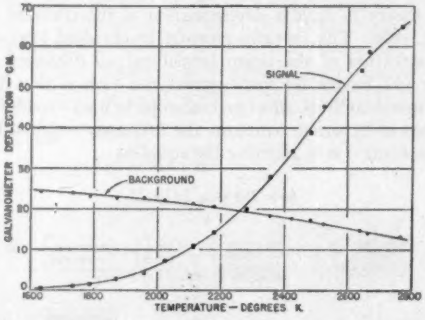

FIG. 33. Dependence on tungsten oven temperature of galvanometer signal due to metastable hydrogen atoms and background deflection due to photo-electrons. The pressure in the source chamber given by Knudsen gauge was approximately constant during the measurements. The signal curve corresponds roughly to that for an oven pressure of 10^{-3} atmos in Fig. 5.

[65] J. Schwinger, Phys. Rev. **76**, 790 (1949).

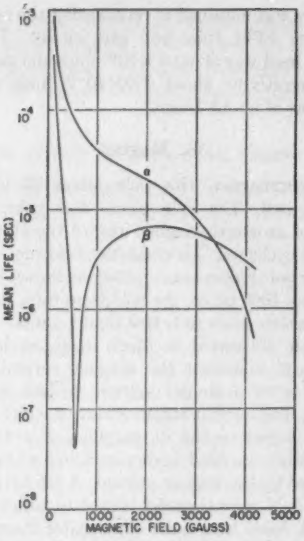

FIG. 34. Theoretical mean lives of metastable states α and β for atoms from source at 2500°K moving perpendicular to a magnetic field. The calculations assume a level shift of 1060 Mc/sec, and neglect quenching other than that due to motional electric field.

G. OPERATION OF THE NEW APPARATUS

41. General Considerations

In taking a resonance curve, typical operating conditions are: source temperature, 2550°K; bombarding voltage, 10.8 v; bombarding current, 200 μamp; gas pressure in the source chamber, 7.5×10^{-4} mm Hg for hydrogen and 5×10^{-4} mm Hg for deuterium; gas pressure in the detector chamber about 3×10^{-5} mm Hg, and some intermediate value in the bombardment chamber. Under these conditions, the signal due to metastable atoms is from 100- to 140-cm galvanometer deflection when the apparatus is considered usable. Fluctuations may amount to a few millimeters on favorable occasions.

Although larger signals can be obtained at higher gas admission rates, it was found that objectionable fluctuations in signal occur when the source chamber pressure is greater than about 8×10^{-4} mm Hg. At equal pressures, deuterium gives about 50 percent more signal than hydrogen. Consequently, although the deuterium working pressure is taken lower than for hydrogen, the signal is steadier, and the data are more accurate.

Similarly, larger signals can be obtained by elevating the temperature of the hydrogen dissociator, as can be seen from Fig. 33. The adopted temperature is one that gives long life of the tungsten tube and fairly large

signals without unduly heating the apparatus. In this figure, the curve labelled "background" is about twice as large as would be obtained at present because of some subsequent improvements in the electron gun. The curve labelled "signal" corresponds roughly to the middle curve of Fig. 5.

In contrast to behavior with the apparatus described in Part I, operation of the electron bombarder is only slightly dependent on the magnetic field when it is greater than about 50 gauss. This is presumably due to the much more homogeneous magnetic field in the present apparatus. Nevertheless, the signal due to metastable atoms is still quite dependent on the magnetic field.

As explained in Sec. 16, the motional electric field $\mathbf{E}=(\mathbf{v}/c)\times\mathbf{H}$ causes a quenching of the two metastable states α and β at different rates. The lifetimes of these states may be calculated according to Eq. (42), suitably generalized to allow for the multiplicity of competing states; and the results are shown in Fig. 34.

In addition, there may be quenching due to stray electric fields in the electron bombarder or elsewhere along the beam. These could markedly reduce the magnitude of the signal where there is near degeneracy of the $2^2S_{\frac{1}{2}}$ and $2^2P_{\frac{1}{2}}$ states, which may occur for both α- and β-states at low magnetic fields, and for state β in the vicinity of the crossing point of states β and f in Fig. 14.

Beyond this point, the beam of metastable atoms begins to contain an appreciable fraction of atoms in the lower metastable state. The actual amount is very dependent on the presence of stray electric fields, because of the near degeneracy. Complications which this imposes on the analysis of resonance curves will be considered in Parts III and IV.

42. Excitation Curves for the State $2^2S_{\frac{1}{2}}$

Excitation curves have been very instructive in the study of the relationship of electron bombarder conditions and signal. In addition, they have an intrinsic interest of their own; but unfortunately the present apparatus is not well adapted to taking good excitation curves.

The curves of Fig. 35 labeled "signal" represent the variation of the beam of metastable atoms with electron accelerating voltage, and "background" the corresponding current due to photons. Curves A are taken with the hydrogen dissociator turned on, i.e., for the atomic case, and curves B for the oven at room temperature, i.e., for the molecular case.

The apparent threshold of signal in case A is 9.3 v, which is to be compared to the expected value of 10.2 v. This discrepancy may be attributed to the combined effect of (1) thermionic energy of emission of bombarding electrons, (2) contact potential differences between the tungsten filament and molybdenum anode, (3) reduction of electron energy by space charge, (4) filament voltage drop, (5) recoil dilution factor of Eq. (22) variable with electron bombardment energy, and (6) effects due to charged insulating layers on grid and anode.

Some of these effects contribute merely a constant additive correction to the voltage scale. Thus, (1) should add about $\frac{1}{2}$ v, while (2) should be the difference between the work function between the tungsten filament and molybdenum anode, for clean surfaces $4.5-4.1=0.4$ ev.

The reduction of electron energy due to space charge will in general both distort the excitation curve and change its threshold. If the bombarding current is vanishingly small, the error disappears. In order to be able to use a finite but small current and avoid distortions, the following procedure was adopted. As the nominal energy eV_0 of the electron beam was varied, the bombarding current I was also varied so as to keep the charge density constant. Assuming small space charge, this requires that I and V_0 be related by the equation,

$$IV_0^{-\frac{1}{2}}=\text{const.} \tag{98}$$

In that case, the effective energy eV of the beam would differ by a constant amount from the nominal energy

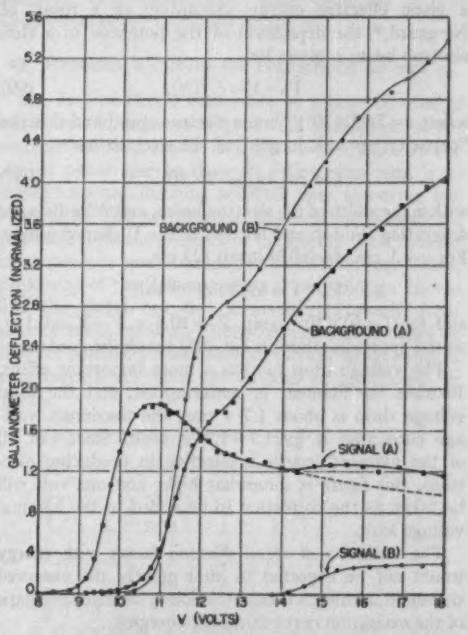

FIG. 35. Excitation curves (for deuterium) giving variations of signal and background with nominal energy of electron bombardment. Curves marked (A) were taken with tungsten oven at 2550°K, while the oven was at room temperature for those marked (B). The curve marked Signal (B) is due to the process of molecular dissociation discussed in Sec. 7, while the hump on Signal (A) starting at 14 ev corresponds to the same process occurring in the molecular gas in the bombardment chamber.

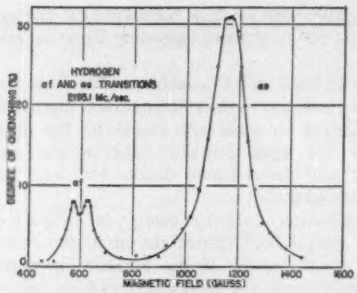

FIG. 36. Observed resonance curves for hydrogen taken at 2195.1 Mc/sec with power chosen to bring the $a\alpha$ peak to about 31 percent quenching. The hyperfine structure of the transition αf is clearly resolved, and the separation is about as expected in Sec. 17, assuming the hfs of the $2^2P_{\frac{1}{2}}$ states to be $\frac{1}{9}$ of that for $2^2S_{\frac{1}{2}}$. A more quantitative test of this ratio must await accurate curve fitting of such data to a theoretical formula.

eV_0, and effect (3) would simply give an additive constant error in the voltage scale. It is, of course, necessary to reduce the data to constant bombarding current, assuming that when the space charge is small, the signal is proportional to the bombarding current at a given effective energy. According to a result of Nergaard,[62] the depression of the potential in a thin electron beam is given by

$$V_0-V=I/(Cv), \tag{99}$$

where $v=5.93\times10^7V^{\frac{1}{2}}$ is the electron speed and C is the "capacity per unit length" of the electron beam,

$$C=2w[4\pi\cdot\tfrac{1}{2}d\cdot9\times10^{11}]^{-1}, \tag{100}$$

with w the width of the electron beam, and d the distance separating the top and bottom of the U-shaped anode. For $w=1$ cm, $d=0.050$ in$=0.127$ cm,

$$V_0-V=6\times10^3IV^{-\frac{1}{2}}\text{ volt}; \tag{101}$$

and for $I=50\times10^{-6}$ amp, $V_0=10.8$ v, $V-V_0=0.1$ v, so the approximations in Eq. (98) should be good.

The voltage drop (4) has a more important effect. Because the filament is centertapped, and the total voltage drop is about 1.7 v rms, the maximum voltage correction is $\frac{1}{2}\sqrt{2}1.7=1.2$ v peak. Since not all of the filament length is effective in producing electrons, this figure is somewhat high; and one volt will be taken as the correction to be added to the nominal voltage scale.

The variation of recoil dilution factor with energy would not be expected to alter greatly the observed threshold, although it might seriously change the shape of the excitation curve at higher energies.

With the corrections estimated above, $0.3+0.4-0.1+1.0=1.6$ ev, the observed threshold would be $9.3+1.6=10.9$ ev, which is too high by 0.7 ev, according to theory. It cannot be said whether this difference is due to errors in the above estimates, or to item (6) discussed in the next section.

In any case, the apparent threshold energy of signal (a) is low by $10.2-9.3=0.9$ ev, so that presumably the apparent threshold energy of signal (B) due to dissociation of molecules should be raised by 0.9 ev, giving $14.2+0.9=15.1$ ev in agreement with the expectations of Sec. 7. It is clear that, compared with the adopted method, the molecular dissociation method of producing metastable atoms directly gives a very unfavorable ratio of signal (B) to background (B) resulting in large fluctuations.

43. Disappearance of the Signal

It was remarked in Sec. 35 that no difficulties with emission poisoning have occurred with the tungsten cathode. However, there has still been considerable difficulty with disappearance of the beam of metastable atoms at various times. If one starts with a clean apparatus having new oil in all the pumps, a month may elapse before the signal becomes unusably small. For

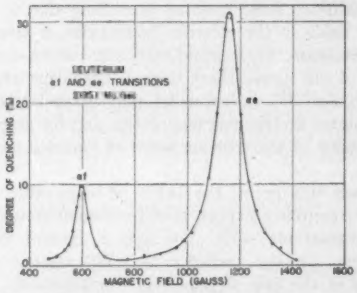

FIG. 37. Observed resonance curves for deuterium taken at 2195.1 Mc/sec with power chosen to bring $a\alpha$ peak to about 31 percent. Each peak is the composite of three unresolved peaks separated by about 9 gauss (compared to about 59 gauss for hydrogen).

a time thereafter, it is possible to regain the signal by heating the anode of the electron bombarder before observations. Subsequently, this does not suffice and it is necessary to heat the anode during the taking of data; and, finally, it becomes impossible to keep a usable signal at all. The remedy in such a situation is to clean the inside of the apparatus thoroughly and replace all of the pump oil.

If the apparatus is in a clean condition, it is observed that as the bombarding current is increased, the signal increases also until a current of about 400 μamp is reached, after which the signal rapidly decreases to a value of only a few centimeters. The background behaves similarly. When the signal has partially disappeared, as described above, the optimum current is less than 100 μamp. At this state, heating the anode will usually restore the optimum current to something like 300 μamp. At later stages this becomes impossible.

The probable explanation of this phenomenon, as already mentioned in Part I. is that the surface of the

anode becomes coated with an insulating substance which acquires a negative charge under electron bombardment. When the poisoning has reached the acute stage, brownish-black deposits become visible on the anode in the region where the electron beam strikes. In some cases, the shadow of the grid wires can be seen on the anode. As a result of the action of the crossed magnetic field and electric field resulting from space charge repulsion, the shadow is somewhat skewed. The fact that deposits form in this way is taken as evidence that they are produced by breakdown under electron bombardment of an organic layer on the anode surface. The substance causing these deposits has not been determined; but it is probably a decomposition product of pump oil vapor, apiezon wax, or solvent vapor which is produced by electron bombardment, reaction with atomic hydrogen, or thermal decomposition. The formation of such visible deposits under electron bombardment is well known[66] to workers in electronics, although they are mostly reported at energies of 12 ev or more, whereas only 10.8 ev is used here. Of course, many of the difficulties experienced with the electron bombarder are peculiar to the low energy required for work just above the critical potential of hydrogen.

Another effect noted has been a varying contact potential of about 0 to 0.6 ev in the rf line between the electrostatic quenching electrode and the center conductor. This phenomenon will be discussed in a later paper in another connection. Visible deposits accumulate on the electrodes of the rf line and on the detector target j. These are in part related to the deposits in the electron bombarder and also to material evaporated directly from the hydrogen dissociator, possibly an oxide of tungsten.

H. OBSERVATIONS

44. Transitions $\alpha\beta$ $2^2S_{\frac{1}{2}}$ $(m=1/2\rightarrow m=-1/2)$

As mentioned in Sec. 16 and illustrated in Fig. 34, the lower $2^2S_{\frac{1}{2}}$ state β is much less metastable than the upper state α for a considerable range of magnetic fields. Consequently, it should there be possible to observe transitions from α to β, since atoms in the β-state do not reach the detector. The corresponding resonance curves should have a width determined by the reciprocal life of the β-state, and as this is considerably longer than the life of the nonmetastable states such as e and f, the $\alpha\beta$-resonances should be much narrower than those for transitions αe, αf, etc. Even at the crossing point of levels β and e, the life of state β is 4×10^{-8} sec according to Fig. 34, so that the half-width ought to be $1/(2\pi\tau)$ or 4 Mc/sec instead of 100 Mc/sec as for transitions to the more highly damped states.

Since the frequency of the $\alpha\beta$-transition is closely given by Eq. (97), a very convenient method for determination of magnetic field in the apparatus should be available.

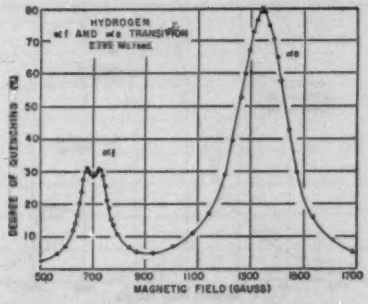

FIG. 38. Observed resonance curves for hydrogen taken at 2395 Mc/sec with power chosen to bring αf peaks to about 31 percent and thereby considerably saturating the αe peak.

Such resonances were sought with the previous apparatus, but, owing to smallness of signal and lack of constancy and homogeneity of the magnetic field, could not be observed. In the present apparatus, the sharp transitions $\alpha\beta$ are easily observable and are used for magnetic field calibration. Some examples of the $\alpha\beta$-resonances are discussed in Sec. 47.

45. Resonance Curves for Transitions αe and αf

The data of Part I were taken at a large number of frequencies in order to map out the entire field of observable transitions such as is shown in Fig. 25. In the present paper and in those to follow, the plan is to concentrate on obtaining accurate data at only a few frequencies. This procedure is based on the assumption that aside from the presence of the shift of the $2^2S_{\frac{1}{2}}$ state and a possible small change in the doublet separation, the theory of the Zeeman effect is well enough known that the shifts can be calculated accurately from measurements made at a few frequencies. In order to allow for possible deviations from theory, measurements are presented for both the αf and αe transitions of Fig. 15.

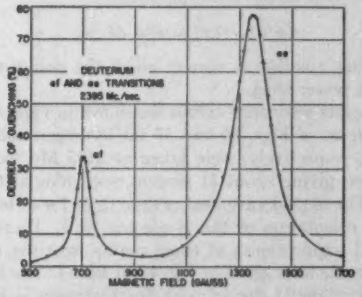

FIG. 39. Observed resonance curves for deuterium taken at 2395 Mc/sec with power chosen to bring αf peak to about 31 percent and thereby considerably saturating the αe peak.

[66] C. H. Bachman, *Techniques in Experimental Electronics* (John Wiley and Sons, Inc., New York, 1948).

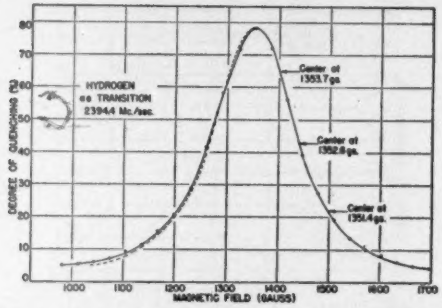

FIG. 40. Detail of $\alpha\varepsilon$ peak (similar to that shown in Fig. 38) broadened by application of excessive rf power. The dotted curve on the left represents the mirror image of the right side of the resonance curve about an arbitrary magnetic field ordinate. The lack of symmetry is presumably due to causes listed in Sec. 45, but in any case is so small that a fairly reliable level shift can be obtained without elaborate corrections.

On account of the variability of signal with magnetic field discussed in Sec. 41, the resonance curves would be considerably distorted if variations in signal were not taken into account. Consequently, at each magnetic field setting, the signal is measured by quenching essentially all of the metastable atoms by the application of an electric field (Sec. 36). The degree of quenching by the radiofrequency field is then expressed as the percentage of the total possible quenching. This procedure also minimizes distortions due to changes in signal produced by other causes such as changing pressure, bombardment current, drift of hydrogen dissociator temperature, detector efficiency, etc. These quantities are usually only slowly variable, so that the process is quite effective. Changes in rf power are corrected by measuring the change in the degree of quenching corresponding to a small change in crystal current. For small changes in power this is proportional to the change in power and gives a slope $d\phi/dI_x$, where ϕ is the percentage of quenching and I_x is the crystal current. This measurement is usually made at some standard point where the quenching is ϕ_0. Then at some different ϕ, one has, at least for small quenching

$$d\phi/dI_x=(\phi/\phi_0)(d\phi/dI_x)_0. \qquad (102)$$

It is thus possible to correct all of the points to the same rf power level.

Complete resonance curves are shown in Figs. 36–39. The curves of Figs. 36 and 37 for hydrogen and deuterium, respectively, were taken at 2195 Mc/sec with rf powers giving about 31 percent quenching at the $\alpha\varepsilon$ peak. The αf peaks are weaker than those for $\alpha\varepsilon$ because of the orientation of the rf electric field. There is a marked improvement of these results over the nearly comparable ones given in Fig. 15 of Part I. The hyperfine structure of the αf peak for hydrogen is clearly resolved as it should be, and the deuterium resonances are noticeably sharper than those for hydrogen owing to the reduced hyperfine structure for deuterium. In Figs. 38 and 39 are shown corresponding results obtained at 2395 Mc/sec with increased rf power so as to bring the peaks αf to 31 percent. The other resonances $\alpha\varepsilon$ are then somewhat broadened owing to rf saturation effects discussed in Sec. 13.

Some general remarks are required on the possible methods of taking data to determine the resonance magnetic fields. Essentially three methods come into consideration here: (1) determination of the magnetic fields for which the quenching is maximum by a study of the neighborhood of the maxima only, (2) measurements made on the sides of the resonances near points of inflection in order to determine a midpoint, and (3) a fit of an entire resonance curve to a theoretical resonance curve containing the resonance fields as parameters to be determined.

The third method is soundest in principle, but in practice necessitates taking an enormous amount of data which would require greater long term stability of the apparatus than has been obtained. An advantage of this method would be that all kinds of shifts and asymmetries could (or should) be included in the theoretical formula.

The first two methods will give erroneous results if there are uncorrected asymmetries and shifts. Both methods are in error equally if shifts are present, while the first errs less in the case of asymmetries. On the other hand, a really precise determination of the level shifts requires that all asymmetries be understood and allowed for, so that the intrinsically higher accuracy of determination of the midpoint by method (2) has led to its selection over method (1).

Among the factors which can lead to asymmetries and shifts, besides those basic to radiation theory, are the following: (1) overlap of nearby resonances, (2) variation of the matrix element for the transition as the magnetic field is varied (due to breakup of L–S coupling), (3) incomplete Back-Goudsmit effect for the hyperfine components, (4) differential quenching of the hyperfine components by motional electric fields, (5) curvature of the Zeeman energy curves, (6) Stark effect, and (7) presence in the beam of a small fraction of atoms in the β-state. A lengthy program of calculations and measurements is required to allow for all such sources of error, and will form the subject of Parts III and IV. For present purposes, however, it suffices to take a more purely empirical point of view. The resonances are actually highly symmetrical. This has been tested in Fig. 40, in which an excessive amount of power has been used to further broaden the $\alpha\varepsilon$ resonance, and thereby increase the chance to observe an asymmetry. Despite this, the centers of the curve obtained at different levels of quenching agree quite closely with each other, and also with the center obtained when using much less power.

A further empirical check was made by comparing the centers for the different resonances $\alpha\varepsilon$ and αf at

2195 and 2395 Mc/sec. On the basis of these experimental tests, and supported by simple estimates of the effect of the errors listed above, we conclude that no corrections are needed to obtain a result with a limit of error of ±5 Mc/sec from the treatment of the data given below.

46. Data and Results

We now turn to a discussion of some data analyzed by the second method above. These measurements were made on runs of generally high caliber, but certain refinements to be described in the later papers were not included. One defect was that the field calibration made at 2395 Mc/sec was not corrected for motional Stark effect. In order to minimize the effects of uncontrolled changes in search coil calibration, crystal sensitivity, etc., points were taken on alternate sides of the curve in a zigzag fashion, so that the center of the curve could be determined at various levels of the curve. This was done graphically on a large scale plot by reflecting one side about a line of ordinates near the center of the peak. Five or six pairs of points were usually selected along the sides of the curve. Each pair of points permits a determination of the shift. The shift is determined on the basis of the theory given in Sec. 15, using in particular, Eqs. (39)–(41).

In the case of the αf peaks, a rough correction for overlap by the $\alpha\varepsilon$ resonance was made.

The results for the $2^2S_{\frac{1}{2}}$ level shift in hydrogen from these runs are presented in the form of a histogram in Fig. 41, in which the nominal internal scatter and discrepancy between results for $\alpha\varepsilon$ and αf give results ranging from 1061 to 1065 Mc/sec. It should be recalled that in using the formulas of Sec. 15, no account is taken of the anomalous magnetic moment of the electron, reduced mass effects, and other corrections mentioned in Sec. 45. In addition, there is a possible error of a megacycle or so in using the $\alpha\beta$-resonance at 2395 Mc/sec for magnetic field calibration without correction for Stark effect. With these possibilities for error in mind, the value for the shift was reported[80] in January, 1949, as 1062±5 Mc/sec with confidence that the finally obtained value would not lie outside this range. Results for deuterium lie in the same range.

47. Observation of Sharp Resonances

As explained in Sec. 39, the sharp transitions $\alpha\beta$ were used to calibrate the magnetic field. These have a markedly different character depending on whether or not the level β is separated from competing levels by their radiation width. An example of the first type, taken at 1995 Mc/sec, is given in Fig. 42, and some of the second type are shown in Figs. 43 and 44. The resonances of the second type are superposed on the broad resonance $\alpha\varepsilon$, as shown in Fig. 45.

One of the sharp resonances is observed for each hyperfine state: two for hydrogen and three for deuterium. A peculiar feature of these transitions is that the quenching is *reduced* when the resonance condition $\omega=\omega_{\alpha\beta}$ is satisfied. In the first type of resonance, this reduction occurs at the minimum on the right of the peak. The maximum is located essentially at the field to be expected if motional Stark effect shifting of the levels is considered. In the second type, the quenching of each hyperfine component is also reduced to a small value when $\omega=\omega_{\alpha\beta}$. The width of the resonance corresponds to the lifetime of the β-state at the crossing point of β and ε as explained in Sec. 44.

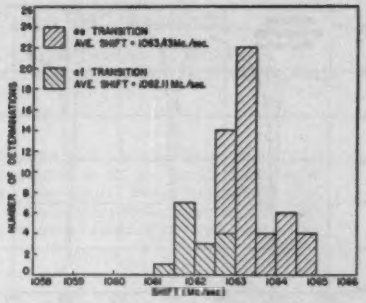

FIG. 41. Histogram showing distribution of results obtained from 61 determinations of $2^2S_{\frac{1}{2}}$ level shift. The difference between results obtained from $\alpha\varepsilon$ and αf would presumably be removed if the corrections for the errors listed in Sec. 45 were applied. The finally determined level shift may be expected to lie in the range 1062±5 Mc/sec.

The theory of these transitions leads to an understanding of the above features. It is rather complicated and will be postponed to Part III. However, one can obtain a physical picture of the process in terms of an electrical analogy with the problem of two coupled resonant circuits shown in Fig. 46, consisting of a primary with parameters L_1, C_1, R_1 and a lossless secondary L_2, C_2 coupled to the first by a mutual in-

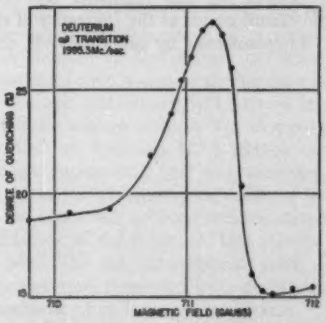

FIG. 42. Example of $\alpha\beta$-transition taken at 1995.3 Mc/sec. The peak shown is the center one of three observed with deuterium separated by about 9 gauss. For hydrogen, two peaks separated by about 63 gauss would be observed. The resonance fields for transitions αf and $\alpha\varepsilon$ at this frequency would be 490 and 970 gauss, respectively.

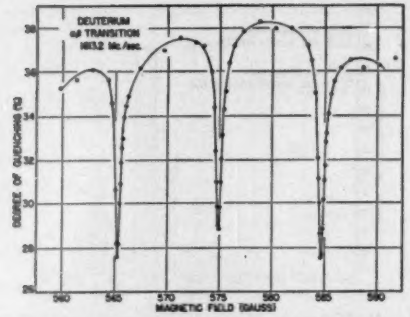

FIG. 43. Sharp resonance curves for transitions $\alpha\beta$ in deuterium at a frequency 1613.2 Mc/sec, for which the broad resonance $\alpha\epsilon$ overlaps the sharp resonance $\alpha\beta$.

ductance M. The resonance frequency $\omega_1=(L_1C_1)^{-\frac{1}{2}}$ of the first circuit corresponds to the transition from α to ϵ, and radiation damping is represented by the

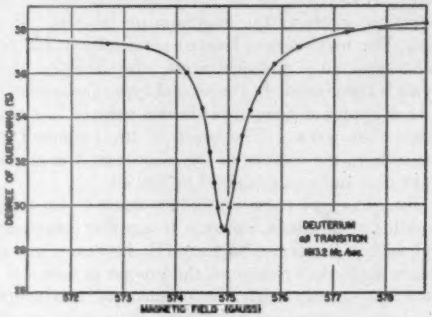

FIG. 44. Detail of the central peak shown in Fig. 43 obtained in another measurement.

resistive element R_1. The resonance $\omega_2=(L_2C_2)^{-\frac{1}{2}}$ of the second circuit occurs at the frequency of the transition $\alpha\beta$. As represented by setting $R_2=0$, the β-state

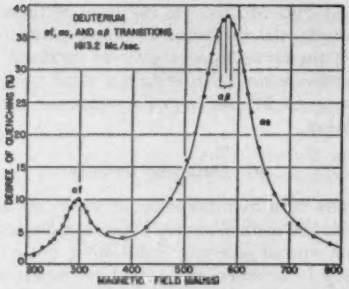

FIG. 45. Panoramic view of resonances αf and $\alpha\epsilon$ in deuterium at 1613.2 Mc/sec showing location and magnitude of sharp resonances of Fig. 43.

does not decay directly. There is no direct coupling from α to β (except by relatively unimportant magnetic dipole radiation), while in the electrical circuit analogy, the second resonator is excited only indirectly by its mutual inductive coupling to the first circuit. In the atomic case, the motional Stark effect provides the coupling between β and ϵ. The input admittance of such a circuit (and hence the power absorbed) has a

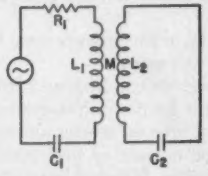

FIG. 46. Electrical circuit analog for interference of transitions $\alpha\epsilon$ and $\alpha\beta$.

broad resonance for $\omega=\omega_{\alpha\epsilon}$, while in a very narrow band about $\omega=\omega_{\alpha\beta}$ the reflected impedance of the lossless secondary is large and reduces the response of the network.

The authors have benefited greatly from the cooperation and assistance of Messrs. N. T. Williams, P. F. Yergin, and J. J. Lentz as well as others mentioned in Part I.

Excited State of Be^9 from the $B^{11}(d, \alpha)Be^{9*}$ Reaction†

D. M. Van Patter, A. Sperduto, K. Huang, E. N. Strait, and W. W. Buechner
Department of Physics and Laboratory for Nuclear Science and Engineering, Massachusetts Institute of Technology, Cambridge, Massachusetts

(Received September 25, 1950)

The alpha-particles from boron bombarded by 1.51-Mev deuterons have been investigated with a magnetic spectrometer. Two groups of alpha-particles have been assigned to the reaction $B^{11}(d,\alpha)Be^9$ with Q-values of 8.018 ± 0.007 and 5.596 ± 0.006 Mev, indicating a virtual state of Be^9 at 2.422 ± 0.005 Mev. The previously unreported alpha-particle group corresponding to this excited state had a natural half-width of less than 7 kev. No additional alpha-groups corresponding to excited states of Be^9 were observed for excitations of Be^9 from 0 to 5.0 Mev.

I. INTRODUCTION

At present, only the one excited state of Be^9 at 2.4 Mev is well-established experimentally. This virtual state was first discovered by Davis and Hafner[1] from the inelastic scattering of 4.5- and 7.1-Mev protons. They reported the level at 2.41 Mev with a half-width of less than 100 kev and found no indication of other levels in Be^9 up to 5.4-Mev excitation. This result has been confirmed recently by Rhoderick,[2] who found only one level at 2.39 ± 0.05 Mev from the inelastic scattering of 4.7-Mev protons.

Guth and Mullin[3] have made a theoretical analysis of the experimental cross section of the $Be^9(\gamma,n)Be^8$ reaction which has a pronounced maximum about 100 kev above the reaction threshold. Their results indicated that the $Be^9(\gamma,n)Be^8$ yield can be accounted for by a bound S-state about 100 kev below threshold (at 1.5-Mev excitation of Be^9).

Mullin and Guth[4] have also analyzed the angular distribution of neutrons from this reaction. They find good agreement with the assumption that the ground state of Be^9 is a doublet ^2P-state and that the level at 2.4 Mev is an unresolved ^2D-state.

It is possible to examine the excited states of Be^9 from an investigation of the $B^{11}(d,\alpha)Be^{9*}$ reaction. The ground-state $B^{11}(d,\alpha)Be^9$ alpha-particles have been observed by Cockcroft and Lewis[5] at 0.55-Mev bombarding energy, and they reported[6] a Q-value of 8.13 ± 0.12 Mev. In their results, there was no indication of an alpha-group corresponding to the 2.4-Mev excited state of Be^9; however, if such an alpha-group were much weaker than the ground-state group, it probably would not have been detected. Using 0.55-Mev deuterons and an enriched B^{11} target, Smith and Murrell[7] found the ground-state $B^{11}(d,\alpha)Be^9$ alpha-group to have a range of 4.6 cm. They observed another alpha-group of 2.8-cm range, which was of about equal intensity from both the enriched B^{11} and B^{10} targets and which Smith and Murrell attributed to carbon contamination from the reaction $C^{13}(d,\alpha)B^{11}$. An alpha-group corresponding to the 2.4-Mev excited state of Be^9 would have coincided with the 2.8-cm alpha-group. However, it should have been six times more intense from the enriched B^{11} target (97 percent B^{11}) as from the enriched B^{10} target (15 percent B^{11}).

Since there had been no report in the literature of any alpha-particle groups from the $B^{11}(d,\alpha)Be^{9*}$ reaction corresponding to excited states of Be^9, it was decided to study this reaction. This has been done using a magnetic spectrometer of high resolution in order to investigate both the states of Be^9 and the possibility that some of the states may be closely spaced doublets.

II. APPARATUS AND EXPERIMENTAL PROCEDURE

The apparatus and experimental procedure were essentially the same as those described in a previous paper,[8] except for some improvements in stabilization and in the analysis of results. A beam of deuterons in the energy range of 1.2 to 1.8 Mev was obtained from an electrostatic accelerator. This beam was then defined in space, direction, and momentum by means of a deflecting magnet and slit arrangement. The target was located between the pole faces of a large annular magnet. A fraction of the charged particles emitted from the target at right angles to the incident beam was deflected through 180 degrees and focused in the uniform field of the annular magnet. The charged particles were recorded on Eastman NTA plates, each plate being exposed successively and each covering a range of 10 percent in energy. During the course of the experiments to be described, an improvement was made in the stabilization of the magnetic field of the annular magnet. With the slit arrangement used, charged-particle groups were measured with an energy spread at half-maximum of as low as 0.21 percent.

Measurements of the magnetic field and radii of curvature of the charged particles determined the momentum of the particles. The magnetic field was

† This work has been assisted by the joint program of the ONR and AEC.

[1] K. E. Davis and E. M. Hafner, Phys. Rev. **73**, 1473 (1948).
[2] E. H. Rhoderick, Proc. Roy. Soc. **A201**, 348 (1950).
[3] E. Guth and C. J. Mullin, Phys. Rev. **76**, 234 (1949).
[4] C. J. Mullin and E. Guth, Phys. Rev. **76**, 682 (1949).
[5] J. D. Cockcroft and W. B. Lewis, Proc. Roy. Soc. **A154**, 246 (1936).
[6] Corrected by M. S. Livingston and H. A. Bethe, Rev. Mod. Phys. **9**, 3 (1937).
[7] C. L. Smith and E. B. M. Murrell, Proc. Cambridge Phil. Soc. **35**, 298 (1939).
[8] Buechner, Strait, Stergiopoulos, and Sperduto, Phys. Rev. **74**, 1569 (1948).

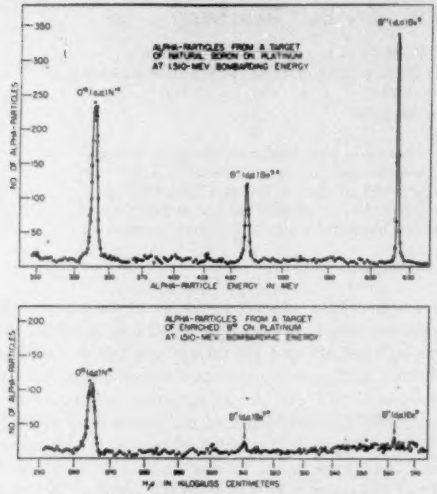
ALPHA-PARTICLES FROM A TARGET OF NATURAL BORON ON PLATINUM AT 1.510-MEV BOMBARDING ENERGY
NO. OF ALPHA-PARTICLES
ALPHA-PARTICLE ENERGY IN MEV
ALPHA-PARTICLES FROM A TARGET OF ENRICHED B10 ON PLATINUM AT 1.510-MEV BOMBARDING ENERGY
NO. OF ALPHA-PARTICLES
MILLIGAUSS CENTIMETERS

FIG. 1. Alpha-particle spectrum from natural boron and enriched B^{10} targets in the energy interval 3.0 to 6.7 Mev. The incident deuteron energy is 1.510 Mev.

measured by a balance-type fluxmeter which was described in a previous paper.[9] The calibration constant for the fluxmeter was determined from the measured radius of curvature of polonium alpha-particles in the magnetic field of the annular magnet. The value of Hr for polonium alpha-particles used as an absolute standard was computed from Briggs' value[10] for the Hr of RaC′ alpha-particles and from Lewis and Bowden's value[11] for the ratio of velocities of RaC′ alpha-particles and polonium alpha-particles. From these measurements, the value of Hr for polonium alphas is 3.3159×10^5 gauss-cm (absolute emu), accurate to 1 part in 5000.

The radii of curvature of the charged-particle groups were determined by measuring with a microscope the track-density distribution on the nuclear-track plates relative to a fixed index mark. The background track density for a given peak was determined at points sufficiently far removed so that the contribution from the reaction peak was negligible. In the case where several peaks were only partly resolved, an analytic resolution of the peaks was made taking into account the peak shape.

The incident deuteron energy was determined from the measurement of the energy of deuteron groups scattered elastically from targets consisting of a thin layer of natural boron evaporated onto a thin film of Formvar. It was found possible to resolve the deuteron groups scattered from B^{10}, B^{11}, C^{13}, and O^{16} nuclei contained in the target and backing.

As will be described in a forthcoming paper, the determination of Q-values was made more precise by an accurate measurement of the median angle of observation as a function of the magnetic field of the annular magnet. This angle varied from $(\frac{1}{2}\pi - 0.0029)$ radians at zero field to $(\frac{1}{2}\pi - 0.0015)$ radians at maximum field. The appropriate corrections were applied to the observed Q-values calculated for a 90-degree angle of observation. In addition, a correction was made for the finite solid angle of observation as well as for the approximation of using the nonrelativistic Q-equation for calculation.

The targets used for the initial survey of the $B^{11}(d,\alpha)Be^9$ reaction were prepared by the evaporation of metallic boron from a carbon crucible onto platinum backings 0.010-in. thick. Both natural boron and boron enriched to 96 percent B^{10} (obtained from Oak Ridge) were used. These targets had an effective thickness for the $B^{11}(d,\alpha)Be^9$ ground-state reaction of less than 13 kev. In addition, targets were made consisting of a thin layer of natural boron evaporated onto a thin film of Formvar. From these latter targets, it was possible to observe deuteron groups elastically scattered from the B^{10} and B^{11} nuclei in the natural boron.

III. RESULTS

A survey was first made of the alpha-particle groups with energies between 3.0 and 6.7 Mev emitted from the natural boron and enriched B^{10} targets on platinum when bombarded by 1.51-Mev deuterons. The results of this survey are shown in Fig. 1. The survey was not extended to lower energy alpha-particles because of the presence of deuterons scattered from platinum. The yields of the alpha-particles from the two targets have been normalized to the same beam bombardment and area counted on the nuclear-track plates. The relative thickness of the two targets was determined from a comparison of the yield of the $B^{10}(d,p)B^{11}$ protons from each target. When corrected for the isotopic abundance of B^{10} in the two targets, the thicknesses of the natural boron and enriched B^{10} targets were found to be equal to within 10 percent.

In Fig. 1, the prominent alpha-group from the natural boron target (81 percent B^{11}) at 6.37 Mev was assigned to the ground-state reaction $B^{11}(d,\alpha)Be^9$. This assignment was made on the basis of the following evidence. From the enriched B^{10} target (four percent B^{11}), a weak alpha-group at this position could barely be distinguished from the continuous distribution of alpha-particles from the reaction $B^{10}(d,\alpha)2\alpha$. The yield of this group increased by a factor of approximately 25 when the natural boron target was substituted for the enriched B^{10} target. Since there is a difference of a factor of 20 in the relative abundances of B^{11} in the two targets, this result is in agreement with the assumption that the 6.37-Mev alpha-group originates from the B^{11}.

[9] Buechner, Strait, Sperduto, and Malm, Phys. Rev. **76**, 1543 (1949).
[10] G. H. Briggs, Proc. Roy. Soc. **A157**, 183 (1936).
[11] W. B. Lewis and B. V. Bowden, Proc. Roy. Soc. **A145**, 250 (1934).

The preliminary Q-value for this group was found to be 8.02 Mev, in close agreement with the value of 8.03 Mev calculated from masses[12] and in fair agreement with the previous experimental value[6] of 8.13±0.12 Mev. The above results indicate that the assignment of this alpha-group to the $B^{11}(d,\alpha)Be^9$ reaction is correct.

A second prominent alpha-group of 4.69-Mev energy was observed from the natural boron target. A weak group of the same energy was observed from the enriched B^{10} target, the yield being about a factor of 10 smaller. If this group were assigned to the $B^{11}(d,\alpha)Be^{9*}$ reaction, it would correspond to an excited state of Be^9 at 2.42 Mev, agreeing with the position of an excited state already established by inelastic proton scattering. However, the ratio of the yields from the two targets was a factor of 2 smaller than expected. In addition, at 1.51-Mev bombarding energy, the position of this 4.69-Mev alpha-group agreed within a few kev with the position of the alpha-group from the $C^{13}(d,\alpha)B^{11}$ reaction with a Q-value of 5.16 Mev. Prior to these experiments, the $C^{13}(d,\alpha)B^{11}$ group had been observed from other targets subjected to long bombardments and had evidently originated from a surface contamination of natural carbon which contains 1.1 percent of C^{13}. It was therefore necessary to eliminate the possibility that the observed alpha-group from the natural boron target was entirely due to the $C^{13}(d,\alpha)B^{11}$ reaction.

To accomplish this purpose, the relative intensities of the $C^{13}(d,\alpha)B^{11}$ and $C^{13}(d,p)C^{14}$ groups were measured at 1.811-Mev bombarding energy from a target of $KC^{13}N$, enriched to 60 percent C^{13}. The ratio of the yields was found to be 5:1. Then, the ratio of the possible $B^{11}(d,\alpha)Be^{9*}$ alpha-group and the $C^{13}(d,p)C^{14}$ proton group was measured from the natural boron target at the same bombarding energy. This ratio was found to be 62:1. This indicated that only eight percent of the alpha-group from the natural boron target could be attributed to the $C^{13}(d,\alpha)B^{11}$ reaction, and the remainder was evidently due to the $B^{11}(d,\alpha)Be^{9*}$ reaction. This also explained the fact that the ratio of the yield of this group from the natural boron and the enriched B^{10} targets was lower than predicted from the abundance of B^{11} in the two targets, inasmuch as part of the weak group from the enriched B^{10} target was evidently due to the $C^{13}(d,\alpha)B^{11}$ reaction.

In the above work, the energy of the $B^{11}(d,\alpha)Be^{9*}$ alpha-group was measured at 1.812-Mev bombarding energy. Combining this result with the original measurements made at 1.510-Mev bombarding energy, it was possible to determine the shift in energy of this alpha-group for a change in deuteron bombarding energy of 302±3 kev. At an angle of observation of 90 degrees, the change of energy of a disintegration particle, ΔE_{out}, due to a change of bombarding energy, ΔE_{in}, is given by:

$$\Delta E_{out}=[(M_{res}-M_{in})/(M_{res}+M_{out})]\Delta E_{in},$$

where M_{res} is the mass of residual nucleus, M_{in} is the mass of bombarding particle, and M_{out} is the mass of disintegration particle.

In the case of the $B^{11}(d,\alpha)Be^{9*}$ reaction, the energy of an alpha-group would change 162±2 kev for a change in bombarding energy of 302±3 kev. For the $C^{13}(d,\alpha)B^{11}$ reaction, the expected change would be 181±2 kev. The observed change in the energy of the alpha-group was 161±4 kev, in agreement with the assignment of this group to the $B^{11}(d,\alpha)Be^{9*}$ reaction. In fact, this result ruled out any target mass other than 11, since a target mass of 10 or 12 would have given an alpha-energy shift of 151 or 172 kev, both of which are outside the limit of error on the measurement. These results indicated that the 4.69-Mev alpha-group from the natural boron target could be assigned unambiguously to the $B^{11}(d,\alpha)Be^{9*}$ reaction.

In the light of this evidence, the results of Smith and Murrell[7] were reexamined. Using enriched B^{11} (97 percent B^{11}) and B^{10} (15 percent B^{11}) targets, they found a 2.8-cm alpha-group that they assigned to carbon contamination on the basis that the yield of this group was about the same from the two targets. The possibility cannot be ruled out that part of the group which they observed was actually due to the $B^{11}(d,\alpha)Be^{9*}$ reaction, but it is evident that they also observed particles from the $C^{13}(d,\alpha)B^{11}$ reaction.

The remaining prominent alpha-group in Fig. 1 of energy 3.42 Mev from the natural boron target was only a factor of 2.5 more intense than the corresponding group from the enriched B^{10} target. This factor was considerably smaller than the factor of 20 for the relative amounts of B^{11} in the two targets and indicated that this alpha-group should not be attributed to the $B^{11}(d,\alpha)Be^{9*}$ reaction. In addition, the Q-value of this group, if assigned to the reaction $O^{16}(d,\alpha)N^{14}$, agreed within 10 kev with the Q-values measured for the same reaction when a target of Formvar (containing oxygen but no boron) was used. However, it was still necessary to rule out the possibility that part of this group could come from the $B^{11}(d,\alpha)Be^{9*}$ reaction. In order to do this, the following experiments were made:

(1) The ratio of intensities of the $O^{16}(d,\alpha)N^{14}$ and $O^{16}(d,p)O^{17}$ groups from a thin Formvar target was measured at 1.510-Mev bombarding energy and was found to be 0.8:1. Then, the ratio of the 3.42-Mev alpha-group and the $O^{16}(d,p)O^{17}$ proton group from the natural boron target was measured at the same bombarding energy and was found to be 1:1. These ratios were considered in agreement with the accuracy of measurement.

(2) The relative yield of this prominent alpha-group from the natural boron target at 1.81- and 1.51-Mev bombarding energy was measured as 3.0:1. The same relative yield was measured from the enriched B^{10}

[12] W. F. Hornyak and T. Lauritsen, Revs. Modern Phys. 20, 191 (1948).

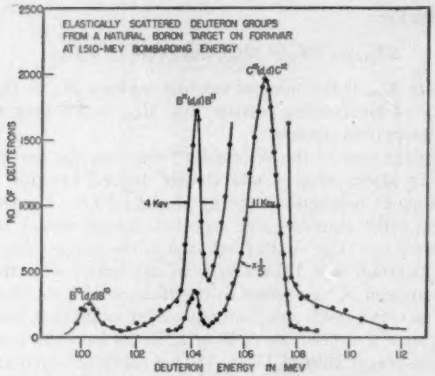

FIG. 2. Spectrum of elastically scattered deuteron groups from a natural boron target on Formvar at 1.510-Mev bombarding energy.

target (four percent B^{11}) and was found to be 3.7:1, in agreement within the error of measurement.

(3) Precise measurements were made on the energy shift of the prominent alpha-group from the natural boron target when the deuteron bombarding energy was changed from 1.203 to 1.811 Mev. The expected change in energy for a $B^{11}(d,\alpha)Be^{9*}$ alpha-group would be 327 ± 2 kev for a change of 608 ± 3 kev in bombarding energy, while that for a $O^{16}(d,\alpha)N^{14}$ group would be 405 ± 2 kev. The observed change in energy was 403 ± 3 kev, in agreement with the assignment of this group to the $O^{16}(d,\alpha)N^{14}$ reaction.

In addition, the observation of the $O^{16}(d,\alpha)N^{14}$ group at a bombarding energy of 1.203 Mev precluded the possibility that a small $B^{11}(d,\alpha)Be^{9*}$ alpha-group might be hidden under the $O^{16}(d,\alpha)N^{14}$ group at 1.510-Mev bombarding energy. From 1.510- to 1.203-Mev bombarding energy, the $O^{16}(d,\alpha)N^{14}$ group shifted 40 kev more than would a possible $B^{11}(d,\alpha)Be^{9*}$ group. Since the half-width of the $O^{16}(d,\alpha)N^{14}$ group was 40 kev at 1.510-Mev bombarding energy, a small $B^{11}(d,\alpha)Be^{9*}$ group would have been resolved from the $O^{16}(d,\alpha)N^{14}$ group at 1.203-Mev bombarding energy.

The above results indicated that the assignment of the 3.42-Mev alpha-group to the reaction $O^{16}(d,\alpha)N^{14}$ was correct. It was concluded that both boron targets contained an appreciable amount of oxygen, the natural boron target containing the greater amount.

Except for the $O^{16}(d,\alpha)N^{14}$ and the two $B^{11}(d,\alpha)Be^{9}$ groups, no other definite group of alpha-particles appeared in the survey shown in Fig. 1. The background between peaks observed from the natural boron target could be accounted for partially by the continuous distribution of alpha-particles from the $B^{10}(d,\alpha)2\alpha$ reaction from the 19 percent of B^{10} in the target. The remainder of the background is considered to come from a certain amount of alpha-particle contamination on the nuclear-track plates, which cannot be completely eliminated from the counting of the track-density distributions. However, this survey indicated that there were no additional alpha-groups with an intensity greater than 0.1 the intensity of the $B^{11}(d,\alpha)Be^{9*}$ group corresponding to the 2.42-Mev level in Be^{9}. The region of excitation of Be^{9} covered in this survey was 0 to 5.0 Mev.

The original survey of the $B^{11}(d,\alpha)Be^{9}$ reaction indicated that the alpha-group corresponding to the 2.42-Mev level of Be^{9} had a half-width of less than 30 kev. However, the contribution of target thickness to this half-width was somewhat uncertain since the elastically scattered deuterons from the platinum backing of the target obscured the deuteron group scattered from the boron. To eliminate this difficulty, a target was prepared by evaporating natural boron onto a thin film of Formvar (containing oxygen and carbon). The spectrum of elastically scattered 1.510-Mev deuterons from this target is shown in Fig. 2. The deuteron groups scattered from B^{10}, B^{11}, and C^{12} are clearly resolved. The intensities of the B^{10} and B^{11} groups are very closely in the ratio of their isotopic abundance in natural boron.

The deuteron group elastically scattered from B^{11} had an observed half-width of 4.6 kev. To calculate the target thickness for the $B^{11}(d,d)B^{11}$ reaction, it was first necessary to subtract the energy spreads caused by the finite solid angle of observation and the geometry of the slit arrangement. As a result, the target thickness was calculated to be 2.8 kev for the $B^{11}(d,d)B^{11}$ reaction and 4.5 kev for the $B^{11}(d,\alpha)Be^{9*}$ reaction.

The $B^{11}(d,\alpha)Be^{9*}$ alpha-group observed from the same target at 1.510-Mev bombarding energy is shown in Fig. 3. This alpha-group had an observed half-width of 14.8 kev. Correcting this energy spread for the finite angle of observation, the half-width was reduced to 11.4 kev. Before an upper limit for the natural half-width of this group could be made, an estimate was required of the energy spread due to the distribution of beam on the target and the aberration of the 180-degree focusing action of the annular magnet. With the improved stabilization of the annular magnet, the narrowest half-width observed from a reaction where the target thickness was negligible had an energy spread of 0.20 percent after correction for the finite solid angle. Most of this spread could be attributed to the distribution of bombarding deuterons on the target. This distribution had a half-width of 0.6 mm, resulting in an energy spread of 0.16 percent.

The above energy spread of 0.20 percent would contribute 9.2 kev to the half-width of the $B^{11}(d,\alpha)Be^{9*}$ peak. Subtraction of this energy spread and the contribution due to target thickness left an upper limit of 5 kev for the natural half-width of the $B^{11}(d,\alpha)Be^{9*}$ alpha-particle group. The upper limit of the natural half-width estimated in this way is probably determined by instrumental factors.

The targets used for the original survey of the

$B^{11}(d,\alpha)Be^9$ reaction had been subjected to long beam bombardments. From previous experience, it had been found that Q-values calculated for (d,α) reactions from such targets were often of the order of 20 kev too low because of a thick surface layer of carbon that evidently increased with bombardment. In order to eliminate this effect, the Q-values for the two $B^{11}(d,\alpha)$ alpha-particle groups were measured from freshly prepared targets that had not been previously bombarded. The Q-values were calculated to be 8.018 ± 0.007 and 5.596 ± 0.006 Mev, respectively, corresponding to the ground state of Be^9 and an excited state at 2.422 ± 0.005 Mev. Both of these Q-values are an average of two independent measurements which agreed to better than 7 kev. The corrections previously described have been applied to these Q-values, the total corrections being -4.7 and -4.1 kev, respectively. The major part of these corrections, about 80 percent, came from the small deviation from 90 degrees of the median angle of observation. The probable error on this correction was only one-sixth of the correction itself.

The magnetic spectrometer used for these experiments was not designed for the accurate measurement of relative intensities of various particle groups. In most cases, the groups to be compared were recorded on different nuclear-track plates, and it was necessary to assume that the experimental conditions had not changed. However, it was found that the yield of a given particle group from the same target can usually be reproduced to better than a factor of 2. The observation of the deuteron group scattered elastically from the B^{11} nuclei of the natural boron target, as shown in Fig. 3, permitted a comparison of the yield of the $B^{11}(d,d)B^{11}$ process with the yields of the two $B^{11}(d,\alpha)Be^9$ groups. At 1.510-Mev bombarding energy the observed relative intensities of these groups were as follows:

$$B^{11}(d,\alpha)Be^9 : B^{11}(d,\alpha)Be^{9*} : B^{11}(d,d)B^{11} = 1.0 : 0.6 : 12.$$

These relative intensities have reproduced several times to better than 20 percent.

In addition, the elastic scattering of both protons and deuterons from B^{10} was observed. At 1.510-Mev bombarding energy, the observed relative intensities of the various scattering processes were:

$$B^{11}(d,d)B^{11} : B^{10}(d,d)B^{10} : B^{10}(p,p)B^{10} = 1.0 : 1.1 : 1.8.$$

These values cannot be considered to be reliable to better than a factor of 2. If one assumes Rutherford scattering for 1.510-Mev protons scattered from B^{10} at a laboratory angle of 90 degrees, it is possible to estimate the differential cross section for the $B^{10}(p,p)B^{10}$ process as 57 millibarns per atom per steradian. After applying a correction for the solid angle of observation in center-of-mass coordinates, the differential cross sections for the $B^{11}(d,\alpha)Be^9$ and $B^{11}(d,\alpha)Be^{9*}$ reactions are calculated to be 2.6 and 1.6 millibarns per atom per steradian. The accuracy of the differential cross sections calculated by this method cannot be stated, since the validity of

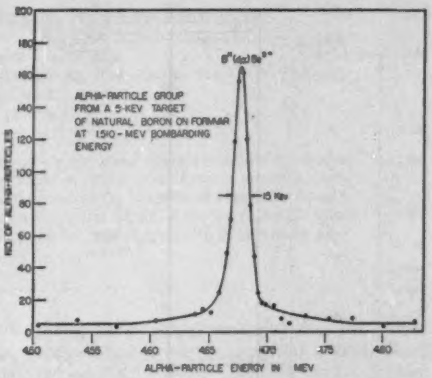

FIG. 3. $B^{11}(d,\alpha)Be^{9*}$ alpha-particle group observed from a 5-kev natural boron target on Formvar.

assuming Rutherford scattering is not known. It is probable that this assumption may be considerably in error, but it provides a convenient way of expressing the observed intensities.

IV. CONCLUSIONS

The results of this investigation indicate that a previously unreported $B^{11}(d,\alpha)Be^{9*}$ alpha-particle group has been observed, corresponding to an excited state of Be^9 at 2.422 ± 0.005 Mev. The reason that this group was not previously reported is probably because of its close proximity to the alpha-particles from the reaction $C^{13}(d,\alpha)B^{11}$. The position of this excited state is in agreement with the values of 2.41 Mev[1] and 2.39 ± 0.05 Mev[2] previously reported from inelastic proton scattering. The differential cross section for this alpha-particle group is of the order of 2 millibarns, of the same magnitude as the differential cross section of 3 millibarns reported by Davis and Hafner[1] for the inelastic scattering of 4.5- and 7.1-Mev protons leading to the same excited level.

No indication has been found to indicate that other states of Be^9 from 0 to 5 Mev are excited by the $B^{11}(d,\alpha)Be^{9*}$ reaction. This result is in accord with the results of Davis and Hafner[1] from inelastic proton scattering. Recently, the inelastic scattering from beryllium of 14-Mev deuterons has been investigated by the M.I.T. cyclotron group.[13] Only one inelastic deuteron group was found, corresponding to an excited state of Be^9 at 2.4 ± 0.3 Mev, with no indication of other excited states from 0 to 5 Mev. There is therefore no evidence from these investigations that any other state of Be^9 from 0 to 5 Mev, except the 2.42-Mev state, is excited by the $Be^9(p,p')$, $Be^9(d,d')$, and $B^{11}(d,\alpha)$ reactions with an intensity greater than 0.1 to 0.2 the intensity of the 2.42-Mev excited state. The above results are

[13] Preliminary measurements, M. I. T. Cyclotron Group.

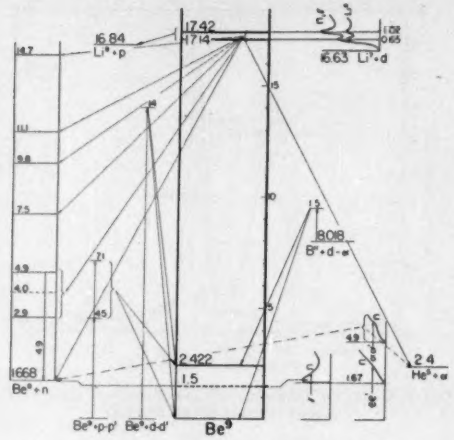

FIG. 4. Energy-level diagram for Be^9. Energies in Mev.

included in the energy-level diagram for Be^9, shown in Fig. 4.

As has been mentioned, it has been proposed that the ground state and the 2.4-Mev excited state of Be^9 may be doublets. The observed half-widths of the $B^{11}(d,\alpha)$ alpha-groups, corresponding to these two states of Be^9, were 20 and 15 kev, respectively. Neither group showed any indication of doublet structure. Analysis of these results indicates an upper limit of 12 and 7 kev for the spacing of possible doublets in the ground state and 2.42-Mev excited state of Be^9, assuming the doublet members to be of about equal intensity.

The upper limit of the half-width of the $B^{11}(d,\alpha)Be^{9*}$ alpha-particle group was calculated to be about 5 kev, corresponding to an upper limit of 7 kev for the natural half-width of the 2.42-Mev excited state of Be^9. This is considerably smaller than the 100-kev upper limit reported by Davis and Hafner.[1] This excited state is virtual, being 0.75 Mev above the threshold for neutron emission. The narrow half-width of this level indicates that neutron emission is improbable and that the state may decay mainly by the emission of gamma-radiation. This result may account for the fact that the 2.42-Mev excited state of Be^9 has not been observed from the $Be^9(\gamma,n)Be^8$ reaction.

We are indebted to Mrs. Cecilia Bryant, Mrs. Hester Sperduto, and Mr. W. Tripp for their assistance in measuring the track-density distributions of the nuclear track plates.

High Energy Cosmic-Ray Showers in Nuclear Emulsions*

L. S. OSBORNE
Physics Department and Laboratory for Nuclear Science and Engineering, Massachusetts Institute of Technology, Cambridge, Massachusetts

(Received August 14, 1950)

A detailed and statistical study of high energy events in nuclear emulsions exposed at high altitudes has given some information on a model to describe the showers found in cosmic rays. There is evidence shown that shower multiplicity increases with primary energy. Differences in the behavior of events from heavy and light nucleus collisions are described. From multiplicity and angular spread of the tracks in individual events, arguments are presented to support a pluromultiple model for meson production in high energy collisions with a nucleus.

I. INTRODUCTION

THE study of cosmic rays by various methods has revealed the occurrence of nuclear interactions wherein many secondary particles of very high energies are ejected, apparently from the collision of an incoming particle with some nucleus. These secondary particles are emitted more or less collimated in a direction opposite to the incoming particle (if such is visible). In some instances the secondary particles have been identified as mesons.[1–4] With the evidence for meson production from nuclear collisions obtained with the cyclotron at Berkeley,[5] it seems reasonable that these high energy showers involve the production of mesons. The development of very sensitive nuclear photographic emulsions has made possible the recording of these high energy showers and the detection of all charged particles, incoming and emitted.[6]

The purpose of this experiment is to study such events from a statistical basis and in detail to provide information for a satisfactory model to explain these events.

II. EXPERIMENTAL PROCEDURE

Eastman NTB3 photographic plates were used in the experiment. The plates were exposed on balloon flights carried out by the Cosmic Ray group of Brookhaven National Laboratory. The data were acquired from four flights at three different geomagnetic latitudes, 31°, 48°, and 57°. In all these flights the balloons ascended to an altitude of about 90,000 feet (15 g/cm² of air) and remained there between four and six hours. The rise time was about 2 hours, the descent 1 hour. The plates were mounted so that the vertical was included in the plane of the emulsion. There was no appreciable material placed over them.

The plates were scanned and all nuclear events recorded. The tracks in a star were further classified by their specific ionization (grain count) into the following sets corresponding to energy ranges of a singly charged particle:

"Minimum"—energy >0.5 mc².
"Near minimum"—energy >0.1 mc², <0.5 mc².
"Medium"—energy <0.1 mc².
"Heavy"—specific ionization greater than that of a singly charged particle of any energy.

Additional measurements were made on stars which showed high minimum track multiplicity. A microscope provided with a tilting stage was used to measure the direction angles of the tracks with respect to the vertical and the plane of the emulsion; the tilting stage allowed easy location and measurements on each minimum ionizing track. The angle with respect to the emulsion plane was corrected for the emulsion shrinkage during development. When a long near-minimum track was found, a scattering measurement was made to determine the mass of the particle. The heavy tracks were examined to determine their charge. If these tracks ended in the emulsion, it was possible to use the methods suggested by Bradt and Peters.[7] When the track left the emulsion, it was possible to establish the minimum charge it could have by comparison with tracks of known Z.

III. STATISTICAL ANALYSIS OF ALL STARS

By adding the total recognizable charge, Z min, carried away by low energy particles (heavy and medium tracks) one obtains an estimate of nuclear charge "boiled off" from the residual excited nucleus. If one examines the stars with 4 or more emitted minimum tracks, it appears that the values obtained for Z min fall into two groups, large and small Z min, as shown in the histogram, Fig. 1. The emulsion of the plates is composed of elements of high and low A as shown[8] in Table I. It is reasonable to suppose that the large or small "boiled-off" charge is an indication of a collision with a high A or low A nucleus; this conclusion assumes that we must have charge production in the light nucleus events. This agrees with similar

* Supported by the joint program of the ONR and AEC.
[1] E. Hayward, Phys. Rev. 72, 937 (1947).
[2] Rochester, Butler, and Runkoron, Nature 159, 227 (1947).
[3] G. D. Rochester, Revs. Modern Phys. 21, 20 (1949).
[4] O. Piccioni, Phys. Rev. 77, 1 (1950); 77, 6 (1950).
[5] E. Gardner and C. M. G. Lattes, Science 107, 270 (1948).
[6] R. W. Berriman, Nature 161, 432 (1948); 162, 992 (1948). R. H. Herz, Phys. Rev. 75, 478 (1949).
[7] H. L. Bradt and B. Peters, Phys. Rev. 74, 511 (1948).
[8] J. H. Webb, Phys. Rev. 74, 511 (1948).

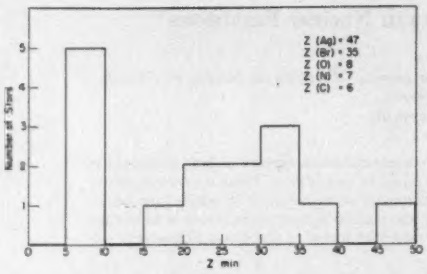

FIG. 1. Histogram of the total charge carried by nonrelativistic particles in stars which show a cone of minimum ionizing particles.

results obtained by Harding[9] and by the Brookhaven group.[10] We obtain a ratio for the number of heavy to light nucleus events with 4 or more emitted minimum tracks of 2.8 (36 to 13). This compares with a total geometrical cross-section ratio of 2.5 expected from the composition of the emulsion. This agreement could be only approximately good, since events of 4 or more minimum tracks could be initiated by incoming particles of different energy ranges in heavy and light nuclei. If we examine events with less than 4 minimum tracks, it is not always possible to judge an event as the product of a light or heavy nucleus collision.

In stars showing collimation of secondary particles, it is possible to determine the existence of an initiating relativistic charged particle. For the stars with no collimation, we have adopted the convention of classifying them as initiated by a relativistic charged particle if a track of minimum ionization is seen in the upper hemisphere.

In Table II we have classified all the stars found in our plates at three latitudes. A comparison of the plates exposed at Cuba with those of the other flights shows a relative depletion in the classes of stars with 4 or less minimum tracks. We can explain this observation if we assume that stars of multiplicities less than about 5 are initiated by protons of energy less than that of the magnetic cutoff at Cuba (8 Bev). This same effect is possibly shown by comparison of the Pennsylvania and Minnesota plates; in this case a multiplicity of about unity corresponds to the cutoff in Pennsylvania. This evidence indicates that the higher energy primaries produce in general a high multiplicity of outgoing minimum tracks. If we take the primary energy cutoff in the vertical direction at 30° geomagnetic latitude as computed by Lemaître and Vallarta[11] at 8 Bev, we conclude that showers with greater than 5 relativistic particles are initiated by primaries of greater than 8 Bev. These data show qualitative agreement with the results of other observers.[10,12]

[9] J. B. Harding, Nature **163**, 440 (1949).
[10] Salant, Hornbostel, Fisk, and Smith, Phys. Rev. **79**, 184 (1950).
[11] G. Lemaître and M. S. Vallarta, Phys. Rev. **50**, 493 (1936).
[12] Camerini, Coor, Davies, Fowler, Lock, Muirhead, and Tobin, Phil. Mag. **40**, 1073 (1949).

IV. ANALYSIS OF VERY HIGH ENERGY SHOWERS

This section presents the details and final results of an experiment previously reported.[13] We have selected 16 of the highest multiplicity showers, 6 from the light nucleus collisions and 10 from heavy nucleus collisions, for analysis.

The tracks are plotted on an angular coordinate system representing the surface of a sphere whose center is the star. Each track is represented on the plot by its point of emergence from the sphere. By using the celluloid plot made in the same way, one can measure directly the angle between any two tracks. Two such plots are shown in Fig. 2, for both a heavy and light nucleus collision. For each of these events we have found the mean latitude and longitude angle for the emitted minimum tracks; this point is the "center of gravity" of the points representing the minimum tracks on the plots. We define the "shower axis" as that direction from the star represented by this point. This direction will not necessarily be the extrapolated direction of the incoming particle; however, the convention allows consistent treatment of events with and without visible incoming tracks.

We have measured the angle, ψ, which each track in the star makes with the shower axis. From these data we have also computed the average angle, $\bar{\psi}$, for the minimum and near-minimum tracks for each event. The values of $\bar{\psi}$ obtained if we had defined the shower axis as the direction of the incoming particle, wherever possible, agree with those computed, within 10 percent (except for $H1$ where there is doubt that the backward-directed minimum track is indeed an incoming particle). This result is to be expected, since these two axes are separated by an angle sufficiently less than $\bar{\psi}$, and a small change in the position of the axis has only a second-order effect on the value of $\bar{\psi}$. A general idea of the angular divergences of these tracks is given by Fig. 3, where we have plotted in a histogram the superimposed angular distributions from all heavy and light nucleus showers. The plot for the heavy and medium tracks illustrates their spherical symmetry, thus leading to the explanation that they are "boiled-off" particles from a residual excited nucleus. In 4 of the light nucleus events there is a pronounced cylindrical asymmetry in the distribution of minimum tracks about the shower axis. The degree of this asymmetry is measured by

TABLE I. Composition of the nuclear emulsions.

Element	Z	A	Percent by weight	Percentage of total nuclear geometric cross section
Ag	47	107	47	38
Br	35	80	34	30.5
C	6	12	8.5	14.5
N	7	14	3.1	5
O	8	16	4.8	7.5
H	1	1	1.2	4.5

[13] Feld, Lebow, and Osborne, Phys. Rev. **77**, 731 (1950).

finding the average component of $\bar{\psi}$, $\bar{\psi}_{max}$, along the major axis of the distribution and $\bar{\psi}_{min}$ along the minor axis. The ratio, $\bar{\psi}_{max}/\bar{\psi}_{min}$, has been computed for these 4 events. The data on each event are presented in Table III.

Eight "near-minimum" tracks were long enough to allow scattering measurements. These measurements were accurate enough to detect the scattering of a non-relativistic particle of 80 Mev or below. Thus, if a near minimum track ($0.1<E/mc^2<0.5$) shows definite scattering, its mass must be less than 800 Mev/C^2. Of the 8 tracks measured, 7 showed no scattering, and one gave a mass measurement of 150 Mev±50 Mev/C^2.

Calculation on a Nucleon-Nucleon Meson-Producing Collision Model

To interpret these data we have computed the expected angular distribution if we assume the simple picture of a nucleon-nucleon collision producing mesons which come off in the center-of-mass system of the two nucleons with a total energy, ϵ, and with an angular distribution given by some even power of $\sin\theta$ or $\cos\theta$. We assume also that all the energy available in the center-of-mass system is used to produce mesons which enables us to compute the maximum multiplicity, M, for a given collision.

TABLE II. Statistical survey of all events found in the nuclear emulsions for various geomagnetic latitudes.

Table IIa
Cuba (lat. 31°) 6.0 c.c. hours of exposed emulsion

Incoming particle	Struck nucleus	Number of outgoing minimum tracks ≥10	5–9	4	3	2	1	0
	heavy	3	2	0				
Minimum	light	0	2	0				
	total	3	4	0	1	4	3	9
	heavy	0	0	0				
Other	light	2	0	1				
	total	2	0	1	4	2	9	50
Total		5	4	1	5	6	12	59

4 π-meson events

Table IIb
Pennsylvania (lat. 48°) 3.6 c.c. hours of exposed emulsion

Incoming particle	Struck nucleus	Number of outgoing minimum tracks ≥10	5–9	4	3	2	1	0
	heavy	1	2	3				
Minimum	light	0	1	1				
	total	1	3	4	4	11	10	14
	heavy	1	1	1				
Other	light	0	0	0				
	total	1	1	1	2	4	10	63
Total		2	4	5	6	15	20	77

3 π-meson events

Table IIc
Minnesota (lat. 57°) 10.8 c.c. hours of exposed emulsion

Incoming particle	Struck nucleus	Number of outgoing minimum tracks ≥10	5–9	4	3	2	1	0
	heavy	3	3	6				
Minimum	light	1	0	2				
	total	4	3	8	12	21	54	65
	heavy	1	4	5				
Other	light	0	2	1				
	total	1	6	6	19	23	54	158
Total		5	9	14	31	44	108	223

16 π-meson events

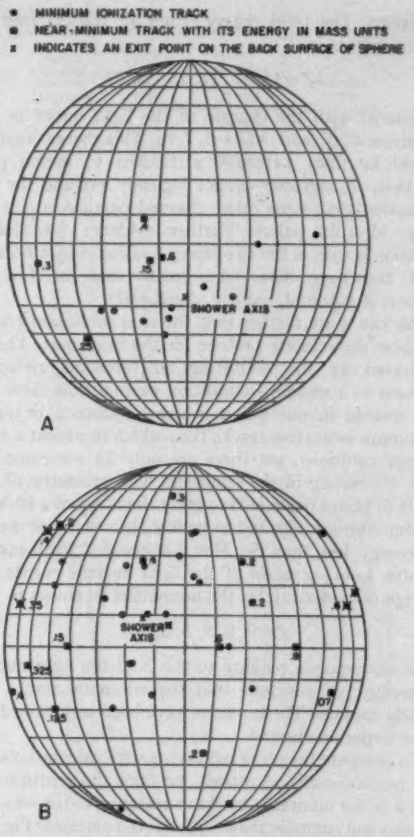

FIG. 2. Shown here for comparison are two typical spherical plots of a light (Fig. A) and heavy (Fig. B) nucleus shower. Figure 2A shows the typical conical asymmetry exhibited by the cone of minimum ionizing particles in 4 of the 6 light nucleus showers.

From these assumptions we calculate $\bar{\psi}$ for the emitted mesons in the laboratory system. The details of the computation are given in the Appendix. In addition, a computation assuming a spectrum, $d\epsilon/\epsilon$, with spherical symmetry was made. The results are plotted in Fig. 4 for various values of meson energy in the center-of-mass system and spherical symmetry as a plot of $\bar{\psi}$ *versus* M. It was found that $\bar{\psi}$ is relatively insensitive to an assumed asymmetry of the type $\cos^{2n}\theta$ or $\sin^{2n}\theta$ (~5 percent for $n=1$). It is also evident from the plotted curves that the results are changed little by the assumption on meson energy.

V. INTERPRETATION OF HIGH ENERGY SHOWERS

The evidence that we are indeed observing meson production comes from an analysis of the light nucleus

collisions. The total charge (from all tracks) emitted in the 6 stars is

$$Z=11, 13, 17, 15, 20, 22,$$

compared with the charges of the light nuclei in the emulsion C, N, and O ($Z=6, 7, 8$). This charge creation would be most naturally attributed to meson production, though one cannot logically exclude the explanation that some other charged particle is created (say, electron pairs). Further evidence for charge creation is seen in the two heavy nucleus events $H9$ and $H11$; the charge observed is greater than the Z of the highest Z material, namely, Ag($Z=47$).

We can state further that the near-minimum tracks in these showers are protons for the most part. This is indicated by the scattering measurement giving 7 protons to 1 meson. In addition we find that there are 156 events in our plates which produce 2 or more minimum ionization tracks (i.e., which represent a high energy collision), yet there are only 23 π-mesons (+ and −) ending in the emulsion. The geometry of the stack of plates represents roughly the range of a 50-Mev meson. Statistically, then, one finds less than one meson of energy less than 50 Mev for every 7 high energy events. Looking again at the light nucleus events the charge carried away by the nonminimum tracks is

$$Z=9, 6, 8, 5, 5, 10.$$

This corresponds roughly to the Z of the light nuclei. Therefore, we conclude that the minimum tracks are mostly mesons. These results have been ascertained by other experimenters.[3,4]

To compare the observed events with calculations for the nucleon-collision model, we take the multiplicity and $\bar{\psi}$ of the minimum tracks as referring to the emitted mesons and compare these with our calculations (Fig. 4). We assume in this comparison that the mesons, if produced by one encounter, are not scattered by additional collisions in the nucleus. The plot points out:

(1) The angular dispersion of relativistic tracks decreases in general with multiplicity.

(2) The events in light nuclei are not inconsistent with a single collision model.

(3) The heavy nucleus events cannot be described by this model. $\bar{\psi}$ is larger by a factor of about 2 from the computed value. This disagreement is difficult to reconcile by other assumptions about the energy and angular distribution of mesons in the center-of-mass system. A less inelastic collision aggravates the disagreement. It has been computed that if all the mesons came off so as to give the maximum angle in the laboratory system, the results would be just satisfied; but this is at the expense of eliminating front to back symmetry in the center-of-mass system. Of the two heavy nucleus collisions giving the lowest $\bar{\psi}$, one is initiated by an α-particle, the other is too close to the emulsion surface to identify the initiating particle. It is not unreasonable to expect that an α-particle initiated shower of the same multiplicity would give a narrower cone of emitted particles.

We conclude that these events cannot be described with a single collision model, particularly if we take into account further indirect evidence:

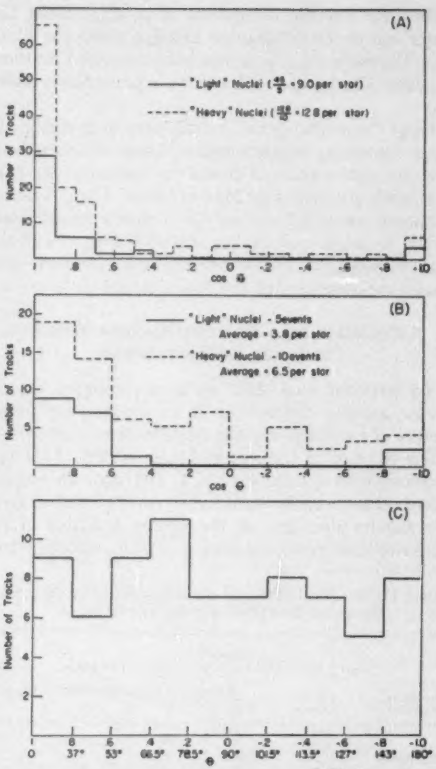

FIG. 3. These histograms show the superimposed angular distribution for all stars in the three categories: minimum ($E>0.5$ mc²) (Fig. A), near minimum (0.1 mc²$<E<0.5$ mc²) (Fig. B), and heavy and medium tracks (Fig. C). These are shown separately for the heavy and light nucleus events to show the greater collimation for the latter. The spherical symmetry of the heavy and medium tracks lends credence to their identification as "boiled-off" fragments.

(1) The average multiplicity of minimum tracks is greater for heavy than light nucleus events.

Heavy nuclei (9 showers):	12.6
Light nuclei (6 showers):	9.1.

This indicates that the extra nuclear material of the heavy nuclei is involved in the process though not in the ratio of nuclear diameters, which is about 2 to 1.

(2) The large number of near-minimum tracks (mostly protons) with forward collimation indicates multiple nucleon interactions.

The other extreme model of successive collisions through the nucleus each producing one meson seems unsatisfactory. A measure of the maximum number of collisions is given by the number of particles which do *not* appear as "boiled-off" particles. We assume a like number of neutrons as protons in this category and take the average A for the light nuclei to be 14. This number, 14 minus $2Z$ min, corresponding to the maxi-

TABLE III. Summary of data on each shower.

Star	Minimum tracks number	Minimum tracks $\bar{\psi}$	Near-minimum tracks Number	Near-minimum tracks $\bar{\psi}$	Heavy tracks Number	Heavy tracks Z_{min}	Z_{min} including near-min tracks	Total observable charge	Incoming minimum track?	$\pi-\psi$ for incoming track	$\bar{\psi}_{max}/\bar{\psi}_{min}$
*L*1	6	34°	2	30°	4	4	6	12	Yes	10°	4.2
*L*2	7	35	3	85	4	4	7	14	Yes	10°	
*L*3	9	17.5	5	43	2	4	9	18	Maybe[a]		
*L*4	10	16.5	4	68	3	3	7	17	No		2.5
*L*5	10	20	5	31	5	5	9	19	No		4.5
*L*6	13	17	5	7	4	4	9	22	No		1.7
*H*1	5	45	9	65	14	27	36	41	Yes?	65°	
*H*2	5	40	10	54	18	26	36	41	Yes	15°	
*H*3	9	44	6	72	20	28	34	43	Yes	20°	
*H*4	10	43	8	74	17	24	32	42	No		
*H*5	11	35.5	1	(137)	11	15	16	27	Yes	20°	
*H*6	12	32	6	38	15	18	24	36	Yes	18°	
*H*7	12	22	6	59	11	17	23	35	α-particle	9°	
*H*8	13	37	8	87	17	19	27	40	No		
*H*9	14	9	5	50	22	43	48	62	Maybe		
*H*10	15	32	4	55	11	22	26	41	Yes	19°	
*H*11	20	25.5	19	65	15	19	38	58	Yes	10°	

[a] The doubt occurs because of the star being near an emulsion surface.

mum number of nucleons ejected in some collision, is for the 6 light nucleus cases: 6, 6, 6, 8, 4, and 6. On the other hand, the amount of excess charge produced is 3, 5, 10, 10, 13, and 15. The last four cases indicate that more than one meson is produced per nucleon involved in the collision. In all this we have not considered the additional possibility that neutral mesons are produced as well.

As mentioned above, we have found a definite asymmetry in the cones of minimum tracks associated with light nucleus collision. To interpret this asymmetry we should inquire whether it is statistically significant. We may imagine the points of emergence of the minimum tracks on the sphere plots as points on a plane with a center at the shower axis. We define the "major axis" of the distribution as the line passing through the shower axis and the point farthest from the center. If cylindrical symmetry were expected, of the remaining points, there should be an equal population in the two quadrants bisected by the major axis, as in the two bisected by the minor axis. We have used this analysis on the six events, including the points from the two stars showing no asymmetry, and find 34 points in the major axis quadrants to 15 for the minor axis. By the laws of probability the chance that this or greater asymmetry is a statistical misfortune of a symmetric distribution is 2.5 percent. These observations could be explained by assuming the cone to be produced by subsidiary cones of a primary plus secondary collision; however, our data cannot confirm such a speculation.

To compare these results with those of other observers, cloud-chamber pictures by Freier and Ney[14] give the result that showers from heavy nuclei show a higher multiplicity of penetrating particles than those from light nuclei, though the average angular dispersions are the same. This is in essential agreement with our data as shown in Fig. 4. Evidence for pluromultiple meson production has also been found in large showers occurring in nuclear emulsions as seen by Kaplon *et al.*[15] and LePrince-Ringuet *et al.*[16]

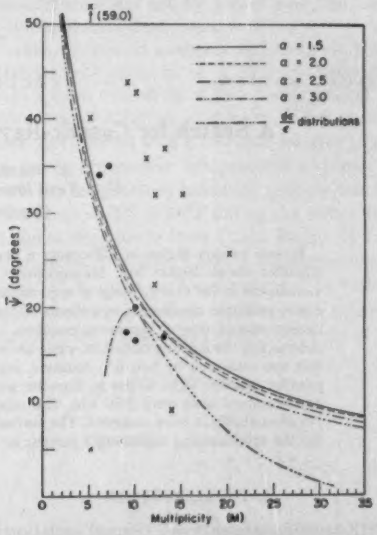

FIG. 4. This plot shows the average dispersion angle, $\bar{\psi}$, for the "minimum" tracks in each event *vs* the corresponding multiplicity. The heavy nucleus events are marked by a (×) and the light nucleus events by a (●). The lines give the predicted multiplicity *vs* $\bar{\psi}$ for a single completely inelastic nucleon-nucleon collision for various center-of-mass meson spectra: (1) monoenergetic mesons of total energy, α, in meson rest mass units: (2) a $d\epsilon/\epsilon$ spectrum.

[14] Phyllis Freier and E. P. Ney, Phys. Rev. 77, 337 (1950).

[15] Kaplon, Peters, and Bradt, Phys. Rev. 76, 1735 (1949).

[16] LePrince-Ringuet, Bousser, Hoang-Tchang-Fong, Jauneou, and Morellet, Phys. Rev. 76, 1273 (1949).

The author is indebted to Dr. E. O. Salant and Dr. J. Hornbostel of the Brookhaven National Laboratory for making these plates available. He wishes to express his thanks to Dr. B. T. Feld for suggesting this experiment and contributing to the analysis of the data. The author wishes to express particular gratitude to Mrs. T. Kallmes and Mr. I. L. Lebow for help in scanning and analyzing the plates.

APPENDIX

We have calculated the average angle of dispersion for mesons emitted in the collision of two nucleons if the mesons are produced in the center-of-mass system of the two nucleons with a single energy and an angular distribution corresponding to the $2n$th power of the sin or cos.

β = velocity of meson in c-of-m system.
β_0 = velocity of c-of-m system.
θ = angle of meson emission in c-of-m system.
ψ = angle of meson emission in laboratory system.

We assume a distribution in the center-of-mass system

$$\text{if} \quad N(\theta)\sim\cos^{2n}\theta\sin\theta d\theta,$$

then,

$$\bar{\psi}=\int_0^\pi \cos^{2n}\theta\psi(\theta)\sin\theta d\theta \Big/ \int_0^\pi \cos^{2n}\theta\sin\theta d\theta,$$

$$\psi(\theta)=\tan^{-1}[(1-\beta_0^2)^{\frac{1}{2}}\sin\theta/(\beta_0/\beta)+\cos\theta].$$

This expression can be integrated exactly

$$\bar{\psi}=(\pi/2)+(\pi/2)(1/\beta_0)(1/\alpha_1-\alpha_2)[G(\alpha_1)=G(\alpha_2)] \quad \beta_0<\beta,$$
$$\bar{\psi}=(\pi/2)(1/\beta_0)(1/\alpha_2-\alpha_1)[G(\alpha_1)-G(\alpha_2)] \quad \beta_0>\beta,$$
$$\alpha_{1,2}=(1/\beta_0\beta)\{1\pm[(1-\beta_0^2)(1-\beta^2)]^{\frac{1}{2}}\},$$
$$G(\alpha)=\left(-\frac{\beta_0}{\beta}\alpha+1\right)\left[\alpha^{2n}+\tfrac{1}{2}\alpha^{2n-2}+\cdots+\frac{1\cdot3\cdots(2n-1)}{2\cdot4\cdots2n}\frac{\alpha^{2n-1}}{(\alpha^2-1)^{\frac{1}{2}}}\right].$$

We can find $\bar{\psi}$ for a distribution, $\sin^{2n}\theta$, from the corresponding $\cos\vartheta$ moments. For instance,

$$\bar{\psi}(\sin^2\vartheta)=\tfrac{1}{2}[3\bar{\psi}(n=0)-\bar{\psi}(\cos^2\vartheta)].$$

For the case $n=0$ (spherical symmetry)

$$\bar{\psi}=[1-(1-\beta^2)^{\frac{1}{2}}](1-\beta_0^2)^{\frac{1}{2}}/\beta\beta_0 \quad \beta_0>\beta,$$
$$\bar{\psi}=1-\{[1-(1-\beta_0^2)^{\frac{1}{2}}]/\beta\beta_0\} \quad \beta_0<\beta.$$

To obtain the curves of Fig. 4, we have assumed various total energies, ϵ, for the mesons in the center-of-mass system. Assuming then a given nucleon total energy, U_0, (laboratory system), we find the velocity of the center-of-mass, β_0,

$$1-\beta_0^2=2Mc^2/(U_0+Mc^2), \quad M \text{ is the nucleon mass.}$$

We find the total energy available in the center-of-mass system and divide by the meson energy to obtain the multiplicity, M_0

$$M_0=[2Mc^2(U_0+Mc^2)^{\frac{1}{2}}-2Mc^2]/\epsilon,$$
$$\epsilon=mc^2/(1-\beta^2)^{\frac{1}{2}}=\alpha mc^2,$$
$$m=\text{meson mass.}$$

The values of $\bar{\psi}$ for the $d\epsilon/\epsilon$ spectrum are obtained by an integration of the above expressions for $\bar{\psi}$ over the center-of-mass meson energy. The resulting curves of M_0 vs $\bar{\psi}$ are shown in Fig. 4.

PHYSICAL REVIEW VOLUME 81, NUMBER 2 JANUARY 15, 1951

A Search for Cosmic-Ray Diurnal Effects at Balloon Altitudes

T. A. BERGSTRALH AND C. A. SCHROEDER
U. S. Naval Research Laboratory, Washington, D. C.
(Received September 25, 1950)

In two balloon flights in Minnesota a search was made for diurnal effects in the cosmic radiation at altitudes above 50,000 feet. Measurements were made simultaneously of the total ionizing radiation, γ-radiation in the energy range of approximately 0.75 to 5 Mev, and fast neutrons. The ionizing radiation and γ-radiation component was measured by means of a central horizontal counter tube surrounded by a closely packed ring of horizontal counters. Coincidences between the central counter and the outer ring determined the ionizing radiation, while anticoincidences gave the intensity of the γ-radiation. The neutron flux was measured by two BF_3 counters, one filled with enriched BF_3, mounted side by side in a vertical paraffin cylinder eight inches in diameter surrounded by Cd. One flight was launched at 12:30 A.M. LCT and remained aloft until 8:30 A.M. The other flight was launched at 6:00 P.M. and landed at 10:00 P.M. No diurnal effects were observed. The statistical accuracy of this measurement is on the order of 1 percent for the total ionizing radiation, 3 percent for the γ-radiation, and 2 percent for the neutron measurement.

I. INTRODUCTION

THE possible existence of a diurnal variation in the cosmic-ray intensity is of considerable interest, since it bears both on the matter of a permanent solar magnetic moment[1] and on the energy spectrum of the primary cosmic radiation. A solar magnetic moment of adequate magnitude to account for the apparent "knee" in the cosmic-ray latitude curve[2] should also give rise to an appreciable diurnal effect.[3,4] Measurements of this effect may provide evidence to aid in the resolution of the present doubtful status of the solar moment. If the absence of a diurnal effect can be established, some other mechanism will be required to explain an energy cut-off at high latitudes.

The relatively low energy particles of 3 Bev or less which would be affected by the solar field contribute very little to the intensity at ground level. These

[1] P. M. S. Blackett, Phil. Mag. **40**, 125 (1949).
[2] L. Jánossy, Z. Physik **104**, 430 (1937).
[3] M. Vallarta, Nature **139**, 839 (1937).
[4] P. S. Epstein, Phys. Rev. **53**, 862 (1938).

particles would also be excluded by the earth's magnetic field at low latitudes. From this it appears that measurements at high altitude and at least intermediate latitude should be most favorable to the detection of this variation.

We carried out a search for the diurnal effect at balloon altitudes in Minnesota (magnetic latitude 56°) in June of 1949. Identical equipment was carried in each of two balloon flights, the first of which was launched at 12:30 A.M. and remained aloft to 8:30 A.M. local civil time. The second flight was flown from 6:00 P.M. to 10:00 P.M. local civil time. Measurements were made of the intensity of the total ionizing radiation, of gamma-radiation in the energy range 75 kev to 5 Mev, and of fast neutrons. No diurnal variation was found in any of the three measurements. The statistical probable error for the total ionizing particle measurement was of the order of 1 percent, for the gamma-radiation of the order of 3 percent and for the neutrons about 2 percent.

II. EXPERIMENTAL APPARATUS

Figure 1 shows the Geiger counter arrangement used for measuring the total ionizing particle intensity and the intensity of the gamma-radiation. This is similar to that used by Perlow[5] in rocket experiments. It consisted of a single horizontal counter (A) surrounded by a closely packed ring (B) of five counters in parallel. A particle penetrating the center counter resulted in a coincidence ($A \cdot B$) between the center counter and the outer ring. An anticoincidence ($A-B$), in which the center counter was discharged but no counter in the outer ring was discharged, would result from a gamma-ray in the energy range 75 kev to 5 Mev approximately.

Figure 2 shows a cross section of the neutron counter. The two proportional counters 1 and 2 were physically identical. Counter 1 was filled to 25 cm pressure with BF_3 enriched to 96 percent of B^{10}. Counter 2 was filled to the same pressure with normal BF_3. The counters were sealed with paraffin into a removable aluminum cylinder as shown to provide for interchangeability of the counters. The large paraffin cylinder, 8 inches in diameter, was covered with sheet cadmium to stop thermal neutrons. The two counters, differing only in the concentration of B^{10}, were used to correct the neutron counting rate for spurious counts due to highly ionizing events not necessarily associated with neutrons in the energy range considered. Preflight calibration with a Ra-Be source was used to establish the ratio of the efficiencies of the two counters for neutrons. Actually, it proved unnecessary to make this correction.

Output pulses from the Geiger counters were fed to diode coincidence and anticoincidence circuits.[6] The ($A \cdot B$) output of this circuitry was scaled by a factor of 16 and the ($A-B$) output by a factor of 8. The proportional counter pulses were amplified and also fed to scaling circuits. A scale factor of 16 was used for the enriched BF_3 counter and a factor of 8 for the normal BF_3 counter.

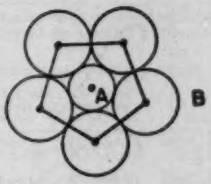

FIG. 1. Geiger counter arrangement for measuring total ionizing particle intensity and the intensity of gamma-radiation.

The counter data after scaling was totalized on four telephone message registers and time reference was provided by a clock. Ambient atmospheric pressure was measured by two mercury manometers, one having a range from zero to 10 cm, and the other calibrated over a range from 5 cm to 76 cm. A photographic type thermometer was used to determine the temperature within the gondola. The entire instrument group was photographed with a 16-mm gunsight camera modified for continuous film motion. Exposures were made at approximately 20-sec intervals by flashing four bulbs mounted in a reflector. The time interval between exposures was set by a cam operated switch driven by the camera gear train.

The entire equipment assembly including electronics and batteries was enclosed in a 30-in. pressure-tight aluminum sphere consisting of two hemispherical sections spun out of 0.030-in aluminum. Prior to flight the sphere was covered with a two-inch blanket of glass wool to prevent excessive temperature changes. By this means the temperature inside the gondola was held within the range of 70° to 80°F during the entire flight.

Both flights were made from Camp Ripley at Little Falls, Minnesota. Two 70-ft General Mills polyethylene cells were used to carry each experiment. The balloons and flight services, including tracking and recovery, were provided by Project Skyhook. Tracking of the

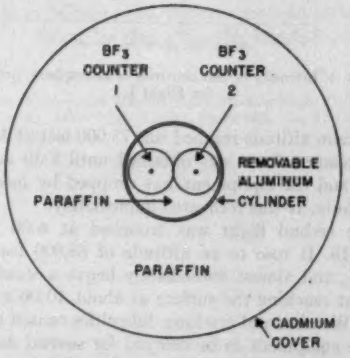

FIG. 2. Cross section of neutron counter.

[5] Perlow, Kissinger, and Schroeder, Phys. Rev. 76, 164 (1949).
[6] Howland, Schroeder, and Shipman, Rev. Sci. Instr. 18, 551 (1947).

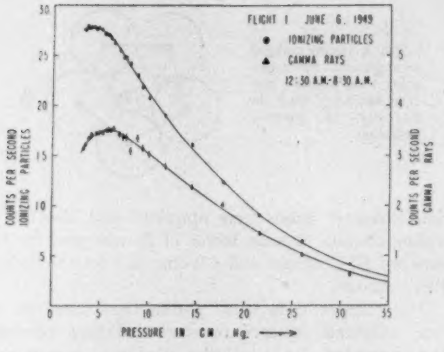

FIG. 3. Intensity of ionizing particles and of gamma-radiation *vs* pressure for Flight 1.

balloons was accomplished by means of theodolites and by a Radio sonde in conjunction with the radar. The Radio sonde also provided altitude data, but the pressure data from the mercury manometers was used for all calculations.

Flight 1 was launched at 12:30 A.M., local civil time, on June 6. This flight climbed to an altitude of approximately 55,000 feet and leveled off until sunrise, when heating of the gas caused a further slow ascent. The

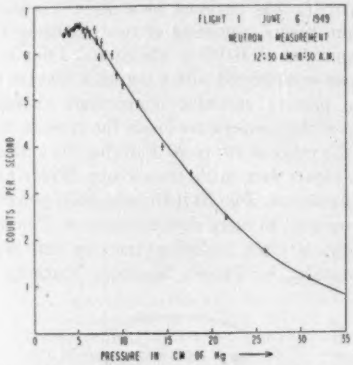

FIG. 4. Intensity of fast neutrons *vs* atmospheric pressure for Flight 1.

maximum altitude reached was 75,000 feet at 3.1 cm of Hg pressure. Data was obtained until 8:30 A.M. local time, and the equipment was dropped by means of a parachute. It was recovered immediately.

The second flight was launched at 6:00 P.M. on June 18. It rose to an altitude of 85,000 feet before sunset, and almost immediately began a steady rapid descent reaching the surface at about 10:00 P.M. local time. Weather and tracking difficulties caused recovery of the equipment to be delayed for several days. The film record was recovered in good condition.

III. RESULTS

The intensities of the three types of radiation which were measured are shown plotted as counting rates *vs* atmospheric pressure in Figs. 3–6. Figures 3 and 4 show the results for Flight 1, and Figs. 5 and 6 for Flight 2. The uncertainties indicated are the statistical probable errors.

The data shown for Flight 1 covers a time period of seven hours, approximately 1:00 A.M. to 8:00 A.M., local time. During this entire period the balloon was ascending. The rate of ascent through the pressure

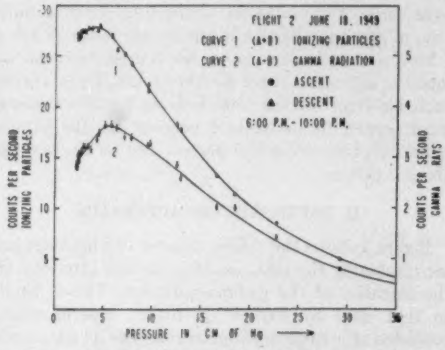

FIG. 5. Intensity of ionizing particles and of gamma-radiation *vs* atmospheric pressure for Flight 2.

interval 6.0 cm to 3.1 cm Hg was very slow, requiring 5 hours of the total period. Sunrise was approximately 0412 when the balloon was at an altitude of 18.5 km.

The curves for Flight 2 include data obtained over a 3-hr period from 6:40 P.M. to 9:40 P.M., local time. Apparently because of a break in one of the balloons, this flight did not remain at peak altitude for any extended period but descended at a rate comparable to the rate of ascent. Data were obtained throughout the

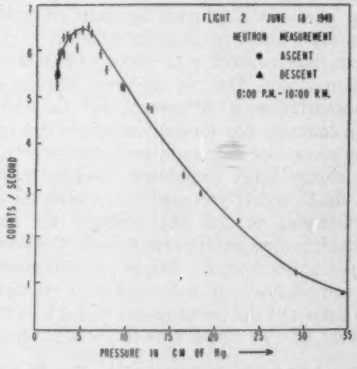

FIG. 6. Intensity of fast neutrons *vs* atmospheric pressure for Flight 2.

TABLE I. Data of Flight 1 corrected to constant pressure by means of the curves of Flight 2. The corrected counting rates are normalized to unity at the peak rate for each type of radiation.

Pressure altitude cm Hg	Local civil time	Normalized intensity Ionizing particles	Gamma rays	Neutrons
7.60 cm	0205	1.005±0.010	0.974±0.027	1.027±0.021
5.77 cm	0259	0.997±0.009	1.000±0.000*	0.979±0.020
5.37 cm	0405	0.993±0.009	0.969±0.022	
5.15 cm	0414			1.000±0.000*
4.70 cm	0454	0.994±0.008	1.018±0.022	1.003±0.015
4.00 cm	0549	1.000±0.000*	1.014±0.023	0.988±0.016
3.56 cm	0652	0.996±0.008	1.046±0.024	1.005±0.018
3.18 cm	0741	0.990±0.008	1.009±0.027	1.016±0.020

* Normalization point.

flight, and agreement between the counting rates for ascent and descent are satisfactory for all three measurements. Sunset occurred at approximately 1950 and an altitude of 21.5 km.

Since the balloons did not remain at a constant pressure level, the data of Flight 1 were corrected to constant pressure by means of the curves of Flight 2. The corrected counting rate was normalized to unity and is shown in Table I. The uncertainties shown are the statistical probable errors. The maximum correction for pressure difference is 15 percent. During the time interval from 2:00 A.M. to 8:00 A.M. on June 6, there was no variation in any of the three measurements which could be ascribed to a diurnal effect.

A comparison can also be made between the intensities of the ionizing radiation at widely separated times of day using ground calibration to correct for counter differences. Table II is a tabulation of the counting rates of ionizing particles for the two flights at an atmospheric pressure of 31 mm Hg, the maximum altitude reached by Flight 1, and at the Pfotzer maximum. The ratio of the effective volumes of the two counters was found by ground calibration to be 1.01 ±0.01. No difference as great as 1 percent was found in the ionizing radiation intensity between 7:40 A.M. and 7:40 P.M., and between 4:05 A.M. and 7:24 P.M., local time.

IV. DISCUSSION

Dwight[7] has recently published calculations on the expected magnitude of the diurnal variation. He assumed a power law spectrum for the incident cosmic

[7] K. Dwight, Phys. Rev. 78, 40 (1950).

TABLE II. Comparison of counting rates for ionizing radiation at different times of day. Corrected for counter differences by means of ground calibration.

	Pressure altitude cm Hg	Local civil time	Counting rate ionizing particles	Corrected counting rate	Ratio
Flight 1	3.18 cm	0741	27.52±0.12	27.52±0.10	1.009±0.012
Flight 2	3.18 cm	1942	27.50±0.19	27.77±0.26	
Flight 1	5.28 cm	0405	27.22±0.13	27.22±0.10	1.002±0.013
Flight 2	5.28 cm	1924	27.00±0.20	27.27±0.28	

radiation and an intensity in the "forbidden directions" of 90 percent of the full intensity.[8] For a solar magnetic moment of 10^{34} gauss-cm^3, he found that the vertical intensity should increase by about 7 percent between 4:00 A.M. and 8:00 A.M., local time, at 56° magnetic latitude. Both the magnitude and the phase of the variation are sensitive to the value of the assumed magnetic moment. When this was reduced to 0.42×10^{34} gauss-cm^3, a decrease of approximately 4 percent in the vertical intensity between 8:00 A.M. and 8:00 P.M. was predicted.

These calculations apply rigorously only to particles entering the earth's field in the vertical direction. Our measurements accepted radiation from all directions. Malmfors[9] has shown that when low energy charged particles are emitted from a sphere into the field of a magnetic dipole their final direction is practically independent of the direction of emission over a very large range about the vertical. The inclusion of a large solid angle should not seriously affect the results of the measurement.

The absence of an appreciable diurnal effect as indicated by these experiments places an upper limit on the value of the solar magnetic moment below that required for the latitude cut-off. Since no effect was noted in any radiation at the day-night line, the sun should not be a source of a significant portion of these radiations.

We wish to acknowledge the aid of our colleagues in the Rocket Sonde Research Branch of the Naval Research Laboratory, and of the personnel of Project Skyhook at Minneapolis. We are especially indebted to Dr. G. J. Perlow for many valuable suggestions on this problem.

[8] Kane, Shanley, and Wheeler, Revs. Modern Phys. 21, 51 (1949).
[9] Malmfors, Arkiv Mat. Astron. Fysik 30A, No. 12 (1944) and 32, No. 8 (1945).

Oscillatory Phenomena in Direct Current Glow Discharges*†

T. DONAHUE AND G. H. DIEKE
The Johns Hopkins University, Baltimore, Maryland

(Received November 29, 1948)

In glow discharges having a positive column with a constant emf and a series resistance, oscillations usually are observed in tube voltage, current, and light intensity. While current and voltage oscillations represent a modulation of only a few percent, the intensity decreases to zero between maxima in the positive column, but there is an appreciable steady component near the cathode. The intensity maxima move as positive striations toward the cathode, or as negative striations with a much higher speed toward the anode. Where positive and negative striations meet they stop for times up to 100 μsec.

The oscillations are often very stable and repeat themselves without change for hours. Often several modes exist and the discharge moves back and forth between them and appears unstable.

The data presented in this paper were obtained chiefly from argon discharges although similar phenomena occur in most other gases over a great range of pressure and current. A discussion of the mechanism producing the phenomena is given.

I. INTRODUCTION

IN the direct current glow discharge through gases at low pressures, the simplest conditions which can prevail are usually taken to be those in which the positive column is homogeneous, and the current is constant. It is well known that such conditions are not always met, and considerable study has been made of oscillations of several types which have been detected in "direct current" discharges. These include the high frequency oscillations of electrons in the space charge plasmas, the moving striations in rare gas and mercury vapor glows and arcs, and low frequency electrical oscillations which have been associated with these striations in a few cases. However, the information concerning these oscillations in the literature is rather fragmentary, and they have remained among the least well understood phases of the subject of electrical discharges in gases.

This is true even in the case of the moving striations in the positive columns of rare gas and mercury vapor glow discharges which were discovered by Abria[1] in 1843. A summary of the information which has been obtained since then can be found in any of the standard treatises on gas discharges[2–4] or in the review of Druyvestyn and Penning.[5] The study of the striations themselves has been made chiefly by means of rotating mirrors or by rotating cameras,[6] although Pupp,[7] who has made a rather extensive study of these phenomena, used also a photo-cell in conjunction with a cathode-ray tube to obtain a record of the fluctuations of light intensity caused by the striations. Electrical oscillations accompanying the moving striations were the subject of investigations by Appleton and West and by Fox.[8]

Owing to the difficulty of obtaining very precise or detailed information from the instruments available for all this work, it was not possible to set forth a satisfactory explanation for the moving striations.[9] As a result they have never really acquired a stature beyond that of a mere curiosity, a manifestation perhaps of a somewhat abnormal situation.

It should also be remarked that almost the same might be said for another example of inhomogeneity in the positive column—the case of the standing striations which appear for certain ranges of pressure and current in discharges through diatomic gases. There are many more experimental data for these striations than for the moving striations.[10] But again a theoretical explanation is lacking. In particular, no relationship has even been discovered between moving striations and those of the stationary type.

Recently, during a survey in this laboratory of short period phenomena in a large number of gas discharges of various types, it became apparent that oscillations are much more common in gas discharges than seemed to have been realized.[11] In fact, so seldom were they absent that it seems quite likely that any theory of discharges which neglects them is defective in some essential way. Therefore, a program to study these oscillations as thoroughly as possible under controlled

* The work of this paper was carried out under ONR auspices. The results were distributed in 1948 as Technical Report No. 1 of this project. Many details not given in the present paper may be found in the report. The results were communicated to the Conference on Gaseous Discharges held in Brookhaven, October 27–29, 1948.

† Revised manuscript received July 31, 1950.

[1] J. J. Thomson, Phil. Mag. 18, 441 (1909). This paper has a complete bibliography of the very early work in this field.

[2] A. v. Engel and M. Steenbeck, *Elektrische Gasentladungen* (Julius Springer, Berlin, 1933).

[3] L. B. Loeb, *Fundamental Process of Electrical Discharge in Gases* (John Wiley and Sons, Inc., New York, 1939).

[4] J. J. Thomson and G. P. Thomson, *Conduction of Electricity through Gases* (Cambridge University Press, London, 1933).

[5] M. J. Druyvestyn and F. M. Penning, Revs. Modern Phys. 12, 87 (1940).

[6] F. W. Aston and T. Kikuchi, Proc. Roy. Soc. 98, 50 (1921). T. Kikuchi, Proc. Roy. Soc. 99, 257 (1921). R. Whiddington, Nature 116, 506 (1925); 126, 467 (1929). B. v. Manen, Physica 1, 968 (1934). A. H. v. Gorcum, Physica 2, 535 (1935).

[7] W. Pupp, Physik. Z. 33, 844 (1932); 35, 705 (1934); 36, 61 (1935).

[8] E. Appleton and A. West, Phil. Mag. 45, 879 (1923). G. W. Fox, Phys. Rev. 35, 1066 (1930); 37, 815 (1932).

[9] See for example the remarks of Druyvestyn and Penning, reference 5, page 169, or of Loeb, reference 3, page 573.

[10] Druyvestyn and Penning, reference 5, p. 166.

[11] Dieke, Loh and Crosswhite, J. Opt. Soc. Am. 36, 185 (1946). H. Y. Loh and G. H. Dieke, J. Opt. Soc. Am. 37, 837 (1947).

conditions seemed desirable and promising. The application of photo-tubes and the oscillograph to the problem offered a promise of gaining more complete information about these oscillations than any technique previously used.

The following paper is a report of results obtained in this study for a number of dc glow discharges. In the earlier survey referred to, ac had been used as a matter of convenience and because during the ac cycle insight can be had into various transitory and break-down phenomena which are not readily observed with dc. But it is, of course, desirable to study the discharge under the simplest and most easily evaluated conditions. These surely obtain when the discharge is through a low pressure gas enclosed in a glass tube and driven by constant batteries. Then, if ever, one should expect a steady time independent discharge.

II. EXPERIMENTAL TECHNIQUE

The experimental arrangement is shown in Fig. 1. The glow discharge is maintained by a bank of batteries B or by a regulated rectifier power-supply in series with a variable resistance R. The discharge tube T is mounted horizontally. Riding beside it on a rack and pinion is the electron multiplier tube P (type 931-A or 1P28) in its housing. Light from a narrow region of the glow is admitted to the sensitive surface of the photo-tube through a narrow slit. Various methods for selecting light from the discharge tube have been used. Sometimes a second slit, almost touching the discharge tube, is placed about 2 cm in front of the slit on the photo-tube housing. A lens or mirror has also been used to focus an image of the discharge on the photo-tube slit. All of these schemes give practically the same results. Output currents from the photo-tube circuit flow through a resistance Y at the input terminals of an oscillograph. Thus the pattern on the cathode-ray tube screen gives the light output near a selected point in the glow discharge as a function of time.

The discharge voltage can be studied as a function of the time merely by bringing leads directly from the electrodes to the oscillograph (i.e., opening K_1 and closing K_2. In a similar manner the current at any point in the circuit can be studied in terms of the voltage variation across a properly chosen series resistance.

Figure 2 shows the results observed in a typical case (discharge in Hg vapor in the presence of 4 mm argon). Oscillations in the light intensity and the tube voltage were observed for all values of the current used (from a few tenths of a milliampere to about 60 ma). Often the fluctuations had the disordered appearance of Figs. 2A and 2B. Under such conditions the positive column seemed to contain striations which jumped about with great disorder and rapidity. But often the fluctuations are quite definitely periodic (Figs. 2C and D). The positive column appears then quite steady and homogeneous to the eye.

There is a very essential difference between the oscillations in the tube voltage and in the light intensity. The voltage fluctuations represent a modulation of a few percent (e.g., in the example of Fig. 2 the amplitude of the oscillations is 5 volts when the tube voltage is about 200 volts). The intensity fluctuations on the other hand represent a 100 percent modulation; i.e., the intensity is zero or very nearly so in the minima. In the ordinary oscillograph traces such as those of Fig. 2 this difference is not apparent as the amplifier in the oscillograph suppresses the dc component. The zero line can be brought out by applying the signal directly to the deflection plates or through a dc amplifier. The same result can be also achieved by interposing an electronic switch between signal and oscillograph (see e.g., Figs. 4, 5, 6).

III. OSCILLATIONS AND MOVING STRIATIONS

That the oscillations mentioned above are closely related to moving striations is apparent from the fact that voltage and intensity oscillations always have the same frequency and always become erratic and regular in the same way. This shows that the two types of oscillations are different manifestations of the same phenomenon.

The voltage fluctuations can thus be used to trigger the driven sweep of the oscillograph (e.g. DuMont type 248 A) which means that the sweep will always begin at the same instant of the cycle. The phase of the intensity oscillations are then observed to depend on the point in the tube from which the light comes. In Fig. 2F the point of observation is 0.34 cm closer to the cathode than in Fig. 2E. The pattern is clearly retarded by the time distance between two successive markers; i.e., 100 μsec. This indicates that the intensity wave travels from the anode to the cathode with a speed of about 34 m/sec and these traveling waves are called

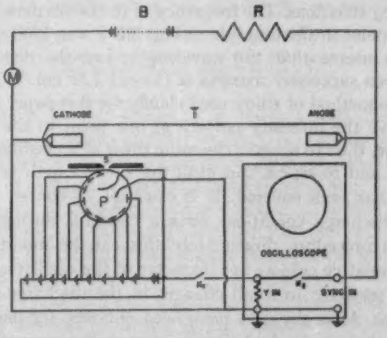

FIG. 1. Diagram of the discharge tube and photo-multiplier tube circuits.

B: Bank of twenty-five or more dry batteries, 45 volts each.
R: Variable resistance, maximum value 42,000 ohms.
M: Milliammeter.
T: Discharge tube.
P: Electron-multiplier phototube.
K_1, K_2: Switches.

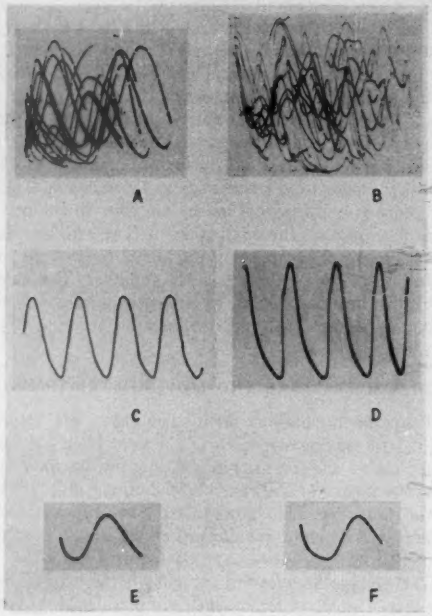

FIG. 2. Voltage and light intensity oscillations in a dc mercury vapor-argon glow discharge. The argon pressure was 4 mm. The sweep-length is 1000 μs with markers every 100 μs for *A*, *B*, *E*, and *F*.

A: Light intensity 4.83 cm from anode; current, 6.00 ma.
B: Voltage oscillation; magnitude 7 volts for same conditions as *A*.
C: Light intensity 11.60 cm from anode; current 6.00 ma.
D: Voltage; amplitude of sharp rise 5.72 *v* for same conditions as *C*. In *C* and *D* the sweep-length is about 3500μs.
E: Light intensity 5.70 cm from anode; current, 5.12 ma.
F: Light intensity 6.04 cm from anode; same conditions as *E*.

The frequency in *E* and *F* is 1333 sec^{-1}.

moving striations. The frequency of the oscillations at a fixed point in the example of Fig. 2E–F was 1300 sec^{-1} which means that the wavelength, i.e., the distance between successive maxima is ($\lambda\nu = v$) 2.55 cm.

The method of study used chiefly for this paper is to observe the intensity pattern at one point in the discharge, then to observe the same thing at a neighboring point and to repeat this until the whole length of the tube has been covered. It is essential, of course, that the discharge conditions remain constant during the whole procedure. Fortunately this can be monitored with relative ease as the character of the oscillations is very sensitive to small changes in the discharge conditions. After the data have been obtained for one set of conditions the discharge parameters like current and pressure can be changed and the discharge analyzed in the same manner for the new conditions.

It seems desirable to study the moving striations and their associated electrical phenomena under as simple conditions as possible. These probably prevail in a monatomic gas and for this reason the glow discharge in argon will be discussed in some detail. We had available four cylindrical tubes[12] of equal dimensions filled with argon at pressures of 2.1 mm, 4.4 mm, 12 mm, and 30 mm respectively. They were made of Pyrex, 15 mm in diameter. The electrodes were small zirconium cylinders of square cross sections with 5 mm sides. The distance between the electrodes was about 42 cm.

We shall take as a typical example the argon discharge at 12 mm pressure which shows most of the interesting phenomena. After this, attention will be called to the differences observed at the other argon pressures. Phenomena observed in other gases like Hg, He, Ne, Kr, Xe, H_2, and air will only briefly be mentioned although examples from such discharges will be used occasionally to illustrate some point.

IV. OSCILLATIONS IN ARGON AT 12 MM PRESSURE

Figure 3 shows the ordinary dc characteristic of the discharge, i.e. the tube voltage against discharge current, both measured with an ordinary dc instrument. The character of the oscillations (stability, frequency, velocity of propagation, etc.) was observed as function of the current over the range 10–200 ma.

Figure 3 gives also the observed frequency of the oscillations. It is immediately apparent that the various values do not lie on one continuous curve. When the current is increased the oscillations may become unstable and with further current increase, or sometimes even after a suitable waiting period at the same current, the oscillations become stable again but with a markedly different frequency. We have thus several *modes* of oscillations. Six such modes are indicated in Fig. 3. For some values of the current several modes can exist. Which one is in evidence at a given time depends on the previous treatment of the tube, e.g. whether a particular value of the current was reached by increasing or decreasing the current. Sometimes the tube moves back and forth between two different modes and a confused picture arises as in Fig. 2A and B. After some time the tube usually will settle on a definite mode. For other current values stable oscillations apparently do not exist under any conditions. Regions in Fig. 3 where no frequencies are indicated are such regions of instability. There are values of current and pressure (not, however, in the range of Fig. 3) where the discharge is entirely free from oscillations (see Figs. 4G and 4H).

Figure 4 shows that the intensity pattern may be quite different for different modes. Figures 4A and 4B represent mode III, 4C mode VI, and 4D mode VII. The wave form of the intensity pattern may also change considerably when different parts of the tube are com-

[12] We are indebted for these tubes to the late Dr. A. C. Rentschler of the Westinghouse Research Laboratories at Bloomfield, New Jersey. Owing to his cooperation a great deal of delay was avoided at a time when facilities for constructing such tubes were not yet available in our own laboratory.

pared. It is usually more or less the same all through the positive column but changes very greatly in character in the parts near the cathode. A study of this behavior reveals valuable clues to the nature of the mechanism which produces the moving striations.

V. ANALYSIS OF THE MOVING STRIATIONS

The low current modes, particularly modes I and III of Fig. 3, in argon at 12 mm reveal some of the characteristic properties of the striations.

There were faint but definite stationary striations visible in the part near the cathode at the low currents whenever the oscillations were stable. The separation d_s of the stationary striations was related to the distance λ between the moving striations by

$$\lambda = nd_s,$$

where n was an integer, usually one or two. The moving striations cross the standing striations. They are broad and move relatively slowly in the bright parts and are much sharper and move faster in the minima of the standing striations. Tables I and II give some of the properties of these striations. Let us look at mode I at a current of 19.20 ma through the tube. The appearance of the discharge is as follows. The distances are measured from the cathode.

Cathode glow	0.22 cm
Cathode dark space	0.70
Negative glow	1.60
Faraday dark space	2.05
Positive column	2.42

Figures 5 and 6 show the appearance of the oscillations at various distances from the cathode. The variation of the curves with position is quite striking as is the complexity of the pattern.

We shall call each of the maxima visible on these traces a "striation." From the time scale on each trace the moment can be determined at which this particular striation reaches the spot of observation. From an inspection of the figures it is obvious that there are several striations of different character passing the spot of observation during each cycle. By comparing a whole set of pictures taken at different parts of the tube it is possible to trace the movement of each striation through the tube. A particular striation will not only move along the tube but may change its amplitude and shape as it moves along.

The results of such analysis are summarized in Fig. 7. The abscissa is plotted as the distance of the place of the observation from the cathode, and the ordinate as the time when a particular maximum passes this spot.

The neighboring spots can be connected by a curve and this curve represents the motion of a particular striation.

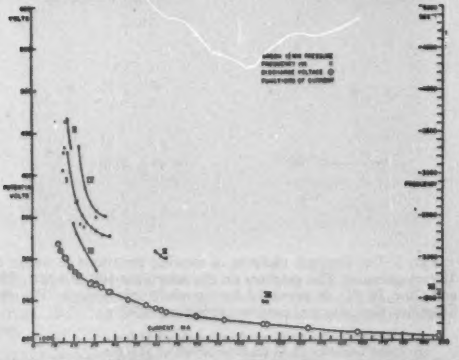

FIG. 3. Total discharge voltage ⊙ and frequency of oscillations x as functions of the current for an argon glow discharge at 12 mm pressure.

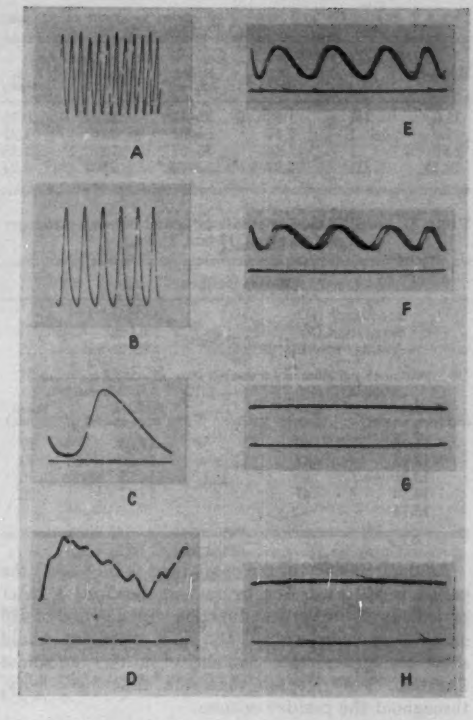

FIG. 4. Voltage and intensity oscillations in argon at 12 mm and 30 mm pressure. Time markers are spaced 100 μs. In C, D, E, F, and G the lower trace is the line of zero intensity provided by an electronic switch.

12 mm pressure

A: Voltage oscillation at 31.0 ma.
B: Light intensity 20 cm from cathode at 31.0 ma; frequency, 1866 sec^{-1}.
C: Light intensity at 114 ma; frequency, 1470 sec^{-1}.
D: Light intensity at 195 ma; frequency, 1665 sec^{-1}.

30 mm pressure

E: Light intensity 25.2 cm from cathode at 95.2 ma; frequency, 2600 sec^{-1}.
F: Light intensity 25.2 cm from cathode at 144.0 ma; frequency, 2460 sec^{-1}.
G: Light intensity 25.2 cm from cathode at 150.0 ma.
H: Light intensity 25.2 cm from cathode at 270.0 ma.

TABLE I. Stationary and moving striations in argon at 12 mm.

Current (ma)	Mode (see Fig. 3)	λ (cm)	Speed (m/sec)	Frequency (sec^{-1})	d_0 (cm)
31.0	III	1.88	25–42	1870	0.94
25.4	I	2.44	56–62	2440	1.22
24.9	I	2.46	55–62	2390	1.23
19.35	III	2.47	53–70	2500	1.24

TABLE II. Speed of moving striations in and between stationary striations argon, 12 mm, 31.0 ma.

Moving striations	
Frequency (ν):	1866 sec^{-1}
Separation (λ):	1.88 cm
Average speed (v av):	35.2 m/sec

Stationary striations and measured speed of moving striations

Minima		Maxima	
Position (cm from anode)	Speed (m/sec)	Position (cm from anode)	Speed (m/sec)
11.98	40	12.35	29
12.92	42	13.29	30
13.86	40	14.23	26
14.80	47	15.17	28
15.74			

As the frequency of the oscillations is 2438 sec^{-1} the period is 410 μsec. The figure has, therefore, a strict periodicity in the vertical direction with a period of 410 μsec. If extended toward the right the figure would show an approximate periodicity in the horizontal direction, less rigorous than the time periodicity, throughout the positive column.

Figure 7 shows that there are two types of striation. The curve of one type slopes up toward the left. This means that these striations move from the anode toward the cathode. The slope is considerable which implies a moderate velocity of propagation which is, moreover, not constant (from 33 to 350 m/sec with an average value of 65 m/sec). This type of striation we call *positive* striation. This is the type of moving striation observed before in many cases. It is marked with a dot over the maxima in the oscillograms of Figs. 5 and 6.

The other type of striation, here called *negative* striation, moves from the cathode toward the anode. Its velocity is much faster than that of the positive striation. The negative striations never seem to have been observed before. All those not marked with a dot in Figs. 5 and 6 are negative striations.

Obviously the positive striation is a positive space charge, the negative striation a negative space charge, which move in the appropriate direction in the electric field which exists within the discharge tube. Presumably the negative charge consists of electrons and because of its high mobility can move faster than the positive space charge consisting of positive ions. We must, however, consider also the possibility of neutralization at the trailing edge of the positive space charge and fresh ionization on the leading edge as a mechanism for motion, in which thus the individual ions do not necessarily move with the same velocity as the center of the space charge.

Whenever a positive striation and a negative striation meet, they neutralize each other and there is then a true plasma formed with the field strength very small. We observe then for a time interval varying here from 20 to close to 100 μsec no motion at all. After this interval a negative and a positive striation each emerge from this plasma travelling in opposite directions.

Figures 5 and 6 represent actual oscillograph traces and Fig. 7 is directly derived from such traces and represents, therefore, the behavior in an actual tube with some irregularities caused by wall conditions.

The method of treating the oscillographic evidence can be better discussed with the help of Fig. 8, which presents drawings of typical oscillograph patterns of light intensity as function of the time for eight positions in the positive column successively closer to the cathode. For each of these the time at which a peak in the intensity occurs is then plotted on the lower right part

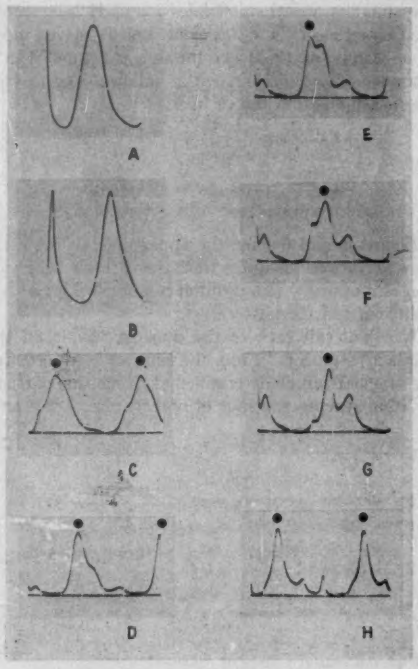

FIG. 5. Oscillograph pictures of moving striations in argon at 12 mm pressure. The markers on the sweep are 100 μs apart. The zero line (*C–H*) is provided by an electronic switch. The dot identifies the principal positive striations (*C–H*).

A: Light intensity 12.45 cm from anode at 31.0 ma.
B: Light intensity 14.75 cm from anode at 31.0 ma.
C–H: Light intensity in positive column at 19.20 ma; frequency, 2438 sec^{-1}.
C: 4.83 cm from cathode.
D: 4.05 cm.
E: 3.80 cm.
F: 3.67 cm from cathode.
G: 3.45 cm.
H: 2.53 cm.

of the figure for the points which are numbered in correspondence with the oscillograph traces. Thus at point (1), closest to the anode, intensity peaks occur at 50, 200, 250, and 450 μsec and are so plotted on the graph. It is seen that at the neighboring points (2), (3), etc., the peak marked (+) occur at successively later times while the other peaks occur earlier but only slightly so. The peak marked (+) moves therefore toward the cathode and represents a positive striation, whereas peaks (*a*) and (*b*) move in the opposite direction but with a much higher velocity and represent negative striations.

If we fix now our attention to peaks (+) and (*a*) we find that they approach each other continually until at point (5) they are only separated by 43 μsec. The intensity does not fall to zero during the time between these peaks near point (5).

At point (6) the two peaks are again more widely separated and through comparison with (7) and (8) it is

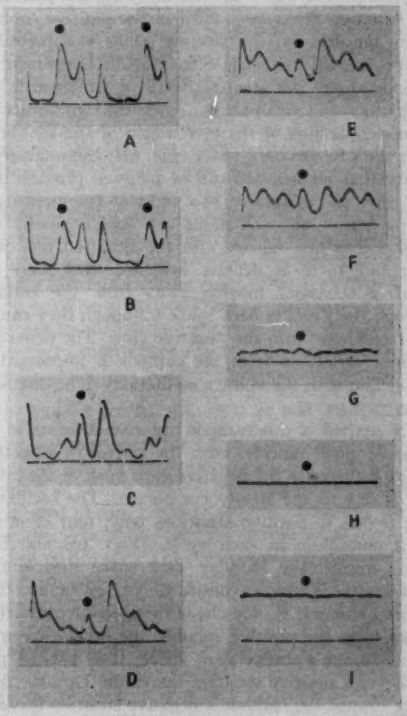

FIG. 6. Oscillograph pictures of moving striations near the cathode in argon at 12 mm pressure. Markers 100μs apart; current, 19.20 ma. The dot identifies the principal positive striations.

A: 2.18 cm from cathode.
B: 2.05 cm (Faraday dark space).
C: 1.89 cm.
D: 1.72 cm.
E: 1.60 cm (Negative glow).
F: 1.36 cm.
G: 1.50 cm.
H: 0.70 cm (Crookes dark space).
I: 0.22 cm (Cathode glow).

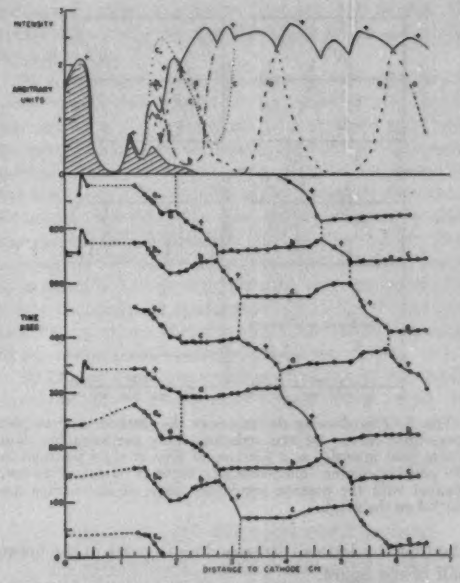

FIG. 7. Time-position curves for the moving striations near the cathode in argon at 12 mm pressure and 19.20 ma current. At the top of the figure is plotted the amplitude of the light intensity for each of these striations as a function of position. These curves are labeled to correspond with the striation paths plotted in the bottom part of the figure. The full curves are not drawn for *b*, *c*, a_4, b_4.

apparent that the left peak is now the negative and the right one the positive striation. This can only be interpreted to mean that at point (5) the striations pause for about 45 μsec. While this happens they are intermingled and form a true plasma. The light intensity drops but not to zero and rises again when they are ready to separate.

In Fig. 8 peaks separated by 400 μsec are designated by the same letter. They are manifestations of the same striation one period apart. In our example there are two negative striations (*a* and *b*) to each positive one. If the distance between points (1) and (8) is 2.5 cm the average speed of the negative striations is 1000 m/sec, that of the positive striations 100 m/sec.

Figure 7, the diagram of an actual tube, is somewhat more complicated than Fig. 8 because different parts of the discharge may be quite different in the behavior of the striations, particularly near the cathode.

As one follows a particular positive striation along the tube in Fig. 7 it meets three negative striations in a cycle. Its intensity is a maximum between the meeting points, a minimum at the meeting points. These intensities of the striations, i.e., the values of the intensity maxima in each oscillogram, are indicated in the upper part of Fig. 7 in which the particular striations are

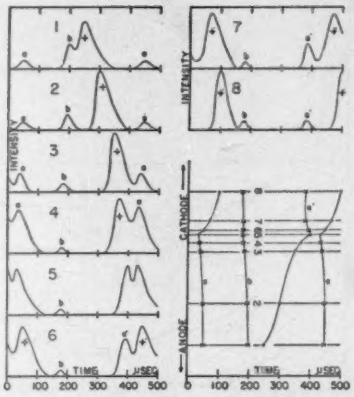

FIG. 8. This drawing demonstrates the method used to plot space-time curves for the striations from oscillographic data giving light intensity as a function of time at eight positions in the positive column. Each intensity curve is numbered to correspond with the position where the times of its maxima are plotted on the graph.

identified by letters corresponding to parts in the lower half of the figure.

The intensity of only one negative striation, the one marked (a) is plotted throughout (dashed line). The intensity curves for the other two (b) and (c), are discontinued where they first meet the positive striation (+). (a), (b), and (c) all originate in the negative glow between 1.75 cm and 2.12 cm from the cathode. At the same points positive striations arise which go into the negative glow. These are marked (a_+), (b_+), and (c_+). The intensity curves, for example of (a) and (a_+), are continuous. A vertical bar indicates on the intensity plots where the change occurs. Only the curves for (+) and (c_+) are continued all the way to the cathode to avoid crowding. The minima between striations are uniformly zero except near the cathode where there is a considerable steady non-oscillating part in the intensity which is indicated by the cross-hatched area. The negative glow, which extends from about 1.05 cm to about 2.05 cm, has a pronounced structure. The division at 1.4 cm has apparently never been noticed previously. One might say that the positive column begins where the steady part in the intensity becomes zero.

The meeting places of the positive and negative striations are at fixed spots in the tube (positive column). Although the amplitudes of the striations are brightest between these meeting points, the average intensity is larger at the meeting points because the striations remain there longer and the intensity does not go down completely to zero while the striations are at rest. The time average of intensity is, therefore, higher near these meeting points and they appear as stationary striations.[13]

[13] This type of stationary striation appears to be different from the typical stationary striations observed in some diatomic gases.

Since all the positive striations meet negative ones always in the same spot it follows necessarily that the number of stationary striations within one wavelength must be an integer, a fact which was mentioned earlier. This wavelength (the distance between points in the tube with the same phase) is constant where the phenomena are truly periodic in space. Where such a periodicity is not established, as in the region near the cathode, or is not interfered with as, for example, in the positive column through local differences in the properties of the tube wall, the wavelength will vary.

Well inside the positive column the negative striations are not very conspicuous as their amplitude is small. They have a uniformly high speed (about 1500 m/sec, see Fig. 9). The time delay at the meeting place with the positive striations is small. The meeting point can always be found from an observation of the positive striations as the maximum of the oscillograph traces is broadest there (Fig. 5A as compared with Fig. 5B). The left part of Fig. 9 gives a fairly typical picture of the situation throughout most of the positive column, where the delay at the meeting points is appreciable.

As is evident from Figs. 5 to 7 the discharge near the cathode shows the greatest detail of structure in the oscillations and this part is of greatest significance for an understanding of the mechanism of the striations.

In the Crookes dark space (Fig. 6H) the intensity is so low that no striation can be followed through it in this case. In the *cathode glow* most of the intensity is steady but weak oscillations are superimposed. The observations are difficult and the situation not quite clear but there is definite evidence that these are negative striations moving away from the cathode through the Crookes dark space (although they cannot be traced here) into the negative glow. The departure of these striations from the cathode is important in connection with the voltage oscillations to be discussed later.

The arrival of this cathode negative striation in the negative glow coincides with the arrival of a positive striation there. In the negative glow most of the intensity is due to the steady component. The oscillating part is due to positive striations only, four of nearly equal amplitude in each cycle, (Figs. 6E and 6F). Going toward the Faraday dark space they change their relative intensities considerably (Figs. 6C and 6D). Figure 7 shows that only one of these positive striations comes from the positive column, the other two originating in the Faraday dark space. It is noticed that whenever a positive striation leaves the Faraday dark space toward the cathode a negative striation leaves it to move in the opposite direction.

The picture near the anode is presented in Fig. 9 for a condition very similar to that of Fig. 7. The current here is slightly higher (19.35 ma) and the frequency a little lower (2425 sec^{-1}). There is no great difference in the structure of the striations in the positive column until very close to the anode. The negative striations

are observed to travel all the way to the electrode. In the present case the positive striations are seen first a very short distance in front of the anode shortly after a negative striation has passed. This is considered to be accidental since there are many cases in which no correspondence can be established between the arrival of negative striations and the departure of positives. Whenever a striation arrives at or leaves the anode a maximum in the tube voltage and a minimum in the current is observed.

There is in this case, and very frequently in others, a definite asymmetry in the positive striations near the anode, alternate ones travelling in a slightly different way. This distinction disappears before much of the positive column is traversed.

Since it is impracticable to present a complete position-time graph here for a tube 40 cm long, we have sketched (Fig. 10) what the striation behavior should be for a tube having only five stationary striations in the positive column. Actual data are represented near the anode and the cathode and in the voltage oscillation, but the central portion of the positive column has been telescoped in such a way that the phase relation between cathode, anode, and voltage oscillations remains correct. The speed of striation motion has been idealized to uniformity. The diminution of the delay time when striations meet in the central part of the positive column is indicated and real. Arrows at the bottom of the figure point to these meeting places; i.e., to the maxima of the stationary striations. The precise correspondence between voltage peaks and striations at the anode and between voltage minima and striations at the cathode should be noted. Here, in contrast to Fig. 9, positive striations leave the anode a long while after negative striations have gone in. It should be also noted that the striations repeat in groups of three. This complex periodicity is quite a common phenomenon.

VI. ARGON AT 2.1, 4.4, AND 30 MM PRESSURE

The phenomena in the argon discharge at pressures of 2.1, 4.4, and 30 mm are essentially the same as those observed at 12 mm pressure. Because of the appearance of different modes, the data are not sufficient to determine the general dependence of the oscillatory phenomena on pressure. For this reason only the significant differences appearing at different pressures will be mentioned which supplement the data observed at 12 mm.

Figures 11 and 12 show the behavior at 2.1 mm and 3.83 ma current. The frequency of the oscillations is 5000 sec^{-1} which makes the period 200 μsec. The average wavelength is 3.39 cm and the average speed 169 m/sec. The striations are very regular. The time position diagram (Fig. 12) is very similar to that at 12 mm (Fig. 7). There are two negative striations to each positive one in the positive column, a weak third one is observed near the Faraday dark space. The speed of the main negative striation is 2300 m/sec and can be measured rather accurately. The left side of Fig. 12 shows the voltage fluctuations about which more will be said in Sec. 7.

At 4.4 mm the oscillations seem at first sight much more complicated than at 12 mm (see Fig. 13). This is due to the fact that there are nine negative striations for every two positive striations. Furthermore, alternate positive striations do not meet negative striations at the same point. The minima of the one set of stationary striations thus produced coincide almost exactly with the maxima of the other set. The positive column thus appears to be entirely homogeneous to the eye. There is an odd effect in the cathode glow when negative striations leave toward the negative glow. From the same point striations can be seen which run around the edge of the cathode and back towards its rear.

At 30 mm there are simple oscillations at the lower currents with the negative striations not much in evidence. At 150 ma the oscillations disappear completely and the discharge is steady (Fig. 4*G*). This state of affairs prevails up to the highest currents (270 ma) at which observations could be made.

VII. CURRENT AND VOLTAGE OSCILLATIONS

It has already been noted that intensity oscillations are always accompanied by voltage oscillations. Also the discharge current shows oscillations.

The relationship between the current oscillations at either electrode, the voltage oscillation across the tube, and the intensity oscillations is most simply studied with a circuit such as that of Fig. 14. When SW_2 is closed, with SW_1 open, the voltage oscillation can be measured. When SW_2 is open and SW_1 closed in position

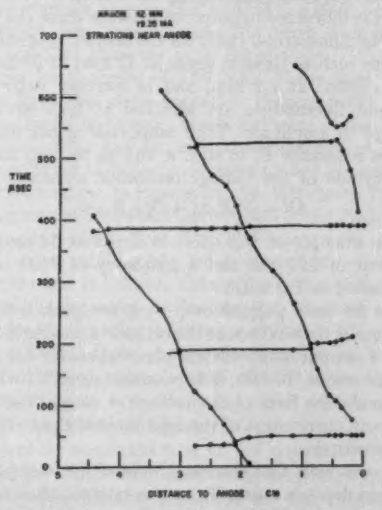

FIG. 9. Time-positive curves for the moving striations near the anode in argon at 12 mm pressure and 19.35 ma current.

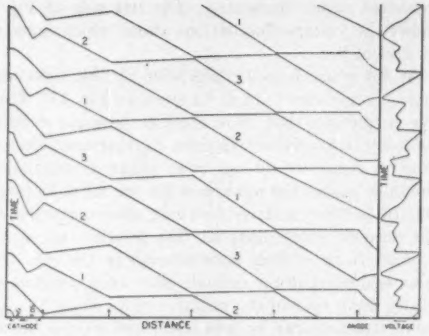

FIG. 10. Plot of time-position curves showing striation behavior completely from anode to cathode. These curves are representative of the motion of striations in general, but a specific case is reproduced only near the anode and cathode and in the voltage oscillation. The curves are drawn as straight lines in the positive column. In an actual case the slope would vary. Arrows locate the maxima of stationary striations.

A the current oscillations at the cathode are displayed on the oscillograph, and similarly those at the anode for SW_1 in position B. R_A and R_C are both 6000 ohms. Because it is not proper to ground permanently any point in this circuit, the trigger for the sweep must come from the photocurrent fluctuations for some convenient and fixed point in the discharge.

For a number of discharges the current and voltage oscillations were compared when the series resistance R was altered and the emf changed to maintain a constant discharge condition; i.e., identical dc ammeter reading and identical striation behavior. The relationship of i_c, the current at the cathode; i_a, the current at the anode; and the difference in potential between these electrodes may be summarized easily for the simpler types of oscillations such as those in argon at 12 mm, at 30 mm, for low current at 2.1 mm, and in mercury vapor. The current fluctuations are identical at both electrodes except in amplitude. Their amplitude varies with the series resistance R, in such a way as to keep ΔV, the magnitude of the voltage oscillation constant, where

$$\Delta V = -[R_c \Delta i_c + (R + R_a)\Delta i_a].$$

An example of this effect in argon at 12 mm for a current of 21.7 ma and a frequency of 3400 sec^{-1} is presented in Table III.

As we have pointed out, a current peak will occur whenever there is seen at the cathode a moving striation and a current minimum will occur whenever one is seen at the anode. In fact, it is possible to predict with fair accuracy the form of the voltage or current oscillation from an observation of the light intensity patterns near the electrodes.

It was seen that the magnitude of the current oscillations depends markedly on the external circuits while the voltage oscillations are much more characteristic of the discharge.

There is strong indication that the voltage oscillations are closely associated with the excitation and ionization potentials of the gas.

The relationship is expressed in Table IV for some of the gases for which data are available. This shows that the voltage oscillations (ΔV) show the same trend as the excitation potentials (V_e). The relationship is not exact and cannot be as the amplitude of the voltage oscillations may depend on the discharge conditions. The values given are typical values. There are often many subsidiary voltage peaks with different amplitudes.

VIII. OSCILLATIONS IN OTHER GASES

Many observations were made on oscillations and moving striations in other gases besides argon. Such oscillations occur under a great variety of conditions in He, Ne, Kr, Xe, Hg vapor, H_2, and air and probably other gases. This shows that the moving striations are a rather universal phenomenon in glow discharges and that any theory of the discharge mechanism should take account of them.

Some of the gases show oscillation phenomena with features considerably different from those observed in argon. We expect to deal with them in a subsequent paper.

A few remarks may be useful on oscillations in mercury vapor discharges. Mercury vapor discharge tubes are in general use now for many purposes, for example, in fluorescent lighting tubes, germicidal tubes, sun lamps, etc. Oscillations and moving striations can be observed easily in most of them and it matters little whether they have a hot or cold cathode.

Almost all such mercury tubes have a rare gas filling in which the discharge is started when the tube is cold. The heat produced by the discharge evaporates the mercury, and the discharge is then almost completely in the mercury vapor. The striations observed in such a tube are then characteristic for mercury vapor and not for the rare gas. This was verified with a tube with a side chamber which could be immersed in liquid air. It took about a week to distill all of the mercury from the main part of the tube through which the discharge passed into the side tube. The removal of the mercury could be verified when the spectrum of the discharge was a pure argon spectrum. The type of oscillations changed then from those typical of a mercury discharge into those typical of argon.

In mercury there was also the tendency for several modes. In the range of currents where the modes overlapped there was a conspicuous tendency toward instability (Figs. 2A and 2B) which was due to a change-over between such modes.

The magnitude of the voltage oscillations is usually between 4 and 5.75 volts although at low currents amplitudes as low as 1.6 volts have been observed.

In one tube two sharply defined modes could be observed which could be excited independently over a

wide current range. The dc characteristics for the two modes are found to be distinctly different. In other mercury tubes more than six different modes could be observed.

Although a large amount of data on mercury discharges is available, there seems to be little point in going into details here. Conditions in an ordinary mercury discharge are not very simple. Unless special precautions are taken the vapor density will depend on the current and, furthermore, the situation is complicated by the presence of the rare gas. A mercury discharge, however, is particularly well suited for observations of the striations in the monochromatic light of a single spectrum line, which will be discussed in the next section.

IX. SPECTROSCOPIC OBSERVATIONS IN THE STRIATIONS

For this purpose a General Electric type H-6 quartz mercury tube was used which has a diameter of about 0.25 cm and the electrodes 2.8 cm apart. The tube was used at low currents (about 1–10 ma). The discharge

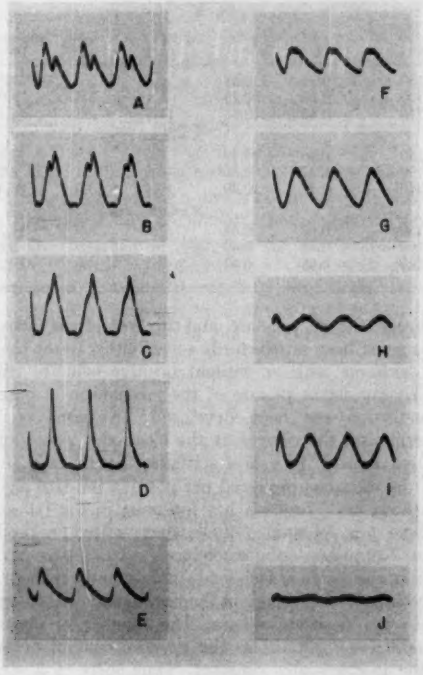

FIG. 11. Light intensity oscillations in argon at 2.1 mm pressure and 3.83 ma current. Time markers are 100 μs apart.

A: 12.54 cm from cathode.
B: 12.24 cm.
C: 12.16 cm.
D: 11.80 cm.
E: 2.68 cm.
F: 2.15 cm from cathode.
G: 2.16 cm.
H: 1.70 cm (Faraday dark space).
I: 1.29 cm (Negative glow).
J: 0.83 cm (Crookes dark space).

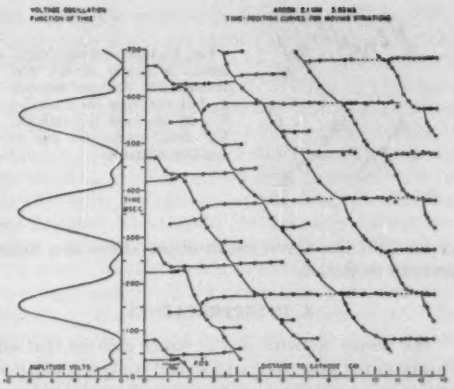

FIG. 12. Time-position curves and voltage oscillation for striations (see Figure 11) in argon at 2.1 mm pressure and 3.83 ma current.

was then a glow discharge and showed typical oscillations. At 2.35 ma, for instance, the frequency was 10750 sec^{-1} and the voltage oscillation as high as 50 volts.

An image of the discharge tube was focused on the entrance slit of a one meter grating spectrograph by means of a system of mirrors indicated in Fig. 15. This made it possible to examine spectroscopically any point in the discharge. An exit slit on the focal curve of the spectrograph would isolate any desired spectral line. A multiplier photo-tube received the light of this line and the output of the photo-tube was analyzed with the oscillograph in the manner described earlier. In this way the five mercury lines at 2537A, 4358A, 4047A, 5461A, and 3660A were investigated. The three lines 4047, 4358, and 5461 have the same initial state (7^3S) with an excitation potential of 7.69 volts. These three lines should have the same excitation characteristics and this was found to be true. The initial state of the 3660 line ($6^3D \rightarrow 6^3P_2$) has an excitation potential of 8.80 volts and is not sufficiently different for any changes in excitation to show up experimentally. Within the limits of experimental errors this line behaves in the discharge like the three visible lines. The 2537 line, on the other hand, has a considerably lower excitation potential (4.9 volts) and it behaves differently in the discharge.

When the intensity oscillations are observed at a given place in the tube, it turns out that the 2537 striation is definitely ahead of the other striations by about 15 μsec. Although this is a small effect it is consistent and unmistakable. Self-absorption, which may be considerable for 2537 if the mercury pressure is high, probably plays no significant part at the low currents (5.6 ma) and short path lengths. Even if there were appreciable self-absorption it is hard to see how this could shift the position of the maximum. We must conclude, therefore, that the atoms responsible for the emission

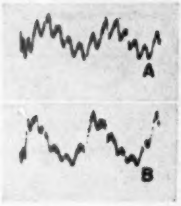

FIG. 13. Light intensity oscillations in argon at 4.4 mm pressure and 8.60 ma current. *A*, 3.31 cm from the cathode; *B*, 3.68 cm from the cathode. The small peaks are due to negative striations.

of the 2537 line travel ahead of the atoms in a higher state of excitation.

X. INTERPRETATION

The results reported in this paper indicate that any theory of the glow discharge should contain oscillations and moving striations as an essential or at least very important feature. For the work here presented shows that oscillations occur almost universally in glow discharges and under conditions hitherto believed to produce stationary discharges. Oscillations and moving striations are not exceptional cases but are almost always present within a large range of pressure and current *whenever a positive column exists*. Therefore, it is to be suspected that they play an essential part in the mechanism of the glow discharge. The rare cases in which striations are absent probably should be regarded as exceptions.

While many of the fundamental properties of the oscillations have been presented in this paper, this work is by no means complete. Work on other important features of oscillating glow discharges has by this time been nearly completed in this laboratory and the results are scheduled for early publication. Thus the experimental data are not yet complete. An attempt to develop a detailed theory of the glow discharge must wait until these further quantitative experimental data are available.

However, the observations reported here do suggest a tentative mechanism which is presented as a working hypothesis for the guidance of further experiments, rather than as a definite theory. This mechanism, which suggests the principal role of the moving striations in sustaining a glow discharge, fits in a qualitative way much that has been discovered about the striations thus far, though it by no means explains everything. In particular, it should be noted that the following sections do not apply to discharges through diatomic gases.

Although the problem of describing the distribution of potential, positive, and negative ion current, and electron temperatures as functions of the total current

TABLE III. Voltage and current oscillations in argon, $p=12$ mm. Direct current: 21.7 ma. Frequency: 3400 sec^{-1} (Mode IV).

Time of peak (μsec)	Δi_a (ma)	Δi_c (ma)	$(R+R_a)\Delta i_a$ (volts)	$R_c\Delta i_c$ (volts)	ΔV (measured) volts
			$R=20{,}000$ ohms		
150	0.36	0.38	9.3	2.3	11.5
190	0.28	0.26	7.4	1.6	8.9
240	0.46	0.43	11.9	2.5	14.4
			$R=12{,}500$ ohms		
150	0.46	0.49	8.6	2.9	11.5
190	0.37	0.36	6.8	2.1	8.9
240	0.56	0.49	10.4	3.0	13.4
			$R=6{,}000$ ohms		
150	0.62	0.64	7.5	3.9	11.3
190	0.48	0.49	5.8	2.9	8.8
240	0.68	0.67	8.1	4.0	12.2

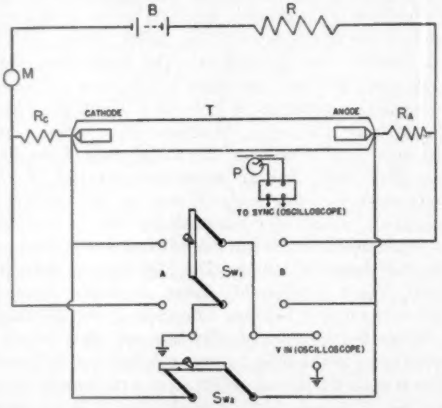

FIG. 14. Circuit diagram for the measurement of voltage oscillations and current oscillations at either end of the tube under the same conditions.

B: Twenty-five dry batteries, 45 volts each.
R: Variable resistance, 0–100,000 ohms.
R_a, R_c: 6000 ohms.
P: Photo-tube.
SW_1: Permits observation of cathode current in position *A*.
SW_2: Permits observation of anode current in position *B*.
SW_3: When closed with SW_1 open permits observations of voltage oscillations.

density, the gas pressure, and the type of gas molecule has never been satisfactorily solved either in the case of a discharge with or without positive column, still a fairly consistent picture of the mechanism of gaseous conduction has been developed. In terms of this mechanism the current at the electrodes would suffer fluctuations in time of a statistical nature only. Each of the electrons produced per positive ion striking the cathode must produce $1/\gamma$ ion pairs in the fall space where γ is the number of electrons emitted per positive ion. The primary and secondary electrons after passing out of the region of high field strength in the cathode fall and after losing energy in the negative glow then travel into the positive column. The number of electrons passing any surface in the positive column per unit time is essentially constant. Thus there is a steady current at the cathode and at the anode.

However, one critical phase of this process has been generally overlooked. There is a difficulty concerning the process whereby the electrons, after passing out of the region of large positive space charge in the fall space

TABLE IV. Relation between the observed voltage oscillations (ΔV) and excitation potentials of the vapor atoms.

	V_e (ev)	V_i (ev)	ΔV (v)
Hg	4.9	10.4	5.4
Kr	9.9	14.0	10.1
A	11.6	15.8	12.4
Ne	16.6	21.6	14.4
He	19.8	24.6	16.6

and losing a considerable part of their energy by excitation in the negative glow, pass into the supposedly uniform field region of the positive column. There is certain to be a considerable accumulation of electrons in the negative glow, for somewhere in this glow the sign of the space charge must change and become negative. There is even good evidence that the electric field becomes negative there. Thus there would actually be a minimum in the potential near the Faraday dark space and a trap would exist for electrons in the negative glow around the corresponding potential maximum. Unless it can be shown that electron diffusion against this field is sufficient, the current delivered to the positive column will not be steady but will decrease as the negative space charge in the negative glow increases and spreads toward the cathode. The attendant decline in the field of the Crookes dark space will then cause the current at the cathode to diminish and presumably the discharge would tend to be extinguished due to the critical nature of the value of the cathode fall.

To arrest this process before it has developed too far it is necessary to find a means of removing the excess electrons which have accumulated in the negative glow. It seems certain that the moving striations of the positive type are regions of high positive space charge which travel toward the negative glow. When one of these striations preceded by a region of high field has come sufficiently close to the trapped electrons the barrier will be lowered and the electrons will be released to travel as a burst toward the positive striation. Such a burst is a negative striation. These striations are indeed observed to originate in the rear of the negative glow (see Fig. 7 at 620 μsec, 510 μsec, and 400 μsec, or Fig. 12). When the electrons leave they apparently leave behind a positive space charge which begins at once to travel toward the cathode through the negative glow. This advancing potential wave raises the cathode fall, causing enhanced emission at the cathode and the resulting flow of electrons appears as a negative striation which travels across the Crookes dark space and meets the oncoming positive striation at the cathode edge of the negative glow. There the positive and negative space charge waves tend to neutralize each other and the process of electron entrapment begins again because the positive striation in the positive column by this time has been neutralized by the negative striation which it drew out of the rear of the negative glow.

A trapping procedure similar to that in the negative glow will also be effective in the positive striation. Obviously, there is high excitation in the positive striation, the electrons losing energy in inelastic collisions, and a concentration of electrons builds up. The flood of electrons in the negative striation feeds so much charge into this trap that a plasma of low total charge density is formed, both striations stop, excitation and light emission decrease, and the positive striation ceases to be an effective agent for the removal of electrons from the negative glow. Once again the discharge current decreases and electrons accumulate in the negative glow.

However, another positive striation will eventually draw close enough to the place where the first pair stopped to release the trapped electrons there. The negative striation is then observed to leave this region and to travel to the oncoming positive striation, causing it to stop in its turn. However, the release of electrons leaves the first positive striation, now somewhat reduced in strength due to loss of ions while it was stopped, free to move again toward the negative glow. It increases in strength until once again it is able to release electrons from the glow.

The cycle described above is then repeated since eventually the second positive striation will lose its trapped electrons as a negative striation to a third and move on toward the cathode and the first trapped striation.

Eventually the first striation becomes free so close to the negative glow that it travels all the way to the

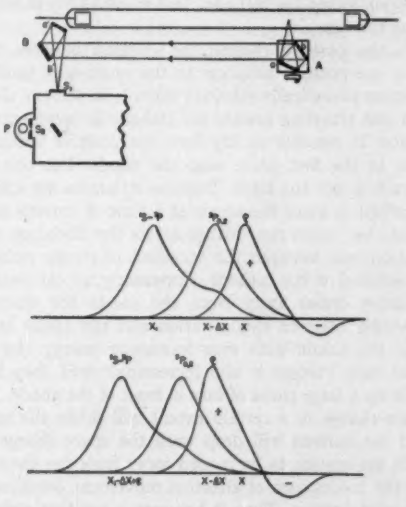

FIG. 15.

Top: Optical system used to observe individual spectral lines in moving striations. *A*: Carriage with pinion which moves on a rack parallel to the discharge tube. *a*, *a'*: Spherical mirrors. *b*, *b'*: Plane mirrors making a 45° angle with *a* and *a'*. s_1, s_2: Entrance and exit slits of a one-meter Eagle grating spectrograph. *P*: Photo-tube.

Bottom: Possible distribution of space charge, ρ, of mercury atoms in the metastable states, $^3P_0$ and $^3P_2$, and the probability of the $^1P \rightarrow {}^1S$ transition at times t and $t+\Delta t$.

cathode edge of the glow where it is met by a negative striation from the cathode. This is usually an occasion of absolute maximum light emission and current in the cathode layers.

The entire cycle is then repeated with the second positive striation now drawing negative striations from the negative glow. The number of negative striations leaving the glow between the times two positive striations reach it determines the number of stationary striations (electron entrapment) per wavelength in the positive column.

The cathode fall, it should be noted, is never so much reduced that the process of ionic bombardment and electron emission at the cathode is greatly impaired. The fluctuations in current are usually only a small percentage of the total current. The negative glow never becomes dark, and there is always a steady undercurrent of electrons through the positive column as is attested by the fact that even while the positive and negative striations are bound to each other and at rest, light emission does not fall completely to zero in that region. This steady stream of electrons, however, is of low energy between positive striations and does not cause any excitation there except during the period when it is enhanced by a negative striation and both current density and field are strong.

It should be emphasized that the time of current maximum at the cathode is that instant at which electron emission is copious due to the reduced negative charge in the negative glow; i.e., when a negative striation leaves the cathode. This is inevitably observed to be the case.

In the positive column the electron bunches pass from one positive striation to the next, each positive striation periodically releasing them from the one ahead of it and traveling toward the cathode between entrapments. It remains to say how the positive striations arise in the first place near the anode. For this the picture is not too clear. Positive striations are always observed to leave the anode at a time of current minimum; i.e., when the voltage across the discharge tube is maximum between the occasions of strong emission (striations) at the cathode. Apparently, as one positive striation draws away from the anode the electrons traveling between this striation and the anode arrive near the anode with ever increasing energy (for the total tube voltage is also increasing) until they have built up a large cloud of ions in front of the anode. This space charge to a certain extent will shield the anode and the current will drop until the space charge has built up enough to be moved away from the electrode by the mechanism of striation movement described in the next section. Thus it becomes a positive striation and sets out for the cathode until it stops a negative striation somewhere near the anode. This negative space charge is usually released to the anode itself when the anode has risen to a potential high enough to draw it away.

Evidence which further supports this qualitative picture has been obtained and will soon be reported.

XI. CUMULATIVE IONIZATION IN MOVING STRIATIONS

At least two important points remain to be discussed. These are the matter of how ionization takes place in the positive column and of why the positive striations move. It is possible that the two processes are related; that the manner in which ionization occurs near a striation tends to cause the positive ion concentration to shift toward the cathode. Suppose, for example, that in a gas the only levels excited to any appreciable extent in the positive column by collisions between electrons and unexcited atoms are those low lying ones of which some are metastable, and that the only effective process by which large numbers can attain higher levels of excitation and ionization is collision between electrons and metastable excited atoms. In other words, electrons with energies much greater than the first critical potential of the gas rarely occur in the field of a positive striation. Then at some instant, if there should exist in the gas the following distribution of ions and excited atoms, such a configuration should tend to preserve itself by moving in the direction of the cathode.

Let there be a positive space charge peak at some point x. Here, for a reason which will become clear, the concentration of metastables should be low, but should rise to a maximum just on the cathode side of x, say at $x-\Delta x$ (Fig. 15). Finally, suppose that at the same moment the rate of production of metastable atoms, due to impacts by electrons which have gained energy in the field of the positive space charge, is greatest still farther toward the cathode at x_1. This situation would exist if the electrons had risen in energy so that the peak in their energy distribution were just above the energy levels of the metastable states when they arrive at x_1. Near x_1, then, much excitation of these levels but little in any higher levels would take place. The electrons leaving x_1, after a sharp drop in energy due to inelastic collisions there, would gain energy again in the region to the cathode side of x where the space charge concentration exists. Thus when they get to $x-\Delta x$ where the concentration of metastables is high they would begin to produce highly excited atoms as well as ions. At x not much ionization would take place due to the low concentration of metastable atoms there and due to the losses in electron energy near $x-\Delta x$. Thus in time a concentration of metastable atoms would be built at x_1, while the ion concentration would rise and the metastable population decline at $x-\Delta x$. At x no new ions are being produced, so the ion concentration there falls due to the various factors which contribute to the loss of ions, such as lateral motion to the walls and recombination in the gas. Beyond x the electrons which even at x could not produce many excited atoms because of their low energy and because of the scarcity of metastable atoms, lose energy in a nega-

tive field and no longer contribute any excitation. Thus after a time Δt the space charge configuration which was at x has moved to $x-\Delta x$, the metastable peak which was at $x-\Delta x$ has moved toward x_1, while the number of metastable atoms at $x-\Delta x$ has declined due to the cumulative excitation and ionization which have removed them. In turn the peak production of metastable atoms is no longer at x_1, but at $x_1-\Delta x\pm\epsilon$ because of the shift in space and perhaps in strength of the source of the local field. Such a mechanism would tend to produce a movement in the striations. Whether it is sufficient to explain the entire motion remains to be determined.

There are two consequences of such a theory which can be tested easily. First of all the speed of the striations should depend on the rate of production of metastable atoms and their consequent removal by collisions into higher states in such a way that the striations are fastest when they are brightest. This is indeed a very noticeable feature of the moving striations. On the other hand, it is not a property uniquely belonging to this mechanism. For if the motion were entirely due to the fact that the striations are positively charged configurations in an electric field, the electric force would be highest when the total number of ions (hence also the number of excited atoms) is highest, and high speed and strong emission would again coincide.

The second consequence would have to do with the spectroscopic study of the striations. In a mercury vapor discharge, for instance, it would be possible at any instant to locate the point x_1, because this point at which the excitation of the metastable levels of the Hg triplet ^3P is at a maximum would also correspond to a maximum in the radiation at $\lambda=2537$A due to transitions from the one level of the three that is not metastable. This peak in 2537A should lie at a given time to the cathode side of the peaks of radiation at all other wavelengths which should *coincide* at the point $x-\Delta x$. The intensity of 2537A emissions at $x-\Delta x$ should surely not be as high as it is at x_1 for a few electrons attain sufficient energy at $x-\Delta x$ to produce the $^3P_1$ level directly and only a fraction (much less than unity) of those atoms raised from $^3P_0$ or $^3P_2$ to higher levels return to the ground state via $^3P_1$. Beyond x all radiation should decrease. Of course, it would be necessary for the peak excitation of the higher levels to reach x_1 in a time short enough that an appreciable population of metastables could still be present there. An interval of about 10^{-5} sec does not seem to be inordinately large.

These are just the results of the investigation in a mercury vapor discharge as described in Sec. IX. In fact, when the oscillograph traces of intensity at 2537A, 4358A, and 3660A are compared, it is difficult to find any interpretation of the results but the one outlined above. It will be noted, finally, that the 4358 and 3660A peaks follow the 2537A past no point by more than 2×10^{-5} sec. There should be a large number of metastable atoms left after a period so short.

The foregoing picture is vague in many respects and will need to be implemented or changed to account for some of the observed phenomena. The chief purpose of the experiments now under way is to gather material with which the further development of the theory can be freed from uncertainties. In particular, it is desirable to develop the theory to such an extent that it will yield quantitative results which can then be compared with the large body of quantitative data furnished by the experiments.

Thermoelectromotive Force of a Superconductor *Versus* the Same Metal in the Non-Superconductive State

M. C. STEELE
Naval Research Laboratory, Washington, D. C.
(Received August 11, 1950)

Measurements of the thermoelectromotive force of superconducting *versus* normal junctions of the same metal have been made for lead, tin, indium, and thallium. The technique used differed in several respects from that employed by previous workers. Results are discussed in light of existing theory. It is found that the data obtained are in good agreement with a relation derived from Fermi-Dirac statistics and the assumption that the Thomson coefficient of a superconductor is zero.

I. INTRODUCTION

A NUMBER of years ago Kok[1] postulated the existence of a thermoelectromotive force at a junction of a superconductor and the same metal in the non-superconductive state. By considering a thermoelectric cycle analogous to the Gorter-Casimir[2] cycle, Kok showed that

$$E \propto H^2, \tag{1}$$

where E is the thermoelectromotive force of the superconducting-normal junction of the same metal and H is the critical magnetic field. Shortly after Kok presented his hypothesis, Keesom and Matthijs[3] measured E as a function of temperature for tin and indium. The experimental results agreed with theory only along broad lines. This was due partially to the limitations in measuring voltages of the order of 10^{-8} v. In the present experiment a new method was used to measure E as a function of critical magnetic field for lead, tin, indium, and thallium. The data obtained for each of these elements has been found to be in disagreement with Kok's hypothesis. However, it is shown that the results are consistent with a relation derived from the free electron theory of metals. A preliminary report[4] of this work has already been given elsewhere.

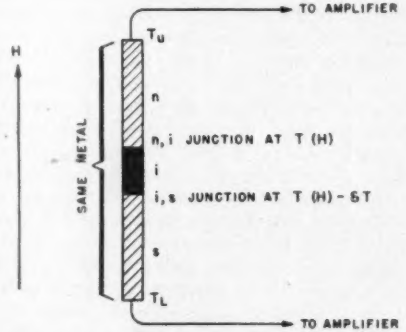

FIG. 1. Basic circuit: n designates the normal state; s, the superconducting state; i, the intermediate state.

II. EXPERIMENTAL METHOD

The previous work of Keesom and Matthijs[3] utilized magnetic shielding to obtain two superconducting-normal junctions at different temperatures. In order to increase the accuracy of voltage measurement, they used from four to six circuits in series. The present experimental arrangement differs from that of Keesom and Matthijs in three respects:

(a) Magnetic shielding is not utilized. (b) There is only one superconducting-normal junction in the circuit. (c) Only one circuit is used.

Figure 1 shows a schematic diagram of the basic circuit. The metal to be studied was connected to a dc voltage amplifier by copper leads. When the temperature of the upper and lower junctions (T_u and T_L, respectively) have been adjusted so that $T_u > T_c > T_L$, (where T_c is the superconducting transition temperature in the absence of a magnetic field) one portion of the metal will be superconducting, another part will be in the intermediate state, and the remainder will be normal. In Fig. 1, $T(H)$ is the transition temperature corresponding to a field H, and δT represents the temperature interval over which there is an intermediate state. Since the specimens used in this experiment were all wires with their lengths much greater than their diameters, and longitudinal fields were employed, it seems reasonable to assume that δT would be negligible compared to $T_c - T(H)$. Throughout the remainder of this development we will set $\delta T = 0$, thereby eliminating the two intermediate state junctions and substituting in their place a single n,s junction at the temperature $T(H)$.

With the condition described above and zero applied magnetic field, the total voltage, $\epsilon(0)$, applied to the amplifier is:

$$\epsilon(0) = \epsilon(Cu,n)_{T_u} + \epsilon(n,s)_{T_c} + \epsilon(s,Cu)_{T_L} + \epsilon_m, \tag{2}$$

where the first three terms on the right-hand side of Eq. (2) represent the voltage contribution of the three

[1] J. A. Kok, Physica **4**, 276 (1937).
[2] C. J. Gorter and H. Casimir, Physica **1**, 305 (1934).
[3] W. H. Keesom and C. J. Matthijs, Physica **5**, 437 (1938).
[4] M. C. Steele, Phys. Rev. **78**, 308 (1950).

junctions at their respective temperatures, and ϵ_m is a miscellaneous voltage due to the remaining part of the circuit. If T_u and T_L are maintained constant while a magnetic field of strength H_1 is applied longitudinally over the entire length of the metal being investigated, the new voltage applied to the amplifier would be:

$$\epsilon(H_1)=\epsilon(Cu,n)_{T_u}+\epsilon(n,s)_{T(H_1)}+\epsilon(s,Cu)_{T_L}+\epsilon_m. \quad (3)$$

It is assumed in Eq. (3) that $\epsilon(Cu,n)_{T_u}$ and $\epsilon(s,Cu)_{T_L}$ are independent of magnetic fields of the order of magnitude of the threshold values. From Eqs. (2) and (3) it follows that:

$$\Delta\epsilon=\epsilon(H_1)-\epsilon(0)=\epsilon(n,s)_{T(H_1)}-\epsilon(n,s)_{T_c}. \quad (4)$$

If we set

$$\epsilon(n,s)_{T_c}=0, \quad (5)$$

Eq. (4) can be written as

$$\Delta\epsilon=\epsilon(n,s)_{T(H_1)}. \quad (6)$$

$\epsilon(n,s)_{T(H_1)}$ is the desired voltage E. If the magnetic field strength is now increased by increments, the observed voltage differences can be summed to give the value[5] of E as a function of $T(H)$. It is of interest to consider the situation in the limit as H approaches the critical field corresponding to the lowest temperature T_L. For this case, the voltage applied to the amplifier would be

$$\epsilon(H(T_L))=\epsilon(Cu,n)_{T_u}+\epsilon(n,s)_{T_L}+\epsilon(s,Cu)_{T_L}+\epsilon_m. \quad (7)$$

Since Eq. (7) shows that under this field condition *all* of the superconducting portion is in the helium bath at the temperature T_L, it follows that the superconducting portion can be removed from the circuit without altering the observed voltage. Therefore, Eq. (7) is completely equivalent to

$$\epsilon(H(T_L))=\epsilon(Cu,n)_{T_u}+\epsilon(n,Cu)_{T_L}+\epsilon_m. \quad (8)$$

If H is made to exceed $H(T_L)$ it should follow that the observed voltage would remain constant since Eq. (8) indicates that ϵ is no longer a function of H. This condition was observed in all our experiments.

This method gives E as a function of H directly. If H is known as a function of T, E can be expressed as a function of T.

III. EXPERIMENTAL DETAILS

A Perkin-Elmer breaker-type dc amplifier was used to measure voltages. The output of the amplifier was connected to a recording milliammeter. With this arrangement, voltage differences of the order of 10^{-9} v could be measured.

Temperature measurements of the copper-normal metal junction and superconducting metal-copper junction were made with carbon thermometers. Although the absolute temperature could be determined only to about 0.01°K with such thermometers, temperature differences of the order of 0.001°K could be detected readily. Since the extent to which the junction temperatures can be held constant is a function of the temperature differences that can be detected, the carbon thermometers were satisfactory for this experiment.

For two of the elements studied (indium and thallium), heat was applied at the upper junction in order to have $T_u > T_c$, while T_L was maintained as low as could be obtained by pumping on the liquid helium. The heater consisted of manganin wire wrapped around the upper junction thermometer.

The magnetic field was furnished by a nitrogen-cooled solenoid which surrounded the helium flask. The solenoid was 23 inches long, $1\frac{3}{4}$ inch i.d. and dissipated about 300 watts for a field of 1000 oersteds. Specimens to be investigated were restricted to a length of 7 inches so that the field was uniform to within one percent over the entire length of the metal. The field strength was known to one percent from previous calibration. The metal being studied was mounted vertically in the helium flask. The liquid helium bath was adjusted so that about half of the sample was immersed. Therefore, the lower junction temperature, T_L, was the same as the bath temperature throughout the experiment.

All the elements used were in cylindrical wire form with diameters ranging from 0.005 to 0.07 in. For both lead and indium two sizes of wire were investigated. Specific information on purity, size, and source is given in Table I.

In the case of the lead 0.032-in. diameter specimen, it was noted that the copper-normal lead junction temperature, T_u, was strongly affected by the application of the magnetic field. In fact, increasing the magnetic field resulted in decreasing T_u by as much as

TABLE I. Data on the materials used.

Element	Purity, percent	Impurities, percent	Diameter, inches	Source
Lead	99.98	Sn 0.008 Sb 0.006 All others: <0.001	0.018 0.032	National Lead Company
Tin	>99.9	Pb~0.04 Fe<0.01 Bi<0.01 V<0.01	0.005	Baker and Company
Indium	99.9	Fe~0.1 Pb<0.01 Sn<0.01 Tl<0.01	0.011 0.014	National Bureau of Standards[a]
Thallium	>99.9	Fe~0.01 Al~0.01 Mo~0.01	0.065	Johnson, Matthey and Company

[a] The author wishes to thank Dr. R. B. Scott, Cryogenics Laboratory, National Bureau of Standards, Washington, D. C., for furnishing not only the indium wire but also valuable information on its superconductive properties.

[5] Because of the assumption of Eq. (5), the absolute value of E will be known up to an additive constant. However, the form of the variation of E with H or T will not be affected by setting this additive constant to zero.

0.6°K. This effect can be explained by the decrease in thermal conductivity of superconducting lead compared to normal lead. The change in T_s made it necessary to apply appropriate corrections to the data. This was done by calibrating the copper-normal lead junction voltage as a function of temperature in the absence of a magnetic field.

IV. EXPERIMENTAL RESULTS

The observed values of E as a function of applied magnetic field are shown in Fig. 2 for lead and Fig. 3 for tin, indium, and thallium. It seemed desirable to treat lead separately, since the maximum voltage observed for lead was an order of magnitude larger than for any of the other three elements. Relative to

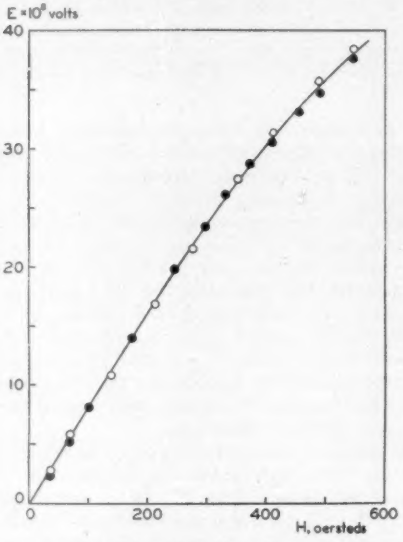

FIG. 2. Thermoelectromotive force of superconducting lead against normal lead as a function of applied magnetic field. ○, 0.018-in. diameter specimen; ●, 0.032-in. diameter specimen.

the effect of specimen size, it is seen that for both lead and indium the results were reproducible for different sizes of the same element.

In order to compare the present results for tin and indium with the values obtained by Keesom and Matthijs,[5] it was necessary to have the temperature corresponding to the applied field. These temperature values were obtained from the magnetic threshold curves of the particular elements. With the exception of indium the temperature values were taken from curves existing in the literature. However, before this was done a number of threshold values were measured[6] for each of the above specimens and within experi-

[6] The resistance method was used for getting threshold values.

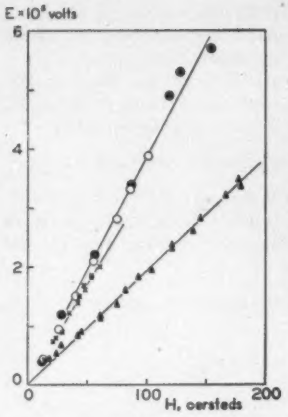

FIG. 3. Thermoelectromotive force of the superconducting-normal junction of the same metal as a function of applied magnetic field. ▲, tin; ○, indium specimen with 0.011-in. diameter; ●, indium specimen with 0.014-in. diameter; ×, thallium.

mental error the results were found to be in agreement with the published curves.

The threshold curves used were obtained from the following sources: Daunt and Mendelssohn[7] for lead; de Haas and Engelkes[8] for tin; and Daunt, Horseman, and Mendelssohn[9] for thallium. Since the indium used in this experiment had a somewhat higher normal transition temperature (3.41°K) than many values given in the literature (3.37°K), its magnetic threshold curve was measured from 1.95°K to 3.41°K. The values found between 3.26°K and 3.41°K were in good agree-

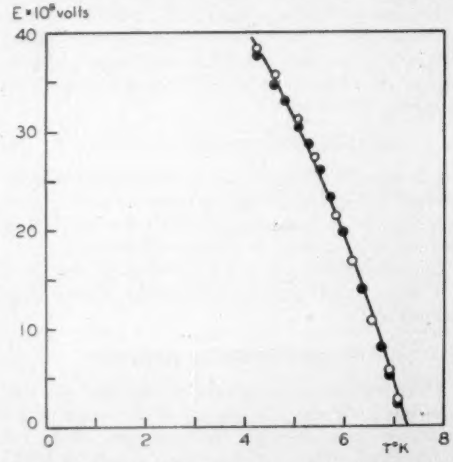

FIG. 4. Thermoelectromotive force of the superconducting-normal junction of lead as a function of temperature. ○, 0.018-in. diameter specimen; ●, 0.032-in. diameter specimen.

[7] J. G. Daunt and K. Mendelssohn, Proc. Roy. Soc. **A160**, 127 (1937).
[8] W. J. de Haas and A. D. Engelkes, Physica **4**, 325 (1937).
[9] Daunt, Horseman and Mendelssohn, Phil. Mag. **27**, 754 (1939).

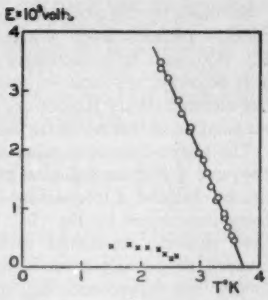

FIG. 5. Thermoelectromotive force of the superconducting-normal junction of tin as a function of temperature. ○, present data; ×, results of Keesom and Matthijs (reference 3).

ment with the measurements of Scott[10] on the same sample of indium.

Figures 4 through 7 show E plotted as a function of T for lead, tin, indium and thallium respectively. The data of Keesom and Matthijs[3] for tin and indium are included in Figs. 5 and 6.

The accuracy of the measured values of E is estimated to be within ± 10 percent.

V. DISCUSSION

It is seen from Figs. 2 and 3 that the present data do not agree with Kok's[1] hypothesis as given by Eq. (1). In fact for tin, indium, and thallium, the results indicate that E is very nearly linear in H. For lead, there is a slight curvature towards the H axis, which is opposite to that predicted by Kok. The disagreement is also evident in the temperature variation of E. If we assume a parabolic relation for the magnetic threshold curve[11] Eq. (1) can be written as

$$E \propto [1-(T/T_c)^2]^2. \tag{9}$$

If E is plotted as a function of T using the relation given by Eq. (9), it is found that there is an inflection point at $T=T_c/\sqrt{3}$ and $dE/dT=0$ at $T=T_c$. None of the curves in Figs. 4 through 7 exhibit either of these properties. This disagreement is evident to the same degree even if the actual threshold curves are used in place of the parabolic assumption for transforming Eq. (1) to a temperature dependence of E. There is a way of explaining this contradiction between theory and experiment if we examine the basis of Kok's hypothesis. Following is the hypothesis used by Kok[1] for the derivation of Eq. (1):

"The difference of the molar free energies of the metal in the two states $\Delta F(=F_s-F_n)$ has the same value as the difference of the molar free energies of the conduction electrons. This hypothesis is equivalent with the plausible assumption that the molar free energy of the lattice does not change at the transition of the metal from the superconductive to the nonsuperconductive state."

The hypothesis, as stated above, implies that there is no interaction between the conduction electrons and the lattice. Actually, we might expect that the interaction between electrons and lattice becomes increasingly significant as the temperature approaches absolute zero. Objections to the assumption of weak coupling between electrons and lattice are given by Tisza[12] in a recent article. Of course, if there is an appreciable interaction between electrons and lattice, Kok's hypothesis would be obviated.

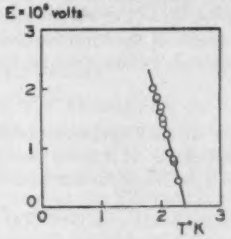

FIG. 7. Thermoelectromotive force of the superconducting-normal junction of thallium as a function of temperature.

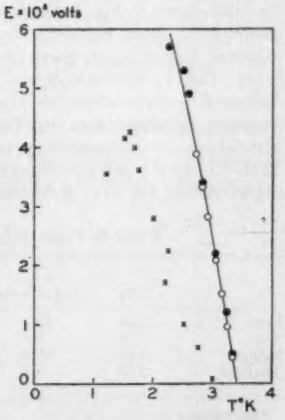

FIG. 6. Thermoelectromotive force of the superconducting-normal junction of indium as a function of temperature. ○, present data for 0.011-in. diameter specimen; ●, present data for 0.014-in. diameter specimen; ×, results of Keesom and Matthijs (reference 3).

It is of interest to remark that the failure of Kok's hypothesis to explain the experimental thermoelectric data presents somewhat of a paradox. The paradox becomes apparent in a qualitative sense when it is considered that an assumption equivalent to Kok's hypothesis has been used successfully for a phenomenological explanation of the specific heat behavior of a superconductor.[13] To demonstrate the paradox analytically, we start with the expression for the thermoelectric power of a normal-superconducting thermocouple of the same metal in terms of the Thomson coefficients of the two states:

$$\frac{dE}{dT}=\int_0^T \frac{(\sigma_n-\sigma_s)}{T}dT, \tag{10}$$

[10] R. B. Scott, J. Research Natl. Bur. Standards **41**, 581 (1948).
[11] For the soft superconductors used in this experiment, the threshold curves can be very nearly represented by parabolas.
[12] L. Tisza, "Theory of Superconductivity" RLE M.I.T. Technical Report (1950); also Phys. Rev. **78**, 342A (1950).
[13] J. de Launay and M. C. Steele, Phys. Rev. **73**, 1450 (1948).

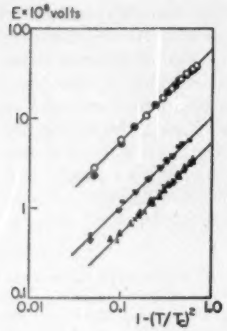

FIG. 8. Log-log plot of E as a function of $1-(T/T_c)^2$. ○, lead (0.018-in. diameter); ●, lead (0.032-in. diameter); ▲, tin; ▼, indium (0.011-in. diameter); ■, indium (0.014-in. diameter); ×, thallium.

where σ is the Thomson coefficient. From the free electron theory of metals[14]

$$\sigma=\frac{-2\gamma T}{3e}-\frac{k^2\pi^2 T}{3e}\left[\frac{l'(\xi_0)}{l(\xi_0)}\right], \tag{11}$$

where γT is the electronic contribution to the specific heat of the metal, e is the electronic charge, $l(\xi)$ is the mean free path of the electron with energy ξ, $l'(\xi)=dl/d\xi$, ξ_0 is the Fermi energy and k is Boltzmann's constant. If the term involving the mean free path is neglected, we can write for the normal state:

$$\sigma_n=-2\gamma_n T/3e. \tag{12}$$

Now we shall assume tentatively that a relation of the form of Eq. (12) holds for the superconducting state. For γ_s we shall further assume the relation:

$$\gamma_s=3\gamma_n T^2/T_c^2, \tag{13}$$

which can be derived[13] from the Gorter-Casimir theory and a parabolic relation for the threshold field. It would then follow that

$$\sigma_s=-2\gamma_n T^2/eT_c^2. \tag{14}$$

From Eqs. (10), (12), and (14) and the boundary condition $E=0$ at $T=T_c$, it would follow that

$$E=(\gamma_n T_c^2/6e)[1-(T/T_c)^2]^2. \tag{15}$$

It is noted that Eq. (15) indicates exactly the same temperature dependence as that predicted by Kok's relation (as expressed by Eq. (9)). Since the present experimental results disagree with Eq. (9) or (15) it behooves us to seek the fallacious assumption in the above development. The most vulnerable point in the derivation of Eq. (15) is the assumption that $\sigma_s\neq 0$, but is, in fact, given by Eq. (14). The experimental results of Daunt and Mendelssohn[15] show that $\sigma_s=0$ (at least for lead).

[14] F. Seitz, *Modern Theory of Solids* (McGraw-Hill Book Company, Inc., New York, 1940).

[15] J. G. Daunt and K. Mendelssohn, Proc. Roy. Soc. **A185**, 225 (1946).

Summing up this situation, we find that the following paradox presents itself. Whereas γ_s as expressed by Eq. (13) leads to a successful explanation of specific heat behavior, the same expression combined with the free electron theory relation for σ leads to an incorrect explanation of thermoelectric behavior.

The above discussion raises the question as to how adequate a phenomenological explanation for the data can be obtained if it is assumed that $\sigma_s=0$, instead of being represented by Eq. (14). Pimentel and Sheline[16] have recently considered such a situation for the analysis of thermocouples composed of two different metals, one superconducting, the other normal. From Eqs. (10) and (12) and the assumption $\sigma_s=0$, we obtain:

$$E=(\gamma_n T_c^2/3e)[1-(T/T_c)^2]. \tag{16}$$

Equation (16) does not exhibit any inflection point, and $dE/dT\neq 0$ at $T=T_c$. It should also be noted that Eq. (16) is in no way dependent upon the parabolic relation for the threshold field. In fact the magnetic field does not enter into the derivation of Eq. (16).

If we designate E_0 as the value of E for T equal to the absolute zero, it follows from Eq. (16) that

$$E_0=\gamma_n T_c^2/3e. \tag{17}$$

It is of interest to note that E_0 as given by Eq. (17) is exactly twice as large as the value that would be obtained if Eq. (15) were valid.

A quantitative test of the form of Eq. (16) can be obtained from the experimental results by plotting E as a function of $[1-(T/T_c)^2]$ on a log-log basis. There should result a straight line with a slope of unity for each element investigated. Figure 8 shows such a log-log plot of the data. It is of interest to note that a single line represents the data for both tin and thallium. Within experimental error the slope of each line in Fig. 8 is unity. Values for E_0 are obtained by extrapolation of the lines shown in Fig. 8. Having obtained E_0, we can compute γ_n from Eq. (17). In Table II numerical values of E_0 and γ_n are given for the elements investigated. The γ_n values obtained in this way can be compared to those determined thermodynamically from magnetic threshold data by Daunt, Horseman, and Mendelssohn.[9] Corresponding values of γ_n given in Table II show good agreement only for lead. If one considers that Eq. (11) is derived from a free electron

TABLE II. Values of E_0 and γ_n.

	T_c°K	$E_0\times10^8$ volts	$\gamma_n\times10^4$ cal/mole/(°K)² Present data	Daunt *et al.*[a]
Lead	7.26	59.	7.7	7.0
Tin	3.72	5.5	2.7	3.95
Indium	3.41	10.4	6.2	3.5
Thallium	2.40	5.5	6.6	2.8

[a] See reference 9.

[16] G. C. Pimentel and R. K. Sheline, J. Chem. Phys. **17**, 644 (1949).

model, it is perhaps not surprising that the agreement is no better than to order of magnitude for the value of γ_n. It is also possible that the term involving the mean free path in Eq. (11) is not negligible. For example, if $l'(\xi_0)/l(\xi_0)$ were independent of temperature, but not negligible, Eq. (10) would lead to:

$$E=\frac{T_c^2}{3e}\left[\gamma_n+\frac{k^2\pi^2}{2}\left(\frac{l'(\xi_0)}{l(\xi_0)}\right)\right]\left[1-\left(\frac{T}{T_c}\right)^2\right]. \quad (18)$$

Equation (18) still preserves the parabolic relation which fits the experimental data nicely. In order to compute γ_n from Eq. (18) one would need information about the behavior of the mean free path at low temperatures. Unfortunately the quantity $l'(\xi_0)/l(\xi_0)$ has not been determined theoretically to date. The differences in the γ_n values shown in Table II and the good fit of experimental data to a parabolic temperature relation suggest (using the free electron model) that the quantity $l'(\xi_0)/l(\xi_0)$ may be independent of temperature rather than negligible. In fact, if we accept the γ_n values of Daunt, Horseman, and Mendelssohn[9] and use the experimentally determined values of E_0 it is found that

$$|l'(\xi_0)/l(\xi_0)|\sim 0.1 \text{ ev}^{-1}$$

for each of the elements used.

VI. EFFECT OF IMPURITIES

In the course of obtaining the data there was occasion to investigate the effect of small amounts of impurity on the value of E. Since the effect observed was so marked it was thought to be significant enough to include the data in this paper. Figure 9 shows a comparison of the results for pure and impure lead. The major impurity in the impure lead was tin (~1.5 percent). It is seen that the maximum voltage observed was a factor of five smaller than the corresponding voltage for the pure material. In addition, the data for impure lead could not be fitted satisfactorily to a parabolic relation of the type given by Eq. (16) and hence was omitted from Table II.

VII. COMPARISON WITH PREVIOUS RESULTS

Keesom and Matthijs[3] had measured E as a function of T for tin and indium by an entirely different procedure. Comparison of results shows that for tin (Fig. 5) there is an order of magnitude difference between the present data and the data obtained previously. For indium (Fig. 6) the two sets of data are at least in agreement to order of magnitude. Part of the disagreement in the case of indium may be due to the different superconducting properties of the samples. Because of the serious disagreement in the case of tin, this laboratory has undertaken to repeat the measurement for tin with an arrangement similar to that used by Keesom and Matthijs. The results of that independent investigation[17] were in very good agreement with the data given in the present paper.

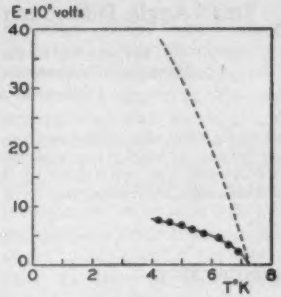

FIG. 9. Effect of impurities on the results for lead. The dashed curve represents results for lead of 99.98 percent purity, while the solid circles give the values obtained for lead of approximately 98 percent purity.

VIII. CONCLUSIONS

The results obtained in this investigation for the temperature variation of the thermoelectromotive force of a superconducting-normal junction of the same metal are consistent with a relation derived from Fermi-Dirac statistics and the assumption that the Thomson coefficient of the superconducting state is zero. It is proposed that the disagreement between experimental results and Kok's hypothesis may be due to interaction between electrons and lattice in the superconducting state.

The author wishes to express his appreciation to Dr. R. T. Webber for having suggested this problem, and to Mr. M. F. M. Osborne for profitable discussions relating to theoretical interpretation. Thanks are also due to Mr. J. Babiskin for help in making many of the measurements.

[17] R. T. Webber and M. C. Steele, Phys. Rev. 79, 1028 (1950).

Small Angle Diffraction of Light by a Glass Cube

A. THEODORE FORRESTER AND LOTHROP MITTENTHAL
University of Southern California, Los Angeles, California
(Received August 8, 1950)

Experiments on the diffraction of light by a glass cube failed to yield results compatible with a theory of Halpern and Gerjuoy. Although it is possible that the anomalously large amount of scattering predicted by the theory could have been counteracted by the effects of the clamping of the cube, this seems very unlikely. The remaining alternative appears to be that the use of Born approximation in the theory is unjustified.

I. INTRODUCTION

IN a recent paper by Halpern and Gerjuoy[1] a formula is derived which is applicable to the diffraction of light from a glass parallelopiped, provided the index of refraction of the surroundings is close to that of glass. When the incident wave is travelling in a direction which is within 0.2° of being parallel to one of the faces, a very large amount of small angle scattering is predicted in the plane perpendicular to this face and containing the direction of the incident beam. For a cube of edge L, their formula for the differential scattering cross section can be written

$$\sigma(\theta,\phi)=\frac{\pi^2}{\lambda^4}(1-\mu^2)^2L^6\frac{\sin^2(\pi L\mathbf{q}\cdot\mathbf{i}_1/\lambda)}{(\pi L\mathbf{q}\cdot\mathbf{i}_1/\lambda)^2}\cdot\frac{\sin^2(\pi L\mathbf{q}\cdot\mathbf{i}_2/\lambda)}{(\pi L\mathbf{q}\cdot\mathbf{i}_2/\lambda)^2}\cdot\frac{\sin^2(\pi L\mathbf{q}\cdot\mathbf{i}_3/\lambda)}{(\pi L\mathbf{q}\cdot\mathbf{i}_3/\lambda)^2}. \quad (1)$$

In this expression λ is the wavelength of the light, μ is the index of refraction of the glass relative to its surroundings, and $\mathbf{i}_1$, $\mathbf{i}_2$, $\mathbf{i}_3$ represent unit vectors in the directions of three mutually perpendicular edges of the cube, as shown in Fig. 1. The vector

$$\mathbf{q}=\mathbf{k}_s-\mathbf{k}_0$$

is the difference between unit vectors in the directions of the scattered and incident waves, and, for small angle scattering, its magnitude is easily seen to be the scattering angle θ. If the vector $\mathbf{k}_0$ lies in one face, as required for the anomalous effect sought in this experiment, Eq. (1) becomes

$$\sigma_1(\theta,\phi)=\frac{\pi^2}{\lambda^4}(1-\mu^2)^2L^6\frac{\sin^2(\pi L\theta\cos\phi/\lambda)}{(\pi L\theta\cos\phi/\lambda)^2}\cdot\frac{\sin^2(\pi L\theta\sin\phi\sin\alpha/\lambda)}{(\pi L\theta\sin\phi\sin\alpha/\lambda)^2}\cdot\frac{\sin^2(\pi L\theta\sin\phi\cos\alpha/\lambda)}{(\pi L\theta\sin\phi\cos\alpha/\lambda)^2}, \quad (2)$$

where α is the angle between $\mathbf{k}_0$ and one of the edges of the face containing $\mathbf{k}_0$, as shown in Fig. 1. At $\phi=0$, the direction for which large scattering is predicted, this equation reduces to

$$\sigma_1(\theta,0)=(\pi^2/\lambda^4)(1-\mu^2)^2L^6\sin^2(\pi L\theta/\lambda)/(\pi L\theta/\lambda)^2. \quad (3)$$

To appreciate the magnitude of this quantity, compare this scattering with the diffraction of light by a square aperture. If $\mathbf{i}_1$ and $\mathbf{i}_2$ represent unit vectors in the directions of the sides of a square, the differential cross section for the aperture is[2]

$$\sigma(\theta,\phi)=\frac{L^4}{\lambda^2}\frac{\sin^2(\pi L\mathbf{q}\cdot\mathbf{i}_1/\lambda)}{(\pi L\mathbf{q}\cdot\mathbf{i}_1/\lambda)^2}\frac{\sin^2(\pi L\mathbf{q}\cdot\mathbf{i}_2/\lambda)}{(\pi L\mathbf{q}\cdot\mathbf{i}_2/\lambda)^2}, \quad (4)$$

where L, here, represents the length of a side of the

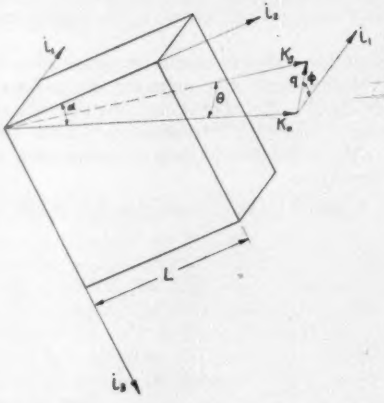

FIG. 1. Quantities involved in the scattering of light by a glass cube.

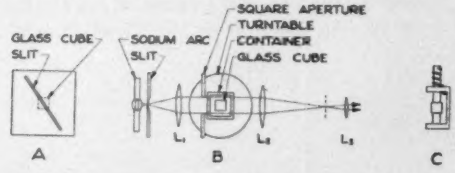

FIG. 2. Schematic diagram of the apparatus showing (a) the light source view of the slit illustrating its orientation with respect to the glass cube, (b) the assembly of the apparatus, and (c) the clamp for the glass cube.

[1] O. Halpern and E. Gerjuoy, Phys. Rev. 76, 1117 (1949).

[2] E.g., Max Born, *Optik* (Verlag. Julius Springer, Berlin, 1933), p. 157.

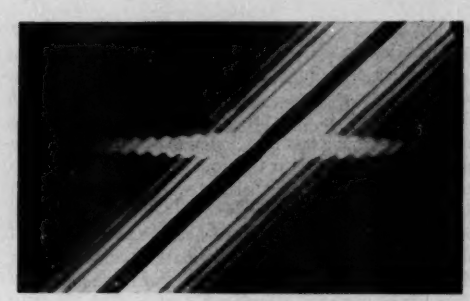

FIG. 3. Expected appearance of the image, according to the theory of Halpern and Gerjuoy. *This picture is a double exposure of two single slit diffraction patterns.* The central image is blocked out.

square. For small angle scattering in a direction parallel to one of the edges, Eq. (4) becomes

$$\sigma_2(\theta, 0) = (L^4/\lambda^2) \sin^2(\pi L\theta/\lambda)/(\pi L\theta/\lambda)^2. \qquad (5)$$

Equations (3) and (5) are identical except for the multiplicative constants, the scattering by a glass cube being greater by the factor

$$\sigma_1/\sigma_2 = \pi^2(1-\mu^2)^2 L^2\lambda^2/\lambda_g{}^4 = 4\pi^2\delta^2 L^2\mu_g{}^4/\lambda^2, \qquad (6)$$

where $\lambda_g = \lambda/\mu_g$ is the wavelength of the light in the glass cube, and $\delta = \mu - 1$ is considered to be small compared with unity. If $L = 0.5$ cm, $\lambda = 5.89 \times 10^{-5}$ cm, and $\mu_g = 1.517$ (the values used in this experiment), $\sigma_1/\sigma_2 = 1$ when $\delta = 8 \times 10^{-6}$. If the index of refraction of the glass cube relative to its surroundings is as large as 1.001, then $\sigma_1/\sigma_2 = 1.5 \times 10^4$. This result is astounding in its magnitude and one that should be easily and strikingly observable.

II. THE EXPERIMENTS

The apparatus used in the attempt to observe this effect is illustrated schematically in Fig. 2. Light from a sodium arc collimated by the slit and lens L_1 and restricted by a square aperture 8 mm on a side, illuminates the 5-mm glass cube immersed in liquid, and is converged to the focus of the 85-cm focal length lens L_2, where it can be viewed with the eyepiece L_3 or recorded photographically.

The adjustment of the collimating system was accomplished with the aid of a telescope equipped with a Gaussian eyepiece. The maximum angular spread in the beam due to error in positioning the slit in this manner is certainly less than 2′, a fact verified by photographs taken with lens L_2 absent. Since Halpern and Gerjuoy predict a large fanning of the beam for angles as large as 12′ between k_0 and the face of the cube, this beam may be considered well collimated for the experiment.[3]

The 5-mm cube was mounted in the "C" clamp illustrated in Fig. 2c, which fitted snugly into an absorption cell filled with a liquid. The glass was crown glass of index 1.5170, which we are able to match quite closely with anisole, whose index is 1.5173. By adding a small percentage of kerosene it was possible, judging from the difficulty of visually locating the cube in the liquid, to match the index more closely than this.

As shown in Fig. 2a, the slit was tipped with respect to the cube. With this arrangement, only a small area of the slit illuminates the glass cube at the correct angle, and the image sought should have the appearance of Fig. 3. As the turntable is rotated, the horizontally diffracted streak should move up or down the slit.

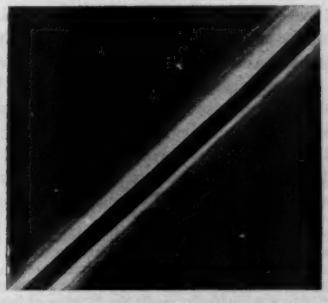

FIG. 4. Diffraction pattern of a glass immersed in anisole, using a tipped slit for the light source.

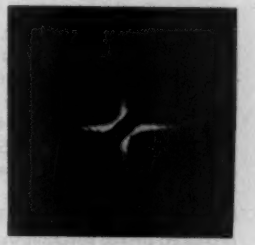

FIG. 5. Diffraction pattern of a glass cube immersed in anisole, using a point source.

In the photograph shown in Fig. 4 no sign of the effect sought can be seen. A comparison of this photograph with photographs made first with the cube absent, and secondly with the cube replaced by an opaque object, indicates that what is observed is simply a combination of the diffraction by the square aperture and by the two slits formed by the edges of the glass cube and the edges of the square aperture.

It is important to note that the angle made between the critical surface of the glass cube and the light coming from one end of the slit differs by 1.5° from the angle with which light from the other end of the slit strikes the face of the cube. Since the fanning out of the beam is predicted for light making an angle as large as ±0.2° with one face, the image should be spread out for about one-fourth of its length. This would be a plainly observable effect.

[3] However, see Sec. III of this paper.

Examinations of the diffraction patterns, using this tipped slit technique, were made visually as well as photographically, with the environment of the cube provided by numerous mixtures of liquids, including some matching the index of refraction of the glass very closely (probably $|1-\mu|<10^{-4}$). In no case was any sign of the sought-after effect observed.

The possibility that the orientation of the cube was sufficiently in error that none of the light illuminated the cube at the appropriate angle can easily be ruled out. Images of the slit produced by total reflection of the light from the faces of the cube could be seen, and the cube was oriented midway between those positions which gave symmetric images on the two sides. This could be done to an accuracy which guaranteed that the appropriate angle of incidence occurred for the light originating near the center of the slit. In addition, the turntable carrying the tube could be rotated continuously during visual observation; and no effect which was not completely symmetrical along all points of the slit could be observed, other than that definitely assignable to the reflection.

Although the expected effect is so large that it should be immediately apparent, we carried the experiment one step further to see if there was not perhaps an effect of the type sought but very much smaller. Accordingly, a point source was approximated by crossing the slit with another. While lacking the observational convenience of the previous arrangement, this offers the advantage that there is no diffracted light from the rest of the slit to mask the effect. In this experiment we obtained a series of photographs, one of which is shown in Fig. 5, with the cube rotated 6′ between each exposure. The only noticeable change produced by the rotation was a faint tailing to the right in some cases and to the left in others. This did not have the symmetry of the predicted effect; and, in some cases, the intensity plainly increased after a certain distance from the center of the pattern instead of falling off steadily. These patterns are completely explainable in terms of total reflections from faces of the cube, if one takes into account the diffraction by the reflecting surface.

In view of the negative results, it is important to examine the experiment very critically for possible weaknesses. The glass cube[4] was inspected carefully for flaws, first between crossed polaroids, and secondly by half-silvering and examining the fringes of equal thickness.[5] In the first test a uniform darkness of the field indicated no anisotropy in the glass, and in the second test sharp straight fringes failed to show any deviations from flatness in the surfaces or any inhomogeneities in the glass. The number of fringes observed in the latter examination indicated a tip of 2′ for the faces examined, but this is of no consequence. Parallelism of the surfaces is not critical in the theory of Halpern and Gerjuoy.

The effect of clamping the cube, as shown in Fig. 2c is difficult to evaluate with certainty. A method of eliminating this as a factor would be to make a clamp of a transparent plastic of index close to that of the glass and then to match the liquid to the plastic; or to imbed the glass cube in a plastic whose index matched its own very closely. However, it is difficult for us to believe that clamping on faces which are not the critical ones for this experiment can eliminate so completely an effect of this magnitude; and neither of these modifications has as yet been attempted.

III. DISCUSSION AND CONCLUSION

A more basic consideration is the effect of a lack of parallelism in the light falling on the cube. If the collimating slit is not precisely in the focal plane of the collimating lens L_1 (Fig. 1b), the light will have an angular spread as it approaches the cube through the square aperture. The experimental procedure followed by us ensured an angular spread of less than 2′, and since the effect sought requires alignment of the beam to within $\pm 12'$, this would appear to be a well-collimated beam. However, since the components of the beam travelling in different directions, because of this effect, would not be randomly phased, it appears reasonable to ask whether it is not possible that an interference of the scattered light corresponding to the various components does not somehow manage to obliterate the effect completely. This cancellation would have to be postulated as one that persisted down to very small angular spreads, because in one set of visual observations the position of the collimating slit was varied continuously about the focal plane of the collimating lens with no appearance of the phenomenon sought.

Furthermore, if this objection is to be raised, it applies equally well to the angular apread introduced by the diaphragm, which in this case is about 0.4′ for the center of the diffraction pattern.

However, the basic assumption of the theory which this experiment is designed to test is that effects of this kind can be neglected, provided the angular spread introduced is small. As soon as the scattering cross section calculated for the cube becomes larger than the physical cross section of the cube, the problem becomes a multiple scattering problem. The beam passing over the latter half of the cube is that scattered by the first half and will have introduced into it a small angular spread. Under these conditions the objection raised to the experiment applies equally well to the theory.[6]

[4] Made for this experiment by Herron Optical Company, Los Angeles, California.

[5] E.g., Tolansky, *High Resolution Spectroscopy* (Pitman Publishing Corporation, New York, 1947), pp. 141–142.

[6] Halpern and Gerjuoy recognized that they were concerned with a multiple scattering problem, but dismissed this as a possible source of error by stating that, as coherent scattering, the angular spread must be less than for incoherent scattering; and that if this is sufficiently small, the "scattered beams are in effect reabsorbed in the main beam." This process cannot be expected to give the correct result for the central beam, i.e., for

In other words, the use of first-order theory (Born approximation) by Halpern and Gerjuoy may not be justified. To decide definitely, a quantitative investigation of the error introduced by the Born approximation is necessary. If this approximation proves valid, an examination of the effects of the mounting is called for.

In any case the theory would be expected to be valid for μ so close to unity that the problem ceases to be a case of multiple scattering, and it is of interest to see to what this criterion is equivalent. If the incident beam, for simplicity, is parallel to four of the faces of a cube, the differential cross section can be obtained from Eq. (2) by setting $\alpha=0$ and plainly has the same form as the scattering from a square aperture expressed in Eq. (4). The transition to multiple scattering will occur when the coefficients of Eqs. (2) and (4) are equal; i.e., when σ_1/σ_2, as expressed in Eq. (6), is less than unity. This condition may be written

$$\delta L/\lambda_0<1/2\pi\mu_0. \tag{7}$$

The quantity δL is the optical path difference between the two paths through the cube and outside the cube. It is perhaps surprising to recognize that this problem does not cease to be a multiple scattering problem until the optical path difference becomes as small as is indicated by this equation. In other terms, a glass cube immersed in a liquid whose index of refraction matches the glass so closely that the optical path through and outside the cube differ by only one-tenth of a wavelength appears to be as effective a diffracting object as an opaque absorber, at least for light striking a face of the cube normally.

It is doubtful whether the index of refraction of the fluid ever matched the glass sufficiently closely in this experiment to satisfy the criterion of Eq. (7), or whether an effect which is the same as the scattering by the aperture would have been noticed in this experiment.

We wish to acknowledge the help of numerous stimulating discussions with Dr. E. Gerjuoy.

angles less than λ/L; but it might be expected to do so for larger angles. Halpern and Gerjuoy were particularly concerned with the angle $(\lambda/\pi L)^{\frac{1}{2}}$, which is about 20′ for the values used here, an angle easily observable with the apparatus used.

PHYSICAL REVIEW VOLUME 81, NUMBER 2 JANUARY 15, 1951

On the Maxima of the Patterson Functions

PHILIP HARTMAN AND AUREL WINTNER
Department of Mathematics, Johns Hopkins University, Baltimore, Maryland

(Received September 11, 1950)

For the case of a one-dimensional crystal (and, therefore, in three dimensions as well) it is possible to construct a counter-example, realizing the following situation: the electron density is the sum of two monatomic distributions, but the number of peaks in Patterson's diagram exceeds three, whereas the standard rule would claim at most three such peaks. Consequently, the usual "addition rule of peaks" is false as a general mathematical theorem. It follows that the explanation of the empirical success of this rule in crystallography lacks to date a mathematical basis, that is, a non-empirical foundation.

I. INTRODUCTION

FOR the sake of simplicity, the following remarks on Patterson's diagram will be formulated, as is usual since Patterson's first publications on the subject, for the case of a one-dimensional crystal. This simplification of the model is not always legitimate in the deduction of positive theorems. It will be legitimate in the following considerations, the results of which will be negative in nature.

Let $\rho(x)$ be a positive periodic function of period a, and let $P(X)$ denote the corresponding Patterson function ("auto-convolution"), defined by

$$P(X)=\frac{1}{a}\int_0^a \rho(x)\rho(x+X)dx. \tag{1}$$

Then $P(X)$ is positive, of period a, and even, that is, $P(X)=P(-X)$. In Fourier terms, the connection between $\rho(x)$ and $P(X)$ is as follows: If

$$\rho(x)=\sum_{h=-\infty}^{+\infty} F_h \exp(-2\pi i h x/a), \tag{2}$$

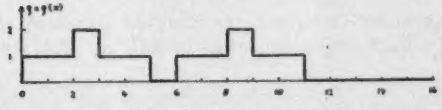

FIG. 1. Graph of $\rho(x)$ for Example 1.

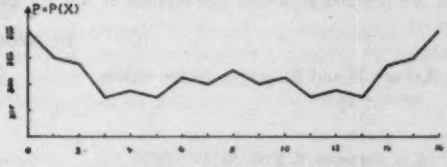

FIG. 2. Graph of $P(X)$ for Example 1.

then

$$P(X)=\sum_{h=-\infty}^{+\infty}|F_h|^2\exp(-2\pi ihX/a). \tag{3}$$

What will be referred to as Patterson's principle are certain statements connecting the "peaks" of the graph of $\rho(x)$ with those of $P(X)$. Some of the empirical discrepancies arising in the applications of this principle are usually excused by an appeal to the slowness of the convergence of the respective series (2), (3). Such effects of slow convergence will not enter into the following considerations. In fact, $\rho(x)$ will be defined directly by a graph, rather than by its Fourier analysis (2), and the graph of $P(X)$ will then be calculated, without any error, directly from (1), rather than from (3).

The crystallographic literature[1] contains the following principle, which will be called the Patterson principle:

If $\rho(x)$ is continuous and has a finite number N of peaks (local maxima) on a period, $0\leq x<a$, say at $x=x_1, x_2, \cdots, x_N$, then $P(X)$ can have peaks only at (or near) the points $X=x_m-x_n+ka$, where $1\leq m, n\leq N$ and $k=0, \pm1, \pm2, \cdots$.

Some writers do not formulate the principle as cautiously as it is formulated above, but state directly or by implication,[2] that $P(X)$ has peaks at, and only at, the points $X=x_m-x_n+ka$.

A corollary of the Patterson principle is that $P(X)$ has at most $N(N-1)$ peaks on the interval $0<X<a$. The less cautiously worded form of this principle would imply that, if the interatomic distances $|x_m-x_n|$ are distinct for distinct pairs of atoms, then $P(X)$ has exactly $N(N-1)$ peaks on the interval $0<X<a$.

It will be shown below that, as a mathematical theorem, the Patterson principle is not true. In fact, the number of peaks of $P(X)$ on the interval $0<X<a$ can be greater than $N(N-1)$; so that the location of a peak of $P(X)$ need not correspond to an interatomic distance $|x_m-x_n|$. It is known that the number of peaks might be less than $N(N-1)$; in fact, Patterson has pointed out that peaks can be "hidden or distorted." However, the possibility of an excess of peaks is not mentioned.

To facilitate the calculation of $P(X)$ from (1), the counter-examples $\rho(x)$ will be given as non-negative, discontinuous functions. Since (1) shows that the Patterson function is changed only slightly when small changes are made in $\rho(x)$, it will be clear from continuity considerations that the given $\rho(x)$ can be replaced by a positive, continuous function (with two well-defined maxima on a period), without invalidating the considerations below.

II. FIRST EXAMPLE

Let $a=16$, and let $\rho(x)$ have the values

$$1,\quad 2,\quad 1,\quad 0,\quad 1,\quad 2,\quad 1,\quad 0$$

on the respective intervals

$$0\leq x<2,\quad 2\leq x<3,\quad 3\leq x<5,\quad 5\leq x<6,\quad 6\leq x<8,\quad 8\leq x<9,\quad 9\leq x<11,\quad 11\leq x<16.$$

The graph of $\rho(x)$ is given in Fig. 1.

The Patterson function $P(X)$, belonging to the function $\rho(x)$ just defined, is continuous; in fact, its graph consists of line-segments joining the pairs of points of coordinates $(X, P(X))$, where $X=0, \pm1, \pm2, \cdots$, for consecutive values of X. The definition, (1), of $P(X)$ shows that the values of $P(X)$ for

$$X:\quad 0,\quad \pm1,\quad \pm2,\quad \pm3,\quad \pm4,\quad \pm5,\quad \pm6,\quad \pm7,\quad \pm8$$

are

$$P(X):\quad \frac{16}{16},\ \frac{12}{16},\ \frac{11}{16},\ \frac{6}{16},\ \frac{7}{16},\ \frac{6}{16},\ \frac{9}{16},\ \frac{8}{16},\ \frac{10}{16},$$

respectively. The graph of $P(X)$ is given in Fig. 2 (abscissae and ordinates are not drawn for the same scale of units).

The Patterson principle predicts that the maxima of $P(X)$ for $-8<X\leq8$ will occur at (or near) some or all of the points $X=0, \pm6$. But it is seen that, while $P(X)$ does have maxima at $X=0, \pm6$, it has, in addition, maxima at $X=\pm4$ and at $X=8$. The maxima at $X=\pm4$ and at $X=8$ do not correspond to "interatomic" distances.

III. SECOND EXAMPLE

Let $a=30$ and let $\rho(x)$ have the values

$$4,\quad 8,\quad 1,\quad 0,\quad 1,\quad 5,\quad 4,\quad 0$$

[1] A. L. Patterson, Z. Krist. **90**, 517 (1935).
[2] Compare, for instance, M. J. Buerger, Proc. Nat. Acad. Sci. **36**, 325 (1950).

on the respective intervals

$$0\leq x<1,\quad 1\leq x<2,\quad 2\leq x<5,\quad 5\leq x<10,\quad 10\leq x<13,\quad 13\leq x<14,\quad 14\leq x<15,\quad 15\leq x<30.$$

A straight-forward calculation shows that the graph of the corresponding Patterson function $P(X)$ consists of the linear segments joining pairs of points of coordinates $(X, P(X))$, where $X=0, \pm1, \pm2, \cdots$, for consecutive values of X. The values of $P(X)$ for

$$X:\ 0,\quad \pm1,\quad \pm2,\quad \pm3,\quad \pm4,\quad \pm5,\quad \pm6,\quad \pm7,\quad \pm8,\quad \pm9,\quad \pm10,\quad \pm11,\quad \pm12,\quad \pm13,\quad \pm14,\quad \pm15$$

are

$$P(X):\ \frac{127}{30},\ \frac{69}{30},\ \frac{23}{30},\ \frac{21}{30},\ \frac{8}{30},\ 0,\ 0,\ 0,\ 0,\ 0,\ \frac{22}{30},\ \frac{21}{30},\ \frac{48}{30},\ \frac{52}{30},\ \frac{16}{30},\ 0,$$

respectively.

For this case, the Patterson principle predicts that the maxima of $P(X)$ for $-15<X\leq15$ will occur at (or near) some or all of the points $X=0, \pm12$, It is seen that $P(X)$ does have maxima at $x=0, \pm13$, but has maxima at $X=\pm10$ also. The latter maxima do not correspond to "interatomic distances."

IV. COMMENTS

These examples show that the Patterson principle cannot be stated as a mathematical theorem. The errors in the usual arguments (see Patterson, 1935) for the validity of Patterson's principle are easy to see. In these arguments it is assumed that $\rho(x)$ is the sum of "atomic functions" $\rho_1(x), \cdots, \rho_N(x)$, each of period a, and each possessing exactly one peak for $0\leq x<a$, the peaks occurring say at $x=x_1, \cdots, x_N$, respectively. This assumption is satisfied by the functions $\rho(x)$ above. In fact, if, in the first example, $\rho_1(x)=\rho_1(x+16)$ has the values

$$1,\quad 2,\quad 1,\quad 0$$

for

$$0\leq x<2,\quad 2\leq x<3,\quad 3\leq x<5,\quad 5\leq x<16,$$

respectively, and if $\rho_2(x)=\rho_1(x-6)$, then $\rho(x)=\rho_1(x)+\rho_2(x)$. In the second example, if $\rho_1(x)=\rho_1(x+30)$ has the values

$$4,\quad 8,\quad 1,\quad 0$$

for

$$0\leq x<1,\quad 1\leq x<2,\quad 2\leq x<5,\quad 5\leq x<30,$$

respectively, and if $\rho_2(x)=\rho_2(x+30)$ has the values

$$0,\quad 1,\quad 5,\quad 4,\quad 0$$

for

$$0\leq x<10, 10\leq x<13, 13\leq x<14, 14\leq x<15, 15\leq x<30,$$

respectively, then $\rho(x)=\rho_1(x)+\rho_2(x)$. The standard arguments then state that each of the functions

$$P_{nm}(X)=\frac{1}{a}\int_0^a \rho_n(x)\rho_m(x+X)dx$$

has peaks at, and only at, $X=x_n-x_m+ka$, where $k=0, \pm1, \cdots$. This statement concerning $P_{nm}(X)$ is not in general true. It happens to be true if $\rho_n(x)$, $\rho_m(x)$ is any pair of the functions $\rho_1(x)$, $\rho_1(x)$, $\rho_2(x)$, $\rho_2(x)$ occurring in the definition of the first example above. But it is not true if $\rho_n(x)$, $\rho_m(x)$ is the pair of functions $\rho_1(x)$, $\rho_2(x)$ occurring in the definition of the second example above.

[It is hardly possible to formulate a necessary and sufficient condition on $\rho_n(x)$, $\rho_m(x)$ which would ensure the truth of the statement concerning $P_{nm}(X)$. A sufficient, but surely not very useful, condition results by requiring the graphs of $\rho_n(x)$, $\rho_m(x)$ to be symmetric relative to the vertical lines through their peaks. In the case of 3-dimensional crystals, this symmetry requirement becomes an assumption of spherical symmetry.]

At the end of the standard arguments, the Patterson principle is "deduced" from the identity

$$P(X)=\sum_{n=1}^{N}\sum_{m=1}^{N}P_{nm}(X).$$

Even if the objections made up to this point are met, the Patterson principle does not follow from this identity. This is shown by the first example above. [The difficulties involved in attempting to deduce the number of peaks of $P(X)$ from the number of peaks of each of the summands $P_{nm}(X)$ are illustrated by the fact that if, in the first example above, $\rho(x)=\rho_1(x)+\rho_1(x-6)$ is modified to be $\rho(x)=\rho_1(x)+\rho_1(x-4)$, the resulting function $\rho(x)$ has three peaks instead of two.]

Since the Patterson principle is not valid as a general mathematical theorem, it becomes an open question whether or not the principle happens to be true for all of the electron density functions considered in crystallography.

We wish to thank Drs. Gabrielle Donnay and J. D. H. Donnay of The Johns Hopkins University for helpful discussions of the crystallographic aspects of the problem and of our objections to the classical rule.

Letters to the Editor

PUBLICATION of brief reports of important discoveries in physics may be secured by addressing them to this department. The closing date for this department is five weeks prior to the date of issue. No proof will be sent to the authors. The Board of Editors does not hold itself responsible for the opinions expressed by the correspondents. Communications should not exceed 600 words in length.

On the Existence of Rossi Second and Third Maxima

P. K. SEN CHAUDHARY
Bose Research Institute, Calcutta, India
October 16, 1950

RECENTLY the controversial existence of a Rossi second maximum has been claimed to be re-established[1-3] along with a third maximum. It appears from the results of Hess[4] and his co-workers that they obtained some evidence of the third maximum at 25 cm of lead, using a triple coincidence arrangement similar to that of Clay.[1] We also have definitely established the existence of second and third maxima. From a careful analysis it seems that the failure of some workers to confirm these maxima may be due to overlapping, firstly by oblique showers when the three counters are arranged very close together near the absorber, and secondly by a greater percentage of side showers of external origin when all the three counters without sufficient vertical separation are placed far below the absorber for narrow-angle showers. Full details will be published soon. We were led to these investigations by the correspondences of these maxima with the anomalies of RaC gamma-ray absorption in lead reported by the author.[5] The absorption coefficient between 16 and 20 cm, particularly at about 24 cm, was found to be far below the theoretical minimum value as shown in Fig. 1, with a rise again after this. This was attributed to some neutral particle either emitted by RaC or created by a photon. This anomaly almost exactly corresponds to the third maximum in the *d*-curve of Bothe[3] which he indicates is due to a long-lived neutretto. Soddy and Russell[6] obtained a hump in the log intensity curve exactly where the Rossi second maximum is obtained and they interpreted these to be due to some peculiar secondary radiation generated in lead and manifesting itself in this locality. They could eliminate these by bringing the electroscope very near the absorber. From these correspondences we[5] suggested that these anomalies and the two maxima have the same origin and probably are due to two groups of unstable neutral particles of low mass produced by the photon. Since RaC gamma-rays are of maximum energy only 2.4 Mev, therefore these neutral particles might be simply positron-electron dipoles behaving like the former before annihilation. According to Heitler[7] the probability of a positron capturing an electron is a maximum when its kinetic energy is 0.5 Mev and consequently a positron-electron dipole with very slight interaction with matter and with this much energy requires a life only about 10^{-9} sec to produce these anomalies and maxima. The two groups may be due to two different lives depending on spin. Wheeler[8] showed that a positron-electron can only form an atom of life about 10^{-6} sec with parallel spin and the probability of its formation is one in a million.

The author is thankful to Dr. D. M. Bose for kindly providing laboratory facilities and to the Imperial Chemical Industries for the grant of a fellowship.

[1] J. Clay, Revs. Modern Phys. 21, 82 (1949).
[2] E. Fenyves and O. Haiman, Nature 165, 244 (1950).
[3] W. Bothe and H. Thurn, Phys. Rev. 79, 544 (1950).
[4] V. F. Hess, *et al.*, Phys. Rev. 58, 1011 (1940).
[5] P. K. Sen Chaudhary, Ind. J. Phys. 22, 341 (1948); Science and Culture 15, 38 (1949).
[6] Soddy and Russell, Phil. Mag. 19, 725 (1910).
[7] W. Heitler, Quantum Theory of Radiation (Oxford University Press, London, 1944).
[8] J. A. Wheeler, Ann. New York Acad. Sci. 48, 219 (1946).

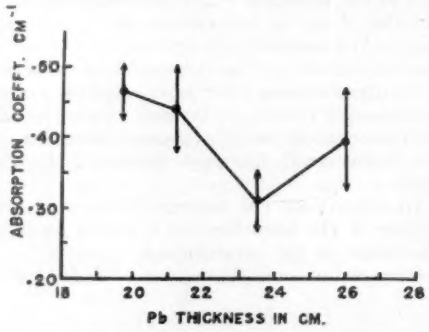

FIG. 1. Absorption coefficient of the RaC γ-ray in lead.

The Cathode Field in Diodes under Partial Space-Charge Conditions with Initial Velocities

A. O. BARUT
Department of Applied Physics, Swiss Federal Institute of Technology, Zürich, Switzerland
October 27, 1950

A FORMULA has been given by Ivey[1] which relates the cathode field, E, in a diode under partial space-charge conditions to the actual diode current density, I, if the initial velocities of the electrons are neglected. We have obtained a more general formula, inclusive of the effects of a homogeneous initial velocity distribution, by a method described below.

If the velocity vector of an electron is denoted by

$$\mathbf{V}=f(x)\mathbf{i}+k\mathbf{j} \tag{1}$$

the equations of motion, and those of the electric field, yield for the function $f(x)$ the differential equation[2]

$$f'^2+4ff'f''+f'''f^2=0. \tag{2}$$

With the initial condition $f(0)=(\partial u_1/m)^{\frac{1}{2}}\cos\varphi$, where u_1 is the initial velocity, the field strength, $E(x)$, and the current density can be calculated in terms of $f(x)$ and its derivatives by the relations

$$E(x)=-(m/e)ff', \tag{3}$$

$$I=\rho V=-(m\epsilon_0/2e)(ff'^2+f^2f''). \tag{4}$$

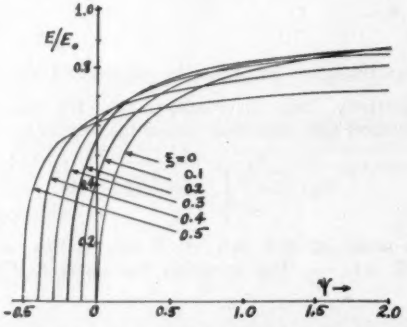

FIG. 1. Dependence of E/E_0 on ψ for various values of ξ.

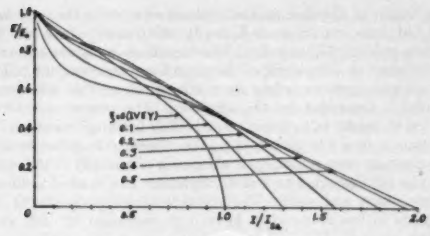

FIG. 2. Dependence of E/E_0 on I/I_{∞} for various values of ξ.

The solution of (2) when inserted into (3) and (4) gives the following general equations[3]

$$(I/I_{\infty})^{\frac{1}{2}}=(1-2\psi)(1+\psi)^{\frac{1}{2}}-(\xi-2\psi)(\xi+\psi)^{\frac{1}{2}} \quad (5)$$

$$E/E_0=(4/3)[(1-2\psi)(1+\psi)^{\frac{1}{2}}(\xi+\psi)^{\frac{1}{2}}-(\xi-2\psi)(\xi+\psi)]. \quad (6)$$

Here I_{∞} is the saturation current density with zero initial velocities according to Child's law

$$I_{\infty}=(4\epsilon_0/9d^2)(\vartheta/m)^{\frac{1}{2}}u_a^{\frac{3}{2}}.$$

E_0 is the value of E in the absence of current flow (i.e., is equal to u_a/d), ξ is the relative initial velocity of the electrons

$$\xi=(u_1/u_a)^{\frac{1}{2}}\cos\varphi \quad (7)$$

and ψ is a parameter specifying the degree of space charge. For $\psi=-\xi$ it follows that $E=0$, so that the space charge is "complete," and for $\psi\to\infty$, $E=E_0(I=0)$. With increasing current density ψ decreases from ∞ to $-\xi$ and the cathode field decreases from u_a/d to zero, as is indicated in Fig. 1.

In the general case a relation between I and E can be obtained by elimination of ψ between Eqs. (5) and (6), the nature of the result being shown in Fig. 2. For zero initial velocities ($\xi=0$) the formula of Ivey is regained

$$\frac{I}{I_{\infty}}=\frac{1}{2}\left\{1\mp\left[1-\frac{27}{4}\left(\frac{E}{E_0}\right)^2\left(1-\frac{E}{E_0}\right)\right]^{\frac{1}{2}}\right\}. \quad (8)$$

The solution of (2) also permits one to calculate the transit times of electrons with initial velocities, and the electron paths for oblique emission under partial space charge.[3]

[1] H. F. Ivey, Phys. Rev. 76, 554 (1949).
[2] A. O. Barut, Z. Angew. Math. u. Phys. (to be published, 1951).

Diverging Integrals in the Self-Charge Problem

J. McCONNELL
St. Patrick's College, Maynooth, Ireland
November 27, 1950

THE polarization of the vacuum arising from the virtual production of electron-positron pairs by an electromagnetic field was examined by Schwinger,[1] who found that the current induced in the vacuum contains a part which leads to a logarithmically divergent but unobservable charge renormalization in the current producing the electromagnetic field. In an investigation of the polarization of the vacuum by the virtual formation of particles with spin zero, Jost and Rayski[2] again found that the induced current includes a logarithmically divergent self-charge term, which moreover has the same sign as that occurring in Schwinger's result. In the calculation of the current induced by the virtual formation of particles with spin 1 having vector coupling with the electromagnetic field, Feldman[3] obtained a quadratic divergence in the self-charge term. He therefore concluded that the cancellation of the diverging self-charge cannot be effected by any superposition of real fields with spin 0, ½, and 1, if no formal regularization procedure is applied.

We have performed the calculation for spin 0 and spin 1 independently, and wish to draw attention to some points in the manipulation of the divergent integrals. For convenience we shall quote from Feldman's paper. In the case of spin 1 he gives the self-charge term of the induced current

$$\alpha/4\pi\cdot(\vartheta_1-\tfrac{1}{2}\vartheta_2)J_\mu(x), \quad (1)$$

where $J_\mu(x)$ is the current producing the external field,

$$\vartheta_1=1/im^3\cdot\int_{-\infty}^{\infty}\exp(im^2z)/z^2\cdot\epsilon(z)dz,$$

$$\vartheta_2=\int_{-\infty}^{\infty}\exp(im^2z)/z\cdot\epsilon(z)dz,$$

$$\epsilon(z)=z/|z|,\quad \alpha=e^2/4\pi,\quad \hbar=c=1.$$

Now these integrals have singularities at $z=0$. Integrating from $-\infty$ to $-z_0'$ and from z_0 to ∞ we deduce that

$$\vartheta_1=2+\vartheta_2+1/im^3\cdot\lim_{z_0\to 0,\ z_0'\to 0}(1/z_0-1/z_0'),$$

$$\vartheta_2=-\lim_{z_0\to 0,\ z_0'\to 0}(\log\gamma m^2z_0+\log\gamma m^2z_0'),$$

where

$$\gamma=1.78.$$

Expression (1) is equivalent to

$$\{2+\tfrac{1}{2}\vartheta_2+1/im^3\cdot\lim_{z_0\to 0,\ z_0'\to 0}(1/z_0-1/z_0')\}(\alpha/4\pi)J_\mu(x). \quad (2)$$

The most strongly divergent terms are imaginary and so must be excluded for physical reasons. In order to make them vanish we are obliged to take the principal values of the diverging integrals, that is, we must put $z_0'=z_0$. Then (2) becomes

$$\{2-\lim_{z_0\to 0}\log\gamma m^2z_0\}(\alpha/4\pi)J_\mu(x), \quad (3)$$

which diverges logarithmically.

The part of the current induced in the vacuum through the formation of electron-positron pairs, which corresponds to (3), is

$$-(\alpha/6\pi)J_\mu(x)\int_{-\infty}^{\infty}\exp(im_e^2z)/z\cdot\epsilon(z)dz$$
$$=\lim_{z_0\to 0}(\log\gamma m_e^2z_0)\cdot\alpha/3\pi\cdot J_\mu(x), \quad (4)$$

where m_e is the electron mass. The sign of the logarithmic divergence is different in (3) and (4). Thus on admitting principal values—which, however, is an additional prescription—it will be possible to cancel the self-charge effects by a superposition of fields of particles with spins ½ and 1, or indeed by a superposition of fields with spins 0, ½, and 1.

However, the advantage gained by the compensation of the self-charge term is offset somewhat by the fact that in the case of vector mesons under consideration there appears also a diverging term

$$-(\alpha/24\pi m^2)\vartheta_2\Box J_\mu(x),$$

to which no term corresponds in the spin 0 or spin ½ cases.

I am indebted to Professor W. Heitler, University of Zürich, for helpful comments.

[1] J. Schwinger, Phys. Rev. 75, 651 (1949).
[2] R. Jost and J. Rayski, Helv. Phys. Acta 22, 457 (1949).
[3] D. Feldman, Phys. Rev. 76, 1369 (1949).

Čerenkov Radiation Counter for Fast Electrons*

JOHN MARSHALL
Institute for Nuclear Studies, University of Chicago, Chicago, Illinois
November 24, 1950

PROPOSALS have been made by Getting[1] and Dicke[2] to use Čerenkov radiation as a means of counting fast charged particles. Also recently Jelley[3] has reported Čerenkov detection of cosmic-ray particles. This letter is a description of an arrangement with which fast electrons, produced by the 48-Mev bremsstrahlung of a betatron, have been counted by the Čerenkov radiation which they produce in Plexiglas or Lucite. The work was undertaken in the hope of developing a velocity discriminating detector to be used with the 450-Mev proton synchrocyclotron under construction at the University of Chicago.

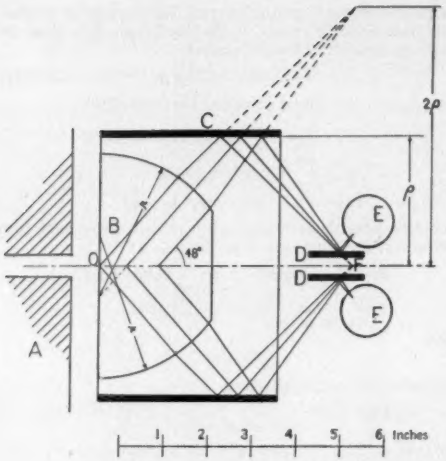

FIG. 1. Counter arrangement (explanation in text).

The arrangement is shown schematically in Fig. 1. The block, A, is a lead collimator through which electrons from a thin ($\frac{1}{8}$-in.) radiator in the betatron beam enter the system. The radiator, B, is made of Lucite or Plexiglas. It is a figure of revolution generated by rotating a circle around an axis in its plane, but not through its center. The radius of curvature, r, is so chosen as to focus the Čerenkov radiation into a sharp ring with a radius of approximately 2ρ, where ρ is the radius of a cylindrical reflector, C, made by silvering a piece of large diameter glass tubing on its inner surface. The cylindrical reflector focuses the light on the axis of the system at F where, in principle, a photo-multiplier could be placed to count the incident particles. Because of noise, it is much preferable to use a fast coincidence system operated by two photo-multipliers. To focus the light on two multipliers, two plane mirrors, D, are used. The photo-multipliers are of type 931-A.

The coincidence and counting circuit can be described briefly as follows. The pulse out of each multiplier was clipped with a 9-in. length of 173-ohm coaxial cable shorted at its far end, and was fed into two Spencer-Kennedy distributed amplifiers in cascade through 173-ohm line. The impedance level was reduced to 100 ohms at the output of the second amplifier and the pulse was clipped again to reduce its width, which at this point was broadened somewhat by the amplifiers. The pulses were then limited in height by a series crystal diode carrying current in a direction opposite to that in the pulse. Finally, the pulses in the two channels were combined at the center of a length of 100-ohm line and fed through a crystal discriminator to a linear amplifier, discriminator, and scaler. This coincidence circuit is similar in principle to one rumored to have been developed by Bell and Jordan.

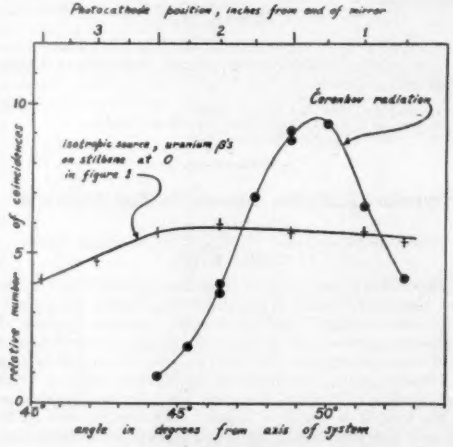

FIG. 2. Angular dependence of coincidence rate.

The Čerenkov counter was set up so that fast electrons, emitted from a lead radiator at about 0.1 radian from the forward direction of a collimated x-ray beam, could enter the system through its collimator after being deflected slightly by a small magnet. The direct x-ray beam was absorbed in 16 in. of lead. Coincidences were observed and it was found that the insertion of enough line in either channel to delay the pulse by 2×10^{-9} sec. reduced the counting rate by a factor 6. The same coincidence circuit excited by uranium betas on stilbene had its counting rate reduced by the same factor by a time delay of about 4×10^{-9} sec. It is apparent that the light pulses are quite short. It is felt that the resolving time obtained is as short as can be expected from the system even from an infinitely fast light pulse.

The counting rate was linear with betatron intensity as indicated by an ionization chamber. An absorption curve in iron taken with good geometry gave a relaxation length of 3.30 ± 0.1 cm, which indicated an effective x-ray energy of approximately 30 Mev.

The position of the multiplier tubes was varied to measure the angle of emission of the light from the forward direction of the electrons. The results are given in Fig. 2. The Čerenkov angle for Lucite ($n=1.5$), with particles of velocity C, should be about 48°. The observed angle indicates a slightly higher index of refraction which may perhaps be explained by assuming that most of the effective light is in the ultraviolet.

A two stilbene crystal coincidence absorber arrangement which should give approximately 100 percent counting efficiency for electrons above 5 or 6 Mev counted at ten times the rate of the Čerenkov counter in the arrangement used. At higher electron energies, the Čerenkov counter should be considerably more efficient than the 10 percent indicated here because of the longer electron ranges and reduced scattering to be expected. A variation of the arrangement described here will be tried with protons from the cyclotron when it comes into operation.

* Work supported in part by the ONR and AEC.
[1] I. A. Getting, Phys. Rev. 71, 123 (1947).
[2] R. H. Dicke, Phys. Rev. 71, 737 (1947).
[3] J. V. Jelley, Harwell Nuclear Physics Conference (September, 1950).

Magnetic Shielding of the Proton Resonance in H_2, H_2O, and Mineral Oil*

H. S. GUTOWSKY AND R. E. MCCLURE
Noyes Chemical Laboratory, University of Illinois, Urbana, Illinois
November 30, 1950

WE have measured the differences in magnetic shielding of the proton magnetic resonance in H_2, H_2O, and mineral oil (Nujol). These particular results are reported at this time because the proton resonances in water and mineral oil are used frequently as standards. The theoretical value[1,2] for the magnetic shielding in H_2 can be combined with these data to reduce other observations to the unshielded proton.

Experimental procedures were similar to those described previously.[3] A major improvement was made by reducing the *total variation* in the field of the permanent magnet to 0.15 gauss over a volume 2 in. in diameter and 1 in. thick. Half-maximum line widths of from 0.03 to 0.08 gauss were observed in these experi-

ments, using 30-cycle modulation. Measurements were made with a dual system, excited by a single oscillator at 27.2 Mc, and incorporating two samples in separate probes in the field. The difference in resonance magnetic fields for the two samples was obtained by measuring alternately the dc field-biasing current necessary to center first one resonance on an oscilloscope and then the other. The small difference in the applied fields at the two samples, due to residual field in homogeneities, was cancelled in the case of H_2O *versus* mineral oil by interchanging samples.

The effects of bulk diamagnetism are appreciable. The field, H_i, in the sample will differ from the applied field H_0, by an amount[4]

$$H_i - H_0 = (\tfrac{4}{3}\pi - \alpha)\kappa H_i = (\tfrac{4}{3}\pi - \alpha)\kappa H_0.$$

Here κ is the volume susceptibility of the sample, and α is the demagnetization factor which is 2π for an infinite cylinder and $4\pi/3$ for a sphere. Spherical samples are indicated but experimental difficulties prevented their use. Instead, "infinite cylinders" 8 in. long and $\frac{1}{2}$ in. in diameter were used for H_2O and mineral oil. Diamagnetic corrections were made using an α of 2π and κ's of -0.70 and $-0.65\pm0.05\times10^{-6}$ cgs units for H_2O and mineral oil respectively. The mineral oil κ was estimated from hydrocarbon data. κ for H_2 may be neglected.

H_2 was observed at 30 atmos in the pressure probe shown in Fig. 1. A photograph of its resonance and that of mineral oil is reproduced in Fig. 2. The phasing of the 30-cycle voltage on the

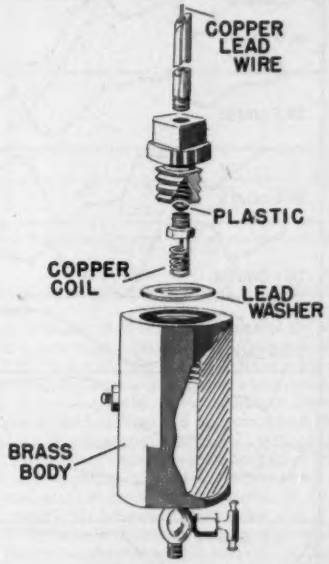

FIG. 1. Pressure probe for nuclear magnetic resonance experiments with gases. A null-T rf bridge was used with this assembly.

x-axis of the oscilloscope is adjusted to superimpose the first relaxation wiggle; this provides a sharper setting point than the resonance line itself. The pressure and reference probes were mounted rigidly in the gap. A length of $\frac{1}{32}$-in. copper tubing connected to the bottom inlet of the pressure probe was used to introduce, or remove hexane from the sample cavity. By comparing its resonance field with that of a hexane sample of the same shape in the reference probe, the difference in applied fields at the two positions was obtained. In all experiments with H_2 the sample in the reference probe was contained in the same Pyrex tube, 8 mm internal diameter and 8 in. long, with a thin glass barrier at the middle, and placed in the same position with

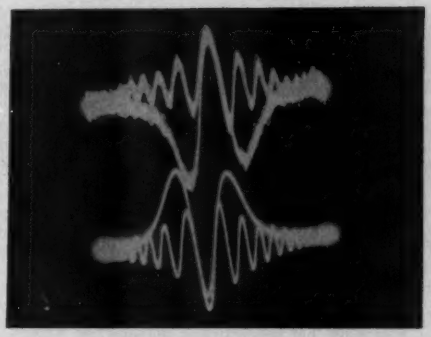

FIG. 2. Proton magnetic resonance lines in H_2 gas at 30 atmos (top) and mineral oil (bottom). The phasing of the 30-cycle reference voltage on the oscilloscope x-axis is adjusted to superimpose the first relaxation wiggles to provide a sharper setting point. Total modulation sweep is about 0.75 gauss.

the glass film below the bottom of the rf coil. For "infinite cylinders" the whole tube was filled.

The results are summarized in Table I. The stated errors are probable errors, which include the calibration of the field-biasing current, uncertainties in the diamagnetic corrections, and the probable error of the measured field-biasing currents themselves. The H_2O *versus* mineral oil results are in good agreement with those of Lindström,[5] whose data are equivalent to the applied

TABLE I. Magnetic shielding of the proton resonance in H_2, H_2O, and mineral oil at 27.1 Mc (6365 gauss). The applied field for mineral oil is higher than for H_2. Field differences are in gauss.

Sample	Difference in applied field corrected for diamagnetism	Fractional effect corrected for diamagnetism	Difference in applied field for "infinite cylinders"	Fractional effect for "infinite cylinders"
Mineral oil (Nujol)	0.0235±0.0020	$(3.7\pm0.3)\times10^{-6}$	0.0150±0.0010	$(2.3\pm0.15)\times10^{-6}$
H_2O (distilled)	0.0020±0.0020	(0.3±0.3)	−0.0075±0.0010	(−1.2±0.15)
H_2 (g, 30 atmos)	0.0000±0.0020	(0.0±0.3)	0.0000±0.0020	(0.0±0.3)

field for H_2O being less than that for paraffin oil by the fractional amount $4.1\pm3.0\times10^{-6}$. The absolute value of the proton magnetic moment is virtually unaffected[6] by the results reported herein, because differences in magnetic shielding constitute only about five percent of the stated error in the most recent determination.[7]

We wish to thank C. J. Hoffman for his assistance with several of the measurements. Equipment was provided by a Grant-in-Aid from Research Corporation.

* Supported in part by the ONR.

[1] N. F. Ramsey, Phys. Rev. **78**, 699 (1950).
[2] G. F. Newell, Phys. Rev. **80**, 476 (1950).
[3] H. S. Gutowsky and C. J. Hoffman, Phys. Rev. **80**, 110 (1950).
[4] W. C. Dickinson, Ph.D. thesis, MIT, Cambridge, Massachusetts (1950).
[5] G. Lindström, Phys. Rev. **78**, 817 (1950).
[6] The value obtained in reference 7 cannot be compared directly with these data as their water sample contained ferric ions.
[7] Thomas, Driscoll, and Hipple, Phys. Rev. **78**, 787 (1950).

The Production of π-Mesons in Proton-Proton Collisions

J. C. GUNN, E. A. POWER, AND B. TOUSCHEK
Department of Natural Philosophy, Glasgow University, Glasgow, Scotland
November 13, 1950

RECENT measurements[1] on the production of π-mesons in 345-Mev $p-p$ collisions have shown that the spectrum of the mesons has a strong maximum near the upper energy limit. This has been attributed to the interaction between the resulting

proton and neutron and to the possible formation of a deuteron.[3] The cross section in the laboratory system was estimated to be 20×10^{-30} cm²/sterad-Mev in the forward direction.[3]

We have carried out calculations which confirm this interpretation. A phenomenological interaction between nucleons has been assumed, following Foldy and Marshak.[4] It proves to be important, however, to give a more accurate account of the nuclear wave functions. The method employed is similar to that used by various authors[5] for the discussion of bremsstrahlung. The interaction Hamiltonian

$$H'=\int \psi^+(x)Q\phi(x)\psi(x)dx$$

between the nucleon and the meson field is written as

$$H'=\int\int[\psi_f^*\sum_{i=1}^{2}Q_i\phi(x_i)\psi_0]dx_1dx_2$$

in terms of the two-particle wave functions ψ_0 and ψ_f of the initial and final state. For nonrelativistic nucleons the 8-component spinor functions can be reduced to 4-component Pauli functions by a procedure in which a certain allowance is made for negative energy contributions. For the nonrelativistic approximation solutions of the appropriate Schrödinger-Pauli equation with empirical potentials V_0 and V_f can be taken. Serber's suggestion for zero interaction in odd states was adopted, but recent refinements in the $p-p$ interaction were not included.

Detailed calculations have been carried out for the case of a pseudoscalar charged meson with pseudovector coupling. The potentials were assumed to be of the Hulthén form

$$V=J^{(a)}e^{-\kappa r}/(1-e^{-\kappa r})$$

for even triplet ($s=3$) and even singlet ($s=1$) states, with $V=0$ for odd states. The result for the cross section corresponding to the formation of a deuteron is approximately

$$\frac{d\sigma}{d\Omega}=\frac{f^2}{v\mu^2}\cdot\frac{b^2(b^2-1)}{\{1+[(b+1)\kappa/2p_0]^2\}^2}\cdot\frac{k^2\kappa^2}{p_0^3}\cdot\left[2\left(\frac{\omega p_0}{kM}\right)^2+\left(\frac{\Delta J}{J^{(a)}}\right)^2-\frac{8\omega}{M}\cos^2\theta\right].$$

Here v is the relative velocity of the protons; $b=MJ^{(a)}/\kappa^2$; $\Delta J=J^{(a)}-J^{(t)}$; k and ω are the momentum and energy of the meson, and p_0 is the initial proton momentum. Inserting values corresponding to Peterson's experiments and taking $1/\kappa=1.17\times10^{-13}$ cm one finds that

$$d\sigma/d\Omega=19f^2(1-0.7\cos^2\theta)\times10^{-30}\text{ cm}^2.$$

The isotropic term dominates near the threshold; both terms are of the same order of magnitude for 345-Mev protons. It will be seen that after transformation to the laboratory system the magnitude of the cross section at 30° is of the observed order (if an experimental energy resolution of 6 Mev is assumed). At 0° the agreement does not appear to be as good. The angular distribution depends on the type of meson theory assumed; the magnitude of the cross section is strongly dependent on the internucleon potential. Singular potentials give large values for the cross section; a square well leads to a reduction by a factor of 50. This is in contradiction with the earlier results of Foldy and Marshak and illustrates the importance of using a reasonably accurate wave function for small separations of the nucleons.

The transitions to the continuous spectrum of the proton-neutron system can be treated in a similar manner. The virtual ^1S-state of the deuteron tends to produce a peak near the upper end of the meson spectrum. This peak, however, is completely masked by the dominating transitions to a final continuous ^3S-state. The differential cross section is approximately

$$\frac{d\sigma}{d\omega d\Omega}=\frac{2f^2}{v\mu^2}\cdot\frac{b^2}{\{1+[(b+1)\kappa/2p_0]^2\}^2}\cdot\frac{kM\kappa^2}{p_0^5}\cdot\left[\frac{2\mu^2}{M^2}-\frac{8\mu k^2}{Mp_0^2}\cos^2\theta\right].$$

In the zero momentum system the continuous spectrum consists of an isotropic part proportional to the meson momentum, k, and a $\cos^2\theta$ term proportional to k^3. One finds by integration that the numbers of mesons produced in the discrete and continuous spectra are of the same order. This is consistent with the observations.

The calculations here reported will be presented more fully elsewhere. They are capable of immediate extension to other meson fields and to more complicated nuclear systems.

[1] V. Z. Peterson, Phys. Rev. **79**, 407 (1950).
[2] W. Barkas, Phys. Rev. **75**, 1109 (1949).
[3] L. W. Alvarez, Harwell Conference, September, 1950.
[4] L. L. Foldy and R. E. Marshak, Phys. Rev. **75**, 1493 (1949).
[5] N. F. Mott, Proc. Camb. Phil. Soc. **27**, 255 (1931).

Nuclear Audiofrequency Spectroscopy by Resonant Heating of the Nuclear Spin System

N. F. Ramsey and R. V. Pound
Department of Physics, Harvard University, Cambridge, Massachusetts
November 1, 1950

In nuclear magnetic induction and resonance absorption experiments, the sensitivity decreases rapidly with decreasing frequency[1] if the size of the sample being tested is kept constant. This decrease in sensitivity is due to various causes including the reduction in the difference in the Boltzmann factor for the states

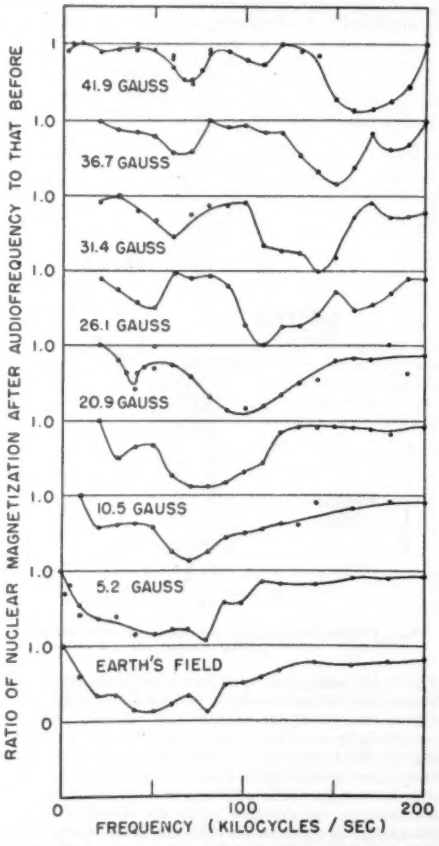

FIG. 1. Audiofrequency spectrum of the LiF in different magnetic fields. The ordinate is the ratio of the strong field Li^7 nuclear magnetization after and before the resonant heating of the nuclear spin system in the indicated magnetic field.

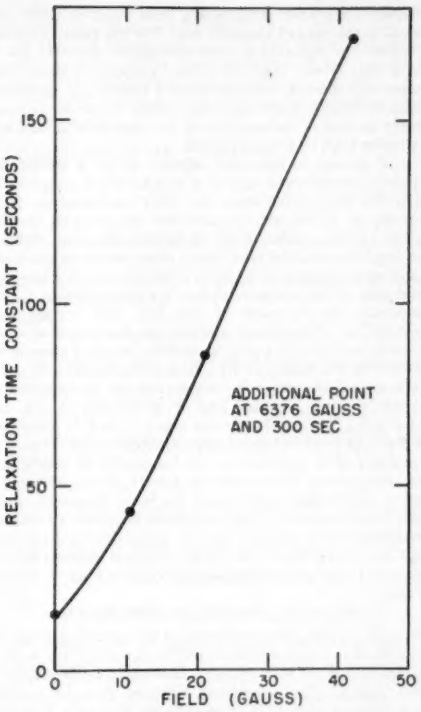

FIG. 2. Relaxation time constant as a function of magnetic field for Li^7 in LiF.

concerned and the reduction in the energy of the photons emitted and absorbed.

Therefore, when one of us (R.V.P.)[2] discovered the long relaxation time of a pure single crystal of LiF, it was suggested by the other (N.F.R.) that such long relaxation times make possible a new nuclear magnetic resonance technique which would have high sensitivity at low frequencies of the oscillating magnetic field. With the new method, the crystal is removed from a strong magnetic field for a time short compared to the relaxation time of the crystal in the absence of a strong field (15 sec for LiF) and during this short time is placed in a weak audiofrequency magnetic field. For one isotope of the crystal, the ratio of the nuclear magnetization immediately before and immediately after the removal from the strong field is measured[2] with a radiofrequency spectrometer. This ratio is then observed as a function of the frequency of the audio-oscillator. The dependence of this ratio on the audio-oscillator frequency presumably arises from resonant heating of the nuclear spin system to a temperature above the low value attained by adiabatic demagnetization when the crystal is removed from the strong magnetic field.

In this way the audiofrequency spectrum of LiF was studied between 20 and 200,000 cycles/sec with the strong field (6376 gauss) observations being of the Li^7 resonance. With audiofrequency magnetic fields of about 0.2 gauss, it was found that resonant heating did not take place below 100 cycles but did occur continuously and completely at frequencies between 1000 cycles and 200,000 cycles. However, when the amplitude of the audiofrequency field was reduced to 0.018 gauss applied for 3 sec, a nuclear audiofrequency spectrum was observed which possessed a broad maximum centered at 50 kc and with a width at half maximum of about 45 kc as shown in the lowest curve in Fig. 1. The first practical application of the 50 kc audiofrequency spectrum of LiF was its indication that the magnetic field reversal in the negative temperature experiments described in an accompanying paper[3] must be accomplished in a time short compared to 1/50 of a msec.

The effect of an external fixed magnetic field on the audiofrequency spectrum was also measured and is shown for different values of the magnetic field between 0 and 42 gauss in the upper curves of Fig. 1. It is of interest to note that the ratios of frequency to field for the two pronounced minima of the highest field curve correspond to nuclear g-factors 5.2 and 2.2 in surprisingly close agreement with the nuclear g-factors 5.26 and 2.17 for F^{19} and Li^7 respectively. The reduction of the subsequent Li^7 magnetization by an oscillatory field appropriate to F^{19} indicates that during or subsequent to the application of the oscillatory field the Li and F spin systems are in at least partial thermal equilibrium.

The effect of the external fixed magnetic field on the relaxation time in the absence of an audiofrequency field is shown in Fig. 2, where the length of time for reduction of the strong field resonance by a factor of two is plotted as a function of the strength of the weak magnetic field in which the sample is stored.

[1] Bloembergen, Purcell, and Pound, Phys. Rev. **73**, 679 (1948).
[2] R. V. Pound, Phys. Rev. **81**, 156 (1951).
[3] E. M. Purcell and R. V. Pound, Phys. Rev. **81**, 279 (1951).

A Nuclear Spin System at Negative Temperature

E. M. PURCELL AND R. V. POUND
Department of Physics, Harvard University, Cambridge, Massachusetts
November 1, 1950

A NUMBER of special experiments have been performed with a crystal of LiF which, as reported previously,[1] had long relaxation times both in a strong field and in the earth's field. These experiments were designed to discover the conditions determining the sense of remagnetization by a strong field when the initially magnetized crystal was put for a brief interval in the earth's field.

At field strengths allowing the system to be described by its net magnetic moment and angular momentum, a sufficiently rapid reversal of the direction of the magnetic field should result in a magnetization opposed to the new sense of the field. The reversal must occur in such a way that the time spent below a minimum effective field is so small compared to the period of the Larmor precession that the system cannot follow the change adiabatically. The experiments in zero field reported above[2] showed a zero field resonance at about 50 kc and therefore the following experiment was tried.

The crystal, initially at equilibrium magnetization in the strong (6376 gauss) field, was quickly removed, through the earth's field, and placed inside a small solenoid, the axis of which was

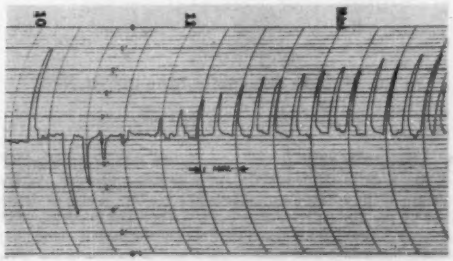

FIG. 1. A typical record of the reversed nuclear magnetization. On the left is a deflection characteristic of the normal state at equilibrium magnetization ($T \approx 300°K$), followed by the reversed deflection ($T \approx -350°K$), decaying ($T \to -\infty$) through zero deflection ($T = \infty$) to the initial equilibrium state.

parallel to a field of about 100 gauss, provided by a small permanent magnet. A 2 μfd condenser, initially charged to 8 kv, was discharged through the coil, with 500 ohms in series, in such a sense that the field in the coil reversed to about -100 gauss, with a time constant of about 0.2 μsec and decayed back to the original field with a time constant of 1 msec. The crystal was quickly returned, through the earth's field, to the strong magnet and the Li^7 resonance sampled. The operation could be done in 2 to 3 sec. A reversed deflection was found and it decayed, through zero, to the equilibrium state with the characteristic 5-min time constant. A typical record is shown in Fig. 1.

The state of spin system just after this treatment is thought to be properly described by a negative spin temperature. The system loses internal energy as it gains entropy, and the reversed deflection corresponds to induced radiation. Statistically, the most probable distribution of systems over a *finite* number of equally spaced energy levels, holding the total energy constant, is the Boltzmann distribution with either positive or negative temperature determined by whether the average energy per system is smaller or larger, respectively, than the mid-energy of the available levels. The sudden reversal of the magnetic field produces the latter situation.

One needs yet to be convinced that a single temperature adequately describes the nuclear spin state. Bearing on this is the fact that the crystal passes through the earth's field after the inverted population is produced, on its way back to the main magnet. The retention of the reversed magnetization requires that the spin-only-state, in the earth's field, have an inverted population and be described by a suitably small ($\sim -1°$K) negative temperature. Thus a very short time is required for the attainment of thermal equilibrium within the spin system itself (not the ordinary T_2, however).

A system in a negative temperature state is not cold, but very hot, giving up energy to any system at positive temperature put into contact with it. It decays to a normal state through infinite temperature.

This and related experiments indicate that the spin system is able to follow changes in even a small field adiabatically unless they occur in a time presumed to be less than about 20 μsec.

[1] R. V. Pound, Phys. Rev. **81**, 156 (1951).
[2] N. F. Ramsey and R. V. Pound, Phys. Rev. **81**, 278 (1951).

Erratum: Experiments on the Effect of Atomic Electrons on the Decay Constant of Be^7. II

[Phys. Rev. **76**, 897 (1949)]

R. F. LEININGER, E. SEGRÈ, AND C. WIEGAND
Radiation Laboratory, Department of Physics, University of California, Berkeley, California

IN Fig. 1 we have erroneously plotted $2\delta e^{\lambda t}$ instead of $\delta e^{\lambda t}$ as indicated on the ordinate scale on the left. The final result is in error by a factor 2 and should read:

$$\lambda(\mathrm{BeO})-\lambda(\mathrm{BeF_2})=(0.69\pm0.03)10^{-3}\lambda(\mathrm{BeO})$$
$$\lambda(\mathrm{Be})-\lambda(\mathrm{BeF_2})=(0.84\pm0.10)10^{-3}\lambda(\mathrm{Be}).$$

On the Nuclear Magnetic Moment of Na^{23}

R. A. LOGAN AND P. KUSCH
Columbia University, New York, New York*
November 30, 1950

A DISCREPANCY occurs between the nuclear g values of[1] Ga and[2] In as determined from measurements on the hfs spectrum of these atoms in the ground state ($^2P_{1/2}$) and as determined by the nuclear resonance method where the nuclei occur in molecules. Foley[3] has discussed the effect of the partial decoupling by the applied magnetic field of the L and S vectors in the $^2P_{1/2}$ state on the nuclear g-value obtained from observational data under the assumption that decoupling does not occur. He concludes that the diagonal magnetic interaction term $m_I g_I \mu_0 H$ which was assumed in finding g_I from the experimental data is to be modified by a small perturbation term which is, itself, proportional to the applied magnetic field. For the cases of gallium and indium the apparent g-value determined from the hfs of atoms is thus greater than the g-value obtained in the nuclear resonance experiments. Foley indicates a satisfactory agreement between the observed and calculated values of the discrepancy, especially in view of uncertainties in the theoretical calculations and a rather large experimental error.

It is of interest to determine whether or not a similar discrepancy appears for the case of a nucleus which occurs in an atom in the $^2S_{1/2}$ state, where the effect considered by Foley cannot appear. A previous measurement[4] has indicated that the apparent nuclear g-value of Cs is, indeed, the same within a rather large experimental uncertainty when measured in a molecule and when measured in an atom in the $^2S_{1/2}$ state. A precision measurement of the g-value of sodium is reported here.

Essentially use is made of the fact that certain lines $(F, m)\leftrightarrow(F, m-1)$ consist of doublets, one component of which arises in the state $F=I+\frac{1}{2}$ and the other one of which arises in the state $F=I-\frac{1}{2}$. The frequency separation of the doublet is $2g_I\mu_0 H/h$ and the mean frequency of the doublet permits determination of the quantity $x=(g_J-g_I)\mu_0 H/h\Delta\nu$, if $\Delta\nu$ is itself known, and hence of g_I/g_J. The $\Delta\nu$ of Na^{23} was found to be $1771.631\pm0.002\times10^6$ sec^{-1} by a method previously described[4] which depends on the existence of a maximum in the frequencies of certain lines in the hfs spectrum. The doublet $(F, 1)\leftrightarrow(F, 0)$ was observed at a field of about 6800 gauss where the mean frequency of the doublet is still sufficiently field dependent to permit an accurate determination of x and the doublet separation becomes large enough ($\sim16\times10^6$ sec^{-1}) to permit accurate measurement in the face of a large over-all frequency ($\sim430\times10^6$ sec^{-1}). We find then that

$$g_J(\mathrm{Na},\ ^2S_{1/2})/g_I(\mathrm{Na},\ ^2S_{1/2})=-2488.39\pm0.15.$$

Since[5] $g_I(H)/g_J(\mathrm{Na},\ ^2S_{1/2})=-15.1927\times10^{-4}\pm0.005$ percent, we find $g_I(\mathrm{Na},\ ^2S_{1/2})/g_I(H)=0.26451\pm0.008$ percent. This is to be compared with Bitter's[6] result $g_I(\mathrm{Na,\ mole})/g_I(H)=0.26450\pm0.01$ percent. The excellent agreement indicates that the apparent nuclear g-value measured in an atom in the $^2S_{1/2}$ state is, in fact, equal to the true nuclear g-value within the diamagnetic correction. Since no effect is here observed, it appears that the effect discussed by Foley accounts for the entire discrepancy observed for atoms in the $^2P_{1/2}$ state.

Determinations of the spin g-value of the electron reported heretofore depend on a measurement of the ratio of the electronic g_J of atoms in different electronic configurations. A combination of our present result with that of Bitter and with the result of Gardner and Purcell[7] for $2g_L/g_I(H)$ yields $g_s/g_L=2(1.00107\pm0.00012)$ under the assumption that $g_J(\mathrm{Na},\ ^2S_{1/2})=g_s$ and that no differential diamagnetic correction is to be applied to the nuclear moment of sodium in an atom and in a molecular configuration. It is of interest that this result does not depend on any assumption as to the g_J-values of P-states. The result agrees with other data on the spin moment of the electron. While it could be improved, a very accurate determination is precluded by the nature of the assumptions.

* This research was supported in part by the ONR.
[1] P. Kusch, Phys. Rev. **78**, 615 (1950).
[2] Private communication from W. G. Proctor.
[3] H. M. Foley, Phys. Rev. **80**, 288 (1950).
[4] P. Kusch and H. Taub, Phys. Rev. **75**, 1477 (1949).
[5] H. Taub and P. Kusch, Phys. Rev. **75**, 1481 (1949).
[6] F. Bitter, Phys. Rev. **75**, 1326 (1949).
[7] J. H. Gardner and E. M. Purcell, Phys. Rev. **76**, 1262 (1949).

Numerical Evaluation of the Fermi Beta-Distribution Function

D. G. E. MARTIN
George Holt Physics Laboratories, University of Liverpool, Liverpool, England
November 30, 1950

ATTENTION has recently been drawn by Feister[1] to methods of calculating the Fermi β-distribution function,

$$f(z,\eta)=\eta^{2+2s}e^{\pi\eta}|\Gamma(1+s+i\eta)|^2.$$

An asymptotic expansion of the gamma-function of the complex argument has been used by Hall.[2]

It does not seem to be widely known that the modulus of the gamma-function of the complex argument can be obtained in terms of the polygamma-functions of real arguments.

Let $1+s=x$, a constant, and put $x+iy=z$, then expanding by a Taylor series:

$$\ln\Gamma(x+iy)=\ln\Gamma(x)+iy\left\{\frac{\partial}{\partial y}\ln\Gamma(x+iy)\right\}_0 -\frac{y^2}{2!}\left\{\frac{\partial^2}{\partial y^2}\ln\Gamma(x+iy)\right\}_0+\cdots$$

$$=\ln\Gamma(x)+iy\psi(x)-\frac{y^2}{2!}\psi'(x)-\frac{iy^3}{3!}\psi''(x)+\frac{y^4}{4!}\psi'''(x)+\cdots$$

where $\psi(x)$, $\psi'(x)$, $\psi''(x)$, $\cdots$ are the polygamma-functions which have been tabulated.[3]

Since

$$\ln\Gamma(x+iy)=\ln Re^{i\phi}=\ln R+i\phi$$

we are interested only in the real part of the expansion, so that

$$\ln R=\ln\Gamma(x)-\frac{y^2}{2!}\psi'(x)+\frac{y^4}{4!}\psi'''(x)-\cdots.$$

This series may be made to converge more rapidly by increasing the argument, x.

Thus

$$\ln R=\ln\Gamma(x+1)-\frac{y^2}{2!}\psi'(x+1)+\frac{y^4}{4!}\psi'''(x+1)-\cdots-\tfrac{1}{2}\ln(x^2+y^2)$$

since by the property of the gamma-function

$$\ln\Gamma(z)=\ln\Gamma(z+1)-\ln z$$

and

$$\Re[\ln(x+iy)]=\tfrac{1}{2}\ln(x^2+y^2).$$

This process may be repeated until these terms converge sufficiently rapidly to give the accuracy desired. In this manner for a given value of x (i.e., a given atomic number) a series in y can be obtained for easy computation of the gamma-function.

Thus for $Z=82$, $x=0.80109$

$$\log_{10}R=1.252\,05-0.050\,26y^2+0.000\,44y^4 -\tfrac{1}{2}\log_{10}(x^2+y^2)[(x+1)^2+y^2][(x+2)^2+y^2][(x+3)^2+y^2].$$

I am indebted to Dr. J. C. P. Miller for this method of computation, which has been used in papers by Martin and Richardson[4] to evaluate Fermi functions for $Z=81$, 82, 83, 84.

[1] I. Feister, Phys. Rev. **78**, 375 (1950).
[2] Harvey Hall, Phys. Rev. **79**, 745 (1950).
[3] H. T. Davis, *Tables of the Higher Mathematical Functions*, (Principia Press, Bloomington, Indiana, 1933, 1935), Vols. I and II. British Association Mathematical Tables. Vol. I.
[4] D. G. E. Martin and H. O. W. Richardson, Proc. Phys. Soc. (London) **LX**, 466 (1948); *ibid.* **A195**, 287 (1948).

On the Decay of the π^- Meson*

L. Lederman, J. Tinlot,† and E. T. Booth
Columbia University, New York, New York
November 29, 1950

THE spontaneous decay of the π^- meson has been observed directly in a cloud chamber. The decay mechanism has been studied and the mass of the μ^- meson measured.

The decay of the π^+ meson at the end of its range has been studied extensively in cosmic rays[1] and with accelerators.[2] Because of the very large probability for capture of the π^- meson in nuclei,[3] its decay properties can only be studied in flight.

π^- mesons produced by the bombardment of an internal carbon target with 385 Mev protons were collimated by a 2×10 in. hole in the six-foot thick concrete shielding. A 16-in. cloud chamber with a magnetic field of 4040 gauss was exposed to this beam. A preliminary run with a ¼″ Pb plate showed that the beam included fast electrons as well as π^- and μ^- mesons. The most probable momentum of the incoming particles was 180 Mev/c.

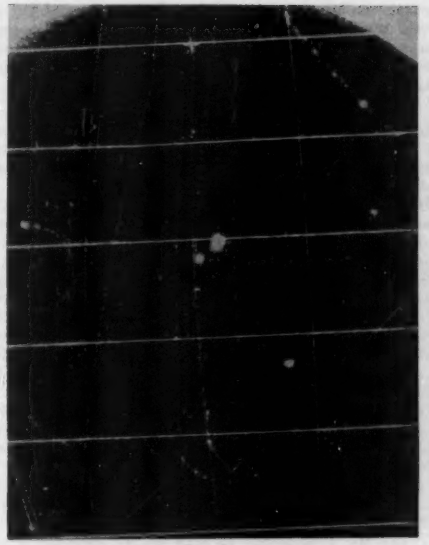

Fig. 1. Cloud-chamber photograph of the meson beam showing a typical decay-in-flight.

Fifty cases of apparent decay-in-flight were observed in the gas of the cloud chamber (Fig. 1). The requirement for identification was an abrupt deflection of a track by more than 5°. The track was required to be well illuminated and at least one inch from the walls of the chamber. The most probable angle of deflection observed was 12°. With the exception of four cases, all of the events are consistent, within the experimental errors, with the kinematics of decay-in-flight for the process:

$$\pi^-\rightarrow\mu^-+\nu^0, \qquad (1)$$

where ν^0 is a neutral particle of small rest mass.

Twenty-eight examples were selected for detailed analysis on the basis of measurability of both arms of the deviated track.

Table I. Mass measurements of the μ^- meson.

No.	$M\mu^-$ (Mev)	$\Delta M\mu^-$ (Mev)
1	100.8	10.1
2	126.0	18.3
3	106.2	7.3
4	114.2	42
5	103.5	7.1
6	105.1	14.2
7	106.5	6.1
8	119.5	10.0
9	116.2	11.3
10	112.0	6.5
11	105.7	7.4
12	95.6	23
13	116.8	6.2
14	108.0	6.0
15	114.7	7.0
16	96.6	50
17	104.7	5.0
18	116.7	8.4
19	105.0	7.3
20	98.6	8.9
21	105.9	5.0
22	108.5	5.1
23	104.6	4.0
24	110.5	6.4
25	60.2	10.0
26	Imaginary	a
27	Imaginary	a
28	Imaginary	a

a These masses remain imaginary within the limits of the uncertainties in the measurements.

The momenta before and after deflection were measured with an average precision of ±12 percent. Angles of deflection were measured in space by stereoscopic reprojection to ±2°. In the case of a $\pi-\mu$-decay-in-flight, the mass of the μ-meson is given by:

$$m_\mu^2=m_\pi^2+2p_\pi^2-2p_\pi p_\mu\cos\theta - 2\{(m_\pi^2+p_\pi^2)(p_\pi^2+p_\mu^2-2p_\pi p_\mu\cos\theta)\}^{\frac{1}{2}}. \quad (2)$$

Equation (2) assumes that the neutral decay product has zero rest mass.[2] The results of this independent measurement of the μ^- mass in terms of the π^- mass are given in Table I. The π^- mass used[4] is $276m_e$.

The last four masses are obviously not consistent with the remaining observations. They are attributed to large angle scattering or some other process not consistent with Eq. (1). The weighted mean value of the included cases is $m_\mu-=210\pm3m_e$. When the probable error of the π^- mass[4] ($\pm6m_e$) is included, the weighted mean value becomes $m_\mu-=210\pm6m_e$. This is to be compared with independent measurements of the meson masses.[2,4] The Berkeley work discussed in the last reference gives the most precise results for the π^+, π^-, and μ^+ mesons. Their method was not applied to the μ^- meson. This is due to the fact that the μ^- mesons do not originate in the target.

There is, of course, the possibility that some of the included cases belong to other processes than normal $\pi-\mu$-decay. The rather small spread in individual values, in view of the errors, seems to make this improbable.

The authors wish to thank Professor G. Bernardini for many valuable discussions on this letter. Also, we wish to thank Messrs. H. Byfield and J. Kessler for their assistance in the taking of this data, and Mr. J. Spiro and his staff for the operation of the cyclotron.

* Assisted by the joint program of the AEC and ONR.
† Now at the University of Rochester, Rochester, New York.
[1] Lattes, Occhialini, and Powell, Nature 160, 453, 486 (1947).
[2] See Gardner, Barkas, Smith, and Bradner, Science 111, 191 (1950); and Bradner UCRL 486 for excellent summary and references.
[3] Menon, Muirhead, and Rochat, Phil. Mag. 41, 583 (1950).
[4] Smith, Barkas, Bishop, Bradner, and Gardner, Phys. Rev. 78, 86 (1950).

Paramagnetic Resonance Absorption in Potassium Dissolved in Liquid Ammonia*

CLYDE A. HUTCHISON, JR., AND RICARDO C. PASTOR
Institute for Nuclear Studies and Department of Chemistry, University of Chicago, Chicago, Illinois
November 27, 1950

IT is well known that in solutions of certain metals in liquid NH_3 the metal atoms dissociate into electrons and positive metal ions.[1,2] The magnetic susceptibilities of these solutions have been studied by various workers.[3-5]

We have observed paramagnetic resonance absorption in a solution of K in liquid NH_3. The experiment was performed at 23°C and at a frequency of 23,700 Mc. A sample of 6.7×10^{-3} cm³ of the solution containing 4.8×10^{-6} mole of K (concentration of K was 0.7 mole l^{-1}) was placed in a Pyrex capillary and mounted at the midpoint of a resonant section of rectangular wave guide oscillating in the $TE_{1,0,2}$ mode. At this concentration the atomic susceptibility of K is about that expected for an electron gas free to move throughout the volume of the solution.[3-5] The resonance absorption was displayed on an oscilloscope using a sawtooth modulation on the repeller of the klystron. Frequencies were measured to an accuracy of 1 part in 10^4 by means of a wave meter calibrated against harmonics of a 5 Mc crystal controlled oscillator using techniques described by Good.[6] Simultaneously the proton resonance frequency in a sample of H_2O separated from the NH_3 solution by the wall of the wave guide was determined. The g-factors were computed from the measured ratio of proton frequency to electron frequency using Taub and Kusch's[7] value $(1.51927\pm0.00008)\times10^{-3}$, for this ratio for electron spin and using 2.0023 as the g-factor for electron spin. The g-factor was found to be 2.0012 with an average deviation of 0.0002 from the mean of nine measurements. A sample of diphenyl picryl hydrazyl $[(C_6H_5)_2N-NC_6H_2(NO_2)_3]$ was placed in a similar container and similarly located and the g-factor was found to be 2.0037 with an average deviation of 0.0001 from the mean of six measurements in agreement with the measurements of Holden *et al.*[8]

The Q of the cavity was seriously reduced by introduction of the sample and intensities of the absorption relative to other substances are therefore not as yet known.

The absorption is very narrow having a half-width at half-maximum absorption of approximately 0.3 Mc corresponding to 0.1 gauss. Measurements on a sample of diphenyl picryl hydrazyl gave a half-width at half-maximum absorption of 1.2 gauss in agreement with the measurements of Holden *et al.*[8]

Further studies of the dependence of the magnetic resonance on temperature and concentration are in progress.

We wish to thank C. L. Arnow for construction of electronic equipment used in this research; A. Kowalsky for the synthesis of the diphenyl picryl hydrazyl; and W. E. Good for much helpful advice in the construction and operation of the apparatus.

* Research assisted by the office of Naval Research.
[1] Kraus, J. Franklin Inst. 212, 537 (1931).
[2] Johnson and Meyer, Chem. Rev. 8, 273 (1931).
[3] Freed and Thode, Nature 134, 774 (1934).
[4] Huster, Ann. Physik 33, 477 (1938).
[5] Freed and Sugarman, J. Chem. Phys. 11, 354 (1943).
[6] Good, Scientific Paper 1538, Westinghouse Research Laboratories, East Pittsburgh, Pennsylvania (August 1, 1950) (unpublished).
[7] Taub and Kusch, Phys. Rev. 75, 1481 (1949).
[8] Holden, Kittel, Merritt, and Yager, Phys. Rev. 77, 147 (1950).

Second Shock in Liquid Helium II?*

F. REINES
University of California, Los Alamos Scientific Laboratory, Los Alamos, New Mexico
November 24, 1950

CONSIDERATION of the variation of the speed of second sound with temperature[1] suggests the possibility of the existence of a peculiar type of shock wave in liquid HeII. In a medium in which the velocity is a monotonic decreasing function of temperature, a finite positive temperature pulse will develop into a triangular pulse with a discontinuity at its trailing side. A negative temperature pulse can be expected in such a medium to develop a sharp leading edge. Depending on the direction of propagation of a finite sinusoidal pulse, it will either develop into an inverted N-shape wave or a sawtooth form with the discontinuity at the center. The extent to which a smooth finite pulse in liquid HeII will actually distort toward the limiting forms indicated in this discussion is governed by other dissipative mechanisms. In view of the high velocity dispersion in liquid HeII at temperatures below 1°K and from 1.7°K to the λ-point, such distortions might be observable, for example, for pulses of maximum amplitude ~0.02°K in a medium at 0.5°K after a linear travel of perhaps 10 cm.

If a sharp discontinuity of the type discussed here does form in liquid HeII, it should be expected to have the velocity, V, given by the equation

$$V=(\rho v_n-\rho_0 v_{n0})/(\rho-\rho_0),$$

where ρ is the density of normal liquid He component and v_n is the material velocity of normal liquid He component. The subscript ^{0} refers to conditions ahead of the shock. Symbols without subscripts are appropriate to conditions behind the shock front.

A more detailed discussion of these questions is in preparation.

* Work done under the auspices of the AEC.
[1] J. R. Pellam, Phys. Rev. 75, 1183 (1949); 76, 869 (1949). K. R. Atkins and B. V. Osborne, Phil. Mag. 41, 1078 (1950).

On the Lamb Shift for Spinless Electrons

W. A. NEWCOMB AND F. ROHRLICH
Laboratory of Nuclear Studies, Cornell University, Ithaca, New York
November 24, 1950

IN 1947 a relativistic calculation of the Lamb shift was carried out by Dyson.[1] Since the covariant formulations of quantum electrodynamics were not well developed at that time, he achieved

an important simplification of these calculations by neglecting the spin of the electron; the assumption that this approximation would not lead to a numerical result very different from the correct value seemed to be plausible.

Because of the inherently noncovariant character of the method of computation the renormalization of the infinite self-energy integrals turned out to be ambiguous. Two alternatives offered themselves: the "wave packet" and the "single particle" subtraction prescription. The difference of the $2s$- and the $2p$-level displacements was found to be

$$D=\frac{1}{3\pi}Z^4\alpha^3Ry\left(\mathrm{L}-\ln 2+\frac{13}{36}+\frac{4}{15}\ln 2+\frac{\epsilon}{12}-\frac{1}{40}\right) \quad (1)$$

where $\epsilon=2$ and -1, respectively, for the two alternatives, and L is the difference of the logarithms of the $2s_{1/2}$ and $2p_{1/2}$ levels involving the nonrelativistic average excitation energies $k_0(n, l)$. For hydrogen L was found to be[3]

$$\mathrm{L}=\ln\frac{mc^2}{k_0(2,0)}-\ln\frac{Ry}{k_0(2,1)}=7.7215-0.0300\pm 0.0008$$

and therefore Dyson's formula gives

$$D=1045\text{ Mc and }1011\text{ Mc} \quad (2)$$

for the two subtraction prescriptions.

In order to resolve this ambiguity a covariant calculation is necessary. The Feynman method offers a particularly simple procedure for this purpose. We find for the $2s$-level shift

$$D_s=\frac{1}{3\pi}Z^4\alpha^3Ry\left(\ln\frac{mc^2}{k_0(2,0)}-\ln 2-\frac{3}{4}+\frac{5}{6}-\frac{1}{40}\right) \quad (3)$$

and for the $2p$-level shift

$$D_p=\frac{1}{3\pi}Z^4\alpha^3Ry\ln\frac{Ry}{k_0(2,1)}. \quad (4)$$

The relative shift is therefore

$$D=D_s-D_p=\frac{1}{3\pi}Z^4\alpha^3Ry\left(\mathrm{L}-\ln 2+\frac{1}{12}-\frac{1}{40}\right). \quad (5)$$

The term $-3/4$ in Eq. (3) comes from the evaluation of the Feynman diagrams; the term $5/6$ from the second-order calculation which is nonrelativistic and hence is identical with that for spin $1/2$; the term $-1/40$ represents the vacuum polarization. For hydrogen one finds from (5)

$$D=956\text{ Mc}. \quad (6)$$

As was anticipated, this value is rather close to that found for spin $1/2$, which is $1051.4-67.8=983.6$ Mc, 67.8 Mc being the contribution of the electron spin.

Comparison of (1) and (5) shows that neither of the two alternative subtraction procedures is correct. The term $(4/15)\ln 2$ in (1) is easily traced back to a term of the form

$$\int|\nabla^2\psi|^2d\tau \quad (7)$$

which originates in a somewhat doubtful expansion in the noncovariant method. It involves the kinetic energy of the free particle and should be omitted. When this is done we notice that Dyson finds a p-level shift

$$D_p=\frac{1}{3\pi}Z^4\alpha^3Ry\left(\ln\frac{Ry}{k_0(2,1)}+\frac{\epsilon}{96}\right)$$

which leads us to take $\epsilon=0$ when compared with (4). Formula (1) then has only $[\mathrm{L}-\ln 2-(1/12)-(1/40)]$ in the bracket, which is still incorrect. We conclude that there seems to be no simple way in which to obtain the correct result from the ambiguous noncovariant calculation.

After this work was completed the authors noticed a paper by Sasaki and Suzuki[3] who obtain instead of (5)

$$D=\frac{1}{3\pi}Z^4\alpha^3Ry\left(\mathrm{L}-\ln 2+\frac{5}{48}-\frac{1}{40}\right) \quad (8)$$

which yields 3 Mc more than (6). They use the Schwinger-Tomonaga formalism which makes the computations very much more complicated than by the Feynman method, which perhaps increases the chance of making errors.

[1] F. J. Dyson, Phys. Rev. **73**, 617 (1948).
[2] Bethe, Brown, and Stehn, Phys. Rev. **77**, 370 (1950).
[3] M. Sasaki and R. Suzuki, Prog. Theor. Phys. **4**, 485 (1949).

Two Crystal Spectrometer Results with Uncollimated γ-Rays

JOE KEAGY BAIR, FRED C. MAIENSCHEIN, AND WILLIAM B. BAKER
Fairchild Engine and Airplane Corporation, NEPA Division, Oak Ridge, Tennessee
November 20, 1950

FIGURE 1 shows the γ-ray spectra of Cs^{137} and Co^{60} as obtained on a two crystal Hofstadter[1] type spectrometer. Amplifier gains were different for the two curves. The instrument used differs from that described by Hofstadter in that no collimation was necessary and that considerably larger NaI crystals were used.

The point source of gamma-rays was located several inches from a 1-in. diameter, 1-in. high Compton-electron counting crystal. The degraded-gamma-counting crystal, 1.5 in. in diameter and 1.5-in. high, was located 2.75 in., center to center, from the one-in. crystal and at an angle of about 150° with the direction of the incident gamma-rays. The large crystal was shielded from the direct beam to reduce its count rate. The resolution is essentially equivalent to that obtained here with the same apparatus but employing a well-collimated source. The use of larger crystals and an uncollimated source permit greatly increased sensitivities. The data on Co^{60} were taken with a 0.25 mC source and required one hour of counting time. Experimental and calculated efficiencies agree, giving a figure of about 0.003 counts/sec in the peak for unit flux at the Compton scattering crystal.

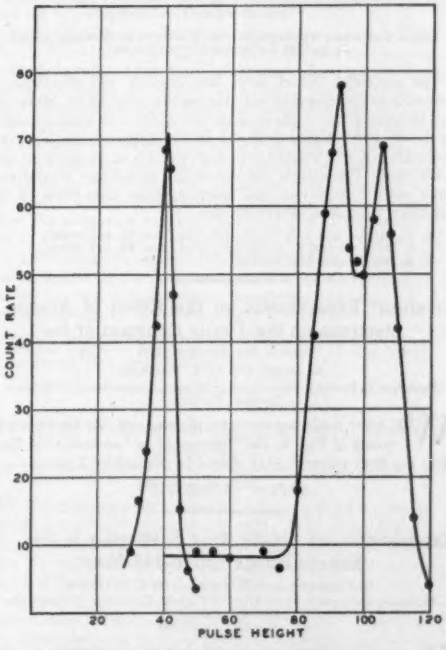

FIG. 1. Cs^{137} and Co^{60} spectra taken with a two crystal spectrometer using large crystals and an uncollimated source.

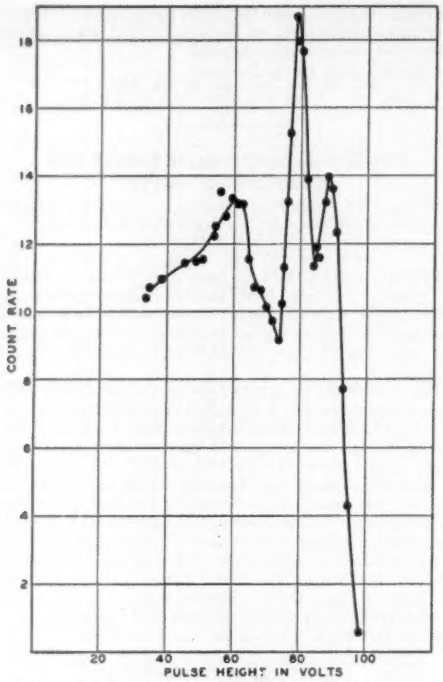

FIG. 2. Co^{60} single crystal spectra taken with 1½-in. diameter crystal 1½ in. high and an uncollimated source.

The successful use of large NaI crystals and uncollimated sources is in disagreement with the results obtained by McIntyre and Hofstadter[2] on single crystals but agrees with those obtained by P. R. Bell.[3] Figure 2 shows an uncollimated, single-crystal spectrum of Co^{60} obtained with a crystal 1.5 in. in diameter and 1.5-in. high. Presumably the uniformity of the raw crystal material, surface conditions, and mounting have more effect on the resolution than does the crystal size.

[1] R. Hofstadter and J. A. McIntyre, Phys. Rev. 78, 619 (1950).
[2] J. A. McIntyre and R. Hofstadter, Phys. Rev. 78, 617 (1950).
[3] P. R. Bell, *Science* 112, 7 (1950).

Erratum: Experiments on the Effect of Atomic Electrons on the Decay Constant of Be^7

[Phys. Rev. 75, 39 (1949)]

E. SEGRÈ AND C. E. WIEGAND
Radiation Laboratory, Department of Physics, University of California, Berkeley, California

WE have made an error in plotting, as the experimental points of Fig. 2, $2\delta e^{\lambda t}$ instead of $\delta e^{\lambda t}$ as indicated. Similarly the final value of $\Delta\lambda/\lambda$ should be divided by 2 giving

$$\Delta\lambda/\lambda=(-1.5\pm0.9)10^{-4}.$$

Experiments on Elastic $p-p$ Scattering in the Energy Range 120 to 345 Mev*

O. CHAMBERLAIN, E. SEGRÈ, AND C. WIEGAND
Radiation Laboratory, Department of Physics, University of California, Berkeley, California

November 20, 1950

IN a previous paper[1] we described some experiments on $p-p$ scattering at 340 Mev made with gas proportional counters.

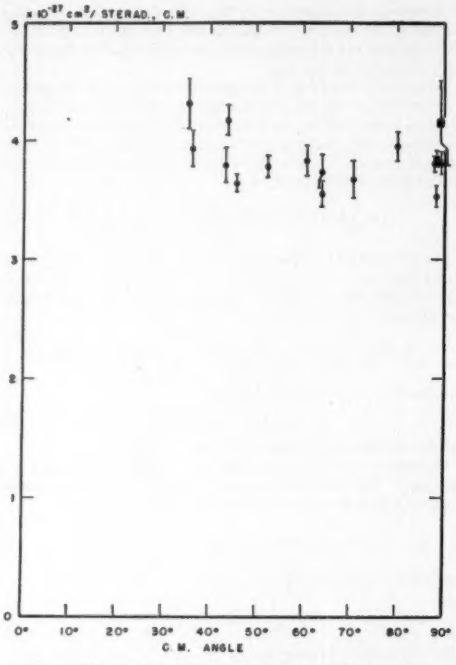

FIG. 1. Differential scattering cross section in the center-of-mass system as a function of the angle in this system.

We have now improved and extended the measurements by using stilbene scintillation counters in coincidence and by varying the energy of the beam by the use of lithium absorbers.

In view of the interest in these results as shown in recent theoretical papers we have decided to publish the results to date. Details on the experiments and extension to smaller angles will follow later.

The results at 345 Mev are summarized in Fig. 1 which gives the differential scattering cross section in the center-of-mass system as a function of the angle in this system. The cross section is normalized in the usual way such that the total scattering cross section σ_s is given by

$$\sigma_s=\tfrac{1}{2}\int_{4\pi}\sigma(\phi)d\omega_\phi=\tfrac{1}{2}\int_0^\pi\sigma(\phi)[2\pi\sin\phi d\phi].$$

Table I gives the differential cross sections of $\sigma(\phi)$ (center of mass system) for incident proton energy, E, in the laboratory coordinate system, at angle ϕ (center-of-mass system) from the beam direction. The symmetry of the problem in the center-of-mass system guarantees that $\sigma(\phi)=\sigma(\pi-\phi)$.

TABLE I. Differential scattering cross sections at reduced energies. Quoted errors are standard deviations from counting statistics only.

E (Mev)	ϕ (degrees)	$\sigma(\phi)$ (10^{-27} cm² sterad⁻¹)
119	63	4.0 ±0.4
119	78	4.2 ±0.4
119	89	3.95 ±0.12
164	61	4.1 ±0.4
164	89	3.8 ±0.3
249	48	3.5 ±0.3
249	63	3.7 ±0.2
249	78	3.69 ±0.15
249	87	3.64 ±0.11

The errors shown in Fig. 1, as well as those quoted in Table I, are the standard deviations due only to the statistical counting errors. The other errors, which must be superimposed on those shown, are for the most part systematic errors which affect all of the cross sections equally. These errors do not alter the angular distribution very much. We believe that the systematic errors amount to five percent (probable error) in the experiments at 345 Mev, and to 10 percent in the experiments at lower energy.

* This work was performed under the auspices of the AEC.
[1] O. Chamberlain and C. Wiegand, Phys. Rev. 79, 81 (1950).

A Note on Rainwater's Spheroidal Nuclear Model*

E. Feenberg and K. C. Hammack
Washington University, St. Louis, Missouri
November 20, 1950

A SPHEROIDAL core offers possibilities for large nuclear quadrupole moments. Coupling between the total angular momentum of the whole nucleus and the symmetry axis of the core is required to maintain a nonspherical charge distribution with respect to external fields. Rainwater[1] has shown that the model of an odd particle in a spheroidal potential well generated by a spheroidal core has the required coupling and a minimum energy associated with a definite departure from the spherical shape. The energy of the spheroidal system contains a quadratic term in the eccentricity from the change in surface and Coulomb energies of the core and a linear term from the shift in the eigenvalue of the extra-core particle. The linear term can be derived simply as follows.

A potential well of constant depth in a spheroidal region of constant volume is defined by the equations

$$V(s)=-D, \quad s<R \qquad =0, \quad s\geqq R \tag{1}$$

$$s=[\lambda(x^2+y^2)+z^2/\lambda^2]^{\frac{1}{2}}. \tag{2}$$

The eccentricity, ϵ, is defined by the equation

$$\epsilon=-\lambda+1/\lambda^{\frac{1}{2}} \cong-\tfrac{3}{4}(\lambda-1) \quad \text{when} \quad |\lambda-1|\ll 1. \tag{3}$$

For small values of ϵ the eigenvalue of a particle in a spherical well can be computed from first-order perturbation theory employing the normalized solution $\psi_0(x, y, z)$ of the unperturbed problem with the result

$$\begin{aligned} E(\epsilon)-E(0)&=\int\int\int|\psi_0(x,y,z)|^2[V(s)-V(r)]d\tau \\ &=\int\int\int V(r)[|\psi_0(x/\lambda^{\frac{1}{2}}, y/\lambda^{\frac{1}{2}}, \lambda z)|^2 \\ &\qquad -|\psi_0(x,y,z)|^2]d\tau \qquad (4) \\ &=-\tfrac{1}{2}eD\int\int\int_R\left[\frac{\partial}{\partial x}x+\frac{\partial}{\partial y}y-2\frac{\partial}{\partial z}z\right] \\ &\qquad \times|\psi_0(x,y,z)|^2d\tau \end{aligned}$$

the integration in the last line of Eq. (4) extending over a spherical region of radius R. Using Gauss' theorem and introducing spherical coordinates, Eq. (4) reduces to

$$\begin{aligned} \Delta E&=-\tfrac{1}{2}eDR^3\int\int(1-3\cos^2\theta)|\psi_0(R,\theta,\varphi)|^2\sin\theta d\theta d\varphi \\ &=\tfrac{1}{2}eDR^3\mathfrak{R}_{nl}^2(R)\frac{\frac{1}{2}l(l+1)-m^2}{(l+\frac{3}{2})(l-\frac{1}{2})} \end{aligned} \tag{5}$$

in which $\mathfrak{R}_{nl}(r)$ is the normalized radial function.

An asymptotic formula valid for $x_0=(2MD)^{\frac{1}{2}}R/\hbar\gg 1$ is easily derived for levels near the bottom of the well. The result is

$$\tfrac{1}{2}DR^3\mathfrak{R}_{nl}^2(R)\cong T_{nl}\left(\frac{x_0}{1+x_0}\right)^2 \tag{6a}$$

$$T_{nl}=\hbar^2\omega_{nl}^2/2MR^2. \tag{6b}$$

Here T_{nl} is the kinetic energy of a particle in a well of infinite depth and ω_{nl} is the nth zero of a Bessel function of order $l+\frac{1}{2}$.

Using $D=28.3$ Mev and $R=A^{\frac{1}{3}}e^2/2mc^2$, the right-hand member of Eq. (6a) is too large by 25 to 40 percent for levels at the top of the occupied spectrum. For example at $A=100$, $x_0=7.64$, $T_{14}=32$ Mev and

$$\begin{aligned} &\tfrac{1}{2}DR^3\mathfrak{R}_{14}^2(R)=20 \text{ Mev} \\ &T_{14}[x_0/(1+x_0)]^2=25 \text{ Mev}. \end{aligned} \tag{7}$$

Rainwater finds the asymptotic formula

$$\Delta E_{n,\,l\pm 1}\cong-\tfrac{1}{4}T_{nl} \tag{8}$$

(valid for $l\to\infty$ and $D=\infty$) by a somewhat obscure and complicated procedure. The present calculation checks Rainwater's result under his limiting conditions, but yields a greatly reduced coefficient of ϵ when Eq. (5) is evaluated accurately. Using the numbers quoted above for $A=100$,

$$\begin{aligned} \Delta E_{1,4,\pm 4}&\cong-21\epsilon \text{ Mev (Eq. (8))} \\ &\cong-10\epsilon \text{ Mev (exact)}. \end{aligned} \tag{9}$$

The possibility of excessive quadrupole moments, mentioned by Rainwater, is probably eliminated by the accurate calculation.

* Assisted by the joint program of the ONR and AEC.
[1] J. Rainwater, Phys. Rev. 79, 432 (1950).

Addendum: The Disintegration of Ti^{45}

[Phys. Rev. 80, 360 (1950)]
M. Ter-Pogossian, C. S. Cook, F. T. Porter, K. H. Morganstern, and J. Hudis
*Washington University.** *St. Louis, Missouri*

WHEN the proof for the above-mentioned article was returned to the American Institute of Physics, a note to be added to the article was attached. This note is mentioned in footnote 10 but was not printed at the end of the article. Its content was as follows:

Since this paper was submitted, an article describing the work at Illinois has appeared.[1]

Because the elimination of Sc^{46} as an impurity was exceedingly difficult in the current research, the authors feel that the Compton and photo-electrons of Fig. 6 of Kubitschek's paper possibly may be attributed to Sc^{46}. The line at 780 kev is in perfect position to be the K-shell photo-electron line of the 890-kev gamma-ray from Sc^{46}. By drawing the line through the lower energy experimental points in a slightly different manner, it is possible to attribute all to Compton electrons from the 890-kev gamma-ray of Sc^{46}. Also it is difficult to understand the mechanism which would give a more intense L-shell photo-electron line than K-shell photo-electron line as appears to be the case in Fig. 6 of Kubitschek's article.

In a private communication, Dr. Kubitschek has indicated to us that a check of his photo-electron spectrum reveals the possible indication of a bump at the correct momentum to account for a 450-kev gamma-ray of very low intensity.

* Assisted by the joint program of the ONR and AEC.
[1] Kubitschek, Longacre, and Goldhaber, Phys. Rev. 77, 742 (1950); H. E. Kubitschek, Phys. Rev. 79, 23 (1950).

A Method of Isotopic Separation by (n, γ) Recoil*

L. B. Magnusson
Argonne National Laboratory, Chemistry Division, Chicago, Illinois
November 20, 1950

STUDIES of gamma-recoil atoms have been confined to systems in which the "hot" atoms remain within the phase boundaries of the target material. The factors of "hot" atom reactivity, ordinary thermal reaction exchange, and physical and chemical separation difficulties operate against efficient isotopic separation.

A new method is proposed for utilizing the recoil energy from gamma-emission for isotopic separation. If targets in the form of very thin films could be bombarded with thermal neutrons in vacuum, it seemed probable that an appreciable percentage of the (n, γ) product atoms would have sufficient recoil energy from the

gamma-emission to leave the film. The method is analogous to the collection of daughters of alpha-decay,[1] with the difference that gamma-recoil energy is of the order of a thousand times smaller than alpha-recoil energy.

The method has been given a successful preliminary trial by neutron bombardment of Au^{197} to produce Au^{198}. Targets were prepared on one-inch diameter nickel disks by electroplating gold containing a known trace of Au^{198}. The apparent thickness and total gold content of the deposits were calculated from the measured Geiger activity of the nickel plates. The gold content varied from one to several hundred micrograms. The plates were stacked alternately with clean plates for catching recoils, each plate separated 1/16 in. from the next by a nickel ring. The stack of plates was clamped in a tubular nickel magazine and placed in a quartz tube connected to a vacuum system. After degassing the quartz tube and contents at 150° to a holding vacuum of about 10^{-4} mm the quartz tube was sealed off and placed in the thimble of the Argonne CP-3 reactor for a two-hour bombardment. The gas pressure in the quartz tube after bombardment was 10^{-3} mm.

Known amounts of Au^{197} carrier were added to each target plate and to one-half of each catcher plate and separated chemically to recover active Au^{198} (2.7-day β^-). The remaining halves of the catcher plates together with clean nickel samples and a gold monitor were bombarded at atmospheric pressure to determine if Au^{197} contamination and impurity were present.

Au^{198} activity from gamma-recoil was present on the catcher plates. The maximum yield of recoil atoms was low, about 0.5 percent of the total Au^{198} produced in the target. Apparently the targets were not true films but consisted of relatively large clusters of atoms. Gold is now known to aggregate in deposits of less than a characteristic thickness.[2]

The exact amount, if any, of Au^{197} contamination from the targets could not be determined since the nickel plates were found to contain 2×10^{-6} percent by weight of gold impurity. The activity produced from the gold impurity varied from 10 to 50 percent of the total Au^{198} activities of the catcher plates. From the precision of the gold impurity determination an upper limit of about ten percent of the total Au^{198} can be placed on the amount of Au^{199} arising from Au^{197} contamination.

* Reported in Chemistry Division Quarterly Report, Argonne National Laboratory, July, August, September, 1949 (unpublished).
[1] Rutherford, Chadwick, and Ellis, *Radiations from Radioactive Substances* (Cambridge University Press, London, 1930), p. 156.
[2] R. S. Sennett and G. D. Scott, J. Opt. Soc. Am. 40, 203 (1950).

The Microwave Spectra of the Deutero-Ammonias*

M. T. Weiss and M. W. P. Strandberg
Research Laboratory of Electronics, Massachusetts Institute of Technology, Cambridge, Massachusetts
November 20, 1950

MEASUREMENTS of the inversion-rotation spectra of the deutero-ammonias have been made in the 6000 to 80,000 Mc region. About 35 lines of NH_2D and NHD_2 have been measured and identified. Our results are in agreement with the structural parameters of ammonia as given by Herzberg[1] and with the inversion doubling theory of Dennison and Uhlenbeck.[2] Thus the inversion splittings for the ammonia molecules are approximately as follows: 24,000 Mc/sec for NH_3; 12,000 Mc/sec for NH_2D; 5000 Mc/sec for NHD_2; 2000 Mc/sec for ND_3. A complete list of our observed lines and our interpretation of this spectrum will be published shortly.

Our results are in disagreement with the implied interpretation of a list of low-frequency lines given by H. Lyons *et al.*,[3] and in particular with the assignment of the 5000 Mc/sec lines to the ND_3 inversion spectrum.

* This work was supported in part by the Signal Corps, the Air Materiel Command, and ONR.
[1] G. Herzberg, *Infrared and Raman Spectra* (D. Van Nostrand Company, Inc., New York, 1945), p. 439.
[2] D. M. Dennison and G. E. Uhlenbeck, Phys. Rev. 41, 313 (1932).
[3] Lyons, Kessler, Rueger, and Nuckolls, Phys. Rev. (to be published).

The Mass of S^{32}

Henry E. Duckworth, George S. Stanford, John M. Olson, and Cort L. Kegley
Scott Laboratory of Physics, Wesleyan University, Middletown, Connecticut*
November 30, 1950

THE mass of S^{32} was first measured mass spectrographically by Aston[1] in 1936 who obtained the value 31.9823 ± 0.0003, corresponding to a packing fraction of -5.53 ± 0.09. In 1941 Okuda and Ogata[2] reported a mass of 31.98089 ± 0.00007, representing a packing fraction of -5.98 ± 0.02. This latter value, because of the greater stated precision, has been widely used although it has been in very poor agreement with the mass of S^{32} as computed from lighter masses by means of transmutation data. The discrepancy between the Okuda-Ogata value and that derived from transmutation data has been the subject of a recent letter by Penfold.[3] Within the past few weeks Smith[4] has used his "synchrometer" to obtain for S^{32} the mass 31.9823 ± 0.0010, a value identical with that of Aston, albeit with admittedly poorer precision. As Smith has remarked, "This result indicates, but does not prove" that the Okuda-Ogata value is too low. Our purpose is to describe a measurement of the mass of S^{32} just completed in this laboratory.

TABLE I. Mass of S^{32}.

Present work	31.98237 ± 0.00009
Aston[a]	$31.9823\ \pm0.0003$
Okuda and Ogata[b]	31.98089 ± 0.00007
Smith[c]	$31.9823\ \pm0.0010$
Penfold[d]—deduced from Si^{29}	31.98199 ± 0.00021
Motz[e]—deduced from Si^{29}	31.98224 ± 0.00010

[a] Reference 1.
[b] Reference 2.
[c] Reference 4.
[d] Reference 3.
[e] Reference 6.

Ion Source.—In our experiments the mass of S^{32} was measured by photographing the $(O^{16})_2-S^{32}$ doublet, the same doublet as was used by Aston, Okuda, and Ogata, and Smith. The O_2^+ and S^{32+} ions were obtained in a manner which is thought to be novel. A mixture of SO_2 and O_2 (in the approximate ratio 1:5 by volume) was allowed to leak into the source region, emerging from the leak into a high frequency spark between two platinum electrodes. The number of desired ions formed in the spark was sufficient to enable us to photograph well-matched doublets with exposure times of 5 to 12 minutes.

Mass of S^{32}.—Five doublets were measured and yield for the $(O^{16})_2-S^{32}$ packing fraction difference the value $\Delta f=5.51\pm0.03$. This gives the mass $S^{32}=31.98237\pm0.00009$. A suitable mass scale was provided by the $(Cu^{63})^{++}-(O^{16})_2$ separation, the doubly-charged copper arising from the platinum electrodes where it was present as an impurity. The mass of Cu^{63} was assumed[5] to be 62.95032 ± 0.00041.

Discussion.—The present value for the mass of S^{32} is compared in Table I with other measured and computed values. It is seen to agree remarkably well with the values of Aston and Smith. It is also in good agreement with the value computed by Motz[6] from Si^{29} using some of the very accurate transmutation data recently obtained by Van Patter at M.I.T., and is in fair agreement with the value deduced by Penfold[3] from Si^{30}. The masses of Si^{29} and Si^{30} used in these two calculations were those obtained in this laboratory.[7]

* This letter is based on work done at Wesleyan University under contract with the AEC.
[1] F. W. Aston, Proc. Roy. Soc. (London) A163, 391 (1937).
[2] T. Okuda and K. Ogata, Phys. Rev. 60, 690 (1941).
[3] A. S. Penfold, Phys. Rev. 80, 116 (1950).
[4] L. G. Smith, Phys. Rev. 81, 295 (1951).
[5] H. E. Duckworth and R. S. Preston, to be published.
[6] H. T. Motz (private communication).
[7] Duckworth, Preston, and Woodcock, Phys. Rev. 79, 188 (1950); H. E. Duckworth and R. S. Preston, Phys. Rev. 79, 402 (1950).

Streamer Breakdown and Sparking Thresholds

LEONARD B. LOEB
Department of Physics, University of California, Berkeley, California
November 24, 1950

THE studies of Raether[1] with Wilson cloud chambers and of the writer's students[2] with positive corona have established the reality of the streamer breakdown mechanism of sparks beyond the shadow of a doubt. All sparks showing bright, narrow channels, straight, crooked, or branched, extending down to pressures so low that diffusion yields broad fuzzy channels or glow, unquestionably involve as an important element of the mechanism the positive and negative streamer mechanisms as postulated by Meek and the writer[3] and by Raether.[1]

The streamer mechanism was invoked initially, among other reasons, to account for the formative time lags of the order of 10^{-7} sec observed in slightly overvolted gaps.[3] These could not well be accounted for by the classical secondary Townsend mechanisms. Relatively recently, Gaenger[4] and Fisher[5] and his collaborators attempted to locate the lower pressure and gap length values at which, in uniform fields, transition of the streamer mechanism to the diffuse Townsend spark occurred. They found that down to conditions where the spark appears as a diffuse glow, the breakdown is consistently of the streamer type. Fisher and his collaborators further found that as the applied overvoltage across the plane parallel plate gaps was decreased to a few tenths of a percent in air and N_2, the *formative time lag of sparking rose rapidly from 10^{-7} to 10^{-4} sec* and longer. The curve between overvoltage and time lag was independent of triggering illumination within limits, was independent of pressure, but varied in proportion to gap length. Analogous but more erratic data were observed in O_2. In argon the formative lag was much greater than in air and could be reduced to microseconds only by overvoltages of the order of 100 percent. In argon and O_2 the overvoltage time lag curves were pressure dependent. Such long time lags are incompatible with a sparking mechanism in which the *threshold is set by streamer formation* as originally proposed by Meek[3] and the writer and Raether.[1]

The theory for the temporal growth of a Townsend discharge developed by von Engel and Steenbeck[6] has been elaborated by Bartholomeyczyk[7] and investigated by von Gugelberg[8] in terms of the various secondary γ-mechanisms. The theory and data on γ fix the threshold for a Townsend discharge as $\gamma \exp(\alpha d) = 1$ for a uniform field gap of length d with α the first Townsend coefficient. Above this threshold positive ions accumulate in the gap through a diffusive self-sustaining discharge of low order. It has independently been shown by von Engel and Steenbeck[9] and by Varney, White, Loeb, and Posin,[10] that if the X/p values are such that they lie below the point of inflection of the $[(\alpha/p)-(X/p)]$ curve, the space charge accumulations will enhance the development of the distortion leading to a spark. Near the threshold of the Townsend discharge the space charge build-up takes long time intervals as shown by Schade[11] and von Gugelberg[8] in conformity with theory. The time of build-up rapidly decreases the greater the overvoltage. In fact, Kachickas and Fisher have calculated the formative time lags using Schade's approximation to von Engel and Steenbeck's theory assuming $\gamma \exp(\alpha d) = 1$. The crude theory qualitatively predicted the course of the observed variations of the overvoltage-time lag curves for air and argon remarkably well.

It must thus be concluded that with low values of γ as in air and especially with low values of α and high values of γ as in argon, the Townsend threshold for a space charge build-up sets in at values of X/p and of potentials V *below* those which would initiate streamer formation. Streamer formation requires values of avalanches, $\exp(\alpha d)$, of the order of 10^7 electrons or more. Thus, *spark discharges in uniform fields set in at thresholds for low order Townsend discharges* by creating space charge field distortions. These distortions increase to the point where avalanches reach streamer-forming proportions in midgap, thus yielding sparks as streamer-type breakdown. As overvoltages increase, the temporal rate of space charge production is increased, and the streamer-forming avalanches are produced in progressively shorter time intervals. In air or O_2 the low values of γ require high potentials to give the correspondingly large values of $\exp(\alpha d)$ for Townsend thresholds. Hence, only slight overvoltages are needed in air so that Meek's streamer criterion nearly holds. In argon and other inert gases appreciable values of α set in at such low values of X/p and α is so small, while γ is large, that the Townsend thresholds fall far below streamer thresholds. Thus, Meek's streamer theory cannot apply to such gases.

The physicist must, therefore, reconcile himself to the paradoxical situation of a streamer breakdown mechanism for spark in uniform fields with *a threshold which is set by the conventional Townsend criterion* and *not* by that of *Meek and the writer and of Raether*. If this is done, practically all of the difficulties of the past are reconciled in a single consistent sparking theory.

It must be emphasized that the conditions cited apply to uniform field breakdown. In the intense highly distorted fields near positive points and wires, streamers can and do form as postulated by the writer, Meek, and Raether, and ultimately lead to breakdown. Thresholds for such discharges are set directly by streamer theory and are entirely gas dependent.[12]

[1] H. Raether, Ergeb. exakt. Naturwiss. **30**, 75 (1949).
[2] L. B. Loeb and A. F. Kip, J. Appl. Phys. **10**, 142 (1939).
[3] L. B. Loeb and J. M. Meek, *Mechanism of the Electric Spark* (Stanford University Press, Stanford, 1941).
[4] B. Gaenger, Arch. Elektrotech. **39**, 508 (1949).
[5] L. H. Fisher and B. Bederson, Phys. Rev. **78**, 331 (1950). B. Bederson and L. H. Fisher, Phys. Rev. **78**, 331 (1950). L. H. Fisher and B. Bederson, Phys. Rev. **81**, 109 (1951). G. A. Kachickas and L. H. Fisher, Phys. Rev. **79**, 232 (1950). L. H. Fisher and G. A. Kachickas, *Conference on Gaseous Electronics*, paper D-1 (New York, October 19–21, 1950).
[6] M. Steenbeck, Wiss. Veröffentl. Siemens-Konzerns **9**, 42 (1930). A. von Engel and M. Steenbeck, *Elektrische Gasentladungen* (Verlag. Julius Springer, Berlin, 1934), Vol. 2, pages 179ff. and pages 51–55.
[7] W. Bartholomeyczyk, Z. Physik **116**, 235 (1940).
[8] H. L. von Gugelberg, Helv. Phys. Acta **20**, 250 and 307 (1947).
[9] See reference 6, Vol. 2, pages 51ff.
[10] Varney, White, Loeb, and Posin, Phys. Rev. **48**, 818 (1935).
[11] R. Schade, Z. Physik **104**, 487 (1937).
[12] L. B. Loeb and R. A. Wijsman, J. Appl. Phys. **19**, 797 (1948). L. B. Loeb, Phys. Rev. **73**, 798 (1948).

A Note on the Calculation of the Fermi Function in the Theory of Beta-Decay*

J. Y. MEIT
Department of Physics, Indiana University, Bloomington, Indiana
November 6, 1950

IN view of recent advances in experimental techniques of beta-ray spectroscopy, the accuracy of the calculation of the Fermi function has been investigated by several authors.[1] In fact, it can be calculated as accurately as desired without much effort.

According to Konopinski's formulation[2] of the theory of beta-decay, the number of beta-particles emitted in the momentum range p to $p+dp$ is given by the relation

$$N dp = CF(z, W) p^2 (W_0 - W)^2 dp \qquad (1)$$

where $F(z, W)$ is the Fermi function given by

$$F(z, W) = \frac{4(2pR)^{2s-2} e^{\pi\delta} |\Gamma(s+i\delta)|^2}{|\Gamma(2s+1)|^2} \cdot \frac{1+s}{2},$$

and

$$\delta = \alpha 2W/p. \qquad (2)$$

TABLE I. Comparison of the approximations to the Fermi function.

	S^{35}		$Cu^{64}(\beta^-)$		RaE		
p	$(F/F_K)^{\frac{1}{2}}$	$(F/F_B)^{\frac{1}{2}}$	$(F/F_K)^{\frac{1}{2}}$	$(F/F_B)^{\frac{1}{2}}$	$(F/F_K)^{\frac{1}{2}}$	$(F/F_B)^{\frac{1}{2}}$	$(F/F_F)^{\frac{1}{2}}$
0.2	1.0094	0.9957	1.0209	0.9869	0.2967	0.8524	1.797
0.4	1.0059	0.9952	1.0144	0.9860	0.2927	0.8561	1.764
0.6	1.0034	0.9950	1.0077	0.9852	0.2867	0.8595	1.745
0.8	1.0013	0.9949	1.0021	0.9848	0.2799	0.8620	1.737
1.2	0.9984	0.9949	0.9934	0.9845	0.2666	0.8650	1.738
1.6	0.9964	0.9949	0.9869	0.9843	0.2549	0.8659	1.745
2.4	0.9933	0.9948	0.9775	0.9842	0.2371	0.8668	1.757
3.2	0.9912	0.9948	0.9707	0.9841	0.2242	0.8670	1.759
4.0	0.9896	0.9948	0.9655	0.9841	0.2145	0.8672	1.755
4.8	0.9882	0.9948	0.9613	0.9841	0.2067	0.8673	1.744

We know that[3]

$$|\Gamma(\alpha+i\beta)|=\frac{\Gamma(1+\alpha)}{\alpha}\prod_{n=0}^{\infty}\left[1+\frac{\beta^2}{(\alpha+n)^2}\right]^{-1}, \quad (3)$$

where α and β are real. Making use of relation (3) we have

$$F(z, W)=fp^{2s-2}\varepsilon^{\pi\delta}\prod_{n=0}^{\infty}\left[1+\frac{\delta^2}{(s+n)^2}\right]^{-1}, \quad (4)$$

where f is a factor independent of W. If we set $s=1$, we have the nonrelativistic Kurie approximation

$$F_k=f\varepsilon^{\pi\delta}\prod_{n=0}^{\infty}\left[1+\frac{\delta^2}{(n+1)^2}\right]^{-1} =f2\pi\delta/(1-\varepsilon^{-2\pi\delta}). \quad (5)$$

Therefore

$$F=F_kp^{2s-2}\prod_{n=0}^{\infty}\left\{\left[1+\frac{\delta^2}{(n+1)^2}\right]\Big/\left[1+\frac{\delta^2}{(n+s)^2}\right]\right\}. \quad (6)$$

The infinite product in (6) converges at a reasonable rate. Table I gives the accuracy of the different prevailing approximations for the three typical cases of the light nucleus S^{35}, the medium nucleus Cu^{64} (negatron emission), and the heavy nucleus RaE, and the comparison with the exact calculations. In this table F is an abbreviation for $F(z, W)$ as given in Eq. (6), F_B denotes Bethe's approximation

$$F_B=F_kp^{2s-2}(\delta^2+\tfrac{1}{4})^{s-1}, \quad (7)$$

F_F denotes Fermi's approximation for heavy nuclei

$$F_F=1/p-0.355 \quad (8)$$

where p is the momentum in units of mc.

* This research was assisted by the joint program of the ONR and AEC.
† Present address: National Research Council, Ottawa, Canada.
[1] C. Longmire and H. Brown, Phys. Rev. **75**, 264 (1949); I. Feister, Phys. Rev. **78**, 375 (1950); H. Hall, Phys. Rev. **79**, 745 (1950).
[2] E. J. Konopinski, Revs. Modern Phys. **15**, 209 (1943).
[3] Godefroy, *La Fonction Gamma* (1901), p. 14.

Internal Motion of Hydrogen Absorbed in Tantalum

MARTIN A. GARSTENS
Electricity Division, Naval Research Laboratory, Washington, D. C.
November 30, 1950

THE metals which absorb hydrogen are usually divided into two groups, the so-called good absorbers (Ti, Zr, Th, V, Ta, Pd), which have decreasing solubility of hydrogen with temperature, and the poor absorbers (Ni, Fe, Co, Cu), which have increasing solubility of hydrogen with temperature. The poor absorbers are thought to allow the protons to move freely through the lattice without any effect on the lattice structure whereas the good absorbers are believed to form definite metal hydrides having a different lattice structure from the pure metal. The latter are supposed to have the hydrogen atoms tightly bound to the metal atoms.[1]

Previous observations of nuclear magnetic resonance[2] absorption lines indicated, however, that in tantalum the protons have strong internal motion at room temperature. To verify this result further an experiment was performed to freeze in the proton motion by lowering the temperatures of the tantalum lattice. This was done successfully at a temperature of about 215°K. Beginning with a line width of less than one gauss at room temperatures the line remains narrow down to 215°K. Over a range of 20° about this point it undergoes a pronounced widening, indicating that the protons are being frozen in position.

Thus in the range of temperature where solubility measurements of hydrogen in metals have been made in the past[3] (i.e., from room temperature up) our experiment indicates that the hydrogen atoms are not tightly bound to the metal atoms. In this respect tantalum resembles the poor absorbers.

The tantalum sample was in powdered form and had a hydrogen concentration of 53.5 atomic percent. Previous observation showed that the line width, at least at room temperature, was not affected appreciably by the degree of concentration of hydrogen. However, at this temperature the tantalum line is so narrow as to be determined by the magnetic field inhomogeneity so that small differences in line width due to differences in concentration may be masked.

Specific heat anomalies have been observed in the tantalum-hydrogen system, within the temperature range where our line width changes have been detected.[4] The specific heat curves have maxima in the region 220° to 265°K, the height of the maxima and the temperatures at which they occur being proportional to the amount of dissolved hydrogen. However, only small concentrations of hydrogen have been used in these experiments (i.e., 0 to 12 atomic percent). According to Hagg[5] the structure of the tantalum lattice changes from a body centered cubic lattice to hexagonal close packing at about 12 atomic percent hydrogen. The sample used in our experiment would then have a lattice which is hexagonal close packed. This may account for the fact that the specific heat anomalies occur at slightly higher temperatures than the resonance line width discontinuity.

Kelley[4] suggests that the specific heat anomaly is due "to the differences in the number of possible ways of arranging the hydrogen particles among the positions in the tantalum lattice available at the higher and lower temperatures." This, of course, conforms to the idea that the protons are frozen in at the lower temperatures.

[1] R. H. Fowler and C. J. Smithels, Proc. Roy. Soc. (London) **A160**, 37 (1937).
[2] M. A. Garstens, Phys. Rev. **79**, 397 (1950).
[3] C. J. Smithels, *Gases and Metals* (1937).
[4] K. K. Kelley, J. Chem. Phys. **8**, 316 (1940).
[5] Hagg, Z. physik. Chem. **B11**, 433 (1931).

Erratum: Acceleration of Stripped C^{12} and C^{13} Nuclei in the Cyclotron

[Phys. Rev. **80**, 486 (1950)]

J. F. MILLER, J. G. HAMILTON, T. M. PUTNAM, H. R. HAYMOND, AND G. B. ROSSI
Crocker Laboratory, Divisions of Physics, Medical Physics, Medicine, and Radiology, University of California, Berkeley and San Francisco, California

THE Editors regret a typographical error in the list of authors of this letter as originally printed. "Purnam" should be replaced by "Putnam" as above.

Ratio of the Quadrupole Moments of Cl^{35} and Cl^{37}

S. GESCHWIND, R. GUNTHER-MOHR, AND C. H. TOWNES
Columbia University, New York, New York*
November 14, 1950

RECENT measurements of the ratio of the quadrupole moments of Cl^{35} and Cl^{37} by several observers using different methods are in disagreement by amounts which are considerably

TABLE I. Data on the quadrupole coupling constants of Cl^{35} and Cl^{37}.

Method	$eqQ(Cl^{35})/eqQ(Cl^{37})$
Direct quadrupole transitions in solid *trans*-dichloroethylene CHCl=CHCl	1.2661 ±0.0002[a]
Atomic beam magnetic resonance method, Cl	1.2795 ±0.0008[b]
Microwave spectra of CH_3Cl	1.273 ±0.004[a]
Microwave spectra of FCl	1.2704 ±0.004[d]
Microwave spectra of BrCl	1.2768 ±0.004[e]

[a] H. G. Dehmelt and H. Krüger, Naturwiss. **37**, 111 (1950).
[b] Davis, Feld, Zabel, and Zacharias, Phys. Rev. **76**, 1076 (1949).
[c] Gordy, Simmons, and Smith, Phys. Rev. **74**, 243 (1948).
[d] Gilbert, Roberts, and Griswold, Phys. Rev. **76**, 1723 (1948).
[e] Smith, Tidwell, and Williams, Phys. Rev. **79**, 1007 (1950).

TABLE II. New measurements of the coupling constants.

Substance	Interval	Cl^{35} (Mc)	$eqQ(Cl^{35})$ (Mc)	Cl^{37} (Mc)	$\frac{eqQ(Cl^{35})}{eqQ(Cl^{37})}$
CH_3Cl	$(F=3/2\rightarrow3/2)-(F=3/2\rightarrow5/2)$	18.695	74.77 ±0.015	14.731	1.2691 ±0.0003
$J=0\rightarrow1$ $K=0$	$(F=3/2\rightarrow5/2)-(F=3/2\rightarrow1/2)$	14.952		11.780	
ClCN	$(F_1=1/2\rightarrow3/2)-(F_1=1/2\rightarrow1/2)$	20.843	83.33 ±0.02	16.436	1.2682 ±0.0006
$J=1\rightarrow2$	$(F_1=1/2\rightarrow1/2)-(F_1=3/2\rightarrow3/2)$	16.849		13.333	
GeH_3Cl	$(F=5/2\rightarrow3/2,\ 5/2,\ 7/2)-(F=7/2\rightarrow5/2,\ 7/2,\ 9/2)$	11.734	46.95 ±0.015	9.262	1.2670 ±0.0005
$J=2\rightarrow3$	$(F=5/2\rightarrow5/2,\ 7/2,\ 9/2)-(F=1/2\rightarrow3/2)$	8.418			

outside the limits of the quoted experimental errors. Table I lists the various results obtained hitherto for the ratios of the quadrupole coupling constants, the quoted errors, and the method of measurement.

Probably at least some of the ratios given in Table I are in error. Although the very nice experiment of Dehmelt and Krüger should yield the most accurate ratio, their value is made somewhat doubtful by preliminary results obtained by Wang using the same technique.[1] For the same molecule he obtained 1.2682±0.004. The atomic beam measurement should be rather accurate, but may be questioned because the ratio of magnetic moments of the two Cl isotopes from the same measurement is also distinctly different from the ratio obtained by nuclear induction methods, and this difference is so far unexplained. A recalculation of the theoretical BrCl spectrum and comparison with experimental measurements indicates that perhaps the accuracy of the Cl^{35}/Cl^{37} ratio obtained therefrom has been overestimated.

Because of these uncertainties we have redetermined the ratio $eqQ(Cl^{35})/eqQ(Cl^{37})$ from the microwave spectrum of CH_3Cl, ClCN, and GeH_3Cl. With the very high resolution afforded by a balanced microwave bridge spectrometer,[2] the intervals from which the quadrupole couplings were determined were measured to 8 kc or better, and hence rather accurate values of quadrupole couplings were obtained. The results of these measurements are given in Table II along with the computed quadrupole coupling ratios. These results are averages of as many as five different sets of determinations for a given molecule on as many different days. For no set were values found which would make the quadrupole coupling ratios in GeH_3Cl and CH_3Cl overlap. Although some of the discrepancies shown in Table I are probably due to errors or to the differing types of experiments used, it seems clear from repeated measurements with the same technique on CH_3Cl and GeH_3Cl that the apparent ratio of quadrupole coupling constants of the two Cl isotopes depends slightly on the molecular environment.

The ClCN spectrum is somewhat complex because of the occurrence of two quadrupolar nuclei in the same molecule. The experimental results were fitted to a theoretical calculation which included all known effects of important size except for a possible magnetic coupling between the nitrogen nucleus and the molecular rotation.

The two measured intervals in GeH_3Cl^{35} did not agree exactly with the spacings expected for pure quadrupole coupling. This deviation was attributed to a magnetic coupling of the type $c(\mathbf{I}\cdot\mathbf{J})$ with $c=-4\pm3$ kc. Inserting this very small correction, one obtains for this molecule $\frac{eqQ(Cl^{35})}{eqQ(Cl^{37})}=1.2670\pm0.0005$. Similarly, if a magnetic coupling of the form $c(\mathbf{I}\cdot\mathbf{J})$ is assumed for Cl in CH_3Cl, the constant c would have the very small value, 0.4 ±0.8 kc.

The only other pair of isotopes for which the quadrupole moment ratios have been measured with some accuracy is Br^{79} and Br^{81}, which in BrCN and CH_3Br seem to agree within experimental accuracy of one part in 2500.

The authors are grateful for a generous gift from Dr. A. H. Sharbaugh of GeH_4 from which the GeH_3Cl was made, and the loan by Professor H. C. Wolfe of a 2K50 oscillator of unusually high frequency.

* Supported jointly by the Signal Corps and the ONR.

[1] T. C. Wang, Columbia University, private communication.

[2] Columbia Radiation Laboratory Report, June 30, 1949, unpublished.

Polarization of the Nucleus by Electric Fields*

G. R. GUNTHER-MOHR, S. GESCHWIND, AND C. H. TOWNES
Columbia University, New York, New York

November 14, 1950

THE preceding letter[1] shows that the ratio of quadrupole moments of Cl^{35} and Cl^{37} in CH_3Cl appears to be slightly different from that found in GeH_3Cl. It will be shown below that the most reasonable explanation of this difference is a fictitious quadrupole moment due to anisotropic polarization of the Cl nuclei by molecular electric fields.

Two molecular effects which might change the apparent ratio of the quadrupole moments from one molecule to another are the pseudoquadrupole effect discussed by Foley[2] and the variation in zero-point vibration with isotopic mass.

A reasonable estimate of the pseudoquadrupole effect makes it too small to account for the observed change by a factor of 10^4. In order to obtain an effect of the correct magnitude, electronic levels within 1 cm^{-1} of the molecular ground state would need to be assumed.

From measured changes of quadrupole coupling with vibration in several molecules, an upper limit for the expected change in quadrupole coupling due to isotopic mass variation is one part in 2500. If the observed effect were due to zero-point vibrations in GeH_3Cl the change in Cl quadrupole coupling per quantum of vibration energy would need to be −10 percent. Actual rough measurement shows this change to be +3 percent ±3 percent. Although the effect of vibration in CH_3Cl has not been measured specifically, the quadrupole coupling change per vibrational excitation would have the ridiculously large value of 20 percent if it is to explain the variation in apparent quadrupole moment ratios, and hence this explanation is ruled out.

Two other effects which can produce a variation in the apparent quadrupole moment ratio are a second-order perturbation of the electronic levels by the nuclear quadrupole coupling and a penetration of the nuclear volume by electronic charge. The variation due to either one of these effects, however, would be much too small to account for the observed discrepancy.

A reasonable explanation of the discrepancy is that a polarization of the Cl nuclei occurs in the molecular electric fields. If the nuclear polarizability depends on the direction of polarization with respect to the spin axis of the nucleus, then the classical

energy of polarization can be shown to be

$$W_p=-\frac{1}{6}\left[(\alpha_s+2\alpha_s)\left(\frac{e\rho}{r^4}\right)_{Av}\right]+\frac{(\alpha_s-\alpha_s)}{12}\times\left[\frac{e\rho(3\cos^2\theta_m-1)}{r^4}\right]_{Av}P_2(\cos I,J),$$

where α_s=polarizability along the nuclear axis, α_s=polarizability perpendicular to the nuclear axis, ρ=charge density (outside the nucleus considered), r=distance from center of nucleus to charge, θ_m=angle between molecular axis of symmetry and charge, I=nuclear spin, and J=angular momentum of molecule. The quantum-mechanical equivalent of $\alpha_s-\alpha_s$ is

$$\alpha_s-\alpha_s=\frac{2I(I+1)}{2I-1}\sum_n\frac{[|\mu_{on}|_{M=I}]^2-[|\mu_{on}|_{M=I-1}]^2}{E_n-E_0},$$

where E_0 and E_n are the nuclear energies in the ground and excited states, respectively, and $|\mu_{on}|_{M=I}$ is the z-component of the dipole matrix element between these two states for the magnetic quantum number $M=I$.

With the above definition of $\alpha_s-\alpha_s$, the proper expression for the anisotropic part of the polarization energy for a nucleus on the axis of a symmetric molecule is

$$W=\tfrac{1}{4}e(\alpha_s-\alpha_s)\mathrm{p}\left(\frac{3K^2}{J(J+1)}-1\right)\left[\frac{\frac{3}{4}C(C+1)-I(I+1)J(J+1)}{2I(2I-1)(2J-1)(2J+3)}\right],$$

where $C=F(F+1)-I(I+1)-J(J+1)$,

$$\mathrm{p}=\left[\frac{\rho(3\cos^2\theta_m-1)}{r^4}\right]_{Av}=2(E_z^2-E_x^2)_{Av}.$$

E_z is the electric field at the nucleus parallel to the molecular axis due to all charges outside the nucleus.

Hence the polarization coupling constant $\frac{1}{4}e(\alpha_s-\alpha_s)\mathrm{p}$ is equivalent to a quadrupole coupling constant eqQ and distinguishable only because p depends on the inverse fourth power of r, while q depends on the inverse cube. The ratio of apparent quadrupole moments of Cl^{35} and Cl^{37} isotopes will be

$$\frac{Q_{35}+\frac{1}{4}(\alpha_s-\alpha_s)_{35}(\mathrm{p}/q)}{Q_{37}+\frac{1}{4}(\alpha_s-\alpha_s)_{37}(\mathrm{p}/q)},$$

which will vary when p/q varies unless

$$Q_{35}/(\alpha_s-\alpha_s)_{35}=Q_{37}/(\alpha_s-\alpha_s)_{37}.$$

The lowest known energy level of Cl^{35} is 0.6 Mev, while the lowest for Cl^{37} is 2.7 Mev,[3] so that their polarizabilities may be somewhat different. Assuming a single-particle model, the difference of the matrix elements

$$[|\mu_{on}|_{M=I}]^2-[|\mu_{on}|_{M=I-1}]^2$$

will be of the order of $e^2r_n^2$, where r_n is the nuclear radius, and hence $(\alpha_s-\alpha_s)$ for Cl^{35} can be approximated, with $E_1-E_0=0.6$ Mev. Although a number of higher levels may contribute to α_s, they would probably not affect the difference $(\alpha_s-\alpha_s)$ appreciably. From the use of Hartree wave functions[4] for K^+ and K^{++} it is found that for a 3p-electron $\langle 1/r^4\rangle_{Av}\approx 7.5(\langle 1/r^3\rangle_{Av})^{4/3}$, so that p can be estimated from the known value of q. Hence $\frac{1}{4}e(\alpha_s-\alpha_s)\mathrm{p}$ for Cl^{35} in CH_3Cl would be approximately 0.20 Mc, or 1/550 of eqQ. If, therefore, the ratio p/q changes by 90 percent between CH_3Cl and GeH_3Cl, the observed discrepancy of one part in 600 in the $Cl^{35}Cl^{37}$ quadrupole moment ratio would be produced.

In the particular case of K^+ and K^{++}, Hartree wave functions[4] indicate that p/q for the 3p-electrons changes by only three percent. However, this value may differ considerably from the change between the CH_3Cl and the GeH_3Cl molecules.

A rather large possible error should be allowed for the above estimate of the size of the polarization effect because of uncertainties, not only in p/q but also in the dipole matrix elements and the nuclear energy levels. The lowest known Cl^{35} level is 0.6 Mev, but investigation might reveal other lower levels in either Cl^{35} or Cl^{37}.

One of the authors has benefited from discussions of polarization effects with I. I. Rabi and A. Bohr. Thanks are also due to Mr. L. C. Aamodt for calculations.

* Work supported jointly by the Signal Corps and ONR.

[1] Geschwind, Gunther-Mohr, and Townes, Phys. Rev. 81, 288 (1951).
[2] H. M. Foley, Phys. Rev. 72, 504 (1947).
[3] D. E. Alburger and E. M. Hafner, Brookhaven Laboratory Report BNL-T-9 (July 1, 1949) (unpublished).
[4] W. Thatcher, Proc. Roy. Soc. (London) 172, 242 (1939).

A Canonical Transformation in the Theory of Particles of Arbitrary Spin

W. A. HEPNER
Department of Mathematics, Imperial College of Science and Technology, London, England

October 20, 1950

MUCH of the work in the theory of elementary particles of arbitrary spin[1] is based on the assumption that the relativistic spin operator is of the form

$$I_{\mu\nu}=(\sigma_k,\gamma_k)=\text{const}\cdot i(\beta_\mu\beta_\nu-\beta_\nu\beta_\mu) \qquad k=1,2,3;\quad \mu,\nu=1,2,3,4. \tag{1}$$

It may therefore be of interest to point out a general condition under which this form of the spin operator can be derived as a result. Also, the knowledge of this condition provides a desirable short-cut in the otherwise lengthy derivation of the commutation relations of the β_μ and in work on the solutions of the wave equation, particularly for the higher spins.

The equations expressing the relativistic invariance of the linear first-order wave equation are

$$\begin{aligned}&[\beta_i,\sigma_i]=0,\quad [\beta_i,\sigma_k]=i\beta_l,\quad [\beta_l,\sigma_i]=0,\\ &[\beta_i,\gamma_k]=0,\quad [\beta_k,\gamma_k]=i\beta_4,\quad [\beta_4,\gamma_k]=-i\beta_k,\end{aligned} \tag{2}$$

where $[A,B]=AB-BA$, and (i,k,l) are in cyclic order. On the other hand, the commutation relations between the components of the relativistic (6-vector) spin operators are

$$\begin{aligned}&\text{(a)}\ [\gamma_i,\sigma_i]=0; \quad \text{(b)}\ [\gamma_i,\sigma_k]=i\gamma_l,\\ &\text{(c)}\ [\gamma_i,\gamma_k]=i\sigma_l; \quad \text{(d)}\ [\sigma_i,\sigma_k]=i\sigma_l.\end{aligned} \tag{3}$$

The similarity existing between Eqs. (2a, b) and (3a, b) suggests that the equations can be solved by the following S-transformation

$$\gamma_k=\lambda S\beta_kS^{-1}, \tag{4}$$

where

$$S\sigma_kS^{-1}=\sigma_k,\quad S\beta_4S^{-1}=\beta_4, \tag{4'}$$

with λ as a (real) number. It follows from Eqs. (2d, e, f) that

$$[(S^{-1})^2\gamma_kS^2+\gamma_k]\beta_\mu-\beta_\mu[(S^{-1})^2\gamma_kS^2+\gamma_k]=0. \tag{5}$$

The operator $[(S^{-1})^2\gamma_kS^2+\gamma_k]$ thus commutes with the whole complex generated by the β_μ and is, therefore, a multiple of the unit operator. Since from (3b), $\mathrm{Spur}(\gamma_k)=0$, it follows that

$$S^2\gamma_k+\gamma_kS^2=0, \tag{6}$$

whence also

$$S^2\beta_k+\beta_kS^2=0, \tag{7}$$

S^2 thus commuting with all of the β_μ. It can be deduced, therefore, that S^2 is a constant multiple of the operator η_4 the existence of which is necessary for the covariance of the wave equation under reflections of the three space axes.

Applying the canonical transformation (4) and (6) to (2f) and (3c), the important expression (1) is now obtained as a result.

An immediate consequence of the canonical S-transformation is the equality of the characteristic equations of $\lambda\beta_\mu$ and σ_k. For, owing to the complete parity of all four β_μ, the characteristic equations of σ_k and γ_k are the same and, according to (4), so are the characteristic equations of γ_k and $\lambda\beta_k$. Also, the four operators γ_k and $\lambda\beta_4$ satisfy the same commutation relations as do the four $\lambda\beta_\mu$. This knowledge effects considerable simplification not only in the derivation of the commutation relations of the β_μ, but also in the construction of solutions of the wave equation from the elementary solutions in the rest system by Lorentz transformations.

The expressions for the canonical transformation (4) in the cases of the Dirac electron, the Duffin-Kemmer meson, and Bhabha's particle of spin 3/2 are represented by

$$S=\text{const}\cdot\exp(i\tfrac{1}{4}\pi\beta_4). \tag{8}$$

In particular

$$\begin{aligned} S_{\text{electron}}&=(1-i\beta_4)/\sqrt{2}\\ S_{\text{meson}}&=1-i\beta_4-\beta_4^2\\ S_{3/2}&=\frac{1}{2\sqrt{2}}\left(\frac{5}{2}-\frac{13}{3}i\beta_4-2\beta_4^2+\frac{4}{3}i\beta_4^3\right). \end{aligned} \tag{9}$$

The inverse operators are obtained simply by replacing i by $-i$.

[1] H. J. Bhabha, Revs. Modern Phys. 17, 200 (1945).

An Unusual Nuclear Event*

PAUL R. BARKER
University of Michigan, Ann Arbor, Michigan
October 16, 1950

A NUCLEAR event, unusual in that it produces two electron showers but no charged penetrating particles, has been observed in a cloud chamber operated at sea level. Figure 1 shows one of the stereoscopic views. The nuclear event appears to have been initiated by particle A, which has the proper orientation to have triggered the chamber by passing through the counter telescope directly above. This track is of approximately minimum ionization and therefore it seems improbable that it represents a particle projected upward from the point of interaction. The energies and directions of the two showers, B and C, are consistent with the assumption that each shower was initiated by one of the photons resulting from the decay of a neutral π-meson of extremely short lifetime. No high energy charged particles are produced and therefore most of the kinetic energy of the initiating particle is given to the neutral meson, if one assumes that there are no other energetic neutral particles. It is improbable that there is more than one neutral meson, since then there would be at least two more photons which would have to be emitted in such directions as to escape detection. A rough estimate, based on range and ionization, indicates that the energy of the three heavily ionizing particles, assumed to be protons, is 5 percent±5 percent of the energy present in the showers. Thus, allowing an equal energy for neutrons, the meson receives about 90 percent±10 percent of the total energy.

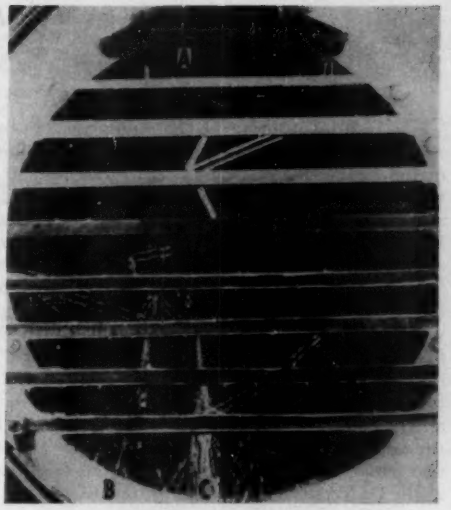

FIG. 1. Nuclear interaction producing two energetic photons but no energetic charged particles.

The nuclear interaction takes place in a $\frac{1}{4}$-in. aluminum plate. Shower B starts in a $\frac{1}{4}$-in. brass plate, and shower C starts in the first of four $\frac{1}{4}$-in. lead plates. The separation of positive and negative ions in the clearing field indicates that the showers occurred at the same time as the nuclear event. The axes of the showers intersect at approximately the point of the nuclear interaction and make angles of 13° and 4° with the direction of particle A. From the numbers of electrons produced, it was estimated that the energies of showers B and C are 300 Mev and 1000 Mev respectively. Assuming that a meson of 140-Mev rest energy decays into two photons with energies of 300 Mev and 1000 Mev, one finds that the total included angle should be 15°, which compares favorably with the measured angle of 17°.

If the meson receives most of the energy of the incident particle, it should continue very closely in the direction of that particle. Thus a further check can be made of the consistency of the above assumptions. It can be shown that photons emitted at angles of 13° and 4° to the direction of motion of the meson will have energies of 270 Mev and 850 Mev, which values are in good agreement with those given previously.

* This work was financed in part by the joint program of the ONR and AEC.

Proceedings of the American Physical Society

Minutes of the 1950 Thanksgiving Meeting at Chicago, November 24–25, 1950

THE 301st meeting of the American Physical Society was held at Chicago, in the buildings of the University of Chicago (with one session at the Museum of Science and Industry), on Friday and Saturday, November 24 and 25, 1950. This will be remembered by those who were there as a frozen meeting; it was not the coldest in the history of the Society (this dismal eminence will probably always be retained by the Cambridge meeting in the winter of 1933–1934) but it was cold enough. No blame for the weather (which was still worse in regions from which many members came) attaches to the Local Committee, which was able to make adequate and amazingly good arrangements for the largest meeting ever held in Chicago—twenty-two sessions of which six were simultaneously held at the University both on the Friday afternoon and on the Saturday afternoon, comprising three symposia, seven other invited papers and one hundred and ninety-two ten-minute papers. The Institute for Nuclear Studies lent us the services of some of its staff, and very particular gratitude is due to Dorothy C. Johnson of that Institute for supervising the entirety of the very complicated planning. The attendance at the meeting was at least 625.

The text of the Bulletin, apart from the preliminary pages, is republished intact in the following pages; errata will follow if any are submitted by the speakers. Mention is here made that the three symposia were provided by three of our Divisions (Electron Physics, High-Polymer Physics, Solid State Physics) and that the invited speakers were Enrico Fermi, Alexander Langsdorf, Jr., E. M. Lyman, N. F. Mott, J. R. Platt, H. T. Richards, and Frederick Seitz.

The banquet of the Society was held in Ida Noyes Hall of the University of Chicago on the Friday evening, with an attendance of 226. K. K. Darrow gave a memorial address in honor of John T. Tate, late Managing Editor of the Society and Editor of *Physical Review*; and N. F. Mott spoke under the title "Science and Government."

The Council met on the Sunday following. To Fellowship were elected twenty candidates, and to Membership three hundred and thirty-seven; their names are appended. It named the first officers (to serve for 1950–1951) of the new Division of Chemical Physics: R. S. Mulliken (Chairman), J. G. Kirkwood (Vice-Chairman), J. R. Platt (Secretary), F. G. Brickwedde (Treasurer), J. E. Mayer, H. H. Nielsen, O. K. Rice (additional members of Executive Committee).

The Nominating Committee, called into special session after the death of John T. Tate, had nominated S. A. Goudsmit as his successor in the post of Managing Editor of the American Physical Society, which carries with it the Editorship of *Physical Review*. After conferring with the Council, Dr. Goudsmit accepted nomination to this important, responsible, and difficult position; his name will appear on the election-ballot. The Council will provide him with the services of an Assistant Editor and the requisite secretarial help. Dr. Goudsmit will remain on the staff of Brookhaven National Laboratory, and the editorial office will be located at the laboratory site. This will be a great contribution by Brookhaven and the Atomic Energy Commission to the science of physics.

A letter from H. A. Barton to Robert L. Clark (Director, Manpower Office, Executive Office of the President, National Security Resources Board, Washington, D. C.), dated November 8, 1950, will soon be published in *Physics Today*. Concerning this letter, the Council directed the Secretary to send the following message of Messrs. Barton, Clark, and G. R. Harrison, and to publish it in these Minutes:

"The Council of the American Physical Society cannot endorse the letter of H. A. Barton of November 8, 1950. The Council also is disturbed by the conclusions, which, it has reason to suppose, are being reached as a result of the 'manpower meeting' held at the building of the National Academy of Sciences in Washington on November 13, 1950. The President of the Society has been empowered to appoint a Committee to study these questions."

Following are printed the lists of the candidates elected to Fellowship and to Membership in the American Physical Society on November 26, 1950.

Elected to Fellowship: Valentin Bargmann, H. S. Brown, R. J. Cashman, R. W. Engstrom, Kasimir Fajans, Simon Freed, R. Frerichs, J. J. Hopfield, D. F. Hornig, D. W. Kerr, Leona Marshall, H. A. Oetjen, D. M. Robinson, F. D. Rossini, H. W. Russell, S. S. Sidhu, A. L. Sklar, J. S. Smart, J. W. Stout, and A. L. Turkevitch.

Elected to Membership: Georgette Albouy, Perry B. Alers, Harry C. Allen, Jr., Saul Altshuler, Mohammad R. Amin, Donald J. Anthony, Charles H. Arrington, Jr., Kenneth C. Bandtel, Stanley E. Barden, John P. Barry, George W. Barton, Jr., Van W. Bearinger, Max Bender, Francis A. Benedetto, Donald J. Berets, Ted G. Berlincourt, Hilmer W. Besel, Daniel N. Beshers, Jacob Bigeleisen, R. Byron Bird, John W. Bittner, Henri Bizette, Frank J. Blatt, Henry V. Bohm, Martin Boloten, Charles A. Boyd, Thomas J. Boyd, Jr., Franklin H. Branin, Jr., John L. Braud, Robert G. Breene, Jr., Richard T. Brice, Ronald A. Brightsen, Sidney Brooks,

Robert H. Brout, Hugh N. Brown, Karl L. Brown, Warren L. Buck, Wayne A. Burnett, William A. Butler, Fredric W. Cagle, Jr., Thomas R. Carver, Yvette Cauchois, Martin Caulton, Paul T. Chan, Ernst H. Cherrington, Jr., Robert L. Christensen, Robert W. Christy, David D. Clark, Francis H. Clark, Joe S. Clark, Wesley A. Clark, Jr., Robert S. Codrington, Bowman C. Collins, Richard H. Comer, Barnett C. Cook, Edward L. Corcoran, Richard C. Cornelius, Myron L. Corrin, Lester Corrsin, John P. Cox, Alba D. Craft, David J. Craig, William H. Cramer, Edwin A. Crosbie, Abbey B. Cullen, Jr., Vaughn E. Culler, Irene Joliot-Curie, John P. Curtis, Richard E. Cutkosky, Melvin A. Dachs, Nicolo Dallaporta, Marian Danysz, William C. Davidon, Costa de Beauregard, Kent G. Dedrick, Joseph de Heer, Herbert De Staebler, Jr., Daniel P. Detwiler, Robert W. Deutsch, George W. Dickson, Hendrik Dijkstra, Edward E. Dodd, Robert C. Doerner, Marcia Doolittle, Nancy Dorny, John A. Doughty, John Bernard Drahmann, Maurice Dubin, Bernard J. Dunn, David B. Dutton, Henry T. Dybvig, Frank S. Eby, Milton C. Edlund, Dean S. Edmonds, Jr., Gert Ehrlich, Allen R. Ellis, M. Zaki El-Sabban, Charles R. Emigh, Theodore C. Engelder, Frank Evans, George T. Ewan, Walter J. Fader, Kenneth Fearnside, John S. Fostor, Jr., Erwin Fues, Osmund T. Fundingsland, LeRoy R. Furlong, William B. Gager, William J. Galloway, Richard A. Gardner, Wolfgang Gentner, Murray Gershenzon, Peter G. Gibbs, Charles G. Gilbart, Neel W. Glass, Alfred E. Glassgold, Maurice Glicksman, Donald V. Gnau, Izabella Goldin, Yves Goldschmidt-Clermont, Garry D. Gordon, Raymond A. Grandey, Edward F. Greene, Richard D. Greene, David F. Griffing, John S. Grosso, Leonard I. Grossweiner, Richard Grover, Harry E. Gunning, Beat Hahn, William R. Harp, Jr., William M. Harris, Don E. Harrison, Jr., Herbert A. Hauptman, Satio Hayakawa, Walter Helly, Ernest M. Henley, Frank Herman, Jack M. Hirshon, James G. Holbrook, John H. Holland, Robert J. Horsley, Charles M. Howe, Horace A. Howe, Yee-Chuang Hsu, Elsa L. Huber, Donald R. Hutchinson, Francis E. Jablonski, Herbert L. Jackson, P. Jacquinot, Ali Javan, Frederick A. Johnson, John L. Johnson, Lawrence W. Jones, Karl T. Jonsson, J. Paul Jordan, James Joseph, Walter R. Kane, Manuel A. Kanter, Henry J. Karam, Arthur L. Karp, Sidney W. Kash, Margaret M. Kearns, John M. Kennel, Frank Keywell, Henry A. Kierstead, William J. King, Jr., Harrold B. Knowles, Jr., George F. Koster, Alfred A. Kraus, Jr., Wallace S. Kreisman, Ulrich E. Kruse, Edward T. Kubu, Melvin Labitt, Robert A. Lad, Stanley A. Landeen, Almon E. Larsh, Jr., Kalervo V. Laurikainen, Norman H. Lazar, Sidney Lees, William Z. Lemnios, Meyer Lepor, Edward J. Leshan, Charles A. Levine, Henry R. Lewis, David A. Liberman, Philip G. Lichtenstein, William T. Lindsay, Jr., Herbert G. Lipson, Elton L. Litchfield, Ernst M. Loebl, Nelson A. Logan, Marvin Lubin, Frederick A. MacMillan, Hormoz M. Mahmoud, Richard T. Mara, Stanley Marder, Hershel Markovitz, Irvin Marshall, Paul T. Matthews, Eugene K. Maun, John G. Mavroides, Donald S. McClure, Joel W. McClure, John G. McCubbin, Robert W. McMurrough, Per E. Melin, Alfonso Merlini, Lewis E. Miller, Richard C. Miller, Alfred P. Mills, Marvin H. Mittleman, George Moe, Lynn R. Momo, Dewey Moore, Henry M. Morgan, Tetsu Morita, William E. Mott, Ambuj Mukerji, Burton H. Muller, Olen A. Nance, Robert K. Nesbet, Gertrude F. Neumark, Jack B. Niedner, Eunice Niles, Martin Nisenoff, Lawrence C. Noderer, James F. Norton, Walter A. Oberheim, Nathan Ockman, George F. O'Neill, Alan Oppenheim, David G. Ott, William Patterson, Jr., Ronald S. Paul, Harry M. Peek, Michael J. Pentz, Miles T. Pigott, Donald K. Pollock, Donald A. Pontarelli, Albert G. Prodell, Vetury Ramakrishna Rao, Alfred G. Redfield, Frederick P. Reding, Rowland W. Redington, Stanley F. Reed, Willard A. Reenstra, Harvey N. Rexroad, Herman Ritow, Thomas R. Robillard, David Z. Robinson, George W. Robinson III, Harold B. Robinson, Jr., Jack Rosen, John C. Rowley, Byron W. St. Clair, Raymond C. Sangster, Harry Schiff, Frederick W. Schmiedeshoff, Jr., Otto Schnepp, Glen E. Schrank, Frank Schroeder, Helmut Schwarz, Stephen M. Shafroth, David S. Selengut, John H. Shaw, Kurt E. Shuler, Ronald J. Sladek, Donald M. Slager, Lawrence M. Slifkin, Ernst R. Smith, Sheldon D. Softky, Nicholas Solimene, Abraham Sosin, Robert S. Speck, Ross L. Spoerlein, Ellen L. Spotz, Harold Staras, Jesse E. Stareck, Howard L. Steele, Jr., Joseph M. Stein, Stanley Stein, Martin Steinberg, David P. Stevenson, Thomas H. Stix, Hugh F. Stoddart, Martin L. Storm, Virgil L. Stout, Edward N. Strait, Jr., Oliver F. Swift, Hoang Tchang-Fang, Newton A. Teixeira, Kent M. Terwilliger, Raphael M. Thaler, Manuel A. Thangaraj, Robert H. Thompson, John S. Thomsen, Robb M. Thomsen, William A. Thornton, Jr., Kiyo Tomiyasu, Richard K. Trask, John G. Tryon, Leo D. Tuck, Jean C. Turgeon, Paul Urban, Richard H. vanHaagen, J. Van Kranendonk, Nico F. Verster, Jack H. Waggoner, Jr., Darcy Walker, Martin Walt, Robert K. Wanless, Michael S. Watanabe, Marshall T. Watson, Robert T. Watson, Francis H. Webb, Jr., Alfons Weber, Yung T. Wei, Marvin S. Weinstein, Paul Weiss, Donald R. Westervelt, Peter K. Weyl, Angus C. Whittier, Charles E. Whittle, Thuler O. Willy, Oscar B. Wilson, Jr., Robert D. Worley, James M. Wyckoff, Yako Yafet, Leo Yaffe, Chen N. Yang, Robert L. Younkin, Joseph S. Yudelson, Robert L. Zimmerman, Carl F. Zobel, and Gus T. Zorn.

KARL K. DARROW, *Secretary*
American Physical Society
Columbia University
New York 27, N. Y.

Errata Pertaining to Papers B6, B10, C2, H2, K11, L5, V1, V5, and Session N

B6, by T. R. Roberts and Alfred O. Nier. The measured value should be $S^{32}=31.9823\pm0.001$, a result which indicates that the value of reference 1 is too low rather than too high.

B10, by Guy C. Omer. This research was supported in part by the ONR.

C2, by G. Dejardin and R. Falgon. D. Dejardin should read G. Dejardin. This error also appeared in the Index of the Bulletin.

H2, by L. G. Schulz. L. G. Schultz should read L. G. Schulz. This error also appeared in the Index of the Bulletin.

K11, by Goldhaber, Williamson, Jackson, and Laubenstein. In the fourth line from the bottom the cross section should read 0.14×10^{-24} cm²/steradian.

L5, by A. S. Nowick. A. S. Novick should read A. S. Nowick. This error also appeared in the Index of the Bulletin.

V1, by Alexander Langsdorf, Jr. The name of the speaker should be Alexander Langsdorf, Jr. with only one f. This error also appeared in the Index of the Bulletin.

V5, by Pasternack, McReynolds, Weiss, and Corliss. In the table, 0.10 should read 0.14 and 0.18 should read 0.39.

Session N. The name of the chairman should be W. G. Shepherd.

PROGRAMME

FRIDAY MORNING AT 10:30

Mandel Hall

(I. I. RABI presiding)

Invited Papers

A1. High Energy Nuclear Events. ENRICO FERMI, *University of Chicago.* (45 min.)
A2. Electronic distribution in alloys. N. F. MOTT, *University of Bristol.* (30 min.)

FRIDAY MORNING AT 10:00

Eckhart 133

(L. A. TURNER presiding)

Papers Not Classed Elsewhere

B1. The Use of Conducting Extensions of Small Pool-Type Cathodes in Arcs. B. PEARSON DELANY AND PAUL L. COPELAND, *Illinois Institute of Technology.*—Lufcy and Copeland[1] found that the stability of arcs with pool-type cathodes was increased markedly by confining the cathode spot within a glass constriction. One of the disadvantages of this structure is the difficulty of establishing a discharge within the constriction. In one part of the present work, constrictions formed from semi-conductors confine the cathode spot to a limited area of the pool surface. In another part of this work, the constriction is formed by a glass tube pulled down into a taper. A drop of liquid at the small end serves as cathode pool, and the conducting extension in this case is made by coating the interior wall of the taper with a thin film of metal in electrical contact with the pool. In either of these arrangements, a glow between the extended cathode structure and an anode placed several centimeters above it is readily established. Under favorable circuit conditions, transition to an arc is rapid. When the arc is operated at low currents, an increase in the stability of the arc with reduction of the pool area within the constriction is observed.

[1] C. W. Lufcy and P. L. Copeland, J. App. Phys. 16, 740 (1945).

B2. Control of Low Current Arcs by Conducting Constrictions. PAUL L. COPELAND AND B. PEARSON DELANY, *Illinois Institute of Technology.*—A constriction of resistance material in contact with a cathode pool serves as a very useful control electrode when an electrical connection is made to the part of the structure extending away from the pool. An arc may be initiated by applying a positive potential which is very much less than that required for the formation of a glow. In this work experimental arcs have been started and operated from a 50-volt d.c. source. With a current of an ampere or more, the arc continues after the potential is removed from the control electrode. When a positive potential is maintained on the control electrode, the anode current may be reduced to the order of 100 milliamperes. The current carried by the control electrode in this case may be about 50 milliamperes. When the anode current is low, the removal of the potential from the control electrode results in the rapid extinction of the arc.

B3. Stability of Short Arcs in Oxygen, Hydrogen, and Helium. W. M. BRUBAKER, *Westinghouse Research Laboratories.*—An arc drawn between separating contacts is known to be very unstable, in the absence of oxygen, in the usual power circuit. To study this instability experiments have been made in which a four-ampere arc in a 125-volt d.c. resistive circuit was repeatedly restruck between separating contacts. Various metals were used as cathodes, with spectroscopically pure carbons as anodes, in various gases. Data have been obtained showing the dependence of average arc duration after ignition on the cathode material and on the pressure and kind of surrounding atmosphere for a number of metals in oxygen, hydrogen, and helium. Oxygen exhibits an extraordinary stabilizing influence for most metals, whereas in hydrogen the mean life of the arc is generally less than ten milliseconds even at atmospheric pressure.

B4. Electron Loss Cross Sections for Hydrogen Atoms Passing Through Hydrogen Gas. S. K. ALLISON, J. H. MONTAGUE, AND FRED RIBE, *University of Chicago.*—Measurements have been made of the electron-loss cross section in hydrogen gas for hydrogen atoms moving with kinetic energies between 45 kev and 329 kev. The proton beam from a high voltage accelerator was passed through a thin window (8–15 kilovolts thick in various cases) and entered a chamber which could be filled with a known pressure of hydrogen gas. The chamber was located between the pole faces of a magnet capable of producing a field up to 8000 gauss. On emerging from the window the beam contained a neutralized fraction of hydrogen atoms. When hydrogen gas was admitted, some of these atoms were stripped of their electron and the proton thus formed bent out of the beam by the magnetic field. This attenuation of the beam could be expressed as an electron-loss cross section which varied from $6.6_4\times10^{-17}$ cm^2 to $2.2_1\times10^{-17}$ cm^2 per hydrogen atom at the limiting energies quoted above. Between 120 kev and 329 kev the cross section was found to vary approximately as E^n, where E is the kinetic energy of the atom, and n is $-0.70\pm.05$.

B5. A Versatile All-Metal 60° Mass Spectrometer. RUSSELL BALDOCK AND JOHN SITES, *Oak Ridge.*—A mass spectrometer has been constructed of stainless steel and uses aluminum gaskets for the vacuum seals. The VFM 100 D. P. I. diffusion pump is backed by a Welch 1405 forepump. A cold trap is held at −60°C by a refrigerator compressor system charged with freon 22. In addition, a liquid nitrogen trap may be used. The overhead mounted magnet has an Alnice iron yoke, with

16 individually wound, air-cooled coils. The magnet is supplied directly from a 2 kw G. E. amplidyne, which is controlled by an electronic regulator. Magnetic scanning is accomplished with a motor-driven helipot in the input comparison circuit of the amplidyne regulator. The source and receiver are modifications of the commonly used Nier type. Data on mass spectra may be recorded on an L and N Speedomax, read from a galvanometer scale, or taken using a bucking potentiometer on the grid of the VX-41A electrometer tube. Preliminary work has been done on appearance potentials and mass cracking patterns of calutron charge materials.

B6. The Mass "Synchrometer" and Measurement of the Mass of S^{32}.* LINCOLN G. SMITH, *Brookhaven National Laboratory*.—A new method has been developed for accurately measuring the rotation period (T) of ions in a uniform magnetic field. After passing through a slit 180° from the source, ions are subjected to an electric field of small extent in space and time. Thus is formed a short bunch having reduced energy and free to execute a large number (n) of rotations in the same plane without striking the source. Reestablishment of the electric field at time nT later further reduces the energy of the bunch so that it strikes a detector. Electronic measurement of the interval between two applied voltage pulses for maximum current to the detector yields a value of the ionic mass. From measurement of the time difference for S^+ and O_2^+ bunches ($n=40$, $nT=840$ μsec.) formed in SO_2, a value $S=32.9823 \pm 0.0010$ agreeing with Aston's has been obtained. This result indicates, but does not prove, that a more recent value[1] is too high. Results to date have been obtained in a small preliminary instrument. A larger "synchrometer" employing higher fields, believed capable of a precision of 10^6 or better is being designed.

* Research carried out at Brookhaven National Laboratory, under the auspices of the U. S. AEC.
[1] T. Okuda and K. Ogata, Phys. Rev. 60, 690L (1941).

B7. On the Dissociation of Oxygen Molecules in the Upper Atmosphere. TA-YOU WU, *National Research Council, Canada*.—It has been shown by Moses and Wu[1] that on the basis of the conditions for steady state, namely, (a) constancy of number concentrations of atoms and molecules, (b) constancy of temperature, and the barometric equation, it is possible to determine the temperature and the concentrations of the oxygen atoms and molecules as functions of height, provided the temperature and the temperature gradient are given at a certain height where the theory holds. Further calculations have been carried out. The variation of the degree of dissociation with height obtained differs from the results of Rakshit[2] and of Penndorf.[3] The causes for the difference between the theory of Moses and Wu and those of Rakshit and Penndorf are pointed out. It is shown that Penndorf's result would correspond to the following situation: an atmosphere with the normal proportion of N_2 and O_2, which is separated by horizontal, transparent partitions so that, while radiation can come down, the atoms and molecules after dissociation cannot redistribute themselves. The basic assumptions of the three theories are discussed.

[1] H. E. Moses and T. Y. Wu, Phys. Rev. 78, 333 (1950).
[2] H. Rakshit, Ind. J. Phys. 21, 57 (1947).
[3] R. Penndorf, J. Geophys. Res. 54, 7 (1949); Phys. Rev. 77, 561 (1950).

B8. A Contribution to the Theory of Bose-Einstein Liquids. C. V. HEER AND J. G. DAUNT, *Ohio State University*.—Smoothed potential models for liquid He^4 and liquid He^3 in which each are considered as ideal Bose-Einstein and Fermi-Dirac gases situated in potential wells of potential $-\chi_4^\circ$ and $-\chi_3^\circ$, respectively, are considered. It is shown that the lambda transition temperatures, T_λ, of solutions of such liquids can be calculated. The calculated values of T_λ, as a function of concentration of He^3, appear to be in satisfactory agreement with the observed values. Detailed calculations have been made of the vapor pressures of such smoothed potential liquid models of He^4 and He^3 in solution. The results indicate that, in the temperature range above 1°K for solutions of not too high concentration of He^3, the total vapor pressure would be higher than that given by Raoult's law for temperatures both above and below the λ-temperature of the solution. In this way the experimental results for the vapor pressure of such solutions, first emphasized by Taconis, *et al.*, can be explained and good agreement between theory and experiment is evident.

B9. The Velocity of Second Sound in He^3-He^4 Mixtures. ERNEST A. LYNTON* AND HENRY A. FAIRBANK, *Yale University*.**—Extending our preliminary measurements,[1] we have obtained the velocity of second sound in He^3-He^4 mixtures for temperatures between 1.24°K and 1.95°K and He^3 concentrations ranging from 0.09 percent to 0.80 percent. Even with these small concentrations of He^3 the second sound velocity at lower temperatures was found to be much larger than that for pure He^4, the difference increasing with decreasing temperature and increasing concentration, in general agreement with Pomeranchuk's predictions.[2] At 1.26°K, e.g., the velocity was 19.08 meters/second for pure He^4, 24.04 m/sec. for 0.41 percent He^3, and 27.09 m/sec. for 0.80 percent He^3, while at temperatures above 1.95°K the difference between pure He^4 and the various concentrations of He^3 was less than the experimental error of one percent.

* Du Pont Company Postgraduate Fellow.
** Assisted by the ONR.
[1] E. A. Lynton and H. A. Fairbank, Phys. Rev. 79, 735 (1950).
[2] I. Pomeranchuk, J. Exp. Theor. Phys. USSR 19, 42 (1949).

B10. The Cosmological Constant as Derived from a Cluster of Galaxies. GUY C. OMER, JR., *University of Chicago*.—Clusters of galaxies are assumed to arise from small fluctuations in the initial density at the beginning of the expansion of the universe. A non-homogeneous, spherically symmetric cosmological model is considered which has a cluster at the coordinate orgin and is surrounded by a homogeneous expanding field. The interior of the cluster can be oscillating and presently contracting. The periphery of the cluster must be monotonically expanding. There must be a transition zone which is asymptotically expanding to the Einstein static state. Since matter in the neighborhood of this transition zone is expanding or contracting at a very slow rate, a break in the density-radius curve of the cluster is to be expected. The location of this break would be determined by the ratio of the cosmological constant to the average mass of a galaxy. The cluster of galaxies in Coma Berenices was investigated with the Palomar 48″ Schmidt telescope. A break was found in the density curve as integrated from the counts of galaxies projected against the sky. If the average mass of these galaxies is of the order of 10^9 that of the sun, than the cosmological constant is of the order of $+10^{-18}$ (lt-yrs)$^{-2}$.

B11. The Space-Time World and Physical Laws. ROBERT E. BASS, *University of Toledo*.—The existence of physical systems for immensely long periods is so basic and conspicuous in fact in the entire universe that this existence itself is a characteristic property of the cosmos. Continued existence or development of a physical system will, however, not follow from an initial state, unless simultaneous quantities in that state are connected by particular mathematical relations. Such relations are not causal laws and are irreducible to causal laws alone.[1] Furthermore, those relations are irreducible to probability laws. Less entropy and more available energy of a system at an earlier state will not enforce the actual validity of those relations at a later state. Hence there are two distinct basic kinds of order in the physical world: (I) An order of facts succeeding each other in time, (II) Such an order of simul-

taneous facts that systems can develop and continue to exist. Examples for the occurrence of II are: Non-vanishing mean mass density in the universe, stability of galaxies and of the solar system, and specific relations between simultaneous facts in biological organization.

[1] R. E. Bass, Phys. Rev. **79**, 201 (1950).

B12. General Theory of Current Stabilizers. J. J. GILVARRY AND D. F. RUTLAND, *Rand Corporation and Institute for Numerical Analysis, N.B.S.*—The general theory of the linear four-terminal current stabilizer is developed by specifying an arbitrary stabilizer by four parameters (current-stabilization factor t, internal resistance r, equivalent shunt resistances q for open-circuited output and p for short-circuited output) which are necessary and sufficient for a complete specification. The current statilization factor t can be expressed as $t=sr$, where s is the voltage-stabilization ratio of the current stabilizer viewed as a voltage stabilizer. By means of an equivalent circuit derived[1] for the general voltage stabilizer, the general solution is obtained for the problem of expressing the over-all performance parameters of a current stabilizer in terms of parameters of the stabilizer itself and the load and supply resistances. Two special cases are discussed: one is the current-stabilizer analogue of a type of voltage stabilizer for which Hunt and Hickman[2] have given the theory; the other is the passive current stabilizer. Confirmatory experimental results are presented.

[1] J. J. Gilvary and D. F. Rutland, Phys. Rev. **80**, 129(A) (1950).
[2] F. V. Hunt and R. W. Hickman, Rev. Sci. Inst. **10**, 6 (1939).

B13. Head Wave Produced by a Point Source. E. GERJUOY, *University of Southern California.*—A very careful analysis has been made of the reflection of a pulse of sound from a point source in one non-absorbing liquid separated from a second non-absorbing liquid by an infinite plane boundary, thereby clarifying the mechanism of propagation of the head wave which arises when the index of refraction is < 1. The head wave is shown to be a consequence of deviations between geometrical and wave propagation, which cause rays incident at the critical angle to be refracted along the surface with finite amplitude. It is shown *without approximation* that the head wave in the first medium is precisely the wave required to satisfy the boundary conditions for this refracted wave in the second medium. That the head wave does actually form plane wave fronts in the first medium, reflected from the surface at the critical angle, is shown by using Huyghens' principle. Finally it is shown *without approximation* that a pulse of sound is received in the first medium at a time corresponding to propagation along the surface with the wave velocity of the second medium. The possibility of direct experimental confirmation of the existence of the head wave in the analogous electromagnetic problem will be discussed.

FRIDAY MORNING AT 11:30

Breasted Hall

(J. R. PLATT presiding)

Optical Physics and Microwave Spectroscopy

C1. Interference Films on Glass. SCOTT ANDERSON, *The Anderson Physical Laboratory.*—Interference films on optical glass have been studied by means of channelled spectra. The variation of thickness and refractive index was measured as a function of time in an acid bath. The thickness change followed a definite function of time which is concave toward the time axis but does not conform to a diffusion mechanism. The refractive index shows an initial decrease followed by an increase which remains about equal to that of the base glass as the film thickness increases. These results indicate that the interference film forms by a narrow region of great disorganization moving as a "front" into the base glass. As the front moves into the glass, the constituents left behind reassemble themselves in a configuration very similar to that present in the original glass.

C2. Use of Image-Converting Tubes in Infra-Red Spectroscopy. D. DEJARDIN AND R. FALGON, *Université de Lyon.*—Various image-converting tubes have been combined with spectrographs in such a way that the visible image of an infrared portion of a spectrum appears on a luminescent screen. Such images have been photographed on orthochromatic plates with the aid of a chamber provided with an objective of large aperture. Among the spectra thus examined in the near infra-red are those of argon, mercury, hydrogen, etc. We had the best results with a three-electrode tube similar to the *Bildwandler* of the A.E.G., operated with a total voltage of about 13,000. This detector is so sensitive that we were able to record, with exposures of 20 minutes or less, prismatic spectra extending as far out as 12,100A (mercury) and also grating spectra of rather high dispersion. In the latter case the resolving power is good enough to bring out clearly the detailed structure of the bands of the first positive system of nitrogen, particularly that of the band (0,0) toward 10,500A. The spectrograms are comparable in quality with photographs made directly on special plates. The photo-sensitive layer has to be sharply cooled when the instrument is used for the study of the light of the night sky, as we are using it now.

C3. The Variability of Atomic Polarizabilities. FRANK MATOSSI, *Naval Ordnance Laboratory.*—In previous papers it has been proposed to consider the atomic polarizability α not as a constant but as dependent on the field strength or on the distance between neighboring atoms. Only then can the observed depolarization factors of symmetric Raman lines of diatomic molecules be accounted for. This idea is now applied to triatomic symmetric and unsymmetric linear molecules (OCO, SCS, OCS, NCS, NNO, NNN). The method used involves the knowledge of the force constants and is applicable to bond-stretching vibrations only. In all cases, it is possible to derive, from Raman effect and Rayleigh scattering data, reasonable values for the variation of the polarizability with the atomic distance. These values vary somewhat with the molecule from which they are derived, due possibly to the uncertainty of the force system. The values of $d\alpha/dr$ are between 0.6 and 2.5×10^{-16} cm^2 for N, C, and O; for S, they are between 3 and 8×10^{-16} cm^2. This is equivalent to a change of the atomic radius of not more than about 10 percent.

C4. The Mass of S^{35} from Microwave Spectroscopy.* W. S. KOSKI,** T. WENTINK, JR.,*** AND V. W. COHEN, *Brookhaven National Laboratory.*—The $J=1\rightarrow2$ rotational transition for

OCS has been observed in molecules containing S^{34} and S^{36}. The OCS^{36} frequency is 23457.403±.011 mc/sec. From the frequencies and the recently measured frequencies[1] of OCS^{32} and OCS^{34}, we have evaluated the isotopic mass difference ratios $(m^{36}-m^{32})/(m^{34}-m^{32})$ and $(m^{36}-m^{32})/(m^{33}-m^{32})$, the values being 1.50156±.00015 and 2.99882±.00030, respectively. From these and the masses of the stable isotopes the value of m^{36} is calculated to be 34.97898±.00032, which compares favorably with the value 34.97907±.00045 as computed from nuclear reaction data.[2] The C−O and C−S bond distances have also been calculated to be 1.1637 and 1.5582A, respectively.

* Research carried out under contract with the U. S. AEC.
** Now at Johns Hopkins University, Department of Chemistry.
*** Now at Cornell University, Ithaca, New York.
[1] S. Geschwind (unpublished).
[2] W. Low and C. H. Townes (to be published in *The Physical Review*).

C5. A Reduction in the Doppler Width of Microwave Absorption Lines. GEORGE NEWELL AND R. H. DICKE, *Princeton University.*—Since the natural width for transitions at microwave frequencies is negligible, the resolution of microwave spectroscopy and the stability of frequency standards based on microwave absorption lines is limited ultimately by the Doppler breadth of the lines. This paper describes a method capable in principle of reducing that breadth indefinitely. Microwave radiation with wave-length λ traverses the absorbing gas in the X direction as an approximately plane wave. A system of charged grids establishes a stark effect in the gas which is spacially periodic with a repeat distance of λ/2 along the x-axis and which oscillates in time with an audio-frequency ν. The influence of the periodic stark effect is such that, with sufficiently weak fields, that component of the absorption which is modulated with the frequency ν is due entirely to molecules having X components of velocity lying in narrow ranges about the values $\pm\nu\lambda/2$. The broad absorption line is therefore replaced by two narrow symmetrically placed responses. The method is being tested with the ammonia inversion lines in apparatus designed to give a tenfold improvement in line width. Preliminary results will be reported.

C6. Microwave Spectra of Deutero-Ammonias. H. LYONS, M. KESSLER, L. J. RUEGER, AND R. G. NUCKOLLS, *National Bureau of Standards.*—Measurements of the spectra of the deutero-ammonias previously reported[1] have been extended with an improved spectrograph. Approximately 100 lines of NH_2, NDH_2, and ND_2H have been found in the region from 3100 to 17,000 Mc and are part of a program to provide precise reference standards to lower frequencies than previously available. A major group of lines tentatively assigned to ND_2 appears in the region of 5000 Mc in agreement with the calculations and data of Manning and of Loubser, Klein, and Townes.[2] Additional lines are expected when higher concentrations of NDH_2 and ND_2H are used. Separation of the ND_2 lines is being attempted so that analysis of the spectrum can be made. Many hyperfine lines have been resolved with spacings slightly different from NH_2 as expected. Line-width parameter measurements are under way. A representative list of the stronger lines in Mc follows: 3192; 3865; 4720; 5962; 6461; 7561; 8284; 9007; 9518; 10,844; 11,400; 12,150; 12,778; 13,210; 13,626; 13,923; 14,102, 14,566; 15,132; 15,772; 16,497. Helpful discussions with C. H. Townes are gratefully acknowledged.

[1] Harold Lyons, Phys. Rev. 76, 161 (1949); J. App. Phys. 21, 59 (1950).
[2] M. F. Manning, J. Chem. Phys. 3, 136 (1935). J. H. N. Loubser and J. A. Klein, Bull. Phys. Rev. 78, 348 (1950). C. H. Townes (private communication).

FRIDAY MORNING AT 10:30

Kent

(A. C. G. MITCHELL presiding)

Beta-Emitters, Neutron Through Technetium

D1. Measurement of K-Capture to Positron Ratios by Proportional Counter,* J. TOWNSEND,† *Washington University.*—Several investigations have used proportional counters to study the low energy range of beta-spectra; the present work deals with their use in determining K-capture to positron ratios. A source, suitably placed inside a proportional counter, which decays both by orbital-electron capture and by positron emission, will emit x-rays, Auger electrons, and positrons that are absorbed by the counter gas in such a manner that every disintegration is counted. The height of the resulting counter pulse is in each case directly proportional to the energy of the emitted radiation; the pulse-height distribution can therefore by analyzed to give the ratio of K-capture events to positron emissions. Gaseous sources are found to yield much better spectra than the thinnest obtainable solid sources, due presumably to absorption and scattering of Auger electrons in the backing. For gaseous sources, a correction is to be expected to account for reduction in path length of positrons emitted by gas molecules near the counter wall; under certain conditions, however, this wall correction can be neglected. These conditions will be discussed and results will be presented for Zn^{65}.

* Assisted by the joint program of the ONR and the AEC.
† AEC Predoctoral Fellow.

D2. Beta-Spectrum of the Neutron. J. M. ROBSON, *National Research Council, Chalk River.*—The beta spectrum of the neutron has been measured by a spectrometer method. A collimated beam from the Chalk River pile passes between two magnetic lens spectrometers arranged end to end. An electrostatic collecting system deflects the low energy protons from the neutrons decaying in the beam into the proton magnetic lens spectrometer where they are focused onto the first electrode of an electron multiplier. Some of the beta-particles from the decaying neutrons enter the other magnetic lens spectrometer set up as a beta-spectrometer with a scintillation counter as detector. Coincidences are obtained between the scintillation counter and the electron multiplier when a delay is introduced in the scintillation counter channel to compensate for the transit time of the protons through the proton spectrometer. These coincidences disappear if a boron shutter is placed in the beam or if the proton spectrometer is defocused. By obtaining the coincidence rate as a function of the focusing current in the beta-spectrometer, the beta-spectrum of the neutron has been obtained. The spectrum is of the allowed shape with an end point of 782±13 kev.

D3. Air Absorption of P^{32} Beta-Particles. R. K. CLARK AND S. S. BRAR.—The spatial distribution of the energy ab-

sorbed from beta-emitters is of interest in biological experimentation and in calibration of survey equipment. Measurements in air from point sources yield information which is helpful in these connections. The ionization produced in air by a P^{32} source has been studied as a function of the distance from the source. The measurements were made in a large room. The active material was dried on aluminum foil (about 200 $\mu g/cm^2$) suspended by fine wires to minimize possible scattering by the mounting. The ionization was measured with cylindrical chambers of 1-liter and 10-liter volume, the walls of which were .0003" thick. The importance of a number of sources of error has been evaluated. These include the effect of the earth's magnetic field, chamber-wall symmetry, and the chamber-supporting stem. Comparison will be made between the experimental results and the ionization to be expected on the basis of the known P^{32} spectrum and the stopping power of beta-particles.

D4. β-Spectrum of K^{40}. L. Feldman and C. S. Wu.—Greuling's[1] comparison of the theoretical half-life of K^{40} with the observed value, based on $\Delta J=4$ and $W_0=3.6$ mc^2, has been extended and leads to the result that the four interactions which give compatible half-lives, $3T$, $3A$, $4T$, and $4V$, also predict the same unique energy spectrum. This spectrum is determined by the correction factor $C_3=q^6+7q^4p^2+7q^2p^4+p^6$. The beta spectrum of K^{40} was measured in the solenoid spectrometer with a resolution of 9–10 percent using a KCl source approximately 2.5 mgm/cm² thick. The K^{40} was enriched to 7.13 percent at Oak Ridge under the supervision of C. P. Keim. The Kurie plot is curved concave towards the energy axis but yields a straight line down to about 500 kev when corrected by the C_3 factor. The end point is 1325±20 kev. Comparative studies with an inert KCl source containing Y^{91} activity indicate that the deviation which sets in at 500 kev is very probably due to source thickness. These results are in essential agreement with those reported by other observers.[2]

[1] E. Greuling, Phys. Rev. 61, 568 (1942).
[2] Bell, Weaver, and Cassidy, Phys. Rev. 77, 399 (1950); D. E. Alburger, Phys. Rev. 78, 629 (1950).

D5. Electron Capture in K^{40}. V. L. Sailor, J. J. Floyd, and L. B. Borst.—Characteristic K_α x-rays have been observed associated with electron capture in naturally radioactive potassium (K^{40}). A Pontecorvo type high gain proportional counter, filled with a krypton-methane mixture, proved efficient in discriminating between the 2.9 kv x-rays and the nuclear beta-particles. The ratio of disintegration constants for electron capture to beta emission $\lambda_\alpha/\lambda\beta$ is thought to be less than 20 percent, probably consistent with complete decay through an excited state and hence by gamma-ray emission to the ground state of A^{40}.

D6. Branching Ratio in K^{40}. D. C. Hess, H. Brown, C. Patterson, and M. G. Inghram, *Argonne National Laboratory and Institute for Nuclear Studies.*—The ratio of beta-emission to K-capture in the decay of potassium 40 has been determined to be 7.9±.3 by measurement of the relative abundance of argon 40 and calcium 40 in an old mineral. Known amounts of argon 36 and calcium 48 were added to different aliquots of 10^8-year-old Stassfurt sylvite. The argon was then removed from the sample by melting at 1050°C for one hour. The isotopic constitution was compared with that of the original tracer with a mass spectrometer. The calcium was extracted by a stage of fractional crystallization followed by two oxalate precipitations. Its isotopic spectrum was compared with the original tracer using a surface ionization source. The presence of argon 38 and calcium 44 in the naturally occurring elements permitted a measurement of the radiogenic purity of the products. Comparison of the branching ratio thus measured with the counting value of Sawyer and Wiedenbeck[1] indicates that there was little loss of argon 40 during geologic time. We wish to thank Professor W. W. Watson of Yale for supplying the A^{36}. The Ca^{48} was supplied by the Y-12 Plant at Oak Ridge under allocation from the Atomic Energy Commission.

[1] G. A. Sawyer and M. L. Wiedenbeck, Phys. Rev. 79, 490 (1950).

D7. The High Energy Beta-Spectrum of Sc^{46}. Fred T. Porter and C. Sharp Cook, *Washington University.**—An investigation of the high energy negatron group of Sc^{46} has been made with a 13-cm radius of curvature semi-circular magnetic spectrometer. Spectrometer sources were prepared from an Oak Ridge sample of Sc^{46}. Two different chemical procedures for the purification of scandium were carried out with portions of the original sample. These, along with an unpurified portion, yielded three sources all of which resulted in identical spectral shapes. A high energy group of negatrons was found. The end point appears to be 1.2±0.1 Mev and the abundance of the higher energy group about 0.9 percent. Both these figures are lower than those reported by Peacock and Wilkinson.[1] The lower end point modifies the disintegration scheme[1] by reversing the order of the gamma-rays, the high energy beta-group still going to the first excited state of Ti^{46}. Comparison of the areas of the internal conversion lines with those of the beta-spectra indicates internal conversion coefficients of 1.36×10^{-4} for the 0.89-Mev gamma-ray and of 6.07×10^{-3} for the 1.12-Mev gamma-ray.

* Assisted by the joint program of the ONR and the AEC.
[1] Peacock and Wilkinson, Phys. Rev. 74, 297 (1948).

D8. Problems Related to Neutron-Rich Short-Lived Arsenic Isotopes.* Ronald A. Brightsen, Kalman Shure, Charlie Fisher,** and Charles D. Coryell, *Massachusetts Institute of Technology.*—The neutron-rich arsenic isotopes $40h$ As^{77} and $90m$ As^{78} are well known.[1] Our separations from targets for the $Br^{81}(n,\alpha)As^{78}$ reaction confirm the $90m$ activity characterized in fission,[1,2a] checking also the radiation characteristics, although others report a $65m$ period. Our studies of arsenic separated from other fission products by Winsberg's volatilization method[2b] indicate however, prominent occurrence of an additional arsenic activity of about $40m$ period which probably has a germanium parent of $\sim 2h$ period. Three isotones of As^{78} are known to display isomerism (Ge^{77}, Br^{80}, Rb^{82}). The $40m$ activity is probably another As^{78} produced in high yield in β-decay and in low yield in the (n,α) reaction. An alternate possibility is that it is As^{79}, although Butement[4] reports a $9m$ activity from $Se^{80}(\gamma,p)As^{79}$. The arguments for assignment, genetics, and energetics will be elaborated.

* Supported by the joint program of the ONR and the AEC.
** Research Fellow from the Commissariat à l'Energie Atomique (Paris) under the M.I.T. Foreign Students' Summer Project.
[1] Way, Fano, Scott, and Thew, *Nuclear Data* (Nat. Bur. Stand. Circ. 499, U. S. Printing Office, 1950).
[2] E. P. Steinberg and D. W. Engelkemeir, Paper 54; L. Winsberg, Paper 228, Nat. Nucl. En. Series (McGraw-Hill Book Company, Inc., New York, 1950), Vol. 9, Div. IV.
[3] A. H. Snell, Phys. Rev. 52, 1007 (1937); Sagane, Kojima, Miyamoto, and Ikawa, Proc. Phys. Math. Soc. Japan 21, 660 (1939).
[4] F. D. S. Butement, Nature 165, 149 (1950).

D9. The Disintegrations of Br^{84} and Br^{83}.* L. M. Langer, *Indiana University,* and R. B. Duffield, *University of Illinois.*—The 32-minute activity of Br^{84} and the 2.4-hour activity of Br^{83} were separated from the other fission products produced on irradiating uranyl nitrate, enriched in U^{235}, in the thermal column of a nuclear reactor. The beta-spectra of both activities were studied in a magnetic lens spectrometer. Br^{84} emits a complex beta-spectrum which can be resolved into at least four groups with end points and relative intensities of 4.679 Mev (40 percent), 3.56 Mev (9 percent), 2.53

Mev (16 percent), and 1.72 Mev (35 percent). The absence of beta-gamma coincidences above 3.6 Mev suggests that the 4.7 Mev transition is directly to the ground state of Kr^{84}. The spectrum of this group does *not* have the forbidden shape which one might expect from the predictions of the nuclear shell model and from the relatively high value of the comparative half-life (log ft. = 7.75). It is suggested that the 32-minute half-life may be that of a metastable level ($p_{3/2}$, $g_{9/2}$) feeding a very short lived (<5-sec.) ground state ($p_{3/2}$, $p_{1/2}$) of Br^{84}. The Br^{83} transition yields a simple straight-line Fermi plot consistent with its being an allowed transition from the $p_{3/2}$ ground state of Br^{83} to the $p_{1/2}$ ground state of Kr^{83}. The end point is 0.940 Mev and log ft. = 5.0.

D10. Radiations from Mo^{99} and Tc^{99m}. ROBERT CANADA AND MERLE E. BUNKER, *Indiana University.*—The radiations from Mo^{99} (67 hours) and its metastable daughter Tc^{99m} (6 hours) have been measured in a magnetic lens spectrograph. The beta-ray spectrum consists of a group with an end-point energy of 1.23 Mev, one of 0.445 Mev, and possibly a third lower energy group. The relative intensities of the 1.23-Mev to 0.445-Mev groups are 4:1. Gamma-rays have been found at 0.040, 0.140, 0.181, 0.367, 0.741, and 0.780 Mev. The gamma-rays at 0.040, 0.140, and 0.181 are internally converted. The spectrum of Tc^{99} consists of one internally converted gamma-ray at 0.140 Mev. A disintegration scheme is proposed.

FRIDAY AFTERNOON AT 2:15

Cobb 110

(W. H. ZINN presiding)

Beta-Emitters, Ruthenium Through Gold

E1. Radioactivities of Ru^{105} and Rh^{105}.* R. B. DUFFIELD, *University of Illinois*, AND L. M. LANGER, *Indiana University.*—A lens spectrometer and coincidence methods have been used to study the disintegration of Ru^{105} (4.5 hr.) and Rh^{105} (36.2 hr.). The beta-spectrum of Ru^{105} is simple, with an end point of 1.150±0.006 Mev. The beta is followed by a gamma-ray transition of 0.726 Mev to a previously unobserved metastable level in Rh^{105}. This isomer decays to the ground state of Rh^{105} by emission of a converted gamma-ray of about 0.1 Mev (absorption measurement) with a half-life of 45 seconds. The ground state of Rh^{105} emits a simple beta-spectrum with an end point of 0.570±0.005 Mev. No gamma-ray appears to be associated with this decay.

* Research done at the Los Alamos Scientific Laboratory of the University of California under the auspices of the AEC.

E2. Half-Life of the Long-Lived Tc^{99}. A. H. JAFFEY, SHERMAN FRIED, N. F. HALL, AND L. E. GLENDENIN, *Argonne National Laboratory.*—The half-life of Tc^{99} has been determined on materials isolated both from fission products and from neutron-irradiated molybdenum. The beta-particle measurements were made on aliquots of solutions deposited on thin rubber-hydrochloride films. The concentrations of the solutions were determined by dissolving known weights (several milligrams) of known compounds—NH_4TcO_4 and Tc metal. The beta-counts were made absolute by comparison with Co^{60} and RaDEF standards. The Co^{60} sources were standardized by coincidence counting and by comparison with Bureau of Standards samples. The RaDEF sources had been standardized[1] by alpha-counting RaF. Owing to the large upswing of the absorption curves at small absorption, comparison with RaE required the use of a low absorption counter; variation of specific ionization with electron energy required the use of high gas density in the detector. Because of the great similarity in absorption curves, comparison of Tc^{99} and Co^{60} was relatively simple. The result was a specific activity of 3.78×10^4 d/m/microgram, or a half-life of 2.12×10^5 years, with an estimated error of ±2 percent.

[1] T. B. Novey, Rev. Sci. Inst. 21, 280 (1950).

E3. A Lower Limit on the Half-Life of Sn^{124}. J. S LAWSON, JR., *University of Illinois.*—The double beta-decay of Sn^{124} has been investigated in a cloud chamber, with an isotopically enriched sample percent (83 Sn^{124}) weighing 0.268 g, obtained from Oak Ridge. A sensitive time of 0.47 second per picture was used, in taking 8794 pictures which were then searched twice for possible events. Thirty-nine such events were found and examined by stereoscopic reprojection. All these two track events were found to have one or more of the following faults: (1) different track origins, (2) two apparent tracks due to one electron circling through foil twice, (3) two tracks due to splitting of one by sweep field, and (4) tracks of different ages. The 10 best-looking of these "possible events" were critically examined for further confirmation of their not being the event sought. It was found that in all cases the two electrons had very nearly the same direction, and that the total kinetic energy was about 500 kev. Thus, no events were seen of the type reported by Fireman.[1] As conservative estimates of the useable solid angle in the chamber predict a yield of at least 5 events for a half-life of 10^{16} years, and none were seen; the half-life is probably greater than this.

[1] E. L. Fireman, Phys. Rev. 75, 323 (1949).

E4. New Antimony Isotopes in Fission.* ALEXIS C. PAPPAS,† *Massachusetts Institute of Technology.*—Previous work[1] on antimony activities in fission disclosed the occurrence of ~5-min. Sb^{128} and that Sb^{130} and Sb^{131} both have <10-min. half-lives. Attention has been turned to this element in connection with further studies[2] of fission-yield perturbations resulting from closed-shell effects.[3] After short irradiation of UO_3 with thermal neutrons and fast chemical separation of antimony by solvent extraction ($SbCl_3+Cl_2$ into isopropyl ether; $SbCl_3+N_2H_4$ into $H_2O-NaNCS$, ether wash), the activity of the solution was observed. Four species were identified of ~50 sec., 2.0-min., 4.4-min., and 23.1-min. half-lives. In separate experiments, fission mixtures were rapidly freed of tellurium, and successive tellurium separations made for genetic identification. Activity-time curves of 30-min. Te^{131}—8.0-day I^{131} showed the occurrence of 23-min. Sb^{131}. Curves of 66-min. Te^{132}—22-hr. I^{132} showed 4.4-min. Sb^{132}. Energetic considerations lead to probable identifications as Sb^{130} for the 2.0-min. activity and $Sb^{134,135}$ for ~50-sec. activity.

* Supported by the joint program of the ONR and the AEC.
† Fellow of the Royal Norwegian Council for Scientific and Industrial Research from the University of Oslo.
[1] P. H. Abelson, Phys. Rev. 56, 1 (1939).
[2] A. C. Pappas and C. D. Coryell, abstract E5.
[3] L. E. Glendenin and C. D. Coryell, Phys. Rev. 75, 337 (1949); Phys. Rev. 77, 755 (1950).

E5. Excited States of Prometheum^{147} Appearing in the Disintegration of Neodymium. W. S. EMMERICH AND J. D. KURBATOV, *Ohio State University.*—Energy levels in Pm^{147} following the beta-disintegration of Nd^{147} have been studied. Commercially supplied, spectroscopically pure neodymium was activated by neutrons at the Oak Ridge National Laboratory of the AEC. The aged, activated neodymium was investigated with a permanent magnet spectrograph for internal conversion electrons. The observed groups of monoenergetic electrons were found to have energies of 46.0 ± 0.2, 84.5 ± 0.3, and 89.9 ± 0.5 kev. The decrease in intensity of these lines corresponds to a decay period of ~11 days. Applying the binding energies for K, L, and M electrons of prometheum gave the energy of the photon as 91.5 ± 1.0 kev. The N_k/N_l was found to be 2.5. Including the previously reported upper energies of the complex beta-disintegration of Nd^{147} and the emitted photons,[1-3] a scheme of disintegration will be proposed.

[1] G. T. Seaborg and I. Perlman, Rev. Mod. Phys. **20**, 585 (1948).
[2] Cork, Shreffler, and Fowler, Phys. Rev. **74**, 240 (1948).
[3] C. E. Mandeville and E. Shapiro, Phys. Rev. **79**, 391 (1950).

E6. The Decay of Yb^{169}.* A. W. SUNYAR AND J. W. MIHELICH, *Brookhaven National Laboratory.*—It has been reported[1] that following K-capture in Yb^{169} (33-day), a converted gamma-ray of 400 kev is emitted, leading to an isomeric state of 1 μsec. lifetime, which decays to the ground state by emission of an internally converted gamma-ray of 190 kev. Recent work[2] has revealed the presence of several gamma-rays. We have investigated the decay scheme by scintillation counter coincidence techniques. Approximate K/L ratios for the conversion lines obtained with a 180° permanent magnet-type spectrograph are of aid in assigning a level scheme. Only K and L x-rays of Tm and no gamma-rays precede the isomeric state. The lifetime of the isomeric state is 6.0×10^{-7} sec., in agreement with an independent measurement by Fuller.[3] The isomeric state is probably 307 kev above the ground state and decays by three alternative means: (1) the 307-kev ground state transition, (2) a 177-kev gamma-ray followed by a 130-kev gamma-ray, (3) a 198-kev gamma-ray followed by a 109-kev gamma-ray.

* Work performed at Brookhaven National Laboratory, under the auspices of the AEC.
[1] S. De Benedetti and F. K. McGowan, Phys. Rev. **74**, 736 (1948).
[2] Cork, Keller, Rutledge, and Stoddard, Phys. Rev. **78**, 95 (1950).
[3] E. W. Fuller, Proc. Phys. Soc. London **63A**, 1044 (1950).

E7. Radioactivity of Ta^{180}.* W. L. BENDEL,† HUGH BROWN, AND ROBERT A. BECKER, *University of Illinois.*—Eight-hour Ta^{180} in thin foil samples was obtained by the probe method[1] in the 22-Mev betatron through a gamma-n process. Use of a 180° spectrometer showed the presence of a strong beta-minus component with end point near 600 kev, with some evidence for another with end point near 700 kev. Auger lines, intense x-rays, and critical absorption techniques confirm the K-capture process reported by Oldenberg.[2] Positrons were sought, and found to be absent. Coincidence techniques reveal gamma-gamma, gamma-beta, and electron-gamma coincidences. In addition to these are found prominent L and M conversion lines and a weaker K line, all attributed to a strong 92-kev transition. Also, a weak line was found, which was attributed to the conversion of a 103-kev gamma-ray. A tentative partial decay scheme will be presented. Detailed measurements yield a half-life of 8.15 hours for this activity.

* Assisted by the joint program of ONR and AEC.
† AEC Predoctoral Fellow.
[1] Becker, Kirn, and Buck, Phys. Rev. **76**, 1406 (1949).
[2] O. Oldenberg, Phys. Rev. **53**, 35 (1938).

E8. Disintegration Scheme of Re^{186}. FRANZ R. METZGER AND R. D. HILL, *University of Illinois.**—The radiation emitted in the decay of Re^{186} has been investigated using scintillation counters and β-ray spectrographs. Appreciable numbers of $\beta-\gamma$, $X-\gamma$ and $X-X$ coincidences were observed, but no $\gamma-\gamma$ coincidences[1] could be detected. The main features of our disintegration scheme are the following. In 90 percent of the disintegrations, Re^{186} decays by β^--emission into Os^{186}, and in the remaining 10 percent by K-capture into W^{186}. A 25-percent partial β^--spectrum of 930-kev end point is followed by a 137-kev γ-ray. A 3-percent branch of K-capture is succeeded by a 123-kev γ-ray. All the other disintegrations observed lead directly to the ground states of the product nuclei. From a search for $\gamma-\gamma$ coincidences, we conclude that there is less than one positron for every 10^6 Re^{186} disintegrations. For the 137-kev γ-ray we measured $\alpha_K=0.35\pm0.1$ and $N_K/N_L=0.6\pm0.1$. The corresponding values for the much weaker 123-kev γ-ray are ~0.45 and ~0.6. Based on these conversion data we interpret both γ-rays as electric quadrupole transitions.

* Supported in part by the joint program of the ONR and AEC.
[1] Beach, Peacock, and Wilkinson, Phys. Rev. **76**, 1585 (1949).

E9. Beta-Spectrum and Internal Conversion for Au^{198} and Cb^{95}. C. Y. FAN *University of Chicago.*—The β-spectra of 2.7-day Au^{198} and of 35-day Cb^{95} have been studied with the double lens β-spectrometer of this laboratory.[1] For Au^{198}, the β-spectrum is allowed with end point at 0.961 Mev. The gamma-ray has energy $E\gamma=0.411$ Mev and internal conversion coefficients $\alpha_K=2.9$ percent, $\alpha_{L+M}=1.2$ percent. These values are in accord with those obtained by Siegbahn and Hedgram[2] and by Saxon and Heller.[3] In the case of Cb^{95}, the β-spectrum was also allowed with end point at 0.163 Mev. The gamma-ray having energy $E\gamma=0.771$ Mev showed a total internal conversion $\alpha_{K+L+M}=0.18$ percent. The L conversion line was not resolved, but the ratio $\alpha_K/\alpha_L=2.3$ could be estimated.

[1] H. M. Agnew and H. L. Anderson, Rev. Sci. Inst. **20**, 869 (1949).
[2] K. Siegbahn and A. Hedgran, Phys. Rev. **75**, 318 (1949).
[3] D. Saxon and R. Heller, Phys. Rev. **75**, 909 (1949).

FRIDAY AFTERNOON AT 2:15

Judd 126

(R. S. MULLIKEN presiding)

Invited Paper

F1. Regularities in the Ultraviolet Spectra of Large Molecules. J. R. PLATT, *University of Chicago* (30 min.)

Molecular Spectra

F2. Raman and Infra-Red Spectra of $CHBrCl_2$ and $CDBrCl_2$. SANTIAGO R. POLO, FORREST F. CLEVELAND, RICHARD B. BERNSTEIN, ARNOLD G. MEISTER, AND ROBERT H. SHERMAN, *Illinois Institute of Technology.*—Raman displacements ($\Delta\nu$), quantitative depolarization factors, semi-quantitative relative intensities (I), and infra-red wave

numbers (ν) have been obtained for $CHBrCl_2$ and $CDBrCl_2$ in the liquid state. The $CDBrCl_2$ sample contained about 60 percent of $CHBrCl_2$. The infra-red spectra were obtained with a Perkin-Elmer 12C spectrometer equipped with NaCl optics, and the region scanned was 700–4000 cm^{-1}. For $CHBrCl_2$, $\Delta\nu$ and I values have been reported by Bonino and Brüll, Kohlrausch and Köppl, and Glockler and Leader; and their data are in substantial agreement with the present results. However, no depolarization or infra-red data for $CHBrCl_2$ and no Raman or infra-red data at all for $CDBrCl_2$ could be found in the literature. The present $\Delta\nu$ values in cm^{-1} for the fundamental frequencies of the two compounds are:

$CHBrCl_2$ 220, 220, 329, 602, 719, 761, 1171, 1214, 3022;
$CDBrCl_2$ 220, 220, 329, 580, 700, 735, 872, 904, 2253.

The 220 cm^{-1} line corresponds to two unresolved fundamentals. The present ν and $\Delta\nu$ values are in very close agreement. The depolarization factors were obtained by the well-tested single-exposure method previously used in this laboratory. Infra-red work with KBr optics, calculation of thermodynamic properties, and normal coordinate treatments for the two molecules are in progress.

F3. Raman and Infra-Red Spectra of $CHClBr_2$ and $CDClBr_2$. Donald A. Pontarelli, Forrest F. Cleveland, Richard B. Bernstein, Arnold G. Meister, and Robert H. Sherman, *Illinois Institute of Technology.*—Raman displacements ($\Delta\nu$), semi-quantitative relative intensities (I), and quantitative depolarization factors for the liquid, and infra-red wave numbers (ν) for both liquid and gas have been obtained for $CHClBr_2$ and $CDClBr_2$. The $CDClBr_2$ sample contained about 40 percent $CHClBr_2$. Both Beckman IR-2 (KBr optics) and Perkin-Elmer 12C (NaCl optics) spectrometers were used and the region scanned was 400–4000 cm^{-1}. For $CHClBr_2$, $\Delta\nu$ and I values have been reported by Glockler and Leader; and their values are in good agreement with the present results, except for the 1190- and 3020-cm^{-1} lines, for which the present values are, respectively, 4 and 3 cm^{-1} less than their's. Also, ν values have been reported by Emschwiller and Lecomte; but their results are not in very good agreement with the present data. No depolarization factors for $CHClBr_2$ and no Raman or infra-red data at all for $CDClBr_2$ were found in the literature. The present $\Delta\nu$ values in cm^{-1} for the fundamental frequencies of the two compounds are:

$CHClBr_2$ 168, 201, 279, 569, 659, 750, 1146, 1190, 3020;
$CDClBr_2$ 168, 201, 279, 545, 635, 725, 853, 888, 2252.

The present ν and $\Delta\nu$ values are in excellent agreement. Normal coordinate treatments and calculation of thermodynamic properties for the two molecules are in progress.

F4. Raman Spectral Data for $CBrClH_2$. Alfons Weber, Forrest F. Cleveland, and Arnold G. Meister, *Illinois Institute of Technology.*—Raman displacements ($\Delta\nu$), quantitative depolarization factors (ρ), and semiquantitative relative intensities (I) have been obtained for liquid $CBrClH_2$. Results of previous Raman investigations by Bacher and Wagner, Wagner, and Delwaulle and Francois are in substantial agreement with the present results. The infra-red results of Emschwiller and Lecomte and of Plyler also are in very good agreement with the present and previous Raman data. The present depolarization factors were measured by the well-tested single-exposure method used in this laboratory and substantiate the values of Wagner and of Delwaulle and Francois. A new Raman line at 460 cm^{-1} has been found; it is probably the first overtone of the 228 cm^{-1} fundamental. The present $\Delta\nu(I)\rho$ values for the fundamentals are: 228(68)0.41; 603(100)0.16; 729(5)0.54; 854(very weak); 1128(1)0.85; 1227(1)0.32; 1407(5)0.66; 2989(44)0.23; 3056(4)0.84. A normal coordinate treatment and calculation of the thermodynamic functions are in progress. Neither force constants nor experimental or calculated thermodynamic functions are available in the literature.

F5. Raman and Infra-Red Spectral Data and Calculated Thermodynamic Properties for CH_3I. Paul F. Fenlon, *Armour Research Foundation,* Forrest F. Cleveland, and Arnold G. Meister, *Illinois Institute of Technology.*—Raman displacements, semiquantitative relative intensities, and quantitative depolarization factors have been obtained for all of the fundamental frequencies of CH_3I in the liquid state. The depolarization factors were determined with the well-tested single-exposure method previously used in this laboratory. The infra-red wave numbers for both liquid and gaseous CH_3I in the region 400–4000 cm^{-1} also have been determined, with both Beckman IR-2 (KBr optics) and Perkin-Elmer 12C (NaCl optics) spectrometers. Present values for the spectral data were compared with the results of previous investigators in order to decide upon the most probable values of the fundamental frequencies. The fundamental frequencies so obtained were then used to calculate the thermodynamic properties—heat content, free energy, entropy, and heat capacity—for eleven temperatures from 200° to 1000°K, to a rigid rotator, harmonic oscillator approximation. Force constants are being determined by the Wilson FG matrix method; and the constants thus obtained will be tested by calculation of frequencies for CD_3I, four of which are known.[1]

[1] Ch. Courtoy, Ann. soc. sci. Bruxelles 60, 122 (1946).

F6. Force Constants and Calculated Thermodynamic Properties for Some Trifluoromethanes. Charlotte E. Decker, Arnold G. Meister, and Forrest F. Cleveland, *Illinois Institute of Technology.*—Force constants have been determined for the CF_4 and CF_3H molecules, by the Wilson FG matrix method and a potential energy function containing all possible second-degree terms. These force constants were then used to predict the fundamental frequencies of CF_3D, for which no experimental values could be found in the literature. The frequencies so obtained should be reliable to within 2 percent of the calculated values. The F matrix elements have been obtained for the type E fundamental vibrations of CF_3Cl and the determination of the F matrix elements for the type A_1 vibrations is in progress. The available Raman and infra-red data for CF_4, CF_3H, and CF_3Cl were collected and critically examined, in comparison with the results of the normal coordinate treatments, in order to decide upon the best values for the fundamental frequencies. These frequencies were then used to calculate the heat content, free energy, entropy, and heat capacity for the three compounds for the ideal gaseous state at one atmosphere pressure for temperatures ranging from 50 degrees below the boiling point to 1000°K. Similar calculations also are being made for CF_3D in order that fairly good tentative values of the thermodynamic properties might be available for this molecule, pending the experimental determination of its fundamental vibrational frequencies.

F7. Infra-Red Spectra and Calculated Thermodynamic Properties for Some Trichloromethanes. John R. Madigan and Forrest F. Cleveland, *Illinois Institute of Technology.*—Continuing previous work on the trichloromethanes, wave numbers and estimated relative intensities of the infra-red absorption bands of CCl_3H, CCl_4, and CCl_3Br have been obtained with a Beckman IR-2 spectrophotometer (KBr optics). For CCl_3H and CCl_4, bands were found in the regions 660–3100 and 700–1300 cm^{-1}, respectively, for both liquid and vapor. Previous data for the gas were obtained in only one investigation for each of the two molecules, and then only 3 bands were obtained for CCl_3H and 1 for CCl_4; we obtained 5 bands for each. For CCl_3Br, bands were found in the region 400–1600 cm^{-1} for the liquid only. With gaseous frequencies

used whenever possible, heat content, free energy, entropy, and heat capacity values were calculated for the ideal gaseous state at 1 atmos. pressure for nine temperatures from 298.16° to 1000°K, to a rigid rotator, harmonic oscillator approximation. Previous calculations of some of these had been made for CCl_3H and CCl_4 by Vold, by Yost, and by Lord and Blanchard; but, since they used more liquid frequencies and older values of the bond distances and angles, their values are all slightly larger than the present values. The present calculated entropies are in good agreement with the few experimental values.

F8. Frequency Assignment, Force Constants, and Calculated Thermodynamic Properties for 1,1,1-Trichloroethane. M. ZAKI EL-SABBAN, ARNOLD G. MEISTER, AND FORREST F. CLEVELAND, *Illinois Institute of Technology.*—A normal coordinate treatment for H_3C-CCl_3 was carried out by the Wilson FG matrix method and a reasonable set of force constants was obtained. The calculations indicated that one of the doubly degenerate vibrations should correspond to the wave number 363 cm^{-1}, which was not observed in the present investigation and has been regarded as doubtful by previous investigators. The calculations also indicated that the wave number corresponding to the carbon-carbon stretching vibration is 1035 cm^{-1}. The values finally adopted for the A_1 and E fundamentals are: A_1—343, 522, 1035, 1378, 2939; E—241, 363, 716, 1077, 1434, and 3005 cm^{-1}. These were used to calculate the heat content, free energy, entropy, and heat capacity for the ideal gaseous state at one atmosphere pressure for nine temperatures from 298.16° to 1000°K. Comparison with the experimental values of the entropy given by Rubin, Levedahl, and Yost[1] indicated that a reasonable value for the torsional frequency is 207 ± 19 cm^{-1}.

[1] T. R. Rubin, B. H. Levedahl, and D. M. Yost, J. Am. Chem. Soc. 66 279 (1944).

F9. Vibrational Spectra and Assignments for Dimethyldiacetylene. SALVADOR M. FERIGLE, FORREST F. CLEVELAND, AND ARNOLD G. MEISTER, *Illinois Institute of Technology.*—Previous work on the $H-C\equiv C-C\equiv C-H$ (DA) and $H_3C-C\equiv C-C\equiv C-CH_3$ (DMDA) molecules indicated a smaller value for the force constant of the central C—C bond than would be expected from the bond length determined by electron diffraction. Also, difficulty was experienced in obtaining a satisfactory set of force constants for the doubly degenerate vibrations. In an attempt to clear up these difficulties, we have obtained new Raman and infra-red data for DMDA in both CCl_4 and benzene solutions. Depolarization factors were obtained by the new well-tested single-exposure method, the most significant result being the value 0.84 obtained for the 475-cm^{-1} line, previously assigned as a polarized A_1 fundamental. Consequently, the assignment of this line must be changed. The assignment of the 644-cm^{-1} band of DA also seems questionable, for comparison with the data of a number of molecules containing the $-C\equiv C-H$ group indicates that it should have been assigned as a bending mode. The low value previously indicated for the C—C force constant is thus no longer certain. Some of the assignments have now been changed and a normal coordinate treatment is in progress to see if satisfactory force constants can be obtained.

FRIDAY AFTERNOON AT 1:30

Museum of Science and Industry

(W. L. DAVIDSON presiding)

High-Polymer Physics

G1. High Poiymer Model Including Van der Waals Forces. EUGENE GUTH, *University of Notre Dame,* AND HUBERT M. JAMES, *Purdue University.*—In the elementary statistical theory of rubber, considered as a network of flexible molecular chains, forces between the molecules are neglected, except as they control the volume of the system. Actually, these forces tend to align neighboring molecules, producing partial crystallization at low temperatures. We have studied a model in which the molecular chains are treated as consisting of links which exert on all neighboring links (of the same or of different chains) on orienting force derived from a potential $A\cos^2\theta$, θ being the angle between the axes of the two links. With A negative, neighboring links then tend to become parallel or antiparallel. The effect of these orienting forces has been discussed in the Bragg-Williams approximation. They produce a first-order transition, a rotational freezing, at a temperature which is higher the higher the degree of cure and the more the material is stretched. The sharp transition predicted by this theory, in contrast to the observed behavior of freezing rubber, is due to the uniformity of conditions in the material implied by use of the Bragg-Williams approximation. This type of model may, however, be useful in discussing the effect of van der Waals forces above the freezing point.

G2. Statistical Theory of Large Deformations of Rubber-like Materials.* MING CHEN (WANG) YU AND EUGENE GUTH, *University of Notre Dame.*—In the elementary statistical theory of rubber elasticity, the material is assumed to consist of a network of molecular chains, for each of which the configuration function (number of possible configurations as a function of the separation of its ends) is of Gaussian form. For a pure homogeneous deformation of a unit cube into a cuboid with edges L_x, L_y, L_z, the theory yields an elastic energy proportional to the sum of the squares of the relative lengths L_x, L_y, L_z, to the absolute temperature, and to a factor depending on distribution functions characterizing the unstretched network. If the configuration functions for the molecules are not Gaussian, the elastic energy can be expanded in powers of the three invariants of L_x, L_y, L_z, with coefficients depending on the distribution functions that characterize the unstretched network. These distribution functions imply relations between the coefficients in the expansion of the elastic energy. A linear function of two, and a polynomial in all three invariants with arbitrary coefficients have been proposed by Mooney and Rivlin, respectively, on a phenomenological basis. The relation of this phenomenological theory to the statistical theory will be discussed and comparisons with experiment will be made.

* Supported in part by ONR.

G3. Visco-Elasticity of Rubber. R. B. BLIZARD,* *Massachusetts Institute of Technology.*—A theory has been developed for the elastic behavior of rubber in the frequency range above that at which creep is important and below that at which it behaves like a hard solid. The rubber chains are treated as

springs in a viscous medium, and a general expression is obtained for the contribution to modulus of a single section of chain as a function of its length and terminations. A statistical estimate is made of the number of chain segments having given length and terminations. A modulus function is found for the group of chains with each kind of termination and these are added in the proper amounts to give the form of the modulus *vs.* frequency curve for any amount of cross-linking. Measurements of shear modulus were made at frequencies between 0.012 and 750 cycles/sec. Agreement is good if a pure viscosity is added to the theory. Kirkwood's theory agrees about as well. Although the two theories are fundamentally different, they give nearly the same result in the range for which there are good data. Measurements on a series of samples made from the same monomer with varying polymerization and cross-linking should eliminate at least one theory. Both theories predict that at low frequencies the imaginary part of the modulus is proportional to frequency. Experiment indicates that it approaches a nearly constant value, thus setting a lower frequency limit on the validity of the theories.

* Now at Sperry Gyroscope Company, Great Neck, New York.
[1] J. Chem. Phys. **14**, 51–56 (1946).

G4. A Study of Crystallite Sizes in Polymers by a Light Scattering Method.* F. Bueche and P. Debye, *Cornell University.*—A tractable relation for the angular scattering of light by cylindrical inhomogeneities of any size has been found. This relation has been applied to the angular light scattering curves observed for several polymers during various stages of crystallization. The results so obtained indicate that the polymers contain crystallites, or aggregates thereof, which are of the order of thousands of angstroms large. Modified quenching experiments have been performed. These together with observed changes in crystallite size as the polymer is heated indicate that small crystallites are stable only at low temperatures. Measurements of the size of crystallites in a crystallizing supercooled polymer have also been made. Near the melting point it is found that after an induction period the number of crystallites increases in the manner reported by others. However, the average size of the crystallites remains constant within experimental error. This indicates that the crystallites do not grow indefinitely and that their rate of growth at these temperatures is far larger than the rate of crystal nucleation.

* The work reported in this paper was done in connection with the Government Research Program on Synthetic Rubber under contract with the Office of Rubber Reserve, Reconstruction Finance Corporation.

G5. Stress-Temperature Studies of the Second-Order Transition in Rubbers.* R. S. Witte and R. L. Anthony, *University of Notre Dame.*—The apparent second-order transition occurring in rubbers was studied by observing the dependence of stress upon temperature and time in samples held at various constant extended lengths. The rubber stocks studied were a natural rubber gum stock, a butyl gum stock, a GR-S loaded stock, and a Hycar OS-10 loaded stock. All samples were stretched to the desired extended length at room temperature and permitted to relax until only a negligible time rate of stress relaxation remained. The temperature was then lowered and the stress observed as a function of temperature and time. Rapid stress relaxation was observed slightly below the transition temperature, Tm; but no stress relaxation was observed at temperatures a few degrees above Tm nor well below Tm. For both the butyl and Hycar OS-10 stocks Tm was observed to depend strongly upon extension, higher extensions resulting in lower values of Tm. No such dependence upon extension was observed for three different extensions of the natural rubber stock. The interpretation of the results will be discussed.

* Supported in part by ONR.

G6. Study of High Polymers by Nuclear Magnetic Induction.* B. A. Mrowca and L. V. Holroyd, *University of Notre Dame.*—Quantitative data on nuclear magnetic resonance line widths have been obtained for several high polymers. The line widths were measured at room temperature in a field of approximately 7000 gauss at a frequency in the neighborhood of 30 Mc. The narrowness of the line width obtained for unvulcanized natural rubber and GR-S shows that "free" rotation of molecules containing proton groups in these materials is comparable to that of protons in water. Vulcanization or carbon black loading produced a broadening of the observed line widths, indicating that either process tends to impede "free" rotation. The line widths for several polymers were observed as a function of temperature. The temperature range was chosen to include the "second-order transition region." As expected, the line widths were found to increase with decreasing temperature through this region.

* Supported in part by ONR.

G7. Velocity and Attenuation of Sound in Plexiglas.* J. Gaffney and A. A. Petrauskas, *University of Notre Dame.*—Using an improved pulsed ultrasonic technique the velocity and attenuation of sound in polymethyl methacrylate (Plexiglas) were measured as functions of temperature at frequencies of one and two megacycles. The temperature range investigated extended from 20°C to 95°C. Preliminary results indicate that with the present equipment velocities can be measured to a precision of about 0.03 percent. It was found that the velocity in Plexiglas decreases gradually at first with increasing temperature, and then more rapidly at higher temperatures. The attenuation increases with increasing temperature. In the frequency and temperature range investigated no definite evidence in support of a second-order transition in Plexiglas was found either in the velocity or in the attenuation measurements.

* Supported in part by ONR.

G8. Visco-Elastic and Flow Properties of Polyisobutylene.* Herbert Leaderman and R. G. Smith, *National Bureau of Standards.*—The retarded-elastic shear compliance $\Psi(t)/G$ and the flow behavior have been measured for low molecular weight isobutylene polymers ($\bar{M}_n = 6.5\times10^3$ to 7.0×10^4) and a copolymer ($\bar{M}_n = 1960$). For each material, the viscosity η and the time-scale for retarded elastic behavior vary in the same way with temperature; thus, for a given material the retarded elastic behavior at different temperatures can be represented by a single curve if $\Psi(t)/G$ is plotted against $\log(t/\eta)$. This curve varies slightly with molecular weight; $\Psi(t)$ can be represented by a function of the type

$$1-\exp[-(t/\tau)^m],$$

where m is about 0.5. For polyisobutylene, $\log\eta$ varies linearly with $1/T$°. The non-Newtonian flow can be expressed in terms of an "internal shear modulus" G_i following Ferry;[1] G_i is not very temperature-dependent. G_i and G are of the same order of magnitude and decrease with increase in molecular weight.

* Supported by ONR and Office of The Quartermaster General.
[1] J. D. Ferry, J. Am. Chem. Soc. **64**, 1334 (1942).

G9. Relation of Tensile Strength to Brittle Point in Plasticized Polymers. R. F. Boyer, *The Dow Chemical Company.*—Several current theories concerning the efficiency of plasticizer action predict a brittle point lowering proportional to the ratio w_1/M_1, where w_1 is the weight fraction of plasticizer of molecular weight M_1. The constant of proportionality is presumably a property of the base plastic. The tensile strength also decreases linearly with the same ratio, and again the proportionality constant should depend only on the base polymer. Hence, one would expect a linear relation between tensile strength and brittle point which should be relatively inde-

pendent of molecular weight and plasticizer type. Actual data on plasticized polyvinyl chloride confirms roughly this linear relationship. However, the lines for different plasticizers are shifted quite markedly along the brittle point scale. This behavior suggests in a different way the probable importance of plasticizer diffusion rate in brittle point lowering.

Business Session of the Division of High-Polymer Physics

FRIDAY AFTERNOON AT 2:15

Mandel Hall

(A. VON HIPPEL presiding)

Symposium of the Division of Solid-State Physics
Formation of the Solid State by Crystallization

H1. Crystallization Phenomena in Metals. J. H. HOLLOMON, *General Electric Company.* (45 min.)

H2. Crystallization Phenomena in Ionic Materials. LEROY SCHULTZ, *University of Chicago.* (45 min.)

H3. Crystallization Phenomena in Organic Materials. R. W. G. WYCKOFF, *National Institutes of Health.* (45 min.)

FRIDAY AFTERNOON AT 2:15

Kent Theatre

(S. K. ALLISON presiding)

Nuclear Analyzers and Accelerators: Nuclear Magnetic Resonance

I1. The Design and Construction of a Spherical Electrostatic Analyzer.* D. S. CRAIG, C. P. BROWNE, AND R. M. WILLIAMSON, *University of Wisconsin.*—A spherical electrostatic analyzer has been constructed for use with the Wisconsin cylindrical analyzer[1] for accurate measurements of Q values. The focusing properties of such an instrument have been described by Purcell.[2] This instrument permits the use of a large solid angle, approximately 4.4×10^{-3} steradian for a target 1 mm in diameter, while at the same time having a high resolving power. The calculated resolution is 1000 for 1-mm object and image apertures. The plates, constructed of meehanite cast iron, are only a portion of an entire sphere, being 90° of the sphere along the path of the particles and having a 60° aperture. The mean radius of the plates is 45.95 cm—the gap 0.48 cm. The analyzer has been designed to fit over the cylindrical analyzer and to accept particles at an angle of 135° from the bombarding beam. The voltage between the plates required to focus a singly charged particle of energy E is $E/47.86$ volts.

* Work supported by the AEC and Wisconsin Alumni Research Foundation.

[1] Warren, Powell, and Herb, Rev. Sci. Inst. 18, 559 (1946).
[2] E. M. Purcell, Phys. Rev. 54, 818 (1938).

I2. Measurements and Resolution Tests of a Spherical Electrostatic Analyzer.* C. P. BROWNE, D. S. CRAIG, R. M. WILLIAMSON, AND D. J. DONAHUE, *University of Wisconsin.*—Dimensional measurements and operational tests have been made on the spherical analyzer described in the preceding paper. The figure of the plates has been determined and the spherical gap mapped. The assembled analyzer has been tested for alignment, focus, and resolution using elastically scattered protons of 0.5- to 1-Mev energy. Monoergic protons scattered from thin targets are focused by the analyzer. A plot of the number of particles entering the detector *vs.* the voltage across the spherical gap gives the resolution. A shutter allows small sectors of the total gap to be tested individually. A sharp focus is obtained and all sectors focus particles of the same energy for a given gap voltage. Preliminary results indicate a resolution of 500 with 1-mm object and image apertures.

* Work supported by the AEC and Wisconsin Alumni Research Foundation.

I3. Energy and Phase Distributions of Emitted Electrons for a Linear Accelerator Constructed of Constant Wave Speed Sections. JAMES SWIHART AND EDWARD AKELEY, *Purdue University.*—The new proposed Purdue accelerator is to be made in three sections with $\beta=0.7$, 0.96, and 1.0. Curves giving energy and phase as functions of initial phase and distance along the guide for constant initial energy of 50 kev had been computed* for the first two sections. The case of $\beta=1.0$, where the solution is expressable in terms of elementary functions for particles moving on the axis, has now been considered. The curves, which had already been computed* for the first two sections, have now been extended through the third section, making it possible to obtain the final phase and energy distribution in the accelerator in term of the distribution of the entering electrons. The energy distribution, at the end of two meters of the third section for a uniform initial phase distribution, shows 33 percent of the particles from 3.08 Mev to 7.13 Mev, and 18 percent from 7.03 Mev to 7.13 Mev; 7.13 Mev was the maximum energy at this point in the tube. Graphs will be shown of the energy-distance, phase-distance, and energy and phase distribution curves.

* The axial motion of an electron in a constant wave velocity section of a linear accelerator. David Caplan and Edward Akeley, Paper D3, Mexico City meeting.

I4. Electron Loading in Ion Accelerating Tubes. I.* C. M. TURNER, *Brookhaven National Laboratory.*—A new, or at least newly recognized phenomenon has been encountered in ion accelerating tubes having internal diameters larger than normally used heretofore. This phenomenon is that of "electron loading" or back electron current appearing under suitable conditions of voltage and vacuum, and has been a source of difficulty in tubes built for both of the Brookhaven electrostatic accelerators. The outstanding characteristics of this phenomenon are the following. (a) It sets in at a definite voltage threshold as evidenced by the sudden appearance of x-rays and increased current drain. (b) It increases approximately as the sixth power of the voltage and hence acts as an effective voltage limiter. (c) The threshold is found to be sharply dependent on tube pressure, increasing with increasing tube pressure. (d) H_2, He, N_2, and A affect the threshold in approximate proportion to the mass of gas present. Numerous tests suggest that the electrons in question are emitted from regions at the cathode end of the tube where field lines from the tube terminate. A possible mechanism to account for this emission is discussed in the following paper.

* Work performed under the auspices of the AEC.

I5. Electron Loading in Ion Accelerating Tubes. II.* JOHN P. BLEWETT, *Brookhaven National Laboratory.*—The experiments described by Dr. Turner in the preceeding paper indicate that the spurious electron emission observed in positive ion accelerating tubes is a surface effect and is associated with surface layers of reasonably volatile materials, probably pump oils or other organic vapors. These phenomena have been reproduced in a parallel plane diode whose electrodes were about one millimeter apart. The electron currents appeared in the range between 2 and 30 kilovolts, so that the fields were of the order of tens of kilovolts per centimeter. Fields of this order appear at the electrodes of conventional Van de Graaff accelerating tubes. The electron current varied about as the sixth power of the voltage just as in the case of the current observed at high voltages. The effect depends on field, not total voltage; it is relatively independent of temperature around room temperature; and it is strongly affected by surface contaminations. Arguments will be presented to show that this effect is identical with the Malter effect.

* Work performed under the auspices of the AEC.

I6. Properties of the Ranger. DAVID L. HILL, *Vanderbilt University.*—I shall describe the Ranger, developed in 1944–45 at the Argonne National Laboratory to measure distributions-in-range of heavy particles released in nuclear reactions. Four pillbox-shaped proportional grid-counters, operating usually under 0.05 atmosphere of CO_2, and connected to a coincidence-anticoincidence network, detect, with resolutions limited only by straggling, particles with ranges in NTP air between 0.15 and 200 centimeters (0.15 to 200 cm). A remote control mechanism within the gas-tight envelope common to the counters and the source plate (which may, e.g., rest in a neutron or gamma-ray beam fired from a chain reactor) permitted the variation by steps as small as 0.03 cm. of absorbers both between the source and the first counter and between the first and second counters without disturbing the common gas mixture or altering the source-counter geometry, and without radiological hazard. We have successfully applied the Ranger to the measurement of several neutron, proton, and alpha-particle spectra. The gated electronic channels for the counter signals are adjusted to determine the maximum and minimum pulses passed. Thus the instrument selects protons or alpha-particles or other ions by counting only those charged particles producing a chosen specific ionization at a given distance from the end of their range.

I7. Regenerative Deflector for Synchrocyclotron.* J. L. TUCK AND L. C. TENG, *The University of Chicago.*—The deflection of a synchrocyclotron beam can be obtained through the increasing radial oscillation induced by repeated passage through a locally increased magnetic field at one point on the stable orbit and a similarly reduced field at another. The azimuthal separation between these two perturbations is made about 90°. Graphical plotting shows that by suitably shaping the field perturbations, the separation between consecutive orbits can reach about 1.5″ after ~25 revolutions for a 450 Mev proton beam at 76″ stable radius, while at the same time, the growth of the vertical oscillation can be suppressed. This is sufficient for the beam to clear the mouth of a magnetic shielding channel. It is found also that after ~10 passages through the perturbations, all the protons are forced into the same phase of radial oscillation. This gives the expectation of a high efficiency. The deflected proton pulses are of extended duration.

* Supported by the joint program of the ONR and AEC.

I8. A Recording Radiofrequency Spectrometer for Nuclear Quadrupole Studies.* N. A. SCHUSTER AND G. E. PAKE, *Washington University.*—A recording r-f spectrometer, similar in function to that of Pound,[1] has been constructed for studying electric quadrupole splittings of nuclear resonances. The circuit consists of an r-f oscillator, untuned r-f amplifier, detector, audio amplifier, and a simplified phase-sensitive detector of a design which minimizes the effect on balance of tube characteristics, reference-voltage amplitude, and audio-voltage amplitude. The apparatus is used with a permanent magnet which provides a constant field of 7300 gauss. A well-resolved quadrupole splitting of the Li^7 resonance has been obtained from a single crystal of $LiAl(SiO_3)_2$ (Spodumene). Although the resonance of Li^6 (7.3 percent natural abundance) has been obtained from the same crystal, the quadrupole doublet is not well resolved. On the basis of analysis of the width of the unresolved Li^6 resonance, a tentative value for the magnitude of the ratio $Q(Li^6)/Q(Li^7)$ will be given.

* Assisted by the joint program of the ONR and AEC.
[1] R. V. Pound, Phys. Rev. 79, 685 (1950).

I9. Magnetic Shielding of H^1 and F^{19} Nuclei in Molecules.* H. S. GUTOWSKY, C. J. HOFFMAN, AND R. E. MCCLURE, *University of Illinois.*—It has been suggested[1] that the magnetic shielding of a given nucleus chemically bound to other atoms in various simple covalent compounds depends systematically on the position in the periodic system of the other atoms. Nuclear magnetic resonance measurements have been made of the magnetic shielding of the H^1 nucleus in most of the covalent hydrogen compounds of types CH_4, NH_3, H_2O, HF, and H_2, and also for the F^{19} nucleus in similar fluorine compounds. The range in magnetic shielding observed thus far for the proton resonance is 0.11 gauss; anhydrous HF and HI are at the limits with the latter exhibiting the largest shielding. In the case of the fluorine resonance, the range is 3.7 gauss with limits at F_2 and SF_6; SF_6 has the largest shielding. The total field for these measurements was about 6375 gauss. The results confirm the periodicity of the shielding; in a given period the shielding decreases with Z, while in a given group the shielding increases with Z. As the covalent radii follow the same trends, the magnetic shielding may be related directly to the covalent radii.

* Supported in part by the ONR.
[1] H. S. Gutowsky and C. J. Hoffman, Phys. Rev. 80, 110 (1950).

I10. Nuclear Magnetic Resonance of Protons Absorbed Into Metallic Palladium.* R. E. NORBERG, *University of Illinois.*—The nuclear magnetic resonance absorption signal has been observed at 30 mc/sec. for mobile protons loaded into palladium wire by means of a glow discharge. The signal is due to those protons included in the skin depth and is ob-

served by the use of a bridge technique with the wire used either as the sample coil or as the termination of a quarter wave-length coaxial line. The coaxial line signal is comparable to that obtainable with the coil. If the tip of the line is immersed in water, a strong liquid resonance is observed. A narrow hydrogen-palladium line width ($\sim\frac{1}{10}$ gauss) is observed,[1] which broadens with increasing concentration and with decreasing temperature. The relaxation time, as determined by saturation measurements, is several seconds and is apparently due to the conduction electrons. The resonant frequency is shifted with respect to that for water. At low loads the shift is due primarily to the bulk paramagnetism of the palladium and is a function of the orientation of the sample in the field. At high loads and negligible Pd susceptibility, a small paramagnetic shift is probably due to the conduction electrons.[2] The results will be discussed with respect to possible structures of the H-Pd system.

* This work has been supported in part by the ONR.

[1] M. A. Garstens, Phys. Rev. 79, 397 (1950).
[2] W. D. Knight, Phys. Rev. 76, 1259 (1949).

FRIDAY AFTERNOON AT 2:15

Breasted Hall

(GREGOR WENTZEL presiding)

Theoretical Physics, Mainly Nuclear

J1. Interference Effects in Gamma-Gamma Polarization Correlation. M. FUCHS AND E. S. LENNOX, *University of Michigan.*—Ling and Falkoff[1] have suggested that the experimental angular correlation[2] of Sr^{88} can be fitted by a mixture of magnetic dipole and electric quadrupole for one transition and a pure magnetic dipole for the other. They show that the relative phase δ for M.D. and E.Q. ranges from 0° to 58° and with each phase there are two choices for $|\beta/\alpha|$, the relative amplitude of E.Q. to M.D. in the mixed transition. We investigate the question of whether one could sharpen the choice of δ and $|\beta/\alpha|$ by the usual polarization correlation experiment in which either quantum of the cascade goes to the polarization sensitive detector. We find: (a) I_θ/I_φ (Hamilton's notation) depends upon η, the relative efficiency for counting when the pure or mixed quantum goes to the polarization detector. (b) For the case of Sr^{88} where $\eta \approx 1$, one might determine δ and $|\beta/\alpha|$ within narrow limits if I_θ/I_φ is large. If $I_\theta/I_\varphi \approx 1$, we can narrow the choice of $|\beta/\alpha|$, but δ remains undetermined.

[1] D. S. Ling and D. L. Falkoff, Phys. Rev. 76, 1639 (1949).
[2] E. L. Brady and M. Deutsch, Phys. Rev. 72, 870 (1947); 74, 1541 (1948).

J2. Level Densities in Light Nuclei. C. L. CRITCHFIELD AND S. OLEKSA, *University of Minnesota.*—The theory of the density of energy levels was investigated originally from a statistical point of view by Bethe.[1] Subsequently, many authors have continued the investigation; and, in particular, Bardeen has taken the effect of exchange forces into consideration for heavy nuclei. For lighter nuclei the statistical approach is questionable; and more explicit methods of counting levels have been applied for medium weight nuclei ($A<60$) assuming constant spacing of single particle kinetic energies, and for very light nuclei ($A\leqq 16$). Most of our precise experimental data, however, lie in the region $16\leqq A\leqq 40$. In order to determine the regions of validity of the statistical method in the latter range we have made an explicit determination of the levels in the independent particle model of $Neon^{20}$ with a ground state of $s^4p^{12}d^4$. Principal contributions to excitation were considered to be the differences in kinetic energy (calculated for finite potential well) and the effect of the symmetry of the wave function on the potential energy. In counting the levels, however, we allowed only the degeneracy of total angular momentum. The relation between our results and statistical calculations will be presented.

[1] Bethe, Rev. Mod. Phys. 9, 82 (1937).

J3. Graphs of Internal Conversion Theory.* PETER AXEL AND R. F. GOODRICH, *University of Illinois.*—The purpose of this paper is to show and explain the essential features of a series of graphs on internal conversion coefficients. The graphs will be circularized as a Navy Report. The data are not new, but the presentation illustrates some features of the theory of particular interest to the experimentalist. For example, it is apparent that the theory can be tested most easily in the low Z region, since, despite possible mixtures, there are large regions of K conversion coefficients which are not admissable according to theory. On the other hand, mixtures can be studied in the high Z region. Graphs are presented which attempt to extend the exact values for K conversion coefficients to lower energy by extrapolation using approximate calculations as a guide. The partial validity of the approximate theory of electric conversion at low energy is illustrated graphically. At 150 kev the maximum error is 58 percent for $Z=30$ and $l=5$; it is less for lower l and higher Z. Graphs are also presented of the electric K to L ratio at several Z values.

* This work was sponsored under a joint ONR-AEC contract.

J4. High Energy Bremsstrahlung and Pair Production. G. PARSEN, *University of Chicago.*—Calculations of the cross section for high energy bremsstrahlung have been carried out without the use of the Born approximation, but by reducing the problem to the calculation of the exact elastic scattering of electrons and positrons. That this procedure may be possible is suggested by the usual perturbation calculation, in which bremsstrahlung is pictured as a two-step process, one of which is the scattering of the electron by the nucleus. In the elastic scattering of electrons, the BA (Born approximation) has been found to be considerably in error for heavy elements. Correspondingly large deviations should be expected and were found at the larger angles in the angular distribution of the bremsstrahlung. However, at the smaller angles where most of the bremsstrahlung is concentrated, the BA leads to little error, so that the BA should give the integrated cross section correctly at sufficiently high energies. It was estimated that the error in the integrated cross section is at most of the order of about $(m/E)^{\frac{1}{2}}$, where E is the incident energy of the electron. Screening effects were neglected, but it is felt that the inclusion of screening would not affect this result very much. Similar considerations were carried through for pair production.

J5. On the Theory of Forbidden β-Transitions. R. H. GOOD, JR. AND G. E. UHLENBECK, *University of Michigan.*—By using the WKB approximation for the relativistic radial wave functions, the following problems regarding the shape

of forbidden β-spectra were investigated: (I) The validity of Fermi's cut-off method for the radial wave functions. A nuclear model with uniform surface charge was considered, and the wave functions evaluated strictly at the origin. Although in some terms of the formulas for the forbidden spectra the change compared to the usual formulas is appreciable, the over-all effect on the shape is usually minor. (II) The effect of the screening of the atomic electron cloud on the shape of forbidden β-spectra. It turns out that the effect of screening is inappreciable for the correction factors, and the only change needed in the formulas for the shape is a modified $F(Z, W)$ as has been discussed earlier for allowed transitions.

J6. Consequences in H^2 of the H^3, He^3 Moment Anomaly. NORMAN AUSTERN, *University of Wisconsin.*—If the three-body magnetic moment anomaly is assumed to be a two-nucleon "interaction moment," the associated operator can be established without reference to its origin, a detailed theory of the nuclear interaction mechanism being avoided. Of those operators with the correct transformation properties under rotations and reflections of coordinates and under interchange of nucleons, only that one is retained which contributes to the H^2, He^3 moments in the pure symmetric ^3S state and does not contribute to the deuteron moment:

$$\Delta\mathbf{M} = (e\hbar/2Mc)\tfrac{1}{2}\Sigma_{\alpha,\beta}(\sigma_\alpha - \sigma_\beta)\tfrac{1}{2}(\tau_\alpha - \tau_\beta)\Phi(|\mathbf{r}_\alpha - \mathbf{r}_\beta|).$$

As $\Delta\mathbf{M}$ is correlated in some way with the interaction mechanism the unknown function, Φ must be short range. The operator $\Delta\mathbf{M}$ can be used to compute the corresponding effects for other nuclear systems: both changes in static moments and in magnetic dipole transition probabilities. A 4-percent increase is found for the theoretical NP (magnetic dipole) capture cross section, which offers a cleancut test for $\Delta\mathbf{M}$. This prediction is nearly independent of the shape of Φ if the shape is not unreasonable.

J7. Some General Angular Correlation Formulas. STUART P. LLOYD, *University of Illinois.*—It is shown that the angular correlation function of two successive particles emitted by a nucleus can be found explicitly as a function of the angular momenta of the three nuclear levels and the multipole orders of the two radiations, using the function $W(abcd; ef)$ introduced by Racah[1] to describe a certain sum of products of vector-addition model coefficients. The essence of the method is the use of the invariance property of the correlation under rotations of the coordinate system used to describe the particles. The $W(abcd; ef)$ involved are fairly simple in the physically interesting cases where the multipole order is the lowest or next lowest allowed. The author has obtained the $\gamma-\gamma$, γ-conversion electron and conversion electron-conversion electron angular correlation functions in these cases (including the polarization-polarization and magnetic 2^L-electric 2^{L+1} interference terms) in a form suitable for numerical calculation, for arbitrary multipole orders of the emitted particles. The method is general and covers all cases in which two successive particles are emitted (the second quickly) by a system which is initially randomly oriented. The extention to correlations in β-decay is straightforward.

[1] Giulio Racah, Phys. Rev. 62, 438 (1942).

J8. Excitation and Disintegration of Nuclei by the Coulomb Field of Positive Particles.* CHARLES J. MULLIN AND EUGENE GUTH, *University of Notre Dame.*—General formulas for the cross section for the 2-pole excitation (or disintegration) of a nucleus by the electric field of a non-relativistic positively charged projectile have been obtained by using the Born approximation; the finite size of the nucleus has been taken into account. For electric dipole excitation a more accurate evaluation has been made in which the initial and final states of the charged projectile are described by the exact Coulomb field wave functions. The cross section for electric 2-pole excitation of a nucleus by the field of a charged projectile is proportional to the corresponding photo-excitation cross section; the proportionality factor may be interpreted as the number of virtual electric 2-pole quanta in the field of the charged projectile. In the electric dipole case, the cross section for the inelastic scattering of a charged projectile is shown to be proportional to the cross section for the production of continuous x-rays by deflection of the projectile in a Coulomb field. Thus, a relation is established between the virtual quanta representing the Coulomb field of the projectile and the real quanta of the x-ray spectrum corresponding to the scattering process.

* Supported in part by the ONR.

J9. On the Canonical Constraints in Covariant Field Theories.* JAMES L. ANDERSON, PETER G. BERGMANN, AND ROBERT PENFIELD,† *Syracuse University.*—In the canonical formulation of the field equations of a fully covariant field theory, it is necessary to prescribe a number of algebraic constraints between the canonical field variables which must be satisfied on a space-like hypersurface and which will then remain satisfied elsewhere by virtue of the canonical field equations. There are four primary constraints and at least four secondary constraints, defined as Poisson brackets between the primary constraints and the Hamiltonian. The secondary constraints correspond to the second subsidiary condition in electrodynamics. In general, the primary constraints are not by themselves separated momentum densities, as the first subsidiary condition is in electrodynamics. But we have been able to prove that such a separation can always be effected with the help of an appropriately chosen canonical transformation. We shall show the construction of the generating functional. The result of this separation is a considerable simplification of the structure of the theory. We are continuing the investigation of the secondary constraints.

* Supported by ONR.
† Now at Harpur College.

J10. Covariant "Photon-Vacuum." F. J. BELINFANTE, *Purdue University.*—Let ^{H} denote Heisenberg representation (with state vector Φ) and let $^\sigma$ denote interaction representation (with $\Psi[\sigma]$). It was pointed out earlier that the "photon-vacuum" condition $^H\mathcal{A}_\perp^{(+)\mu}(x)\Phi=0$ or $^\sigma\mathcal{A}_\perp^{(+)\mu}(x)\Psi[\sigma]=0$ is not rigorously covariant with $\partial_\mu{}^H A^\mu(x)\Phi=0$. These conditions lead to an electronic "kinetic self-energy,"[1] and to a Rydberg constant contrary to experimental results.[2] It is now suggested that the rigorously covariant condition $^\sigma\mathcal{A}_\perp^{(+)\mu}(x)\Phi=0$ (with $\partial_\mu{}^\sigma A^\mu(x)\Phi=0$) be used instead. Since (neglecting integrals at infinity) we may put $^\sigma A = {}^H A - {}^H A_{\text{ret}}$, the new condition means equality of the "field of photons" (in the sense of Heisenberg representation) to the retarded field: it means absence of "photons without source." Instead of being simply a "photon-vacuum" condition, this condition may well be valid for *all* states, even more fundamentally than the Lorentz condition. Only when sources of incident photons are arbitrarily "left out of consideration," the new condition should be dropped, unless we want to exclude "incident photons." The applicability of the new condition is being studied.

[1] F. J. Belinfante, Phys. Rev. 79, 201A (1950).
[2] F. J. Belinfante, Science 111, 711 (1950); R. T. Birge, Phys. Rev. 79, 193, 1005 (1950).

J11. The Irreducible Volume Character of Events. B. T. DARLING, *Mendenhall Laboratory of Physics, Ohio State University.*—It is proposed that the creation, continued existence, and annihilation of particles be considered as aspects of a material process, that this process—through which a transformation from non-particle (field) to particle occurs—is governed by the *same* structure, whether the transformation involves the creation of one or of several particles (of same or of different natures), or of their motion in continued existence.

It is assumed that this material process requires an irreducible volume in space-time. The mathematical formulation of the theory consists of a two-step correspondence type of generalization of the wave equations (Dirac, Proca, etc.) which are first converted into self-adjoint difference equations (thereby introducing a fundamental length ω) and then averaged over the four-dimensional rotation group. The resulting integro-difference equation in the Dirac case possesses a spectrum of masses among which are presumably the electron, proton, and μ-meson (predicted mass 218.76 e.m.); and the fundamental length ω agrees with the classical diameter of the electron. All of the particles have the same magnitude of charge and are electrically stable. This stability and the non-existence of any particle between the electron and μ-meson allows the conclusion that the μ-meson must decay into an electron and two neutrinos.

J12. The Values of the Fundamental Atomic Constants and Integral Relationships. ENOS E. WITMER, *University of Pennsylvania.*—If we assume that M_p/m is 1836 and hc/e^2 is $2^2\times37/11$ *exactly* and use the best experimental values of h/e, R_∞, c, and M_p in mass units, we can calculate very accurate values of most of the other atomic constants. Following Bearden and Watts,[1] we take c as $(2.997898\pm0.000009)\times10^{10}$ cm/sec., h/e as $(1.37928\pm0.00004)\times10^{-17}$ erg sec. e.s.u.$^{-1}$, and M_p as 1.0075835 m.u. This yields the following values of the more important atomic constants: F, 9652.36 ± 0.28 e.m.u. equiv^{-1} (Phys.); e, $(4.80198\pm0.00015)\times10^{-10}$ e.s.u.; e', $(1.601782\pm0.000046)\times10^{-20}$ e.m.u.; h, $(6.62327\pm0.00040)\times10^{-27}$ erg sec.; N, $(6.02601\pm0.00035)\times10^{23}$ (Phys.); m, $(9.10706\pm0.00053)\times10^{-28}$ gm; e'/m, $(1.758835\pm0.000051)\times10^{7}$ e.m.u. gram^{-1}; $1/\alpha$, 137.04687. Also we take the magnetic moment of the proton to be $(1876/671)(1-\alpha/2\pi)\mu_N$. These values are in excellent agreement with all experimental values.

[1] J. A. Bearden and H. M. Watts, *A Reevaluation of the Fundamental Atomic Constants* (The Johns Hopkins University, Radiation Laboratory, July 31, 1950).

J13. The Macroscopic Neutral Meson Field. WALTER W. WADA, *University of Michigan.*—Taking the neutral vector meson field for consideration, an attempt is made to establish a macroscopic neutral vector meson field for nuclear matter corresponding to the macroscopic electromagnetic field in Maxwell theory by exploiting the analogy between the two fields. In the low energy region of nuclear force mesons (140 Mev−300 Mev), where the deBroglie wave-length is long compared with the average inter-nucleonic distance in nuclear matter, it was possible to derive macroscopic neutral Proca field by the process of averaging similar to that employed by Lorents in deriving Maxwell equations from his microscopic electromagnetic equations. Following Bhabha's treatment[1] of the classical equations of motion of a nucleon in an external neutral vector meson field, dispersion law has been obtained both in the vector and tensor coupling between the field and the nucleon. It is found that ϵ arising from the mesonic electric polarization moment in the vector coupling is practically unity, whereas μ obtained from the mesonic magnetic polarization moment in the tensor coupling could be considerably larger than unity in the region of meson energy considered owing to the existence of resonance in the scattering formula.

[1] H. J. Bhabha, Proc. Roy. Soc. London, **A178**, 314 (1941).

Invited Paper

J14. Energy Levels of Mirror Nuclei. H. T. RICHARDS, *University of Wisconsin.* (30 min.)

FRIDAY AFTERNOON AT 2:15

Eckhart 133

(D. J. HUGHES presiding)

Bremsstrahlung; Scattering; Stopping Power

K1. Proton Bremsstrahlung at 145 Mev.* JAMES ROUVINA AND RICHARD WILSON, *University of Rochester.*—A 145-Mev proton beam was intercepted by a Be target. γ-rays and neutrons from the target were collimated in the cyclotron fringing field which removed charged particles. γ-rays were detected by counting the pairs from a thin Pb materializer with a telescope of scintillation counters. Absorption of the primary radiation in Pb and Al showed a negligible number of neutron counts at 90° and 180° to the proton beam. Absorption of the secondary electrons in copper indicates that the spectrum of γ-radiation has a maximum near 50 Mev. If we assume that the spectrum is of the form $(\frac{1}{2}E_0-\nu)^{\frac{1}{2}}\nu^{n-2}d\nu$, corresponding to a nuclear potential varying as $1/r^n$,[1] we find $n=3\pm1$. The ratio of intensities at 90° to 180° is 2.8 ± 0.7 after correction for the different spectra at the two angles. The total cross section is found to be 4×10^{-30} cm² per nucleon within a factor of 2.

* This work was supported by the AEC.
[1] A. Simon, Phys. Rev. 79, 573, 1950.

K2. Bremsstrahlung Cross Section of 61-Mev Electrons in Lead.* C. D. CURTIS, *University of Illinois.*—Radiation straggling was used to measure the absolute cross section and the shape of the high energy end of the bremsstrahlung spectrum for electrons in lead. After scattering from the target of an 80-Mev betatron, electrons emerged through the "donut" wall. After collimation and magnetic analysis, the electron flux had a mean energy of 61 Mev and a half-intensity total spread of about 13 Mev. Energy loss occurred when the electrons passed perpendicular to a 3100-gauss magnetic field through 5- or 15-mil lead foils in a 9-in. cloud chamber. The photographed tracks were steroscopically analyzed. Only large energy losses were recorded. Partial analysis of the data to date show:

Theory[1]		Experiment	
$h\nu/(E_0-mc^2)$	$\sigma\times10^{24}$ cm²/Mev	$h\nu/(E_0-mc^2)$	$\sigma\times10^{24}$ cm²/Mev
0.975	0.3	0.95−1.00	0.23 ± 0.05
0.925	0.6	0.90−0.95	0.60 ± 0.08

Total observed cross sections for pair creation by electrons and electron-electron scattering are of the same order as theory.

* Assisted by the joint program of ONR and AEC.
[1] W. Heitler, *The Quantum Theory of Radiation.*

K3. An Improved Calorimeter for Calibration of 320-Mev Bremsstrahlung.* E. L. PIPER AND G. A. PRICE, *University of Illinois.*—Observations of photo-nuclear reactions with bremsstrahlung from the betatron and absolute measurements of corresponding cross sections have indicated the desirableness of an absolute measurement of bremsstrahlung intensity. A new calorimeter used in measuring the power of the x-ray beam was a thermopile consisting of two identical lead cylinders multiply connected with chromel-alumel wire. The evacuated system was placed in the beam in such a way that one of the cylinders intercepted all of the collimated beam while the other received no radiation. A parallel plate ionization chamber measured the bremsstrahlung ionizing power immediately behind ¼" Pb. Preliminary tests with this chamber provide a second prescription for measuring bremsstrahlung flux.[1] The chamber consisted of three parallel Al foils each 0.016" thick with 4" diameter active area and 0.120" air gap separating them. At the ion chamber the diameter of the collimated x-ray beam was ¼". The center foil voltage was measured with a Victoreen model-70 electroscope.

The x-ray energy flux is 0.0012 joules per e.s.u. of ionization per cm air path length.

* Assisted by the Joint Research and Fellowship Program of the ONR and AEC.
[1] D. W. Kerst and G. A. Price, Phys. Rev. 79, 725 (1950).

K4. Z Dependence and Angular Distribution of Bremsstrahlung from 17-Mev Electrons.* L. H. LANZL AND A. O. HANSON, *University of Illinois.*—The cross section for bremsstrahlung production as a function of atomic number, Z, has been measured using a 16.93-Mev focused electron beam from a 22-Mev betatron. The incident electrons impinged on thin targets of $Z=4$, 13, 29, 47, 79, which had the same $N(Z^2+Z)$. The x-ray beam thus produced was cleared of electrons by means of a magnet. Two detectors were used to measure the radiation. Using the radioactivity induced in Cu^{63} [(γ, n), threshold 10.9 Mev], which measures the upper end of the x-ray spectrum where screening is negligible, the cross section was found to vary as (Z^2+Z), within the experimental error of about 2 percent. Using a thick-walled aluminum ion chamber, which detects low as well as high energy quanta, the x-ray yield from the targets was found to decrease with Z, Be giving a yield 1.4 times that from Au. The angular distribution of radiation intensity was measured with a small ion chamber for Au targets of various thicknesses. Experimental measurements gave angles of half-intensity slightly less than those predicted by Schiff's theory. The central radiation intensity, as a function of Au thickness, shows a maximum at 0.035 inch.

* Assisted by the joint program of the ONR and AEC.

K5. Nuclear Radii from Electron Scattering Measurements.* A. O. HANSON, E. M. LYMAN, AND M. B. SCOTT, *University of Illinois.*—The measurements on the elastic scattering of 15.7-Mev electrons, reported at an earlier meeting, have been repeated and are now estimated to be accurate to about 5 percent. These measurements give cross sections for light nuclei at 30 degrees, which are about 5 percent higher than those calculated including the radiative correction.[1] The difference may not be significant, since it is just within the experimental error. The scattering from the heavier elements at large angles was compared with the scattering by a uniform nuclear charge distribution of finite size as calculated by Elton[2] and Acheson.[3] The scattering from silver and gold is reduced to 0.7 and 0.5 of that for a point charge which corresponds to nuclear radii of about 0.75 and 0.62 of those found from neutron measurements. These small radii for the nuclear charge densities may indicate that nuclei are built up of dense central cores surrounded by less dense outer regions and may be useful in understanding the success of the shell model of the nucleus.

* Assisted by the joint program of the ONR and AEC.
[1] J. Schwinger, Phys. Rev. 76, 790 (1949).
[2] L. R. B. Elton, Phys. Rev. 79, 412 (1950).

K6. Electron-Electron Scattering at 15.7 Mev.* M. B. SCOTT, A. O. HANSON, AND E. M. LYMAN, *University of Illinois.*—The angular distribution and momentum of 15.7-Mev electrons scattered by atomic electrons was investigated at eight angles between 10° and 43° in the laboratory system (70° to 150° in the center-of-mass system). Electrons from the 22-Mev betatron were focused by a magnetic lens on 1- and 2-mil nylon scattering foils. The scattered electrons were defined by a gold-lined aperture and detected by a Geiger counter. The electrons scattered from electrons were separated from electrons elastically scattered from nuclei by a Nier type 75° magnetic analyzer, since the energies involved are quite distinct. Preliminary analysis of the data indicates good agreement with the theory of Møller[1] as to angular distribution and energy of the scattered electrons.

* Assisted by the joint program of the ONR and AEC.
[1] C. Møller, Ann. d. Phys. 406–14, 531 (1932).

K7. Measurement of Multiple Scattering of 15.7-Mev Electrons.* E. M. LYMAN, A. O. HANSON, L. H. LANZL, AND M. B. SCOTT, *University of Illinois.*—The angular distribution of multiply scattered 15.7-Mev electrons has been measured for Be and Au foils. The experimental equipment is the same as that used in the electron-electron scattering measurements by Scott, Hanson, and Lyman. The scattered beam was defined by a $\frac{1}{32}$" diameter hole 10" from the scattering foil and detected by an air ionization chamber. The distributions have $1/e$ widths of 2.58° and 3.76° for Au foils of 18.66 and 37.28 mg/cm², and 3.06° and 4.25° for Be foils of 257 and 491 mg/cm². These values are at least 10 percent narrower than calculated by Snyder and Scott[1] is we replace Z^2 in their theory by Z^2+Z, except where Z applies to shielding. In another experiment using x-ray film as a detector, the widths of the film density distributions were slightly narrower than those given above. The scattering by the Aufoils was also measured from 6° to 30°, which is the region of single scattering increased slightly by multiple scattering. The ratio of the scattering from the thick foil to that of the thin foil was $2+95/\theta^2$ from $\theta=9°$ to 30°.

* Assisted by the joint program of ONR and AEC.
[1] H. S. Snyder and W. T. Scott, Phys. Rev. 76, 220 (1949).

K8. A Cloud Chamber Study of Positron-Proton Collisions.* K. H. MORGANSTERN AND H. P. HOTZ, *Washington University.*—The large-angle scattering of positrons from hydrogen nuclei has been studied in order to obtain an experimental comparison of the angular variation in cross section with the Rutherford distribution (modified for spin),

$$\csc^4(\theta/2)[1-(v^2/c^2)\sin^2(\theta/2)]$$

in the case of positrons. A 10-millicurie Na^{22} source was used to provide the positrons, which were rendered monoenergetic and collimated by means of a wedge-shaped magnetic field and slit system. The beam of positrons, which entered the cloud chamber through a half-mil polyethylene window, was pulsed to coincide with the expansions of the chamber. The cloud chamber was filled with a hydrogen-alcohol mixture at a gauge pressure of 10 pounds per square inch. Results will be reported for positrons of two energies, 200 kev and 450 kev; preliminary results at the lower energy show agreement with the Rutherford law.

* Assisted by the joint program of the ONR and AEC.

K9. Scattering of Protons by Tritium.* R. S. CLAASSEN, G. D. FREIER, AND W. R. STRATTON, *University of Minnesota.*—The differential cross section for the scattering of protons from tritium has been measured in the energy range 2.5 to 3.5 Mev and the angular range 41.8° to 163° in the laboratory system. Protons accelerated by the Minnesota electrostatic generator were scattered and counted in a small volume

(about 1 standard cc of gas) non-planar scattering chamber with an angular range of 17° to 163°. The center-of-mass differential cross section considered as a function of scattering angle shows a broad minimum at 100° in the above energy range. These measurements are in reasonable agreement with those of Hemmendinger, *et al.*[1] in the region of overlapping energy. The small volume chamber designed to utilize small quantities of rare gases as target nuclei in scattering and disintegration angular distribution experiments will be described.

* This work was supported in part by the ONR.
[1] Hemmendinger, Jarvis, and Taschek, Phys. Rev. **76**, 1137 (1949).

K10. On the Low States of He^5 and Li^5. ROBERT K. ADAIR, *University of Wisconsin.*—An analysis of the experimental material on the scattering of protons[1,2] and neutrons[3] by alpha-particles indicates that the low states of He^5 and Li^5 consist of an inverted $P\frac{1}{2}-P\frac{3}{2}$ doublet with a splitting of the order of 3 Mev. The phase shifts can be fitted with single level dispersion formulas:

$$\delta_{l,j}=\tan^{-1}\frac{\gamma_{l,j}^2[1/F_l^2(a)+G_l^2(a)]}{E_r-E}-\tan^{-1}\frac{F_l(a)}{G_l(a)},$$

where F_l and G_l are the regular and irregular particle wave functions. Both the Li^5 and the He^5 data were best fitted by using the same value for a, the reaction radius, and for γ^2, the reduced width, consistent with the assumption of charge independent interaction. An E_r of 2.65-Mev proton bombarding energy was obtained for the ground state of Li^5, while the lowest level of He^5 occurred at 1.3-Mev neutron energy. The $P\frac{3}{2}$ levels seemed to lie 3 or 4 Mev higher. So large a splitting may be evidence for the importance of velocity dependent forces.

[1] Freier, Lampi, Sleator, and Williams, Phys. Rev. **75**, 1345 (1949).
[2] C. L. Critchfield and D. C. Dodder, Phys. Rev. **76**, 602 (1949).
[3] Bashkin, Petree, and Mooring, unpublished.

K11. Elastically Scattered Protons from Carbon.* GERSON GOLDHABER,† R. M. WILLIAMSON, H. L. JACKSON,‡ AND M. J. W. LAUBENSTEIN, *University of Wisconsin.*—Excited levels in N^{13} were investigated by observing the yield, at an angle of 164°, of protons elastically scattered from carbon. Bombarding energies from 0.3 Mev to 4.0 Mev were observed. A 90° magnetic analyzer was used to separate proton groups from carbon and the nickel backing. Only two resonances at 456-kev and 1.7-Mev proton energy, previously known[1,2] from the $C^{12}(p,\gamma)N^{13}$ reaction, were found. The differential cross section for elastic scattering at the two peaks was 0.54×10^{-24} and 0.94×10^{-24} cm²/steradian, respectively. Absolute cross sections were determined to ±25 percent. Between the resonances, the yield maintains a level of 0.14×10^{-25} cm²/steradian which is well above Rutherford scattering. Following the second resonance region, a lower plateau of 0.063×10^{-24} cm²/steradian extends to about 3.5 Mev.

* Work supported by the AEC and the Wisconsin Alumni Research Foundation.
† Now at Columbia University, New York, New York.
‡ Kimberly Clark Fellow.
[1] W. A. Fowler and C. C. Lauritsen, Phys. Rev. **76**, 314 (1949).
[2] D. M. Van Patter, Phys. Rev. **76**, 1264 (1949).

K12. Stopping Power and Energy for Ion Production for 340-Mev Protons.* C. J. BAKKER AND E. SEGRÈ, *University of California, Berkeley.*—The relative mass stopping power for 300-Mev protons of H (in $(CH_2)_x$), Li, Be, C, Al, Fe, Cu, Ag, Sn, W, and Pb have been measured. They are in the ratios 2.634; 1.062; 1.024; 1.124; 1.000; 0.906; 0.875; 0.789; 0.751; 0.680; 0.660; 0.630. For heavier substances the Bethe stopping power formula fits with experiments assuming $I/Z=9.2$ ev. (I average ionization energy, Z atomic number.) We measured also the energy spent per ion pair produced by 340-Mev protons. For the following gases it is, in ev per ion pair: H_2, 35.3; He, 29.9; N_2, 33.6; O_2, 31.5; Ne, 28.6; A, 25.5; air, 33.3.

* This work was performed under the auspices of the AEC.

Invited Paper

K13. Scattering of 16-Mev Electrons. E. M. LYMAN, *University of Illinois.* (25 min.)

FRIDAY EVENING AT 7:00

Ida Noyes Hall

(I. I. RABI presiding)

Banquet of the American Physical Society

After-dinner speeches

John Torrence Tate. K. K. DARROW, *Bell Telephone Laboratories.*

(Title to be announced). N. F. MOTT, *University of Bristol.*

SATURDAY MORNING AT 10:00

Eckhart 133

(CYRIL S. SMITH presiding)

Metals

L1. The Half-Life of Positrons in Metals.* S. DE BENEDETTI AND H. J. RICHINGS, *Carnegie Institute of Technology.*—The annihilation of slow positrons in a metal occurs only by recombination with the conduction electrons because of the electrostatic repulsion between the positrons and the ions. Thus the annihilation high-life should be longest in the alkali

metals where the density of free electrons is small. If one neglects the electrostatic attraction between the free electron and the positron, the computed half-life in K is 6×10^{-9} sec. If one considers the electrostatic effect but neglects the modulation of the wave functions due to the crystal lattice (Fermi gas of free electrons), the computed value is 3×10^{-10} sec. for positrons at rest. The real half-life probably lies between these two limits. An experimental attempt to detect the difference in half-life of positrons absorbed in metallic K and Pb has been performed. The method consists in a delayed coincidence measurement of the shift in time between the entrance of a fast positron and the emergence of an annihilation γ from the absorbers. Preliminary measurements indicate that the difference is smaller than 10^{-9} sec. We are presently improving our techniques with the hope of detecting a measurable effect.

* This work was done under the joint auspices of the AEC-ONR.

L2. Change in Electrical Resistivity of Pure Copper Single Crystals as a Function of Cold Work.* J. W. MICHENER AND J. S. KOEHLER,† *Carnegie Institute of Technology.*—Single crystals of pure copper (99.999 percent Cu) were grown in the shape of standard cylindrical tensile specimens (0.18-in. diameter) by means of the Bridgman method in a vacuum furnace. Resistivities are measured at liquid hydrogen temperatures by passing a known current through the samples and measuring the voltage developed between two wires soldered to each sample. Data will be presented for four samples, a fifth is always measured but is not strained so that it serves as a reference standard in order to correct for small temperature differences. The samples are pulled in simple tension in increments of approximately 10 percent resolved shear strain. Strain is measured by using fiducial marks consisting of light scratches produced by a razor blade. Resolved shear stress and strain are determined using x-ray orientation data. Laue back reflection patterns are obtained after each increment in strain. Stress-strain curves will be presented as well as curves of resistivity *versus* resolved shear strain and elongation.

* This work supported in part by contract with ONR.
† Now at University of Illinois, Urbana, Illinois.

L3. Line Widths for Cold Worked Metals.* CHARLES S. BARRETT, *University of Chicago* AND MARJORIE A. BARRETT, *De Pauw University.*—Integral line widths were measured for filed powders of face-centered cubic metals using CuKα and a Geiger-counter spectrometer. Filings were prepared at different temperatures and immediately quenched. The 200 Kα line widths in $^\circ\theta$, after correction by subtracting integral widths of recrystallized filings, may be grouped thus: (a) 0.02–0.20 (b) 0.21–0.40 (c) 0.41–0.50 (d) 0.51–0.69. The grouping and filing temperatures (°C) were: (a) Al ("2*S*"), 20°, −195°; Al alloy "24*S*-*T*," 20°; Cu, 20°; Ag, 20°; Cu—2.9 percent Si, 450°; (b) Cu, −195°; Cu—2.9 percent Si, 350°; Cu—8.5 percent Zn, 20°; Cu—1.89 percent Si, 20°; (c) Cu—30 percent Zn, 20°; Ag—7 percent Sb, 20°; (d) Cu—2.9 percent Si, −195°; Cu—4.2 percent Si, 20°; Ag—11 percent Sn, 20°. All samples known by oscillating crystal methods[1] to have stacking faults are in (d); other in which faults were suspected are in (c) and those believed fault-free are in (a) or (b). Thus, faults cause significant widening in some cold-worked alloys, though this cause of widening has usually been ignored.

* Work supported in part by ONR, U.S.N., at University of Chicago.
[1] C. S. Barrett, Trans. A.I.M.E. 188, 123 (1950).

L4. Stress-Strain Curves of Pure Copper Single Crystals as a Function of Temperature.* J. B. WACHTMAN, JR. AND J. S. KOEHLER,† *Carnegie Institute of Technology.*—Single crystals of 99.999 percent copper were grown in pairs in the shape of standard cylindrical tensile specimens by the Bridgeman method in a vacuum furnace. The two members of each pair had the same orientation and the different pairs had different orientations. After a 20-hour vacuum anneal at 1000°C the crystals were strained either at room temperature or in a boiling bath of liquid nitrogen. Strain was determined by measuring the separation of light scratches. All strain measurements were made at room temperature and it was assumed that the strain determined this way was equivalent to the true low temperature strain (i.e., that the thermal expansion coefficient is independent of cold work). The rate of loading was constant. It was found that the stress-strain curve for identical crystals was, within the accuracy of measurement, the same at liquid nitrogen temperature as at room temperature. Data on crystals strained partly at low temperature and partly at room temperature will be presented as well as stress-strain curves at constant temperatures.

* This work supported in part by ONR contract.
† Now at University of Illinois, Urbana, Illinois.

L5. Internal Friction Arising from the Precipitation of Zinc in an Aluminum-Zinc Alloy. A. S. NOVICK, *University of Chicago.*—Torsion experiments on an aluminum-zinc alloy (40 percent zinc) at frequencies of about one cycle per second show that precipitation may give rise to a very large internal friction. Specimens freshly quenched from a solution temperature of 450°C show negligible damping at room temperature, but subsequent aging at an intermediate temperature results in increased internal friction depending upon the time and temperature of aging. The observed internal friction is a rapidly increasing function of the temperature of measurement and does not yield a peak. Values as high as $Q^{-1}=0.2$ have been observed; this result is considerably larger than the height of the well-known grain boundary peak. In addition, the dynamic shear modulus has been observed to *increase* after aging by as much as 20 percent over the corresponding value in the quenched state. The observed effects seem to be independent of the grain size and the state of cold work of the specimen and are, therefore, attributed entirely to the precipitation of zinc from solid solution. The manner by which relaxation may be produced by atomic movements at the surfaces of precipitate particles will be discussed.

L6. Contribution from the Institute of Metals. C. ZENER, *University of Chicago.*—Arguments are presented for the thesis that the entropy of activation ΔS for self-diffusion will always be positive, and a method is given for estimating its order of magnitude. All experimental values of D_0 for self-diffusion are in accord with a positive ΔS. The same arguments are applicable to chemical diffusion provided such diffusion occurs homogeneously throughout the lattice. Nearly all the determined values of D_0 for chemical diffusion, other than those obtained at this laboratory, require a negative ΔS. We conclude that in such cases diffusion was not homogeneous, and that the larger D_0 values characteristic of a positive ΔS will be obtained when very small concentrations are used in large grain-sized specimens.

L7. Precipitation of Carbon and Nitrogen in Cold-Worked Alpha-Iron. S. HARPER, *University of Chicago.*—The precipitation of carbon and nitrogen from supersaturated solution in cold-worked α-iron has been studied by means of internal friction measurements of the amount of solute in the material. The precipitation rate has been studied as a function of such variables as time, temperature, amount of cold work, and the degree of supersaturation. The results obtained indicate that the precipitate involved is not the normally appearing iron carbide or nitride phase but is a concentration of the solute atoms around dislocations in the iron. Quantitative agreement is found with a postulated dislocation model of this process,[1] the results permitting estimates of dislocation densities which are in accord with previous estimates. The temperature dependence of the precipitation is in accordance with an activa-

tion energy of 20,000 cal./mole in the case of carbon and 17,200 cal./mole in the case of nitrogen, in agreement with published data for the activation energies of diffusion of these elements in body-centered cubic iron.

[1] A. H. Cottrell and B. Bilby, Proc. Phys. Soc. (London) Series A, 62 (1), 49 (1949).

L8. Effect of Inclusions on Coercive Force of Iron. L. J. DIJKSTRA AND C. WERT.—A theoretical study is made of the contribution to the coercive force H_c by non-magnetic inclusions distributed at random in a ferromagnetic matrix. The following effects which impede the movement of the domain walls are examined: (1) The surface tension effect, (2) the effect of internal magnetic poles. It is found that H_c depends both on the volume fraction of inclusions and their state of dispersion. For a given volume fraction of inclusions the largest effect occurs for particles whose diameter is about the wall thickness δ. For this diameter the contribution to H_c due to (1) is smaller than, but comparable to that due to (2). Measurements of H_c have been made using a dispersion in iron of Fe_3C in the shape of spheres, the diameter of which could be varied over the desired range. The maximum effect on H_c is found for a particle size of about 1200A, indicating a value of δ of about this magnitude. This is in agreement with the theoretical value. For this diameter the measured value of H_c is found to agree well with the calculated value.

L9. New Approximation Method for Treatment of Order-Disorder Transitions. HUBERT M. JAMES AND LLOYD D. FOSDICK, *Purdue University*.—The order-disorder problem of the square Ising array in two dimensions has been discussed by an extension of Bethe's method. A 3×3 section of this array is considered, and account is taken of (a) the tendency of interaction with external atoms to induce short-range order, as well as long-range order, in the outer sites of this section, and (b) the differing control of long-range order exerted by this interaction for non-equivalent sites in the outer shell. The theory thus involves three parameters instead of the one parameter of Bethe's theory. This more careful treatment of short-range order greatly improves the accuracy of the method, which in an elementary manner yields results comparable to those of Kramers and Wannier, and much superior to those of other approximation methods. The predicted Curie point is some seven percent higher than the exact value. The short-range order is in good agreement with the exact results of Onsager for all temperatures, with maximum error around the Curie point. The theory predicts a specific heat varying like $(T-T_c)^{-\frac{1}{4}}$ as T approaches the Curie temperature T_c from below, whereas other approximation methods predict finite values; Onsager's exact result varies as $-\log|T-T_c|$.

L10. On the Mechanism of Heat Transfer from a Solid to a Gas. H. B. WAHLIN AND CHARLES D. HENDRICKS, JR., *University of Wisconsin* (*Presented by* MR. HENDRICKS).—When a palladium filament is heated in hydrogen to a fixed temperature it is found that the energy input necessary to maintain the temperature is independent of the pressure down to a pressure of about 4 cm or less. If helium is substituted for the hydrogen the energy input increases with increasing pressure at least up to 20 cm which is about the limiting upper pressure which can be used without convection effects setting in. Nitrogen and air also show a similar pressure dependence. When nickel was substituted for palladium the same general effect was observed. This suggests that the heat loss is determined by the condensed layer on the metal, and in the case of hydrogen a stable layer is established which is independent of the pressure above 4 cm. In helium, nitrogen, and air this is not the case.

L11. Ferromagnetic Resonance Measurements on Stressed Thin Nickel Films. J. ROSS MACDONALD,* *Oxford University*.—Previous measurements by Griffiths and Standley[1] on thin annealed nickel films at wave-lengths of 1.23 and 3.04 cm showed the possibility of considerable dependence of the Landé g-factor upon film thickness. Present measurements indicate these results were largely caused by thickness-dependent isotropic plane tension. Measurements were made at 1.25 cm on nickel films from 0.05 to 3 microns thick evaporated on mica. Resonance observations on both sides of the films showed the resonance magnetic field, $H_0{}'$, could be as much as 900 oersteds larger on the film side first evaporated on mica and still attached to it than on the free side, for films thicker than 0.3 micron. When a modified resonance condition: $\hbar\omega=g\mu_B\left\{\left[H_0{}'+\left(4\pi I_0+\frac{3\lambda T_0}{I_0}\right)\right]H_0{}'\right\}^{\frac{1}{2}}$ accounting for isotropic plane stress, T_0, was used in conjunction with a T_0 value calculated from differential contraction between nickel and mica on cooling after evaporation, g-values found for the two sides, with no stress correction applied to the free side, were both very nearly equal to the bulk-nickel g-value. Finally, peeling films free from the mica reduced the initial resonance field difference between the two sides to zero, eliminating the possibility that difference was partly due to magnetocrystalline anisotropy and preferred crystalline orientation.

* Rhodes Scholar; now at the Armour Research Foundation, Chicago, Illinois.

[1] J. H. E. Griffiths, *Oxford Conference on Microwave Spectroscopy*, July, 1948.

SATURDAY MORNING AT 9:30

Kent Theatre

(J. D. FERRY presiding)

Symposium of the Division of High-Polymer Physics
Solidification and Crystallization in Polymers

M1. Introductory Remarks on Polymerization. J. D. FERRY, *University of Wisconsin*. (20 min.)

M2. Formation of Solids by Vitrification. J. R. VAN WAZER, *Monsanto Chemical Company*. (30 min.)

M3. Experimental Methods for Determining the Extent of Crystallization in Polymers. I. FANKUCHEN AND H. MARK, *Polytechnic Institute of Brooklyn*. (40 min.)

M4. Effect of Polycrystalline Texture on Properties of Crystalline Polymers: Role of Nucleation in the Crystallization Process. TURNER ALFREY, JR., *Dow Chemical Company*. (40 min.)

SATURDAY MORNING AT 9:30

Mandel Hall

(W. C. SHEPHERD presiding)

Symposium of the Division of Electron Physics

N1. Principles Involved in the Performance and Design of Betatrons. D. W. KERST, *University of Illinois.* (30 min.)

N2. Electron Counting: A New Low-Current Measuring Technique. A. S. EISENSTEIN, *University of Missouri.* (30 min.)

N3. Optical and Thermal Electronic Processes in Barium Oxide. R. L. SPROULL, *Cornell University.* (30 min.)

N4. Induced Conduction in Diamond. G. C. DANIELSON, *Iowa State College.* (30 min.)

SATURDAY MORNING AT 10:00

Rosenwald 2

(MARCEL SCHEIN presiding)

Artificial and Natural Mesons: Cosmic Rays

P1. Energy and Angular Distribution of π-Mesons Produced by Gamma-Rays from the 340-Mev Synchrotron.* B. T. FELD, J. S. CLARK, D. H. FRISCH, I. L. LEBOW, AND L. S. OSBORNE, *Massachusetts Institute of Technology.*—Targets of CH_2, CD_2, and C were simultaneously exposed to gamma-rays from the synchrotron. Mesons are detected in Eastman NTB (200μ-) emulsions, embedded in aluminum. Plates were placed at 45°, 90°, and 135° to the beam, two per angle, adjacent to each target. All mesons stopping in the emulsion are recorded. The meson energy is determined from the thickness of material traversed. Positive π-mesons undergo π-μ-decay; negatives produce stars (except for a known fraction).[1] The plates cover, in six energy intervals, the range 28–70 Mev. Corrections are applied for the different solid angle subtended by each interval. 4–500 mesons are recorded per plate. The data from the C-target are used to obtain (by subtraction) the distributions from H and D. The carbon spectrum is flat over the energy interval covered. Negative to positive ratio shows slight increase with energy, with values in fair agreement with pseudoscalar theory. These results agree, in general, with latest published Berkeley data.

* Assisted by the joint program of the AEC and ONR.
[1] Adelman and Jones, Phys. Rev. 75, 1468 (1949).

P2. The Relative Yield of 20-Mev π⁺-Mesons from Seven Elements. DONALD CLARK, *University of Rochester.*—A preliminary measurement has been made of the relative yields of 20-Mev π^+-mesons from seven targets bombarded by the 240-Mev proton beam of the Rochester cyclotron. The mesons emitted at 150°±15° are focused by the magnetic shim of the cyclotron fringing field and detected outside of the cyclotron chamber by a telescope of four scintillation counters. The meson trajectories are defined by a channel in a brass shield and the range by an adjustable absorber placed between the second and the third crystals. Counts correspond to mesons stopping in the third crystal, the first three crystals being in coincidence and the fourth in anticoincidence.

	A	$A^{2/3}$	$\frac{A^{2/3}}{A^{2/3}_{Be}}$	measured yield 20-Mev π^+
Be	9.02	4.33	1.00	1.00±0.13 (all normalized to Be)
C	12.00	5.25	1.21	1.33±0.13
Al	27.00	9.00	2.08	2.4 ±0.3
Cu	63.6	15.9	3.67	3.7 ±0.4
Ag	107.9	22.7	5.25	4.0 ±0.5
W	184.0	32.3	7.45	4.4 ±1.0
Pb	207.2	34.9	8.06	3.6 ±0.8

Corrections are made for the background. The yield per nucleus is a smooth function of A. This work was supported by the joint program of the ONR and AEC.

P3. Evidence for the Multiple Production of Mesons in a Single Nucleon-Nucleon Collision.* MARCEL SCHEIN, J. J. LORD, AND JOSEPH FAINBERG, *University of Chicago.*—Evidence has been obtained for the multiple production of mesons in a single nucleon-nucleon collision in a photographic emulsion exposed to the cosmic radiation at an altitude of 95,000 ft. The nuclear encounter in which the mesons were created was produced by a primary proton of 3×10^{12} ev energy. Directly in line with the incident proton, 7 particles of minimum ionization were emitted in a central core with an angular divergence of 0.003 radian. In addition, 8 other minimum ionization particles were emitted in a wider diffuse cone of 0.13 radian angular divergence. Most of the particles in the central core had energies in excess of 250 Bev, while those in the diffuse cone were of much lower energies as determined by small angle scattering measurements. Both the angular and the energy distribution of the emitted particles is in good agreement with the assumption that in the center-of-mass system the mesons are emitted in two distinct cones of angular width of about 30° forward and backward with reference to the direction of the primary proton. The average multiplicity of 15 agrees with the recent calculation by Fermi, and according to his prediction about one-half of the particles could be made up of nucleon-antinucleon pairs.

* Assisted by the joint program of ONR and AEC.

P4. Photons Emitted in the Capture of μ⁻-Mesons. E. P. HINCKS, *Chalk River Laboratory.*—G-M counters and coincidence circuits are used to detect photons with energies ~1–10 Mev emitted when μ^--mesons are stopped in various absorbers. The counter arrangement, which is surrounded by 3 in. lead, is, top to bottom: tray A; 90 g/cm² lead; tray B; meson absorber; tray C; 10 g/cm² lead; tray D; 10 g/cm² lead; tray E.

A meson traversing A and B and stopping in the absorber with the emission of a photon that is detected by the lead-covered tray D (or E) gives the anticoincidence $(ABD-C-E)$ (or $(ABE-C-D)$). With increasing thicknesses of lead absorber the rate $(ABD-C-E)+(ABE-C-D)$ shows a regular increase not associated with either the stopping or decay of positive mesons. No increase is observed with aluminum absorbers. The effect is attributed to photons from the atomic and nuclear capture of negative mesons. From the observed rates the average total energy emitted in γ-rays is estimated as about 9 Mev per negative meson stopped in lead. Results will be given for several elements. They are consistent with the observations of Chang,[1] and with the absence of high energy photons noted by Piccioni.[2]

[1] W. Y. Chang, Rev. Mod. Phys. 21, 166 (1949); Proc. Echo Lake Symposium, Office of Naval Research, November, 1949.
[2] O. Piccioni, Phys. Rev. 74, 1754 (1948).

P5. Multiple Events Produced by High Energy Cosmic Rays in Liquid Hydrogen at 90,000 Feet.* MARCEL SCHEIN AND M. VIDALE, *University of Chicago.*—A counter experiment has been carried out to study the production of mesons in high energy proton-proton collisions. The apparatus was flown from Chicago on September 6, 1950 with a General Mills balloon. It reached an altitude of 90,000 feet and floated at that height for 4½ hours. A spherical metal Dewar flask 30 cm in diameter was filled with liquid hydrogen which was obtained through the courtesy of Dr. Earl A. Long of the Institute for the Study of Metals of the University of Chicago. Above the hydrogen, four crossed trays of counters were mounted in order to determine accurately the direction of the particles incident upon the hydrogen. Below the Dewar flask extended trays of counters detected multiple events occurring in the hydrogen. The discharge of each individual counter was in coincidence with a fourfold master pulse and was registered separately on a moving photographic film. The results of this experiment will be discussed.

* Assisted by the joint program of the ONR and AEC.

P6. High Energy Cosmic-Ray Stars. FRANK B. MCDONALD, *University of Minnesota.*—A study has been made using nuclear emulsions exposed at 18 grams residual atmosphere, geomagnetic latitude 55°N, of cosmic-ray stars with three or more shower particles (apparent emitted tracks with ionization ranging from minimum to 1.5 min.). It was found that most events of this type were induced by single or double charged particles assumed to be protons and alpha-particles but with some of the lower energy events being induced by neutral radiation. The ratio of proton/alpha-induced events is in agreement with the ratio of proton/alpha-primary flux as reported by various workers.[1–3] Zenith angle distribution of the initiating track has been obtained, and calculated mean free paths will be given. The approximate zenith angle distribution of the neutral star-inducing radiation has been obtained by assuming that the shower axis preserves the direction of the incident particle. The angular distribution of the minimum ionization tracks with respect to the shower axes has been measured, and comparisons with existing meson theories will be given.

[1] Freier, Lofgren, Ney, and Oppenheimer, Phys. Rev. 74, 1818 (1948).
[2] M. A. Pomerantz and F. L. Hereford, Phys. Rev. 76, 997 (1949).
[3] Bradt and Peters, Phys. Rev. 77, 54 (1950).

P7. Altitude and Latitude Variation of Star Production.* J. J. LORD (*Introduced by* MARCEL SCHEIN), *University of Chicago.*—The variation with altitude of the rate of production of stars in photographic plates was measured from mountain elevations to 94,000 feet at geomagnetic latitude $\lambda \simeq 54°$N. The type of particle initiating each star was determined and showed that the total flux of star producing protons decreased rapidly from 94,000 feet to 11,500 feet and was compatible with an absorption mean free path (m.f.p.) of 145 g/cm². The total flux of star-producing neutrons showed a maximum near 70,000 feet and then decreased with altitude with an absorption mean free path of 170 g/cm². Similar altitude dependence measurements were made at $\lambda \simeq 28°$N and showed that the rate of production by neutrons of stars of 3 to 9 prongs at 94,000 feet was 0.19 of the corresponding value at $\lambda \simeq 54°$. This demonstrates that 81 percent of the small stars must be due to the primary protons in the energy interval given by the geomagnetic cut-off at $\lambda \simeq 54°$ and $\lambda \simeq 28°$ (1 to 8 Bev for protons and for α-particles and heavy nuclei 0.35 to 3.5 Bev per nucleon). The total flux of star-producing protons varies by a factor of 3.0 between these two latitudes at 94,000 feet and shows that 67 percent of the proton initiated stars are due to primary particles of energies given above.

* Assisted by the joint program of the ONR and AEC.

P8. Diurnal Variation of Heavy Nuclei in the Cosmic Radiation.* J. LITWIN, J. J. LORD, AND MARCEL SCHEIN, *University of Chicago.*—Measurements of the flux of heavy nuclei have been made from photographic plates exposed by a free balloon at an elevation of 94,000 feet at geomagnetic latitude 55°N. Two groups of Ilford G5 plates were exposed in a vertical position. Both groups of plates reached an elevation over 90,000 feet at 7:50 P.M., May 22, 1950 and the first group (1) was released by parachute at 5:45 A.M. the next day. The second group of plates (2) was then released at 12:10 P.M. the same day. The balloon was kept at an almost constant ceiling altitude by a ballast release mechanism and a temperature compensated barometer gave pressure readings accurate to 1 mb. The flux of heavy nuclei at night was determined from the plates of group (1) and the flux during the day from the difference between the intensity of tracks on the plates of groups (2) and (1). It was found that the ratio between the flux of heavy nuclei during the day to that at night was $2.5 \pm .3$ for all heavy nuclei of $Z \simeq 10$ to $Z \simeq 26$. Data will be given regarding the flux of heavy nuclei with Z less than 10.

* Assisted by the joint program of the ONR and AEC.

P9. Rates of Star Formation and the Flux of Primary Heavy Nuclei During the Solar Flare of August 2, 1950. JOHN E. NAUGLE AND GEORGE W. ANDERSON, JR., *University of Minnesota.*—The flux of primary nuclei with charge ≥ 10 and star formation rates during the solar flare of August 2, 1950, were measured by means of Ilford G-5 photographic emulsions. The exposure was of 3 hours duration at an average depth in the atmosphere of 16 g/cm². Comparison of the flux of heavy nuclei with previous data[1] showed no differences attributable to the flare. Significant increases were observed in the rates of production of some types of stars. Control data was obtained from a closely similar flight during a period of normal solar activity.[2] The prong spectrum and the relative number of stars initiated by neutral and charged radiation will be discussed. Similar effects were observed following the solar flare of May 10, 1949, by other workers.[3]

[1] P. S. Freier, thesis, 1950, University of Minnesota.
[2] J. E. Naugle, thesis, 1950, University of Minnesota.
[3] Lord, Elston, and Marcel Schein, Phys. Rev. 79, 540 (1950).

P10. Measurements on Relativistic Cosmic-Ray Particles with Photographic Emulsions. L. VOYVODIC AND E. PICKUP, *National Research Council, Ottawa.*—Relativistic cosmic-ray particles (observed in Ilford G5 emulsions which had been exposed for several hours at about 85,000 feet) have been analyzed by measurements on the grain density and multiple Coulomb scattering, using the scattering method developed at Bristol by Fowler.[1] Preliminary results will be given for the production spectra of charged and neutral mesons at this altitude. Some evidence has been found for a relativistic increase in grain density of about 10 percent above the minimum, which appears to be in qualitative agreement with ionization loss theories when polarization effects are taken into

account. The accuracy of energy determinations from multiple scattering measurements has been improved by a new calibration using electron pairs formed by the 17.6-Mev γ-ray from protons on lithium.

[1] P. H. Fowler, Phil. Mag. 41, 169 (1950).

P11. An Experimental Attempt to Detect the Dirac Magnetic Monopole. WILLEM V. R. MALKUS, *University of Chicago.*—Dirac* has shown that the charge of a magnetic monopole compatible with quantum mechanics must be an integral multiple of (137/2)e e.m.u. If this monopole is created by cosmic radiation in the atmosphere it would quickly reach terminal velocity in the earth's field due to its large and velocity-independent energy loss. A solenoid directed along the local field lines in an exposed place is used to accelerate any such particle to five hundred Mev. A nuclear emuslion is placed below the solenoid to record the heavy tracks any monopoles would leave. The negative results of this experiment are interpreted as setting an upper limit on the arrival rate of monopoles at the surface of the earth of 10^{-10} per cm^2 per sec., corresponding to a maximum cross section for their production by primary cosmic-ray protons of 3×10^{-26} cm^2.

* P. A. M. Dirac, Phys. Rev. 74, 817 (1948).

P12. The Intensity of the Soft and of the Hard Component of the Cosmic Radiation at Geomagnetic Latitudes of 28°N and 55°N.* M. VIDALE AND MARCEL SCHEIN, *University of Chicago.*—Two sets of identical counter telescopes have been flown with General Mills balloons at geomagnetic latitudes of 28°N and 55°N. The first flight was launched on November 19, 1949 from the deck of an aircraft carrier of the U. S. Navy. The equipment landed in the ocean and was prompty recovered by helicopter. The second one was launched from Minneapolis, Minnesota on June 5, 1950. Both flights had a relatively slow rate of rise and floated at the maximum altitude for several hours. The intensity of the hard component (capable of traversing 12 cm of lead) and of the total flux of the cosmic radiation was measured as a function of altitude. Three counters below 12 cm of lead registered the production of penetrating showers. The intensity of the hard component shows a flat maximum at an atmospheric pressure of 9 cm Hg at 28°N geomagnetic latitude and a maximum at about 3 cm Hg for 55°N. Comparison of the results obtained at the two latitudes gives, at a pressure of 1.6 cm Hg, a latitude effect of 3.85 for the total vertical flux, of 2.75 for the hard component and of 1.5 for penetrating showers.

* Assisted by the joint program of the ONR and AEC.

Invited Paper

P13. Scintillation-Counter Analysis of the Charge Spectrum of Primary Cosmic Rays. E. P. NEY, *University of Minnesota.* (30 min.)

SATURDAY MORNING AT 10:00

Breasted Hall

(F. W. LOOMIS presiding)

Reactions of Transmutation, Tritium Through Aluminium

Q1. The α-Particle Energy Distribution from the $T+T$ Reaction. K. W. ALLEN, E. ALMQVIST, J. T. DEWAN, AND T. P. PEPPER, *Chalk River Laboratory.*—A preliminary study of the energy distribution of the α-particles from the reaction $T+T=\alpha+2n+11.4$ Mev has already been reported.[1] The yield of this reaction for 240 kev triton bombarding energy is very small and considerable difficulty was experienced in studying the upper end of the α-particle spectrum due to the presence of 3.5 Mev $T+D$ α-particles from deuterium contamination on the target. It has now been found that a layer of titanium evaporated on to molybdenum backing and maintained at 400°C gives very little D contamination while providing sufficient yield for a detailed study of the $T+T$ α-particles with a thin window proportional counter and pulse analyzer. These measurements, combined with magnetic analysis data previously obtained, give the shape of the $T+T$ α-particle spectrum over the range 0.7 to 3.8 Mev. The distribution has a broad maximum at about 2.9 Mev. The intensity of an α-particle group which would correspond to the formation of a dineutron with lifetime $>3\times10^{-21}$ sec. is less than 1 percent of the continuum.

[1] Allen, Almqvist, Dewan, Pepper and Sanders, Phys. Rev. 79, 209(A) (1950).

Q2. A Precise Determination of the Reaction Energies of Light Elements.* E. N. STRAIT, D. M. VAN PATTER, A. SPERDUTO, AND W. W. BUECHNER, *Massachusetts Institute of Technology.*—Measurements have been made of the reaction energies of more than thirty ground-state transitions induced by proton and deuteron bombardment of light elements. The reactions studied include the (d, p), (d, α), and (p, α) reactions, and the individual Q-values have been determined to precisions that are between 4 and 14 kev. A total of sixteen stable nuclei from lithium through sulfur were used as targets. The reaction products were analyzed by means of 180-degree focusing in the field of a large annular magnet. In these measurements, careful consideration has been given to possible sources of error, such as the effects of geometry and of surface contaminants. Several of these reaction energies are of particular importance for establishing accurate mass values. These include the $O^{16}(d, \alpha)N^{14}$, $C^{13}(d, \alpha)B^{11}$, and $Li^7(p, \alpha)\alpha$ reactions, the Q-values for which are 3.112 ± 0.006, 5.160 ± 0.010, and 17.340 ± 0.014 Mev, respectively.

* This work has been assisted by the joint program of the ONR and AEC.

Q3. Disintegration of Lithium by Tritons. T. P. PEPPER, K. W. ALLEN, E. ALMQVIST, AND J. T. DEWAN, *Chalk River Laboratory.*—The 250 kv accelerator is being used to study the disintegration of the lithium isotopes by tritons. The mass 3 component of the ion beam, normally containing about 30 percent tritons, bombards targets of ^{6}LiF or $^7Li_2SO_4$ and the energies of the disintegration products emitted at 90° to the beam are measured either by magnetic analysis or by means of a thin window proportional counter and pulse analyzer. With Li^7 the following reactions have been observed:

$$Li^7+T=2\alpha+2n+8.79 \text{ Mev} \quad (1)$$

$$=He^4+\alpha+9.75 \text{ Mev} \quad (2)$$

Two groups of α-particles corresponding to the formation of He^6 in the ground state and in an excited state 2.0 Mev above ground appear superposed on a continuous background of α-particles from (1). The intensity of the α-group from He^6 is about five times greater than that from the ground state. The yield of reaction (2) is considerably less than that of (1). In the disintegration of Li^6, three reactions have so far been observed.

$$\begin{aligned} Li^6+T &= 2\alpha+n+16.03 \text{ Mev} \\ &= Li^7+D+0.98 \text{ Mev} \\ &= He^5+\alpha+15.2 \text{ Mev} \end{aligned}$$

The 3-body disintegration has the largest yield.

Q4. Simple Capture of Alpha-Particles. BERT J. TOPPEL,† PAUL A. ROYS, AND W. E. BENNETT, *Illinois Institute of Technology.*—Gamma-rays have been observed from the simple capture of alpha-particles in lithium. The gamma-ray energies were too large, up to seven Mev, for simple capture in Li^6, but not inconsistent with the reaction $Li^7(\alpha, \gamma)B^{11}$. Three resonances were observed at bombarding energies of 0.401, 0.819, and 0.958 Mev. The corresponding excited states in B^{11} are at 8.90, 9.16, and 9.25 Mev. The yields were too small to use thin targets, but the resonances appeared as steps in the thick target yield curve. The slope of the steps was instrumental for the first two resonances and suggested a width of about 6 kev for the upper resonance. The thick target counting rates above the steps were compared with the counting rate from simple capture of protons in a thick lithium target at 0.54 Mev, the ratios being 0.9, 9, and 60×10^{-4}. Among the other light elements, only Be and B yielded gamma-rays when bombarded by 1.4 Mev alpha-particles, but in these cases the sharp resonances characteristic of simple capture were absent.

† AEC Predoctoral Fellow.

Q5. Search for Be^7 States Using the Li^6 Technique. GEORGE R. KEEPIN, JR.,* *University of California, Berkeley.*—In Be^7, the mirrored counterpart of the single 480 kev excited state in Li^7 is well established at 429 ± 15 kev. However, two additional levels in Be^7 have been reported[1] in spectrum studies on neutrons from LiCl and LiF bombarded with 5.1 Mev (cyclotron) protons. Subsequently others using similar techniques at lower E_p have not found such levels. We have employed the Li^6 technique[2] to measure $Li^7(p, n)Be^7$ neutron spectra in an extended search for any additional levels in Be^7. The possibility of a proton energy threshold for excitation of these additional levels led us to extend E_p from 3.00 Mev up to 4.35 Mev. Approximately 10,000 disintegrations have been measured; an average value of 433 ± 26 kev for the level excitation in Be^7 is obtained. Though some of the data (to be presented) suggests a level intermediate between 433 kev and the ground state, no corresponding group was considered sufficiently resolved to be so identified with certainty. Applying a tentative cross-section correction, no group other than the known level is observed with more than 15 percent of ground state intensity.

* Now at University of Minnesota, Minneapolis, Minn.
[1] J. Grosskreutz and K. Mather, Phys. Rev. 77, 580 (1950).
[2] G. Keepin, Jr. and J. Roberts, Rev. Sci. Inst. 21, 163 (1950). G. Keepin, Jr., UCRL 790 (1950).

Q6. An Experimental Determination of the Half-Life of Be^8. C. H. MILLAR AND A. G. W. CAMERON, *Chalk River Laboratory.*—An Ilford type E1, 100 micron, nuclear research emulsion was exposed under paraffin and cadmium to 240 roentgens of γ-rays from the University of Saskatchewan betatron operating at 26.7 Mev. In a study of 12 cm^2 of this plate, 303 4-pronged α-particle stars from the photo-disintegration of O^{16} were found. Upon analysis, 119 stars were identified as having Be^8 as an intermediate disintegration product, and 27 of these showed a measurable displacement of the Be^8 nucleus prior to its break-up into two α-particles. From a consideration of these statistics and the conditions of observation a value of the half-life of Be^8 of $(5.3\pm1.1)\times10^{-14}$ sec. was obtained.

Q7. Angular Distribution of Neutrons from $Be^9(p, n)B^9$. H. T. RICHARDS, M. J. W. LAUBENSTEIN, V. R. JOHNSON, F. AJZENBERG, AND C. P. BROWNE, *University of Wisconsin.*—Protons from the Wisconsin electrostatic generator, after passing through a cylindrical electrostatic energy analyzer, were used to bombard a thin beryllium foil. Neutrons were detected by a shielded energy insensitive long counter one meter from the target. The neutron yield has been studied both as a function of angle (0° to 150° in the laboratory coordinates) and as a function of proton energy (threshold $E_p=2.059$ Mev to $E_p=4$ Mev). The neutron yield after conversion to center of mass coordinates is isotropic only very close to threshold. In the vicinity of the known resonance at $E_p\sim2.5$ Mev the neutron yield shows maxima at 0° and 135° (c.m. coordinates). For $2.75<E_p<3.4$ Mev, the neutron cross section shows a single maximum at 115°. Above 3.4 Mev the yield at 0° and 135° increases rapidly as though another resonance is being approached. Absolute cross-section measurements will be reported.

* Work supported by the AEC and by the Wisconsin Alumni Research Foundation.

Q8. Energy Levels of B^{10}.* FAY AJZENBERG, *University of Wisconsin.*—A 50-kv foil of Be was bombarded by 3.436 Mev deuterons. The neutron spectrum was observed by means of nuclear emulsions placed at 10 cm from the target, and at angles of 0° and 80° to the beam. Almost 3000 tracks have been measured. Strong evidence is found for levels of B^{10} at 0.73, 3.61, 4.78, 5.13, 5.91, and 6.11 Mev, assuming $Q=4.35$ Mev for the $Be^9(d, n)B^{10}$ reaction. It is probable that levels also exist at 5.57, 5.68, 6.33, 6.57, and 6.80 Mev. The intensity and width of the neutron group corresponding to a level at 5.13 Mev indicate possible multiplicity. Similar evidence points to a doublet at 6.11 Mev. The 0° data, statistically poor for high neutron energies, indicates multiplicity in the region of the previously reported level at 2.18 Mev.[1] This is confirmed by the 80° data which shows two distinct neutron groups corresponding to $E_x=1.82$ and 2.24 Mev. No neutron groups corresponding to levels at 1.46 and 2.89 Mev were found. This result is in disagreement with the equally-spaced levels, harmonic oscillator picture of B^{10}.[1]

* Work supported by the AEC and the Wisconsin Alumni Research Foundation.
[1] Rasmussen, Hornyak, and Lauritsen, Phys. Rev. 76, 581 (1949).

Q9. Excited States of C^{11} and C^{12}.* VIRGIL R. JOHNSON, *University of Wisconsin.*—Thin (100 kev) targets of B^{10} and ordinary boron on tantalum backings were bombarded with monoenergetic deuterons of 3.44 Mev and 3.69 Mev energy. Eastman NTA 200 micron nuclear emulsion plates were mounted 10 cm from the target at 0° and at 80° with respect to the incident beam. Altogether about 3000 tracks have been measured. The neutron groups definitely assigned to the $B^{10}(d, n)C^{11}$ reaction give energy levels in C^{11} at 1.9 Mev, 4.3 Mev, 4.85 Mev, 6.48 Mev, 6.83 Mev, 8.45 Mev, and 8.70 Mev. Other much weaker intensity groups are observed whose assignment is still uncertain. The work on the $B^{11}(d, n)C^{12}$ reaction shows well-defined groups corresponding to C^{12} levels at 15.14 Mev, 15.59 Mev, and 16.12 Mev and much broader poorly defined groups giving a C^{12} excitation of 4.6 Mev, 7.3 Mev, 9.7 Mev, 10.4 Mev, and 11.9 Mev. There are also other possible unresolved levels in C^{12} between 12 Mev and 15 Mev excitation.

* Work supported by the AEC and the Wisconsin Alumni Research Foundation.

Q10. Energy Levels in C^{13} from $Be^9(\alpha, n)C^{13}$. JAMES H. ROBERTS AND WILLIAM H. GUIER, *Northwestern University.*—The neutron energy spectrum from the $Be^9(\alpha, n)C^{13}$ reaction using a thin Po alpha-source and then Be target was measured by the proton recoil method in Kodak NTA nuclear emulsions. The target was 0.25 mg/cm² thick. Photographic plates were mounted about 10 cm from the target in the forward, backward and 90° positions. To date 308 acceptable tracks have been measured in the forward direction and 321 tracks in the backward direction. Four neutron groups were found and were labeled A, B, C and D. Group A corresponds to a transition to the ground state in C^{13}. The Q of the reaction for transition to the ground state used was 5.76 Mev. Table I gives the results of the experiment. E_n is neutron energy and ϵ is the energy in C^{13} above the ground state.

TABLE I.

Group	Forward direction			Backward direction		
	E_n	Q	ϵ	E_n	Q	ϵ
A	—	—	—	7.37	5.80	−.04±.2
B	6.30	1.37	4.4±.2	3.70	1.44	4.3 ±.2
C	3.30	−1.34	7.1±.4	—	—	—
D	2.35	−2.16	7.9±.6	—	—	—

Q11. Interaction of Fast Neutrons with Nitrogen.* C. H. JOHNSON AND H. H. BARSCHALL, *University of Wisconsin.*—Using the method previous described,[1] cross sections for the $N^{14}(n, p)C^{14}$ and $N^{14}(n, \alpha)B^{11}$ reactions were determined for neutron energies from 150 to 2100 kev. Neutrons from the $Li^7(p, n)Be^7$ reaction entered a nitrogen-filled ionization chamber whose axis was at 30° to the proton beam. A "long counter," also at 30°, monitored the neutron flux. Disintegrations in the ion chamber were counted by observing pulses larger than biases set in accordance with pulse height distributions found using a differential discriminator. Resonances were observed in the (n, p) reaction at 500, 640, 995 and 1415 kev; and in the (n, α) reaction at 1415 and 1800 kev. The same resonances produced by the second neutron group from the $Li^7(p, n)Be^7$ reaction indicate that the excited state of Be^7 lies 431±5 kev above the ground state and that the intensity of neutrons relative to the main group of neutrons at 30° is 9, 10, and 12 percent at proton energies of 2.75, 2.89, and 3.66 Mev, respectively.

* Work supported by the AEC and the Wisconsin Alumni Research Foundation.
[1] H. H. Barschall and M. E. Battat, Phys. Rev. 70, 245 (1946).

Q12. Energy Level at 31 kev in Al^{28} from $Al^{27}(d, p)Al^{28}$ Reaction.* H. ENGE,** D. M. VAN PATTER, W. W. BUECHNER, AND A. SPERDUTO, *Massachusetts Institute of Technology.*—The $Al^{27}(d, p)Al^{28}$ and $Al^{27}(d, \alpha)Mg^{25}$ reactions have been studied by bombarding thin aluminum targets with 1.2-, and 1.8-Mev deuterons. Protons emerging at 90 degrees with the incident beam were analyzed in a 180-degree single focusing magnetic spectrometer using nuclear-track plates as recorders. The proton group in the expected position for the Al^{28} ground state appeared to be double. Two alpha-particle groups from $Al^{27}(d, \alpha)Mg^{25}$ were observed on the same plates, and each was single within the present resolution of the apparatus. The high-energy member of the proton doublet was assigned to the ground state of Al^{28} with a measured $Q = 5.494 \pm 0.010$ Mev. The low-energy member was assigned to an excited state at 31.2±2.0 kev with a relative yield of 55 percent of the ground-state yield. The possibility that contaminants in the target produced one of the proton peaks was ruled out by voltage shift and by test runs on magnesium and silicon targets. The relative-yield figure does not change appreciably with changes in the bombarding energy from 1.2 to 1.8 Mev.

* This work has been assisted by the joint program of the ONR and AEC
** On leave of absence from the University of Bergen, Bergen, Norway

SATURDAY AFTERNOON AT 2:00

Breasted Hall

(E. M. LYMAN presiding)

Reactions of Transmutation Concluded: Photon-Induced Nuclear Reactions

R1. Energy Levels of Si^{28} Excited by Alphas on Mg^{24}.*† S. G. KAUFMANN, F. P. MOORING, L. J. KOESTER, AND E. GOLDBERG, *University of Wisconsin.*—Energy levels of Si^{28} have been studied at this laboratory by means of the bombardment of Al^{27} by protons.[1,2] When analysis of the results proved ambiguous, it was thought that alphas on Mg^{24} would offer a simpler approach to the problem. Alphas particles produced by the Wisconsin electrostatic generator were used to bombard thin $Mg^{24}F_2$ targets evaporated onto spectroscopically pure graphite backings. The reaction products separated by a 90° magnetic analyzer were observed at a laboratory angle of 164°±5°. Excitation curves for the reaction $Mg^{24}(\alpha, \alpha)Mg^{24}$ and $Mg^{24}(\alpha, p)Al^{27}$ have been obtained. The $Mg^{24}(\alpha, p)Al^{27}$ and the $Al^{27}(p, \alpha)Mg^{24}$ yield curves[2] show an excellent correspondence in structure. A preliminary Q-value of −1.62 Mev for the reaction $Mg^{24}(\alpha, p)Al^{27}$ has been obtained.

* Work supported by the AEC and the Wisconsin Alumni Research Foundation.
† Mg^{24} was produced by the Y-12 Plant, Carbide and Carbon Chemicals Corporation, on allocation by the Isotopes Division of the AEC.
[1] Bender, Shoemaker, Kaufmann, Bouricius, Phys. Rev. 75, 273 (1949).
[2] Shoemaker, Faulkner, Kaufmann, Bouricius and Mooring (to be published).

R2. Magnetic Analysis of the $P^{31}(d, \alpha)Si^{29}$ and $Si^{30}(d, p)Si^{31}$ Reactions.* P. M. ENDT,** D. M. VAN PATTER, AND W. W. BUECHNER, *Massachusetts Institute of Technology.*—The Q-values of eight hitherto unobserved alpha-particle groups due to the $P^{31}(d, \alpha)Si^{29}$ reaction, corresponding to the ground state and to seven excited states of Si^{29}, have been determined with a magnetic spectrometer by bombardment of a thin zinc-phosphate target with 1.8-Mev deuterons. These Q-values, accurate to about 20 kev, are: 8.170; 6.884; 6.126; 5.727; 5.086; 4.539; 4.080; and 3.211 Mev. These values have not been corrected for possible surface contamination. The level scheme of Si^{29} was checked by bombarding a thin quartz target with 1.8-Mev deuterons and measuring the energies of seven proton groups resulting from the $Si^{30}(d, p)Si^{31}$ reaction. The Q-values for this reaction, accurate to about 10 kev, are: 6.246; 4.973; 4.224; 3.820; 3.180; 2.626 and 1.312 Mev, in reasonable agreement with the recent range measurements of Motz and Humphreys.[1] The positions of the excited states of Si^{29} found from the $P^{31}(d, \alpha)$ and the $Si^{30}(d, p)$ reactions agree within 25 kev.

* This work has been assisted by the joint program of the ONR and AEC.
** On leave from the University of Utrecht, Holland.
[1] H. T. Motz and R. F. Humphreys, to be published.

R3. Preliminary Investigation of Ion Recoil Energy Following K-Capture Disintegration of A^{37}.* G. W. RODEBACK AND J. S. ALLEN, *University of Illinois.*—Using the recently determined $A^{37}-Cl^{37}$ mass difference[1] and assuming conservation of momentum by a neutrino and the nucleus, the K-capture disintegration of A^{37} should give an energy of about 10 e.v. to the recoil nucleus.

An attempt to verify this by a time-of-flight measurement of the Cl^{37} ions has been made using a gaseous source of A^{37} at sufficiently low pressures. The initiating event is taken as the emission of an Auger electron following K-capture and is detected by an electron multiplier. The Cl^{37} ion traverses a field-free distance, and after a rapid acceleration is detected by a second electron multiplier. Counts are made of delayed coincidences which are recorded simultaneously over 18 consecutive time intervals by a multi-channel analyzer.[2]

Present results give a peak on the coincidence-count *versus* time-delay curve which agrees as to position and spread with the predicted values. The additional peaks which occur at later times are not believed to be instrumental in nature and are being further investigated. The zero-time coincidences which occur are probably due to photons emitted by part of the disintegrations.

* Assisted by the joint program of the ONR and the AEC.
[1] H. T. Richards and R. V. Smith, Phys. Rev. 74, 1257 (1948).
[2] Recently developed by J. S. Allen and P. B. Smith.

R4. Proton Bombardment of Copper. C. W. MALICH AND J. C. HARRIS,* *Naval Research Laboratory.*—The Naval Research Laboratory Van de Graaff has been used to bombard copper targets with protons ranging in energy from 1 to 2 Mev. A hard gamma radiation is observed. The thick target yield increases nearly exponentially; no sharp resonances have been observed. At 2 Mev the yield is comparable to that from a thick aluminum target. The energy of the gamma-ray is estimated as roughly the same as the $Al(p, \gamma)$ radiation. Preliminary checks for contamination effects have disclosed no appreciable ones.

* Now at Ohio State University.

R5. The Reaction $Mn^{55}(p, n)Fe^{55}$.* J. J. G. MCCUE AND W. M. PRESTON, *Massachusetts Institute of Technology.*—Protons from the Rockefeller electrostatic generator at M.I.T. have been used to bombard Mn^{55}. The proton energies ranged from the threshold near 1.2 Mev up to 2.05 Mev with a resolution of 4 kev, and up to 2.72 Mev with a resolution of 15 kev. The experiment gives information about the (p, n) resonance levels in the compound nucleus Fe^{55}. Below 1.75 Mev, a number of isolated peaks in the yield curve rise from a weak continuum. The half-widths of these peaks are equal to the resolution used, showing that the level widths are less than 4 kev. Above 1.75 Mev, the spacing of the peaks decreases abruptly and the individual resonances are no longer resolved from one another.

* This work was partially supported by a joint program of the ONR, BuShips, and the AEC.

R6. A Method for the Study of γ-p Reactions.* J. HALPERN AND A. K. MANN, *University of Pennsylvania.*—Scintillation counters have been applied to the detection of photo-protons resulting from targets bombarded by the X-ray beam of the University of Pennsylvania 25 Mev betatron. Each detector consisted of an RCA 5819 photo-tube, a silver activated ZnS screen supported in a vertical plane by a glass backing, and an hemispherical aluminum reflector containing a thin window to permit the entrance of photo-protons. Two counters, operated independently, were contained in a scattering chamber completely shielded by 4 inches of lead, through which the collimated X-ray beam passed. With this arrangement, integral bias curves obtained without a target show the background to be X-ray pile-up plus a small heavy particle component which does not exceed 0.1 counts per *r*. Increased pile-up due to X-ray scattering from targeta does not interfere with the detection of heavy particles. The heavy particles resulting from irradiation of targets have been identified as protons by several methods. This apparatus is applicable to the measurement of $\gamma-p$ excitation functions, angular distributions and yields.

* Supported in part by the joint program of the ONR and AEC.

R7. Yields of Photo-Protons from Various Elements.* A. K. MANN AND J. HALPERN, *University of Pennsylvania.*—The techniques described in the preceding abstract have been used for a study of the relative yields of photo-protons from various elements. Elements investigated were in the form of metal foils of natural isotopic composition. Foil thicknesses were chosen such that target absorption was approximately the same (5 Mev) for all targets. The experimental arrangement allowed targets to be irradiated successively under constant conditions. The data of the experiment are a series of integral bias curves, each curve corresponding to a given target. The relative yields of photo-protons are determined from a comparison of the integral bias curves. Preliminary data on eighteen elements ($Z \leq 50$) indicate that the relative yield increases by a factor of approximately 100 as Z increases from 4 to 28, and then decreases to a value, at $Z = 50$, about one-tenth that of the maximum at $Z = 28$. The relative yield data obtained in this experiment can be compared directly with the known data for photoneutrons.

* Supported in part by the joint program of the ONR and AEC.

R8. Average Photo-Neutron Resonance Energy in Cu^{63} and C^{12}. H. W. KOCH, J. MCELHINNEY, AND J. A. CUNNINGHAM, *National Bureau of Standards.*—The absorption coefficients for the x-rays producing the $Cu^{63}(\gamma, n)Cu^{62}$ and the $C^{12}(\gamma, n)C^{11}$ reactions have been measured. X-rays from a 50-Mev betatron were confined by a lead aperture to a cone whose apex angle was 15 minutes. $\frac{1}{16}$" square monitors and detectors of the element under investigation were placed in the x-ray cone at 146 cm and 546 cm respectively from the x-ray target. Absorbers of lead and aluminum were placed immediately behind the monitor sample, so that the maximum scattering angle at the absorber subtended by the detector was only about 30 minutes. The observed absorption curves were exponential having the following absorption coefficients: in aluminum absorbers, $\tau = .0220(\pm.0004)$ cm²/g for the Cu^{63} resonance; in lead absorbers, $\tau = .0592(\pm.0005)$ cm²/g for the Cu^{63} resonance and $\tau = .0643(\pm.0013)$ cm²/g for the C^{12} resonance. On the basis of these coefficients and the absorption curves as functions of energy in lead and aluminum supplied by Miss Gladys White, the average energy for the Cu^{63} photo-neutron resonance is given as 17.2 ($\pm.4$) Mev and that for C^{12} as 22.1 (± 1.5) Mev. The details of the experiment will be presented and a comparison of the results will be made with the values found by other methods.

R9. Nuclear Excitation of Indium^{115} by Thin Target X-Rays. EDWIN J. SCHILLINGER, JR.,*† B. WALDMAN AND W. C. MILLER, *University of Notre Dame.*—Energy levels in the In^{115} nucleus have been investigated over the energy range of 1.0 Mev. to 2.3 Mev. by means of the continuous x-ray spectrum produced by mono-energetic electrons incident upon thin targets. Conclusive evidence for levels at 1.08 ± 0.02 Mev., 1.47 ± 0.02 Mev., and 1.60 ± 0.02 Mev. has been found. The first two of these levels are a corroboration of the results of Miller and Waldman[1] while the third is reported for the first time. The isochromat theory of Guth[2] has been further verified from threshold to 1.47 Mev. Above 1.65 Mev. the evidence indicates closely spaced levels of small cross sections and/or a breakdown in the isochromat theory. An over-all cross section of about 10^{-24} cm² has been computed for the process at 1.4 Mev., using a gold foil of 30 mg./cm². The investigation em-

ployed a magnetic deflection technique. This work was partially supported by the joint program of the ONR and AEC.

* Now at De Paul University, Chicago, Illinois.
† This work was performed under an AEC Predoctoral fellowship.
[1] W. C. Miller and B. Waldman, Phys. Rev. **75**, 425 (1949).
[2] E. Guth, Phys. Rev. **59**, 325 (1941).

R10. X-Ray Excitation of Ag^{107} and Ag^{109}. E. J. Wolicki,* B. Waldman, and W. C. Miller, *University of Notre Dame.*—X-rays, produced by electrons from the Notre Dame Electrostatic Generator, were used to excite the separated isotopes of silver to their respective metastable states. The electron energy was varied between 0.8 Mev and 2.3 Mev. The thresholds for x-ray excitation of both Ag^{107} and Ag^{109} were found to be below 0.80 Mev. An activation level in Ag^{107} was found at 1.285±.018 Mev. An activation level in Ag^{109} was found at 1.210±.018 Mev. The over-all cross section (i.e., per incident electron on thick gold target) is of the order of 10^{-34} cm² for both isotopes at 1.4 Mev. The activity of each isotope was followed for about seven half-lives. The half-life of Ag^{107} † was found to be 44.0±1.0 sec. The half-life of Ag^{109} † was found to be 40.0±1.0 sec. These measurements are in agreement with those of Bradt *et al.*[1] and the isotope assignment of Helmholtz.[2] This research was supported in part by the Joint Program of the ONR and AEC. The separated isotopes were furnished by Dr. A. C. Helmholtz, Radiation Laboratory, University of California.

* AEC Predoctoral fellow. Now at University of Iowa.
[1] Bradt *et al.* Helv. Phys. Acta **20**, 153 (1947).
[2] Helmholz, Phys. Rev. **70**, 982 (1946).

Saturday Afternoon at 2:00

Eckhart 133

(R. L. Sproull presiding)

Thermionic Emission and Allied Topics

S1. The Non-periodic Deviation from the Classical Schottky Effect.* E. A. Coomes and W. B. LaBerge *University of Notre Dame.*—The Guth-Mullin theory[1,2] for deviations from the Schottky law for thermionic emission has satisfactorily accounted for observed periodic deviations.[3] This theory also contains a monotonic term which causes the predicted slope of the Schottky line to decrease with applied field, rather than remain constant as given by classical theory. At 1500 deg. K this non-periodic deviation should be about 1.5 percent for the reflection effect alone[1] and decrease to a much smaller value when the tunnel effect is included in the theory.[2] Accurate Schottky plots taken on polycrystalline tantalum filaments at 1500 deg. K seem to show deviations of this type. When the patch effects are taken into account, the effect is of the order of one percent.

* This work was sponsored by U. S. Navy Bureau of Ships.
[1] E. Guth and C. J. Mullin, Phys. Rev. **59**, 575 (1941).
[2] E. Guth and C. J. Mullin, Phys. Rev. **61**, 339 (1942).
[3] See e.g., R. L. E. Seifert and T. E. Phipps, Phys. Rev. **53**, 493 (1938).

S2. Schottky Deviations for Polished Tantalum.* G. B. Finn and W. B. LaBerge, *University of Notre Dame.*—Periodic Schottky deviations in thermionic emission from patchy surfaces of polished tantalum have been investigated for fields up to 50,000 volts/cm at a temperature of about 1500°K. The phase and amplitude of the deviations were found to be in substantial agreement with the theory.[1] The Schottky line showed the two changes in slope predicted by patch theory.[2] Deviations were computed using the experimental slope appropriate to the field region. This data on polished tantalum is in good agreement with previous data on unpolished tantalum[3] indicating that polishing does not alter the phase or amplitude of the deviations from the Schottky line nor the occurrence of patch breaks.

* This work sponsored by the U. S. Navy Bureau of Ships.
[1] E. Guth and C. J. Mullin, Phys. Rev. **59**, 575 (1941).
[2] J. A. Becker, Rev. Mod. Phys. **7**, 95 (1935).
[3] Coomes, Munick, and LaBerge, Phys. Rev. **79**, 233 (1950).

S3. Schottky Deviations for Thoriated Tungsten.* E. G. Brock and Fr. Houde, *University of Notre Dame.*—Measurements of the thermionic emission from thoriated tungsten in the Schottky region have been made on a 5-mil filament with fields up to 150,000 volts-cm^{-1}. This filament was studied after being flashed to the clean state and also when contaminated by diffusing thorium onto the surface. The filament temperature range was 1000°K to 1800°K for both clean and contaminated conditions. Periodic deviations and patch breaks in the Schottky line were found which are in substantial agreement with those observed for tantalum by Coomes, Munick, and LaBerge.[1]

* This work sponsored by the U. S. Navy Bureau of Ships.
[1] Coomes, Munick, and LaBerge, Phys. Rev. **79**, 233 (1950).

S4. Thermionic Emission from a Single Crystal Copper Cathode.* David W. Juenker, *University of Notre Dame.*—Preliminary Schottky emission data have indicated that precise thermionic measurements on a single crystal copper cathode surface may be possible. A copper anode and cathode of identical crystal orientation were mounted with plane parallel surfaces 1 mm apart in a diode. The crystals were grown from seed by the Bridgman method. Outgassing was accomplished by heating to 900°C for about 100 hours, by means of the radiation from a tungsten filament. With measuring apparatus found satisfactory in previous Schottky deviation work,[1] a Schottky plot was obtained. The thermionic current at about 900°C was of the order of 10^{-11} amp. cm^{-2}, which agrees well with the value computed using Anderson's figure for the work function.[2]

* This work was sponsored by the U. S. Navy Bureau of Ships.
[1] Coomes, Munick, and LaBerge, Phys. Rev. **79**, 233 (1950).
[2] P. Anderson, Phys. Rev. **76**, 388 (1949).

S5. The Electrolytic Preparation of Single Crystal Copper Cathodes for Electron Emission Studies.* G. J. Baldwin, *University of Notre Dame.*—Single crystal cathodes of copper have been prepared for photoelectric and thermionic emission experiments. Cylinders of single crystal copper[1] were mechanically processed by the standard metallurgical method to obtain plane end and side surfaces of desired crystallographic direction. The surfaces were electrolytically polished[2] in order to removed the disturbed mechanically polished layers. Etching was avoided during the unsteady period at the beginning of the anodic polishing period by adjusting the voltage at 2 volts at the start and maintaining that value throughout the run. Finally the emission surfaces were outgassed by vacuum heating. After each step in the preparation of the cathodes the

emission surfaces were examined by x-ray and photo-micrograph in order to determine the effect of the process on the surface condition.

* This work was sponsored by U. S. Navy Bureau of Ships.
[1] A. A. Petrauskas and F. Gaudry, J. App. Phys. 20, 1257 (1949).
[2] P. A. Jacquet, Nature 135, 1076 (1935).

S6. Thermionic Emission Properties of Barium Sulfide.* W. GRATTIDGE, *University of Missouri.*—Barium sulfide as a thermionic emitter has been investigated previously[1,2] though in no quantitative manner. Specimens of BaS have been prepared by heating either the hydrosulfide or the sulfate in a reducing atmosphere at temperatures of 800°C and 1200°C respectively. Using the materials as cathodes on 1001 pure nickel base metal in diodes with plane parallel geometry, Richardson plots indicate a work function for all specimens of 2.2 ev with A constant varying between 4150 and 0.29 depending on the age of the specimen and the method of preparation. The products of evaporation from a heated barium sulfide-coated platinum ribbon have been examined in the mass spectrometer. This study indicates the formation of some oxide after contact with air. The variation of material evaporated as a function of temperature, assuming the ionization probabilities of the sulfide and oxide to be approximately the same, shows the sulfide to be considerably less volatile than the oxide. The latent heat of vaporization of the sulfide is about 97 kcal mole^{-1}.

* Supported in part by the ONR.
[1] O. W. Richardson, Phil. Mag. 22, 669 (1911).
[2] G. W. Fox and F. M. Bailey, Phys. Rev. 59, 174 (1941).

S7. Correlation of D.C. and Microsecond Pulsed Emission.* FRANK A. HORAK, *University of Missouri.*—D.c. and microsecond pulsed emissions, using plane parallel geometry diodes, were investigated for (BaSr)O coated cathodes on base metals of pure nickel, 0.2 percent Si-Ni, 4 percent Si-Ni, and 4.6 percent W-Ni. Zero field thermionic emissions were determined by (1) d.c. retarding potential, (2) d.c. Schottky, and (3) pulsed Schottky plots. All tubes were life-tested under quiescent conditions at 1125°K. Richardson plots were used to determine the work functions and the A constants. Comparison was made of the characteristic emission current density values, j_0 at 650°K. This temperature is in range over which both d.c. and pulsed currents were measurable. This range of current overlapping was about one order of magnitude in most cases. The work function and the A constants obtained by the three above mentioned methods were essentially the same. The most active cathodes were those of the W-Ni base metal, and the least active were those of pure nickel and the 0.2 percent Si-Ni. X-ray diffraction methods were used to confirm the presence of an interface. A possible explanation will be presented for the observed dependence of emission on type of base metal and life in terms of interface formation.

* Supported in part by ONR.

S8. The Evaporation of BaO from Pt, Ta, W, Mo, and Ni.* L. T. ALDRICH,† *University of Missouri.*—The material evaporated from various base metals coated with BaO and heated over wide ranges of temperature has been studied with a high resolution mass spectrometer. The results of the temperature variation indicate that more than 99 percent of the material evaporated from the BaO-Pt system is BaO and an even greater proportion of that evaporated from the BaO-Ta system is Ba. In order of decreasing Ba/BaO evaporated, the base metals were Ta, W, Mo, Ni, and Pt respectively. The relative amount of BaO evaporated was found to depend on the amount of low temperature aging in the first three of these. High mass peaks which are attributed at least in part to evaporation have been identified as: Ba_2O^{++}, Ba_2O^+, $Ba_2O_2^+$, on all metals but Ta, and $BaMoO_4^+$, $BaWO_4^+$, and $BaTaO_3^+$ have been found on Mo, W, and Ta respectively. No barium compounds containing Ni or Pt were found. Isotopic identification of these compounds was possible in most of the above cases.

* Supported in part by the ONR.
† Present address: Department of Terrestrial Magnetism, Washington, D. C.

S9. Conductivity Measurements of (BaSr)O.* J. R. YOUNG, *University of Missouri.*—Conductivity measurements of (BaSr)O on base metals of Pt, pure Ni, and Mg-Ni have been made at different temperatures in order to test the predictions of the recent Vink-Loosjes theory.[1] The tube design was similar to that used by Vink. Conductivity was determined from d.c. voltage-current characteristics over the temperature range 1150°K to 260°K at different states of activity. The experimental results do not agree in the following respects with those reported by Vink. (1) In many cases there is no difference in the general shape of the V-I curves over the temperature range studied. (2) The low temperature break in the curve $\ln\sigma$ *vs.* $1/T$ does not appear at 800°K except in low states of activity; in some cases it occurs as low as 550°K. (3) Corrections applied by assuming the low temperature (region 1) conduction mechanism to be in parallel with the higher temperature (region 2) conduction mechanism do not change the slope of region 2 to agree with the probable work function in many cases. Also this correction affects only a portion of region 2 introducing still another break if applied.

* Supported in part by ONR.
[1] Loosjes and Vink, Philips Res. Rep. p. 449, December, 1949.

S10. Emission of Neodymium and Neodymium Oxide Ions from a Hot Filament Source. R. G. JOHNSON AND W. C. CALDWELL, *Iowa State College.*—With Nd_2O_3* on a tungsten filament in the source of a mass spectrometer NdO^+ ions may be detected when the filament is below 1850°C. If the temperature is increased to 1850°C and the pressure is maintained below 10^{-6} mm of mercury, Nd^+ ions are observed. With the temperature of the filament still 1850°C and the pressure increased above 10^{-6} mm of mercury NdO^+ ions appear; the relative abundance of NdO^+ ions to Nd^+ ions increases as the pressure increases. These effects are interpreted to mean the removal of either oxygen from the neodymium oxide lattice or adsorbed oxygen from the surface of the neodymium oxide under the conditions of elevated temperature and reduced pressure. The measurements are being extended to attempt to verify the Born cycle for neodymium by measuring the work functions for the neodymium ion, the neutral neodymium atom, and the electron from neodymium oxide and by using the available value for the ionization potential of neodymium.

* Dr. F. H. Spedding kindly furnished the neodymium oxide.

S11. Experiments Relating to the Interaction of Slow Electrons and Surface Films of Potassium Chloride. DIETRICH DOBISCHEK AND HAROLD JACOBS, *Evans Signal Laboratories.*—Experimental diodes were constructed which contained a rotating anode, an oxide-coated cathode and a potassium chloride source. The ionic crystal was evaporated to the anode, to form an uncontaminated surface film. The film was then rotated in front of a previously activated oxide cathode, from which thermionic emission could be obtained. The potassium chloride film was bombarded by electrons with energies ranging between 0.5 ev to 20 ev. It was found that when electrons attained an energy equivalent to the heat of formation of the potassium chloride, decomposition of the alkali chloride occurred. This was illustrated by a sharp and characteristic "slumping" cathode emission at 4.5 ev. In addition, several smaller peaks of rising and falling cathode emission were measured at lower characteristic anode voltages (1.0 ev and 2.5 ev).

S12. Interpretation of the Interaction of Slow Electrons and Surface Films of Potassium Chloride. HAROLD JACOBS AND DIETRICH DOBISCHEK, *Evans Signal Laboratories.*—In the

bombardment of thin films of potassium chloride, it was found that at critical anode energies the electron emission from the cathode was affected. At the energies of about 1.0 and 2.5 ev, either rising emission or falling emission of a temporary nature was observed. At 4.5 ev, the cathode was relatively, permanently damaged with respect to its thermionic emission. By means of several types of calculations, it was shown that charges, due to trapped electrons in the surface film of potassium chloride, could enhance or lower the current from the cathode. At critical kinetic energies of the bombarding electrons, 1.0 and 2.5 ev, the electrons trapped in the potassium chloride could be released, resulting in a rising cathode current. The energies required for the release of the trapped electrons by bombarding electrons were found to be very near the same as the energies required by photons, as described by Hilsch and Pohl in their work on F centers and F′ centers in potassium chloride. It was further concluded that the electron affinity of the evaporated ionic crystal must be very small, i.e., <0.5 ev.

SATURDAY AFTERNOON AT 2:00

Kent Theatre

(CLARENCE ZENER presiding)

Invited Paper

T1. Dislocations and Lattice Defects. FREDERICK SEITZ, *University of Illinois.* (30 min.)

Solids Other Than Metals

T2. Some Optical Properties of NaCl:Pb Phosphors. JAMES H. SCHULMAN, ROBERT J. GINTHER, AND CLIFFORD C. KLICK, *Naval Research Laboratory.*—Absorption and luminescence phenomena in NaCl:Pb phosphors have been found to be rather complex. Melt-grown NaCl:Pb has an asymmetrical, 2730A-peaked absorption band. The variation of emission spectrum with wave-length of excitation within this band shows that it consists of two poorly resolved absorption bands, one peaking at 2730A and the other at 2900A. At low lead concentrations, irradiation into the first of these causes a near ultraviolet emission peaking at 3200A; irradiation into the second causes a visible emission peaking at about 4500A. At high lead concentrations, irradiation into the first band gives a second near ultraviolet emission band peaking at 3850A in addition to the one peaking at 3200A. Precipitated NaCl:Pb shows all the above phenomena, and in addition, has an excitation band peaking at 2600A, producing simultaneously a 3300A-peaked emission and a visible emission. The NaCl:Pb phosphors are unstable, deteriorating after a few days at room temperature and more rapidly at 130°. X-irradiation of these phosphors destroys the above absorption and emissions, and gives a print-out effect due apparently to the formation of colloidal lead. The x-rayed material can be excited by near ultraviolet to give a red emission, peaking at about 6100A.

T3. Exciton-Enhanced Photoelectric Emission from F-Centers in Alkali Iodides near 85°K. L. APKER AND E. TAFT, *General Electric Research Laboratory.*—The frequency variation of an exciton-enhanced photoelectric emission from F-centers in KI has been measured at 300°K in previous work.[1] The photoelectric yield showed a sharp peak at $h\nu = 5.66$ ev, a point practically coincident with the first fundamental optical absorption maximum of KI. At 85°K this absorption peak shifts to about 5.80 ev and becomes sharper, as shown by Fesefeldt; the photoelectric yield, however, then shows two maxima separated by a sharp minimum near the optical peak. Thus, it appears that the yield at first increases with increasing optical absorption, reaches a maximum for an absorption constant near 10^6 cm^{-1}, and decreases as the absorption increases further. An explanation may be based on a hypothesis used by Fano[2] in another connection. He suggests that excitons are destroyed at free surfaces. A sparsity of F-centers near the surfaces of these samples may also be involved. Optical absorption data and similar photoelectric results will be given for RbI, for which a quantitative treatment has been worked out by Hebb.

[1] Apker and Taft, Phys. Rev. 79, 964 (1950).
[2] U. Fano, Phys. Rev. 58, 544 (1940).

T4. Mechanism of Exciton-Enhanced Emission of Photo-Electrons in RbI. MALCOLM H. HEBB, *General Electric Research Laboratory.*—The yield of photo-electrons from RbI observed by Apker and Taft (preceding abstract) is discussed. The reversal near the first maximum in the optical absorption is interpreted with the following model. Excitons produced by absorption of photons in the crystal diffuse without loss of energy to F-centers where they eject electrons and are annihilated. Age theory is used to treat the diffusion of the electrons from their points of origin with gradual loss in energy. It is assumed that an electron reaching the surface with sufficient energy to escape is certain to do so. Destruction of excitons by competing processes at the surface can lower the yield of electrons originating near the surface and give the reversal in total yield when the optical absorption length is small. A paucity of F-centers near the surface can also contribute to the effect. To fit the observations, it is necessary to assume a dead layer at the surface ~140A thick. The length characteristic of electron escape is ~40A. The mean free path of the electrons in the slowing down process is ~10A.

T5. On the Transition Probability for Photoelectric Emission from Semiconductors. H. B. HUNTINGTON* AND L. APKER, *General Electric Research Laboratory.*—An adaptation of Makinson's[1] theory of photoelectric emission from metals is used to treat simple semiconductor models. In one case, a (100) surface of a simple cubic structure is considered. The probability of excitation from a state of initial energy ϵ lying near ϵ_0, the top of an occupied band, is found to be proportional to $\epsilon_0 - \epsilon$. For a density of states having the normal form, $n(\epsilon) \propto (\epsilon_0 - \epsilon)^{\frac{1}{2}}$, the energy distribution of the emitted electrons is thus dominated at higher energies by a factor $(\epsilon_0 - \epsilon)^{\frac{1}{2}}$. Since this result is in good agreement with experimental results obtained for *Te* and other monatomic semiconductors, it is suggested that the relation derived above holds also for these more complicated crystals. This point of view permits a unique interpretation of the graphical techniques previously used in analyzing photoelectric data and assigns a theoretical value of $\frac{1}{2}$ to the parameter m.[2]

* Work done on summer leave from Rensselaer Polytechnic Institute.
[1] R. E. B. Makinson, Phys. Rev. 75, 1908 (1949).
[2] Apker, Taft, and Dickey, Phys. Rev. 74, 1462 (1948).

T6. Fermi Levels in Semiconductors. GUY W. LEHMAN, *Purdue University.*—In nucleon-irradiated semiconductors additional donator and acceptor states appear.[1] The Fermi level changes as a function of the total number N of defects intro-

duced. When more donator levels than acceptor levels are introduced, *P*-type material changes to *N*-type during bombardment. For equal numbers of donators and acceptors (interstitial and lattice vacancies) produced, with activation energies of 0.15 ev and 0.05 ev respectively, the Fermi level in all cases approaches the limiting value 0.275 ev above the middle of the forbidden gap as *N* increases: initially *N*-type material is converted to *P*-type material and initially *P*-type material shows decreasing resistance if the initial concentration of impurities is moderate as observed in Ge. A model corresponding to bombardment-induced transmutations[2] producing three acceptor impurities for each donator shows that *N*-type material is converted into *P*-type and *P*-type material shows decreasing resistance, again as observed in Ge after heat treatment to remove lattice imperfections.

[1] K. Lark-Horovitz, *et al.*, Phys. Rev. **73**, 1256(A) (1948).
[2] Cleland, Lark-Horovitz, and Pigg, Phys. Rev. **78**, 814(L) (1950).

T7. The Preparation of Thin Films of NiO with Lithium Impurity.* N. C. JAMISON AND T. R. KOHLER, *Philips Laboratories, Inc.*—Verwey, Haayman, and Romeyn[1] have shown that by substituting Li for Ni in the NiO lattice the conductivity of the oxide may be varied through a wide range; conventional sintering methods were used and the electrical properties of materials containing up to 9 atomic percent Li were reported. In the present work mixtures of Ni and Li were laid down on polished fused quartz disks by simultaneous vacuum deposition. The metallic films were converted to the oxide by heating to 500°C in a stream of N_2 containing a small amount of O_2. Satisfactory semiconducting films were obtained in the thickness range from a few hundred to 3000A. The lithium content was varied from 2 to 48 atomic percent; the composition was established by chemical means. X-ray measurements made on an NiO film yielded the lattice constant 4.17(1)A in good agreement with other determinations for NiO. From the sharpness of the diffraction lines it was estimated that the size of the crystallites was about 1000A.

* Supported in part by the ONR.
[1] Verwey, Haayman, and Romeyn, Chem. Weekblad **44**, 705 (1948); also Philips Research Reports **5**, 173 (1950).

T8. The Electrical Properties of Thin Films of NiO with Lithium Impurity.* T. R. KOHLER AND N. C. JAMISON, *Philips Laboratories, Inc.*—Resistance measurements made on 38 semiconducting films of $Li_xNi_{1-x}O$ established the relationship between the resistivity and the lithium content in the range, 2 to 48 atomic percent. The curve shows a broad minimum in the neighborhood of 30 atomic percent, the minimum value of resistivity being 5Ω-cm. The temperature coefficient of resistance was measured for the interval 30 to 60°C; the value of B in the expression $\sigma = A' \exp -B/T$ decreased from 3800°K to 2600°K with increasing lithium content (2 to 48 atomic percent). A plot of $\log A'$ as a function of the lithium content has a maximum value corresponding to about 28 atomic percent. The shape of the curve is approximately the same as the log of the product, $(Ni^{++} \times Ni^{+++})$, plotted as a function of lithium content if it is assumed that for each Li substitution one nickel ion becomes trivalent. Six samples on which thermoelectric measurements were made (lithium content <30 atomic percent) indicated hole conduction. The results of noise measurements and resistance at high frequency will also be reported.

* Supported in part by the ONR.

T9. The Temperature and Pressure Dependence of the Dielectric Constant of Cubic Crystals. E. BURSTEIN, PAUL L. SMITH, AND B. HENVIS, *Naval Research Laboratory.*—The optical and static molar polarizabilities of most solids, including the alkali halides, are appreciably dependent on temperature and pressure.[1] This arises from the dependence of the frequency and strength of their absorption bands in the ultraviolet and infra-red on the interatomic distance and amplitude of vibration of their atoms. At optical frequencies the contribution to the change in dielectric constant from the change in molar polarizability is generally smaller than the contribution from the change in number of atoms per unit volume except for crystals such as MgO, ZnS, and diamond where the bonding is appreciably homopolar. At low frequencies, however, the contribution from the change in molar polarizability is almost always larger than the contribution from the change in number of atoms per unit volume. The only known exceptions to this among cubic crystals are the thallium halides. The optical processes underlying these phenomena will be discussed.

[1] E. Burstein and P. L. Smith, Ind. Acad. Sci. **28**, 377 (1948); S. Mayburg, Phys. Rev. **79**, 375 (1950); and G. N. Ramachandran, Ind. Acad. Sci. **25**, 481 (1947).

T10. An Attempt to Determine the Degree of Vitrification in Rapidly Cooled Aqueous Solutions.* B. LUYET, *St. Louis University.*—When an aqueous solution, such as a 1-*M* sucrose solution, is cooled at the rate of several hundred degrees per second—by immersion of thin layers (0.01 cm thick) in liquid nitrogen—it "vitrifies" i.e., it solidifies in the amorphous state. If one decreases the concentration of the solute, vitrification becomes increasingly difficult, since the velocity of crystallization increases. An attempt was made to record the degree of incipient crystallization in the following manner: 1. The junction of a thermocouple was inserted in the thin layer of solution to be immersed in liquid nitrogen; 2. The output of the thermocouple was amplified with a d.c. amplifier of a gain of 10,000; 3. The amplified signal was transmitted to a cathode-ray oscillograph and recorded photographically. The freezing curves thus obtained (with about 0.5 mg of solution cooled to −195° in 0.3 sec.) show a clear-cut crystallization plateau at low sucrose concentrations and in pure water; this plateau is less and less marked as the sucrose concentration is increased and it disappears when the concentration reaches about 50 percent.

* Work supported by Research Corporation.

SATURDAY AFTERNOON AT 2:00

Mandel Hall

(E. P. NEY presiding)

Cosmic-Ray Showers; Scintillation Counters; Cloud Chambers

U1. Altitude Dependence of Penetrating Showers. HAROLD K. TICHO, *University of California, Los Angeles.*—A detector of penetrating showers was constructed, which consists of a 1.71-ton lead block with counter trays placed at various levels. The electronic apparatus records penetrating showers and displays counters tripped in the lower trays by means of a hodoscope. To reach the lowest tray a shower particle must penetrate 630 g/cm² of lead. This equipment was flown in a B-29*

at 30,000 feet and at 37,000 feet and was operated at White Mountain (altitude 10,000 feet). At each altitude approximately 10,000 counts were obtained. The decrease of shower intensity with atmospheric depth is exponential with $\lambda = 120$ g/cm² in agreement with Tinlot.[1] The hodoscope data made it possible to classify the showers as to their size, but no significant change from $\lambda = 120$ g/cm² was observed for large showers. Extrapolation to the top of the atmosphere with $\lambda = 120$ g/cm² yields 0.011 primaries (cm² sterad. sec.)$^{-1}$ capable of producing recordable penetrating showers, in fair agreement with rocket results.[2] It appears therefore that the cross section for penetrating shower production in air remains one-half of the geometric cross section up to energies ~30 Bev.

* The flight time was made available by the ONR and the Air Forces.
[1] J. Tinlot, Phys. Rev. **74**, 1197 (1948).
[2] J. A. Van Allen and S. F. Singer, **78**, 819 (1950).

U2. Study of Showers Produced in Lead, Carbon, and Beryllium. G. DEL CASTILLO* AND W. Y. CHANG, *Purdue University*.—The cloud chamber and control unit, previously used for studying absorption of μ-mesons by thin foils,[1] have been set to study showers containing penetrating particles produced in Pb, *c*, and Be. In both series of the following experiments, ten one-inch *c*-plates have been above the chamber. In the first series two one-inch *c*-plates and three ½-inch Pb-plates were alternately placed inside the chamber. Two trays of counters, each connected for coincidence of two particles, were placed vertically underneath the chamber and separated by one-inch Pb. Another tray was put on the top of the chamber to form a fivefold coincidence shower detector. Many of the showers so selected are large showers. In the second series, two one-inch Be-plates and one ½-inch Pb-plate below have been inside the chamber. One tray of counters connected for two particle coincidence was set immediately below the chamber and followed after 3.5-inch Pb by a single tray. Two more trays on the top of the chamber served with the others as a fivefold coincidence unit. More small showers are selected in this way. Showers produced in these three elements will be compared and discussed.

* Supported in part by Purdue Research Foundation and Mexican Research Commission C.I.C.I.C.
[1] W. Y. Chang and J. R. Winckler, Rev. Sci. Inst. **20**, 276 (1949).

U3. Nuclear Interactions in Gold of Secondary Particles emitted in Penetrating Showers.* A. J. HARTZLER, *University of Chicago*.—A large counter-controlled cloud chamber containing 16 gold plates totaling 308 g/cm² in thickness was operated at an altitude of 11,500 feet. The mean free path for nuclear collisions in gold of the ionizing secondary particles was found to be 230 ± 60 g/cm². 17 percent of the nuclear events observed in making this determination were large angle scatterings of a penetrating secondary particle with no observable disintegration products emerging from the gold plate in which the collision occurred. The momenta of secondary particles used in this determination ranged between 10^9 and 10^{10} ev/c and less than 11 percent of them were protons. The lowest energy penetrating shower which has a high probability of tripping the counter coincidence circuit used is estimated to be 1.5×10^{10} ev. 88 ± 3 percent of the penetrating showers observed in the experiment showed the presence of one or more electron cascades. The average multiplicity of high energy penetrating secondaries emitted in nuclear collisions of an average energy of 3×10^{10} ev was found to be 7 ± 1. The corresponding multiplicity of secondary particles of a group of penetrating showers of 6×10^{10} ev average energy was 11 ± 2.

* Assisted by the joint program of the ONR and AEC.

U4. Absorption in Air of Cosmic Radiation Producing Large Bursts under Thick Absorbers at 11,500 Ft. Elevation.* THOMAS G. STINCHCOMB, *University of Chicago*.—Using a Carnegie Model C meter together with counters to detect air showers, experiments on bursts greater than 200 particles under a spherical absorber of 122 g/cm² Pb were carried out at Climax, Colorado. Corrections were made for bursts produced by energetic μ-mesons and by air showers. A barometric coefficient for vertical radiation of -1.9 (± 0.4 percent) per mm Hg was obtained. This is equivalent to an absorption mean free path of 74 ± 17 g/cm². Using an additional iron shield which absorbed radiation entering at zenith angle from 0° to 15°, 22.5°, or 30°, the zenith angle dependence of burst-producing radiation was found to be that resulting from a mean absorption path of 72 ± 13 g/cm². This large absorption indicates that elastic scattering is nearly zero for these energies which are estimated to be 6×10^{10} ev or greater, and that these bursts originate mostly from primary protons. The flux of the burst producing radiation at Climax is extrapolated and found to agree with flux estimates for particles of this energy at the top of the atmosphere.

* Assisted by the joint program of the ONR and AEC.

U5. On the Particles Producing High Energy Nuclear Interactions in Gold.* MELVIN B. GOTTLIEB,† *University of Chicago*.—A large multiplate counter-controlled cloud chamber containing 300 g/cm² of gold was used for the study of penetrating showers at an altitude of 11,500 ft. Showers above a minimum energy of about 15 Bev initiated by both ionizing and non-ionizing particles could be observed. At least 83.5 percent of the shower producing particles (SPP) were found to be ionizing. From the distribution of events in the plates of the chamber, the mean free path in gold of the SPP was found to be 145 ± 3 g/cm². The observed projected zenith angle distribution corresponds to an absorption mean free path in air of 70 to 90 g/cm². The flux of the SPP of $(1.7 \pm 1) \times 10^{-6}$ particles cm^{-2} sec.$^{-1}$ sterad.$^{-1}$, when compared with the flux of primary protons at the top of the atmosphere, yields an absorption mean free path of 77 ± 5 g/cm². It is very unlikely that only a small fraction of the energy of a SPP be lost in the chamber.

* Assisted by the joint program of the ONR and AEC.
† Now at the State University of Iowa.

U6. Particle Localization by Means of a Scintillation Detector.* LUKE C. L. YUAN AND H. L. POSS, *Brookhaven National Laboratory*.—A long tube with flat ends containing scintillation liquid[1] is placed between two photo-multipliers. Neglecting reflection from the side walls, the intensity of light received at a photo-multiplier from a scintillation is proportional to the solid angle subtended by the photo-cathode at the scintillation point. The ratio of two coincident pulses will then determine the location of the scintillation along the tube independent of light intensity (particle energy). The pulse ratio was obtained by feeding one pulse to the vertical deflection plates and the other to the horizontal ones of an oscilloscope and measuring the inclination angle of the trace. The trace amplitude is related to the particle energy dissipated in the liquid. Preliminary results on the localization effect were obtained using cosmic rays. The coincidence pulse from a Geiger-counter telescope perpendicular to the scintillation detector was used to unblank the oscilloscope. Uncertainty resulting from statistical variations of the photo-multipliers were measured by means of a light source placed at various distances between the photo-multipliers to simulate scintillations. Possible applications of the localizer to angular correlation and cosmic-ray measurements will be discussed.

* Work done under the auspices of the AEC.
[1] H. Kallman and M. Furst, Phys. Rev. **79**, 857 (1950).

U7. Scintillation Counter for High Energy Particles.* FRANCIS X. ROSER AND THEODORE BOWEN (*Introduced by* MARCEL SCHEIN), *University of Chicago*.—The purpose of this experiment is to investigate the response of an anthracene crystal to high energy mesons falling into four energy ranges,

going from 13 to 24, 24 to 52, 52 to 147, and greater than 147 Mev. A fourfold Geiger-Müller counter coincidence circuit initiates the sweep of an oscilloscope. The pulses from two scintillation counters are delayed and appear at the sweep together with delayed pulses from Geiger-Müller trays, which determine the range of the mesons in lead absorbers. An efficiency of better than 95 percent has been found. Measurements of the proportionality are under way and will be discussed.

* Assisted by the joint program of the ONR and AEC.

U8. Scintillation Counter Efficiencies at Short Resolving Times.* M. R. CLELAND, C. E. WHITTLE, A. L. HUGHES, AND P. S. JASTRAM, *Washington University.*—When scintillation counters employing organic crystals or solutions and photomultiplier tubes are used in conjunction with fast coincidence circuits for high resolution delayed-coincidence studies of beta- and gamma-rays, it is found that as the resolving time is reduced in the neighborhood of 10^{-9} second a point is reached at which the coincidence counting efficiency diminishes rapidly. This point determines the maximum resolution at which the system is useful. A study of several counter systems reveals that this effect depends upon both the scintillation material and the type of photo-tube used. Typical values for minimum resolving times (loss of $1/e$ of the coincidences) are as follows:

Phosphor	Photo-tube	τ-minimum
Anthracene crystal	RCA 5819	20×10^{-9} sec.
Terphenyl xylene solution	RCA 5819	9×10^{-9} sec.
Terphenyl xylene solution	RCA 1P28	3×10^{-9} sec.

Annihilation gamma-quanta from Na^{22} positrons are used to produce simultaneous excitation of the two counters. The photo-multiplier output pulses are amplified and equalized in height, and are limited in width by reflection in a length of shorted coaxial cable. A conventional crystal-diode coincidence circuit is used. The band width of the circuit is 200 megocycles.

* Assisted by the joint program of the ONR and AEC.

U9. Scintillation Decay Times.* ARNE LUNDBY, *University of Chicago.*—A delayed coincidence circuit has been used for determining the decay times of some scintillation crystals and in a search for delayed nuclear transitions in the region $10^{-10}-10^{-7}$ sec. The coincidence circuit consisted of two 1P21 photo-multipliers, the output pulses from which were fed into 100-ohm coaxial cables terminated at the input of distributed amplifiers. The output from the amplifiers was applied to a germanium diode bridge coincidence circuit. The average lifetimes of 1,4-diphenyl-butadiene and *p*-terphenyl were found to be 4×10^{-9} sec. The rate of decay did not change when 2.5 g (resp. 5.2 g) of *p*-terphenyl was dissolved in one liter of phenylcyclohexane (resp. xylene). Further decay times measured were: *t*-stilbene, 5.7×10^{-9} sec., anthracene, 24×10^{-9} sec., and napthalene, 60×10^{-9} sec. The operation of the coincidence circuit was checked by measuring the time of flight of light over a distance of about one meter, and by determining the decay time of ThC′. When light piping was employed, the resolving power was reduced due to multiple scattering of the photons in the light pipe.

* Supported by the joint program of the ONR and AEC.

U10. Observations on Diffusion Cloud Chambers.* E. C. FOWLER, D. H. MILLER, R. P. SHUTT, AND A. M. THORNDIKE, *Brookhaven National Laboratory.*—Recent studies of the operation of continuously sensitive diffusion cloud chambers[1] seem to establish their usefulness for demonstrations as well as a research tool. The arrangement and operation of such chambers will be discussed. Experiments with different temperature gradients across a diffusion chamber will be described. With a filling of air and methanol and a temperature gradient of 7°C per cm, cosmic-ray tracks near minimum ionization are straight, sharp, and of good contrast. Photographs of cosmic rays and gamma-ray-induced tracks will be shown. No electric sweeping field is necessary when cosmic rays are observed, but radiations five to ten times as strong will make the chamber temporarily insensitive to track production. Here an electric sweeping field greatly speeds up resensitization. The effects of different gases and vapors used in diffusion chambers have been investigated. The most important result is that with gases of low atomic number, such as helium and hydrogen, a diffusion chamber will not behave stably at or near atmospheric pressure, but at higher pressures good results can be obtained.

* Work performed at Brookhaven National Laboratory under the auspices of the AEC.
[1] A. Langsdorf, Rev. Sci. Inst. 10, 91 (1939).

U11. A Continuously Sensitive Cloud Chamber. T. S. NEEDELS* AND C. E. NIELSEN, *Ohio State University.*—A cloud chamber is described which has a thin horizontal layer continuously sensitive to ion tracks. Supersaturation is maintained in this layer by the principle of vapor diffusion from a hot to a cold surface.[1] This sensitive region is close to the cold surface. The chamber as we have used it is a two-liter glass beaker that sits on dry ice, and which is covered at the top with cardboard wet with alcohol. The alcohol is at room temperature and provides the vapor. Either ethanol or propanol works well. The gas is atmospheric air. A vertical electric field is applied across the sensitive region. This field adds more ionizing events to the sensitive region. When vapor diffusion starts there is about a 15-minute wait during which the air is made dust-free by continuous condensation. Electron and proton tracks in a magnetic field have been photographed from above through a glass-covered hole in the cardboard. The light source is an *H*-6 Hg arc lamp behind a glass lens both placed at the level of the sensitive region.

* Now at Los Alamos, New Mexico.
[1] A. Langsdorf, Rev. Sci. Inst. 10, 91 (1939).

U12. Condensation Efficiency of Ions in the Wilson Cloud Chamber. CARL E. NIELSEN AND THEODORE S. NEEDELS, *Ohio State University.*—We have determined visually the minimum expansion necessary for condensation upon ions ("ion limit") in a Wilson cloud chamber using the following alcohols mixed in various proportions with water: ethanol, *n*- and iso-propanol, 1- and 2-butanol, and 1- and 2-pentanol. We have measured photographically condensation efficiency, defined as the fraction of ions of one sign made observable as drops in an expansion, using various mixtures with water of ethanol and *n*- and iso-propanol. The measurement depends upon the count of drops photographed in clusters of positive and negative ions separated by an electric field. It was concluded some years ago: "With mixtures not too far from 70 percent ethyl alcohol, all positive ions serve as condensation nuclei when negative ions begin to be effective. If a field is used to separate positive and negative ions, the presence of a negative track is evidence that all positive ions are represented by drops in the positive track." The same is true of water mixtures with *n*- or iso-propanol, with the qualification that the negative drops must be at least one-fourth as numerous as the positive drops.

U13. Upward Diffusion Cloud Chamber. O. H. WEDDLE AND C. E. NIELSEN, *Ohio State University.*—It is possible to construct two kinds of stable diffusion cloud chambers. The vapor may be diffused downward through a sufficiently dense gas from a hot source on top to a cold plate on the bottom, or the vapor may be diffused upward through a lighter gas from a hot source on the bottom to a cold plate on top. A chamber of

the latter type has been operated; tracks of ionizing particles have been seen and photographed. The chamber consists of a heated glass bottom and cooled metal top with a glass cylinder clamped between. A region sensitive to ions occurs near the top plate. Pictures were taken through the glass bottom. Propyl alcohol vapor and other vapors have been diffused through helium or hydrogen. A mixture of water and propyl alcohol diffused through helium has given the best results. Diffusion cloud chambers must be operated with ionization intensity appropriate to the vapor supply.

U14. Depth of Sensitive Region in Diffusion Cloud Chambers. W. E. NEXSEN, JR., O. H. WEDDLE, AND C. E. NIELSEN, *Ohio State University.*—In the first continuously sensitive cloud chambers studied at this laboratory tracks could be observed in only a very thin region close to the cold surface. In order to increase the usefulness of the chamber we have studied factors influencing depth of sensitive region. We have investigated the use of multivapor systems, the use of various geometries and the use of different temperature gradients. One chamber used consisted of a crystallizing dish inverted in a pie plate containing a pool of *n*-propanol. A watch glass containing a small pool of propanol was suspended within the chamber and close to the top. The apparatus was placed on a block of dry ice and the top heated gently by a lamp. A relatively deep region was obtained in the upward diffusion chamber when a water-alcohol mixture was employed in such a way that the vapor composition was a function of the height. This resulted in a variation of the ion limit with height. When the variation was such that a more favorable vapor mixture occurred lower in the chamber, the sensitive region was considerably deepened.

U15. Wave-Guide Linear Accelerator with Continuous Dielectric Loading. GAIL T. FLESHER AND GEORGE I. COHN, *Illinois Institute of Technology.*—With the advent of the high power klystron, the linear accelerator becomes an increasingly important research tool; thus investigation of new types is in order to further increase its efficiency. This paper examines the continuous dielectric loaded type to determine its practicability for these uses. By the solution of Maxwell's equations in the guide, the accelerating field is found in terms of the physical dimensions, the dielectric and metal characteristics, and the power input. For equal power inputs the accelerating field attainable is found to be comparable to those for the disk-loaded type. A certain characteristic length is found which determines whether operation should be traveling wave or standing wave. Over a certain range, an increase of dielectric constant allows a higher loss tangent to be tolerated. Practical problems such as heat dissipation are considered. Most of the work has been done for the two coaxial region guide, but other promising configurations will be discussed.

SATURDAY AFTERNOON AT 2:00

Rosenwald 2

(LEONA MARSHALL presiding)

Invited Paper

V1. Distribution of Scattered Neutrons from Various Elements. ALEXANDER LANGSDORFF, JR., *Argonne National Laboratory.* (30 min.)

Neutrons

V2. Fast Neutron Cross Sections and the *n-n* Interaction. ROBERT JASTROW, *University of California, Berkeley.*—Nuclear cross sections for fast neutrons[1] have been examined for possible information on the *n-n* interaction. These cross sections level off to constant values above 150 Mev, in place of the continued decrease with increasing energy which would be expected from a finite nucleon-nucleon interaction, providing evidence for a short-range singularity in this interaction. Indirect evidence for the equality of the *n-n* and *p-p* interactions can be obtained from calculations of these high energy plateaus, based on Serber's model of the transparent nucleus.[2] The results are in agreement with experiment for both light and heavy elements provided one assumes $\sigma_{nn} = \sigma_{pp}$. The energy dependence of the neutron-nucleus cross section at intermediate energies agrees reasonably with that calculated from a nucleon-nucleon interaction containing a repulsive core of radius 1.0×10^{-13} cm, but is in qualitative disagreement with calculations based upon the representation of the nucleus by a finite potential well. This work was performed under the auspices of the AEC.

[1] J. DeJuren, University of California, Radiation Laboratory Report UCRL-736.
[2] Fernbach, Serber, and Taylor, Phys. Rev. **75**, 1352 (1949).

V3. Total Cross Sections of Be, B, O, and F for Fast Neutrons.* C. K. BOCKELMAN, *University of Wisconsin.*—Previous studies of the cross sections of Be and O as a function of neutron energy[1] have been extended to higher energies. The cross sections were calculated from transmission measurements. Neutrons were obtained from the Li(p, n) reaction; the effect of the low energy neutron group is believed to have been negligible. In the range from 0.2 to 1.4 Mev, two resonances were found for Be. Three levels in O were observed below 1.4 Mev in good agreement with the results of the Minnesota group;[2] the values of the cross section at the maxima indicate that a compound state with a total angular momentum of $\frac{1}{2}\hbar$ is formed in each case. Similar experiments revealed one level in B for neutron energies below 1 Mev, while evidence for at least seven resonances was found for F in the energy interval from 0.01 to 0.7 Mev. The assignment of reduced widths to the levels observed is possible in some cases.

* Work supported by the AEC and the Wisconsin Alumni Research Foundation.
[1] Adair, Barschall, Bockelman, and Sala, Phys. Rev. **75**, 1124 (1949).
[2] Freier, Fulk, Lampi, and Williams, Phys. Rev. **78**, 508 (1950).

V4. The Coherent Scattering Cross Section and Nuclear Resonances of Tellurium. C. J. HEINDL, I. W. RUDERMAN, *Columbia University;* AND R. J. WEISS, *Brookhaven National Laboratory.*—Recent small angle neutron scattering measurements[1] show that the coherent scattering cross section of tellurium is much smaller than the free scattering cross section. This can be explained by assuming that one of the tellurium

isotopes has a strong resonance and a negative scattering length. Transmission measurements on normal isotopic tellurium with the Columbia neutron velocity spectrometer confirm the presence of a strong resonance at 2.2 ev, and a number of smaller resonances at higher neutron energies. Further transmission data on an enriched sample of tellurium containing 76.5 percent of Te^{125} are being obtained to determine if the resonance at 2.2 ev is to be attributed to this isotope. The incoherent, and from it the coherent,[2] cross sections of tellurium are being determined by a scattering experiment with the neutron spectrometer. This experiment utilizes an annular bank of BF_3 counters placed at an angle of 18° with respect to the neutron beam. Only incoherently scattered neutrons are counted when the incident neutron energy is greater than 2.5A. Thus, the incoherent cross section may be determined as a function of neutron energy.

[1] See paper by R. J. Weiss to be given at this meeting.
[2] P. J. Bendt and I. W. Ruderman, Phys. Rev. 77, 575 (1950).

V5. Single Crystal Neutron Monochromators.* S. Pasternack, A. W. McReynolds, R. J. Weiss, and L. Corliss, *Brookhaven National Laboratory.*—The effectiveness of a single crystal neutron monochromator depends both on the peak reflectivity at the Bragg angle and on the ratio of the rocking curve width to the angular spread permitted by the collimating system (provided that the former is the smaller angle). In connection with designing such a monochromator for a neutron diffraction apparatus at Brookhaven, some exploratory determinations of these factors were made on several single crystals, using the Oak Ridge neutron diffraction apparatus. The following results were obtained:

Crystal	Reflecting plane	Peak reflectivity of a thick crystal	Rocking curve width (min.)
NaCl	200	0.10	8
Ni	111	0.16	60
Pb	111	0.22	20
Fe	100	0.18	8

For the Brookhaven instrument, whose collimator has a spread of 15 to 20 minutes, it appears that a lead crystal should yield about five times more intensity than rock salt. Transmission measurements were also made through some of these crystals at and near the Bragg peaks. The relationship of the results to the dynamical theory of x-ray scattering as modified for neutrons by Bacon, Lowde, and Thewlis, and to the theory of inelastic scattering, will be discussed.

Research carried out under contract with AEC.

V6. Small Angle Scattering of Thermal Neutrons (Experimental).* A. W. McReynolds and R. J. Weiss, *Brookhaven National Laboratory.*—Broadening of a neutron beam by small angle scattering in transmission through finely divided materials was studied as a function of neutron wave-length and number, size, and index of refraction of particles. Dependence on these parameters confirmed the above theoretical considerations, for ρ large and small. A well-collimated beam was reflected from a mirror adjusted to the critical angle of 3A neutrons and allowed to traverse the powder samples. The beam contour was plotted with a slit mounted on a comparator before a BF_3 proportional counter. By immersing the sample in a liquid of known index of refraction the phase of slow neutron scattering and the coherent cross section could be determined. The phases of P, Si, Cr, Se, Ru, Mo, Pd, Cb, Bi, and Te were found to be positive. The coherent cross sections of Cr and Si indicated little isotopic or spin incoherence. Small angle scattering from carbon blacks yielded results agreeing with x-ray scattering and showed the scattered central maximum superimposed on the undeviated beam. Quantitative agreement with the total cross section for small angle scattering per particle was obtained and substantiated the R^4 dependence. The small angle scattering by ferromagnets discovered by Hughes was corroborated.

* Research carried out under contract with AEC.

V7. Small Angle Scattering of Thermal Neutrons (Theoretical).* R. J. Weiss and S. Pasternack, *Brookhaven National Laboratory.*—The differential and total cross sections for small angle scattering of thermal neutrons by spheres have been calculated. Asymptotically the results are identical with those obtained from geometrical optics (refraction) or from the Born approximation (diffraction), depending on whether the difference, ρ, between the neutron phase change in traversing the particle diameter and the phase change in traversing the same distance in vacuum is large or small, respectively. For large values of ρ the angular dependence of the differential cross section is a function only of δ, the difference from unity of the index of refraction; and the total cross section is $2\pi R^2$. For small ρ the central diffraction maximum has a half-width proportional to λ/R; the total cross section being $\pi R^2\rho^2/2$. When the sphere is part of a conglomerate, coherence effects must be considered for ρ small, but for ρ large the scatterings can be considered independent. In the latter case the multiple refraction theory of Von Nardroff is approximately valid. The above considerations may be applied to shapes other than spheres, and to ferromagnetic domains.

* Work performed under contract with AEC.

V8. Inelastic Scattering of Thermal Neutrons.* David A. Kleinman, *Brookhaven National Laboratory.*—The one-phonon cross sections, often principally responsible for the inelastic scattering, were calculated for a number of materials as a function of the incident neutron energy E for several crystal temperatures T. To shorten the calculations the integrals, equivalent to those given by Weinstock, were evaluated graphically on specially ruled paper. This method is still laborious owing to the large number of integrals, so the method of integrating over reciprocal lattice points was developed following a suggestion by Pomeranchuk and Akhieser. This leads to the formula

$$\sigma=\sigma_0\frac{m}{M}\frac{E}{\theta}\left[F\left(\frac{E}{\theta},\frac{T}{\theta}\right)-\tau f(\tau)G\left(\frac{E}{\theta},\frac{T}{\theta}\right)\right],$$

where $\tau=(m/M)(E/\theta)\phi(T/\theta)$ is essentially the Debye-Waller temperature exponent. Tables have been prepared of $F(E/\theta, T/\theta)$ and $G(E/\theta, T/\theta)$ as well as $\phi(T/\theta)$ and $f(\tau)$ permitting rapid calculation of the one-phonon cross section. The validity of the reciprocal lattice integration requires sufficient incident energy to involve a large number of crystal planes in the scattering process, but fortunately the tables agree quite well with the more laborious calculation even at the lowest energies.

* Research carried out at the Brookhaven National Laboratory under the auspices of the AEC.

V9. On the Coherent Scattering of Slow Neutrons by Fluids in the Critical Region. Louis Goldstein, *Los Alamos Scientific Laboratory.*—The theory of coherent scattering of x-rays in fluids may be used to describe their coherent scattering of slow neutrons. The formalism is based on the explicit use of the fluid correlation function which expresses the local concentration or density inhomogeneity around a given atom or molecule. In the limit of long wave radiation, e.g., visible light and of small angle slow neutron or x-ray scattering the fluid structure factor becomes independent of the details of the scattering process and the correlation. It then depends only on the density fluctuations of the fluid resulting from statistical thermodynamics. It is thus expected that as the temperature increases toward the critical temperature the scattering pattern of the slow neutrons should change considerably.

The slow neutron critical opalescence should manifest itself through an increasingly large small-angle scattering. For a simpler interpretation of the scattering process monatomic liquids might prove preferable. In view of the unsettled status of both theoretical and experimental aspects of the critical opalescence of visible radiation, it is suggested that the investigation of the slow neutron scattering by fluids in the critical region could yield information which might prove helpful for a better understanding of critical phenomena.

V10. Neutron Energy Measurements With Non-Collimated Neutrons Using Li^6-Loaded Photographic Plates.* J. H. ROBERTS, E. NAKAJI, AND W. SOLANO, *Northwestern University.*—Work on neutron energy measurements with Li^6-loaded plates has been previously reported.[1] The feasibility of measurements with this same tool for non-collimated neutrons is under investigation. The method used is to rotate the plates in a beam of neutrons produced by $Li^7(p, n)Be^7$ using protons from an electrostatic generator. The plate rotation mocks up a condition of isotropic incidence. Exposures have been made to neutrons of 200, 400, 600, and 1000 kev. Stationary plates are exposed simultaneously to give a comparison of resolution for collimated and non-collimated neutrons. At 200 kev the resolution for the two cases appears to be the same (histograms of 100-kev width at half-maximum). At 400 kev the resolution obtained with isotropic neutrons appears to be slightly worse than with collimated neutrons for which the histogram width at half-maximum is about 150 kev. At 600 and 1000 kev the resolution for collimated neutrons remains about the same as at 400 kev, but for isotropic neutrons appears somewhat worse. Observer bias will partly explain this fact. 100μ-thick *C*2 emulsions are used for this work. Exposures were made by J. Morris Blair at the Argonne National Laboratory.

* This work is supported by AEC Contract No. AT(11-1)-66.

[1] G. R. Keepin, Jr., and J. H. Roberts, Phys. Rev. **76**, 154 (1949), and Rev. Sci. Inst. **21**, 163 (1950).

V11. A Counter for Fast Neutrons.* P. S. JASTRAM, A. H. BENADE, M. R. CLELAND, AND A. L. HUGHES, *Washington University.*—A scintillation counter has been constructed that has an average efficiency of the order of 50 percent for neutrons in the range 1 to 10 Mev. The scintillation material is a solution of terphenyl, in a concentration of 2 grams per liter, dissolved in xylene. The container comprises a brass cylinder with a quartz window soldered in one end and a thin dural window in the other. Aluminum foil placed against the inner wall serves to improve the light-gathering efficiency; mineral oil between the quartz window and the surface of the photomultiplier tube reduces reflections by maintaining a nearly constant index of refraction in the light path. The cylinder is about 6 cm in length and 4 cm in diameter. The neutrons are obtained from a 3-millicurie polonium-beryllium source. The maximum energy of these neutrons is 11 Mev. A pulse-height distribution calculated from published Po-Be neutron energy distributions, and neutron-proton cross sections, is in rough agreement with the measured distribution.

* Assisted by the joint program of the ONR and AEC.

V12. The Coherent Neutron Scattering Cross Sections of Iron and Its Isotopes. W. C. KOEHLER, C. G. SHULL, AND E. O. WOLLAN, *Oak Ridge National Laboratory.*—The coherent neutron scattering cross sections of Fe, Fe^{54}, Fe^{56}, and Fe^{57} have been determined from neutron diffraction measurements. Since there are ferromagnetic scattering effects with iron, the contribution of the magnetic scattering to the observed intensities must be subtracted to obtain the nuclear scattering cross sections which are reported here. In the case of normal Fe, and Fe^{56}, diffraction peaks were observed at sufficiently large values of $\sin\theta/\lambda$ so that the magnetic contributions to the intensities were small. For the other two samples, where only a few reflections were observed, the data were fitted to the form factor curve of Wick and Steinberger[1] and extrapolated to large angles. The effective nuclear scattering amplitudes obtained in this way were corrected for isotopic content with the results shown in Table I. Although the principal measurements were made with the reduced metal samples, additional measurements on isotopically enriched samples of Fe_2O_3 were necessary to establish the relative phases of scattering.

TABLE I.

Isotope	Coherent scattering amplitude (10^{-12} cm)	Coherent scattering cross section (barns)
Fe^{56}	+0.999	12.6
Fe^{54}	+0.42	2.2
Fe^{57}	+0.23	0.64
Fe	+0.956	11.5

[1] J. Steinberger and G. C. Wick, Phys. Rev. **76**, 994 (1949).

SATURDAY AFTERNOON AT 2:00

Cobb 110

(R. L. ANTHONY presiding)

High-Polymer Physics

W1. Mechanical Properties of Substances of High Molecular Weight. IX. Non-Newtonian Flow and Stress Relaxation in Concentrated Polyisobutylene and Polystyrene Solutions. F. W. SCHREMP, JOHN D. FERRY, AND WARREN W. EVANS, *University of Wisconsin.*—A coaxial cylinder apparatus serves to measure the apparent viscosity of a concentrated polymer solution at various shearing stresses and to follow the relaxation of stress after sudden cessation of flow. The dependence of rate of strain ($\dot{\gamma}$) on shearing stress ($\mathfrak{T}$) can be represented by the equation $\dot{\gamma} = k_1 \sinh k_2 \mathfrak{T}$. The constant k_2 is almost independent of temperature, and decreases with increasing concentration. The course of the stress relaxation depends on the steady state value of $\dot{\gamma}$ preceding cessation of flow. By assuming a logarithmic distribution function Φ of elastic mechanisms which are relaxed by hyperbolic sine flow mechanisms, it can be shown that $\Phi \cong -(d\mathfrak{T}/d\log t)/2.303 k_1 t\, 2\tanh^{-1}\{(\dot{\gamma}/k_1)/(1+[1+(\dot{\gamma}/k_1)^2]^{\frac{1}{2}})\}$, where t is the elapsed time. Values of Φ obtained from this equation are independent of the rate of shear. The reduced distribution function, $\Phi_r = \Phi T_0/Tc$, plotted against the logarithm of the reduced relaxation time, $\tau_r = \tau c T/T_0\eta$, where T is the absolute temperature, $T_0 = 298°K$, c is the concentration in g/cc. and η the viscosity at zero stress, is independent of temperature and concentration over the ranges studied for each of three polymer samples.

W2. Mechanical Properties of Substances of High Molecular Weight. X. The Relaxation Distribution Function in Polyisobutylene and Its Solutions. JOHN D. FERRY, EDWIN R. FITZGERALD, MYRLE F. JOHNSON, AND LESTER D. GRANDINE, JR., *University of Wisconsin.*—Previous twin transducer measurements of the dynamic rigidity and viscosity of a polyisobutylene sample of viscosity-average molecular weight 1.2 million have been extended over a wider temperature range, and previous wave propagation data on solutions of this polymer in xylene have been extended by transducer measurements at lower concentrations. Values of the relaxation distribution function are derived from all these data, and compared with values obtained from (a) the stress relaxation measurements on solutions described in the preceding abstract, (b) stress relaxation data on solid poly-isobutylene of Andrews and Tobolsky, and (c) dynamic measurements on butyl rubber by Nolle and by Guth. When reduced to a common reference state at 25°C by the assumption that all relaxation processes depend identically on temperature and concentration, the results of the six types of measurement are consistent in order of magnitude and provide a picture of the distribution function over twelve cycles of logarithmic time. It appears to have a plateau from 0.1 to 10^4 sec. with a sharp rise at shorter times and a sharp drop at longer times.

W3. Precipitation of Polymers from Solution: The Role of Molecular Weights in the Kinetic Process. D. R. MOREY, *Eastman Kodak Company.*—The kinetics of nucleation, and of further growth of a nucleus, are examined theoretically for the case of polymer chains in dilute solution. The chains are assumed to have a moderate degree of kinking only, such as is expected with cellulose esters. The analysis is carried out primarily to examine the role which molecular weights play in the "average ' which is effective in determining the precipitation point. This average, termed the gamma-average, is not the average of the chain lengths in the precipitate phase, but it represents the "selection mechanism" which, operating over the chains in the solution phase, determines which shall precipitate. The gamma-average has the form

$$M_\gamma = \left[\frac{\Sigma N_i M_i^4 e^{dM_i}}{\Sigma N_i e^{dM_i}}\right]^{\frac{1}{3}},$$

and hence weights heavily the longer chains. Numerical cases are worked out showing substantial agreement with experiment.

W4. Sedimentation Equilibrium in Concentrated High-Polymer Solutions. M. WALES, *University of Wisconsin.*—It has been found that sedimentation equilibrium may be obtained rapidly in polymer solutions of concentration as high as 20 percent by weight, using a Svedberg equilibrium ultracentrifuge. The conditions are such that the ratio of concentrations at the ends of the sedimenting column is small (1.05−1.1). Equilibrium is usually approached more rapidly in concentrated solutions under these conditions than in solutions of medium dilution (*ca.* 0.5 percent). The osmotic pressures of concentrated solutions can be calculated from sedimentation equilibria, although there is a systematic error if the higher virial coefficients are functions of molecular weight distribution. The calculated osmotic pressures are independent of centrifuge speed. For a polystyrene fraction in butanone, the second virial coefficient agreed very well with that obtained by Schick *et al.*[1] while the third coefficient was considerably higher. Measurements were also performed with the system polyvinyl acetate-butanone.

[1] Schick *et al.*, J. Am. Chem. Soc. **72**, 530 (1950).

W5. Electrical Properties of Some Carbon Black-Oil Suspension.* M. J. FORSTER AND D. J. MEAD, *University of Notre Dame.*—The d.c. conductivity and a.c. (1000 c.p.s.) properties of suspensions of *R*-40 carbon black in transformer, silicone and linseed oils, and suspensions of Shawinigan black in linseed oil, were studied as functions of time, carbon black concentration, and rotational speed of test cell. The d.c. conductivity was also studied as a function of voltage. Immediately after agitating the suspension, both a.c. and d.c. conductivities increase rapidly with time, then level off and approach a saturation value. For the d.c. conductivity this value increases with increasing voltage in all suspensions studied except the highest concentrations (10 percent by weight), which obey Ohm's law. The rate of approach to saturation is independent of voltage, but depends on carbon black concentration. Increasing the concentration increases the conductivity. Increasing the speed of rotation decreases the conductivity. Form factors for the carbon black particles are calculated from the dynamic values of the dielectric constant by Voet's method. Agglomeration factors are then determined. At low speeds the agglomeration factor decreases rapidly with increasing speed. At higher speeds it approaches unity asymptotically. The theoretical interpretation of the results will be discussed.

* Supported in part by the ONR.

W6. Quantum-Mechanical Resonance between a Pair of Oscillator Sets which are out of Tune. H. JEHLE, *University of Nebraska.*—Consider an oscillator set 1I, 2I (molecule I) which is coupled with another set 1II, 2II (molecule II) by means of a weak dipole dipole interaction μ. Suppose all oscillators have equal frequency κ for vanishing interactions μ, λ, and study the influence of strong coupling λ in between the oscillators of each set, $H=\frac{1}{2}(q_{1I}^2+q_{2I}^2+q_{1II}^2+q_{2II}^2)+\frac{1}{2}\kappa^2(q_{1I}^2+q_{2I}^2+q_{1II}^2+q_{2II}^2)+\lambda(q_{1I}q_{2I}+q_{1II}q_{2II})+\mu(q_{1I}q_{1II}+q_{1I}q_{2II}+q_{2I}q_{1II}+q_{2I}q_{2II})$. We get an attraction between the molecules I and II, strongly dependent on λ, the more so if the molecules incorporate many identical oscillators each, instead of the two in the present example. In that case the excited levels are lowered towards the ground level which results in an enormous increase in the partition function and attraction. Though a detuning δ of the type $\kappa_{1I}=\kappa_{2I}=\kappa+\delta$, $\kappa_{1II}=\kappa_{2II}=\kappa-\delta$ will not change the attraction (just as in the case of but a single oscillator per molecule), all other types of detuning make the strong attraction practically disappear, e.g., the type $\kappa_{1I}=\kappa+\delta$, $\kappa_{2I}=\kappa$, $\kappa_{1II}=\kappa-\delta$, $\kappa_{2II}=\delta$, as well as $\kappa_{1I}=\kappa+\delta$, $\kappa_{2I}=\kappa-\delta$, $\kappa_{1II}=\kappa+\delta$, $\kappa_{2II}=\kappa-\delta$, and $\kappa_{1I}=\kappa+\delta$, $\kappa_{2I}=\kappa-\delta$, $\kappa_{1II}=\kappa$, $\kappa_{2II}=\kappa$.

SUPPLEMENTARY PROGRAMME

SP1. Cloud Chamber Operation down to −40°C. CARL E. NIELSEN AND THEODORE S. NEEDELS, *Ohio State University*. (To be given at the end of Session U if the Chairman rules that time permits.)—We have refrigerated a Wilson cloud chamber of the rubber diaphragm type in order to investigate its behavior when it is cold. Observations made include the following: In the vapor of a 3:1 ethanol-water mixture tracks of good quality were obtained at all temperatures down to −25°C. A slightly greater useful expansion range was found at the lower temperatures, but the minimum expansion required to catch ions changed little. In pure water vapor only liquid drops appeared providing that the temperature during expansion was not lower than −40°C. When temperatures below −40°C occurred, small ice crystals were formed. Our observations support Fournier d'Albe's[1] conclusion that the ice is a result of freezing of liquid droplets, not of direct crystallization from the vapor.

[1] E. M. Fournier d'Albe, Quart. J. Roy. Meteor. Soc. **75**, 1 (1949).

SP2. Measurements of the Stress in Nickel Films with a New Oscillation Magnetometer. J. ROSS MACDONALD, *Oxford University*. (To be given at the end of Session J if the Chairman rules that time permits.)—Using a new oscillation magnetometer,[1] isotropic planar stress has been measured in thin nickel films evaporated on mica and still attached thereto. Magnetometer measurements were carried out on films which ferromagnetic resonance experiments indicated had virtually no cross-sectional stress dependence and on the same film disks used in the resonance measurements. Under these conditions, magnetometer measurements yield, independent of knowledge of the volume of magnetic material in a disk, the factor $(N_y-N_x)I_0=(4\pi I_0+3\lambda T_0/I_0)$, which also occurs in the resonance condition. For all films, T_0 was found to be positive, indicating tension, and ranged from zero to 1.2×10^{10} dynes/cm², the breaking stress of nickel. It was largest in unannealed films near 0.3 micron thick and smallest in annealed films of more than 1.5 microns thickness. Independent determination of the quantity $(N_y-N_x)I_0$ allowed accurate ferromagnetic resonance g-values to be computed and showed that the g-value of nickel films is independent of film thickness and stress and is 2.20 ± 0.02, the same value as that found for bulk nickel sheets.

[1] J. H. E. Griffiths and J. R. Macdonald, J. Sci. Inst. (to be published).

SP3. Fast Neutron Resonances in Boron and Fluorine. HARVEY B. WILLARD,* WILLIAM M. PRESTON, AND CLARK GOODMAN, *Massachusetts Institute of Technology*. (To be given at the end of Session V if the Chairman rules that time permits.)—The response of a small, enriched BF_3 counter to fast neutrons (0.1 to 2.1 Mev) was measured with a resolution of 25 kev using the $Li^7(p,n)Be^7$ reaction in conjunction with the Rockefeller electrostatic accelerator. Three resonances, appearing at 1.26, 1.66, and 2.04 Mev, were ascribed to charged particle reactions in B^{10} or F^{19}. Since such resonances imply the resonances for the formation of a compound nucleus, the total cross sections of B^{10}, B^{11}, and F^{19} were measured with the same resolution for neutrons of 0.5 to 2.1 Mev. B^{10} exhibits no resonances, B^{11} shows a strong resonance at 1.28 Mev, while F^{19} has resonances at 0.95, 1.24, 1.66, and 2.04 Mev. It is consistent with the observed data to assume that the resonances in the response of the BF_3 counter are due to F^{19}. On the basis of available mass tables the most probable reaction is $F^{19}(n,\alpha)N^{16}$ ($Q\approx+3$ Mev). The resonance in B^{11} at 1.28 Mev and the resonance in F^{19} at 0.95 Mev are probably caused by resonance scattering. This work was supported in part by the ONR and BuShips.

* Gulf Oil Corporation Fellow.

SP4. Activities and Fission Yields in Chains of Masses 129 to 134.* ALEXIS C. PAPPAS† AND CHARLES D. CORYELL, *Massachusetts Institute of Technology*. (To be given at the end of Session E if the Chairman rules that time permits.)—As part of a study of the distribution of fission yield along the decay chains[1a] and perturbations in fission yields connected with nuclear shell-stabilizations,[1b,c] fission chains involving antimony,[2] tellurium, and iodine are being systematically studied radiochemically for characterization of half-lives, genetic relations, and fission yields (both independent and cumulative). Data are given below, with new values for half-life in bold-face and new values of the cumulative fission yields in percent in parentheses: 32-day Te^{129m} (0.23); 30-hr. Te^{131m} (0.45); 25-min. Te^{131} (2.5); 8.0-day I^{131} (3.0); **77.7**-hr. Te^{129} (4.5); 66-min. Te^{133} (4.5); **22.4**-hr. I^{133} (5.2), independent yield (0.5); **44m** Te^{134} (6.9); **52.5**-min. I^{134} (7.8). The fission yields have a precision of about eight percent of the values recorded. The cumulative yields at iodine of chains 131, 132, 133, and 134 are in fair agreement with the values for xenon of Thode *et al.*[3]

* Assisted by the joint program of the ONR and AEC.
† Fellow of the Royal Norwegian Council for Scientific and Industria Research from the University of Oslo.
[1a] Glendenin, Coryell, and Edwards, Paper 52, Vol. 9, Div. IV, Nat. Nucl. En. Series, McGraw-Hill, 1950; [b] Phys. Rev. **73**, 357 (1949); [c] **77**, 733 (1950).
[2] A. C. Pappas, Abstract (**E4**).
[3] Macnamara, Collins, and Thode, Phys. Rev. **78**, 129 (1950).

Author Index to Papers Presented at the Chicago Meeting

Adair, Robert K.—K10
Ajzenberg, Fay—Q8
Aldrich, L. T.—S8
Alfrey, Turner, Jr.—M4
Allen, K. W., E. Almqvist, J. T. Dewan, and T. P. Pepper—Q1
Allison, S. K., J. H. Montague, and Fred Ribe—B4
Anderson, James L., Peter G. Bergmann, and Robert Penfield—J9
Anderson, Scott—C1
Apker, L. and E. Taft—T3
Austern, Norman—J6
Axel, Peter and R. F. Goodrich—J3
Bakker, C. J. and E. Segrè—I2
Baldock, Russell and John Sites—B5
Baldwin, G. J.—S5
Barrett, Charles S. and Marjorie A. Barrett—L3
Bass, Robert R.—B11
Belinfante, F. J.—J10
Bendel, W. L., Hugh Brown, and Robert A. Becker—E7
Blewett, John P.—I5
Blizard, R. B.—G3
Bockelman, C. K.—V3
Boyer, R. F.—G9
Brightsen, Ronald A., Kalman Shure, Charlie Fisher, and Charles D. Coryell—D8
Brock, E. G. and Fr. Houde—S3
Browne, C. P., D. S. Craig, R. M. Williamson, and D. J. Donahue—I2
Brubaker, W. M.—B3
Buechc, F. and P. Debye—G4
Burstein, E., Paul L. Smith, and B. Heavis—T9
Canada, Robert and Merle E. Bunker—D10
Claassen, R. S., G. D. Freier, and W. R. Stratton—K9
Clark, Donald—P2
Clark, R. K. and S. S. Brar—D3
Cleland, M. R., C. E. Whittle, A. L. Hughes, and P. S. Jastram—U8
Coomes, E. A. and W. B. LaBerge—S1
Copeland, Paul L. and B. Pearson DeLany—B2
Craig, D. S., C. P. Browne, and R. M. Williamson—I1
Critchfield, C. L. and S. Oleksa—J2
Curtis, C. D.—K2
Danielson, G. C.—N4
Darling, B. T.—J11
De Benedetti, S. and H. J. Richings—L1

Decker, Charlotte E., Arnold G. Meister, and Forrest F. Cleveland—F6
Dejardin, G. and R. Falgon—C2
DeLany, B. Pearson and Paul L. Copeland—B1
del Castillo, G. and W. Y. Chang—U2
Dijkstra, L. J. and C. Wert—L8
Dobischek, Dietrich and Harold Jacobs—S11
Duffield, R. B. and L. M. Langer—E1
Eisenstein, A. S.—N2
El-Sabban, M. Zaki, Arnold G. Meister, and Forrest F. Cleveland—F8
Emmerich, W. S. and J. D. Kurbatov—E5
Endt, P. M., D. M. Van Patter, and W. W. Buechner—R2
Enge, H., D. M. Van Patter, W. W. Buechner, and A. Sperduto—Q12
Fan, C. Y.—E9
Fankuchen, I. and H. Mark—M3
Feld, B. T., J. S. Clark, D. H. Frisch, I. L. Lebow, and L. S. Osborne—P1
Feldman, L. and C. S. Wu—D4
Fenlon, Paul F., Forrest F. Cleveland, and Arnold G. Meister—F5
Perigle, Salvador M., Forrest F. Cleveland, and Arnold G. Meister—F9
Fermi, Enrico—A1
Ferry, J. D.—M1
——, Edwin R. Fitzgerald, Myrle F. Johnson, and Lester D. Grandine, Jr.—W2
Finn, G. B. and W. B. LaBerge—S2
Fleaher, Gail T. and George I. Cohn—U13
Forster, M. J. and D. J. Mead—W5
Fowler, E. C., D. H. Miller, R. P. Shutt, and A. M. Thorndike—U10
Fuchs, M. and E. S. Lennox—J1
Gaffney, J. and A. A. Petrauskas—G7
Gerjuoy, E.—B13
Gilvarry, J. J. and D. F. Rutland—B12
Goldhaber, Gerson, R. M. Williamson, H. L. Jackson, and M. J. W. Laubenstein—K11
Goldstein, Louis—V9
Good, R. H., Jr. and G. E. Uhlenbeck—J5
Gottlieb, Melvin B.—U5
Grattidge, W.—S6
Guth, Eugene and Hubert M. James—G1
Gutowsky, H. S., C. J. Hoffman, and R. E. McClure—I9
Halpern, J. and A. K. Mann—R6
Hanson, A. O., E. M. Lyman, and M. B. Scott—K5
Harper, S.—L7
Hartzler, A. J.—U3
Hebb, Malcolm H.—T4
Heer, C. V. and J. G. Daunt—B8
Heindle, C. J., I. W. Ruderman, and R. J. Weiss—V4
Hess, D.C., H. Brown, C. Patterson, and M. G. Inghram—D6
Hill, David L.—I6
Hincks, E. P.—P4
Hollomon, J. H.—H1
Horak, Frank A.—S7
Huntington, H. B. and L. Apker—T5
Jacobs, Harold and Dietrich Dobischek—S12
Jaffey, A. H., Sherman Fried, N. F. Hall, and L. E. Glendenin—E2
James, Hubert M. and Lloyd D. Fosdick—L9
Jamison, N. C. and T. R. Kohler—T7
Jastram, P. S., A. H. Benade, M. R. Cleland, and A. L. Hughes—V11
Jastrow, Robert—V2
Jehle, H.—V6
Johnson, C. H. and H. H. Barschall—Q11
Johnson, R. G. and W. C. Caldwell—S10
Johnson, Virgil R.—Q9
Juenker, David W.—S4
Kaufmann, S. G., F. P. Mooring, L. J. Koester, and E. Goldberg—R1
Keepin, George R., Jr.—Q5
Kerst, D. W.—N1
Kleinman, David A.—V8
Koch, H. W., J. McElhinney, and J. A. Cunningham—R8
Koehler, W. C., C. G. Shull, and E. O. Wollan—V12
Kohler, T. R. and N. C. Jamison—T8
Koski, W. S., T. Wentink, Jr., and V. W. Cohen—C4
Langer, L. M. and R. B. Duffield—D9
Langsdorff, Alexander, Jr.—V1
Lanzl, L. H. and A. O. Hanson—K4
Lawson, J. S., Jr.—E3
Leaderman, Herbert and R. G. Smith—G8
Lehman, Guy W.—T6
Litwin, J., J. J. Lord, and Marcel Schein—P8
Lloyd, Stuart P.—J7
Lord, J. J.—P7
Lundby, Arne—U9
Luyet, B.—T10
Lyman, E. M.—K13
——, E. M., A. O. Hanson, L. H. Lanzl, and M. B. Scott—K7
Lynton, Ernest A. and Henry A. Fairbank—B9
Lyons, H., M. Kessler, L. J. Rueger, and R. G. Nuckolls—C6
Macdonald, J. Ross—L11, SP2
Madigan, John R. and Forrest F. Cleveland—F7
Malkus, William V. R.—P11
Malich, C. W. and J. C. Harris—R4
Mann, A. K. and J. Halpern—R7
Matossi, Frank—C3
McCue, J. J. G. and W. M. Preston—R5
McDonald, Frank B.—P6
McReynolds, A. W. and R. J. Weiss—V6
Metzger, Franz R., and R. D. Hill—E8
Michener, J. W. and J. S. Koehler—L2
Millar, C. H. and A. G. W. Cameron—Q6
Morey, D. R.—W3
Morganstern, K. H. and H. P. Hotz—K8
Mott, N. F.—A2
Mrowca, B. A. and L. V. Holroyd—G6
Mullin, Charles J. and Eugene Guth—J8
Naugle, John E. and George W. Anderson, Jr.—P9
Needles, T. S. and C. E. Nielsen—U11
Newell, George and R. H. Dicke—C5
Nexsen, W. E., Jr., O. H. Weddle, and C. E. Nielsen—U14
Ney, E. P.—P13
Nielsen, Carl E. and Theodore S. Needles—U12
—— and Theodore S. Needles—SP1
Norberg, R. E.—I10
Novick, A. S.—L5
Omer, Guy C. Jr.—B10
Pappas, Alexis C.—E4
Pappas, Alexis C. and Charles D. Coryell—SP4
Parzen, G.—J4
Pasternack, S., A. W. McReynolds, R. J. Weiss, and L. Corliss—V5
Pepper, T. P., K. W. Allen, E. Almqvist, and J. T. Dewan—Q3
Piper, E. L. and G. A. Price—K3
Platt, J. R.—F1
Polo, Santiago R., Forrest F. Cleveland, Richard B. Bernstein, Arnold G. Meister, and Robert H. Sherman—F2
Pontarelli, Donald A., Forrest F. Cleveland, Richard B. Bernstein, Arnold G. Meister, and Robert H. Sherman—F3
Porter, Fred T. and C. Sharp Cook—D7
Richards, H. T.—J14
——, H. T., M. J. W. Laubenstein, V. R. Johnson, F. Ajzenberg, and C. P. Browne—Q7
Roberts, James H. and William H. Guier—Q10
——, J. H., E. Nakaji, and W. Solano—V10
Robson, J. M.—D2
Rodeback, G. W. and J. S. Allen—R3
Roser, Francis X. and Theodore Bowen—U7
Rouvina, James and Richard Wilson—K1
Sailor, V. L., J. J. Floyd, and L. B. Borst—D5
Schein, Marcel and M. Vidale—P5
——, J. J. Lord, and Joseph Fainberg—P3
Schillinger, Edwin J., Jr., B. Waldman, and W. C. Miller—R9
Schremp, F. W., John D. Ferry, and Warren W. Evans—W1
Schulman, James H., Robert J. Ginther, and Clifford C. Klick—T2
Schultz, Leroy—H2
Schuster, N. A. and G. E. Pake—I8
Scott, M. B., A. O. Hanson, and E. M. Lyman—K6
Seitz, Frederick—T1
Smith, Lincoln G.—B6
Sproull, R. L.—N3
Stinchcomb, Thomas G.—U4
Strait, E. N., D. M. Van Patter, A. Sperduto, and W. W. Buechner—Q2
Sunyar, A. W. and J. W. Mihelich—E6
Swihart, James and Edward Akeley—I3
Ticho, Harold K.—U1
Toppel, Bert J., Paul A. Roys, and W. E. Bennett—Q4
Townsend, J.—D1
Tuck, J. L. and L. G. Teng—I7
Turner, C. M.—I4
Van Wazer, J. R.—M2
Vidale, M. and Marcel Schein—P12
Voyvodic, L. and E. Pickup—P10
Wachtman, J. B., Jr. and J. S. Koehler—L4
Wada, Walter W.—J13
Wahlin, H. B. and Charles D. Hendricks, Jr.—L10
Wales, M.—W4
Weber, Alfons, Forrest F. Cleveland, and Arnold G. Meister—F4
Weddle, O. H. and C. E. Nielsen—U13
Weiss, R. J. and S. Pasternack—V7
Willard, Harvey B., William M. Preston, and Clark Goodman—SP3
Witmer, Enos E.—J12
Witte, R. S. and R. L. Anthony—G5
Wolicki, E. J., B. Waldman, and W. C. Miller—R10
Wu, Ta-You—B7
Wyckoff, R. W. G.—H3
Young, J. R.—S9
Yu, Ming Chen (Wang) and Eugene Guth—G2
Yuan, Luke C. L. and H. L. Poss—U6
Zener, C.—L6